Vol. 184, June 30, 1986
Complete in one issue

ISSN 0003-2670

ANALYTICA CHIMICA ACTA

International journal devoted to all branches of analytical chemistry

ELSEVIER

ANALYTICA CHIMICA ACTA

International journal devoted to all branches of analytical chemistry
Revue internationale consacrée à tous les domaines de la chimie analytique
Internationale Zeitschrift für alle Gebiete der analytischen Chemie

PUBLICATION SCHEDULE FOR 1986

	J	F	M	A	M	J	J	A	S	O	N	D
Analytica Chimica Acta	179	180	181	182 183/1	183/2 184	185	186	187	188	189	190	19

Scope. *Analytica Chimica Acta* publishes original papers, short communications, and reviews dealing with e aspect of modern chemical analysis both fundamental and applied.

Submission of Papers. Manuscripts (three copies) should be submitted as designated below for rapid and effi handling:

Papers from the Americas to: Professor Harry L. Pardue, Department of Chemistry, Purdue University, West Lafay IN 47907, U.S.A.

Papers from all other countries to: Dr. A. M. G. Macdonald, Department of Chemistry, The University, P.O. Box Birmingham B15 2TT, England. Papers dealing particularly with computer techniques to: Professor J. T. C Universität Bern, Pharmazeutisches Institut, Baltzerstrasse 5, CH-3012 Bern, Switzerland.

Submission of an article is understood to imply that the article is original and unpublished and is not being consid for publication elsewhere. Upon acceptance of an article by the journal, authors will be asked to transfer the copy of the article to the publisher. This transfer will ensure the widest possible dissemination of information.

Information for Authors. Papers in English, French and German are published. There are no page cha Manuscripts should conform in layout and style to the papers published in this Volume. Authors should co Vol. 170 for detailed information. Reprints of this information are available from the Editors or from: Elsevier Edit Services Ltd., Mayfield House, 256 Banbury Road, Oxford OX2 7DH (Great Britain).

Reprints. Fifty reprints will be supplied free of charge. Additional reprints (minimum 100) can be ordered. An form containing price quotations will be sent to the authors together with the proofs of their article.

Advertisements. Advertisement rates are available from the publisher.

Subscriptions. Subscriptions should be sent to: Elsevier Science Publishers B.V., Journals Department, P.O. 211, 1000 AE Amsterdam, The Netherlands. Tel: 5803 911, Telex: 18582.

Publication. *Analytica Chimica Acta* appears in 13 volumes in 1986. The subscription for 1986 (Vols. 179–19 Dfl. 2730.00 plus Dfl. 312.00 (p.p.h.) (total approx. US $1192.94). All earlier volumes (Vols. 1–178) except Vol and 28 are available at Dfl. 231.00 (US $90.59), plus Dfl. 15.00 (US $5.88) p.p.h., per volume.

Our p.p.h. (postage, packing and handling) charge includes surface delivery of all issues, except to subscribers i U.S.A., Canada, Japan, Australia, New Zealand, P.R. China, India, Israel, South Africa, Malaysia, Thailand, Singa South Korea, Taiwan, Pakistan, Hong Kong, Brazil, Argentina and Mexico, who receive all issues by air del (S.A.L. — Surface Air Lifted) at no extra cost. For the rest of the world, airmail and S.A.L. charges are available request.

Claims for issues not received should be made within three months of publication of the issues. If not they cann honoured free of charge.

For further information, or a free sample copy of this or any other Elsevier Science Publishers journal, readers i U.S.A. and Canada can contact the following address: Elsevier Science Publishing Co. Inc., Journal Inform Center, 52 Vanderbilt Avenue, New York, NY 10017, U.S.A., Tel: (212) 916-1250.

0003-2670/86/$

Printed in The Netherlands

ANALYTICA CHIMICA ACTA
VOL. 184 (1986)


RESPECT COPYRIGHT
BERNE
CONVENTION
100 YEARS
1886-1986
ENCOURAGE CREATIVITY

ANALYTICA CHIMICA ACTA

International journal devoted to all branches of analytical chemistry

ELSEVIER Amsterdam–Oxford–New York–Tokyo

Anal. Chim. Acta, Vol. 184 (1986)

0003-2670/86/$0

Printed in The Netherlands

Analytica Chimica Acta, 184 (1986) 1—19
Elsevier Science Publishers B.V., Amsterdam — Printed in The Netherlands

COMPUTER-MEDIATED REDUCTION OF SPECTRAL PROPERTIES TO MOLECULAR STRUCTURES
General Design and Structural Building Blocks

MORTON E. MUNK*, RANDY J. LIND and MICHAEL E. CLAY
Department of Chemistry, Arizona State University, Tempe, AZ 85287 (U.S.A.)
(Received 29th November 1985)

SUMMARY

A basic design is outlined for the conversion of the aggregate spectral properties of an organic compound of unknown structure to a set of compatible alternative molecular structures which is small in number and exhaustive in scope. The process is built around a precisely defined unit of substructure. A procedure is described for the exhaustive generation of the set of these fragments from any specified group of elements and allowed valences. A versatile, user-friendly data-management system (FOCISS) provides a convenient means of manipulating these fragments and correlating their structure and properties. Extensive carbon-13 n.m.r. data are in place and applications of FOCISS to fragment-oriented searches are illustrated. The creation of a subset of chemically-stable fragments is also described.

Over the past two decades, there have been substantial improvements in computer-based methods for the storage, retrieval and correlation of spectral data and structural properties. The application of these techniques to automated inference of structural features from spectral data followed naturally. More recent work has focussed on merging the process of structural inference with molecular structure generation. The CHEMICS [1, 2] and STREC [3] programs are among the earliest examples of such merged programs and accept as input, data from several spectroscopic sources; DARC-EPIOS [4—6], the GENOA-based system [7, 8] and ACCESS [9] draw largely on high-integrity, computerized libraries of assigned carbon-13 n.m.r. spectra and as such are limited by the scope of the substructures in their data bases. Our efforts in this field are centered around the group of computer programs collectively known as CASE.

Goal of the CASE system

In developing a plan for the merger of the methods of structural inference [10—13] and molecule assembly [14—17] that comprise the CASE system, the first need was to define the goal explicitly. In common with other current efforts in the application of the techniques of artificial intelligence to the solution of complex chemical problems, the overall goal of this work is to

0003-2670/86/$03.50

increase the productivity of the chemist. Specifically, it is desirable to reduce the time required to elucidate the structure of an organic compound by developing computer software that can directly reduce the molecular formula and spectral properties of a compound of unknown structure to a set of plausible alternative structures that is small in number but exhaustive in scope. In the computer-assisted process envisaged, the chemist first becomes involved in the structure elucidation at the stage of this small set of compatible structures. The only step remaining is the distinction between these alternatives. Given a manageable number of alternative structures, this is a task at which the chemist excels and can generally complete in a short time. The chemist is spared the most time-consuming component of the process, that of reaching the stage of a manageable number of plausible alternatives. Thus, for the foreseeable future, the chemist is a central participant and the system is still described as Computer-Assisted Structure Elucidation (CASE).

GENERAL ORGANIZATION OF THE CASE SYSTEM

Given the diversity of molecular architecture encountered in nature and the imagination of the synthetic chemist in creating new molecules, the need for computerized structure-elucidation systems with no substructural limitations is clearly evident. Because all such computer programs depend on relationships between subspectra and substructure, purposefully compiled spectral libraries can be a rich source of such information. Unfortunately, the scope of currently available libraries falls short of the diversity of substructure required, and it is probable that it will be so for some years. Thus, library-dependent systems, which can retrieve only those substructures present in the compounds of the library, may fail to include the correct structure among those proposed. In the present work, exhaustiveness receives high priority; the scheme favored, therefore, has no substructural limitations in treating the large majority of organic compounds. This assures the presence of the correct structure among those produced by CASE.

The general organization (Fig. 1) calls for an initial step in which the molecular formula of the compound of unknown structure and its aggregate spectral properties are reduced to a shortlist of "basic units of structure." In subsequent steps, larger structural fragments are inferred from the observed spectral properties, and structural inferences that cannot be expressed in terms of substructure are also derived from the input. Finally, the basic units of structure derived in the initial step are subjected to a constrained structure-generation process to produce the set of molecular structures compatible with the spectral data input. The larger structural fragments and the inferences, all of which may be overlapping in information content, serve as the major constraints on the process. In this paper, the initial step is considered.

The shortlist of "basic units of structure" compatible with the molecular formula and observed spectral data could be derived in one of two ways: (1) build these fragments directly from the spectral data; or (2) prune from a

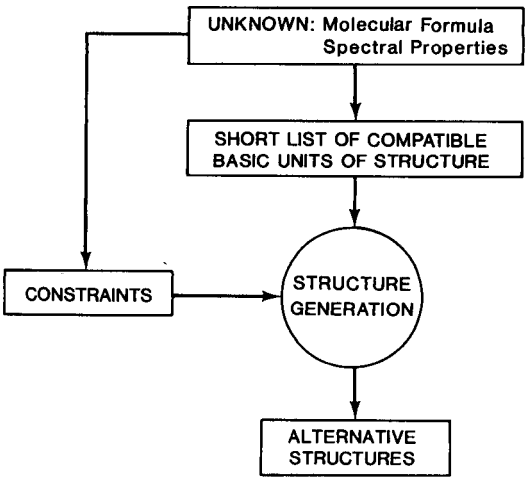

Fig. 1. Organization of the CASE system.

list of "basic units of structure" those that are incompatible with the observed spectral data. The latter was selected because it is more readily amenable to the attainment of exhaustiveness. That requisite is met in principle by pruning from an exhaustive list of basic units of structure. Such an approach imposes two demands on the nature of that structural unit. First, it must be large enough to possess sufficiently distinctive spectral properties. Secondly, it must be small enough such that the number of all possible structural units is manageable. Clearly, these are conflicting conditions and optimizing them necessarily requires compromise. A third condition was imposed for ease of generating and manipulating these structural units: uniformity in structural nature. These three requirements are most readily accommodated by an atom-centered substructure model which is built of concentric layers of "element groups" surrounding a central "element group." (An "element group" defines a specific non-hydrogen atom, the number of attached hydrogen atoms and each partial bond by which it can join to other element groups. For example, there are three possible oxygen element groups, —OH, —O—, and =O.) The designation n-ACF is defined here as an atom-centered fragment so constituted, where n is equal to the number of concentric layers of element groups about the central element group. In this substructural model, only outermost-layer element groups possess residual valence. It is the optimization of the first two requirements that establishes the boundary of the atom-centered fragment (ACF) for the present purpose at one concentric layer of element groups (hereafter designated as a 1-ACF).

The 1-ACF is a precisely defined unit of substructure which can be exhaustively generated, conveniently canonicalized and represented internally, readily combined into larger fragments or molecules, and correlated with its spectral properties.

Generation of exhaustive 1-ACF list

An algorithm was developed for the exhaustive generation of 1-ACFs compatible with elemental type and valence limits set by the user. The building blocks of 1-ACFs in this procedure are element groups. For the present initial study, the elements found in the large majority of organic compounds were considered: carbon, hydrogen, oxygen, nitrogen(III), sulfur(II) and each of the halogens. Common structural units not permitted by these limits, e.g., nitro (monocoordinate), sulfone (dicoordinate) and phosphate (tricoordinate), can be conveniently included by treating them as "super" element groups. Only the nitro group was included at this time, making a total of 27 element groups (Table 1). This list of 27 element groups represents the only constraint on the scope of the molecular structures that can be treated, and that constraint is controlled by parameters in the program; it is not intrinsic to the method. It should be noted that although used here for 1-ACF generation, the algorithm described below is applicable to the generation of atom-centered fragments bearing more than one concentric layer of element groups.

The algorithm designates each of the 27 element groups in turn as a 1-ACF center and connects to it all possible combinations of element groups such that: (1) only like partial bond types join together; (2) all bonding sites of the central element group are satisfied; and (3) at least one bonding site of at least one first-layer element group remains open.

Each element group (EG) is assigned an identification number (*EGID*) and

TABLE 1

The element groups

EGID[a]	EG[b]	*CN*[c]	*BT*[d]	*EGID*[a]	EG[b]	*CN*[c]	*BT*[d]
1	$-CH_3$	1	1	15	$-NO_2$	1	1
2	$=CH_2$	1	2	16	$-CH_2-$	2	1
3	$\equiv CH$	1	3	17	$-CH=$	2	1, 2
4	$-NH_2$	1	1	18	$=C=$	2	2
5	$=NH$	1	2	19	$-C\equiv$	2	1, 3
6	$\equiv N$	1	3	20	$-NH-$	2	1
7	$-OH$	1	1	21	$-N=$	2	1, 2
8	$=O$	1	2	22	$-O-$	2	1
9	$-SH$	1	1	23	$-S-$	2	1
10	$=S$	1	2	24	$>CH-$	3	1
11	$-F$	1	1	25	$>C=$	3	1, 2
12	$-Cl$	1	1	26	$>N-$	3	1
13	$-Br$	1	1	27	$>C<$	4	1
14	$-I$	1	1				

[a]Element group identification number. [b]Element group. [c]The number of other element groups to which the element group may bond. [d]The partial bond types (1 = single, 2 = double, 3 = triple) that comprise the element group.

classified according to its coordination number (*CN* value) and the multiplicity of each of its bonding sites, i.e., single ($BT = 1$), double ($BT = 2$) or triple ($BT = 3$). Whereas a given EG can belong to only one *CN* subset, it will be a member of more than one *BT* subset if $CN > 1$ and the bonding sites are of more than one bond type (Table 1). The final partitioning of element groups that is used directly in 1-ACF generation is based on *BT* subset membership. Bond type arrays $BTARY_{BT=1}$, $BTARY_{BT=2}$ and $BTARY_{BT=3}$ each contain EGs bearing single, double and triple bonding sites, respectively (Table 2). Within each array, EGs are arranged in order of ascending *EGID* value. Each array is assigned an array limit (N_{max}) and an initialization pointer (1*CN*2) to designate the first listed element group with $CN > 1$. Thus, $N_{max} = 20$, 8 and 3, and $1CN2 = 10$, 5 and 3 for $BTARY_{BT=1}$, $BTARY_{BT=2}$ and $BTARY_{BT=3}$, respectively. Once an EG has been selected as a central element group, the first-layer EGs for each possible 1-ACF are determined by stepping through the appropriate bond-type array for each bonding site of the central EG. The "appropriate" bond-type array is that which matches the bond multiplicity of the bonding site. A stepwise summary of the process of 1-ACF generation starting with dicoordinate central element groups ($CN = 2$) is illustrative of the procedure (both $-CH_2-$ and $-CH=$ should be considered as central EGs).

TABLE 2

The bond-type arrays

$BTARY_{BT=1}$			$BTARY_{BT=2}$			$BTARY_{BT=3}$		
Array position	*EGID*	*CN*	Array position	*EGID*	*CN*	Array position	*EGID*	*CN*
1	1	1	1	2	1	1	3	1
2	4	1	2	5	1	2	6	1
3	7	1	3	8	1	3 ($= N_{max}$ = 1*CN*2)	19	2
4	9	1	4	10	1			
5	11	1	5 (= 1*CN*2)	17	2			
6	12	1	6	18	2			
7	13	1	7	21	2			
8	14	1	8 ($= N_{max}$)	25	3			
9	15	1						
10 (= 1*CN*2)	16	2						
11	17	2						
12	19	2						
13	20	2						
14	21	2						
15	22	2						
16	23	2						
17	24	3						
18	25	3						
19	26	3						
20 ($= N_{max}$)	27	4						

Step 1: Set $EGID_c$ to the ID number (Table 1) of the currently selected central EG (a dicoordinate EG in this example).

Step 2: Set CN_c to the coordination number of the currently selected EG (Table 1).

Step 3: Set BT_1 equal to the bond-type value of the bonding site of lowest bond multiplicity and assign subsequent BT_j values to remaining bonding sites in order of ascending bond type values; for a dicoordinate central EG, only BT_1 and BT_2 values are assigned.

Step 4: For each BT_j, create an EG array ($BTARY_j$) containing all members of the subset with the assigned bond type value of BT_j; for a dicoordinate central EG, $BTARY_1$, and $BTARY_2$ will be created; their BT values may or may not be equal.

Step 5: Let N_j be the pointer to select a first-layer EG from $BTARY_j$. Initialize N_j values as follows: (a) set $j = 1$ and initialize $N_1 = 1CN2$, i.e., begin EG selection within $BTARY_1$ at the array position equal to $1CN2$; (b) set $j = j + 1$ and initialize N_2 to a value of 1, i.e., to array position 1 within $BTARY_2$.

Step 6: Let the value of $EGID_c$ define the central element group of the newly generated 1-ACF and each N_j value a first-layer element group (each N_j value is a position pointer in $BTARY_j$).

Step 7: Increment N_j values as follows: (a) set $j = 1$; (b) increment the value of N_j by 1; (c) test the value of N_j against N_{max} for $BTARY_j$ (the maximum allowed array position; see Table 2); (d) if $N_j \leqslant N_{max}$, then repeat step 6, else go to (e); (e) set $j = j + 1$; (f) increment the value of N_j by 1; (g) test the value of N_j against N_{max} for $BTARY_j$ and reset N_{j-1} to $1CN2$ (its original initialized value, see step 5a); (h) if $N_j \leqslant N_{max}$, then test N_j against N_{j-1}, else go to step 8; (i) if $N_j \leqslant N_{j-1}$, then to step 6, else set N_{j-1} equal to N_j and then go to step 6.

Step 8: Compare the bond-type values of BT_1 and BT_2; if $BT_1 \neq BT_2$, then go to step 10, else go to step 9.

Step 9: Exchange the contents of arrays $BTARY_1$ and $BTARY_2$, and exchange the values of BT_1 and BT_2: (a) initialize N_1 and N_2 as in steps 5(a) and 5(b); (b) reset N_{2max} such that only monocoordinate EGs are allowed, i.e., $N_{2max} = 9$ [for a dicoordinate central EG, if $BT_1 \neq BT_2$, BT_1 must originally be equal to 1 (step 3) because the only possible bond-type combinations are 1 and 2, and 1 and 3; dicoordinate EGs are excluded to prospectively eliminate redundancy]; (c) go to step 6.

Step 10: Increment $EGID_c$ by 1: (a) test value of $EGID_c$ against $EGID_{max}$ (Table 1); (b) if $EGID_c \leqslant EGID_{max}$, then go to step 2, else STOP.

In this procedure, it is the creation of element-group subsets based on bond-type membership ($BTARY_j$, step 3) that assures that only partial bonds of identical bond multiplicity will be linked in joining first-layer EGs to a

central EG. The overall generation process, which requires only a few seconds of CPU time on a Prime 450 computer, also prospectively eliminates the formation of molecules (e.g., CH_3—CH_2—CH_3) and duplicate fragments. The former is precluded in step 5 by initializing the first array pointer N_1 to begin the selection of element groups with those having a coordination number greater than one. Thus, at least one first-layer EG will possess a partial bonding site.

Intrinsic to the stepwise procedure that accounts for exhaustiveness in 1-ACF generation is the potential for redundancy. This can occur when the central element group possesses more than one partial bond of the same bond type (e.g., —CH_2—). In these cases, the contents of at least two $BTARY_j$ arrays will be identical (step 4). Unless prospectively precluded, redundancy results because two different permutations of EGs may in fact be the same combination of EGs, e.g., with —CH_2— as the central EG, the outcome N_1 = 11, N_2 = 10, generated prior to N_1 = 10, N_2 = 11, gives the same 1-ACF. By the simple measure of including step 7(i), i.e., by ensuring that N_j never falls below the value of N_{j+1} when they are re-initialized (step 7f, g), this occurrence is prevented, i.e., the latter permutation, N_1 = 10, N_2 = 11, is bypassed. Central EGs with no two bond types alike do not of course suffer from this problem. With unlike bond types, N_j, which is initialized to a value equal to *1CN2*, can never fall below N_{j+1} (see Table 2, e.g., for BT = 1, N_1 is initialized to a value of 10 which is greater than $N_{2\max}$ = 8 for BT = 2), and therefore in step 7(i), the "else" statement is never invoked.

Step 9 applies only to those cases of central EGs of $CN > 1$ where more than one bond type is represented. There are four such EGs, with *EGID* = 17, 19, 21, and 25. With these central EGs, step 9, which calls for an exchange of the contents of arrays $BTARY_1$, and $BTARY_2$ (and their BT_j values as well) after all permissible values of N_2 have been considered ($N_{2\max}$ = 8 for $BTARY_{BT=2}$ and $N_{2\max}$ = 3 for $BTARY_{BT=3}$; see step 7(h)), is required for exhaustiveness. Consider —CH= as central EG. Before exchange, only single-bond-containing EGs with CN > 1 are joined to the central EG, i.e., EGs in array $BTARY_{BT=1}$ with $N_1 \geqslant 10$. The 1-ACFs which combine monocoordinate EGs from array $BTARY_{BT=1}$ with di- and tri-coordinate EGs from $BTARY_{BT=2}$ are not generated because of the device (step 5(a)) that excludes molecule formation. The exchange (step 9) corrects this deficiency. After exchange, initialization of $BTARY_1$ (which now contains members of the BT = 2 EG subset) and resetting $N_{2\max}$ ($BTARY_2$ now contains members of the BT = 1 EG subset) to exclude EGs with $CN > 1$, precludes any duplicate 1-ACFs.

Given the elemental and valence limits described earlier, a total of 13,703 1-ACFs were generated by a computer program written to implement the above algorithm. Support for the veracity of this number was obtained by the application of the principles of combinatorial mathematics [18]. The 1-ACF generation may be viewed as a summation of all valid combinations of EGs (first-layer EGs) with each of the 27 EGs (central EG). Each of the

TABLE 3

Summation formulae for 1-ACFs

EG type	Number of EGs in subset	Summation equation	Number of 1-ACFs[b]
E—	9	$n(a_1 - a'_1)$[a] = 9(20 — 9)	99
E=	4	$n(a_2 - a'_2)$ = 4(8 — 4)	16
E≡	2	$n(a_3 - a'_3)$ = 2(3 — 2)	2
—E—	4	$n(\Sigma a_1 - \Sigma a'_1)$ = 4(210 — 45)	660
—E=	2	$n(a_1 * a_2 - a'_1 * a'_2)$ = 2(160 — 36)	248
—E≡	1	$n(a_1 * a_3 - a'_1 * a'_3)$ = 1(60 — 18)	42
=E=	1	$n(\Sigma a_2 - \Sigma a'_2)$ = 1(36 — 10)	26
—E<	2	$n(\Sigma\Sigma a_1 - \Sigma\Sigma a'_1)$ = 2(1540 — 165)	2750
=E<	1	$n(a_2 * \Sigma a_1 - a'_2 * \Sigma a'_1)$ = 1(1680 — 180)	1500
>E<	1	$n(\Sigma\Sigma\Sigma a_1 - \Sigma\Sigma\Sigma a'_1)$ = 1(8855 — 495)	8360

[a] a_i = number of element groups having membership in BT_i, where i = 1 (single bond), 2 (double bond), or 3 (triple bond); a'_i = number of element groups at the intersection of BT_i and CN = 1. [b] The number of 1-ACFs derived from all EG types is 13,703.

27 EGs can be classified into one of the ten subsets of EG types shown in Table 3 on the basis of coordination number and partial bond types. These parameters in turn define the appropriate summation equation for each of these EG classes. The approach taken in developing each equation is to calculate for each EG class: (1) the total number of first-layer EG combinations consistent with coordination number and bond-type requirements; and (2) the number of complete molecules that are possible. The latter is achieved by considering only monocoordinate EGs as eligible first-layer EGs. Subtraction of the latter number from the former gives the number of valid 1-ACFs. Thus, in Table 3, a'_i and a_i (where i is bond type (BT) of 1, 2, or 3) correspond to the number of EGs in the subset with $BT = i$ and the number of monocoordinate EGs in the subset with $BT = i$, respectively. Table 3 lists the number of valid 1-ACFs derived from each central EG type. Summing the results yields a total of 13,703 unique 1-ACFs, in consonance with the number of 1-ACFs generated by the computer program.

Representation and management of 1-ACFs

Storage and manipulation of 1-ACFs are facilitated by using a canonicalized 1-ACF representation appropriate to a 32-bit word. An array of element-group identification numbers (EGIDs, Table 1; a maximum of five is required) is packed into a 10-digit computer word such that: (1) the central EGID occupies the first two-digit integer number field; (2) the first-layer EGIDs fill succeeding two-digit number fields in order of increasing multiplicity of the bond by which the element group joins to the central element group; and (3) EGIDs for first-layer element groups with the same bond multiplicity are arranged in ascending order. This format also forms the basis

of a convenient, structurally illuminating representation of 1-ACFs for the chemist. Thus, for 1-ACF

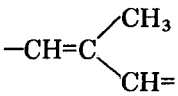

the computer representation is 25011717, and the linear representation is C(—CH_3)(—CH=)=CH— or C(CH_3)(CH=)=CH. (Single bonds are implied if no designation is provided.)

The filing structure for 1-ACFs and their properties is sketched in Fig. 2. A direct-access file contains the 1-ACF structure words, arranged in order of ascending identification numbers (ACFID), each of which is followed by a set of data pointers to the properties file. This file is designed to store structural, spectral, chemical and/or physical properties of each 1-ACF. Finally, an inverted file is included in which these properties can serve as record keys.

A user-friendly data-management system called FOCISS (fragment-oriented chemical information search system) serves a number of functions, among them, the correlation of information in the above-described files. In this application, an editor, which includes a series of versatile and rapidly executed commands for substructure searches, permits the creation of coherent subsets of 1-ACFs. Searches based on element type, element groups, and partial or generalized 1-ACFs are possible and, in addition, Boolean file-merging can be done on the resulting subsets.

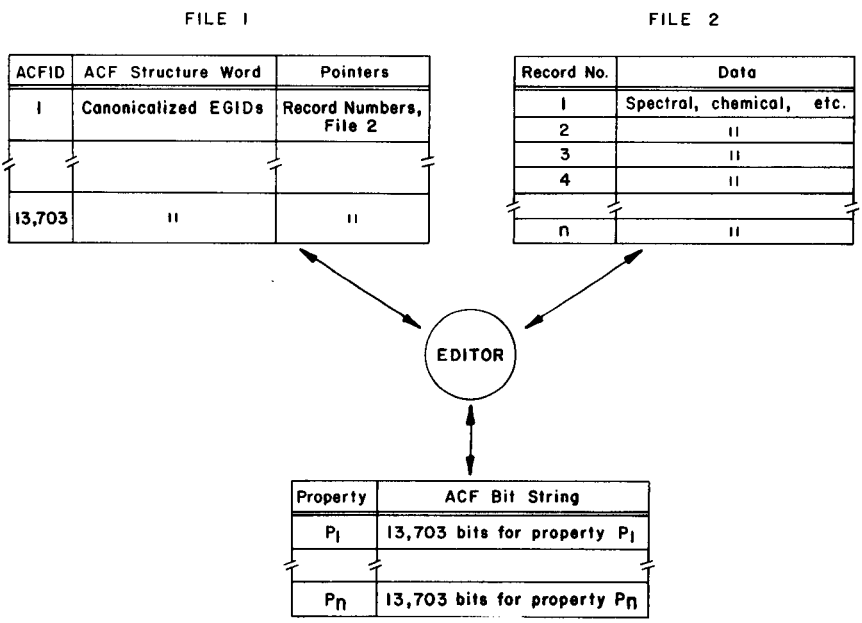

Fig. 2. Filing structure for 1-ACFs.

The chemically stable 1-ACF list

The generator builds valid 1-ACFs based only on coordination number and bond-type considerations; chemical stability is not taken into account by that program. Thus, as expected, the exhaustive list of 1-ACFs includes a number of 1-ACFs that would be expected to confer significant chemical instability on molecules containing them. A plan for computer-assisted structure elucidation, which in its initial step prunes 1-ACFs that are not compatible with observed spectral data, would benefit from a pre-pruning of these "chemically unstable" 1-ACFs. The subset of such 1-ACFs had, therefore, to be identified. Obviously, the state of knowledge pertaining to chemical stability is dynamic in nature and, in part, the boundaries of chemical stability depend on the user's frame of reference and the history of the chemical unknown in question. Thus, a "chemically stable" 1-ACF list is an individual statement of chemical stability that can be tailored to particular needs.

The FOCISS editor offers a convenient and rapid procedure for pruning the exhaustive file of 1-ACFs. Subfiles of 1-ACFs expected to lead to chemical instability were created. These subfiles are listed in Table 4 according to the major structural class to which they belong. Column 2 (1-ACFs excluded), which describes the structural features of the "unstable" 1-ACFs, is followed by an example of an excluded 1-ACF. The justification for the exclusion is also given.

The "generalized 1-ACF" for each subset of "unstable" 1-ACFs that is shown in column 2 of Table 4 comprises an input statement to FOCISS and is a precise statement of the boundaries of chemical stability intended by the chemist. Thus, in the structural class designated "acetal/ketal," aldehyde and ketone hydrates ($-CH(OH)_2$, $>C(OH)_2$) are not excluded because some natural products occur as such, but the mono and diamino analogs ($C(OH)NH_2$, $C(NH_2)NH_2$) are excluded. The same 1-ACF may confer chemical instability on some types of compounds in which it resides, but not others. Such 1-ACFs cannot be excluded, even though at times their inclusion may result in the generation of implausible molecular structures. Consider the 1-ACFs, $-CH=C(OH)-CH=$ and $>C=C(OH)-CH=$: each may constitute either the enol form of a conjugated ketone, which is not considered the preferred tautomer, or a phenol, which is the preferred tautomeric form. Thus, these 1-ACFs are not excluded; however, 1-ACFs such as $CH_2=C(OH)CH=$, $-CH=C(OH)CH_2-$, $-CH=CH(OH)$ and $>C=CH(OH)$ (the latter two constituting the enol tautomer of aldehydes), which cannot be contained as part of a phenol moiety, are excluded. In contrast, the isoamide tautomer ($-N=C-OH$) of the amide functionality ($-NH-C=O$) is not preferred even as part of an aromatic system (e.g., 2-hydroxypyridine preferentially exists as the pyridone).

The union (Boolean OR) of all of the 1-ACF subsets produced was followed by the creation of its complement (Boolean NOT), a "chemically stable" 1-ACF file containing 5058 entries. The composition of this particular

1-ACF file reflects the needs of chemists working on natural products who may isolate compounds from complex mixtures of biological substances with exposure to aqueous medium. (Substances that are sensitive to hydrolysis or are oxidizing in nature are unlikely to survive such an environment.) However, with the editor, the user can conventiently change the composition of this file to reflect the needs of differing problems.

A 1-ACF-ORIENTED CARBON-13 N.M.R. DATA BASE

Carbon-13 n.m.r. spectroscopy is one of the most powerful of currently available probes of the molecular structure of organic compounds. The inclusion of large libraries of assigned carbon-13 n.m.r. spectra in the Chemical Information System (CIS) [19, 20] and the DARC-PLURIDATA system [21], and the development of the large Bremser carbon-13 n.m.r. database [22—24] are but one reflection of this fact. These computer-based libraries among other applications, serve as a source of correlations between structural and spectral properties.

Because the chemical shift of a carbon atom is influenced by its surrounding atomic neighbors, the atom-centered fragment is an ideal substructural model around which to build such structure/spectra correlations. The published compilations of Bremser **[25]** are the most extensive available. The most recent of these reports [26] lists the chemical-shift ranges of carbon-centered fragments with one concentric layer of neighboring atoms that were retrieved from a collection of 58,000 carbon-13 n.m.r. spectra. Although related, the one-sphere atom-centered fragments in this compilation do not correspond directly to 1-ACFs as defined herein. Additional information, beyond that expressed by the 1-ACF (e.g., the distinction between a "double bond" and an "aromatic bond") is provided, but these fragments themselves are generally not as structurally explicit as the element-group-based 1-ACF, in that the hydrogen multiplicity and hybridization of first-layer atoms are not specified.

The work of Jezl and Dalrymple [27] represents an early application of such correlations to the assignment of structure using the carbon-13 n.m.r. spectrum of an unknown. More recent studies include the work of Dubois et al. [4], Zippel et al. [28], Bremser and Fachinger [9] and Gray et al. [7]; the latter is the only one to include the configurational environment of the resonating carbon atom in the encoded atom-centered fragment.

In anticipation of relating the structural environment of 1-ACFs to their carbon-13 n.m.r. spectral characteristics, the CIS carbon-13 n.m.r. library was meged into FOCISS. In preparation for this task, all possible 1-ACFs were extracted from each of the approximately 7300 compound entries in the CIS carbon-13 n.m.r. library. Associated with each of the carbon-centered 1-ACFs extracted is the following information: its ACFID; the CIS connection table number and compound identification number from which it was derived; the literature reference from which the spectral data were acquired;

TABLE 4

Chemical unstable 1-ACFs

Structural class[a]	1-ACFs excluded[b]	Example	Basis for exclusion[c]
A. Aldehyde/Ketone			
1. Acetal/ketal	V—C(Y)Z V = X, —NH_2, —SH, —NO_2 Y = C, —H Z = O, N, S	NH_2—CH(CH_2—)O—	A
2. Thioketone	S=C(Y)Z Y, Z = —C≡, —CH<, —CH_2—, —CH_3, —N=, —H	S=C(CH_3)CH_2—	D
3. Enol	=C=C—Y Y = —OH, —NH_2, —SH	=C=CHOH	D
	CH_2=C(Y)C Y = —OH, —NH_2, —SH	CH_2=C(OH)CH=	D
4. Imine	HN=C(Y)Z Y = C Z = C, —H	HN=CH—CH_2—	A
B. Acid			
1. Acid halide	V=C(Y)Z V = O, S, =NH Y = X, —NO_2 Z = any EG	O=C(Cl)CH_2—	A
2. Isoamide	V=C(Y)Z V = NH=, —N= Y = C Z = —OH	NH=C(CH_2—)OH	D
	—N=C(Y)Z Y = C(sp^3, sp) Z = X, —SH, —NO_2	—N=C(SH)CH_2—	D
	HN=C(Y)Z Y = C Z = O, —N=, S, X, —NO_2	HN=C(Cl)CH_2—	A
3. Thioacid	S=C(OH)Y Y = C	S=C(OH)CH_2—	D
4. Orthoacid	V = CWYZ V = —OH, —NH_2, —SH W = C, —H Y, Z = O, N, S, X, —NO_2	HO—CH(O—)$_2$	C
5. Orthocarbonate	Y_2CZ Y = O, N, S, X, —NO_2 Z = O, N, S	—O—C(Cl)$_2$O—	A, C
6. Carbonic acid	V=C(Y)Z V = O, S, =NH Y = —OH, —SH Z = O, N, S	O=C(OH)NH—	C
	—N=C(OH)Y Y = O, N, S, X, —NO_2	—N=C(OH)NH—	D

TABLE 4 (continued)

Structural class[a]	1-ACFs excluded[b]	Example	Basis for exclusion[c]
	—N=C(Y)Z Y = X, —NH_2, —SH, —NO_2, —H Z = X, —SH, —NO_2	—N=C(NH_2)SH	D
	HN=C(Y)Z Y = O, —N=, S, X, —NO_2 Z = O, N, S, X, —NO_2, —H	HN=C(Cl)NH—	A
7. Enol acid	CH_2=C(Y)Z Y = —OH, —NH_2, —SH Z = O, N, S, X, —NO_2	CH_2=C(OH)S—	D
	V=C(Y)Z V = >C=, —HC= Y = —OH Z = O, N, X, —SH, —NO_2	—HC=C(OH)NH_2	D
	V=C(Y)Z V = >C=, —CH= Y = —NH_2, —SH Z = X, —NH_2, —SH, —NO_2	—HC=C(NH_2)SH	D
8. Ketene/carbon dioxide	Y=C=Z Y = C, N Z = O, N, S	—CH=C=O	A
9. Ynol	—C≡C—Z Z = —OH, —NH_2, —SH	—C≡C—SH	D
C. Heteroatom-Heteroatom Bonds			
1.	Y—O—Z Y = O, S, X, —NO_2 Z = any EG	Cl—O—CH_2—	B
2.	Y—N=Z Y = X, —NH_2, —SH, —NO_2 Z = any EG	Cl—N=CH—	A, B
3.	V—N(Y)Z V = O, N(sp^3), S, X Y, Z = any EG, —H	Cl—NH—CH_2—	B
4.	Y=N—Z Y = =C=, =NH, =S Z = any EG	NH=N—O—	A, C
5.	O=N—Y Y = —O—, —NH—	O=N—O—	A, D
6.	Y—S—Z Y = O, N(sp^3), X, —SH, —NO_2 Z = any EG	HS—S—NH—	B
7.	S=Y Y = =N—, =C=	S=C=	C
8.	Y—N(NO_2)$_2$ Y = any EG	—CH_2—N(NO_2)$_2$	B

[a]Structural class in the broadest sense, including derivatives and heteroatom analogs. [b]V, W, Y, and Z are first-layer element groups. X is a halogen, i.e., F, Cl, Br or I. Where V, W, Y, or Z is identified as an element symbol (e.g., O), all element groups of that element that are compatible in bond type with the central element group are implied. [c]A, water instability; B, oxidizing agent; C, spontaneous decomposition; D, rearranges.

and the chemical shift and signal multiplicity of the central carbon atom and each first-layer carbon atom. Any additional noteworthy structural or spectral features of a particular reference library compound may be added. Approximately 56,800 carbon-centered 1-ACFs were found, representing 1158 different 1-ACFs. These were arranged in order of ascending ACFID numbers. Within each ACFID subset, the entries were sorted according to increasing chemical shift of the central carbon atom. From these data, four reference files were created and merged into FOCISS.

The first, a master file, has 56,800 entries, each of which is assigned to one random-access record and contains the appropriate ACFID number and all of the above-described information associated with that particular 1-ACF. A second file, a mapping file, contains the record pointers relating each ACFID number to its subset of records in the master file. Each record in the third file is keyed to a specific substructural feature, e.g., one first-layer methyl group, two first-layer methyl groups, a carbonyl group. Bit maps (with bits 1—13703) indicate the presence or absence of these structural features in each of the 13,703 1-ACFs. The fourth file is a set of 250 records, each of which corresponds to a 1-ppm chemical shift interval and contains a 13,703 bit string to indicate for each possible 1-ACF whether one or more of the extracted 1-ACFs with the same ACFID number has a central carbon atom signal within that 1-ppm interval. The chemical-shift range begins with —10 ppm and ends at 240 ppm downfield of the reference standard tetramethylsilane.

These four files permit on-line queries of two types. If CSASSIGN (chemical shift assign) is called, options are provided that permit the input of either a single 1-ACF or a group of structurally related 1-ACFs. CSASSIGN returns the chemical-shift range for the central carbon atom of the 1-ACF or group of 1-ACFs by surveying the chemical shifts of all 1-ACFs in the data base that are compatible with the input. The second routine, ACFASSIGN, accepts a chemical shift or chemical-shift range and, using the fourth file described above, produces a list of 1-ACFs which have a central chemical shift compatible with the input.

Two input options are most commonly used with CSASSIGN: a simple, linear representation of a specific 1-ACF or a file of structurally-related 1-ACFs created with the editing capabilities of FOCISS described earlier. For example, in a specific 1-ACF query about —O—CH_2—CH<, the output records the minimum chemical shift (0.9 ppm) and maximum chemical shift (55.4 ppm) of the central methylene carbon found in the data base for the specified 1-ACF, the average chemical shift (29.3 ppm), the standard deviation (6.1), the mode (29.0 ppm) and the number of hits (2773) for that 1-ACF in the data base. The user can also request a histogram displaying the distribution of chemical shift values (Fig. 3). Generally, these plots display Gaussian-like distribution when the number of occurrences is large. At times, more subtle structure/spectra correlations may be discerned. In the example shown in Fig. 3A, the histogram suggests the presence of two regions: that

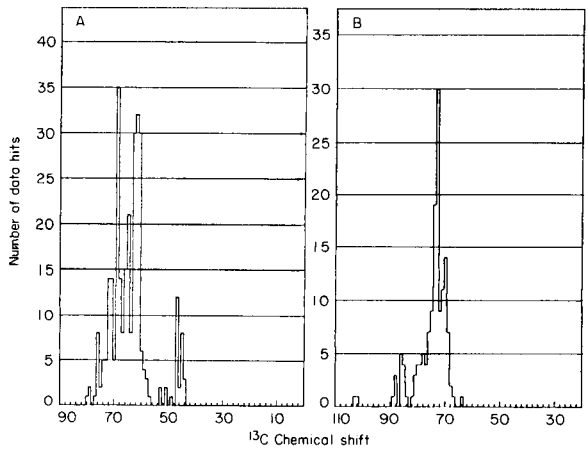

Fig. 3. Histograms displaying distribution of chemical shifts in the data base for: (A) the 1-ACF CH_2(—O—)(—CH——); (B) the hydroxyl-bearing carbon atom of tertiary non-allylic alcohols. (No hits were observed in the region of lower field than shown here.)

from 43 to 53 ppm containing 30 occurrences and that from 56 to 81 ppm containing 2734. Using a structure-display routine, each of the 30 compounds corresponding to the high-field region was examined, revealing that in each case the central methylene-carbon atom was part of an epoxide ring. None of the compounds in the low-field region contained the central methylene-carbon atom in an epoxide ring.

The CSASSIGN query which produced the histogram shown in Fig. 3B, identifies the observed chemical-shift range for the hydroxyl-bearing carbon atom of tertiary, non-allylic alcohols. Using the editing capabilities of FOCISS, a file containing the 19 fragments in the chemically stable 1-ACF list that characterize this functionality is created, i.e., C(G1)(G1)(G2)OH, where G1 can be CH_3, CH_2, CH or C, and G2 can be CH_2, CH or C. The search for all occurrences of these nineteen 1-ACFs in the data base produces a total of 147 hits, with a chemical shift range of 64.4—102.8 ppm. The histogram shown indicates that 98% of the hits fall between 65 and 89 ppm. Examination of the structures corresponding to the two "outliers" at about 102.5 ppm revealed a hydroxyl-bearing carbon atom in an unusually strained environment in each case (Fig. 4).

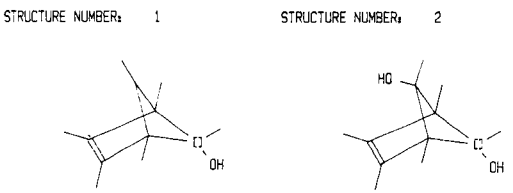

Fig. 4. CASE display of compounds corresponding to outlying 1-ACFs at 102.5 ppm.

CSASSIGN also provides output options that list the actual reported chemical shift of the central carbon for each of the 147 occurrences in ascending order, and the literature references from which these data are derived.

In using the second routine, ACFASSIGN, the user must specify the source file of valid 1-ACFs to be searched for each query on chemical shift or chemical-shift range, e.g., the chemically stable 1-ACFs or any user-created file. Entry of a chemical shift or chemical-shift range and signal multiplicity results in a listing of each 1-ACF (with two or more occurrences in the data base) which has signal multiplicity and chemical-shift range for the central carbon atom compatible with the entered data. The output consits of a graphic display of each 1-ACF identified, its ACFID, the minimum and maximum chemical shift for the central carbon atom, and the number of occurrences of that 1-ACF in the data base. A search using the chemically-stable 1-ACF file may, in some regions of the spectrum return a large number of 1-ACFs. Thus, a more constrained search space that better reflects the particular problem at hand may be advantageous. In addition, ACFASSIGN gives the user the option of entering a molecular formula if the query is related to the spectrum of a specific compound. In that case, the source file, usually the chemically stable 1-ACF list, is automatically pruned of fragments inconsistent with that composition prior to the search.

In a commonly used search mode, the complete carbon-13 n.m.r. spectrum (i.e., the observed chemical shift and multiplicity of each signal) and the molecular formula of the unknown compound are entered. ACFASSIGN first prunes the source file of 1-ACFs based on the molecular formula and then treats each signal as an entirely separate entry in exactly the manner described above.

Table 5 summarizes the output of an actual ACFASSIGN search conducted in connection with an unknown compound of natural origin containing only carbon, hydrogen and oxygen. To assist in the identification of plausible 1-ACFs with an observed central-carbon chemical shift of 102.3 ppm (singlet), the window of the query was widened to a range of 100.0—105.0 ppm and the known molecular formula of the compound ($C_{14}H_{20}O_5$) was also entered. Using the chemically stable 1-ACF file as the search space, ten 1-ACFs compatible with the chemical shift range, signal multiplicity and molecular formula were identified. Without the entry of the molecular formula, the number of hits was 473.

CONCLUSIONS

An element-group-based, atom-centered fragment, having as its boundary the first concentric layer of element groups about the central element group, is proposed as the basic unit of structure in a computer system designed to reduce the spectral properties of a compound of unknown structure to their structural implications. The established boundary condition is a workable

TABLE 5

Summary of ACFASSIGN query
(Input: 100.0—105.00 ppm (singlet); molecular formula $C_{14}H_{20}O_4$.)

1-ACF[a]	Chemical-shift range (ppm)		No. of hits
	Minimum	Maximum	
1. C(—O—)(=C--)(—CH_3)	101.6	168.4	17
2. C(—O—)(—O—)(—CH_3)(—CH_3)	96.9	118.8	22
3. C(—O—)(—OH)(—C---)(—CH_3)	104.4	108.4	4
4. C(—OH)(—C---)(—C---)(—CH_3)	102.3	102.8	2
5. C(—O—)(—OH)(—C---)(—CH_2—)	99.2	103.0	2
6. C(—O—)(—OH)(—C---)(—CH--)	94.4	110.9	2
7. C(—O—)(—OH)(—CH--)(—CH_2—)	96.1	108.8	2
8. C(—O—)(—O—)(—CH--)(—CH_2—)	104.0	109.7	3
9. C(—O—)(—O—)(—C---)(—CH_2—)	105.1	105.1	1
10. C(—O—)(—O—)(—C—=)(—CH--)	103.4	104.1	2

[a]Designated by linear code.

compromise between the need for a structural unit large enough to possess a distinctive chemical environment relative to its spectral properties, and small enough to keep the number of all possible structural units to a manageable level. Exhaustive generation of such 1-ACFs, followed by pruning based on a set of rules about chemical instability led to approximately 5000 1-ACFs.

These structural units can be easily manipulated by the computer and conveniently assigned spectral properties by linking FOCISS to available spectral libraries. (Structural units not present in the compounds of the library cannot, of course, be assigned in this way.) For example, CSASSIGN is of value in the assignment of carbon-13 chemical-shift ranges to 1-ACFs. Given present limitations in our version of the CIS carbon-13 n.m.r. data base, only about 1500 1-ACFs in the chemically-stable list of about 5000 can be assigned realistic chemical-shift ranges by this method. However, these 1500 1-ACFs are among the most prevalent occurring in organic compounds. In general, at least 25 occurrences of a given 1-ACF in the data base are required for chemical-shift range assignment. Prediction-based approaches to the assignment of spectral properties of 1-ACFs are being explored.

Although the procedure for making structural inferences is based on 1-ACFs with assigned spectral properties, it should be noted that the overall strategy described for automated structure elucidation is workable and rigorous even if some 1-ACFs have no assigned properties. The only consequence of such omissions may be the presence of some molecular structures that are, in fact, incompatible with the observed spectral properties, and should have been excluded. Thus, the structure elucidation system is designed to take full advantage of the information contained in current data bases,

but it is not limited by their deficiencies. The user still retains the assurance that no plausible structure is overlooked.

ACFASSIGN is envisaged as an aid to the chemist in the interpretation of carbon-13 n.m.r. spectra. Its value in this regard will, of course, be enhanced as the data base is enlarged in scope. However, the data-base dependence of ACFASSIGN precludes its direct application to CASE because the search is not exhaustive, i.e., it cannot report 1-ACFs that are absent from the compounds of the reference library.

The authors are indebted to B. D. Christie and A. H. Lipkus for revealing discussions in the preparation of this manuscript, and to the National Institutes of Health (NIH Grant GM 21703) and The Upjohn Company for their financial support of this project. This paper was presented in part at the 1984 International Chemical Congress of Pacific Basin Societies, Honolulu, Hawaii, December, 1984, Abstract 08C05.

REFERENCES

1 S. Sasaki, I. Fujiwara, H. Abe and T. Yamasaki, Anal. Chim. Acta, 122 (1980) 87.
2 H. Abe, I. Fujiwara, T. Nishimura, T. Okuyama, T. Kida and S. Sasaki, Comput. Enhanced Spectrosc., 1 (1983) 55.
3 L. A. Gribov and M. E. Elyashberg, Crit. Rev. Anal. Chem., 8 (1979) 111.
4 J. E. Dubois, M. Carabedian and I. Dagane, Anal. Chim. Acta, 158 (1984) 217.
5 J. E. Dubois, M. Carabedian and B. Ancian, C. R. Hebd. Seances Acad. Sci., Ser. C, 290 (1980) 369.
6 J. E. Dubois, M. Carabedian and B. Ancian, C. R. Hebd. Seances Acad. Sci., Ser. C, 290 (1980) 383.
7 N. A. B. Gray, C. W. Crandell, J. G. Nourse, D. H. Smith, M. L. Dageforde and C. Djerassi, J. Org. Chem., 46 (1981) 703.
8 R. E. Carhart, D. H. Smith, N. A. B. Gray, J. G. Nourse and C. Djerassi, J. Org. Chem., 46 (1981) 1708.
9 W. Bremser and W. Fachinger, Magn. Reson. Chem., 23 (1985) 1056.
10 H. B. Woodruff and M. E. Munk, J. Org. Chem., 42 (1977) 1761.
11 M. O. Trulson and M. E. Munk, Anal. Chem., 55 (1983) 2137.
12 J. Zupan and M. E. Munk, Anal. Chem., 57 (1985) 1609.
13 C. A. Shelley and M. E. Munk, Anal. Chem., 54 (1982) 516.
14 A. H. Lipkus and M. E. Munk, J. Chem. Inf. Comput. Sci., 25 (1985) 38.
15 M. E. Munk, C. A. Shelley, H. B. Woodruff and M. O. Trulson, Fresenius' Z. Anal. Chem., 313 (1982) 473.
16 C. A. Shelley and M. E. Munk, Anal. Chim. Acta, 133 (1981) 507.
17 C. A. Shelley, T. R. Hays and M. E. Munk, Anal. Chim. Acta, 103 (1978) 121.
18 N. Ya. Vilenkin, Combinatorics, Academic Press, New York, 1971.
19 J. Zupan, S. R. Heller, G. W. A. Milne and J. A. Miller, Anal. Chim. Acta, 103 (1978) 141.
20 G. W. A. Milne and S. R. Heller, J. Chem. Inf. Comput. Sci., 20 (1980) 204.
21 J. E. Dubois and J. C. Bonnet, Anal. Chim. Acta, 112 (1979) 245.
22 W. Bremser, H. Wagner and B. Francke, Org. Magn. Reson., 15 (1981) 178.
23 CNMR-Information System, INKA Information System, Karlruhe.
24 BASF ^{13}C-NMR Spectral Data Base, BASF Ludwigshafen.
25 W. Bremser, B. Franke and H. Wagner, Chemical Shift Ranges in Carbon-13 NMR Spectroscopy, Verlag Chemie, Weinheim, 1982.

26 W. Bremser, Magn. Reson. Chem., 23 (1985) 271.
27 B. A. Jezl and D. L. Dalrymple, Anal. Chem., 47 (1975) 203.
28 M. Zippel, J. Mowitz, I. Köhler and H. J. Opferkuch, Anal. Chim. Acta, 140 (1982) 123.

Analytica Chimica Acta, 184 (1986) 21—31
Elsevier Science Publishers B.V., Amsterdam — Printed in The Netherlands

PATTERN RECOGNITION BASED ON FUZZY OBSERVATIONS FOR SPECTROSCOPIC QUALITY CONTROL AND CHROMATOGRAPHIC FINGERPRINTING

MATTHIAS OTTO* and HANS BANDEMER

Department of Chemistry and Department of Mathematics, Bergakademie Freiberg, Leipziger Strasse, 9200 Freiberg (German Democratic Republic)

(Received 31st October 1985)

SUMMARY

The quality of multicomponent samples from one or several groups of samples can be monitored by a pattern recognition method. The method is based on profiles of sample quality, which are obtained by means of a multicomponent analytical technique (e.g., ultraviolet spectroscopy or chromatography), and data reduction is done with the aid of fuzzy set theory. The advantages of the method in cases of overlapping and non-additive signals are outlined for quality control of analgesic tablets by ultraviolet spectroscopy. Its performance in the case of highly uncertain data patterns is demonstrated for classification of protein samples by chromatography.

Spectroscopic and chromatographic methods are used to characterize multicomponent samples with respect to chemical components and their concentrations. Apart from the need to report accurate component concentrations, the analyses are frequently applied to ensure the quality of a final product (e.g., by comparing the metal pattern of a steel sample with that of a certified standard) or to classify a complex sample by means of its chromatographic profile used as a "fingerprint". The required data-processing schemes are essentially methods of pattern recognition based on supervised learning techniques [1]. However, the commonly used methods, such as the k-nearest neighbour, the measurement of nearness to the centre of gravity, or the linear learning machine, are not very suitable for solving the problem envisaged because at best only a gross description of the class shape is possible, and the ratio between objects (samples) and features (sensors) is far from being about 3:1.

Individual class-modelling techniques are of more use, as was shown by Wold et al. [2] who used the SIMCA approach for fingerprinting human brain tissues profiled by means of gas chromatography. The SIMCA method is based on principal components analysis [3]; any known class is associated with an individual mathematical model (e.g., a plane or cube) which is then used to decide whether a sample pattern falls within or close to the class. Despite its good performance in many examples [1—3], the SIMCA method has

0003-2670/86/$03.50

drawbacks, arising from the relatively simple (hard) class models that are constructed by using confidence intervals around each model. Furthermore, its application is restricted to cases where the number of abstract components is less than either the number of samples or the features. For example, the SIMCA method will fail with chromatographic profiles if the variability of repeated signal patterns measured on the same sample type is so high that not every peak appears for each sample.

To overcome these limitations, a new approach to the problem based on the theory of fuzzy sets [4, 5] is considered here. Fuzzy set theory has been successfully applied in econometrics [6] and remote sensing [7] but has been adapted to analytical problems only by Blaffert [8] who used it for spectral library search in the infrared range.

With this theory, class shape can be described by models that are highly adaptable to the actual experimental class data. In this paper, the theory of pattern recognition by fuzzy sets is outlined. The practical utility of the method is demonstrated for quality control of pharmaceutical products based on monitoring their ultraviolet spectra and for classifying protein samples by means of their chromatographic patterns.

THEORY

Quality control by pattern recognition

In order to classify an unknown sample with respect to a standard composition or to a group of similarly composed samples, a training set of samples must first be analyzed. After the signal profiles (spectra or chromatograms) have been digitized at p sensor positions (here, sensors mean wavelength or retention data), every sample data vector is characterized by a point in the p-dimensional space (Fig. 1). In the second phase, the grouping of data obtained (the classes) are surrounded by individual class models, e.g., by constructing confidence cylinders as shown in Fig. 1. Finally, the unknown samples are classified by fitting them to the class models, e.g., by multiple regression techniques.

For the application of fuzzy set theory, the following data-specification scheme is the starting point. (A mathematical presentation of fuzzy set theory can be found in the monograph by Dubois and Prade [5]; the basic notions have been outlined by Blaffert [8].) The signal profiles of the training set sample overlap severely as shown in Fig. 2 for the molecular spectra in the u.v. range. Figure 2 gives some impression of the variability and uncertainty of the profiles. When the number of such profiles is increased and the figure is looked at from a distance so that the separate lines are blurred, the spectra appear as various shades of grey; a single point becomes darker as more lines run into one another in its neighbourhood. Hence the shade of grey at a point can be used to represent the possibility that true profiles meet that point. This means, however, the greyish picture can be regarded as a fuzzy set, the membership function of which is defined by the shade of grey assigned within the interval [0, 1]. Thus, the membership function (m.f.)

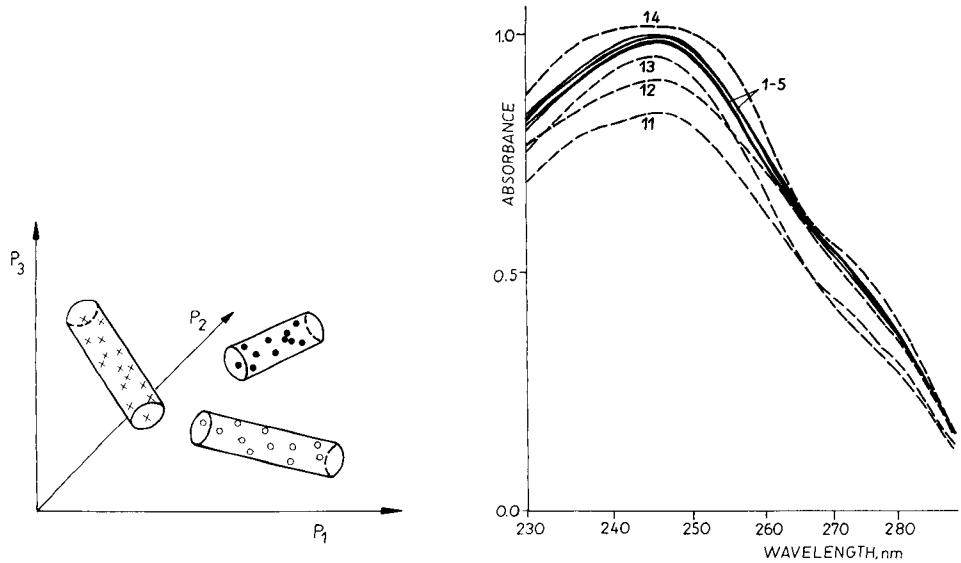

Fig. 1. Sample characterization by its p-dimensional sensor pattern depicted for $p = 3$: (×) class 1; (○) class 2; (•) class 3.

Fig. 2. Ultraviolet spectra for mixtures of caffeine, propyphenazone and phenacetin. The compositions of the mixtures are given in Table 1.

can be written as $m(., x): S \to [0, 1]$, where S represents the signal set and x is a point of the feature axis X.

The special problem in the present case is to specify m when the number of training profiles is low; as always, expert knowledge must be used to specify this function.

Specification of membership functions

Four procedures are presented to specify membership functions of fuzzy sets depending on the training profiles given.

The simplest method (method A) consists of the well known "hard-window" approach [4, 5, 8]. If $s_i(x)$; $i = 1(1)n$ are the given training profiles, then the m.f. is specified (cf. Fig. 3a) by

$$m(s; x) = \begin{cases} 1 \text{ for } \min_i s_i(x) \leqslant s \leqslant \max_i s_i(x) \\ 0 \text{ elsewhere} \end{cases}$$

A more sensible method (method B) starts by specifying the most possible value $s(x)$ for every x and a parameter value $b(x)$ of broadness. Then the m.f. is specified symmetrically to $s(x)$, taking into account the parameter $b(x)$, (cf. Fig. 3b) by

$$m(s; x) = \exp\{-[s - s(x)]^2/2b^2(x)\} \qquad (1)$$

It is noted that specifying this bell-shaped curve does not mean adopting a

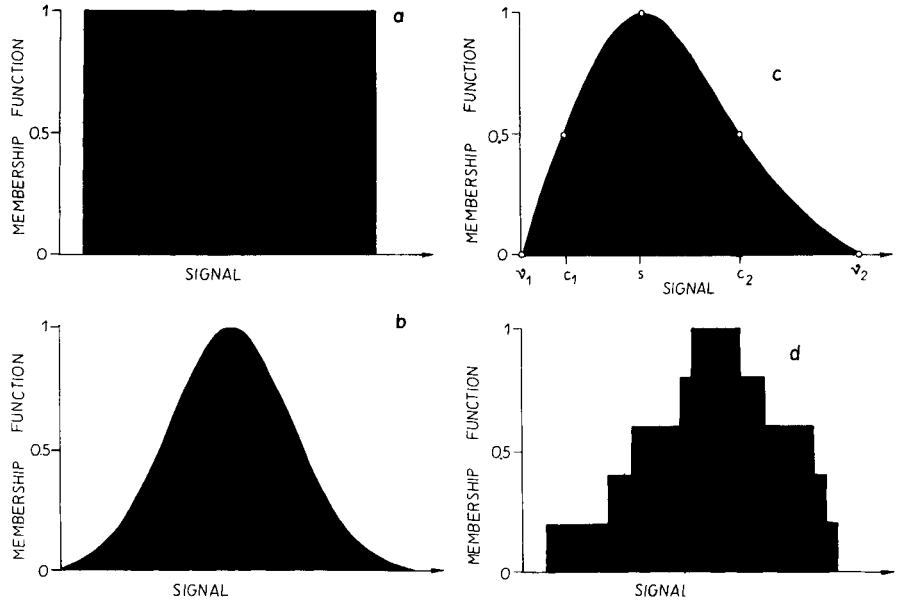

Fig. 3. Specification of membership functions for modelling grey-shaded figures: (a) hard-window approach; (b) bell-shaped curve; (c) cubic spline approximation using the points at membership values of 0, 0.5 and 1; (d) mathematical morphological model by means of moving a structuring element (line segment) along the intensity axis.

Gaussian model or following a statistical line. In another approach (method C), the most possible value $s(x)$ is specified for every x, with $m(s(x); x) = 1$, and cross-over points $c_r(x)$ are specified with $m(c_r(x); x) = 0.5$ as well as initial vanishing points $v_r(x)$ with $m(v_r(x); x) = 0$ defined to have non-vanishing points in their neighbourhood, $r = 1, 2$. The five points $v_1(x)$, $c_1(x)$, $s(x)$, $c_2(x)$, $v_2(x)$ are connected by a cubic spline (Fig. 3c).

A data-orientated procedure (method D) is based on means from mathematical morphology [9]. For this, a structural element (e.g., a line segment L of appropriate length) is moved along the signal axis at sensor position x, and the number of events involving crossing profiles of the training set are counted; stepped membership functions are produced, as shown in Fig. 3(d). If $L(s)$ is defined as the line segment when its midpoint has the position s, then

$$m(s; x) = (1/c) \text{ card } [s_i(x): s_i(x) \in L(s)] \tag{2}$$

where c is some constant to renormalize m to the interval $[0, 1]$ and card stands for cardinality, i.e., the number of elements in the following set. This method is advisable if no useful prior knowledge is available or if the experimental data should or must be used on their own for further treatment.

Classification of samples

Once the fuzziness of measurements has been specified, the method is ready for use in classifying unknown samples by monitoring their signal

profiles and matching the digitized signals to the membership function (m.f.) of the sensors.

The m.f. of the unknown sample is denoted by $m_u(s; x)$ and may be crisp with $m_u(s_u(x); x) = 1$ along the graph $s_u(x)$ and zero elsewhere. Then the intersection of the fuzzy sets with

$$m_m(s; x) = \min[m(s; x), m_u(s; x)] \tag{3}$$

gives a vector of concordant values $m_m(s; x_j)$; $j = 1(1)p$ which can be aggregated to one final value (the degree of containment) to characterize the quality of the sample. The easiest way, considered here, is to use the arithmetric mean

$$g(m; m_u) = (1/p) \sum_{j=1}^{p} m_m(s; x_j) \tag{4}$$

Other aggregation operators have been described [10]. Thus, finally a value ranging between 0 and 1 is obtained which describes the quality of a sample. From experience and test experiments, it can be decided which value must be reached for the sample to qualify as fitting within specified tolerance limits or as being outside these limits.

The approach is so general that it can be applied to any spectroscopic or chromatographic or even electroanalytical method which provides signal patterns. The method is especially useful in cases of signal overlap or when it is impossible to reproduce the whole signal pattern accurately, e.g., with chromatograms from samples of biological origin.

EXPERIMENTAL

Apparatus and computations

Ultraviolet spectra were recorded on a double-beam scanning Model M40 spectrophotometer (VEB Carl Zeiss Jena) and the digitized values were transferred to the computer off-line.

Chromatographic data were taken from high-performance liquid chromatography (h.p.l.c.) of proteins in urine, as reported elsewhere [11].

Computations were done on a SM 4/20 model digital computer (Tesla) programmed in FORTRAN. For graphics, a Commodore 64 microcomputer connected to a model 1541 floppy disk was used; the program was written in BASIC and machine language. The final program is available from the authors on request.

Procedure

Ultraviolet spectra were measured for typical compositions of analgesic tablets consisting of caffeine, propyphenazone, phenacetin, papaverine hydrochloride and phenobarbital. The mixtures were prepared from 0.1% (w/v) stock solutions of the components by appropriate dilution with

twice-distilled water in a 50-ml volumetric flask. The solution then was placed in 0.5-cm cuvettes and the spectra were recorded between 230 and 290 nm every 5 nm.

RESULTS AND DISCUSSION

Spectroscopic quality control

As a spectroscopic application of monitoring the quality of multicomponent samples, u.v.-spectroscopy was used to characterize the component mixtures typically present in analgesic tablets. Although the components are limited to 3—5 in such systems, their analysis is difficult because the spectra overlap strongly so that laborious multivariate calibration techniques combined with multiple regression [12] or principal components analysis [13] become obligatory.

With the fuzzy set approach, calibration is restricted to setting up the system by repeated measurements of a standard sample that contains the individual components at the tolerable concentration levels. Figure 2 (solid lines) shows the spectra of five standard samples which were used to construct the membership function. These functions were first specified by the morphological method [9]; a line segment L was moved along the absorbance axis at 13 wavelength positions x_j. The graphs obtained were quite similar to that shown in Fig. 3(d). Thus a function of the type of Eqn. 1 was chosen to specify the m.f. The parameter of broadness, $b(x)$, was based on the actual standard deviation at the sensor position x calculated from the five repeated measurements; the varying widths of the grey shades at different wavelengths were taken into account. When the standard spectra were matched to the m.f.'s themselves, values higher than 0.5 were obtained for the degree of containment measured by the arithmetic mean (Eqn. 4) (Table 1, mixtures 1—5).

There is no obvious difference between the results whether the stepped m.f. or the bell-shaped m.f. was used. This was also true when the mixtures analyzed varied in composition within ±2% (Table 1, mixtures 6—10) or when outliers were investigated, as given in Table 1 for mixtures 11—14 (cf. Fig. 2). Mixtures 6—10, which varied in composition within the tolerance limits of ±2%, gave similar degrees of containment as the training mixtures and are classified correctly as being of the expected quality. All the outliers show clearly lower degree of containment so that in the present example a degree of containment of 0.5 could be fixed to guarantee the quality of a tablet.

An attempt was made to construct a grey-shaded picture by summing the concentration-weighted spectra of the pure components according to the Lambert-Beer law. This procedure failed, however, because the individual spectra were not additive. The superposition of component spectra gave experimental absorbances which were about 5% lower than expected theoretically.

TABLE 1

Quality control of analgesic tablets by means of u.v. spectra and fuzzy set theory

No.	Concentrations[a]			Degree of containment	
	Caffeine	Propyphenazone	Phenacetin	Method B	Method D
Training mixtures					
1	0.2	0.6	1.2	0.672	0.644
2	0.2	0.6	1.2	0.830	0.608
3	0.2	0.6	1.2	0.627	0.624
4	0.2	0.6	1.2	0.548	0.593
5	0.2	0.6	1.2	0.784	0.675
Mixtures with concentration deviations up to 2%					
6	0.196	0.588	1.176	0.617	0.579
7	0.204	0.612	1.224	0.568	0.525
8	0.204	0.588	1.224	0.739	0.638
9	0.192	0.612	1.176	0.625	0.608
10	0.204	0.612	1.200	0.670	0.640
Outliers					
11	0.2	0.45	1.0	0	0.004
12	0.3	0.6	1.0	0.147	0.149
13	0.1	0.45	1.2	0.003	0.013
14	0.2	0.45	1.4	0.133	0.159

[a]One unit corresponds to 20 μg ml^{-1}.

The sensitivity of the approach was further evaluated by analyzing a five-component system consisting of caffeine, propyphenazone, phenacetin, papaverine and phenobarbital. The latter two components are present at about a tenth of the concentration of the others, which renders their quality inspection more difficult. The results for mixtures where papaverine deviated from the true concentration by 50% (mixture 7, Table 2) and phenobarbital by more than 100% (mixture 9) are represented in Table 2 along with predictions of the standards themselves. From the values for the degree of containment, it can be concluded that these mixtures with high variations (7 and 9) were recognized by both methods B and D as being outside the tolerance limits, i.e., the degree of containment is less than 0.5 with method B (bell-shaped m.f.) and less than 0.9 for method D (morphological approach). In this example, method D seems to be more sensitive to the quality of sample because even mixture 6, which contained 10% more papaverine, shows a different degree of containment compared to the parallel determinations of mixtures 1—5. Further experience with the two methods, however, is needed to confirm this finding.

Other applications can be envisaged, e.g., in the identification of steel and alloy samples by means of energy-dispersive x-ray fluorescence analysis [14]. In that case, several classes (samples having the same metal pattern) would be of interest and their membership functions would have to be stored on file.

TABLE 2

Quality control of a five-component mixture by u.v. spectroscopy

No.	Concentrations[a]		Degree of containment	
	Papaverine	Phenobarbital	Method B	Method D
1	0.032	0.068	0.668	0.985
2	0.032	0.068	0.518	0.969
3	0.032	0.068	0.833	0.941
4	0.032	0.068	0.749	1.000
5	0.032	0.068	0.903	1.000
6	0.035	0.068	0.712	0.849
7	0.048	0.068	0.409	0.565
8	0.032	0.090	0.637	0.981
9	0.032	0.151	0.012	0.016

[a]One unit corresponds to 20 μg ml^{-1}. For all mixtures (1—9) the concentrations of caffeine, propyphenazone and phenacetin were 0.2, 0.6 and 1.2, respectively.

Classification of samples analyzed by chromatography

The proposed fuzzy set approach is especially advantageous for cases in which the repeatability of signal patterns is so poor that peaks can be missed completely or the signal positions and intensities vary very significantly between samples of one class. Such patterns are often encountered in the chromatographic analysis of complex samples, e.g., tissues, micro-organisms or proteins. The advantage of the fuzzy set approach originates from comparing data sets rather than data vectors (cf. [8]).

In the present work, typical liquid chromatograms taken from protein analysis [11] were considered. If an attempt is made to arrange the retention data as a vector for input in a SIMCA treatment, it quickly becomes clear that there is no straight order of retention data. Visual inspection of retention patterns between the three groups shows quite different patterns (Fig. 4a—c). These patterns were used to construct the m.f.; the retention data were fuzzed on the basis of a bell-shaped curve as described in Eqn. 1. In order to account for the decrease in reproducibility of retention values with increasing retention time (t_R) in the chromatogram, the peak width (b) of the m.f. was varied by the linear model $b = 0.02t_R + 0.01$. The m.f. obtained in this way is shown for the group (c) pattern in Fig. 4(d).

To estimate the discriminating ability of the fuzzy set modelling of classes of protein samples, patterns of the three groups of samples were matched to each group. The data for the patterns are given in Table 3 along with the degrees of containment which were calculated according to Eqn. 4. As can be seen, the three sample patterns are classified within the classes from which they originated with high (>0.9) degrees of containment. The most difficult classification occurred with the pattern from class 3, for which the degrees of containment were quite similar for all three classes. However, the

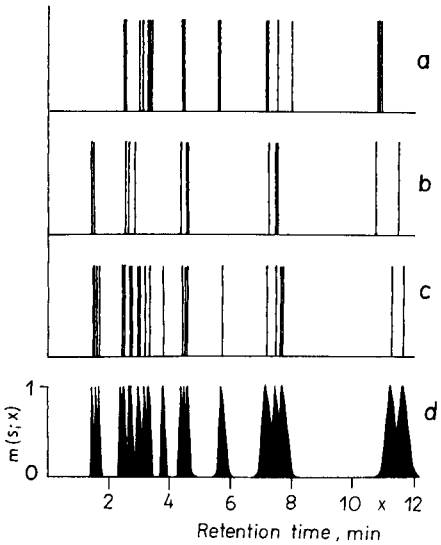

Fig. 4. (a—c) Peak retention data for three groups of urine samples. (d) Class membership function for group (c) based on bell-shaped fuzzing of retention data. In (d), the peaks represent membership functions ranging between 0 and 1 rather than chromatograms.

TABLE 3

Classification of chromatographic patterns based on fuzzy observations

Class	Retention data (min)							
1	2.45	3.06	3.25	4.54	5.67	7.15	11.29	—
2	1.38	1.47	2.60	2.83	4.51	7.47	10.67	11.45
3	1.47	2.45	2.60	3.14	3.30	3.74	4.54	—

Class origin	Degree of containment obtained by matching against class number		
	1	2	3
1	0.98	0.45	0.60
2	0.54	0.96	0.59
3	0.81	0.78	0.93

most probable class, 3, was ranked first as expected. If the ranking were worse, the m.f. would have to be tuned further to guarantee correct sample classification.

The classification scheme was also evaluated for data sets in which both the training and unknown samples were fuzzed. This procedure shifts the degrees of containment closer to unity, i.e., the results become less ambiguous; however, it does not improve the differentiation in ranking unknown samples. Therefore, the data are not presented here.

The proposed method could also be applied to data from pyrolysis gas chromatography of tissues where the number of peaks in the chromatograms can be quite high but very uncertain, e.g., 24 samples with 131 ± 16 peaks each [15]. The number of peaks (features) had to be reduced substantially in order to fit within the constraints of classical pattern-recognition methods, and a time-window peak-matching routine was developed to obtain a suitably populated data matrix. The method [15] was based on dividing the pyrogram into a set of intervals and assigning a formal identity to each peak in the intervals by using a previously updated cumulative reference file. This method solved the problem partly. The fuzzy set approach would be simpler because no data preprocessing would be necessary to generate the input data vectors and the original data could be handled as sets, i.e., fuzzy sets.

Conclusions

Classification of multicomponent samples based on measurements with multicomponent techniques and on data reduction with fuzzy set theory is not restricted to selective analytical methods and highly precise measurements. If the signal profiles are interpreted as fuzzy observations, sample classification is possible in cases of non-additive component signals, overlapped signals, non-random data distribution and even when the signal order is uncertain.

The general method has already been shown to be useful in spectral library searches [8]. Here, it proved successful for classifying samples with complex chromatographic patterns even without consideration of the intensity data in the chromatogram. Extension of the method to take into account both retention and intensity data would be straightforward and has, in fact, been outlined by Blaffert [8] for i.r.-component identification.

The authors thank H. Schellenberg (Pharmaceutical Quality Control, Leipzig) for helpful discussions as well as J. Wagner, U. Steinbrück (Medical Clinic, Karl-Marx-University, Leipzig) and J. Čoupek (LP, Praha) for providing chromatographic protein data.

REFERENCES

1 L. Kryger, Talanta, 28 (1981) 871.
2 S. Wold, E. Johansson, E. Jellum, I. Bjornson and R. Nesbakken, Anal. Chim. Acta, 133 (1981) 251.
3 S. Wold and M. Sjöström, in B. R. Kowalski (Ed.), Chemometrics, Theory and Applications, ACS Symp. Ser. 52, 1977.
4 L. A. Zadeh, Fuzzy Sets, Inf. Control, 8 (1965) 338.
5 D. Dubois and H. Prade, Fuzzy Sets and Systems: Theory and Application, Academic Press, New York, 1980.
6 H.-J. Zimmermann, Proc. Oper. Res., 6 (1976) 99.
7 P. Bois, IEEE Trans. Geosci. Remote Sensing, GE-22 (1984) 692.
8 T. Blaffert, Anal. Chim. Acta, 161 (1984) 135.
9 J. Serra, Image Analysis and Mathematical Morphology, Academic Press, London, 1982.

10 K.-D. Schwab, Dissertation, Peter Lang Verlag, Frankfurt am Main, 1983.
11 J. Wagner, J. Čoupek and U. Steinbrück, IX. Symposium Chromatographie in der klinischen Biochemie, Rostock, 1985.
12 C. W. Brown, P. F. Lynch, R. J. Obremski and D. S. Lavery, Anal. Chem., 54 (1982) 1472.
13 M. Otto and W. Wegscheider, Anal. Chem., 57 (1985) 63.
14 J. Koskinen and T. Numento, Technical Paper: X-MET 840 brochure, Outokumpu Electronics Division, Finland, 1981.
15 J. A. Pino, J. E. McMurray, P. C. Jurs, B. K. Lavine and A. M. Harper, Anal. Chem., 57 (1985) 295.

Analytica Chimica Acta, 184 (1986) 33—51
Elsevier Science Publishers B.V., Amsterdam — Printed in The Netherlands

UNEQ: A DISJOINT MODELLING TECHNIQUE FOR PATTERN RECOGNITION BASED ON NORMAL DISTRIBUTION

M. P. DERDE and D. L. MASSART*

Laboratory of Pharmaceutical and Biomedical Analysis, Farmaceutisch Instituut, Vrije Universiteit Brussel, Laarbeeklaan 103, B-1090 Brussels (Belgium)

(Received 13th January 1986)

SUMMARY

UNEQ, a method for supervised pattern recognition based on the assumption of multivariate normally-distributed groups, is presented. The method belongs to the group of so-called class-modelling techniques, i.e., classification functions are developed for each of the training classes separately, on the basis of the similarities between the objects within a group. New classes can therefore be entered easily into a classification problem. The method allows also easy detection of outliers. For each individual sample, the degree of connection with all the training classes can be defined. If for a given sample, this degree of class membership is low for all the classes, the object is considered as an outlier. The mathematical background of UNEQ is described. The validation of the derived classification functions in terms of sensitivity, specificity and efficiency is discussed. The method is illustrated and compared to SIMCA (another class-modelling technique) by means of a data set that concerns the classification of olive oils according to their area of origin, based on fatty acid patterns. It is concluded that the UNEQ method can be very useful for classification purposes but requires the populations to be homogeneous as is the case for other techniques. For the olive-oil data set, the performance of UNEQ is similar to or even better than SIMCA.

An important aim of the collection of chemical results about sets of objects or samples is the classification of these samples into different categories, e.g., the classification of food products according to origin or quality or the classification of patients into categories of diseases (in which case the classification is referred to as medical diagnosis). For this purpose, supervised pattern recognition techniques have been introduced in analytical chemistry. The final aim of these methods is the development of classification functions or decision rules. According to whether the decision rules emphasize the differences between the classes or the similarities within each class, a distinction can be made between discriminating and modelling supervised techniques. The linear learning machine [1], for instance, is a typical discriminating technique, while SIMCA [2] is the prototype of a class-modelling technique. In this paper, a method called UNEQ, belonging to the second group of methods, is presented. Recently, other new class-modelling techniques have also been proposed [3, 4].

0003-2670/86/$03.50

The aims of UNEQ

There are many different supervised pattern-recognition techniques. For practical applications, the question then arises which technique should be chosen. One criterion is of a mathematical nature: when techniques make assumptions about the training groups, e.g., normality of data, these conditions should be fulfilled as far as possible in order to derive reliable classification rules. There are also other important criteria that should be taken into account. Coomans et al. [5] gave a summary of requirements that should be fulfilled to obtain decision rules that can be used in medical practice. Some of these are particular to medical diagnosis problems, others are more general and apply to most supervised situations. The latter criteria can be summarized as follows.

(1) The method should allow new training classes to be entered easily into the classification problem. This means that the decision rules for the classification in a given class should not depend on the other classes in the training set. This avoids repeating the learning process for all the training classes each time a new group is entered into the classification procedure.

(2) If the classification rule is used for the classification of samples for which no learning group was analysed, or for samples with aberrant patterns (e.g., because of measurement errors), then these samples should be detected and classified as outliers.

(3) It is not sufficient that the output of the classification procedure consists of the classification of the samples into one of the training classes; one should also obtain some idea about the probability of the classification being correct.

(4) It should be possible to detect redundant parameters. In many applications, it is not obvious which variables should be used to discriminate between different groups. This often results in the characterization of the objects by a lot of parameters. However, it may be that not all of these are necessary for the classification problem under study. In general, the reliability of the classification functions decreases when irrelevant parameters are introduced, thus it is advisable to eliminate such parameters. In elimination of parameters, however, it should be realised that the set of parameters optimal for making a distinction between, for instance, groups A and B, can be useless for discriminating between groups A and C.

Criteria 1 and 2 lead to the conclusion that disjoint modelling techniques should be preferred, i.e., techniques that construct, on the basis of the similarities between the objects, a separate class model for each class independently from all the other classes in the training set. Eventually, in the selection of a classification technique, practical considerations must also be considered. The people applying the decision rule in practice are not necessarily experts in the field of pattern recognition. This means that the decision rules should be easy to handle, and that the methods used to derive them should not be too sophisticated, at least in concept, so that the user understands how they work. The method, or the decision rule obtained, should

nowadays be easy to implement on a microcomputer. The program should ask as little input and decision from the user as possible. Moreover, the output results should be represented in an easily understandable way; rather than numbers and tables, the output should consist of plots or histograms.

As will be demonstrated, the UNEQ class-modelling technique satisfies these requirements to a great extent.

BASIC CONCEPTS

The first step in any classification procedure obviously consists of the collection of data for a group of samples with known classification. The data obtained for each single object k constitute a pattern and can be represented by a pattern vector X_k, with $X_k' = [x_{1k}, \ldots, x_{pk}]$, x_{ik} representing the value of the ith variable for the kth object. The pattern vectors of all the training objects are arranged into a data matrix, the structure of which is given in Fig. 1. On the basis of this training or learning set, a decision rule is subsequently formulated. Each of the objects, characterized by p variables, can be considered as being situated in a p-dimensional space, the axes of which are given by the p variables. The position of an object in this pattern space is given by its pattern vector X_k. The general aim of class-modelling techniques is to define in the pattern space for each of the training classes a "class-box" such that for instance 95% of the relevant population falls inside the appropriate class-box.

UNEQ assumes that the class population has a multivariate normal distribution. The class box obtained with UNEQ then coincides with a multivariate normal confidence interval around the population mean at a predefined level of significance. If a class box is constructed at the 5% level of significance, objects lying outside the class box have a probability less than 5% of belonging to the class and will therefore be considered as not belonging to that class.

Geometrically, the classification of a new object is made by comparing the situation of that object in the pattern space with that of the class-boxes. Three kinds of classification decision are possible (see Fig. 2): (a) an object is situated inside the class-box of only one class and is then unambiguously classified as belonging to that class; (b) an object is situated in more than one class-box, which happens when classes overlap and when the object is situated

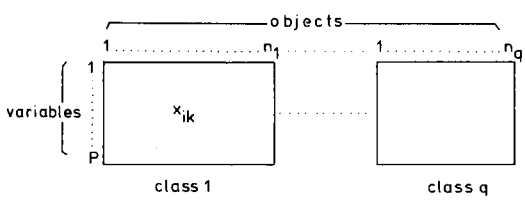

Fig. 1. Matrix representation of a training set: p, number of variables; q, number of classes in the training set; n_q, number of objects in the training set for class q; x_{ik} value of the ith variable for the kth object.

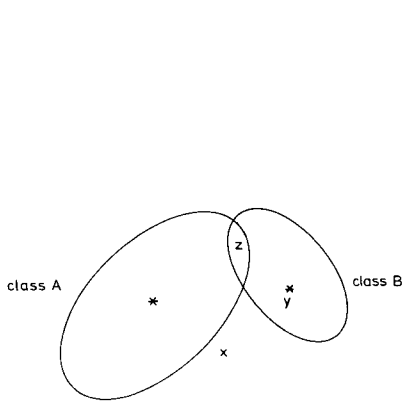

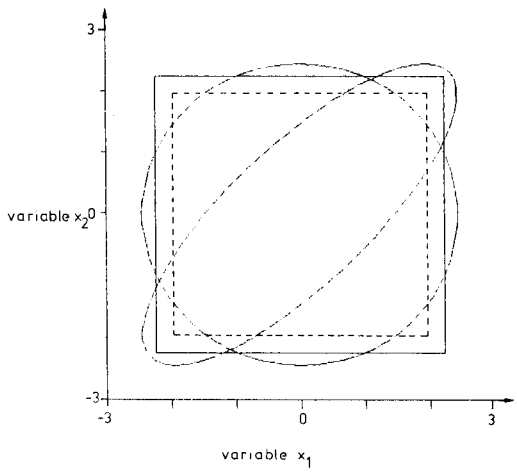

Fig. 2. Geometric illustration of the UNEQ classification in a bivariate situation. Object X is an outlier; object Y is uniquely assigned to class B; object Z falls inside both class models and is therefore not uniquely classified.

Fig. 3. Multivariate and multiple-univariate confidence intervals for a bivariate population with u (0, 0) and $\Sigma = (1, \rho, 1)$: (– – –) 95% confidence interval on the variables in a univariate approach; (——) 95% confidence interval in the multiple-univariate approach. The circle is the 95% bivariate confidence interval ($\rho = 0$) and the ellipse is the 95% bivariate confidence interval ($\rho = 0.8$).

in the overlap region of the concerned classes, so that object cannot be uniquely assigned to a single class; (c) an object is situated outside all class boxes, in which case it is considered an outlier, i.e., it belongs to a class for which no learning group was analysed. Obviously, as the class-boxes are constructed for each class separately, independently of all the other classes in the study, new classes can be introduced easily, without influencing the decision rules (i.e., the shape of the class-boxes) obtained for the classification towards the other classes.

On the basis of the distance of an object from the centroid of a class Q, the probability $P(X/Q)$ that objects belonging to the class are situated nearer to the centroid than the classified object can be calculated; $[1 - P(X/Q)]$ is a measure of class membership of the object concerned. Objects lying on the surface of a class-box developed at the 5% level of significance have a degree of class membership of 0.05; for objects situated outside the class model, the degree of class membership is less than 0.05 while for these situated inside the model the degree of class membership is higher than 0.05. The higher the degree of class membership, the more reliable the classification decision is. UNEQ meets the criteria 1, 2 and 3 given above; criterion 4, concerning the identification of irrelevant parameters, can be approached by combining UNEQ with a principal components analysis as will be discussed in a subsequent paper.

Multivariate versus univariate confidence intervals

One could wonder why multivariate confidence intervals should be used instead of a combination of univariate ones. Figure 3 shows why for a bivariate situation, provided that the class is bivariate normally distributed. The dashed straight lines represent the limits of the 95% univariate reference range for both parameters x_1 and x_2 separately. The use of the combination of both univariate ranges in order to decide whether a sample belongs to the corresponding class would mean looking to see if the sample falls into the rectangular part of the plot. The circle represents the bivariate 95% confidence interval when no correlation exists between the two parameters. It is clear that even in this simple situation the multivariate and the univariate range do not coincide. The main reason is that when two observations are used in order to decide whether or not a sample belongs to a class at a certain α-level (e.g., 0.05) each of the univariate ranges should be made wider, namely corresponding to the 97.5% level of confidence. The α-risk of the combined decision rule then indeed amounts to 0.05 ($1 - 0.975^2$). In a 20-parameter situation, with comparisons made at the 95% level of confidence for each separate variable, one would expect that only 36% of the samples would fall inside the twenty 95% normal ranges while 64% ($\alpha = 1 - 0.95^{20}$), can be expected to show abnormalities in at least one test. It is necessary to adapt the ranges of the univariate confidence intervals to the number of ranges that will be taken into account simultaneously in order to reach the predefined level of significance. The full straight lines in Fig. 3 represent the limits to be used in a bivariate decision problem at the 95% level of confidence. It should be noted that although the α-level (i.e., the probability that an object belonging to the class falls outside the confidence limits) is the same for the bivariate approach (circle) as for the multiple univariate approach (rectangle), the two confidence regions do not coincide totally. In the bivariate approach an extreme value in one parameter, situated outside the univariate confidence interval for that parameter, may be compensated by an observation near the centroid in the other, whereas samples that satisfy the conditions of both univariate reference ranges but are situated very near to the borders of both these ranges are considered as outliners in the bivariate approach.

When variables are correlated pairwise, the difference between the two approaches is more pronounced. The ellipse in Fig. 3 represents the 95% bivariate confidence interval when the correlation between x_1 and x_2 amounts to 0.8. The multiple univariate confidence interval is still limited by the full straight lines, i.e., the same as for the uncorrelated variables. Though the univariate and the bivariate ranges both enclose 95% of the objects belonging to the class, the area of the pattern space they occupy differs greatly. The bivariate range is almost totally situated inside the univariate confidence region. Objects situated in the small parts that are excluded by the univariate but not by the bivariate approach, are those that lie along the edges of the major axis of the ellipse, i.e., they are objects that follow closely the major

trend within the class. Therefore, the probability that objects belonging to the class are situated in these parts is relatively large. As the univariate approach excludes some parts of the bivariate range, it has to include some other part of the pattern space in order to reach the same confidence level. However, as the probability density is lower in any other part of the pattern space, the univariate range has to include a much larger area of the pattern space than the parts of the bivariate range it excludes. The area occupied by the univariate range is therefore always larger than the area of the corresponding multivariate range. For standardized variables (e.g., $u_1 = u_2 = 0$; $\sigma_1 = \sigma_2 = 1$), the univariate range occupies a relative area of 20.1. When the variables are uncorrelated, the bivariate range occupies a relative area of 18.8 whereas for correlated variables ($\rho = 0.8$) this relative area is only 11.3. This difference between the two approaches increases with an increasing number of variables. For three uncorrelated standardized variables, the relative volume of the univariate confidence region is 109.2 while in the multivariate approach it is only 91.5. The difference also increases with increasing confidence level (e.g., $\alpha = 0.01$; $\rho = 0$; area of bivariate range = 28.9; area of univariate approach = 31.6). When the univariate and multivariate confidence regions are both constructed at the same level of confidence, the probability of considering objects as outliers when they are not, is the same for both and amounts to α. However, the larger is the part of the pattern space enveloped by the confidence limits, then the higher the probability that objects not belonging to the class will fall inside its limits and will therefore be considered erroneously as belonging to the class (e.g., the larger the β-error is).

MATHEMATICAL BACKGROUND

The notations used throughout this paper follow the proposals made by Kowalski [6]. As UNEQ develops class models for each class separately, the index referring to the class is omitted to avoid excessively complex symbols.

When a population, characterized by p variables, is normally distributed in a multivariate way, the distribution in the p-dimensional hyperspace of the individuals belonging to that population is described by the density function $f(x_1, \ldots, x_p)$:

$$f(x_1, \ldots, x_p) = [(2\pi)^{p/2} |\Sigma_p|^{1/2}]^{-1} \exp \langle -1/2 \{(X-\mu)' \Sigma_p^{-1} (X-\mu)\} \rangle \qquad (1)$$

The shape of this function is defined by two parameters: μ, the population mean vector, is a parameter of location, indicating the situation of the centroid of the population in the pattern space; Σ_p, the population variance covariance matrix, is a parameter of spread, indicating the dispersion of the individuals around the centroid:

$$\Sigma_p = \begin{bmatrix} \sigma_1^2 & \rho_{12}\sigma_1\sigma_2 & \cdots & \rho_{1p}\sigma_1\sigma_p \\ \rho_{12}\sigma_1\sigma_2 & \sigma_2^2 & \cdots & \\ \vdots & \vdots & & \vdots \\ \rho_{1p}\sigma_1\sigma_p & \cdots & & \sigma_p^2 \end{bmatrix} \quad \mu = \begin{bmatrix} \mu_1 \\ \mu_2 \\ \vdots \\ \mu_p \end{bmatrix}$$

In the simplified case of a bivariate population, the inverse of the variance covariance matrix is given by the matrix

$$\Sigma_2^{-1} = (1 - \rho_{12}^2)^{-1} \begin{bmatrix} 1/\sigma_1^2 & 0 & -\rho_{12}/\sigma_1\sigma_2 \\ 0 & & 0 \\ -\rho_{12}/\sigma_1\sigma_2 & 0 & 1/\sigma_2^2 \end{bmatrix} \tag{2}$$

which converts, after substitution into Eqn. 1, the expression for the distribution function into (3):

$$f(x_1, x_2) = \left(2\pi \left|\Sigma_2\right|^{1/2}\right)^{-1} \exp\left\langle -1/2 \left\{ \frac{1}{(1-\rho_{12}^2)} \left[\left(\frac{x_1 - \mu_1}{\sigma_1}\right)^2 + \left(\frac{x_2 - \mu_2}{\sigma_2}\right)^2 \right.\right.\right.$$

$$\left.\left.\left. - 2\rho_{12}\left(\frac{x_1 - \mu_1}{\sigma_1}\right)\left(\frac{x_2 - \mu_2}{\sigma_2}\right)\right]\right\}\right\rangle \tag{3}$$

The terms within the { } brackets represent an ellipse with the center at the points μ_1 and μ_2, i.e., the centroid of the bivariate normal population. Pairs of points for which this expression has the same value (i.e., points situated on the contour of the same ellipse) all have the same value of the normal density function and are isodensity contours. In the generalized situation (i.e., when p variables are present), the same quantity represents isodensity ellipsoids ($p = 3$) or hyperellipsoids ($p > 3$).

The square root of the expression between the braces in the exponent of the multivariate normal distribution is called the generalized distance D (or the Mahalanobis distance D^2):

$$D^2 = (X - \mu_x)\Sigma_p^{-1}(X - \mu_x) \tag{4}$$

where D is a measure of the distance of the objects with coordinates given by the vector X towards the centroid of the population. When the population has a multivariate normal distribution, D^2 has a chi-square distribution with p degrees of freedom. For pairwise uncorrelated variables, this can easily be proven as the variance covariance matrix then reduces to a diagonal matrix, the elements on the diagonal being the variances of the variables. Consequently, D^2 can be written as

$$D^2 = \sum_{i=1}^{p} [(x_i - \mu_i)/\sigma_i]^2$$

As the marginal distributions of a multivariate normal distribution have univariate normal distributions, D^2 is then equal to the sum of the squares of p standardized normally distributed variables which is indeed chi-square distributed. When the variables are correlated, the same property applies. It is possible to apply, to each set of p correlated variables, an orthogonal transformation such that the derived p new variables are uncorrelated. This is the fundamental theorem on which principal components analysis is based, in which the new variables are called principal components. If p uncorrelated variables y_i ($i = 1, \ldots, p$) are obtained by an orthogonal transformation of p correlated variables x_i ($i = 1, \ldots, p$) then the relation between both groups of variables is given by the equation $\mathbf{Y} = \mathbf{L}'\mathbf{X}$ or $\mathbf{X} = \mathbf{L}\mathbf{Y}$, in which $\mathbf{L}'$ represents the transformation matrix. $\mathbf{L}'\mathbf{L} = \mathbf{I}$, as the transformation is orthogonal.

If D_y is defined as the generalized distance between an object with y coordinates ($y_1, y_2, \ldots, y_p$) and the mean vector μ_y, it can be shown that $D_y^2 = D_x^2$. If $\bar{\mathbf{Y}}$ is defined as the mean score matrix of the y variables, consisting of N identical columns each corresponding to μ_y, and $\bar{\mathbf{X}}$ as the mean score matrix of the x variables, then the variance covariance matrix of the x and y variables is given, respectively, by

$$\Sigma_p(x) = 1/N(\mathbf{X} - \bar{\mathbf{X}})(\mathbf{X} - \bar{\mathbf{X}})' \text{ and } \Sigma_p(y) = (1/N)(\mathbf{Y} - \bar{\mathbf{Y}})(\mathbf{Y} - \bar{\mathbf{Y}})'$$

The notation used here supposes a finite population (size N). Although this is usually not true, this option was chosen in order to avoid complicated notations.

The two matrices are related by $\Sigma_p(y) = \mathbf{L}'\Sigma_p(x)\mathbf{L}$ because

$$\Sigma_p(y) = (1/N)(\mathbf{Y} - \bar{\mathbf{Y}})(\mathbf{Y} - \bar{\mathbf{Y}})' = (1/N)\mathbf{L}'(\mathbf{X} - \bar{\mathbf{X}})[\mathbf{L}'(\mathbf{X} - \bar{\mathbf{X}})]'$$

$$= (1/N)\mathbf{L}'(\mathbf{X} - \bar{\mathbf{X}})(\mathbf{X} - \bar{\mathbf{X}})'\mathbf{L} = \mathbf{L}'\Sigma_p(x)\mathbf{L}$$

and

$$\Sigma_p^{-1}(y) = [\mathbf{L}'\Sigma_p(x)\mathbf{L}]^{-1} = \mathbf{L}^{-1}\Sigma_p^{-1}(x)(\mathbf{L}')^{-1} = \mathbf{L}'\Sigma_p^{-1}(x)\mathbf{L}$$

as $\mathbf{L}' = \mathbf{L}^{-1}$, $\mathbf{L}$ being an orthogonal matrix.

Therefore:

$$D_y^2 = (Y - \mu_y)'\mathbf{L}'\Sigma_p^{-1}(x)\mathbf{L}(Y - \mu_y) = [\mathbf{L}(Y - \mu_y)]'\Sigma_p^{-1}(x)[\mathbf{L}(Y - \mu_y)]$$

$$= (X - \mu_x)'\Sigma_p^{-1}(x)(X - \mu_x) = D_x^2 \qquad (5)$$

as $\mathbf{L}(Y - \mu_y) = \mathbf{L}Y - \mathbf{L}\mu_y = X - \mu_x$

For the uncorrelated y variables, expression D_y^2 has a chi-square distribution with p degrees of freedom, and so this also applies for the generalized distance, calculated on the basis of the correlated x variables. This means that, even when the variables are correlated, the quantity D^2 has a chi-square distribution, e.g., the quantity remains invariant under a principal axis rotation. Equation 5 indicates that this invariance property holds for any linear orthogonal transformation of the original variables and not only for the principal axis rotation, because L can represent any orthogonal matrix.

Because D^2 has a known distribution, it is possible to calculate which value D^2 can have to exclude only 5% of individuals belonging to the class. This value is called D^2_{crit}. Objects for which D^2 is larger than D^2_{crit} have a degree of class membership lower than 0.05 and are therefore considered as outliers to that class at the predefined level of significance of 5%. This also means that the shape of the class-box is given by equation

$$D^2_{\text{crit}} = (X - \mu_x)' \Sigma_p^{-1} (X - \mu_x)$$

representing an ellipsoid in the pattern space with the population mean as centre.

Properties of the generalized distance

A main property of the generalized distance is that the internal dispersion within a group of data is taken into account in the computation of the distance between individuals and the population centroid. For example, with the bivariate population,

$$D^2 = (X - \mu)' \Sigma_p^{-1} (X - \mu)$$

$$= [(x_1 - \mu_1)/\sigma_1]^2 + \langle \{[(x_2 - \mu_2)/\sigma_2] - \rho_{12}[(x_1 - \mu_1)/\sigma_1]\}(1 - \rho_{12}^2)^{-1/2} \rangle^2$$

In the computation of the generalized distance, the part of the second variable which is explained by the first variable is subtracted. If the variables are uncorrelated, the generalized distance reduces to the Euclidian distance of the standardized variables, and therefore the generalized distance can be considered as a generalization of the Euclidian distance.

A second property of the generalized distance is its invariance with respect to scaling of the variables. In matrix notation, scaling is a premultiplication of the data matrix X with a $p \times p$ diagonal matrix $\mathbf{D}(1/a)$, the elements on the diagonal being the reciprocals of the scale factors a_i:

$$\mathbf{D}(1/a) = \begin{bmatrix} 1/a_1 & 0 & \dots & 0 \\ 0 & 1/a_2 & \dots & \vdots \\ \vdots & \dots & \dots & \vdots \\ 0 & \dots & \dots & 1/a_p \end{bmatrix}$$

$\mathbf{Z} = \mathbf{D}(1/a)\mathbf{X}$ or $\mathbf{X} = \mathbf{D}(1/a)^{-1}\mathbf{Z} = \mathbf{D}(a)\mathbf{Z}$ and $(\mathbf{Z} - \bar{\mathbf{Z}}) = \mathbf{D}(1/a)(\mathbf{X} - \bar{\mathbf{X}})$

where $\mathbf{Z}$ is the $p \times n$ matrix of the scaled x_{ik} values. The relationship between the covariance matrices of the z and the x variables is given by

$$\Sigma_p(z) = (1/N)(\mathbf{Z} - \bar{\mathbf{Z}})(\mathbf{Z} - \bar{\mathbf{Z}})' = (1/N)\mathbf{D}(1/a)(\mathbf{X} - \bar{\mathbf{X}})(\mathbf{D}(1/a)(\mathbf{X} - \bar{\mathbf{X}}))'$$

$$= (1/N)\mathbf{D}(1/a)(\mathbf{X} - \bar{\mathbf{X}})(\mathbf{X} - \bar{\mathbf{X}})'\mathbf{D}(1/a)' = \mathbf{D}(1/a)\,\Sigma_p(x)\mathbf{D}(1/a)$$

because $\mathbf{D}(1/a)' = \mathbf{D}(1/a)$,
and by

$$\Sigma_p^{-1}(z) = \mathbf{D}(1/a)^{-1}\,\Sigma_p^{-1}(x)\mathbf{D}(1/a)^{-1} = \mathbf{D}(a)\,\Sigma_p^{-1}(x)\mathbf{D}(a)$$

Therefore

$$\mathbf{D}_z^2 = (Z - \mu_z)'\,\Sigma_p^{-1}(z)(Z - \mu_z)$$

$$= [\mathbf{D}(1/a)(X - \mu_x)]'\mathbf{D}(a)\,\Sigma_p^{-1}(x)\mathbf{D}(a)[\mathbf{D}(1/a)(X - \mu_x)]$$

$$= (X - \mu_x)'\mathbf{D}(1/a)\mathbf{D}(a)\,\Sigma_p^{-1}(x)\mathbf{D}(a)\mathbf{D}(1/a)(X - \mu_x)$$

$$= (X - \mu_x)'\,\Sigma_p^{-1}(x)(X - \mu_x) = D_x^2$$

Practically, this means that the units in which the observations are expressed do not affect the value of the generalized distance and therefore do not influence the decision rules applied in this technique. Moreover, as a translation of the origin of the original axis does also not influence the generalized distance, this implies that a Z-transform (or autoscaling) of the original data will not affect the classification rules.

In some supervised techniques, the scaling of the variables, which is needed to make the range between the different parameters comparable, has an important effect on the classification results. In discriminating techniques, scaling can only be done over the entire data set. Class-modelling techniques, however, have the additional possibility of scaling each training class separately. Therefore, an additional decision must be made before a classification rule can be deduced. As demonstrated for the class-modelling technique SIMCA [7], classification results depend on the way scaling is done.

Population versus sample values

In practice, the population parameters u and Σ_p are unknown and should therefore be estimated by the mean vector $\bar{X}$ and the variance covariance matrix S of a sample of size n. The sample value of D^2 is then denoted by

$$d^2 = (X - \bar{X})'\mathbf{S}_p^{-1}(X - \bar{X})$$

However, as shown by Defrise-Gussenhove [8, 9], an unbiased and consistent estimate of D^2 is given by the equation

$$\tilde{d}^2 = [(n - p - 2)/n]d^2 - p/n \tag{6}$$

where n is the sample size. As $\bar{X}$ and S are random variables, d^2 is also a random variable. The exact sampling distribution of d^2 was also derived [8, 9]. On the basis of this sampling distribution, the variance of D^2 and its estimate were calculated:

$$\text{Var}\,(d^2) = [2n^2(D^2)^2 + 2(n-2)(p + 2nD^2)]/[(n-p-2)(n-p-4)]$$

$$\text{Var}\,(\tilde{d}^2) = [2n^2(D^2)^2 + 2(n-2)(p + 2nD^2)]/[n^2(n-p-4)] \tag{7}$$

Figure 4 represents the variance on the estimate of D^2 as a function of D^2 for several combinations of sample size and number of variables. It shows clearly that the reliability of the estimation of the distance of an object towards a class decreases when the sample size decreases, or when the number of variables increases or when objects are situated farther away from the population centroid. On the basis of Eqn. 7, it is possible to calculate with UNEQ not only the distance between objects and a class centroid but also the confidence on this distance. Furthermore, Eqn. 7 can be used to formulate a criterion for defining the minimum sample size, given p variables, necessary to obtain relevant classification results.

APPLICATION OF THE METHOD

Data set

To illustrate the technique and to compare its performance with SIMCA, UNEQ was applied to a data set provided by Forina and co-workers [10, 11] concerned with the origin of olive oils. In this set, 572 virgin olive oil samples originating from nine different regions in Italy, namely, three northern

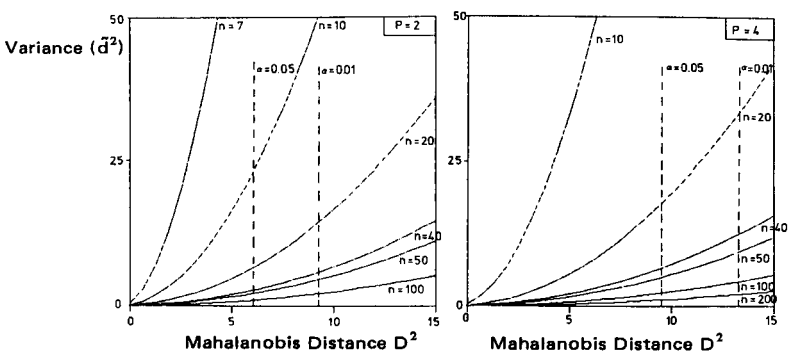

Fig. 4. Variance on the estimated value of the generalized distance $\tilde{d}^2$ as a function of the real (unknown) generalized distance D^2 for several combinations of sample size and number of variables.

regions (Umbria, East Liguria, West Liguria), four southern regions (North Apulia, South Apulia, Calabria, Sicily) and two Sardinian regions (inner and coastal), are characterized by the percentage distribution of eight fatty acids (palmitic, palmitoleic, stearic, oleic, linoleic, eicosanoic, linolenic and eicosenoic acid). To compare the performance of supervised techniques for discriminating the oils from different regions, classification rules were developed for East and West Liguria, North Apulia and Calabria. The procedure used to develop SIMCA classification rules for both of the first two of these classes was discussed in an earlier paper [12].

Computer programs

The computer program UNEQ, written in FORTRAN 77, is designed for use on PDP 11/70 operating under UNIX. For the comparison of UNEQ with the SIMCA method, the SIMCA-2T package [13] running on a CDC CYBER 170/750 was used.

Validation criteria

To evaluate the performance of decision rules and to compare different supervised techniques, validation criteria must be defined. Most frequently, the validity of decision rules is expressed in terms of recognition and prediction rate. The recognition rate represents the rate of correctly classified training objects, i.e., objects on which the development of the decision rules are based; the prediction rate is the rate of correctly classified test objects, i.e., objects with known classification not used in the development of the decision rules. The procedure for determining both these rates depends on the available number of samples with known origin compared to the number of variables by which they are characterized. For large data sets, the sample can be split randomly into a training and a test set of equal size. When the ratio of samples to variables is less favourable, as in the oil data set, it is not advisable to split the sample into two equal parts because the reliability of the derived decision rules would decrease too much. One scheme that can be followed is to make a random selection of part of the data set for developing the decision rule and then to use this rule for the classification of training and test objects. This procedure should be repeated several times. If only one object is deleted each time and the procedure is repeated until all objects are deleted once and only once, this is called the "leave one out" or "jackknife" classification. Recognition (prediction) rate will then be the overall percentage of correctly classified training (test) objects.

Prediction and recognition rate are both measures of the reliability of the classification rules. However, as the latter is obtained on the basis of objects used in the development of the decision rules, it is a biased criterion. The prediction rate is a more realistic criterion of validity. A large discrepancy from the recognition rate indicates an overfitting of the training set, because the sample constituting the training set is not representative of the population from which it is drawn, or because the technique used to derive the decision rule is not suitable for the problem under study.

Though prediction and recognition rates can be used as validation criteria for all supervised techniques, their meaning is different for discriminating and modelling techniques. For a 2-class problem for instance, a discriminating technique yields four possible decision outcomes that can be represented in a 2 × 2 decision table:

	Belonging to class A	Belonging to class B
Classified as A	true A	false A
Classified as B	false B	true B
	$n1$	$n2$

where $n1$ and $n2$ are the numbers of samples belonging to class A and B, respectively. Depending on whether this table is defined on the basis of the training or the test set, the ratios (true A)/$n1$ and (true B)/$n2$ correspond to the recognition or prediction rate of class A and B, respectively, reflecting the separability of both classes. When the two classes are clearly separated, these ratios closely approximate 100%.

The use of a modelling technique for the same problem yields eight possible decision outcomes which can be represented in a 4 × 2 decision table:

	Belonging to class A	Belonging to class B
Classified:		
Uniquely A	true A	false A
Uniquely B	false B	true B
A and B (i.e., situated in the overlap region)	true A	true B
Outlier	false (not A) = false outlier	false (not B) = false outlier

For each class separately, a 2 × 2 decision table can be constructed:

	Belonging to class A	Not belonging to class A
Classified as A	true A	false A
Classified as (not A)	false (not A)	true (not A)

The ratio (true A)/$n1$ is the prediction (or recognition) rate of the model for class A. In analogy with medical decision-making, where this kind of decision table is used to evaluate the performance of diagnostic tests [14], the prediction rate can also be referred to as the sensitivity of the model.

As class models are developed at a predefined level of significance (e.g., 5%), this implies that one expects only 95% of the objects belonging to the population to fall inside the class box and 5% to fall outside of it. In statistical

terms, the percentage of objects belonging to the population that is expected to fall outside the model is called the Type I error α, i.e., the prediction and recognition rate are expected to approach the predefined level of confidence $(1 - \alpha)$. A discrepancy between the actual prediction rate and $(1 - \alpha)$ is a second indication that an unrepresentative sample was taken to construct the class box, or that the constraints for the modelling technique concerned are not fulfilled. The criterion that indicates the dissimilarity between a class and all other classes of the data set is the ratio (false A)/(not belonging to A), which is comparable to the Type II error β of statistical tests. In analogy with statistics, $(1 - \beta)$ = true (not A)/(not belonging to A) can be called the specificity of the model. When "not belonging to A" is replaced by "objects belonging to B" in the decision table, this ratio becomes the specificity index of class A with respect to class B.

The specificity index $(1 - \beta)$ depends on α, the predefined level of significance. The smaller α, the larger the boundaries of the class model are and therefore the larger the degree of overlap between the class boxes. Care should therefore be taken to compare specificity indices on the same level of significance. A possible criterion for the global performance of a model is the efficiency. In medical decision-making, the efficiency is the ratio of all results that are correct, i.e., the ratio [(true A) + true(not A)] /($n1$ + $n2$). Defined in this way, the efficiency index depends on the number of samples in both classes. If the sample sizes $n1$ and $n2$ are proportional to the size of the population from which they are drawn, then the efficiency index will be a realistic reflection of the rate of correct classifications that are obtained with the class model. If, however, $n1$ and $n2$ are not proportional to the population size, the efficiency index may be misleading. A highly sensitive but poorly specific model can yield a high efficiency index if $n1$ is much larger than $n2$. If, in reality, the number of objects that do not belong to population 1 is much larger than the number of objects that do belong to it ($N1 \ll N2$), the real efficiency of the class model will approximate the specificity index instead of the sensitivity index which was calculated from the training procedure. Therefore, it is preferable to evaluate the efficiency as the mean of the specificity and sensitivity indices when one has no prior information about the probability of class membership.

RESULTS AND DISCUSSION

Class models were developed for two southern (North Apulia n = 25, Calabria n = 56) and two northern (East n = 50 and West Liguria n = 50) regions. To evaluate the specificity of the models towards oils from other regions, a distinction can be made between the southern and northern Italian (including Sardinian) oils because these two categories can be distinguished on the basis of a single variable, ecosenoic acid. This acid is absent in the latter group and always present in the former group of oils. For the development of the SIMCA models, the separate scaling procedure was

applied, because previous investigations indicated this to be the most appropriate approach for this data set [7]. Validation of the UNEQ and the SIMCA model was done by use of a procedure in which each time a fixed part of the samples belonging to the class was used as test set. Because the variables in this data set are expressed as a percentage of the total fatty acid content, thus adding to 100%, the variance-covariance matrix is singular so that it cannot be inverted. Therefore, the UNEQ models were developed on the basis of seven variables for the southern regions and six variables for the northern regions (as for these, ecosenoic acid was not detected). The variable not taken into account was the one with the highest coefficient of variance (linolenic acid for the Ligurian regions; palmitic acid for North Apulia, and econsenoic acid for Calabria). Table 1 summarizes the behaviour of both types of class models.

Sensitivity of the models

The sensitivity of the Calabrian UNEQ model approaches the α value at both levels of significance, thereby indicating that the method is appropriate for this class. The North Apulian and East Ligurian UNEQ models perform well at the 95% confidence level but most samples falling outside the 95% range also fall outside the 99% range, resulting in relatively poorer behaviour of the models at this level. For East Liguria, this is due to inhomogeneities within the data set, as was indicated by the SIMCA method which yielded a stable class-box only on the basis of 43 out of the 50 samples belonging to this class. For the North Apulian model, the limited sample size compared to the number of variables, which always produces less reliable classification results, may cause the lower sensitivity at the 99% level of confidence. The West Ligurian UNEQ model performs very poorly, even at the 95% level of significance. The Kolmogorov-Smirnov test, applied to each of the variables separately, showed that two variables could not be considered to be normally distributed ($\alpha = 0.05$). Moreover, PCA indicated this group to be composed of two subgroups. The SIMCA models perform worse than the corresponding UNEQ models for three of the four classes (Calabria, North Apulia, East Liguria). For the Calabrian oils, this is due to the fact that a stable class model was obtained only on the basis of 50 out of the 56 samples, whereas for the East Ligurian group only 43 samples could be used. With SIMCA, the inhomogeneity problem within the West Ligurian class was approached by modelling both subgroups separately by one principal component. In order to compare the UNEQ and the SIMCA model for West Liguria, a UNEQ model was also developed for each of the subgroups of this class separately. This approach, however, does not improve the class sensitivity significantly, probably because of the sensitivity of the UNEQ method to large deviations of the normality of the variables. It should, however, be realised that it is often possible to apply, prior to the development of class-models, transformations to the variables in order to make their distribution normal [15]. It would be worthwhile to investigate whether the

TABLE 1

Comparison of the sensitivity, selectivity and efficiency of the UNEQ and SIMCA models for the oil data, at the 95% and 99% levels of confidence

	Value of the index (%)			
	95% confidence limit		99% confidence limit	
	UNEQ	SIMCA	UNEQ	SIMCA
Sensitivity				
Calabria	92.9	85.7	100.0	89.3
N. Apulia	92.0	88.0	92.0	88.0
E. Liguria	91.8	70.0	93.9	84.0
W. Liguria				
one model	82.0		90.0	
two models	86.0	86.0	86.0	90.0
Selectivity				
Calabria to				
N. Apulia	100.0	88.0	100.0	84.0
S. Apulia	99.0	88.8	97.1	75.7
Sicily	86.1	75.0	69.4	63.9
Sardinia	100.0	100.0	100.0	100.0
N. Italy	100.0	100.0	100.0	100.0
North Apulia to				
Calabria	100.0	98.8	96.4	87.5
S. Apulia	100.0	100.0	100.0	100.0
Sicily	86.1	97.2	83.3	88.9
Sardinia	100.0	100.0	100.0	100.0
N. Italy	100.0	97.3	100.0	90.7
East Liguria to				
W. Liguria	100.0	100.0	96.0	100.0
Umbria	62.7	100.0	31.4	92.2
S. Italy	99.3	99.5	97.6	98.6
West Liguria (one model) to				
E. Liguria	98.0		92.0	
Umbria	100.0		100.0	
S. Italy	100.0		100.0	
West Liguria (two models) to				
E. Liguria	100.0	100.0	98.0	100.0
Umbria	100.0	100.0	100.0	100.0
S. Italy	100.0	100.0	100.0	100.0
Efficiency				
Calabria	95.6	87.5	98.7	82.6
N. Apulia	95.6	96.8	94.3	92.9
E. Liguria	84.8	90.0	73.8	92.1
W. Liguria				
one model	93.3		94.0	
two models	95.3	95.3	94.7	96.7

low sensitivity of both the UNEQ and the SIMCA models improves after transformation of the non-normal distributed variables.

Specificity of the models

The specificity index reflects the separability of classes on the basis of the class-models developed. For the South Italian regions, the largest overlap of the UNEQ models occurs with the Sicilian oils. This was to be expected from PCA because the Sicilian region appears to be very diffuse. The separability of the other South Italian oils is high. The specificity towards the North Italian oils is 100%. The specificity of the SIMCA models for these regions is lower than that of the corresponding UNEQ models, except for North Apulia towards Sicily. The behaviour of the Calabrian model is surprising, because this seems to include a large number of Apulian but also of South Italian oils. As the SIMCA model was developed on the basis of the 50 most similar samples of this class, thereby automatically yielding more compact class-boxes, one would expect a higher specificity. Concerning North Apulia, SIMCA does also not allow a complete separation from the North Italian oils as could be expected from the univariate approach in which a complete separation between northern and southern Italian oils can be made on the basis of the absence or the presence of ecosenoic acid. Obviously, the information provided by this parameter becomes lost in the multivariate SIMCA approach.

The West Ligurian UNEQ and SIMCA models are very specific towards other classes. With SIMCA, a complete separation is obtained; with UNEQ there is only a small degree of overlap. The East Ligurian UNEQ model performs well towards the West Ligurian and the southern Italian regions but encloses a large part of the Umbrian class. The SIMCA model is much more specific in this case; this is as expected because this model was obtained on the basis of the 43 most similar samples belonging to this class. As this yields more compact class-boxes, the probability of overlap with other classes is lower, e.g., the class-boxes will probably be more specific. Neither the UNEQ nor the SIMCA model for East Liguria allows a complete separation from southern Italy whereas the univariate approach does. Neither with SIMCA (when a separate scaling procedure is used) nor with UNEQ is it possible to develop class models including a variable that has a constant value for all the samples of the class. With both techniques, the models for northern Italy were therefore developed without considering the variable ecosenoic acid; the discriminating ability of this variable was therefore lost. Obviously, when highly discriminating discrete variables are available, a combined uni- and multi-variate approach must be used.

Efficiency of the models

For each of the class models, the efficiency index was also calculated. As we had no idea about the relative proportions of the olive oils produced in the diverse regions of Italy, which would be a good indication of the a priori

probability of class membership, the efficiency index was calculated as the mean of the sensitivity and specificity indices. For each of the classes, the efficiency was calculated on the basis of the sensitivity index of the concerned model and its specificity for the other classes from the same region (e.g., southern or northern Italy).

As an illustration of the method, class models were developed and compared at two different levels of significance. Obviously, for practical purposes, the significance level should be fixed on the basis of the training procedure. This level can be chosen on the basis of the sensitivity and the specificity indices. As already explained, these two parameters are strongly related. Very sensitive classes are obtained when large class-boxes are used, e.g., when a relatively high confidence level is taken. As a result of this, the specificity may be low because the probability of overlap with other classes will increase. The choice of the cut-off point depends on the "cost" of a misclassification. If the assignment of a sample to a class to which it does not belong would be a more serious mistake than to consider a sample erroneously as an outlier, the boundaries of the class-boxes should be made narrow, i.e., at an α-level that produces high specificity. If the opposite is true, the models should be constructed at a much higher level of confidence. If the different types of misclassification have about the same consequences, the α-level that yields the highest efficiency should be selected.

In general, it can be concluded that the UNEQ method can be very useful for oil classification purposes but requires the populations to be homogeneous (as is the case for SIMCA). Inhomogeneity within the data set is quickly reflected in a decrease of the sensitivity index. In general, the performance of the UNEQ model is comparable or even better than the corresponding SIMCA model. One data set is, of course, not enough to make a reliable judgement about a technique. In later papers, the results of a simulation study will be presented and the effects of the number of variables and deviations from normality will be discussed in more detail. Attention will also be given to the graphical representations that can be used when modelling techniques are applied.

Helpful discussions with E. Defrise-Gussenhove and L. Kaufman are gratefully acknowledged, as is the financial support of the FGWO (Fonds voor Geneeskundig Wetenschappelijk Onderzoek).

REFERENCES

1 N. J. Nilson, Learning Machines, McGraw-Hill, New York, 1965.
2 S. Wold and M. Sjostrom, in B. R. Kowalski (Ed.), Chemometrics: Theory and Application, American Chemical Society, Washington, 1977, p. 243.
3 I. Juricskay and G. E. Veress, Anal. Chim. Acta, 171 (1985) 61.
4 C. Armanini and M. Forina, Model-Centered Bayesian Analysis: Applications in Food Data Analysis, Paper presented at Computereinsatz in der Analytik, September, 1985, Jena.

5 D. Coomans, I. Broeckaert, M. Jonckheer and D. L. Massart, Method. Inf. Med., 22 (1983) 93.
6 B. R. Kowalski, in Chemometric Newsl., 10 (1983) 4.
7 M. P. Derde, D. Coomans and D. L. Massart, Anal. Chim. Acta, 141 (1982) 187.
8 E. Defrise-Gussenhove, Bull. Inst. R. Sci. Nat. Belg., 31 (26), (1955) 1.
9 E. Defrise-Gussenhove, INED, Paris, 1976, p. 131.
10 M. Forina and E. Tiscornia, Ann. Chim. (Rome), 72 (1982) 143.
11 M. Forina and C. Armanino, Ann. Chim. (Rome), 72 (1982) 127.
12 M. P. Derde, D. Coomans and D. L. Massart, J. Assoc. Off. Anal. Chem., 67 (1984) 721.
13 S. Wold, Simca-2T Program Package for Simple Modelling of Class Analogy, Research group for Chemometrics, Institute of Chemistry, Umea University, Sweden, 1977.
14 R. S. Galen and S. R. Gambino, Beyond Normality: the Predictive Value and Efficiency of Medical Diagnosis, Wiley, New York, 1975.
15 J. C. Boyd and D. A. Lacher, Clin. Chim., 28 (1982) 1735.

Analytica Chimica Acta, 184 (1986) 53—64
Elsevier Science Publishers B.V., Amsterdam — Printed in The Netherlands

BACKGROUND SUBTRACTION FOR FLUORESCENCE DETECTION IN THIN-LAYER CHROMATOGRAPHY WITH DERIVATIVE SPECTROMETRY AND THE ADAPTIVE KALMAN FILTER

DAVID D. GEROW and SARAH C. RUTAN*

Department of Chemistry, Box 2006, Virginia Commonwealth University, Richmond, VA 23284-0001 (U.S.A.)

(Received 12th December 1985)

SUMMARY

Background signals must be removed from analyte responses before reliable qualitative and quantitative results can be obtained. For cases in which a reliable estimate for the background response cannot be obtained, the combination of two mathematical approaches yields accurate quantitative results. First-derivative spectrometric methods, in conjunction with a curve-resolution approach based on the adaptive Kalman filter, are used to compensate for difficulties caused by background responses which are not reproducible. Derivative spectrometric techniques reduce the relative magnitude of low-frequency systematic deviations in the spectra. In this case, this has the effect of localizing model errors to restricted regions of the spectra, which in turn meets the major requirement for successful utilization of the adaptive Kalman filter. The approach is applied to fluorimetric detection for thin-layer chromatography in the quantification of polynuclear atomatic hydrocarbon compounds. Results are given which demonstrate that this combined approach yields accurate estimates for concentrations of components in overlapped chromatographic zones. A derivative spectrometric approach in conjunction with a regular Kalman-filter fit gives less accurate results, and an adaptive Kalman filter used to fit the raw spectral data fails to give any reliable quantitative information. The combined approach using derivative spectrometry and the adaptive Kalman filter is shown to give 8-fold lower detection limits for anthracene when compared to traditional background-subtraction methods.

The removal of background signals from analyte responses is an important step in many quantitative procedures. If the background contribution to the analyte response is reproducible, and can be measured in the absence of the analyte, the background contribution can be removed by simple subtraction. In this case, the detection limit is governed by the amount of noise in the background-subtracted response. If the background response is irreproducible or cannot be measured reliably in the absence of the analyte, then these simple methods yield unreliable results, and the detection limits are degraded. In this paper, a combination of two approaches, derivative spectrometry and the adaptive Kalman filter, is used to obtain reliable qualitative and quantitative results when these problems occur.

0003-2670/86/$03.50

Methods which involve the use of first and higher derivatives can be used to enhance signals with rapidly changing responses over signals with slower variations in response [1, 2]. Tahboub and Pardue [2] have shown that derivative spectrometric methods can be combined with curve-resolution methods utilizing linear least-squares to give good quantitative results in u.v.-visible spectrometry when the background response is a light-scattering component with a relatively constant response in the spectral region of interest. For the case in which the background response is not constant, such as in-situ fluorescence detection of species on thin-layer chromatographic plates, derivative spectrometry must be used in conjunction with background subtraction. If the variations in the background signal are limited to variations in a d.c. offset level, the derivative of the spectrum of the background will be reproducible, and this approach should work well in correcting for the variability in the background responses. If the derivative of the background spectrum is not reproducible, a higher-order derivative must be used, which may degrade the detection limit for the method, and may not improve the reproducibility. Another approach for background subtraction has been developed for situations in which a good model for the background response is not available; however, the assumption is made that the background response is essentially featureless [3].

The Kalman filter is a recursive least-squares algorithm which has been used for the resolution of overlapped responses from voltammetric and spectrometric experiments [4—7]. When an accurate model is available for the individual components contributing to the overall response, accurate estimates for the concentrations for each of the components can be obtained from the Kalman-filter algorithm. Methods involving an adaptive Kalman filter can be used in some instances to obtain reliable results if the model is incomplete or inaccurate [8—10]. The main restriction for the adaptive Kalman filter is that the model information must be accurate for some wavelength region in the spectral response [8].

The approach for background subtraction described here is a combination of the two methods described above. In the studies described here, derivative spectrometry has the effect of localizing model errors to certain regions of the spectrum, which allows the adaptive Kalman filter to be used to remove background responses for qualitative and quantitative purposes.

Thin-layer chromatographic (t.l.c.) methods are widely used as relatively simple methods for qualitative screening, and for quantitative purposes. Quantitative results are usually obtained by using in-situ spectrometric detection. Fluorescence spectrometry is widely used because of its inherently low detection limits. The fluorescent background of silica gel t.l.c. plates is relatively large, and this affects the detection limits of the in-situ approach. In addition, this background fluorescence signal may vary from plate to plate, and from location to location on a single plate. In the studies described here, the combined derivative/adaptive-Kalman-filter approach is investigated as a method for background subtraction and quantitation of

polynuclear aromatic hydrocarbons (PAH) which have been separated with the use of t.l.c. methods [11].

THEORY

Adaptive Kalman filter

The Kalman filter is a recursive, linear least-squares algorithm which allows overlapped spectral responses to be resolved, provided that a good model for the individual responses which contribute to the overlapped response is available. The model used for the Kalman filter is comprised of two equations which describe the chemical system and the measurement process respectively:

$$\mathbf{X}(k) = \mathbf{I} \cdot \mathbf{X}(k-1) + \mathbf{w}(k) \tag{1}$$

$$Z(k) = \mathbf{H}^T(k) \cdot \mathbf{X}(k) + v(k) \tag{2}$$

Here, $\mathbf{X}(k)$ is a vector which contains elements corresponding to the current best estimates for each of the component concentrations. The matrix, I, is the identity, so that Eqn. 1 states that the concentrations are invariant with the index k, which in this case is a counter indicating the emission wavelength for the fluorescence intensity measurement, $Z(k)$. The row vector, $\mathbf{H}^T(k)$ consists of elements corresponding to each of the species contributing to the overall spectral response of a mixture. These elements are essentially values of the slopes for the calibration plots for each wavelength at which a fluorescence measurement has been made. The vector, $\mathbf{w}(k)$, and the scalar, $v(k)$, are noise contributions to the system model and the measurement model, respectively. The measurements are processed one at a time, and a concentration estimate for each component is obtained after each step, using the algorithm given in Table 1. This algorithm is the Potter-Schmidt square-root algorithm, which has been used successfully to alleviate difficulties caused by computer round-off errors [9, 12, 13]. When a good model is available for each of the components contributing to the spectrum, reliable concentration estimates can be obtained. In cases for which the model is incorrect or incomplete, the regular Kalman filter algorithm fails. In this case, an adaptive Kalman-filter algorithm can be used [8—10], provided that the model is valid for some portion of the spectral response. Equation 5 in Table 1 is used to recalculate R, the variance in the measurement process, for each wavelength, k. In spectral regions where the model is invalid, the calculated measurement variance will become large and the filter is closed to subsequent measurements.

EXPERIMENTAL

Fluorescence spectrometry

A Farrand MK-2 spectrofluorimeter, equipped with a t.l.c. scanning device and computer interface, was used to collect the data. This instrument was

TABLE 1

Algorithm equations for the square-root Kalman filter

State estimate extrapolation:

$$\mathbf{X}(k|k-1) = \mathbf{I} \cdot \mathbf{X}(k-1|k-1) \tag{3}$$

Square-root covariance estimate extrapolation:

$$\mathbf{S}(k|k-1) = \mathbf{I} \cdot \mathbf{S}(k-1|k-1) \cdot \mathbf{I}^T \tag{4}$$

Adaptive measurement variance:

$$R(k) = 1/m[\sum_{j=1}^{m} \nu(k-j) \cdot \nu(k-j)] - [\mathbf{H}^T(k) \cdot \mathbf{S}(k|k-1)]^2 \tag{5}$$

where $\nu(k) = Z(k) - \mathbf{H}^T(k) \cdot \mathbf{X}(k|k-1)$ (6)

Kalman gain:

$$\mathbf{K}(k) = a\mathbf{S}(k|k-1) \cdot \mathbf{G}(k) \tag{7}$$

where $\mathbf{G}(k) = \mathbf{S}^T(k|k-1) \cdot \mathbf{H}(k)$ (8)

$$1/a = \mathbf{G}^T(k) \cdot \mathbf{G}(k) + R(k) \tag{9}$$

$$d = 1/\{1 + [aR(k)]^{1/2}\} \tag{10}$$

State estimate update:

$$\mathbf{X}(k|k) = \mathbf{X}(k|k-1) + \mathbf{K}(k)[Z(k) - \mathbf{H}^T(k) \cdot \mathbf{X}(k|k-1)] \tag{11}$$

Square-root covariance update:

$$\mathbf{S}(k|k) = \mathbf{S}(k|k-1) - ad\mathbf{S}(k|k-1) \cdot \mathbf{G}(k) \cdot \mathbf{G}^T(k) \tag{12}$$

used with slits on each monochromator which yielded a bandpass of 10 nm. The spectrofluorimeter was interfaced to a Compupro 816-D computer equipped with an 80286 CPU and an 80287 math co-processor, a 12-bit A/D/A board (I/O Technology), a parallel interface board (Interfacer 2), 512 kb of static RAM memory, a 40-Mb hard disk, and 5¼-in. and 8-in. floppy disk drives. Data collection programs were written in the C programming language. These programs allowed for the collection of fluorescence excitation and emission spectra, which could be stored on disk for subsequent display and data processing. Fluorescence intensity data (expressed as relative intensity) were obtained at 1-nm intervals. Chromatographic data were collected with a Hewlett-Packard integrator.

Stock solutions of benzo[a]pyrene, anthracene, and perylene were prepared from chemicals of at least 99% purity by dissolution in cyclohexane. The spectra of these compounds in solution were obtained and stored on floppy disk.

Thin-layer chromatography

The standard solutions of PAH compounds described above were separated on C-18 reversed phase t.l.c. plates (Whatman). Methods for the t.l.c.

separation of PAH compounds were adapted from procedures described by Butler et al. [14] and Sawicki [15]. Sample aliquots of 500 nl were used, and an 80% (v/v) methanol/water solution was used to develop the plates. Typically, two consecutive developments of 15 min each were used. For mixtures containing anthracene, benzo[a] pyrene and perylene, the anthracene zone was well resolved from the other two zones. Under these chromatographic conditions, however, perylene and benzo[a]pyrene were found to coelute. Spectra of the PAH compounds after chromatographic separation were obtained in-situ by positioning the t.l.c. scanning drive so that the maximum emission was observed. Once the scanner had been positioned at the elution maximum, an emission spectrum was obtained, with the excitation wavelength set at 252 nm. An estimate for the background spectral response was obtained for each spectrum by translating the t.l.c. scanning unit in a direction perpendicular to the solvent flow to a "blank" location on the t.l.c. plate. Linear calibration plots for anthracene and perylene were obtained for the concentration ranges used (10^{-7}—10^{-5} M) in this study. The benzo[a]pyrene was found to be relatively photosensitive, and a calibration graph was not obtained for this compound.

Data-processing programs

The adaptive Kalman filter and the Savitzky-Golay derivative smoothing routines were written in PASCAL. The adaptive Kalman-filter program was modeled after the programs described previously [8, 9], with the following modifications. First, a check on the calculated value for the measurement variance, R, was made for each iteration of the Kalman filter. The calculated value was restricted to a minimum value, which was the estimated variance in the fluorescence measurement. The measurement variance was estimated to be 1.0×10^{-7} (in arbitrary units of relative intensity squared), which was obtained by calculating the autocovariance at zero lag of a spectrum of residuals. This appeared to yield values for the covariance matrix elements that were representative of the precision in the concentration estimates, compared to the values obtained in the previous studies [9]. A smoothing window (m) of 6 points was used to average the innovations sequence, ν (see Eqns. 5 and 6 in Table 1). In this study, the corrections to the measurement function, as described previously [8], were not used. A simplex-optimized version of the adaptive Kalman filter was also tested; it was similar to the program reported previously [9]. Both versions were written with use of the Potter-Schmidt square-root algorithm for better numerical stability [9, 12, 13].

The Savitzky-Golay derivative smoothing routine used a 7-point quadratic smooth [16, 17].

The approach for background removal by means of the combination of the first-derivative smooth and the adaptive Kalman filter incorporated the following steps. In step 1, an estimate for the background spectrum is obtained and the first-derivative spectrum is calculated. In step 2, an "unknown" spectrum is obtained, in which the analyte contribution is either a

known standard to be used in the development of a subsequent Kalman filter model, or a true unknown, for which the identity of the compound(s) is unknown; the first-derivative spectrum is calculated. In step 3, the derivative spectrum described in step 1 is used as the model for the adaptive Kalman-filter measurement; the derivative spectrum described in step 2 is used as the measured response (Z) for the adaptive Kalman filter. A single iteration of the adaptive Kalman filter is used with an initial guess for the "concentration" of the background set to 1.0 and an initial guess for the variance of 0.1. In step 4, the final estimate for the "concentration" of the background obtained in step 3 is used to subtract the appropriate fraction of the background response from the analyte response, for both the original spectrum and the derivative spectrum.

The method described above is essentially an approach for qualitative purposes. Once a spectrum, with the optimum amount of background removed, has been obtained, the compound(s) can be identified from the shape of the spectral response. The success of this approach can be evaluated by inspection of the resulting spectra. In addition, this approach can be used to generate a model for subsequent quantification by using the adaptive Kalman filter. A quantitative step can also be used to confirm the validity of the background subtraction method described above.

The approach used here for quantification is summarized by the following steps. In step 1, a derivative model, comprised of the individual derivative spectra, with background responses subtracted using the approach described above, is generated. These derivative spectra are obtained from measurements of standard solutions which have been eluted on a t.l.c. substrate. This model can be comprised of any number of components; currently, the adaptive Kalman filter program can accept a model consisting of up to five components. In step 2, an "unknown" spectrum is subjected to the background subtraction procedure described above, and the resulting derivative spectrum with the background response removed is used as the measured response. In step 3, the simplex-optimized version of the filter program is used to obtain estimates for the component concentrations. This procedure allows the background removal procedure to be evaluated.

RESULTS AND DISCUSSION

Three background spectra, obtained from a developed t.l.c. plate, were measured and stored on floppy disk. These spectra (Fig. 1A) were obtained from different locations on the t.l.c. substrate. These show substantial variations in both intensity and spectral distribution. The lower two spectra (a and b) cross over, which indicates a change in the spectral distribution. The feature at 350 nm in the spectra is due to a cut-off filter which was used to minimize interferences from second-order scattered light. The other features in the spectra arise from the inherent fluorescence of silica gel, from the fluorescence of the binders used in the t.l.c. plates, and from the fact that

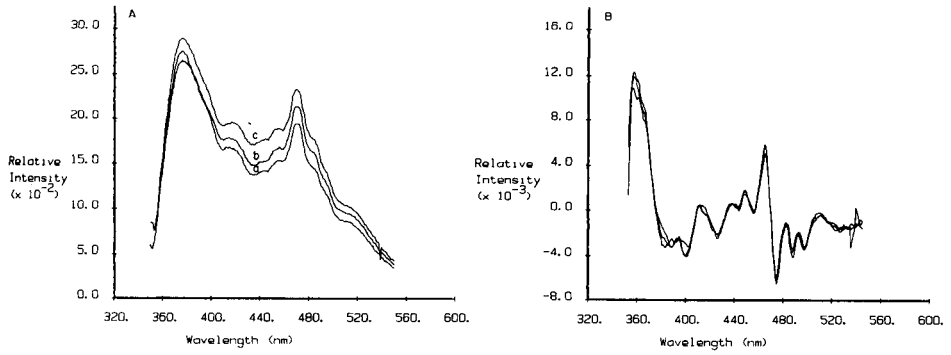

Fig. 1. (A) Background fluorescence spectra of a t.l.c. plate obtained at three locations. (B) First derivatives of these spectra.

the fluorescence spectra are not corrected for the intensity distribution of the light source or the photomultiplier response. Because these spectra show several relatively sharp features, and a significant degree of variability, most approaches for background subtraction that were discussed in the introduction would probably fail.

Derivative spectrometry

The first-derivative spectra for the responses shown in Fig. 1A are shown in Fig. 1B. Most of the variability between the spectra has been eliminated. This suggests that the intensity variations shown in Fig. 1A are largely due to a d.c. offset component in the spectra. The d.c. offset level might be caused by variations in the angle of the incident exciting radiation, e.g., if the plate was slightly tilted with respect to the excitation or collection optics.

Closer examination of Fig. 1B shows that there still is considerable systematic variability between the background responses. This indicates that, while first-derivative spectrometry will aid in eliminating problems caused by variations in the background response, it will not compensate completely for the variability. The signal-to-noise ratios of second- and third-derivative spectra were examined, and it was concluded that the first-derivative approach yielded the best compromise between selectivity and sensitivity.

Quantitative evaluation

To evaluate the performance of the proposed method in the absence of other potential errors, the solution spectra for each of the three compounds were measured and added to the background spectrum (a) shown in Fig. 1A. This generated spectra which could serve as models for quantitative analysis in the presence of the variable background. Here, spectrum (c) in Fig. 1A served as an estimate of the background response in the method for qualitative background removal described in the experimental section. Next, varying amounts of the benzo[a]pyrene and perylene solution spectra were added

to the background response (b in Fig. 1A) and the method for qualitative background removal was used, where spectrum (c) again served as the model for the background response. These spectra simulate the case in which benzo[a]pyrene and perylene coelute on a reversed-phase substrate. Finally, the method for quantification described in the experimental section was used to estimate the "concentration" of each of the two contributing species. The "concentration" estimates and standard deviations for these estimates (obtained from the diagonal elements of the covariance matrix) are given in the final column of Table 2. In addition, "concentration" estimates were also obtained for a regular Kalman filter fit to derivative spectra after simple background subtraction, for a regular Kalman filter fit of the derivative spectra with a model generated from the qualitative approach described in the experimental section, and for an adaptive Kalman filter fit of the undifferentiated spectra. These results are also shown in Table 2.

The standard deviations listed in Table 2 were obtained by taking the square root of the diagonal elements of the covariance matrices. While it has been suggested that the Potter-Schmidt algorithm may yield erroneous values for the covariance matrix elements [18], the results shown here seem to be reliable. These values tend to be somewhat larger for the fits with the derivative/adaptive Kalman filter because of the increase in the measurement variance, R, during filtering regions of the spectra which are prone to model errors.

The results for fitting the undifferentiated spectra with the adaptive Kalman filter were poor in all three cases. The covariance matrix calculation ($\mathbf{P} = \mathbf{S}^T\mathbf{S}$ from Eqn. 12 in Table 1) was unstable, because of the magnitude of the model errors, and no standard deviations are reported. The poor performance observed here is most likely due to the d.c. offset, which would cause the model to be in error over the entire spectral range. This violates the main assumption required for the successful use of the adaptive Kalman filter. The results for fits with the derivative mode after simple background subtraction and the results for derivative mode fits after qualitative background removal

TABLE 2

Comparison of concentration estimates[a]

Component	Relative concentration	Concentration estimates			
		Adaptive Kalman filter	Derivative/ simple subtraction	Derivative/ Kalman filter	Derivative/ adaptive Kalman filter
Perylene	0.5	0.3448	0.5081 (0.0041)	0.5066 (0.0040)	0.4990 (0.0045)
Benz[a]pyrene	1.0	0.8838	1.0234 (0.0048)	1.0082 (0.0048)	1.0028 (0.0056)
Perylene	0.5	0.2938	0.5032 (0.0041)	0.5014 (0.0040)	0.5022 (0.0044)
Benz[a]pyrene	0.2	0.8198	0.2202 (0.0048)	0.2102 (0.0048)	0.2022 (0.0066)
Perylene	0.1	0.3244	0.1155 (0.0041)	0.1231 (0.0040)	0.1006 (0.0046)
Benz[a]pyrene	1.0	0.8070	1.0235 (0.0048)	1.0166 (0.0048)	0.9958 (0.0086)

[a]Standard deviations in parentheses.

are significantly improved. For the first artificial mixture, the benzo[a]pyrene and the perylene contribute approximately equal intensities to the overlapped response, and the derivative/Kalman filter appear to work as well as the derivative/adaptive Kalman filter. In the other two mixtures, the intensity ratio is approximately 10:1, and the non-adaptive fitting methods are not able to estimate the "concentration" of the minor response as accurately. The spectrum and the estimated background response for the third mixture are shown in Fig. 2. Neither benzo[a]pyrene nor perylene shows fluorescence below 380 nm, so that the differences between the two spectra in the region below 380 nm are due solely to variations in the background response. Despite the obvious systematic deviations between the background contributions to the analyte spectrum, and to the model used for the background, the combined derivative/adaptive Kalman filter method can be used to evaluate accurately the contributions from the overlapped species.

In-situ t.l.c. quantification

The above results demonstrate that this combined method can be used to obtain accurate estimates for concentrations in the presence of a poorly modeled background. Next, standard solutions of anthracene, benzo[a]-pyrene and perylene were applied to a t.l.c. plate, along with a solution containing the three compounds at concentrations of 155, 160, and 167 $\mu g\ l^{-1}$, respectively. The standard spectra were subjected to qualitative background removal; the resulting spectra are shown in Fig. 3A—C. In each case, the spectrum is characteristic of each of the compounds. The perylene spectrum (Fig. 3A) shows some deviations in the region from 350 to 420 nm, where a flat baseline should be observed. This is due to systematic variations between the estimated background response and the actual background contribution to the analyte spectrum. Because no assumptions are made about the spectral

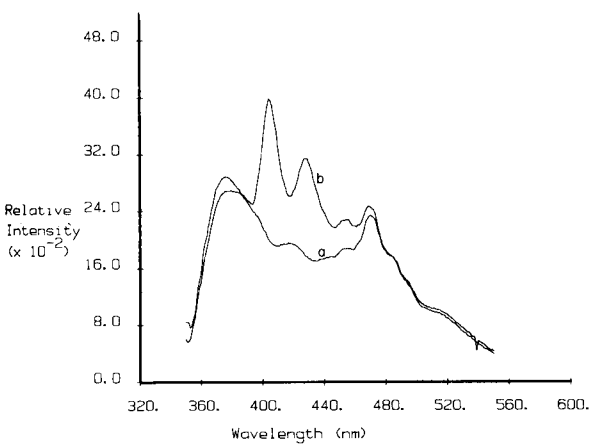

Fig. 2. (a) Model for background fluorescence response of t.l.c. substrate; (b) background response with added benzo[a]pyrene and perlyene.

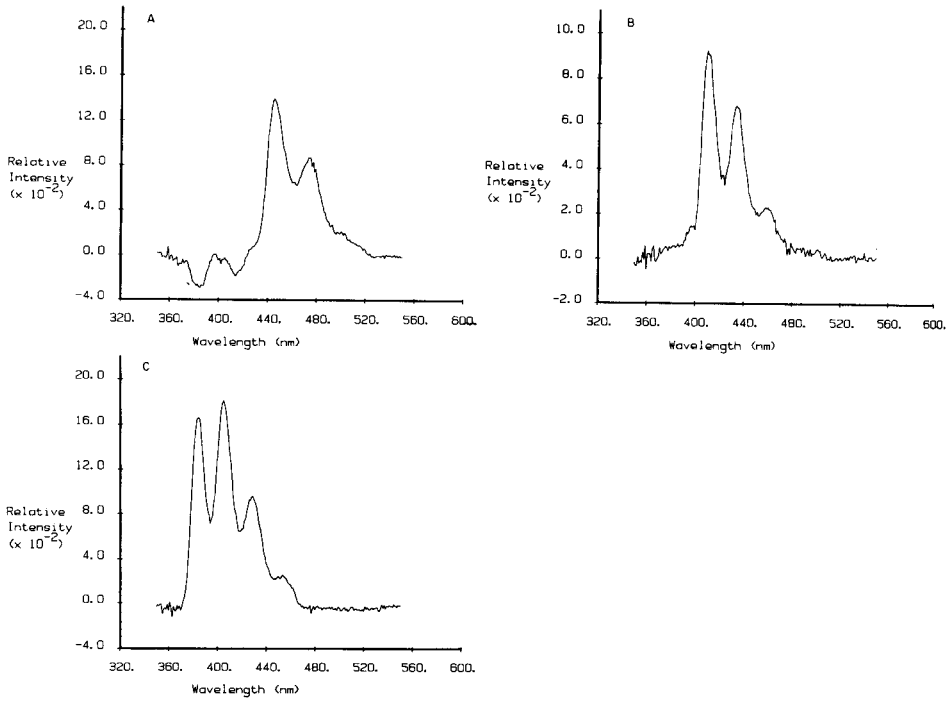

Fig. 3. Responses with background removed: (A) perylene; (B) benzo[a]pyrene; (C) anthracene.

response of the analyte spectrum, these deviations cannot be corrected. Spectra were obtained of the two chromatographic zones observed for the mixture, and the derivative model developed from spectra of the pure components was used to estimate the concentrations in the mixture, using the combined derivative/adaptive Kalman filter method. Anthracene is well resolved from the remaining two components; the estimation error in the concentration of this component is 0.6%. While the perylene and benzo[a]-pyrene appear as a single fluorescent zone on the t.l.c. plate, the R_f values are slightly different. The spectrum of the zone was obtained at the optimal placement for the perylene response, so that in this case only the perylene concentration was determined. Despite the modeling error for the perylene contribution described above, the quantitative derivative/adaptive Kalman filter method yielded an estimation error of only −1.8% for the perylene concentration. No apparent difficulties were caused by the photosensitive nature of the benzo[a]pyrene. The derivative method combined with the regular Kalman filter yielded an estimation error of −26%, and the adaptive Kalman filter approach applied directly to the raw spectral data gave an estimation error of −85%.

Comparison of linear-regression statistics

The limit of detection for anthracene on a t.l.c. substrate was estimated to establish if the method recommended here could be used to improve detectability. Calibration plots were generated by first removing the background response, and then plotting the fluorescence intensity for the band at 402 nm as a function of the concentration of anthracene. The proposed method and simple background subtraction were used to remove the background response from the anthracene spectrum. The parameters for the linear least-squares fits for these two calibration plots are given in Table 3. The proposed method for background subtraction yields an eight-fold reduction in the limit of detection for anthracene over simple background subtraction. The limit of detection observed approaches the limit expected if instrumental noise were the only source of error. While more accurate detection limits can be calculated from repetitive measurements at low concentrations, the estimates given here demonstrate that a significant improvement in detectability is possible. The systematic deviations which arise from the variability of the background responses degrade the detection limit when simple background subtraction is used.

Conclusion

The combination of the two mathematical techniques described here, first-derivative spectrometry and adaptive Kalman filtering, allows for background removal and accurate determination of concentrations in the presence of a poorly modeled background response. The two methods do not compensate for these difficulties when used independently. In the derivative spectra, model errors are effectively localized in specific regions of the spectra, which in turn meets the major requirement for the adaptive Kalman filter. Other approaches, such as the use of higher derivatives, or the inclusion of a d.c. offset component in the Kalman filter model might be used to alleviate these difficulties; however, the combination of the methods described here yields results which are not affected by the higher noise levels observed in higher-derivative spectra, and obviates the need for the assumption of a d.c. offset component in the model. The approach described here should be widely

TABLE 3

Comparison of statistical parameters for different approaches[a]

Method	Slope (10^{-3} M^{-1})	Intercept (10^{+3})	LOD (μM)	Standard error	Correlation coefficient
Proposed	2.758 (0.077)	3.0 (1.9)	1.0	3.0×10^{-3}	0.9988
Simple subtraction	3.40 (0.38)	0.5 (9.7)	8.4	1.5×10^{-2}	0.9813

[a]Standard deviations in parentheses.

applicable when subtraction of background responses with systematic deviations is required.

This research was supported in part by the Grants-In-Aid Program for Faculty of Virginia Commonwealth University. The authors gratefully acknowledge the donation of the Hewlett-Packard integrator by E. I. duPont deNemours & Company, Richmond, VA.

REFERENCES

1 T. C. O'Haver, Anal. Chem., 51 (1979) 91A.
2 Y. R. Tahboub and H. L. Pardue, Anal. Chem., 57 (1985) 38.
3 P. J. Statham, Anal. Chem., 49 (1977) 2149.
4 H. N. J. Poulisse, Anal. Chim. Acta, 112 (1979) 361.
5 T. F. Brown and S. D. Brown, Anal. Chem., 53 (1981) 1410.
6 S. C. Rutan and S. D. Brown, Anal. Chem., 55 (1983) 1707.
7 C. A. Scolari and S. D. Brown, Anal. Chim. Acta, 166 (1984) 253.
8 S. C. Rutan and S. D. Brown, Anal. Chim. Acta, 160 (1984) 99.
9 S. C. Rutan and S. D. Brown, Anal. Chim. Acta, 167 (1985) 23.
10 S. D. Brown and S. C. Rutan, J. NBS Res., 90 (1985) 403.
11 D. T. Kaschani, in W. Bertsch, S. Hara, R. E. Kaiser and A. Zlatkis (Eds.), Instrumental HPTLC, Verlag, New York, 1980, pp. 185—208.
12 P. G. Kaminski, A. E. Bryson, Jr. and S. F. Schmidt, IEEE Trans. Auto. Control, AC-16 (1971) 727.
13 T. F. Brown, D. M. Caster and S. D. Brown, Anal. Chem., 56 (1984) 1214.
14 H. T. Butler, M. E. Coddens, S. Khatib and C. F. Poole, J. Chromatogr. Sci., 23 (1985) 200.
15 E. Sawicki, Talanta, 16 (1969) 1231.
16 A. Savitzky and M. J. E. Golay, Anal. Chem., 36 (1964) 1627.
17 J. Steiner, Y. Termonia and J. Deltour, Anal. Chem., 44 (1972) 1906.
18 S. D. Brown, private communication, 1986.

Analytica Chimica Acta, 184 (1986) 65—76
Elsevier Science Publishers B.V., Amsterdam — Printed in The Netherlands

THE APPLICATION OF PATTERN RECOGNITION TO THE IDENTIFICATION OF PATHOGENS BY LASER-EXCITED FLUORIMETRY

J. T. COBURN, R. A. FORBES, B. S. FREISER, L. BECKER and F. E. LYTLE*
Department of Chemistry, Purdue University, West Lafayette, IN 47907 (U.S.A.)
D. M. HUBER
Department of Botany and Plant Pathology, Purdue University, West Lafayette, IN 47907 (U.S.A.)
(Received 11th November 1985)

SUMMARY

The k-nearest neighbor (*k*NN) approach to pattern recognition was used to evaluate a laser-based method of identifying pathogens based on aminopeptidase profiling. Suitability of the method was tested by evaluating the recognition accuracy for differentiation of four bacterial genera as well as four races within a single species. Even though variations in profile replicates were relatively large, the *k*NN approach successfully differentiated these pathogens. Recognition accuracies of 100% and 92% were achieved for the differentiation of genera and races, respectively. Feature-selection algorithms were used which allowed the rejection of features which did not add useful information towards identification or improve recognition accuracy. Identification of races was facilitated by constructing a data set comprised of only races of one species, because feature selection and weighting were strongly affected by the easily differentiated genera. Methods used for feature selection and weighting were also evaluated.

The time required for diagnosis of many diseases can be governed by the time needed for accurate identification of pathogens. New instrumental approaches which address this problem have reduced the test incubation time, but still require a long growth period to isolate a sufficient quantity of pathogen to begin the test. To circumvent this problem, a method requiring many fewer organisms based on aminopeptidase profiling coupled with improved instrumentation and protocol was recently reported [1]. The aminopeptidase profiling procedure establishes the extent of hydrolysis of a series of amino acid naphthylamide substrates by the pathogen being tested [2]. The bar graph of the extent of hydrolysis versus the substrate hydrolyzed is known as an aminopeptidase profile. The shape of the profile is indicative of the pathogen. Because the accuracy of identification can depend on the profile shape, evaluating the selectivity of the technique is important in assessing its usefulness.

Computer-assisted methods of pathogen identification have been in use for over a decade. Pattern recognition is one general approach which has

0003-2670/86/$03.50

gained favor among clinical microbiologists. Specific variants have included linear discriminant functions [3], quadratic discriminant functions [4] and Bayesian probability theory [5]. With the quadratic discriminant function, 18 tests were used to construct growth inhibition profiles. Concentric ellipses in n-dimensions were then used to assign the most probable class for the test pattern. The data were assumed to follow a normal distribution. The results are impressive with 3726 strains of bacteria being classified into thirty groups with an 88.4% accuracy. With the Bayesian probability approach, 539 isolates were classified as belonging to one of ten species. Assuming a log-normal distribution and choosing a 95% confidence level, five species gave a >90% accuracy, three gave 83—88%, and two gave 72—75%.

The problem with choosing an optimal algorithm for identification of bacteria at the low cell numbers (50 000 cells ml^{-1} compared to a more normal value of 10^7 cells ml^{-1}) used in this study is estimating whether random errors in profiles follow a known probability distribution. After several replicate data sets for one species had been examined, no specific distribution was apparent. As a result, a modified k-nearest neighbor (kNN) approach was utilized because the mathematical decision used to choose a class is based on Euclidian distances alone [6—8], and no assumption of an underlying probability distribution is necessary. Nonlinear mapping was used to display class separations visually [9], and thus provide a confirmation of empirically derived classifications.

The modified kNN method was applied to establish the recognition accuracy of the aminopeptidase profiles generated by the improved methodology [1]. Four genera of pathogens, *Pseudomonas phaseolicola*, *Xanthomonas phaseoli*, *Agrobacterium tumefaciens*, and *Phytophthora megasperma* var. *sojae* were differentiated with 100% accuracy by using only four substrates chosen by the kNN method. Within *Agrobacterium*, four races were identified with 92% accuracy with a possible set of three substrates. The importance of substrate selection and weighting on recognition accuracy will be discussed.

EXPERIMENTAL

Instrumentation and chemicals

The laser fluorimeter was used as described in detail previously [1].

Water was purified by distillation and carbon filtration. The 0.05 M, pH 8.0 borate buffer was made by adding 6 M sodium hydroxide to reagent-grade boric acid (Mallinckrodt). Solids of amino acid naphthylamides kept below 0°C were from Sigma Chemical Company. The β-naphthylamides used were: L-alanyl- (ALA), L-arginyl- (ARG), L-aspartyl (ASP), L-cystinyl-di- (CYS), L-glycyl- (GLY), L-histidyl- (HIS), L-hydroxyprolyl- (HPRO), L-isoleucyl- (ILEU), L-leucyl- (LEU), L-lysyl- (LYS), L-methionyl- (MET), L-phenylalanyl- (PHE), L-prolyl- (PRO), L-pyrrolidonyl- (PYR), L-seryl- (SER), L-tryptophyl- (TRY), L-tyrosyl- (TYR), and L-valyl- (VAL). Stock solutions were 0.001 M in methanol and were stored at 4°C. Working solutions were prepared by a 1:100 dilution in buffer.

Biological samples

Cells of *Pseudomonas phaseolicola* (Burk.) Dowson and *Xanthomonas phaseoli* (Smith) Dowson, obtained from D. J. Hagedorn of the University of Wisconsin-Madison, were washed from 48 h-old beef peptone cultures. Cultures of four races of *Agrobacterium tumefaciens* (Hild.) Starr and Weiss grown on yeast extract peptone were obtained from Stanley Gelvin, Purdue University. The races represented were C58 (no Ti plasmid), A6 + pTiA6 (arg 6), 15 955 + pTil5955, and LBA4404 + pAL4404. Two races of *Phytophthora megasperma* Dresch. var *sojae* Hildeb., PMS 1 (strain 5-58) and PMS 3 (strains 7-76, 84-1-4B, and 84-3-7B) were obtained from David Kuhn, Purdue University. Cell density was adjusted photometrically at 540 nm to 10^7 cells ml^{-1} in 0.005 M borate buffer. An aliquot of the suspension was diluted to the desired cell density of 50 000 cells ml^{-1}. Mycelium of *P. megasperma* was aseptically harvested from liquid V-8 juice broth agar media, weighed, ground in a sintered glass grinder (Tri-R Corp.), and diluted to 0.01 g ml^{-1} in borate buffer. The inoculated substrate samples were incubated for 4 h prior to assaying for hydrolyzed BNA.

Computer software

All of the pattern recognition programs were written for the IBM 9000 lab computer in the IBM version CS-9000 of FORTRAN 77 and used the *k*-nearest neighbor algorithm (*k*NN) [10]. A classifier based on this algorithm predicts the class of an unknown to be the same as that of the majority of its *k*-nearest neighbors. Because of the relatively small size of the data sets, only the first nearest neighbor ($k = 1$) was used to effect classification, and the distance measure used was the Euclidian distance in an N-dimensional feature space. A scaling factor or weighting of the features was found to improve clustering of the classes and in the scheme used the features were weighted differently for each class [11]. With this approach, it is possible to assess the importance of a given feature for each class because uniqueness can be inversely related to the weighting factor. The leave-one-out algorithm [9, 12] was used to generate the recognition accuracies needed by the pattern recognition algorithms.

RESULTS AND DISCUSSION

Precision and accuracy of aminopeptidase profiling

The goal of the research was to establish how well small numbers of microorganisms could be differentiated by aminopeptidase profiling using improved instrumentation and protocol [1]. One method [14] used for differentiation calculated the mean and standard deviations for replicate profiles of both *Pseudomonas phaseolicola* and *Xanthomonas phaseoli* (Fig. 1). A large range in the standard deviations was found. For example, profiles of *Pseudomonas phaseolicola* showed a relative error of 2% for PHE and 70% for TRY. The relative error measured for the same substrate hydrolyzed by different

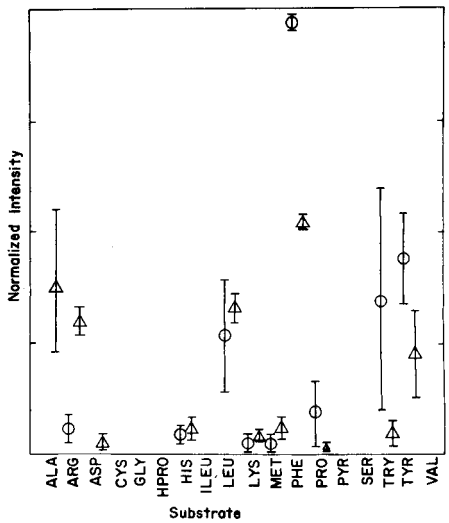

Fig. 1. Average and error brackets for three replicates of amino peptidase profiles of (○) *Pseudomonas phaseolicola* and (△) *Xanthomonas phaseoli.* All data were acquired at 50 000 cells ml and 4 h of incubation.

pathogens also showed a large variation. The LEU showed a larger relative error for *Pseudomonas phaseolicola* than for *Xanthomonas phaseoli.*

The magnitude of the relative error was much greater than that found for instrumental fluctuation (2%) and is probably due to uncontrolled biological sources. There are several such sources of variation in substrate metabolism. For example, certain external parameters may be held constant, but the complexity of the living organism does not rule out the effect of other difficult-to-control environmental factors which may not follow a particular probability distribution. Thus, a different approach was required to evaluate the ability of the profiling method to differentiate organisms.

Pattern recognition

Feature weighting can have a profound effect on recognition accuracies obtained with the *k*NN classifier. The disadvantage of this classifier is its difficulty in correctly classifying patterns at the edges of distributions in hyperspace. In order to overcome this difficulty, it is necessary to increase the separation of distributions of differing classes by feature weighting. A weighting scheme which allows a single feature to be weighted differently for each class uses weighted averages [11, 13]. The weighting factor for a given feature for a given class is the ratio of the weighted average intensity of the feature over all classes to the weighted average intensity of the feature within the given class, where the weighted average intensity is the statistical average, or mean, intensity of a feature multiplied by the number of patterns in which this feature occurs. Because the squared distances along each feature

axis are what are actually weighted, features important for, and unique to, a particular class are minima. For example, the weighting factors applied for the feature substrate phenylalanine in the differentiation of genera are

	Ps	X	A	Ph
PHE	14	41	35	28 880

This substrate is most important for *Pseudomonas phaseolicola* and is not metabolized by *Phytophthora megasperma*. Thus, when an "unknown" which metabolizes phenylalanine is compared along this feature axis to the pattern of the genera *Phytophthoras megasperma*, the distance is exaggerated by the large weighting factor.

The accuracy of identification was improved using the above weighting scheme and by selecting only those substrates that improved the identification accuracy. While the only method which can assure the selection of the optimal subset of features is an exhaustive search, this procedure is not practical in most situations. Often, as in this case, a suboptimal approach is used. Two heuristic methods of substrate selection were used. The first method, successive subtraction, deleted substrates if the accuracy of identification using the leave-one-out algorithm was improved or stayed the same without the substrate. The substrates were deleted beginning with either the first or last substrate to establish whether the order of subtraction had an effect on the recognition accuracy. With this algorithm, either unit weightings or weighted averages were applied and held constant throughout the selection process. The second selection method was forward addition. This method searched all substrates to establish which gave the highest recognition accuracy. After one was selected, another search was done combining the first with each of all other substrates to find the one which improved the accuracy most. The process was continued until there was no longer an improvement in recognition accuracy. With this algorithm, either unit weightings or weighted averages served as a starting point for optimization. Optimization of weightings was performed by using a gradient search algorithm when it was found that a greater reduction in classification error could be obtained by weighting optimization versus addition of a new feature. Two approaches can be used by this algorithm: either a separate space (weight vector) for each class or one space (weight vector) for all classes is optimized.

After the optimal subset of features has been found for a data set, another program was used to give both the recognition accuracies (using the leave-one-out algorithm), and the identities of the nearest neighbors for the data set. The program also has the capability to classify true unknowns against the data set by using its optimal subset of features.

Nonlinear mapping [9] and graphical display of the patterns was used to confirm that the genera and races do indeed cluster, and that the feature selection and weighting algorithms have not produced an artifical fit. The nonlinear mapping algorithm used projects the patterns of a data set from N-dimensional space into a given plane while attempting to preserve the N-space interpattern distances.

The data set

The ability of the aminopeptidase profiling method to differentiate organisms at very low cell numbers was evaluated by obtaining replicate profiles for a series of pathogens. A training set for pattern recognition was formed by using a total of 25 aminopeptidase profiles obtained from *Pseudomonas phaseolicola*, *Xanthomonas phaseoli*, *Agrobacterium tumefaciens*, and *Phytophthora megasperma*. A second, more challenging test was used to evaluate the method. Within the *Agrobacterium* species, three replicates of profiles for four races were measured. The races were C58, A6, 15955, and LBA4404. A critical ratio of greater than three patterns for every feature selected by the *k*NN method [7] was exceeded for both the data set made up of all genera and the subset of profiles from races of *Agrobacterium tumefaciens* with values of six and four, respectively.

Recognition accuracy for genera

An accuracy of 100% was achieved using pattern recognition with substrate selection by the successive subtraction method and substrate weighting (Table 1). It is interesting to note that the profiles of *Agrobacterium* and *Phytophthora* were correctly identified even though the data set contained different races and strains. Substrate weighting and the selection method chosen were both important in improving recognition accuracy. When all substrates were used with no weighting, an accuracy of 80% was obtained. The number of substrates required for differentiation of these genera was drastically reduced by applying the recognition technique. Only four substrates were chosen out of the eighteen available. As often occurs in pattern recognition, an improvement in recognition accuracy was achieved by deleting features in the data set, because they only add "noise" during the identification step.

The weighting scheme used had an effect on recognition accuracy. When the successive subtraction method was used with unit weighting, a different set of substrates was chosen and the recognition accuracy decreased to 84%. By using the same substrates selected by the successive subtraction method with weighting, but employing unit weights, the accuracy degraded to 88%. Likewise, substituting unit weights for the substrates chosen by the forward addition method with weighting degraded the accuracy of the procedure to 80%. Not examining each genera in its unique space also had a deleterious effect on the system. Using one space gave a recognition accuracy of 88%.

The choice of the substrate selection method also affected the recognition accuracy. When the direction of the successive subtraction search was reversed, accuracy was reduced to 88% using six substrates. An accuracy of 88% was also obtained with the forward addition selection method; however, only two substrates were required in this case.

The nonlinear mapping of the genera from the space of all substrates is shown in Fig. 2. It is noted that a fairly good clustering of the genera occurs. Class separation and clustering is improved by selecting four of the 18

TABLE 1

Recognition accuracy for the differentiation of genera

Selection method	Weighting	Substrates	Pathogen[a]	Accuracy (%)	Overall accuracy (%)
Successive subtraction	Yes	ASP, PHE, PYR, VAL	*Ps*	100	100
			X	100	
			A	100	
			Ph	100	
Successive subtraction	No	ARG, LEU, PHE, PRO, TRY, TYR	*Ps*	80	84
			X	75	
			A	83	
			Ph	100	
Forward addition	Yes	PHE, PYR	*Ps*	80	88
			X	50	
			A	100	
			Ph	100	
Forward addition	No	LEU, PHE, PRO	*Ps*	100	88
			X	75	
			A	83	
			Ph	100	
Successive subtraction[b]	No	LEU, PHE, PRO	*Ps*	100	88
			X	75	
			A	83	
			Ph	100	
None	No	All	*Ps*	80	80
			X	75	
			A	83	
			Ph	75	
Successive subtraction[c]	Yes	ALA, ARG, LEU, LYS, PHE, PRO	*Ps*	80	88
			X	75	
			A	100	
			Ph	75	

[a]*Pseudomonas phaseolicola* (*Ps*), *Xanthomonas phaseoli* (*X*), *Agrobacterium tumefaciens* (*A*), and *Phytophthora megasperma* (*Ph*). [b]One set of weights. [c]Reverse search direction.

substrates using successive subtraction with weighted average weightings (100% recognition accuracy). Figure 3 displays an actual 3-dimensional plot of the data using three of the four selected substrates. A good separation of the genera is evidenced; the *Phytophthora megasperma* cluster is at the origin.

Recognition accuracy for races

As mentioned above, three replicates of four races of *Agrobacterium tumefaciens* were entered in the data set. Differentiation of these races was much more difficult than differentiation of the genera (Table 2). When the

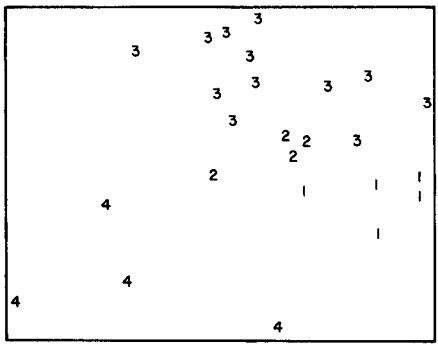

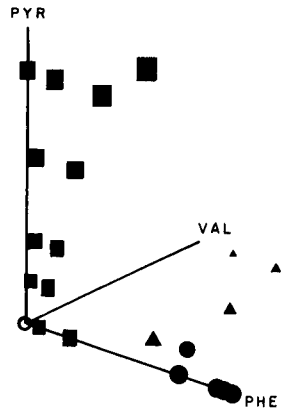

Fig. 2. Nonlinear map of genera from the space of all substrates. Class: (1) *Pseudomonas phaseolicola*; (2) *Xanthomonas phaseoli*; (3) *Agrobacterium tumefaciens*; (4) *Phytophthora megasperma.*

Fig. 3. Plot of genera in the space of three selected substrates: (•) *Pseudomonas phaseolicola*; (▲) *Xanthomonas phaseoli*; (▪) *Agrobacterium tumefaciens*; (○) *Phytophthora megasperma.*

optimum weightings and substrates selected for the differentiation of genera were used, a recognition accuracy of only 25% was obtained. Because such an accuracy would be expected for random race assignment, an alternative method was needed to obtain the race differentiation. Because the substrate selection algorithms optimized the accuracy of genera recognition, a data set of only races of *Agrobacterium tumefaciens* was constructed and new sets of feature weightings and selections were found. The result was an accuracy of 92% for the identification of races with the forward addition method using substrate weighting. The ability to weight and select substrates was especially important in race differentiation. An accuracy of only 8% was obtained without feature weighting and substrate selection.

Weighting factors were smaller for differentiation of races than for genera. A small weighting factor indicated that the substrate was important in the identification of a particular pathogen; and that profiles for the races were much more similar than those of the races. As expected, race differentiation was much more difficult than genera identification. The forward addition method without weighting gave an accuracy of only 75%. Use of only one substrate space gave an accuracy of 83%.

The method chosen for substrate selection also had a large effect on recognition accuracy. The forward addition method gave an accuracy of 92%, while the successive subtraction method had an accuracy of 58%. A reverse successive subtraction run gave an accuracy of only 50%. Note that a different set of substrates was chosen for race differentiation compared to that used for genera differentiation.

TABLE 2

Recognition accuracy for the differentiation of races of *A. tumefaciens*

Selection method	Weighting	Substrates	Pathogen	Accuracy (%)	Overall accuracy (%)
Successive subtraction	Yes	LYS, PRO PYR, TYR	C58	100	58
			A6	33	
			15955	67	
			LBA4404	33	
Successive subtraction	No	ARG, LEU MET, PRO	C58	67	58
			A6	67	
			15955	0	
			LBA4404	100	
Forward addition	Yes	ARG, PRO TYR	C58	100	92
			A6	67	
			15955	100	
			LBA4404	100	
Forward addition	No	ARG, LYS, PRO	C58	67	75
			A6	67	
			15955	67	
			LBA4404	100	
Successive subtraction (one set of weights)	No	ARG, LYS, PRO	C58	67	83
			A6	100	
			15955	67	
			LBA4404	100	
None	No	All	C58	0	8
			A6	33	
			15955	0	
			LBA4404	0	
Successive subtraction (reverse search direction)	Yes	ARG, LYS	C58	67	50
			A6	67	
			15955	67	
			LBA4404	0	
Use of optimum substrates found for recognition of species	Yes	ASP, PHE, PYR, VAL	C58	0	25
			A6	67	
			15955	33	
			LBA4404	0	
Successive subtraction (unit weights)	No	LYS, PRO, PYR, TYR	C58	67	42
			A6	33	
			15955	33	
			LBA4404	33	
Forward addition (unit weights)	No	ARG, PRO, TYR	C58	67	58
			A6	33	
			15955	33	
			LBA4404	100	
Forward addition without gradient search optimization	Yes	ARG, PRO, TYR	C58	100	83
			A6	67	
			15955	67	
			LBA4404	100	

Figure 4 shows the nonlinear mapping of the races from the space of all substrates. Although it appears that some clustering occurs, there is also heavy class overlap because of the similar metabolism of many of the substrates by the differing races. A more distinctive clustering is observed when only those substrates which contribute to the class separation are selected. Figure 5 shows the nonlinear mapping from the three-substrate space chosen by forward addition (yielding 92% accuracy), and a three-dimensional plot of the races in this space is shown in Fig. 6. Except for the distant pattern of C58, the races tend to cluster fairly well.

Because the clustering of the races in the space of all substrates was fairly poor, the possibility exists that an artificial class separation was produced by feature selection, based on accidental correlations in the data set. To test this possibility, class assignments were scrambled such that no two patterns of the same race were assigned to the same class. The feature selection algorithms were applied to this test data set in the same manner as to the true data set. Even when weighted averages were used, the maximum recognition accuracy found for the test data set was 50%, only slightly better than the 33% expected for a random classification.

Recognition strategy

No a priori method was used to choose the optimum selection method. All approaches were investigated to find the method which yielded the highest accuracy. In most cases, weighting the substrates significantly improved recognition accuracy. The greatest improvement in accuracy was obtained by rejection of substrates which did not improve recognition accuracy. All races and strains of *A. tumefaciens* and *P. megasperma* were identified as belonging to the parent genera.

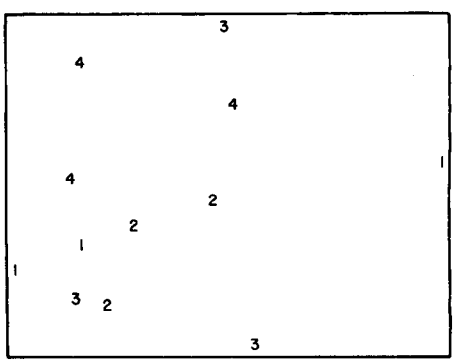

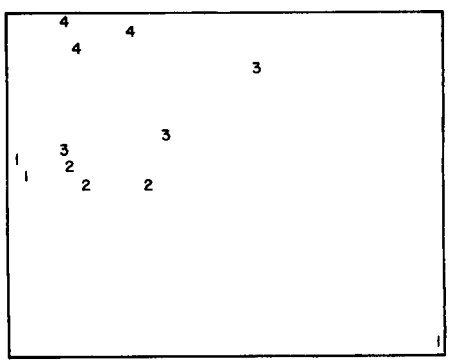

Fig. 4. Nonlinear map of races of *Agrobacterium tumefaciens* from the space of all substrates. Class: (1) C58; (2) A6; (3) 15955; (4) LBA4404.

Fig. 5. Nonlinear map of races of *Agrobacterium tumefaciens* from the space of three selected substrates. Classes as for Fig. 4.

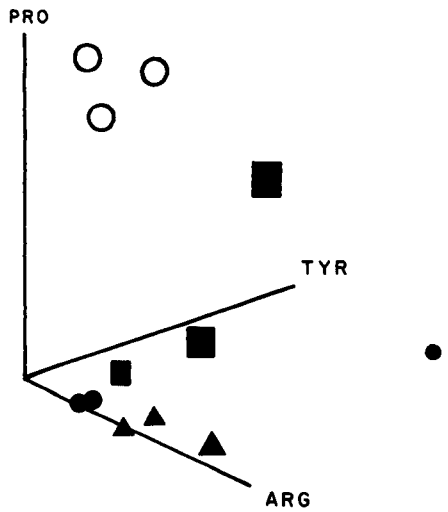

Fig. 6. Three-dimensional plot of races of *Agrobacterium tumefaciens* in the space of selected substrates: (●) C58; (▲) A6; (■) 15955; (○) LBA4404.

An alternative choice of substrates and weightings was required to improve recognition accuracy for races. Accordingly, PYR was chosen as an important substrate for the differentiation of genera. Examination of substrate weightings showed that PYR was needed for the identification of *A. tumefaciens.* But the substrate was not chosen for race differentiation, because more than one race hydrolyzed PYR.

Conclusion

Pattern recognition techniques can be useful tools for the differentiation of pathogens by aminopeptidase profiling. Because the kNN approach does not depend on a known probability distribution, it has an advantage over many statistical methods based on hypothesis testing. Even though the data vary widely for profiles taken on successive days, the modified kNN method was able to recognize consistencies and eliminate substrates which added little information or degraded the recognition. A very practical implication of pattern recognition would be to reduce the number of substrates measured, which would make the aminopeptidase technique less cumbersome. Both the successive subtraction and forward addition methods should be considered to obtain the optimum substrate selection and weightings, because there is no intrinsic reason to choose one over the other. Nonlinear mapping serves as a good check on the validity of the recognition accuracies obtained. Other methods, such as SIMCA and principal components analysis, might also be applied to ensure that there is true class separation. Future applications could inolve a computer-aided, optimized identification of pathogens which are difficult to differentiate. The first step would involve a

survey of all substrates until the species of a pathogen is known and then selection of a subset of substrates to identify the race of the pathogen with new weighting factors.

This work was supported by the National Science Foundation Grant CHE-8320158. R.A.F. and B.S.F. acknowledge support from Lawrence Livermore Laboratory and the Office of Naval Research.

REFERENCES

1 J. T. Coburn, F. E. Lytle and D. M. Huber, Anal. Chem., 57 (1985) 1669.
2 D. M. Huber and M. W. Mulanax, Phytopathology, 59 (1969) 1032.
3 G. Darland, J. Clin. Microbiol., 2 (1975) 391.
4 B. H. Sielaff, J. M. Matsen and J. E. McKie, J. Clin. Microbiol., 15 (1982) 1103.
5 J. H. Godsey, M. R. Matteo, D. Shen, G. Tolman and J. R. Gohlke, J. Clin. Microbiol., 13 (1981) 483.
6 P. C. Jurs and T. L. Isenhour, Chemical Applications of Pattern Recognition, Wiley, New York, 1975.
7 K. Varmuza, Pattern Recognition in Chemistry, Springer Verlag, Berlin, 1975.
8 D. L. Massart, A. Dijkstra and L. Kaufman, Evaluation and Optimization of Laboratory Methods and Analytical Procedures, Elsevier, Amsterdam, 1978.
9 K. Fukunaga, Introduction to Statistical Pattern Recognition, Academic Press, New York, 1972.
10 T. M. Cover and P. E. Hart, IEEE Trans. Inf. Theory, IT-13 (1967) 21.
11 R. A. Forbes, E. C. Tews, B. S. Freiser, M. B. Wise and S. P. Perone, J. Comput. Chem., in press.
12 Q. V. Thomas, R. D. DePalma and S. P. Perone, Anal. Chem., 49 (1977) 1376.
13 R. A. Forbes, E. C. Tews, B. S. Freiser, M. B. Wise and S. P. Perone, Anal. Chem., 58 (1986) 684.
14 J. L. McIntyre, D. Huber, J. Kuc and E. B. Williams, Phytopathology, 65 (1975) 1206.

Analytica Chimica Acta, 184 (1986) 77—85
Elsevier Science Publishers B.V., Amsterdam — Printed in The Netherlands

COMPUTATION OF ACIDITY CONSTANTS OF A POLYPROTIC ACID FROM NUCLEAR MAGNETIC RESONANCE OR U.V.-VISIBLE SPECTROPHOTOMETRIC DATA

GUIDO CRISPONI*, VALERIA NURCHI, TERESA PINTORI and EMANUELE F. TROGU

Istituto di Chimica Generale, Inorganica ed Analitica, Università di Cagliari, 09100 Cagliari (Italy)

(Received 4th November 1985)

SUMMARY

A least-squares program in BASIC is presented for the rigorous calculation of the equilibrium parameters in the dissociation of a polyprotic acid H_qA and of the spectra of all the individual species at equilibrium. The behaviour of the program is discussed for a simulated case involving n.m.r. and for a spectrophotometric study of eriochrome black T.

Potentiometry is the usual method of obtaining the acidity constants of a polyprotic acid [1—5]. However, resort to spectrophotometric or n.m.r. measurements can be useful when it is necessary to obtain not only the acidity constants but also the spectral parameters in studies of the chemical characteristics of the acid, under experimental conditions far removed from those of potentiometric measurements. Furthermore, n.m.r. measurements offer an excellent means of evaluating schemes of microdissociation and of estimating the relative constants [6, 7]. In the evaluation of equilibrium constants from spectrophotometric data, approximate and graphical methods [8, 9] are widely used. In order to simplify the calculations, the data are collected at only one or a few selected wavelengths (or nuclei); in this way, most of the information contained in the system is left unused.

The BASIC program presented here, based on a least-squares procedure, makes it possible to utilize data at several wavelengths (or on several nuclei), so that all the information contained in the system can be exploited. At the same time, both the equilibrium parameters and the spectra of all the individual species at equilibrium can be obtained in a rigorous way. Matrix algebra is used because it is very suitable for the treatment of spectrophotometric data and least-squares problems, and because the matrix notations of BASIC enable the program to be written in a very compact form.

0003-2670/86/$03.50

PRINCIPLE AND CALCULATIONS

For a polyprotic acid H_qA, the dissociation equilibrium is

$$H_qA \overset{K_1}{\rightleftharpoons} H_{q-1}A^- + H^+$$

$$H_{q-1}A^- \overset{K_2}{\rightleftharpoons} H_{q-2}A^{2-} + H^+$$

$$\vdots$$

$$HA^{(q-1)-} \overset{K_q}{\rightleftharpoons} A^{q-} + H^+ \qquad (1)$$

At a given concentration of acid A_t, the equilibrium concentrations of various forms can be obtained from the equations

$$[H_qA] = A_t/(1 + \beta_1/[H^+] + \ldots + \beta_q/[H^+]^q)$$

$$\vdots$$

$$[A^{q-}] = (A_t\beta_q/[H^+]^q)/(1 + \beta_1/[H^+] + \ldots + \beta_q/[H^+]^q) \qquad (2)$$

where $\beta_i = K_1K_2 \ldots K_i$ is the cumulative acidity constant.

At each pH_i value, the measured absorbance $D_{i,j}$ at each wavelength λ_j is assumed to be the sum of the absorbances of the individual contributing species:

$$D_{i,j} = \epsilon_{0,j}[H_qA] + \epsilon_{1,j}[H_{q-1}A^-] + \ldots + \epsilon_{q,j}[A^{q-}] \qquad (3)$$

where $\epsilon_{q,j}$ is the molar absorptivity of the qth component at the wavelength j; when n.m.r. is used, the measured chemical shift is the weighted mean of the shifts of all the species at equilibrium:

$$D_{i,j} = \delta_{0,j}[H_qA]/A_t + \delta_{1,j}[H_{q-1}A^-]/A_t + \ldots + \delta_{q,j}[A^{q-}]/A_t \qquad (4)$$

where $\delta_{q,j}$ is the chemical shift of the jth nucleus in the qth component. If the absorbances (or chemical shifts), D, are measured at n different pH values and at m wavelengths (or nuclei), they can be arranged in a $n \times m$ matrix $\mathbf{D} = \mathbf{C} \times \mathbf{E}$, where $\mathbf{C}$ is the $n \times (q + 1)$ matrix of equilibrium concentrations (or saturation fractions in the n.m.r. case) of the $(q + 1)$ species at equilibrium, and $\mathbf{E}$ is the $(q + 1) \times m$ matrix of molar absorptivities (or chemical shifts of the pure forms).

The matrix of observations $\mathbf{D}$, joined to the $1 \times n$ vector $\mathbf{H}$ of the pH values, contains all the information on the equilibrium and spectral parameters of the acid H_qA. In order to obtain these parameters, a least-squares procedure is used; the function

$$\chi^2 = \sum_{1}^{n}{}_i \sum_{1}^{m}{}_j [D_{i,j} - D_{ci,j}(K_1, K_2, \ldots K_q, \epsilon_{0,1}, \ldots, \epsilon_{q,m})]^2 \qquad (5)$$

where $D_{ci,j}$ is the calculated value of absorbance at the ith pH value and the jth wavelength, has to be minimized with respect to each parameter.

The least-squares Gauss-Newton method could be applied to all the parameters (i.e., q equilibrium constants and $(q + 1) \times m$ spectral parameters) in a

$[q + (q + 1)m + 1]$ dimensional space. However, the high correlation between equilibrium and spectral parameters [10, 11] can cause serious convergence problems, especially with poor initial parameter estimates; furthermore, the Gauss-Newton approach needs prior estimates of all parameters. Therefore, a different least-squares approach was preferred here. This approach was proposed by Feldberg et al. [12] and used earlier in a program for 1:1 adducts [13]. It is based on the mathematical properties of the matrix $\mathbf{D} = \mathbf{C} \times \mathbf{E}$, where the absorbances (or chemical shifts) are linear functions of the spectral parameters, but depend in a non-linear way on equilibrium constants. Therefore, from initial guesses of K values, matrix C can be calculated. Then, by a linear least-squares procedure, matrix E is easily computed as

$$\mathbf{E}(K) = (\mathbf{C}^T \times \mathbf{C})^{-1} \times \mathbf{C}^T \times \mathbf{D} \quad (6)$$

where $\mathbf{C}^T$ is the transpose matrix of C and $(\mathbf{C}^T \times \mathbf{C})^{-1}$ is the inverse matrix of $\mathbf{C}^T \times \mathbf{C}$. Finally, the corresponding $\mathbf{D}_c$ matrix of calculated absorbances (or chemical shifts) is computed together with the associated $\chi^2(K)$, i.e., the minimum value of χ^2 for the set of constants used.

At this point the Gauss-Newton method is applied to calculate the $1 \times q$ vector $\bar{K}$ of the corrections to be applied to the K values:

$$\bar{K} = (\mathbf{Z}^T \times \mathbf{Z})^{-1} \times \mathbf{Z}^T \times (\mathbf{D} - \mathbf{D}_c) \quad (7)$$

where Z is the matrix of derivatives of D with respect to the acidity constants, with the apexes having the usual meaning. The derivatives are calculated by taking into account that E is a function of the acidity constants. To do this, once each constant has been incremented, the new values of E are calculated, and from these the absorbances (or chemical shifts) are calculated.

After the corrections $\bar{K}$ have been applied to the acidity constants, the new value of χ^2 is evaluated and the calculation of the parameters is iterated until the percentage difference of χ^2 between two consecutive cycles is less than a fixed value, up to a maximum fixed number of cycles.

EXPERIMENTAL

Apparatus and reagents

The Cary 219 spectrophotometer used was equipped with a thermostatted cell compartment. The Hewlett-Packard HP-85 personal computer used had 32K memory and was equipped with a ROM MATRIX which allowed the use of the BASIC matrix instructions.

Eriochrome Black T (Erio-T; Merck) was the test substance. Buffer solutions at pH 3, 4, 5, 6, 7, 7.5, 8, 9, 10, 11, 12 and 13, obtained with Carlo Erba Normex buffer solutions, were prepared with Erio-T (2.65×10^{-5} mol dm^{-3}) at a fixed ionic strength of 1 mol dm^{-3} (KCl); all solutions were 2×10^{-4} M in EDTA in order to prevent complexation of Erio-T by traces of metals. The spectra of the solutions were recorded at 25°C in 1-cm quartz cells over the range 350—650 nm; the absorbances were read every 20 nm.

Input/output of the program KACID

The program requires the following features as input: (1) a title for which a file is created containing the input variables, which can then be read as required; (2) an alphanumeric variable, N or U which controls the use of n.m.r. or u.v.-visible data; (3) the number n of experimental points (i.e., the number of pH values examined); (4) the number q of acidic protons in the examined acid; (5) the number m of examined wavelengths (or nuclei); (6) the total molar concentration of the acid; (7) the n values of pH examined; (8) the matrix of absorbances or chemical shifts Y_1 in which each row contains the data at the same wavelength (or nucleus), and each column the data relative to the same pH; and (9) the vector of the pK estimates.

The program gives all the input data as initial output. At each cycle it prints the χ^2 value, the actual values of the optimized constants, the matrix of the spectral parameters $\mathbf{E}(K)$ and the calculation time from the start to that actual moment. At the end of the optimization, the final calculation time is printed together with the following seven features. First is the vector of the equilibrium pK values (partial acidity constants). The second is the variance—covariance matrix $\mathbf{V}_K$, relative to the determination of the equilibrium constants obtained as the scalar product of matrix $(\mathbf{Z}^T \times \mathbf{Z})^{-1}$ by $\sigma^2 = \chi^2/[nm - q - (q + 1)m]$, where $nm - q - (q + 1)m$ is the number of individual measurements minus the number of estimated parameters. The square root of the diagonal element v_{ll} of this matrix gives the errors associated at the lth acidity constant (not at the pK value), while the ratios $[v_{l_1,l_2}/(v_{l_1,l_1} \times v_{l_2,l_2})^{1/2}]^{1/2}$ are the correlation coefficients between the estimates of the l_1th and l_2th dissociation constants, respectively [14, 15]. Other features printed out are the final χ^2 value, the χ^2 value for each individual wavelength (or nucleus), the final matrix E of spectral parameters, the variance—covariance matrix relative to the spectral parameters $\mathbf{V}_s$, obtained as the scalar product of matrix $(\mathbf{D}^T \times \mathbf{D})^{-1}$ by σ^2, and the final matrix $\mathbf{D}_c$.

Simulation of n.m.r. data

The case taken is an acid H_3A with acidity constants $pK_{a1} = 4.18$, $pK_{a2} = 6.01$, $pK_{a3} = 8.97$, having four different protons on A. The chemical shifts (in Hz) with respect to an arbitrary reference are as follows:

	H_1	H_2	H_3	H_4
H_3A	128	150	123	115
H_2A^-	195	164	168	116
HA^{2-}	196	184	174	173
A^{3-}	196	203	191	220

here, H_1 is concerned only with the first deprotonation, H_2 and H_3 are connected with all three deprotonations, and H_4 is connected with the second and third deprotonations. From these values, the chemical shifts of the four protons are calculated over the pH range 2.5—11.5, at 0.5 pH intervals. The

values were rounded to the second decimal place, i.e., an experimental error of about 0.02 was introduced. The calculated values are reported in Fig. 1.

RESULTS AND DISCUSSIONS

The program was tested on the set of simulated n.m.r. data, reported in Fig. 1. First of all, a check was made to see if there was any difference in its convergence capacity when the derivatives were made with respect to the partial or to the cumulative acidity constants. For this purpose, two versions of the program (version I for derivatives with respect to the K_a values and version II for derivatives with respect to the β values) were tested on the same set of data, starting from 27 different initial estimates of the parameters (i.e., all combinations of correct values, values decreased by 10%, and values increased by 10%), for the three partial acidity constants. Such errors were very large on the initial estimates, and so a multiplicative damping factor of 0.5 was introduced in the correction terms.

The difference between differentiation with respect to the K_a values and differentiation with respect to the β values is shown in Fig. 2. The distribution

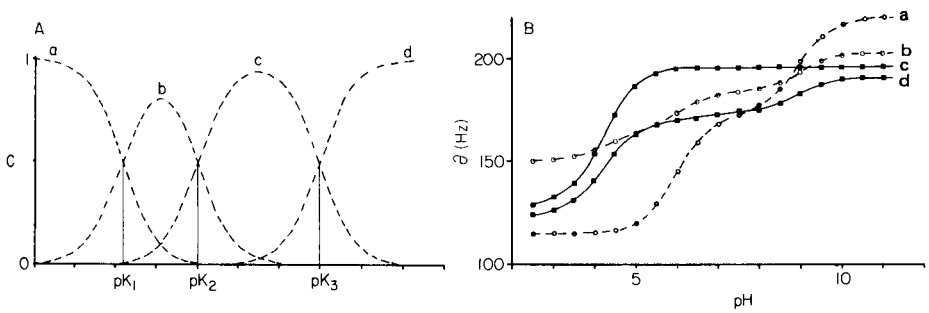

Fig. 1. (A) The distribution functions of an acid, H_3A with $pK_{a1} = 4.18$, $pK_{a2} = 6.01$ and $pK_{a3} = 8.97$: (a) H_3A; (b) H_2A^-; (c) HA^{2-}; (d) A^{3-}. (B) Simulated chemical shifts as a function of pH for the various protons: (a) H4; (b) H2; (c) H1; (d) H3.

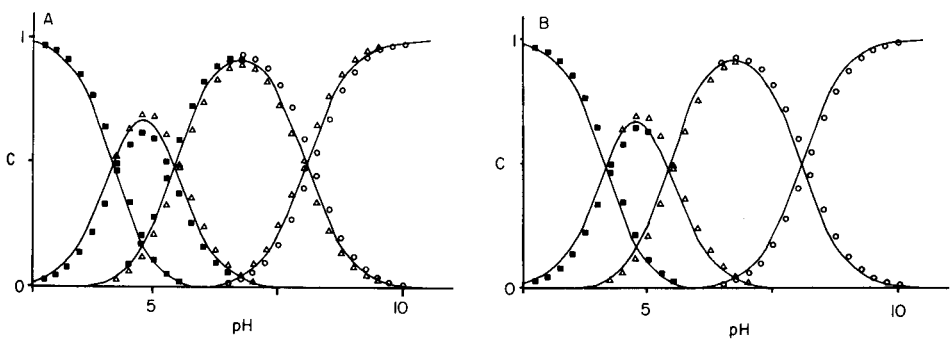

Fig. 2. The distribution functions of the acid H_3A are shown as solid lines. The points indicate where the distribution functions, calculated for an increment of 0.1 unit of each pK in turn (B) or $p\beta$ (A) deviate from the solid lines: (■) pK_{a1} or $p\beta_1$; (△) pK_{a2} or $p\beta_2$; (○) pK_{a3} or $p\beta_3$.

functions calculated with one of the sets of starting parameters, and for an increment of 0.1 units of each constant in turn, are reported. It can be seen that the effect of an increment of pK_{ai} changes the distribution functions of the $(i - 1)$th and ith species around pK_{ai}, while the same increment of $p\beta_i$ changes the distribution functions of the $(i - 1)$th, ith and $(i + 1)$th species in the range beyond $pK_{a(i+1)}$. Therefore, in the former case, the studied pH range can be divided into different ranges, in each of which only the derivatives with respect to only one K_{ai} are clearly different from zero; in the latter case, the range which depends on pK_{ai} is also dependent on $pK_{a(i-1)}$ in the left half, and on $pK_{a(i+1)}$ in the right half. Therefore, only when the derivatives with respect to K_a values are used is a "nearly orthogonal" least-squares design [14] achieved, and this should lead to lower correlation coefficients between parameters and to a better convergence of the iterative procedure.

The results of the calculations with both programs are reported in Table 1 and in Fig. 3. They show that version I always ensures convergence to the correct values, while version II fails to converge in three cases. However, when only one of the initial estimates is wrong, both programs operate in the same way. The correlation coefficients obtained with version I are not significant, whereas very high values are obtained with version II; yet the standard deviations are of the same order of magnitude with both programs. In an orthogonal design, each parameter should converge to the true value by steps which do not depend on the actual values of the other parameters. This is only partly verified when program I is used, the optimization of the one parameter being sometimes greatly affected by the values of the other constants. In fact, when K_{a2} is underestimated, the actual values of K_{a1} and K_{a3} can lead to remarkable overshoots of K_{a2}, whereas when K_{a3} is underestimated, it converged well if K_{a2} is also underestimated; in contrast, when K_{a2} is overestimated, the K_{a3} corrections are too large and also depend on K_{a1}.

TABLE 1

Results of the calculations with programs I and II

Constant	Value found	σ[a]	σ on log value	Correlation coefficient
Results with program I				
K_{a1}	6.6069×10^{-5}	0.0095×10^{-5}	0.0014	$r_{12} = 0.088$
K_{a2}	9.7723×10^{-7}	0.0191×10^{-7}	0.0019	$r_{13} = 0.002$
K_{a3}	1.0715×10^{-9}	0.0020×10^{-9}	0.0019	$r_{23} = 0.360$
Results with program II				
β_1	6.6069×10^{-5}	0.0095×10^{-5}	0.0014	$r_{12} = 0.642$
β_2	6.4565×10^{-11}	0.0160×10^{-11}	0.0025	$r_{13} = 0.456$
β_3	6.9183×10^{-20}	0.0246×10^{-20}	0.0035	$r_{23} = 0.859$

[a]For $\chi^2 = 3 \times 10^{-2}$.

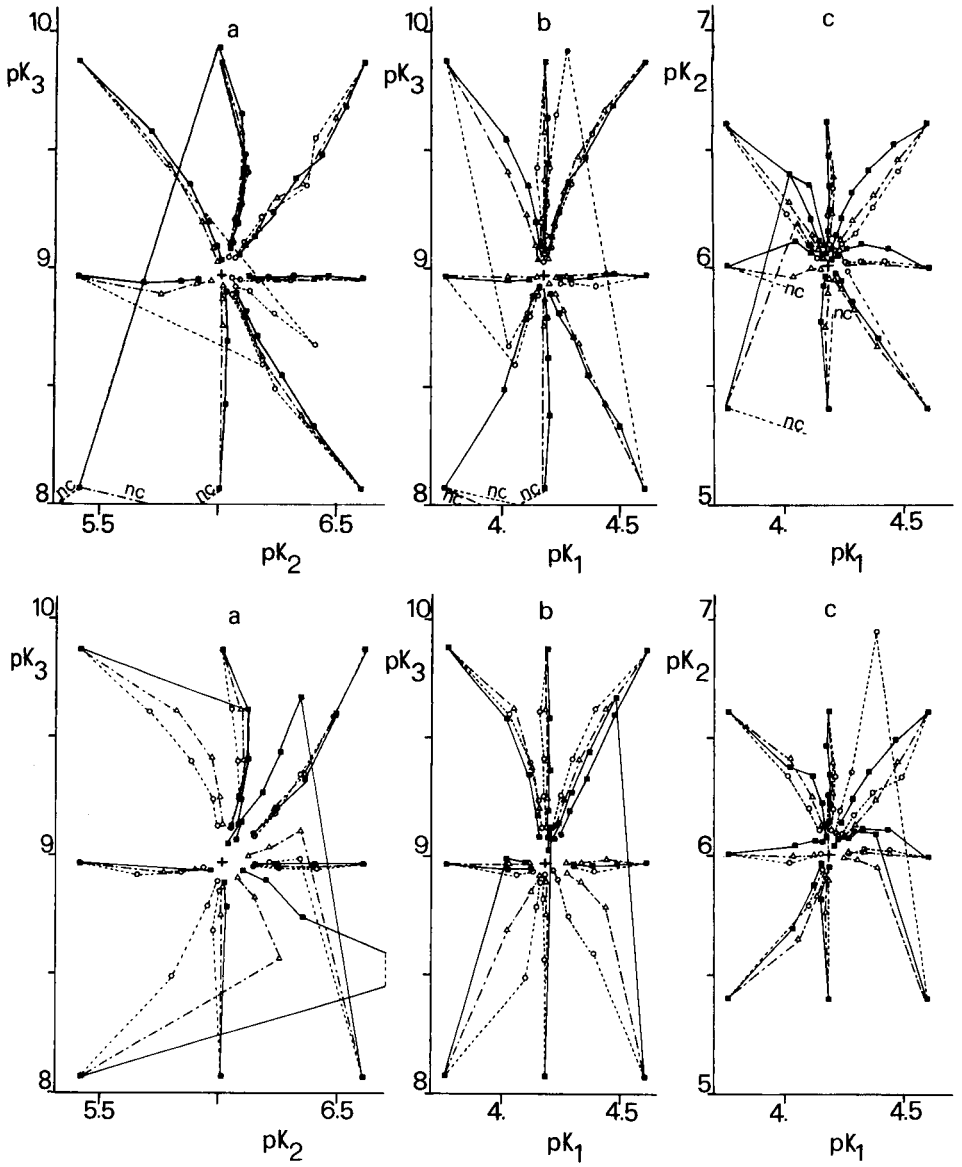

Fig. 3. The pathways of convergence with program I (lower part) and program II (upper part) starting from different estimates of pK_{a_1}, pK_{a_2}, pK_{a_3}. Initial estimates: (△) equal to the true value of the missing constant; (■) greater than the true value; (○) less than the true value.

Such faults in the K_{a2} and K_{a3} optimizations can be understood when the very high errors introduced in the initial estimates are considered; according to their sign, the difference between two consecutive pK_a values can be as much as an order of magnitude; this fact completely ruins the orthogonal

design because of severe overlapping of distribution functions, and therefore the optimization of some parameters becomes difficult.

As far as the use of program II is concerned, a generally slower convergence is found. Three cases of non-convergence are noted, i.e., when (K_{a1}, K_{a2}, K_{a3}), (K_{a2}, K_{a3}) and (K_{a1}, K_{a3}) are underestimated (the estimates of K_{a1} and K_{a2} being equal to the true values in the second and third cases, respectively). The direction of the correction vectors calculated for $\beta_1, \beta_2, \beta_3$ is correct, but the size of $\bar{\beta}_1$ (the correction vector of β_1) reverses the sign of $\bar{K}_{a2}$ and $\bar{K}_{a3}$, leading to non-convergence of the optimization procedure. A similar explanation is valid for the observed overshoots of K_{a3}. As a general rule, it can be said that the interaction between parameters has deleterious effects on convergence when the errors on the initial estimates have the same sign; with program II, errors of opposite sign, however, can given reciprocal compensations which sometimes lead to a convergence better than with program I (some overshoot obtained with program I is completely damped).

On the basis of these findings, and considering that in real cases the errors on the initial estimates are far lower than those introduced in the above study, program I is believed to be more reliable in most real situations. In its final version, a damping factor of 0.25 was introduced in the first four cycles, and of 1 in the following cycles; this ensures a correct mode of convergence even in difficult cases, but there is an increase in computing time.

Finally, the program was tested on a set of spectrophotometric data relative to Erio-T. Some input data are reported in Fig. 4; in Table 2, the calcu-

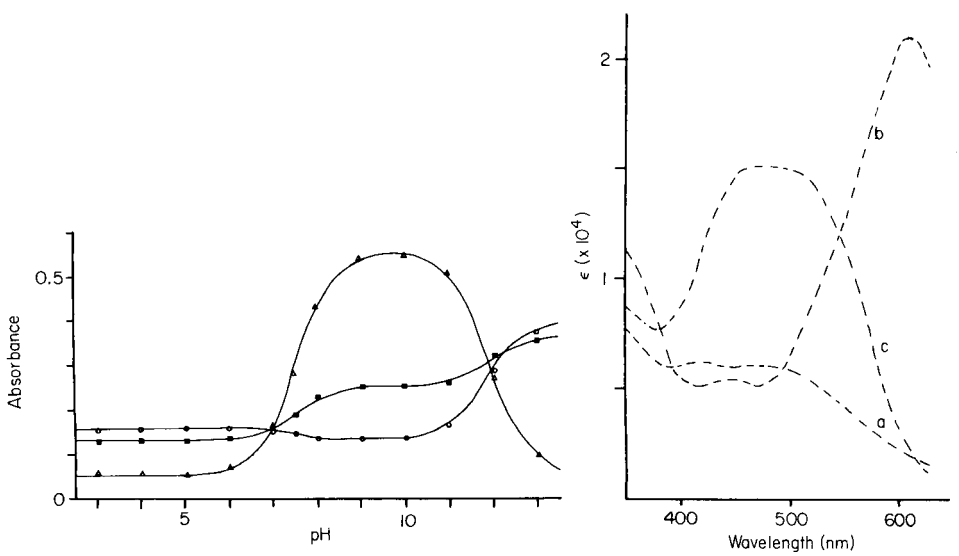

Fig. 4. The absorbances of Erio-T in the twelve test solutions, as a function of pH at different wavelengths: (○) 470 nm; (■) 530 nm; (△) 610 nm. The calculated trends with the optimized parameters are shown as solid lines.

Fig. 5. Calculated spectra of the different forms of Erio-T: (a) H_2A^-; (b) HA^{2-}; (c) A^{3-}.

TABLE 2

Acidity constants for Erio-T

	pK_{a2}	pK_{a3}
Present values	7.57 ± 0.03	11.86 ± 0.04
Earlier values [16, 17]	6.30	11.55

lated acidity constants are reported, and Fig. 5 shows the calculated spectra for the three forms. The acidity constants obtained, as well as the absorptivity values, disagree with those reported in the literature. The spectrum of the H_2A^- species does not show a peak at 520 nm. It seems possible that the older measurements may have been affected by metal impurities which could falsify the final results or that the purities of the Erio-T used were different. Discussion on this point is outside the scope of this paper.

In conclusion, the least-squares program involves separation of the optimization of equilibrium constants from that of spectral parameters and also takes into account the variability of spectral parameters with the acidity constants in the calculation of the derivatives. This approach removes the main divergence factor and generally ensures rapid convergence, thus avoiding the need for more sophisticated approaches, such as the Marquard or Fletcher-Powell algorithms. In this study, the difference between the use of derivatives with respect to K_a or β values has been indicated. This subject requires more careful discussion of its general implication in least-squares programs for the evaluation of stability constants.

The program listing is available from the authors.

REFERENCES

1 E. J. King, Acid-base Equilibria, Pergamon Press, Oxford, 1965.
2 A. Albert and E. P. Serjeant, The Determination of Ionization Constants, 2nd edn., Chapman and Hall, London, 1971.
3 R. F. Cookson, Chem. Rev., 74 (1974) 5.
4 G. Arena, E. Rizzarelli, S. Sammartano and C. Rigano, Talanta, 26 (1979) 1.
5 C. Rigano, M. Grasso and S. Sammartano, Ann. Chim., 74 (1984) 537.
6 A. Loewenstein and J. D. Roberts, J. Am. Chem. Soc., 82 (1960) 2705.
7 U. W. Kesselring and L. Z. Benet, Anal. Chem., 41 (1969) 1535.
8 C. T. Davis and T. A. Geissman, J. Am. Chem. Soc., 76 (1954) 3507.
9 P. Maroni and J. P. Calmon, Bull. Soc. Chim., (1964) 519.
10 T. O. Maier and R. S. Drago, Inorg. Chem., 11 (1972) 1861.
11 G. Carta, G. Crisponi and V. Nurchi, Tetrahedron, 37 (1981) 2115.
12 S. Feldberg, P. Klotz and L. Newman, Inorg. Chem., 11 (1972) 2860.
13 G. Crisponi, P. Deplano, V. Nurchi and E. F. Trogu, Polyhedron, 3 (1984) 1241.
14 O. L. Davies and P. L. Goldsmith, Statistical Methods in Research and Production, Oliver and Boyd, Edinburgh, 1972.
15 N. Draper and H. Smith, Applied Regression Analysis, Wiley, New York, 1966.
16 G. Schwarzenbach and H. Flaschka, Complexometric Titrations, Methuen, London, 1969.
17 G. Schwarzenbach and W. Biedermann, Helv. Chim. Acta, 31 (1948) 678.

Analytica Chimica Acta, 184 (1986) 87—97
Elsevier Science Publishers B.V., Amsterdam — Printed in The Netherlands

AUTOMATION OF THE OPTICAL ALIGNMENT OF A DIODE-LASER SPECTROMETER BY MEANS OF SIMPLEX OPTIMIZATION

H. ABBINK SPAINK and T. T. LUB*

Netherlands Energy Research Foundation (ECN), Westerduinweg 3, P.O. Box 1, 1755 ZG Petten (The Netherlands)

G. KATEMAN

Department of Analytical Chemistry, Faculty of Science, University of Nijmegen, Toernooiveld, 6525 ED Nijmegen (The Netherlands)

H. C. SMIT

Laboratory for Analytical Chemistry, University of Amsterdam, Nieuwe Achtergracht 166, 1018 WV Amsterdam (The Netherlands)

(Received 29th October 1985)

SUMMARY

Optimization of the optical alignment of a tunable diode-laser spectrometer can be automated by using a commercially available Simplex optimization program. This alignment is achieved by displacing a collimation lens placed in front of the laser in three mutually perpendicular directions by motorized positioning equipment. The detector signal, after lock-in amplification, is taken as the optimization criterion. Best parameter settings of the program are discussed on the basis of experimental results. It is demonstrated that the program gives very reliable results in terms of reproducibility of the optimal alignment.

In recent years, many applications of infrared diode lasers in trace gas analysis have been reported [1, 2]. The main advantages of those lasers are high spectral resolution, tunability, high sensitivity, and fast modulation capability. The wavelength of the lasers can be tuned quasi-continuously over a range of 10—100 cm^{-1} by changing the laser temperature and/or current. With these features, diode-laser spectrometry has proved to be valuable for measuring low concentrations (typically at $\leqslant$ppb level [3]) of different molecular species without affecting the sample. A problem associated with these lasers, however, is the optical alignment, which is of great importance for the limits of detection [4]. Although the optical system, once aligned, can remain stable for a long period of time, re-alignment is usually necessary when a sample cell is placed in the optical path or the laser wavelength is changed significantly or another laser is selected. Fine alignment is usually accomplished by adjusting the (XYZ)position of a collimation lens placed in front of the laser. Sometimes other optical components are also involved in the alignment procedure. Even in the relatively simple

case of adjusting only one lens, the alignment can be time-consuming, for the required displacements are typically of the order of several micrometres and are also mutually interdependent. Because of the difficult alignment procedure, diode-laser spectrometers are not very suitable for routine applications and require highly-trained personnel.

In the present paper, it is shown that this problem can be solved by computerizing the system and using a formal simplex optimization procedure for the alignment. The simplex (or polytope [5]) method is frequently used in experimental designs for optimizing N parameters simultaneously [6, 7]. The method has not been applied to laser alignment previously.

THEORY

The optimization procedure described here uses the CHEOPS program [8, 9], which offers many options. The most important of these options are discussed here briefly. The basic principles of the simplex method and its commonest modifications (e.g., Modified Simplex and Super-modified Simplex) have been described fully elsewhere [5—8] and an extensive bibliography is available [7].

Compared to the basic simplex method, in which the worst vertex is reflected in the (hyper)plane formed by the remaining $(N - 1)$ vertices, CHEOPS offers the following options which can be selected indepently of each other [8]. Application of the $(N + 1)$ rule provides for remeasurement of the response if a vertex remains optimal after $(N + 1)$ successive measurements. Weighted centroids can be used for reflection; responses are used as weighting factors for calculation of the centroid so that the simplex will bend towards the direction of the vertices with the highest responses. From the three responses at the original vertex, the reflected vertex and the centroid, the position of an optimal vertex on the line connecting these points can be estimated by using an appropriate fitting function (Fig. 1). The line connecting the vertices can be described mathematically by $X = X_1 + Y(X_c - X_1)$, where X_1 is the worst vertex and X_c the centroid. For $Y = 2$,

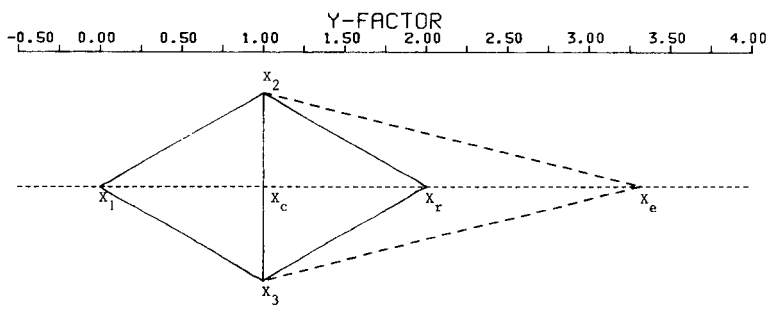

Fig. 1. An example of simplex expansion. Special situations arise for $Y = 0$ (no progress) and $Y = 1$ (degeneracy).

this equation defines the position of the reflected vertex. In the program, the user can select whether the response at X_c is measured or estimated as a weighted average of the $(N-1)$ remaining responses and whether the fitting function should be Gaussian or a second-order polynomial. From the maximum of the fitting function (at $Y = Y_{opt}$), the position of the "optimal vertex" X_e is calculated. If $X_e > X_r$, then X_e is taken as the new vertex; otherwise X_e is rejected and X_r is used. A common problem associated with modified simplex methods is the danger of degeneracy (i.e., loss of one or more dimensions), which can happen quite rapidly when $Y \approx 1$. When $Y \approx 0$, the simplex will make little progress. The problem can be overcome by defining safety intervals around $Y = 0$ and $Y = 1$, e.g., ± 0.25 around 0 and 1 and outer intervals $Y < -2$ and $Y > 4$. The magnitude of the intervals can be defined by the user. When a calculated Y value lies inside a safety interval, the value is reset to the closest boundary value. Despite the use of safety corrections, the simplex can still degenerate during the optimization. In order to estimate the degree of degeneracy, the "symmetry" of the simplex can be defined as the ratio between the radius of a (hyper)sphere that has the same volume as the simplex and the radius of a (hyper)sphere that passes through all vertices of the simplex. The symmetry is scaled between 0 and 1 by taking appropriate multiplication factors (depending on the number of parameters). The symmetry of a perfectly regular simplex is 1, the symmetry of a completely degenerated simplex is 0. Further details on this aspect are easily available [8]. The symmetry can be used as an alternative to the safety margins. After each calculation of Y_{opt}, the symmetry of the new simplex is calculated. When the symmetry threatens to drop below some (user-defined) value, Y_{opt} is adjusted to a value that meets the symmetry condition. In this case, the simplex method is referred to as a "symmetry-controlled simplex".

EXPERIMENTAL

Optics

A complete diode-laser spectrometric system (Spectra-Physics LS-3) is used at ECN (see Fig. 1 of an earlier paper [10]). The aim of the present experiments was to establish the best parameter settings with the simplex program; thus to simplify matters, neither the White cell nor the monochromator was used. All the optimal parameters, with the exception of the initial step sizes, were expected to remain valid when the simplified system, shown in Fig. 2, was extended with other optical components. The initial step sizes would always need re-establishment after any major change in the optical system.

All experiments were done with a narrow-band lead-salt laser (Laser Analytics) which emits in the region 800—910 cm^{-1}, the power being several microwatts. The laser was operated in a single mode, just above threshold. The signal was modulated by chopping the laser current. A low-noise, fast HgCdTe detector (Santa Barbara Research) was used to detect the modulated infrared radiation.

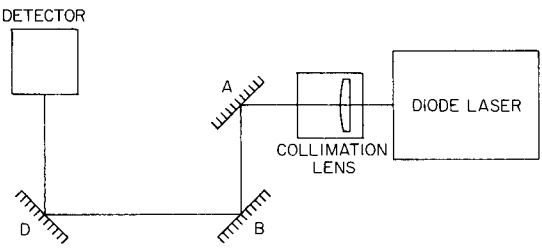

Fig. 2. Simplified optical set-up used for the optimization experiments. Because the laser was mounted on the LS-3 spectrometer, three mirrors (A, B and D) were required to project the laser beam on the detector. Mirrors A and B were retained as in the original equipment at the collimating lens. One mirror in the sample compartment was removed and placed outside the LS-3 assembly (mirror D). The detector was removed and placed in front of mirror D, outside the LS-3.

Electronics

A schematic diagram of the computerized equipment is shown in Fig. 3. Current control and temperature control were done with a laser control module (LCM) and a cryogenic temperature stabilizer (CTS; both from Spectra-Physics). The detector signal was amplified first with a low-noise a.c. preamplifier and then with a lock-in amplifier (Spectra-Physics). The LCM, CTS and lock-in amplifier were modified to permit external computer control of most functions. To control the temperature, current and sweep rate, three stable 16-bit digital/analog converters (DAC; Analogic MP-1916-TC) were used in custom-built interfaces. To set the current modulation amplitude and frequency, 12-bit and 8-bit DAC's, respectively, were used. The interface units can be addressed by a computer via a RS232 serial line. The d.c. signal from the lock-in amplifier was digitized with a standard 12-bit ADC. The maximum sampling rate is 50 Hz. This slow A/D converter will later be replaced by one that allows sampling rates up to 100 kHz. To control the lens position, the three standard micrometer screws of the *XYZ* table were replaced by d.c.-motor actuators (Ardel Motor Mike types 10A-3X for the focus adjustment and 5A-3X for the two other directions). The lens position was read with an accuracy of 1 μm by three Sony Magnescales (type SR-721). A special motor drive unit used a feedback control loop to position the motors at a required value within the accuracy of the Sony Magnescales. The unit was controlled by a computer via a RS232 serial line.

The adjustment screw of the D mirror in the White cell and the steering mechanism of the monochromator were motorized with the aid of stepper motors (Neckar SMG-314 with reduction gearboxes giving 3000 and 750 steps/revolution, respectively). An intelligent interface (Robotic Synergy) was used to control both motors. However, these motors are not included in the alignment procedure described below for two reasons. First, the control of the D mirror was unsatisfactory; because of tolerances and friction forces, the reproducibility at high pathlengths was poor in relation to the sensitivity

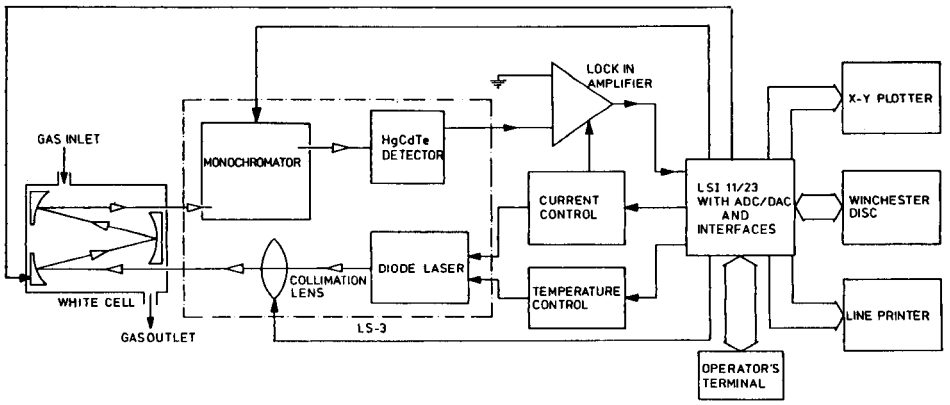

Fig. 3. Schematic diagram of the computerized LS-3 spectrometer.

of the signal to small displacements. Secondly, although the monochromator grating was successfully included in the alignment procedure for some time, it was found recently [11] that it is better to operate the laser in a single mode and eliminate a monochromator from the optical system; accordingly, the monochromator was omitted from the optimization procedure. The computer used was a LSI 11/23 with a floating point processor.

Software

The operating system of the computer is RSX11M, which allows multi-user and multitask operation. The main program developed takes care of all communication between the operator and the laser system. The alignment procedure is also started by this program. The optimization program is largely based on the symmetry-controlled simplex program [8, 9]; the version used is written in FORTRAN-IV. Some modifications were made to adapt it to the experimental environment.

RESULTS AND DISCUSSION

In any optimization problem, the criterion to be used is vital. In the case of diode-laser spectrometry, an obvious criterion would be the signal-to-noise ratio. Direct determination of the *S/N* ratio, however, is impractical in the present set-up, because measurement of the most important noise sources, optical fringing and optical feedback [4], takes too much time. To do this, the laser wavelength must be swept through a sufficiently wide spectral region (compared to the width of an absorption line). The sweep rate is limited by the slow A/D converter; when sampling at 50 Hz the highest frequency occurring in the signal may not exceed 25 Hz (Shannon's theorem) and so the laser wavelength can be swept only slowly. This problem will be solved by using a faster ADC (see above) but here the magnitude of the d.c.

signal from the lock-in amplifier was chosen as the criterion. Fortunately, during many experiments, the maximum d.c. signal appeared to coincide with a minimum fringe amplitude. The coincidence may be explained by noting that fringes and feedback are usually caused by light scattering on optical components; the less scattering (and thus fringes and feedback), the more light will reach the detector.

The initial step size of each parameter must also be defined because this aspect can affect the speed of convergence of the optimization. Appropriate values for the step sizes were chosen as follows: after the optical system had been optimized, a cross-section of the response surface in each direction was made. From these figures, the step sizes were measured as the values for which the response drops to about 90% of the maximum value. Results for the simplified optical set-up (Fig. 2) are shown in Fig. 4; the cross-sections have

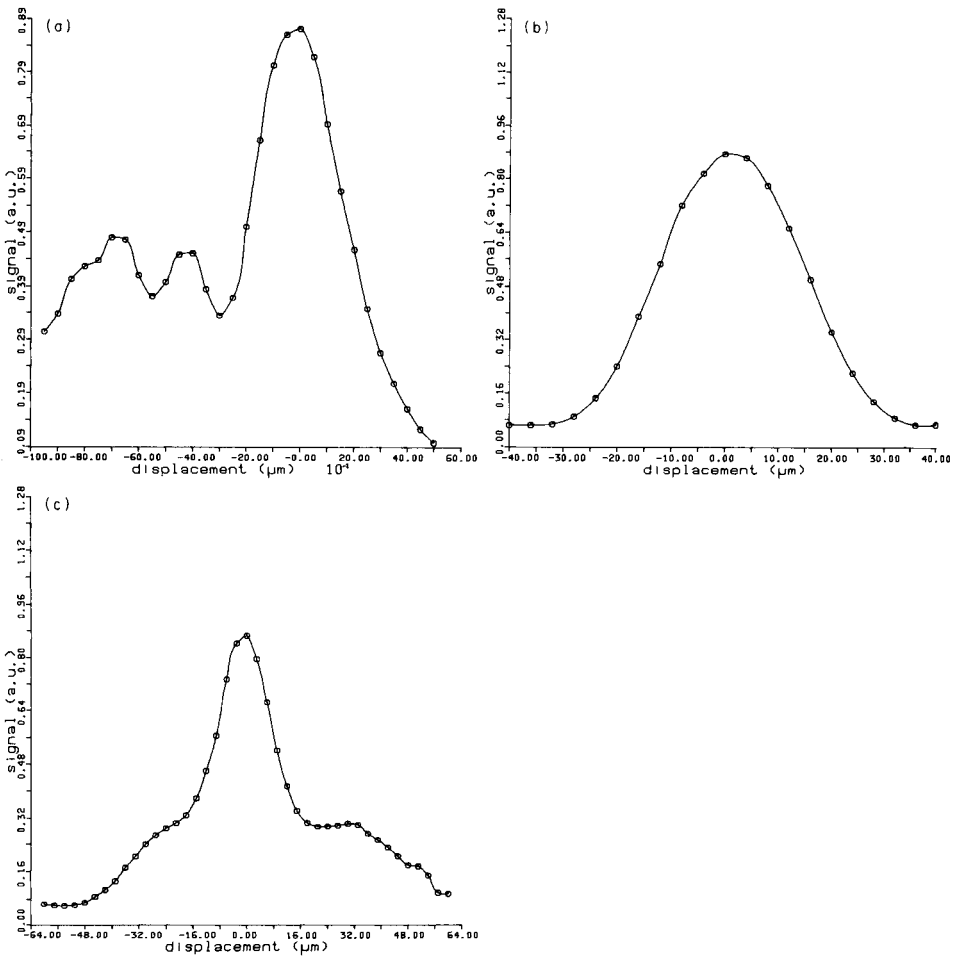

Fig. 4. Intensity distribution of the diode-laser beam in one direction: (a) focus; (b) horizontal; (c) vertical.

approximately Gaussian shapes near the optimum. The step sizes thus found for the focal, horizontal and vertical adjustment were 80, 7 and 4 μm, respectively. Obviously, the values will depend on the optical system, and measurements must be repeated if the system is modified significantly (e.g., inclusion of a White cell).

The program package includes many options for modifying the procedure. The effects of such modifications were studied by changing them one at a time in a sample optimization situation, i.e., the simplex was started from the same position relative to the optimum every time. The starting point was selected as follows: after the position of the optimum had been located by repeating the simplex program (with default parameters) until the result became stable, the lens was displaced over a distance of 100 μm in the focal direction, −10 μm in the horizontal direction and 10 μm in the vertical direction. This point was taken as the starting point for every run of the program. In later measurements, however, the position of the optimum relative to the starting point became unstable (see Tables 1 and 2). Therefore, in an alternative approach, the lens was displaced over a constant distance relative to the optimum found in the previous optimization cycle.

The progress of the simplex was followed by recording the response, the displacement of the motors and the symmetry after each measurement. Examples are shown in Fig. 5. The results are summarized in Tables 1–3. Responses are scaled between 0 and 1. When an experiment took more than 100 measurements, it was terminated manually; this is indicated by ∞ in the

TABLE 1

Effects of different parameter settings in the simplex program[a]

No.	Stop crit.[b]	S[c]	V_c[d]	Refl. type[e]	Final position[f]	V_{opt}[g]	N_{tot}[h]	$N_{0.97}$[i]
1	0.003	0.4	E	W	−115, 5, −9	0.821	34	—
2	0.002	0.4	E	W	−129, 9, −10	0.884	69	28
3	0.002	0.1	E	W	−122, 9, −10	0.884	55	20
4	0.002	0.1	E	W	−115, 8, −10	0.882	56	18
5	0.002	0.1	M	W	−117, 7, −10	0.882	57	36
6	0.002	0.1	E	W	−121, 7, −10	0.878	39	14
7	0.002	0.1	E	N	−116, 7, −11	0.877	∞	—
8	0.002	0.1	E	W	−140, 4, −10	0.877	26	15

[a]The parameter changed with respect to the previous measurement is underlined. The step sizes in the three directions (focus, horizontal, vertical) were 100, 10 and 5 μm, respectively. [b]Stop criterion; responses are scaled to values between 0 and 1. [c]Safety interval (see text). [d]Response at centroid; E(stimated) or M(easured). [e]Type of reflection: W(eighted) or N(ormal). [f]Position of the optimum in μm; initially the optimum was situated at (focus, horizontal, vertical) = (−100, 10, −10). [g](Normalized) response at optimum; initially, a value of 0.882 was found. [h]Total number of measurements. [i]Number of measurements required to reach 97% of the optimal response; if this value was reached after a restart, the number is placed in parentheses.

TABLE 2

Effect of safety interval on speed of optimization[a]

No.	Safety	Final position	V_{opt}	N_{tot}	$N_{0.97}$
1	0.05	−104, 5, −10	0.800	83	18
2	0.1	−100, 4, −10	0.796	59	22
3	0.2	−110, 4, −12	0.798	44	(35)
4	0.3	−94, 4, −11	0.796	60	14
5	0.4	−103, 3, −13	0.797	62	15
6	0.15	−100, 4, −13	0.801	53	(37)
7	0.2	−118, 4, −13	0.796	75	(41)
8	0.1	−115, 3, −12	0.799	43	(31)
9	0.1	−101, 10, −11	0.800	74	(25)
10	0.25	−124, 10, −9	0.795	57	(33)
11	0.4	−61, 10, −9	0.802	27	6

[a]In these measurements, step sizes were 80, 7 and 4 μm. Meanings are as given in Table 1. Two series can be distinguished: 1—8 and 9—11. During the first series, the lens was positioned at (0, 0, 0) as governed by the motor controller at the beginning of each measurement; because of errors in the positioning equipment, the position of the optimum could gradually deviate from (−100, 10, −10). In the second series, the lens was displaced to a position (100, −10, 10) relative to the optimum that was found during the previous run of the program; this point was taken as the new origin. Therefore deviations in the latter case are smaller.

tables. As seen in Fig. 5, the optimization process can be divided in two stages: an initial stage where the response increases rapidly and a further stage where the simplex is near the optimum and the response becomes nearly constant. To express the efficiency of a simplex in both stages, two numbers are given in Tables 1—3: the number of measurements ($N_{0.97}$) required to reach a point where the response is at least 97% of the optimal response, and the total number of measurements (N_{tot}).

With regard to the stop criterion, the simplex is terminated if the deviation of the responses from the average response is less than a certain user-defined value. If this value is too large, the simplex could stop at any point where the slope of the response surface is small; if it is too small, the simplex will never stop because of noise. A suitable value for the stop criterion was 0.002, which was of the same order as the standard deviation of the noise.

The type of reflection was important. In the case of normal reflection, the simplex approached the optimum too slowly, and weighted reflection is preferred. When the response at the point of reflection (centroid) was measured, fewer calculations were required to reach the optimum. However, the total number of measurements remained approximately the same and, because this mainly determines the optimization time, the response can equally well be estimated.

As discussed in the above theoretical part, some safety intervals around $Y = 0$ and $Y = 1$ must be defined in order to prevent the simplex from

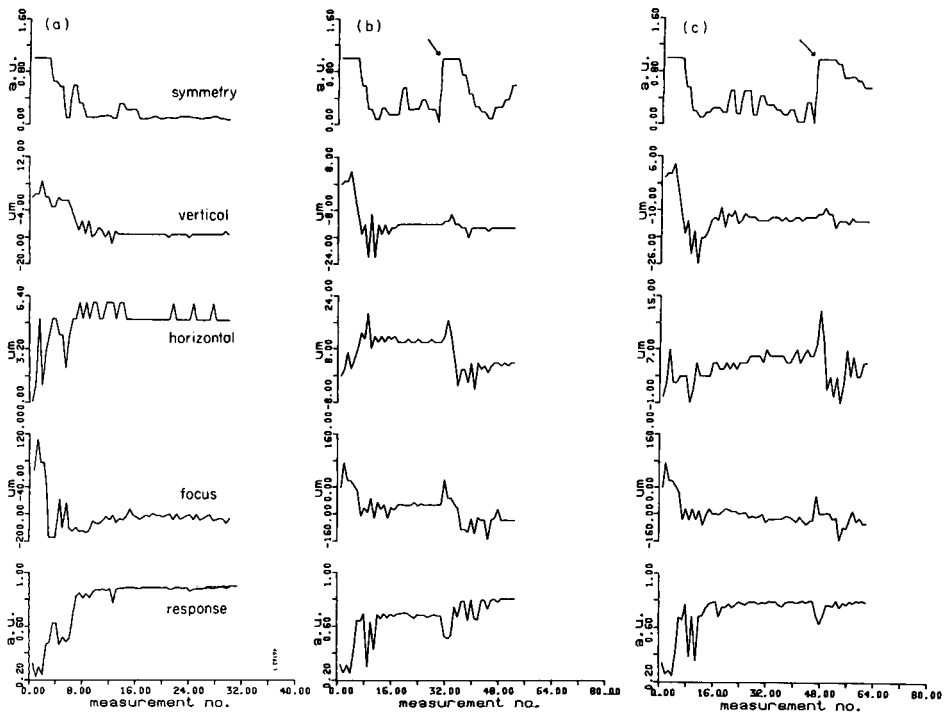

Fig. 5. Progress of different simplexes. (a) With symmetry control; the lens movement dies out, especially in the horizontal and vertical direction. (b) With safety control (S = 0.1); the simplex again contracts too quickly and the arrows indicate restarts. (c) With a higher safety value (0.4); the lens movement now dies out less rapidly.

TABLE 3

Effect of symmetry control on simplex performance

No.	Series[a]	Final position	V_{oot}	N_{tot}	$N_{0.97}$
1	I, 8	−131, 5, −11	0.882	60	19
2	I, 8	−122, 6, −10	0.882	72	(42)
3	II, 8	−96, 3, −13	0.800	27	16
4	II, 8	−97, 11, −9	0.800	49	13
5	II, 11			∞	—

[a]The measurements for studying the effect of symmetry control were part of the measurements given in Tables 1 and 2. The first number refers to the table, the second to the measurement that preceded the symmetry control measurement. Measurement 4 of this table was part of the second series in Table 2. In all cases, the minimum symmetry was set at 0.1.

becoming immobile or degenerating. The safety correction is used to define both intervals. When the safety correction has a value S, the intervals are defined by $[-S, S]$ and $[1 - S, 1 + S]$, respectively. If the calculated value of Y_{opt} lies within a safety interval, Y_{opt} is reset to the closest boundary value. Table 2 shows the effect of the safety value on the efficiency of the simplex. For safety values of $\leqslant 0.2$, the simplex tends to contract too rapidly. In this case, step sizes drop to levels of the order of or below the minimum step size of the motors (1 μm) and the lens no longer moves. This is shown in Fig. 5(b). Because the program considers the lens position as a continuous variable, a strong discrepancy arises between the mathematical model and the physical reality. This produces one of the following situations: (1) if the noise is of the order of the stop criterion, the simplex proceeds indefinitely (it will eventually be stopped by repetitive application of the $N + 1$ rule); (2) if the noise is less than the stop criterion the simplex will stop eventually, though this may not be at the optimum. Obviously both situations are undesirable. Rapid contraction can be counteracted by increasing the value of S. Good results are found for a value of approximately 0.3. Figure 5(c) shows the progress of an optimization with $S = 0.4$.

The use of symmetry control instead of safety correction did not give any improvement. Measurements with a symmetry-controlled simplex gave rather different results for different runs (Table 3). The cause of this irregular behaviour is quite similar to the case of safety corrections with $S < 0.2$: the simplex may contract too rapidly. This is demonstrated in Fig. 5(a). In principle, the symmetry is unrelated to the actual size of the simplex, though it imposes a limit on the speed of contraction (or expansion), but this is merely a side-effect. The safety interval, however, is directly related to the degree of contraction of the simplex. Further, safety correction is less complicated than symmetry correction and is therefore preferred.

Despite all precautions, the symmetry has generally dropped to a low value when the simplex arrives at a point near the optimum (see Fig. 5), so that it no longer searches very efficiently and many measurements may be needed before the simplex finds the optimum. A good solution to this problem is to introduce restart conditions; when the symmetry or the volume of the simplex drops below a certain level, the simplex is restarted from the vertex with the best response. Some of the results presented in Tables 1 and 2 could be obtained only after such a restart. In these cases the $N_{0.97}$ value is placed between brackets.

As can be seen from Tables 1—3, the position found for the optimum is quite reproducible, so that one can be confident that this really is the optimum. This is one of the advantages of automatic alignment; with manual alignment, there is often doubt about the quality of the alignment, for it is difficult to visualize the response surface, which in the present case is defined in 4-dimensional space. The problem worsens as when the number of parameters increases.

In these experiments, the optimization procedure was always started from approximately the same position relative to the optimum. However, when

the automated laser system was actually used for measurements, the method seemed to work equally well for different initial positions.

The total time required for an optimization sequence depends on the speed of the motors and thus on the number of measurements. A sequence of 50 measurements typically takes about 10 min. In daily practice, when the misalignment is less severe than in the situations discussed above, the optimization time is generally less than 5 min. The procedure could be made faster in two ways. In the present system, the d.c. motors can be positioned only sequentially, and simultaneous positioning would be faster. Furthermore, the simplex spends a relatively long time on finding the optimum after it has reached 97% of its final value (which typically takes 15—20 measurements). One reason is that the stop criterion is comparable to the noise amplitude, so that the simplex is deceived by noise. However, the obvious solution to this problem, increasing the stop criterion, increases the chance that the simplex will stop too early (at a point where the slope of the response surface is small) to an unacceptable level. An example is shown in Table 1 for a stop criterion of 0.003. The second reason is that, to find the optimum, step sizes are contracted to a level where they are comparable to the minimum possible step sizes and round-off errors become very large. This quantization of noise produces increasing mismatch between the mathematical model and the physical reality.

In principle, the same technique could be applied to alignment problems with other types of lasers.

The authors are much indebted to Mr. P. J. Kaandorp who carefully developed all interface units. The authors also thank Mr. P. C. C. de Boer for his assistance in the development of the computer system, Mr. C. Lautenbag for developing a stepper motor drive and Mr. P. F. A. van der Wiel for supplying the Simplex program. Mr. R. P. Otjes is acknowledged for testing the automated system in real measurement situations.

REFERENCES

1 D. R. Hastie, G. I. Mackay, T. Iguchi, B. A. Ridley and H. I. Schiff, Environ. Sci. Technol., 17 (1983) 352A.
2 D. T. Cassidy and J. Reid, Appl. Opt., 21 (1982) 2527.
3 D. T. Cassidy and J. Reid, Appl. Opt., 21 (1982) 1185.
4 J. Reid, M. El-Sherbiny, B. K. Garside and E. A. Ballik, Appl. Opt., 19 (1982) 3349.
5 P. E. Gill, W. Murray and M. H. Wright, Practical Optimization, Academic Press, London, 1981.
6 D. L. Massart, A. Dijkstra and L. Kaufman, Evaluation and Optimization of Laboratory Methods and Analytical Procedures, Elsevier, Amsterdam, 1979.
7 S. N. Deming and S. L. Morgan, Anal. Chim. Acta, 150 (1983) 183.
8 P. F. A. van der Wiel, R. Maassen and G. Kateman, Anal. Chim. Acta, 153 (1983) 83.
9 P. F. A. van der Wiel, G. Kateman and B. G. M. Vandeginste, CHEOPS, Elsevier Scientific Software, Amsterdam, 1984.
10 H. Abbink Spaink, T. T. Lub, R. P. Otjes and H. C. Smit, Anal. Chim. Acta, 183 (1986) 000.
11 J. Reid, D. R. Hastie and G. I. Mackay, personal communication.

Analytica Chimica Acta, 184 (1986) 99—106
Elsevier Science Publishers B.V., Amsterdam — Printed in The Netherlands

DETERMINATION OF VOLATILE POLYNUCLEAR AROMATIC HYDROCARBONS IN AIR FROM PARTICULATE PROFILES BY MEANS OF PARTIAL LEAST-SQUARES REGRESSION

J. J. GETHER
Norsoft, Gjerdrumsvei 10b, 0486 Oslo 4 (Norway)
K. E. THRANE*
Norwegian Institute for Air Research, P.O. Box 130 N-2001 Lillestrøm (Norway)
(Received 9th December 1985)

SUMMARY

The possibility of estimating the total (particulate and gaseous) concentrations of volatile polynuclear aromatic hydrocarbons (PAH's) in air on the basis of measured concentrations of PAH's in particles by means of partial least-squares regression (PLS), is discussed. The results show that the estimation can be good for samples exposed to the same source and collected under similar weather conditions.

Ambient air concentrations of polynuclear aromatic hydrocarbons (PAH's) have been reported for many years. In most studies, the pollutants have been collected as particulate matter on glass-fibre filters by high-volume samplers. Significant losses have been shown to occur by this sampling technique, especially for compounds with less than five rings in the molecule [1]. These compounds have high vapor pressures and will be present in both the particulate and gaseous phases at ambient temperatures, but it is thought that most of the losses are due to evaporation from the glass-fibre filter during sampling. The variation in vapor pressure of the different compounds causes selective losses. The degree of loss depends on sampling conditions such as ambient temperature and flow rate, as well as on sample composition, concentrations and properties of the air pollutants. As an example, the relationship between ambient temperature and collection efficiency of a glass fibre filter is illustrated in Fig. 1, which shows that the concentration of volatile PAH's collected on a filter is not representative of the total amount in the ambient air, as has already been pointed out by several authors [1—4]. The evaporation from the filter is influenced by the nature and the amount of the particulate material present. Of course, the PAH compounds may also be lost by reaction with other constituents in the atmosphere and on the filter, in the subsequent isolation and work-up, or in the measurement procedure itself [5].

There are two main reasons for seeking better estimates of the volatile

0003-2670/86/$03.50

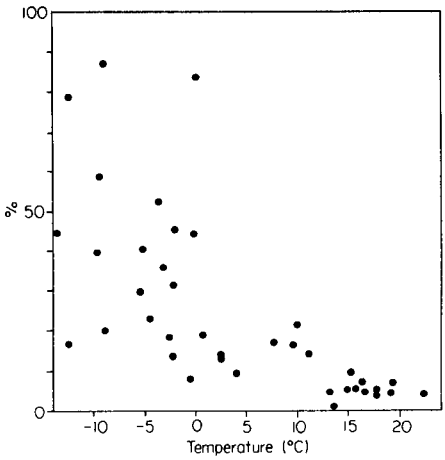

Fig. 1. Relationship between the ambient average temperature during sampling and the amount of particulate fluoranthene as a percentage of the total ambient air concentrations. All samples were collected at the same station by high-volume samplers as described by Thrane et al. [5].

PAH's in air. First, these compounds carry information about the processes leading to their formation and distribution in the atmosphere. Information about their presence enables sources to be better characterized and distinguished [6]. Secondly, some of these compounds or their reaction products or metabolites may be harmful [7], and therefore knowledge of their occurrence is important in assessing possible environmental impact.

Many approaches have been examined in order to estimate the concentrations of the volatile PAH's on the basis of the amount in the particulate phase collected on the filter. Yamasaki et al. [2] indicated that the ratio between the vapor-phase PAH's and the PAH's in the particles, could be described by means of a Langmuir equation. Keller and Bidleman [3] suggested that the vapor pressure of the compounds for the subcooled liquid at 25°C could be used to determine this ratio accurately. This paper presents some results from a study in which partial least-squares regression was applied to a set of PAH data in order to predict the concentrations of the volatile compounds from the profiles in the particulate phase.

MULTIVARIATE DATA ANALYSIS AND PREDICTION

Multicomponent chemical analysis is valuable because one gets to know how each component varies with respect to all others through sets of samples. The interpretation of all this information has only started to become practical with the introduction of computerized data processing. The partial least-squares (PLS) linear regression technique was developed by H. Wold [8]. In multivariate calibration, it can be used to predict one set of properties from

another measured set, by using a learning set of samples for calibration. From the monitoring results for both particulate and volatile PAH's in samples of air, it becomes possible to estimate how accurately the total concentrations of the volatile PAH components can be predicted from measurements of particulate PAH's only. The accuracy of prediction indicates to what extent the two sets of analytical results carry the same information.

A basic notion is that of classes, or groups of samples that are similar in some sense. In supervised learning, a particular set of samples constituting a class may be made up of samples from a particular site, taken under particular conditions of wind and temperature, etc. A class may be thought of as a cloud of points in a q-dimensional space. With q equal to the number of components (variables) measured in each sample, the sample may be represented as a point. A class (cloud) is extended in various directions in this q-space, corresponding to variation in the measured components. Chemometric programs essentially evaluate the directions and extent of variation along each direction for each class, and assign new samples to different classes. Samples that do not fit in any existing class are designated as outliers. The directions of extension are regarded as factors, and together with the extent of variation along each axis, describe a class quite simply and give essential information on class properties.

In 1976 S. Wold [9] introduced the concept of disjoint classes, which means that in a large collection of samples which belong to several classes, each class is treated separately. This is a great advantage because the procedures for data processing become much more robust. The same concept was introduced independently by Bezdek et al. [10] in the Fuzzy c-Varieties clustering algorithms.

Given the concept of a class as a set of points (samples) in a q-dimensional space, the same class can be expressed in another p-dimensional space based on some p other variables measured in the same samples. The first group could be the particulate and the second the total (particulate and gaseous) concentrations of volatile PAH's. If both sets fully describe the class, then rotating and scaling one set of variables would make the two representations of the class coincide. The relationship would then express one set of variables in terms of the other. If the class and this relationship are established by means of a learning set, then it is possible to calculate (or predict) the p values of another set of samples for which the q variables are known. The p values can be the total concentrations of volatile PAH's and the q values the particulate measurements. This means that the amount of total PAH's can be predicted, provided that the learning set and the particulate measurements are available. In real measurements, the two sets of variables only partly measure the same properties, and accentuate particular features of the class. Moreover, the errors present will contribute noise. The overall effect is that a perfect overlap of the two representations of the class is not attainable; there is a residual variance present. This residual variance is a measure of how well one set of variables can be predicted by the other, i.e., the extent to which

they carry the same information. The PLS method was developed so that the variables which most efficiently characterize both representations of the class are emphasized. A full description of the mathematical and computational details is available [11].

In the present work, the program used was the UNSCRAMBLER package developed by Martens and his colleagues at the Norwegian Food Research Institute [12]. This general package is still under development; at present, it can be used to assess the magnitude of the residual variances. In the UNSCRAMBLER program, two subsets of data are used. The learning set consists of the measured concentrations of particulate PAH's (with concentrations of $1-q$) and volatile PAH's (with concentrations of $1-p$) in selected air samples (samples $1, i, \ldots n$). Another selection of air samples ($1, j, \ldots, m$) is then used for testing the prediction of the amount of total PAH's on the basis of the amount in the particles. In the present version of the UNSCRAMBLER program, the residual variance remaining after the prediction is reported.

As more factors are introduced in the model of the underlying physical system, the remaining residuals may be indicated as in Table 1. This example shows the results from a run with 30 samples, with 17 predicting variables (the particulate PAH's) and six variables to be predicted (the volatile PAH's) (see Table 2). Cross-validation is used. The model obtained from the learning set is used to predict the total concentrations of the same volatile PAH in another six samples. The samples were all from the same sampling station and were collected during spring, summer and fall without regard to the variation of the main wind direction. Further description of samples and variables is given below.

The second column in Table 1 shows how the residual variance in the particulate PAH's is reduced as new factors are introduced. The residuals remaining after 4—7 factors are typically about 5% of the initial values, and probably represent random errors in the sampling and chromatographic procedures. The third column shows the corresponding residual variance in the volatile PAH's. In the present case, about 25% of the original residuals re-

TABLE 1

Residual variance of the particulate PAH (*RV1*), the volatile PAH (*RV2*) and the residuals (*R*) when volatile PAH are expressed in terms of the model (*F* is the factor number)

F	*RV1*	*RV2*	*R*
1	1.504	1.204	23.07
2	0.661	0.761	23.95
3	0.514	0.630	20.38
4	0.350	0.586	20.15
5	0.189	0.546	24.37
6	0.138	0.414	33.78
7	0.086	0.339	34.24

TABLE 2

PAH compounds included in the PLS linear regression

Particulate		Particulate		Volatile	
Index	Compound	Index	Compound	Index	Compound
1050	Acenaphthene	1160	Benz(b)fluorene	1010	Naphthalene
1060	Fluorene	1170	Benz(a)anthracene	1040	Biphenyl
1080	Phenanthrene	1210	Benz(e)pyrene	1050	Acenaphthene
1090	Anthracene	1220	Benz(a)pyrene	1060	Fluorene
1110	2-Methylanthracene	1230	Perylene	1080	Phenanthrene
1120	1-Methylphenanthrene	1240	Indeno(1,2,3-cd)pyrene	1090	Anthracene
1130	Fluoranthene	1260	Benz(ghi)perylene		
1140	Pyrene	1280	Coronene		
1150	Benz(a)fluorene				

mains, but 10—15% is more typical. The fourth column gives the residuals when the program attempts to express the volatile PAH's in terms of the model for the particulate PAH's. The prediction accounts for about 16% of the initial variation, and is concerned with factor 3 mostly. As further factors are introduced, the residuals start to increase, showing that these factors have no predictive value, i.e., they express information that is not common to the two sets of measurements.

AIR POLLUTION DATA

The original data, on which this work is based, were collected over a period of 15 months in 1980—1981 in Sundsvall, Sweden, in order to assess the influence of a nearby aluminum plant on the PAH contamination of the ambient air [13]. The PAH's were collected by high-volume sampling. Glass fibre filters were used to collect the particles while the gaseous portions of the volatile compounds were trapped by plugs of polyurethane foam. Individual PAH components were subsequently quantified by means of high-resolution glass-capillary gas chromatography, integration of chromatographic peaks, and conversion to chemical concentrations by means of standard calibration techniques [5]. Ambient temperature, wind direction and air stability were recorded with each sample, as well as the air concentrations of fluoride which is emitted from aluminum plants. During spring, summer and fall, separate day and night samples were collected, while 24-h sampling was done during the winter months.

Data from the study in Sundsvall were entered in a program called ANALYSEDATA [14]. This is a data-base system for measurement data which allows free selection of samples according to both qualitative and quantitative information, as well as graphic displays and preprocessing of data. All data employed in the present work were from a single sampling site.

Seventeen PAH's in the particles were selected for testing the prediction of the total concentrations of six compounds that usually are present in both the particulate and the gaseous phases in an air sample (Table 2). Figure 2 shows an overview of these data in the form of Complot displays from ANALYSEDATA. Each row represents a sample, and each column a particular PAH component. Altogether 49 samples were used for the tests.

LEARNING SETS AND RESULTS

The PLS modelling was tested in five different ways. (1) When all samples were included in the learning set and cross-validation used to assess prediction, poor or no prediction was achieved. (2) Spring/summer/fall samples were used as in (1) and also to predict winter samples; the prediction accounted for 10—25% of the total variance and there was no success for winter samples. (3) Winter samples were used to predict winter and summer samples; the prediction accounted for 10—20% of the total variance in winter samples and summer samples could not be predicted. (4) Selected samples (temperature/wind direction) were used to predict similar samples; prediction accounted for 67% of total variance. (5) As a test against spurious recognition, a learning set was made from particulate PAH and volatile PAH that did not belong to the same air samples; in this case, prediction of all samples was unsuccessful.

DISCUSSION

Air pollution is usually emitted from many sources. It would be expected that the nature of particles and their surface properties, as well as the PAH composition, would depend on their origin, and that the different sources would influence the ratio between volatile and particulate PAH's. Also, if samples reflect a predominating source, this would govern the composition

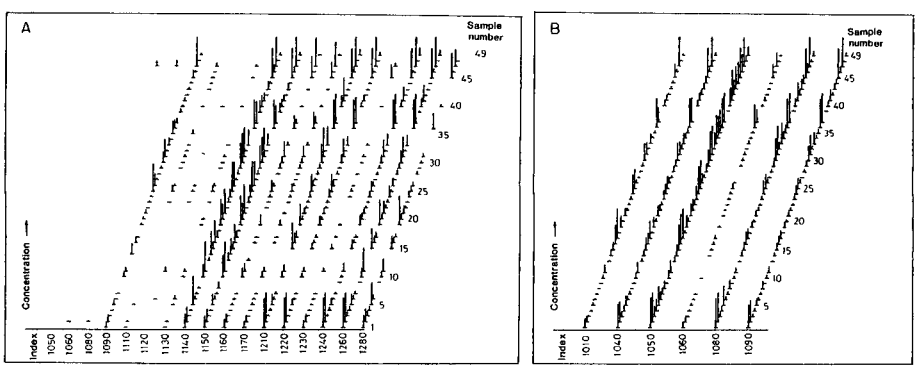

Fig. 2. ANALYSEDATA Complot displays of the PAH data used: (A) particulate PAH; (B) total volatile PAH. The components are arranged along the horizontal axis, identified by the index number in Table 2. The lengths of the vertical lines indicate the concentrations of each PAH in the range 0.01—10 ng m^{-3} for the particulate PAH and 0.01—100 ng m^{-3} for the volatile PAH (larger peaks dipped).

of both the particles and the PAH's in air. Thus one would expect a fair amount of prediction in samples which reflect a common source, and less prediction in samples which are not related. The results seem to support this expectation. This conclusion has two aspects.

In part, it is an indication that the PLS method gives a true and reasonable model of the physical world that underlies the analytical results. This is very encouraging in that no assumption was made about linearity, statistical distribution, etc. of the data. The only factor with influence on the data is the selection of samples to reflect various physical conditions of wind and temperature, followed by normalization by dividing each variable by the mean concentration, so that all variables contribute equally to the total picture. The other aspect is that the volatile PAH's carry their own information about air pollution. Volatile PAH's cannot generally be inferred from knowledge of particulate PAH, temperature, humidity and similar factors unless the nature of the air pollution in the samples is well characterized. In all the tests, most of the prediction is associated with one or two factors (see Table 1). In order to assess the physical reality behind the factors, more detailed studies are required. The dependence of recognition on the selection and weighting of variables, will indicate the physical reality of the factors. It is important that PLS delineates factors, and indicates their importance once their physical nature is known.

At the time of this investigation, the UNSCRAMBLER program was under active development, and was too unwieldy to allow easy interactive operations in combination with selection of different learning sets. As it is further developed, it should prove valuable for interpretation of complex data sets, particularly in combination with a suitable data-base tool for handling such data.

The authors thank H. Martens and C. Irgens for their assistance in using the UNSCRAMBLER program, and the Norwegian Food Research Institute (NINF) for making the program available. The Royal Norwegian Council for Scientific and Industrial Research (NTNF) kindly provided the funding of the study.

REFERENCES

1 K. E. Thrane and A. Mikalsen, Atmos. Environ., 15 (1981) 909.
2 H. Yamasaki, K. Kuwata and H. Miyamoto, Environ. Sci. Technol., 16 (1982) 189.
3 C. D. Keller and T. F. Bidleman, Atmos. Environ., 18 (1984) 837.
4 F. You and T. F. Bidleman, Environ. Sci. Technol., 18 (1984) 303.
5 K. E. Thrane, A. Mikalsen and H. Stray, Int. J. Environ. Anal. Chem., 23 (1985) 111.
6 K. E. Thrane, Proc. APCA 77th Annual Meet., Air Pollution Control Association, San Francisco, CA, (1984) 84-16.6.
7 Committee on Pyrene and Selected Analogues, Board of Toxicity and Environmental Health Hazards, Polycyclic Aromatic Hydrocarbons: Evaluation of Sources and Effects, National Technical Information Service, US Department of Commerce, Springfield, VA, 1983.

8 H. Wold, in J. Gani (Ed.), Perspectives in Probability and Statistics, Academic Press, London, 1975.
9 S. Wold, Pattern Recognition, 8 (1976) 127.
10 J. C. Bezdek, C. Coray, R. W. Gunderson and J. Watson, SIAM J. Appl. Math., 40 (1981) 339, 358.
11 S. Wold, H. Martens and H. Wold, in A. Ruhe and B. Kågström (Eds.), Proc. Conf. on Matrix Pencils, Springer Verlag, Heidelberg, 1982.
12 H. Martens, Norwegian Food Research Institute, personal communication.
13 K. E. Thrane and Wikström, in M. Cook and A. J. Dennis (Eds.), Polynuclear Aromatic Hydrocarbons: Mechanisms, Methods and Metabolism, Columbus, 1984, 1299.
14 J. J. Gether and H. M. Seip, Atmos. Environ., 13 (1979) 87.

Analytica Chimica Acta, 184 (1986) 107—116
Elsevier Science Publishers B.V., Amsterdam — Printed in The Netherlands

EVALUATION OF PATTERN RECOGNITION METHODS BY CRITERIA BASED ON INFORMATION THEORY AND EUCLIDEAN GEOMETRY

DIETRICH WIENKE and KLAUS DANZER*

Sektion Chemie, Friedrich-Schiller-Universität Jena, Steiger 3, 6900 Jena (German Democratic Republic)

(Received 20th December 1985)

SUMMARY

Euclidean geometry and information and fuzzy-set theory are used to develop general criteria for the evaluation of clustering methods. A separation function, describing the geometric clustering in a feature space for a given separation state, is introduced. Suitable clustering algorithms for given data can be selected by using the measure derived. The criteria developed are used in studies of the homogeneity of solids.

Classification and cluster analysis can be dealt with by a large number of possible algorithms. Programs such as ARTHUR [1] contain various methods of pattern recognition, and simple algorithms for microcomputers have been proposed [2]. Preprocessing procedures allow the number of possibilities of studying a data set to be increased. Accordingly, it should be practicable to provide parameters for selecting the most suitable methods of investigating a given data set. Commonly, publications dealing with pattern recognition contain comparisons of several algorithms applied to a set of data; comparison is made qualitatively or by means of method-inherent parameters. However, no scientist can be completely objective with regard to his data.

There are some other unresolved problems such as determination of the significant separation step in the hierarchal cluster analysis, design of valid training sets for classification, and construction of an optimal plan for pattern recognition for a given data set. An optimal plan for pattern recognition involves, first, the best choice of the features pertaining to the problem. Then, preprocessing (scaling, weighting, generation of orthonormalized features) is the second step. After that, clustering enables the data to be examined for any substructures. If some groups which have only numerical character are so found, an attempt can be made to give them chemical meaning. Any such meanings are strongly governed by the features chosen. After this operation, training sets for classification problems can be constructed.

Some authors have suggested the use of information theory [2, 3] or Euclidean geometry [4]. The estimation of probabilities and singularities of the geometrical measurements in the case of clusters with single objects decreases the possibility of application. In this paper, novel criteria are introduced in an attempt to overcome these problems.

0003-2670/86/$03.50

THEORY

The most frequent situation in pattern recognition is that a data set is presented without any information about the inherent structure. Obviously, there is then a large number (Z) of possible ways of separating the objects into groups. These possibilities often have the same probability, Φ_0, or the possibilities can be defined as distributed uniformly because they cannot be evaluated precisely.

After hierarchal clustering, some structure in the data with respect to the algorithm used (e.g., a dendrogram) should be observed. The preliminary uncertainty represented by the information entropy, H_0, decreases then to the uncertainty, represented by entropy H. The information content in such cases is given by Shannon's model:

$$I = H_0 - H$$

with

$$H_0 = -\sum_{s=1}^{Z} \Phi_{0,s} \operatorname{ld} \Phi_{0,s}$$

and

$$H = -\sum_{s=1}^{Z} \Phi_s \operatorname{ld} \Phi_s$$

in which the sums run through all Z possibilities of separation s (states of separation); "ld" means the binary logarithm.

If there is no prior knowledge of the system, all sizes of clusters are possible. Moreover, the n objects may permute between all groups. The total number of Z for all possible separations can be calculated from Stirling's second-order recursive formula [5]:

$$\sum_{i,j=1}^{n} Z(i,j) = \sum_{i,j=1}^{n} Z(i-1, j-1) + Z(i, j-1)$$

Then, H_0 can be expressed as

$$H_0 = \operatorname{ld} \sum_{i,j=1}^{n} Z(i,j)$$

If there is any prior knowledge, e.g., about the number of clusters, the Z number decreases. For instance, the formula of the binomial coefficient yields the same results as Stirling's formula for the case of two groups.

The theory of fuzzy sets [6] can be applied to evaluate the probabilities $\Phi_{0,s}$ and Φ_s as normalized functions applied to the equation

$$\Phi_s = g_s f_s / \sum_{s=1}^{Z} g_s f_s$$

where g_s are arbitrarily chosen weights; in this investigation, g_s was set equal to one. The f_s term is specially defined as the separation function at the sth state of separation. The basic idea is then to interpret $\Phi_{0,s}$ and Φ_s as normalized distances describing one possible state of separation. Clearly, a state of separation of groups is more probable the longer the distances between the groups in the m-dimensional feature space and the closer the objects are placed in relation to their group centroids $c_{k,s}$. Thus the f_s term is defined as the difference of the average distance D_s between each of the groups and the average diameter d_s of all the groups at the sth state of separation: $f_s = D_s - d_s$. All distances are of the Euclidean type and are related to the centroids for the computation of d_s and D_s. Figure 1 shows the geometrical model for a two-dimensional feature space. The separation state s is represented by three clusters. The D_s value is calculated from

$$D_s = (Z \sum_{k,\,l}^{C_s} D_{kl,\,s})/[(C_s - 1)C_s]$$

and for d_s

$$d_s = (\sum_{k}^{C_s} \bar{d}_{s,k})/C_s$$

In these equations, $D_{kl,s}$ is the distance between the centroids of the kth and lth clusters; Z is the total number of separation steps s; $\bar{d}_{s,k}$ is the average diameter of the kth cluster with the centroid $c_{s,k}$; and C_s is the number of clusters.

The separation function f_s is a measure describing the geometric assemblage (clustering) in an m-dimensional feature space for a given separation state s. This function is discrete. It attains a maximum if the objects lie near their group centroids and if there are large distances between the groups. Figure 2 indicates the general behavior of f_s. In this example, data sets with four clusters were chosen (Table 1) and were clustered by using the algorithm given by Kaufman et al. [7]. When the diameters of the clusters decrease but centroids remain at the same position in space (constant D_s), then f_s indicates a growing maximum for $s = 3$ (Fig. 2A). With constant diameters (constant d_s)

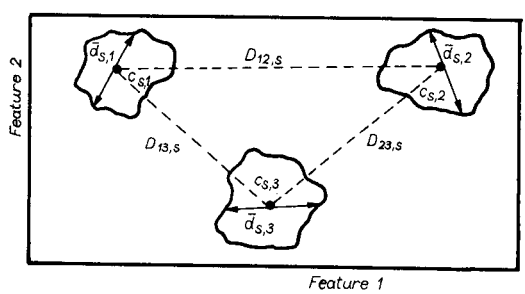

Fig. 1. Geometrical model for the derivation of separation function f_s for the case of two features and three clusters.

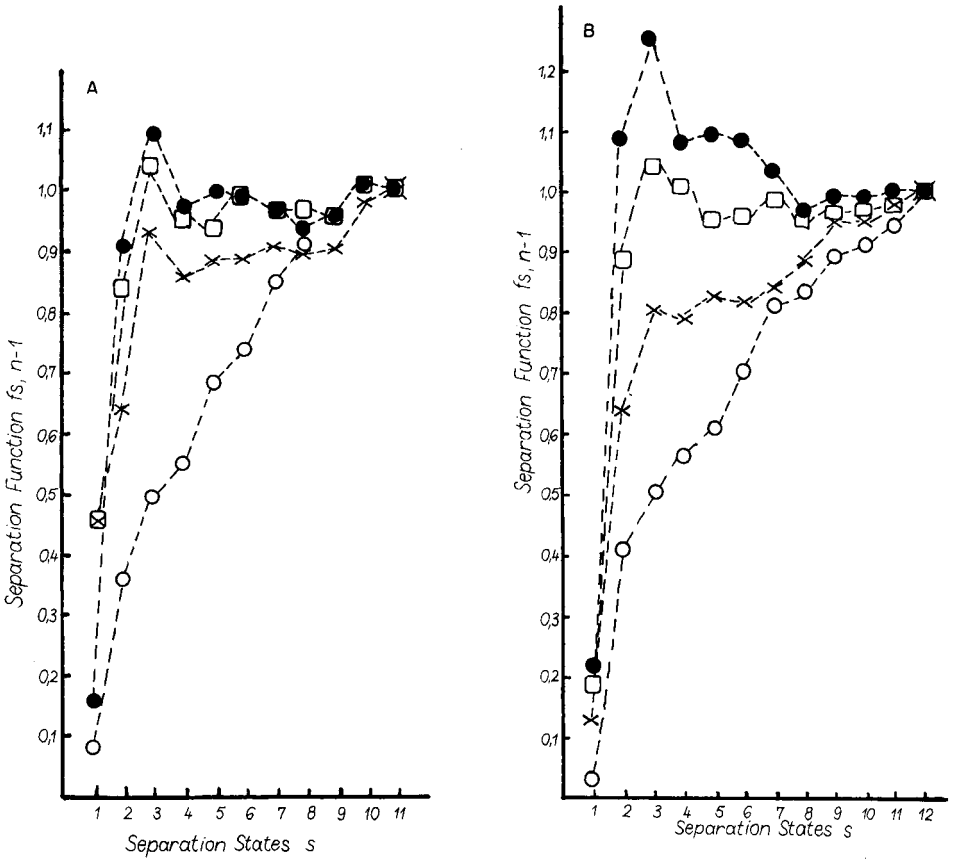

Fig. 2. Separation functions $f_{s,n-1}$ for the data sets given in Table 1: (A) sets 1—4; (B) sets 5—8. For better visualization, the discrete values of function f_s and $f_{s,n-1}$ are connected by dotted lines.

but increasing distances between the groups, the maximum also grows (Fig. 2B). The hierarchal cluster analysis yields $(n - 1)$ separation states for a given set of n objects and therefore contains a residue of uncertainty. When the maximum of f_s is used, it is possible to decide which separation state is inherent to the data set. In practice, the objective section through the dendrogram or tree can be calculated in this way.

By means of the information content, I, or the entropy estimated a posteriori, the whole data structure can be characterized quantitatively. Table 2 includes the four possible cases which exist theoretically for comparison of two results or algorithms A and B for cluster analysis when H and $f_{s,\max}$ are applied. Cases 1—3 are quite clear; the decision is obviously for A. In the fourth case, algorithm B is chosen for further evaluation of the given data because the entropy H characterizes the whole data structure. The following two points are practically important. Clustering of scaled data causes the

TABLE 1

Numerical values of eight synthetic data sets containing two features and twelve (sets 1—4) or thirteen (sets 5—8) objects

SET 1		SET 2		SET 3		SET 4	
0.5	3.0	1.0	3.5	2.5	5.0	4.0	6.5
0.5	4.0	1.0	4.5	2.5	6.0	4.0	7.5
1.5	3.0	2.0	3.5	3.5	5.0	5.0	6.5
1.5	4.0	2.0	4.5	3.5	6.0	5.0	7.5
2.0	11.5	3.5	10.5	4.0	9.5	5.0	8.5
11.0	11.0	9.5	9.5	8.0	8.0	6.5	6.5
11.0	12.0	9.5	10.5	8.0	9.0	6.5	7.5
12.0	11.0	10.5	9.5	9.0	8.0	7.5	6.5
12.0	12.0	10.5	10.5	9.0	9.0	7.5	7.5
8.5	1.0	7.0	2.5	5.5	4.0	4.5	5.0
9.5	1.0	8.0	2.5	6.5	4.0	5.5	5.0
9.5	2.0	8.0	3.5	6.5	5.0	5.5	6.0
SET 5		SET 6		SET 7		SET 8	
2.0	10.0	2.0	10.0	2.0	10.0	2.0	10.0
1.9	5.9	1.5	6.5	1.0	7.0	0.5	4.5
1.9	6.1	1.5	5.5	1.0	5.0	0.5	7.5
2.1	5.9	2.5	6.5	3.0	5.0	3.5	4.5
2.1	6.1	2.5	5.5	3.0	7.0	3.5	7.5
8.9	2.9	8.2	2.5	8.0	2.0	7.5	1.5
8.9	3.1	8.5	3.5	8.0	4.0	7.5	4.5
9.1	2.9	9.5	2.5	10.0	2.0	10.5	1.5
9.1	3.1	9.5	3.5	10.0	4.0	10.5	4.5
9.9	8.9	9.5	8.5	9.0	8.0	8.5	7.5
9.9	9.1	9.5	9.5	9.0	10.0	8.5	10.5
10.1	8.9	10.5	8.5	11.0	8.0	11.5	7.5
10.1	9.1	10.5	9.5	11.0	10.0	11.5	10.5

function f_s to lose its absolute character. Therefore, it is necessary to work with $f_{s,n-1}$, according to the equation $f_{s,n-1} = f_s/f_{n-1}$. The normalization factor f_{n-1} is the value of f_s if the data set is separated into single objects, i.e., it is the average distance between all single objects such that their diameters are infinitesimal. For the comparison of clustering results obtained for data sets with different numbers of objects, it is necessary to normalize H to the n number of objects because H is sensitive to n.

RESULTS AND DISCUSSION

The following examples were computed with MICLU (microcomputer program for cluster analysis) [8]. The program runs on a 64K microcomputer MC-80 (VEB Kombinat Mikroelektronik Gera, G.D.R.) in BASIC. The clustering algorithm is the one proposed by Kaufman et al. [7]. All published data sets were preprocessed by autoscaling before clustering.

Example I

The three data sets A, B and C consist of twelve objects and two features. These sets are represented by their positions in the feature space position (Fig. 3) and by their separation function (Fig. 4). Set A contains twelve clusters (the single objects) and the separation function $f_{s,n-1}$ (A) attains a maximum for the last state s of separation. The separation function $f_{s,n-1}$ (B) shows a sharp maximum for $s = 1$, because set B contains two groups. Set C contains four clusters. The maximum of $f_{s,n-1}$ (C) is attained for $s = 3$. Thus the separation function indicates the number of groups inherent to the data.

Example II

The data set C from example I was clustered by two different algorithms. The first one was that of Kaufman et al. [7], which divides one cluster into

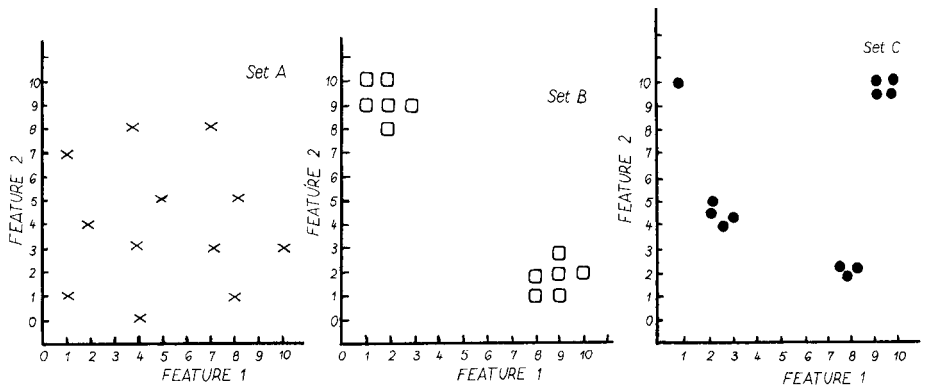

Fig. 3. Representation of three different data sets (A—C) containing twelve objects and two features.

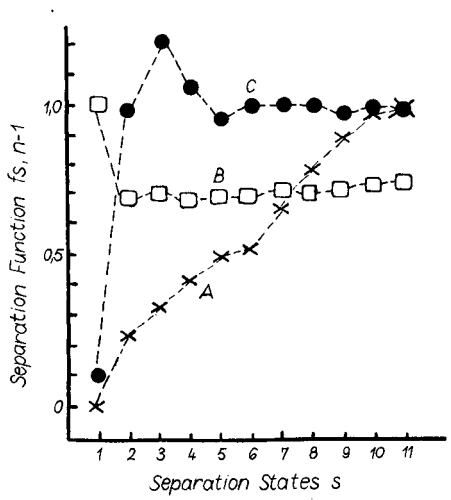

Fig. 4. Separation functions $f_{s,n-1}$ for the data sets A, B, C; the symbols correspond to those used in Fig. 3.

two subclusters by minimizing the average distance from one object to all other objects in the first and in the second subcluster. This algorithm was modified to give a second algorithm, which divides one cluster into two subclusters by minimizing the average distance over all objects in the two subclusters 1 and 2. This was done by using the formulae

$$d_1 = 2 \sum_{i,j}^{n_1} \Delta_{i,j} / [(n_1 - 1)n_1]$$

$$d_2 = 2 \sum_{k,l}^{n_2} \Delta_{k,l} / [(n_2 - 1)n_2]$$

where Δ means the Euclidean distance, n the number of objects in the cluster and d the average distance between all objects in the cluster.

The first algorithm yielded the hierarchal pattern 1 (Fig. 5). The separation function attains a maximum for $s = 3$ having a value $f_{3,\max} = 0.6442$ and an entropy $H = 3.37$ bit. The second algorithm produced the hierarchal pattern 2 (Fig. 5) with $H = 3.43$ bit. It is interesting that the second algorithm runs over the same inherent state of separation (Fig. 5, dashed lines) with four clusters; therefore the $f_{3,\max}$ value is also 0.6442. But the residual data structure is different. According to Table 2, algorithm 1 will be chosen for the separation of the given set C and also for further evaluation of similarities inherent to the set.

Example III

An interesting application of clustering occurs in investigation of the homogeneity of solids. The field of sophisticated analytical characterization of purified and composite materials has expanded rapidly in recent years, given the increasing demands of the microelectronic and optics industries. One kind of investigation is the test of homogeneity by several types of analysis of variance (ANOVA) [9, 10]. The schemes described above can be used for homogeneity studies. The objects of the data set are measurement

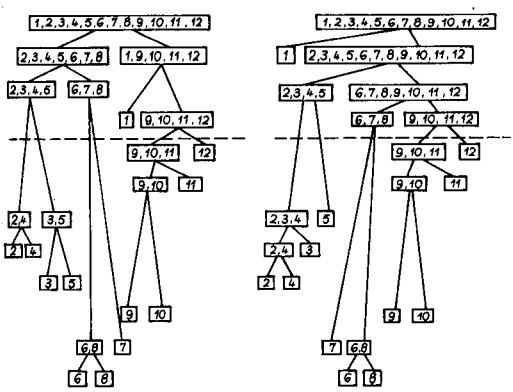

Fig. 5. Data structures of set C obtained by two different algorithms.

TABLE 2

The possible theoretical cases for the evaluation of clustering methods by entropy H and the maximum of separation function $f_{s,\max}$

Result			Separation	
Process A		Process B	Wider[a]	Surer[b]
$f_{\max,A}$	>	$f_{\max,B}$	A	A
H_A	<	H_B		
$f_{\max,A}$	>	$f_{\max,B}$	A	A = B
H_A	=	H_B		
$f_{\max,A}$	=	$f_{\max,B}$	A = B	A = B
H_A	=	H_B		
$f_{\max,A}$	>	$f_{\max,B}$	A	B
H_A	>	H_B		

[a]Wider separation by distance. [b]Surer separation based on information theory.

points at the surface or in the bulk of a solid. The feature vectors are then constructed from the measured situation at those points. The selection of features is based on the question of homogeneity that is to be answered; the features could be the chemical composition, the structure or certain properties at the sample points, or any combination of these. The result of the cluster analysis can be transformed to a favorable representation without distortion of feature space, because the positions of the measurement points on or in the sample are not related to the position of the points in the feature space. However, the separation function derived yields clusters inherent to the data which can be bordered by lines of similarity.

As an example, a rectangular copper sample doped with cobalt and nickel was chosen. At fifteen surface points of the sample, the impurities of nickel and cobalt were determined simultaneously by optical emission spark spectrography. Figure 6 shows all the pairs of concentration as well as the clustering results obtained by MICLU. The separation function indicates three clusters from its maximum for step $s = 2$. The copper sample surface includes inhomogeneities at two corners. This conclusion can be drawn from those few features by a survey of the data. By generalizing the behavior of separation function f_s, it is possible to derive a new idea of homogeneity on the basis of vectors obtained by measurements at different points of the sample.

Ideal homogeneity. The data vectors obtained at the sample points are identical. They lie in the m-dimensional feature space at one point, so that there is only one cluster and the distances to other clusters are zero. The one cluster contains only a single object. The separation function f_s is therefore constant at zero (Fig. 7, line 1): $f_{s,\max} = f_s = D_s - d_s$ for $1 \leqslant s \leqslant (n-1)$.

Partial homogeneity/inhomogeneity. The data vectors obtained at sample

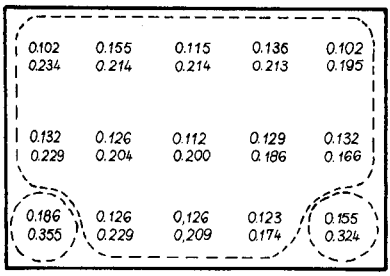

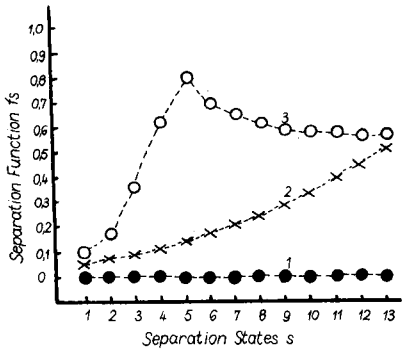

Fig. 6. Surface of a copper sample (original 20 mm × 30 mm) with the nickel and cobalt contents measured at fifteen points. In each pair, the upper number is for nickel and the lower for cobalt, all in % (w/w).

Fig. 7. Qualitative behavior of the separation function f_s for three cases of homogeneity/inhomogeneity. For explanation, see text.

points form significant clusters in the feature space. All points found in the same cluster can be bordered by similarity lines either on the surface or in the bulk sample. The function f_s shows a maximum between the first and the $(n-2)$th state s of separation (Fig. 7, curve 3): $f_{s,\max} > 0$ and $f_{s,\max} \geqslant f_s$ for $1 \leqslant s \leqslant (n-2)$.

Ideal inhomogeneity. The data vectors scatter uniformly in the feature space and do not form significant clusters. All n objects are single clusters and can be bordered by n different lines of similarity. The separation function f_s has its maximum at the last possible state of separation for $s = (n-1)$ (Fig. 7, curve 2): $f_{s,\max} = f_{n-1} \neq f_s$ for $s < n-1$.

Conclusions

The measures described are suitable for indicating the quality of a chosen scheme of pattern recognition for a given data set. The separation function f_s has three advantages. The first is the absence of singularities in the case of single object clusters, and the second is the possibility of using geometry for the calculation of probabilities. The third is that the use of the function is not limited by the number of objects in the data set. The algorithms can be added to every existing computer program for pattern recognition and are also useful for microcomputers. The separation function provides a novel view of overall homogeneity. The values for homogeneity obtained could be displayed by using a small graphics program.

The results of classifications can be evaluated by direct comparisons of the values of the separation function f_s, where s indicates the sth algorithm of classification. The separation function can thus be used as an optimization function for the design of training sets.

REFERENCES

1 B. R. Kowalski, Anal. Chem., 47 (1975) 1152A.
2 C. Liteanu and I. Rica, Anal. Chem., 51 (1979) 1986.
3 K. Varmuza, Pattern Recognition in Chemistry, Springer Verlag, Heidelberg, 1980.
4 E. Kny and G. Nauer, Mikrochim. Acta, III (1983) 399.
5 L. Lovasz, Combinatorial Problems and Exercises, Akademiai Kiado, Budapest, 1979.
6 J. Spal, Aplikace Matematiky, 27 (1982) 326.
7 L. Kaufman, A. Pierreux, P. Russeeuw, M. P. Derde, D. L. Massart, M. R. Detaevernier and G. Platbrod, Anal. Chim. Acta, 153 (1983) 257.
8 D. Wienke, Diplomarbeit, Friedrich-Schiller-Universität Jena, Sektion Chemie, Jena, 1985.
9 K. Danzer, G. Doerffel, H. Ehrhardt, M. Geissler, G. Ehrlich and P. Gadow, Anal. Chim. Acta, 105 (1971) 1.
10 K. Danzer and G. Marx, Anal. Chim. Acta, 110 (1979) 145.

Analytica Chimica Acta, 184 (1986) 117—132
Elsevier Science Publishers B.V., Amsterdam — Printed in The Netherlands

IMPLEMENTATION OF AN EXPERT SYSTEM FOR THE QUALITATIVE INTERPRETATION OF X-RAY FLUORESCENCE SPECTRA

K. JANSSENS and P. VAN ESPEN*

University of Antwerp (UIA), Department of Chemistry, Universiteitsplein 1, 2610 Wilrijk/Antwerp (Belgium)

(Received 16th January 1986)

SUMMARY

The implementation of an expert system for the automated qualitative interpretation of energy-dispersive x-ray spectra is discussed. The first step in the interpretation process is the extraction of the relevant data from the spectrum, which is done by a preprocessor program, written in FORTRAN. The expert system itself consists of three parts. The knowledge base contains specific information on energy-dispersive x-ray fluorescence spectrometry presented in the form of IF/THEN rules. The data base contains the reduced spectral data and an array of certainty factors associated with each element; the certainty factor for an element represents the probability of its being present in the sample from which the spectrum was taken. Finally, the inference engine performs manipulation of the knowledge. For a particular state of the data base, the certainty factors for all the elements are iteratively modified until convergence is reached by using the rules from the knowledge base. During each cycle, the inference engine selects one rule from the knowledge base and executes it. Rules are selected on the basis of the chemical elements contained in their IF part and according to their previously assigned focus levels. Execution of the THEN part of the selected rule modifies the certainty factors of a number of elements. At the end of the interpretation session, the system lists the elements which have a high probability of being present in the sample. Optionally, the user can be provided with explanations of the reasoning steps taken during the interpretation. Application of the expert system to a particular spectrum shows that it is useful for the reliable interpretation of spectral data obtained from electron microprobe analysis of industrial aerosol particles.

The use of computers for instrument control, data acquisition and data evaluation is now widespread. Chemometrics has played an important role in providing the theoretical background and the necessary software. Optimization by Simplex methods [1] and multivariate data treatment and calibration [2] have proved to be very valuable. Although large parts of the data acquisition and interpretation processes have been automated, there are still vital steps in most analytical procedures which have to be done manually in order to obtain reliable results. These steps typically involve decision-making to optimize a certain procedure or to meet certain demands on precision and accuracy. A purely statistical approach does not always yield satisfactory results. In order to make such decisions, one often has to rely heavily on

0003-2670/86/$03.50

experience. This process can be improved substantially by the use of expert systems [3]. An expert system is a computer program which can incorporate considerable amounts of area-specific information and can use this knowledge, similarly to a human expert, to solve problems which cannot be handled by traditional computer algorithms.

An example of partly automated data processing is the characterization by electron-probe microanalysis (EPMA) of particulate material of environmental and/or industrial origin [4]. The chemical characterization involves the evaluation of x-ray spectra measured with a Si(Li)-detector as a result of the bombardment of the individual particles with electrons of keV energy. During the analysis of one sample, typically 1000 or more spectra are generated. This data acquisition can be fully automated [5]. In view of the large number of x-ray spectra obtained, accurate techniques for spectrum evaluation, based on least-squares fitting, require too much operator- and computer-time to be useful [6]. In contrast, simple techniques for spectrum evaluation relying on counts accumulated in predefined energy windows are fast but produce unreliable results because of the often high degree of peak overlap in the spectrum. Nevertheless, an experienced x-ray spectroscopist finds it easy to interpret such x-ray spectra and identify the elements that are present in the sample.

As a solution to this problem, an expert system was developed to assist in the automated interpretation of EPMA spectra. The system consists of two parts: a preprocessor program, written in FORTRAN, and the actual expert system, written in Pascal. No specific "symbolic logic" languages, such as LISP, PROLOG, OPS5 or POP-11, were used. Both programs are implemented on a VAX 11/780, with the VMS operating system. The system typically requires 5 seconds of CPU-time to make an interpretation of an x-ray spectrum.

SPECTRUM PREPROCESSING

The first step in the spectrum interpretation is the extraction of relevant information. This is done by the preprocessor program, written in FORTRAN. The program suppresses noise by using a procedure based on a variable width Savitsky-Golay filter [7] and locates peaks by square-wave convolution of the smoothed data. Peak boundaries and peak widths are determined by using the smoothed first and second derivatives of the spectrum while net peak intensities are calculated by means of a background-correction method based on an algorithm suggested by Clayton [8]. Finally, a list of all possible chemical elements which correspond to the peaks within an energy uncertainty of about 100 eV, is made by comparing the energy of the detected peaks with entries in a library of x-ray lines. These elements are considered as suggestions to the solution by the expert system.

The table generated by the preprocessor corresponding, for example, to the spectrum of Fig. 1 is given in Table 1. Because the information in this table is processed further by the expert system, only crude estimates of the

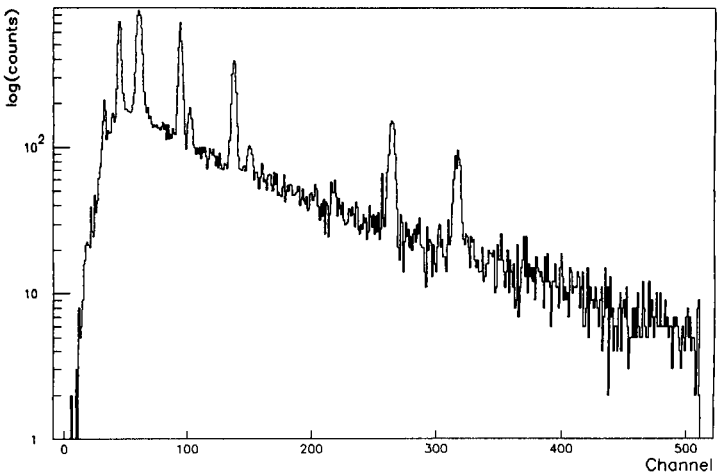

Fig. 1. X-ray spectrum of an industrial aerosol particle obtained by EPMA. The elements Mg, Si, Ca, Cr and Pb are present in detectable concentrations.

actual values are required. The entire preprocessing operation takes about 2 s of CPU-time.

THE EXPERT SYSTEM

The aim of the expert system is to interpret the data in the table produced by the preprocessor and to return the elemental composition of the sample (or particle) associated with that spectrum.

Structure

The expert system can be considered as a conventional production system. It can logically be divided into three distinct subsystems. The first and most important part is the knowledge base, holding (at present) about 200 rules which enable the expert system to perform symbolic reasoning in the field of x-ray spectra interpretation. An example of such a rule is given in Table 2.

The second subsystem is a data base containing information on the spectrum to be interpreted. It also reflects the current state of reasoning by the system. The data base consists of a static and a dynamic part. The static part contains the reduced spectral data. Each spectrum is described by a series of peaks while the relevant characteristics of a peak are stored in a peak frame as shown in Fig. 2. Thus, a whole spectrum is represented in the system data base by means of the spectrum frame of Fig. 3. The dynamic part (its content changes during the reasoning process of the system) consists of a list of all chemical elements. Each element is characterized by a certainty factor. At present, this factor can only have four values: 0.0 (the element is absent), 0.50 (the element may be present), 0.75 (the presence of the element is plausible), 1.0 (the element is present).

TABLE 1

Preprocessor output corresponding to the spectrum in Fig. 1

Spectrum: 001129
Total spectrum intensity (TSI): 54052
Sum of peak intensities: 33273
Total background intensity: 20779
Calibration: 0.00000E + 00 4.00000E − 02
Percentage of intensity from peaks: 61.56%
Percentage of intensity from background: 38.44%

No.	Energy (keV)	Boundary (channel)		FWHM (keV)	Intensity (% of TSI)		Height (counts)	
		Left	Right		Background	Net	Background	Net
1	1.2864 Eu Gd Mg As Ho	23	35	0.106 *M*-α *M*-α *K*-α *L*-α *M*-α	4.160	1.709	87.387	124.613
2	1.7738 Hf Si Re	41	51	0.112 *M*-α *K*-α *M*-α	8.346	9.320	152.841	565.159
3	2.4012 S Pb	53	66	0.190 *K*-α *M*-α	10.999	16.924	165.469	684.531
4	3.7252 Ca Te	89	96	0.113 *K*-α *L*-α	4.618	9.160	121.168	583.832
5	4.0600 Ca Te	99	105	0.080 *K*-β *L*-β	3.845	1.012	116.671	69.329
6	4.9080	121	127	0.280	2.378	0.336	73.300	13.700
7	5.4493 Cr Pm	128	141	0.169 *K*-α *L*-α	4.364	6.811	65.575	327.425
8	5.9666 Eu Cr Pm Gd	146	155	0.187 *L*-α *K*-β *L*-β *L*-α	2.637	1.290	55.522	47.478
9	7.9996	195	208	0.327	2.485	0.437	37.416	5.584
10	8.7100 Re Ho	210	223	0.199 *L*-α *L*-γ	2.159	0.729	31.601	28.399

TABLE 1 (continued)

No.	Energy (keV)	Boundary (channel)		FWHM (keV)	Intensity (% of TSI)		Height (counts)	
		Left	Right		Background	Net	Background	Net
11	10.0075	242	254	0.445	1.462	0.465	22.839	3.161
12	10.5626 Hf As Pb	255	270	0.225 L-γ K-α L-α	1.508	3.984	19.186	132.814
13	11.1696	275	280	0.240	0.472	0.264	16.303	4.697
14	12.6674 Pb Ac	308	322	0.229 L-β L-α	1.098	2.422	15.137	80.863
15	14.8547	366	376	0.203	0.634	0.210	11.978	1.022

The third subsystem, the inference engine, performs the knowledge manipulation. The certainty factors associated with each element in the dynamic part of the data base are modified by means of the rules from the knowledge base, depending on the current state of the data base. As in conventional production systems this is done by executing the following three steps. First, it is necessary to establish which rules are applicable. This is done by a pattern matcher which selects rules having an IF-part which is fully consistent with the facts in the data base. A rule is said to be applicable when its IF part evaluates to TRUE with respect to the current state of the data base. The execution of the THEN part of a rule is here referred to as "applying the rule". The set of applicable rules found by the pattern matcher

TABLE 2

An example of a rule in the knowledge base (Rule 45: check-Fe1)[a]

If:	No Fe was previously found [P(Fe) < 1.0]; a peak at (6.40 ± 0.08) keV is present; a peak at (7.05 ± 0.08) keV is present; Int(7.05)/Int(6.04) is approximately equal to 0.12. No Mn is present [P(Mn) < 0.5]; no Ni is present [P(Ni) < 0.5]; no Sm is present [P(Sm) < 0.5]; no Eu is present [P(Eu) < 0.5]; no Tb is present [P(Tb) < 0.5]; no Er is present [P(Er) < 0.5]; no Tm is present [P(Tm) < 0.5];
Then:	there is evidence (1.0) that the sample contains Fe.

[a]Int(7.05) represents the number of counts in the peak at 7.05 keV; P(Mn) symbolizes the probability that manganese is present in the sample.

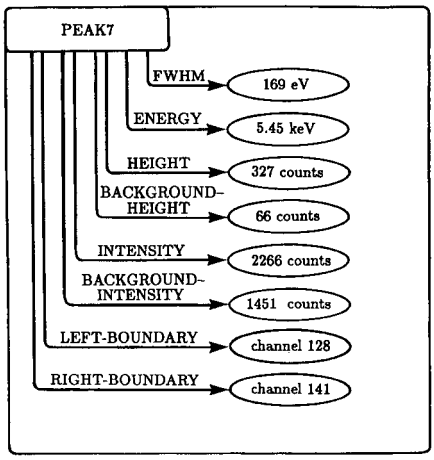

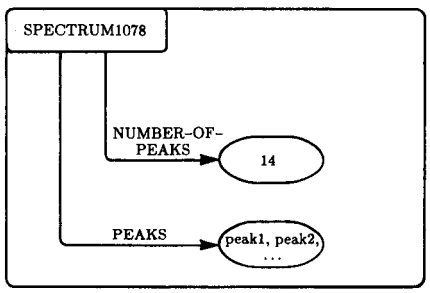

Fig. 2. The relevant characteristics of a peak are represented in a peak frame.

Fig. 3. An entire spectrum can be described by using a spectrum frame consisting of numerous peak frames.

is called the conflict set. If the conflict set contains more than one rule, the inference engine has to decide which of these rules it is actually going to apply. It should be noted that during one cycle, only one rule can be executed, because in doing so, the state of the data base changes, which will produce a different conflict set. This process is termed conflict resolution. In order to do this, a suitable scheme for conflict resolution is needed. In the present case, an hierarchically-structured combination of several distinct procedures was used: (a) the set of rules which have the highest focus level associated with them (see below) is established (the remaining rules are ignored in the later steps); (b) if the reduced conflict set still contains more than one rule, rules are selected on the basis of the use of the most recently changed item(s) in the data base in their conditional part; (c) if more than

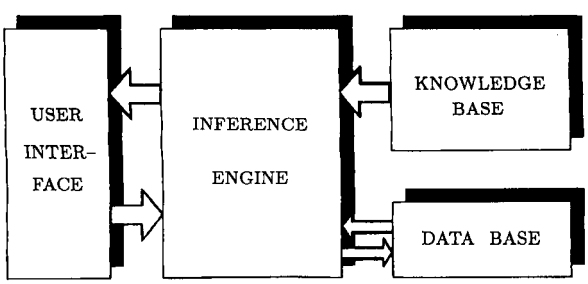

Fig. 4. A production system consists of three parts: a data base containing information about the specific problem, a knowledge base containing more general information, and a control unit (the inference engine) which enables the expert system to infer new data.

one rule is still present in the conflict set after these two reduction steps, one of the rules is selected at random. The system does not use meta-rules to decide which rules have precedence over others; however, a focus level can be associated with each rule. The default value of the focus level is 1. Some rules (those that represent more basic steps in the symbolic reasoning process) have higher focus levels than others. During the selection of one rule from a list of applicable rules, the attention of the system is focused on the rules with the highest focus level. Finally, the THEN part of the selected rule is executed, producing a change in the data base.

This match/select/execute cycle is continued until the data base reaches a state where no more applicable rules are found. After the interpreting session, the system reports the elements having a certainty factor >0.75 as being present in the sample. Thus, the expert system essentially works by decreasing the certainty factors of improbable elements, while increasing the certainty factors for more plausible species. The general structure of the expert system and the relation between the different parts is depicted in Fig. 4.

PASCAL implementation

In order to obtain a clear understanding of the functioning of an expert system, it was decided to implement the system in an all-purpose programming language such as PASCAL, instead of one of the highly specialized symbolic-processing languages like PROLOG or OPS5, which have built-in and thus less comprehensible inference engines.

The data base. Implementation of the static part of the data base in PASCAL was fairly easy using the built-in RECORD declarations. The peak frame of Fig. 2 can be represented by the PASCAL record declarations shown in Table 3.

The dynamic part of the data base is merely an array of certainty factors $CF[Z]$, with Z ranging from 11 to 92, corresponding to the elements sodium up to uranium, respectively. At present, only four discrete values of the CF's (0.0, 0.5, 0.75 and 1.0) are permitted. Information contained in the data base can be retrieved and/or updated by the rules in the knowledge base through a limited number of functions and procedures for interrogating and modifying the data base.

An example of a data base-interrogating function is PRESENT(e, de) which returns TRUE if it can find a peak with energy between $(e - de)$ and $(e + de)$ in the static part of the data base. Another such function is INTENSITY(e, de) which returns the net intensity of the corresponding peak. ELEMENT(z) is a function which returns TRUE if $CF[z] \geqslant 0.5$. Several data base-modifying procedures such as ADD(z), STORE(z) and REMOVE(z) can be implemented. For example, REMOVE(z), STORE(z) and ADD(z) set CF[z] to 0.0, 0.75 and 1.0, respectively. These functions also put their argument (i.e., the atomic number z) at the end of an array "CHANGES" which permits the expert system to keep track of the subsequent data-base modifications. This information is necessary during conflict resultion.

The knowledge base. Each production rule is represented by two PASCAL

TABLE 3

PASCAL record declarations for the peak frame in Fig. 2

```
Type peak descriptor =
   record
      energy: real;
      left boundary: integer;
      right boundary: integer;
      fwhm: real;
      intensity: real;
      background intensity: real;
      height: real;
      background height: real;
      importance: integer;
      possibilities: integer
   end;
Type spectrum descriptor =
   record
      number of peaks: interger;
      peak: array[1.. no of peaks] of
                peak descriptor
   end;
Var spectrum: spectrum descriptor;
```

subprograms: the conditional part of the rule (or pattern to be matched with the current state of the data base) is implemented as a boolean function which can take the value TRUE or FALSE, according to whether the pattern matches or not. The action part of a rule is represented by a procedure. For example, the rule concerning iron mentioned above is represented as shown in Table 4. The IF part of a rule is invariably built from calls to the relatively small number of data base-interrogating functions. Similarly, the THEN part of a rule consists of calls to one of the limited number of data base-modifying procedures. Such an implementation of the knowledge base permits a fairly simple pattern matcher. Only a procedure that sequentially evaluates all the PASCAL functions corresponding to the IF part of the rules and that keeps track of the obtained boolean value (TRUE or FALSE) is required.

In the main program, each rule is referenced by assigning a unique number to the corresponding function and procedure. This assignment takes place during the compilation by a separate program called MODULAN (see Appendix), which generates part of the source code of the inference engine. In general, MODULAN gathers the information needed during the interpretation session which is not explicitly present in the compiled code.

The inference engine

Main routine. The inference engine is the main part of the expert system and coordinates its operation. In the first place, the data base is initialized by reading in a table of spectral data (cf. Table 1). The procedure READ SPECTRAL DATA is called for this purpose. Secondly, the procedure

TABLE 4

Procedure for the rule concerning iron[a]

```
Function check Fe1: boolean;
begin
   if (
      not new el(26)
      and present(6.40, 0.08)
      and present(7.06, 0.08)
      and not element(25) and not element(27)
      and not element(62) and not element(63)
      and not element(65) and not element(68)
      and not element(69)
      and correct ratio(7.06, 0.08, 6.40, 0.08, FeKb/Ka — FeD, FeKb/Ka + FeD)
   then check_Fe1: = true
   else check_Fe1: = false
end;
Procedure act Fe1;
begin
   add(26);
   comment(26, "Kα and Kβ lines present with correct intensity.");
   comment(26, "--> Fe added.")
end;
```

[a]Fe*Kb/Ka* represents the characteristic *Ka/Kb* intensity for Fe while FeD stands for the uncertainty on this number.

READ SYSTEM DATA obtains information needed by the inference engine from background memory during conflict resolution. The actual interpreting session is started by putting the various elements suggested by the preprocessor (cf. Table 1) on the CHANGES array. This is done by the procedure INSTALL POTENTIAL ELEMENTS which also sets the *CF* of these elements to 0.5. Subsequent match/select/execute cycles are handled by the procedure ITERATE. After the iterative interpretation phase, the procedure INFORM is called; this enables the user to obtain information about the reasoning processes performed. The basic skeleton of the inference engine can be represented as outlined in Table 5. (The PASCAL code cited is merely illustrative and for reasons of clarity a number of less relevant statements concerning declaration of variables and subprograms have been omitted.)

The ITERATE procedure. This procedure can be considered as the control part of the expert system. First, it selects applicable rules, then it resolves the resulting conflict set and finally executes the selected rule (see Table 5). The procedure for selecting applicable rules searches the knowledge base by evaluating the boolean functions corresponding to the IF part of the rules. In order to do this, each rule is associated with a unique number. The number corresponding to a rule of which the IF part is TRUE is put on an array of applicable rules; N APPLICABLE denotes the number of applicable rules.

The function EXECUTABLE(RULE NUMBER) returns the value found for

TABLE 5

Basic skeleton of the inference engine with outlines of the important procedures[a]

```
Procedure INFER;
begin
   read spectral data;
   read system data;
   install potential elements;
   repeat
      iterate
   until no applicable rules;
   inform
end;

Procedure SELECT APPLICABLE RULES;
begin
   for rule no.: = 1 to no of rules do
      if executable(rule no.) then
      begin
         n applicable: = n applicable + 1;
         applicable rules[n applicable]: = rule no
      end;
   no applicable rules: = (n applicable = 0)
end;

Procedure ITERATE;
begin
   select applicable rules;
   select highest focus;
   reduce rules (applicable rules, n applicable,
                 last change,
                 selected rule, n selected);
   execute rule(selected rule);
end;

Function EXECUTABLE(RULE NUMBER
INTEGER)[b]: BOOLEAN;
begin
   case rule number of
      1: executable: = check Na;
      2: ...
      ...
      45: executable: = check Fe1;
      46: executable: = check Fe Ni;
      ...
   end;
```

[a]NO APPLICABLE RULES is a boolean variable, the value of which is determined by the procedure SELECT APPLICABLE RULES. [b]The source code for EXECUTABLE (and for EXECUTE RULE, see below) is generated by MODULAN. Check Na, check Fe1, etc. are the names of functions in the data base. The function is boolean.

the IF part of the corresponding rule. It is impossible in PASCAL to declare arrays of functions or procedures, thus the number RULE NUMBER has to be associated with the appropriate function in the explicit (though inelegant) way outlined in Table 5, by means of the function "EXECUTABLE".

If the boolean variable NO APPLICABLE RULES is evaluated as FALSE, the procedures SELECT HIGHEST FOCUS and REDUCE RULES are called, to perform the conflict-set resolution. The SELECT HIGHEST FOCUS procedure determines the maximum of the focus levels of the rules on the APPLICABLE RULES array; it deletes all rules having a focus level less than this number and decrements N APPLICABLE accordingly. The REDUCE RULES procedure is recursive and takes three arguments: an array A1 of integers representing the conflict set at a given stage of the resolution process, an integer *N*A1 representing the number of rules in this set, and CRITERION which is the atomic number of the element to be used as reducing criterion. This returns another array A2 and corresponding integer *N*A2, containing the remaining rules after execution of one step in the resolution process.

At the initial call to REDUCE RULES from within ITERATE, the array A1 is equal to APPLICABLE RULES, while A2 corresponds to the SELECTED RULE array. CRITERION is equal to the last item on the CHANGES array. The REDUCE RULES procedure attempts to reduce the list of rules it receives from ITERATE on the basis of the most-recently-changed item in the data base. It does this by determining which and how many rules use the ele-

ment with z equal to CRITERION in their IF part. As a result, three distinct cases may occur. In the first, no rules in the conflict set use this element; in this case REDUCE RULES calls itself recursively with the initial conflict set as argument; CRITERION is set to the last-but-one item on the CHANGES array. In the second case, more than one rule uses this element; again REDUCE RULES calls itself, but this time with the partly-reduced conflict set as first argument, with the same value for CRITERION as in the first case. In the third case, only one rule uses the element; if this occurs, this rule is immediately returned to the procedure ITERATE (through the array SELECTED RULE) to be used as an argument to the function EXECUTE RULE.

Thus, REDUCE RULES gradually reduces the conflict set by using the entries on the CHANGES array in inverse chronological order. Elements which would cause the conflict set to be deleted completely are disregarded. In doing so, the procedure can exhaust the CHANGES array. When this happens, the inference engine has no criteria left to select one of the rules from the conflict set. It then calls an emergency procedure called SELECT RANDOM, which uses a pseudo-random generator to pick one of the rules from the remaining conflict set. The probability that SELECT RANDOM is called during a loop diminishes as the interpretation session proceeds, because the number of items on the CHANGES array becomes larger. In PASCAL, the REDUCE RULES procedure takes the form shown in Table 6. The SELECT RECENT procedure establishes for each of the rules on the input-

TABLE 6

The REDUCE RULES procedure in PASCAL form

```
Procedure reduce rules(A1: rule array; NA1: integer;
                       criterion: integer;
                       var A2: rule array; var NA2: integer);
begin
  if not changes exhausted then
    begin
      select recent(A1, NA1, criterion, A2, NA2);
      if (NA2 <> 1) then
        begin
          new criterion: = previous(criterion);
          if NA2 <> 0 then reduce rules (A2, NA2, A2, NA2, new criterion)
                      else reduce rules (A1, NA1, A2, NA2, new criterion)
        end
    end
  else
    begin
      NA2: = 1;
      A2[NA2]: = select random(A1, NA1)
    end
end;
```

TABLE 7

The SELECT RECENT procedure

```
Procedure select recent(A1: rule array; NA1: integer;
                        criterion: integer;
                        var A2: rule array; var NA2: integer);
var rule pointer: integer;
begin
   NA2: = 0;
   for rule pointer: = 1 to NA1 do
      if A1[rule pointer] in occurrence set[criterion] then
         begin {add rule number to output array}
            NA2: = NA2 + 1;
            A2[NA2]: = A1[rule pointer]
         end
end;
```

array A1 whether or not it uses the element with z equal to CRITERION in its IF part. In order to do so, SELECT RECENT has to know which elements are used for each rule, or conversely in which IF part of the rules each element of the periodic table will appear. The set of rules that use a particular element in their conditional part is called the "occurrence set" of that element. These sets are generated by the MODULAN program. The SELECT RECENT procedure (Table 7) simply determines the intersection of the set of rules on the array A1 with the occurrence set of the element used as a criterion. The rules in this intersection are returned in the array A2. When the intersection is empty, obviously, the related criterion was not good.

The user interface

Most expert systems are backtracking or goal-directed consultation programs (e.g., MYCIN [9]), where communication between user and system is available and necessary during and after the consultation. As this expert system is intended to interpret x-ray spectra unsupervised, and thus unassisted, the user is never prompted for additional information. However, each time an action part of a rule is executed during this process, an explanatory message is sent to a temporary message board and stored there until the interpretation has finished. Afterwards, these messages can be displayed on a video screen or stored in a file, simply by typing the atomic number or the name of an element. For instance, by typing the message "Fe" or "26", all messages received on the message board concerning iron can be displayed or retrieved for later use.

During the interpretation of a spectrum, the current state of the reasoning process is reflected by the certainty factors associated with each element. Optionally, a periodic table can be displayed on the video screen at the beginning of the session, with all elements and their corresponding certainty factors marked. During the reasoning process, which involves execution of

several rules, and consequent modification of certainty factors, these changes are also reflected in the table displayed; this enables the user to monitor the subsequent changes for each element.

APPLICATION

As an illustration, the line of reasoning followed by the expert system while interpreting the spectrum of Fig. 1 will be discussed. Although this spectrum is relatively simple, in the sense that few peaks overlap, there are some fundamental difficulties in interpreting it by means of traditional window algorithms. This technique can produce a number of erroneous assignments: (a) the Mg-K peak at channel 32, together with the Pb-L_α peak at channel 234 can be assigned to L_α and K_α of arsenic, respectively; (b) the Cr-K_β line at channel 49 can be interpreted as Mn-K_α; (c) the peak at channel 60 can be attributed to S (K-line) and/or to Pb (M_α line); (d) many peaks can be considered as L-lines of elements such as Ho, Eu, Re, Gd, Pm, etc. The expert system, however, uses these partly erroneous suggestions only as initial data and gradually discards implausible candidates. The major deduction steps of the expert system are summarized in Table 8.

During the first cycle of the interpreting session, only two rules (138 and 145) constitute the conflict set, because the attention of the system is focused initially on rules with high focus levels. The use of chromium as reducing criterion selects rule 138 (check Cr0) for application. This rule changes the CF of chromium to 0.75 because both characteristic peaks for Cr are present with a correct K_α/K_β intensity ratio; check Cr0 does not check for the presence of possible interferences on chromium, such as check Fe1 does for iron. The next evaluation cycle results in a conflict set containing only one rule (145, check Ca0) which sets CF[Ca] to 0.75 for similar reasons as does check Cr0. Both check Ca0 and check Cr0 have focus levels of 10, because they represent elementary and rather unconstrained deduction steps.

After the first two cycles, however, no rules with high focus levels are applicable, and the conflict set becomes more extended. In the third cycle, seven rules are applicable. After calcium has been used as reducing criterion (because it is the element with the most recently changed CF), a set consisting of two rules is obtained. From this set, check Ca Te1 is chosen at random; on the basis of CF[Ca] = 0.75 (implying a correct K_α/K_β ratio) and the absence of interferences on calcium other than tellurium, it decides that calcium is certainly present, while tellurium is absent. Accordingly, CF[Ca] is set to 1.0, while CF[Te] becomes 0.0. The next cycle is characterized by a conflict set of six rules, from which check Pb0 is selected. This rule sets CF[Pb] to 0.75 because the M_α, L_α and L_β lines of lead are present with correct relative intensities. The fact that CF[Pb] = 0.75 implies that there are no interfering elements for lead in the sample. During the next two cycles, this conclusion is made explicit by applying the rules check S Pb Ac and

TABLE 8

Major deductions steps taken by the expert system during the interpretation of the spectrum in Fig. 1

Cycle no.	Rule selected	Old situation	New situation	Explanation
1	check Cr0	CF[Cr] = 0.5	CF[Cr] = 0.75	K_α and K_β lines of Cr present with correct K_β/K_α intensity ratio
2	check Ca0	CF[Ca] = 0.5	CF[Ca] = 0.75	K_α and K_β lines of Ca present with correct K_β/K_α intensity ratio
3	check Ca Te1	CF[Ca] = 0.75	CF[Ca] = 1.0	No interferences for Ca besides Te present; CF[Ca] > 0.75
		CF[Te] = 0.5	CF[Te] = 0.0	
4	check Pb0	CF[Pb] = 0.5	CF[Pb] = 0.75	M_α, L_α and L_β of Pb present with approx. correct relative intensities
5	check S Pb Ac	CF[S] = 0.5	CF[S] = 0.0	CF[Pb] > 0.75; CF[S] < 0.75; CF[Ac] < 0.75
		CF[Pb] = 0.75	CF[Pb] = 1.0	
		CF[Ac] = 0.5	CF[Ac] = 0.0	
6	check As Pb	CF[As] = 0.5	CF[As] = 0.0	CF[Pb] > 0.75; CF[As] < 0.75
		CF[Pb] = 1.0	CF[Pb] = 1.0	
7	check Re0	CF[Re] = 0.5	CF[Re] = 0.0	No L_β
8	check Hf0	CF[Hf] = 0.5	CF[Hf] = 0.0	No L_α and no L_β
9	check Ho0	CF[Ho] = 0.5	CF[Ho] = 0.0	No L_α and no L_β
10	check Gd0	CF[Gd] = 0.5	CF[Gd] = 0.0	No L_β
11	check Eu0	CF[Eu] = 0.5	CF[Eu] = 0.0	No L_β
12	check Si	CF[Si] = 0.5	CF[Si] = 1.0	K line of Si present; no interferences present
13	check Mg	CF[Mg] = 0.5	CF[Mg] = 1.0	K line of Mg present; no interferences present
14	check Cr Pm	CF[Cr] = 0.75	CF[Cr] = 1.0	No interferences for Cr besides Pm present; CF[Cr] > 0.75
		CF[Pm] = 0.5	CF[Pm] = 0.0	

check As Pb. In both cases CF[Pb] is set to 1.0; check S Pb Ac removes S and Ac (CF[S] = CF[Ac] = 0) while check As Pb1 sets CF[As] to 0.0.

During the next five cycles, the system removes the improbable elements Re, Hf, Ho, Gd and Eu, using the five corresponding rules which check for the absence of the M_α and/or L_α lines of these elements. After these elements have been removed, the rule check Si, which sets CF[Si] to 1.0 is applied. This rule can only become applicable after Hf and Re have been removed, because the M-line of these elements interferes with the Si-K peak. Similarly, check Mg is applied after it has been ensured that no interferences such as As, Gd, Eu or Ho are present. In the final cycle, only one rule is applicable, i.e., "check Cr Pm" which works similarly to "check Ca Te1"; Pm is removed, while CF[Cr] becomes equal to 1.0. After this has been done, the expert system displays the results of the interpretation for the spectrum in (Fig. 1) showing that the sample contains Si, Mg, Ca, Cr and Pb.

CONCLUSION

The implementation of an expert system for the interpretation of energy-dispersive x-ray spectra has been demonstrated. The proposed method seems fast enough to be useful in the interpretation of large sets of spectral data. The program can be used for the reliable interpretation of spectral data obtained from the electron microprobe analysis of industrial aerosol particles. It should also be useful in the analysis of complex x-ray spectra by non-linear least-squares fitting. In this case, the expert system can provide the fitting procedure with the necessary information about the elements to be used in the fitting model.

A major drawback of the system lies in the large number of rules that are required. Currently, about 200 rules are implemented but for a fully operational system which is capable of dealing with all situations up to 2000 rules may be required. It may be possible to reduce the number of rules by using a more systematic representation of the x-ray spectral information in the knowledge base. Another problem arises from the fact that information about peak ratios is used in the conditional parts of the rules. Although considerable uncertainty is allowed for these ratios, cases of severe absorption may cause the expert system to produce an erronous interpretation. However, in such a situation similar misinterpretations are likely to be made by human experts.

The planning of the inference engine is quite similar to the interpretative reasoning used by an expert x-ray spectroscopist. The automated process could be improved by implementing a scheme that also selects rules based on the number of conditions present in their IF parts. Clearly, rules with a large number of conditions should acquire a higher priority of execution than rules characterized by a small number of constraints. As this expert system is currently in full development, this general plan was not integrated in the control part of the inference engine. Sometimes, certain conditions in the

IF part of a rule appear to be redundant after a time; however, these superfluous conditions would cause the rules in which they appear to obtain a higher priority than rules without them, thus distorting the selection of rules during an interpreting session. At a later stage, this general scheme will certainly be used in conflict resolution.

APPENDIX

The MODULAN program

If the inference engine is to be successful in conflict resolution, it needs additional information about the rules in the data base which is not present in the compiled code of the rules. Basically, the inference engine needs to know the number and names (entry points) of all the functions and procedures present in the knowledge base. To permit efficient manipulation of the rules during the match/select/execute cycle, each rule has to be associated with an integer number.

The MODULAN program acquires this information by analyzing the source code of the knowledge base. It makes a list of all functions and procedures present in the knowledge base and assigns numbers to them. On the basis of this list, it produces the necessary declarations for these routines in the main program and also writes the lengthy case-statements appearing in the EXECUTABLE and EXECUTE RULE routines. For each chemical element, ranging from Na ($Z = 11$) to U ($Z = 92$), a list is made of rules which refer to the *CF* of this element in their conditional part. These lists are called "occurrence sets" MODULAN also evaluates the focus level associated with each rule. Finally, it stores the information concerning the occurrence sets, together with the focus data in background memory, which can be read by the inference engine via the READ SYSTEM DATA procedure. The application of MODULAN enables the inference engine to be updated automatically each time changes are made in the knowledge base (e.g., addition of new rules). Furthermore, the user who wants to update or change the knowledge base need only employ the correct syntax and semantics in writing/updating the rules without requiring knowledge about the internal functioning of the inference engine.

K. J. and P. V. E. are research fellows of the Belgian National Science Foundation (N.F.W.O.).

REFERENCES

1 S. L. Morgan and S. N. Deming, Anal. Chem., 46 (1974) 1170.
2 M. Sjostrom, S. Wold, W. Lindberg, J. Persson and H. Martens, Anal. Chim. Acta, 150 (1983) 61.
3 J. Fox, Trends Anal. Chem., 4 (1985) 9.
4 G. S. Frits, J. J. McCarthy and R. J. Lee, Microbeam Anal., II (1981) 57.
5 B. Raeymaekers, P. Van Espen and F. Adams, Mikrochim. Acta, II (1984) 437.
6 P. Van Espen, 1984 Analytical Electron Microscopy Workshop, San Francisco, U.S.A., 1984.
7 H. P. Yule, Nucl. Instrum. Methods, 54 (1967) 61.
8 E. Clayton, private communication.
9 B. G. Buchanan and E. H. Shortliffe (Eds.), Rule-Based Expert Systems, The MYCIN Experiments of the Stanford Heuristic Programming Project, Addison-Wesley, Reading, Massachusetts, 1984, p. 331.

Analytica Chimica Acta, 184 (1986) 133—142
Elsevier Science Publishers B.V., Amsterdam — Printed in The Netherlands

PROCEDURE FOR BACKGROUND ESTIMATION IN ENERGY-DISPERSIVE X-RAY FLUORESCENCE SPECTRA

KARSTEN NORMANN THOMSEN, JETTE NØRGAARD PEDERSEN and NIELS PIND*

Department of Chemistry, Aarhus University, Langelandsgade 140, 8000 Aarhus C (Denmark)

(Received 7th August 1985)

SUMMARY

A method for semi-automatic background estimation in energy-dispersive x-ray fluorescence spectra is outlined. Two cubic splines were investigated and the spline called the Butland interpolant was chosen for further investigation. Prior to the calculation of the spline, peak regions are set up, and suitable knots are defined outside the peak regions. To set up the peak regions, an automatic peak-search routine and a calibration equation are used. For a given peak, the latter relates the full width at half maximum (FWHM) to the peak centre. In turn, the size of the peak regions are defined by the FWHM multiplied by a constant given by the user. The method was tested on several types of spectra. It was found that the optimal size of the peak region decreased with increasing peak density. Reproducibility tests showed that the standard deviation of the summation of counts within a peak region and after background subtraction was less than would be expected from the counting statistics.

Energy-dispersive x-ray fluorescence spectrometry is well suited for quantitative elemental analysis. The peak areas of the characteristic lines are used for quantitative work. The peak area calculation involves two problems: (1) estimation of background; (2) deconvolution of overlapping peaks. The present paper deals with the background estimation only. A procedure is outlined for the estimation and subtraction of the background prior to peak evaluation. The proposed procedure is reproducible and the simple formulae used make it suitable for small computers.

Several algorithms have been proposed for the estimation of the background in γ- and x-ray spectrometry [1—5]. Bank et al. [1] use a cubic spline interpolation in the program QUEST. The spline connects knots chosen by a combination of a minimum search and manual selection of channels. The background thus obtained is subtracted from the spectrum prior to deconvolution of peaks. A parabolic background was used by Koskelo et al. [2] in the SAMPO80 program; each peak was described by five parameters, of which three were known in advance from a calibration procedure. For each peak, the remaining two parameters and the three parabolic parameters were calculated simultaneously by a χ^2 minimization procedure. Marageter et al.

0003-2670/86/$03.50

[3] described the peak structure as a sum of four terms, including asymmetry of the Gaussian peaks. The background is parabolic and it also includes contributions from the absorption edges of the major elements. All parameters are determined simultaneously by an iterative least-squares procedure. Burgess and Tervo [4] used a filter fit procedure and subtracted the background prior to spectrum deconvolution. Tervo et al. [5] made use of the local minima in the large background regions between peaks in γ-ray spectra. The background was constructed by correcting the counts in the minimum channels and connecting knots so obtained by a cubic spline.

The program for peak-area calculations, FWHMCAL [6], used in this laboratory, is based on a stepwise procedure. The first step is to estimate and subtract the background, the second to find peak centres, the third to calculate the FWHMs and the fourth to calculate the amplitudes and then the peak areas. The stepwise peak-area calculation simplifies the calculations and makes the program construction very suitable for small computers. In order to improve the first step of the procedure, it was found convenient to implement an automatic procedure for the background subtraction. Further, it was found that a procedure based on a cubic spline would fit the requirement of simple calculations. Hence, for background estimation, the two procedures described by Tervo et al. [5] and Bank et al. [1] were implemented in the FWHMCAL program. The peak density in x-ray spectra is often greater than in γ-ray spectra, and the peak width measured in channels of peaks in x-ray spectra is also larger than in γ-ray spectra. Hence, the original procedure for detection of knots proposed by Tervo et al. [5] did not work properly and had to be modified. Further, for the procedure in QUEST [1], the need for the user to intervene in the selection of knots was inappropriate for an automatic procedure. Hence, only the minimum search routine used in QUEST [1] was implemented. Both procedures were tested on spectra of varying peak densities. The procedure based on the work of Tervo et al. [5] was found to be the most suitable.

METHOD OF BACKGROUND ESTIMATION

Localization of peak regions

An automatic peak-search routine [7] localizes the peaks. The routine demands two parameters given by the operator. The first parameter gives an approximate value of the full width at half maximum (FWHM) of the peaks in the spectrum, while the second parameter indicates the noise level in the spectrum. Small peaks caused by noise fluctuations are thus omitted from the peak list. Peaks are detected only if the centre channel is a local maximum.

The FWHM for each peak is calculated from a previously established calibration equation relating FWHM and peak centre [6], $\log (F) = aC + b$, where F and C are the FWHM and centre, respectively, for a given peak. This relation is purely empirical. The theoretical relation requires that $\log (F)$ be replaced by F^2 [8]. Because of its better linearity, the above equation was

chosen for the FWHM calibration. The deviation from theory is caused by the increasing separation of lines, e.g., $K_{\alpha 1}$ and $K_{\alpha 2}$ lines [6], which for fluorescence energies less than 25 keV are treated as a single line.

Finally, a third parameter (hereafter called the FWHM factor) is given. The FWHM factor and the calculated FWHM value for each peak are multiplied, and a region of this size is placed symmetrically around the peak centre. When two of these peak regions overlap, they are combined to one larger region.

Selection of channels used for background estimates

Once the peak regions have been found, useful channels in the remaining background regions have to be selected as knots for a cubic spline. Two automatic algorithms were investigated. The first algorithm (the LM algorithm) is a modification of the procedure proposed by Tervo et al. [5]. It finds a few local minima on each side of a peak region. The minimum search is initialized at the limit of the peak region, and a local minimum is detected if the counts Y_i in channel X_i obey the relationship $Y_{i-1} > Y_i < Y_{i+1}$, where X_i and X_{i+1} are adjacent channels. The search for minima on one side of a peak region is terminated after the detection of three minima or when the limit for an adjacent peak region is exceeded. This procedure is applied to both sides of all peak regions. As a result, an array indicating minima channels is obtained. Finally, the peak region boundaries are moved to the closest local minima.

The minima thus found are extremes of a stochastic process, and the counting values are adjusted to give a more reliable value in the following way. A region of eleven channels is placed symmetrically around each minimum channel. When this small region overlaps a peak region, the boundary of the small region is moved to the boundary of the peak region. The average count in the channels within the small region is calculated and assigned to the minimum channel. In turn, the set of channels and the assigned values in these are used as the knots for the background estimate.

The other algorithm (the GM algorithm) is taken from the procedure of Bank et al. [1]. The global minima between two peak regions are used as knots. A global minimum is detected if the counts Y_i in channel X_i obey the rule $Y_i < Y_j$, where Y_j represents the counts in all the remaining channels (X_j) in the background region defined by two adjacent peak regions. Finally, the channels with the global minima and the counts in these channels are used for the background estimate.

Background estimates

For the background estimates, the Butland interpolant was implemented as given by Tervo et al. [5]. The Butland interpolant is a cubic spline, which passes through the knots, and the slope (first derivative) is a continuous function. For each polynomial interpolation between two knots, the coefficients are determined from the values and slopes in the knots. The slope in a

knot is evaluated as a weighted mean of two adjacent simple slopes. It is a condition that the resulting slope be zero if the two adjacent slopes have different signs.

The spline (hereafter called spline 2) used by Bank et al. [1, 9] was also implemented. For this spline, it is a condition that the curvature (second derivative) also be a continuous function. The coefficients for the spline between two knots are here evaluated simultaneously from a set of linear equations set up from the conditions of continuity. Formulae for the calculation of the two types of cubic splines are given in the Appendix. Finally, in the peak regions, the splines produce a background which is subtracted from the measured spectrum data. Outside the peak regions, the spectrum is nullified.

EXPERIMENTAL

Apparatus and samples

The energy-dispersive x-ray spectrometer is based on secondary target excitation. The spectrometer and the software used for data acquisition have been described recently [6, 10, 11].

A sample containing Ti, Zn, Sr and Mo was used for the FWHM calibration. The background procedures were tested on a variety of samples. Simple single-element samples of lead, tantalum or tungsten (Goodfellow Metals), as well as a pellet of a mixture of selenium (Merck 99.5%) and x-ray mix powder (Chemplex) with a selenium content of 1.5% (w/w) were analyzed. The complex spectra obtained from multi-element samples (e.g., SRM 1201, Hastelloy, U.S. National Bureau of Standards) and a coal fly ash were also investigated.

Measurements

All measurements were made with a silver secondary target. The x-ray generator setting was 45 kV for all samples except for the SRM 1201, where a setting of 40 kV was used. The current setting was adjusted to give equal dead time for the FWHM calibration spectra and the spectra to be investigated. A FWHM calibration spectrum was acquired prior to the acquisition of a sample spectrum. The counting time was chosen to give suitable counting statistics; typical counting times were 500 s for the FWHM calibration sample, 300 s for lead, tantalum and tungsten and 2000 s for the multi-element samples. In the case of selenium, four spectra were obtained for acquisition times of 100 s, 1000 s, 10 000 s and 100 000 s, respectively.

Programs

The routines for background estimates were implemented in the program FWHMCAL [6], which contains routines for plotting, peak searching [7], FWHM calibration, peak-area calculation, etc. The peak list given by the peak search can be inspected, and the operator may add peaks to the list or delete peaks from the list. Finally, the operator has to choose which algorithm is to be used for the selection of knots, and which cubic spline is to be used.

First, FWHMCAL is initiated by the FWHM calibration spectrum, from which an energy calibration and a FWHM calibration are obtained. Next, the unknown spectrum is processed stepwise by FWHMCAL: (1) a peak list is obtained by the automatic search routine; (2) the peak list may be revised by the operator; (3) FWHM values are calculated from the equation $\log (F) = aC + b$; (4) peak regions are defined; (5) the background in the peak regions are estimated and subtracted from the spectrum, and the spectrum is nullified outside the peak regions; (6) the peaks are described as pure Gaussians for which the centre and FWHMs for each peak are known, hence the amplitudes can be calculated by a simple least-squares procedure; (7) peak areas are obtained; (8) results are printed.

The program VAP [10] was used in the analysis of SRM 1201; VAP is based on the fundamental parameter technique in the case of a mono-energetic excitation source [12]. Further, in the cases where all elements are determined by one target, no previous calibration of the spectrometer is necessary. This is feasible, because the spectrometer calibration constant is treated as a scaling factor, the sum of all weight fractions for the elements in the sample being equal to one. Hence, the calculation of the calibration constant is included in the iterative procedure [10].

RESULTS AND DISCUSSION

The cubic spline and algorithm for knot selection

The backgrounds estimated by the Butland interpolant and the LM algorithm are shown in Figs. 1—3; backgrounds obtained by the cubic spline

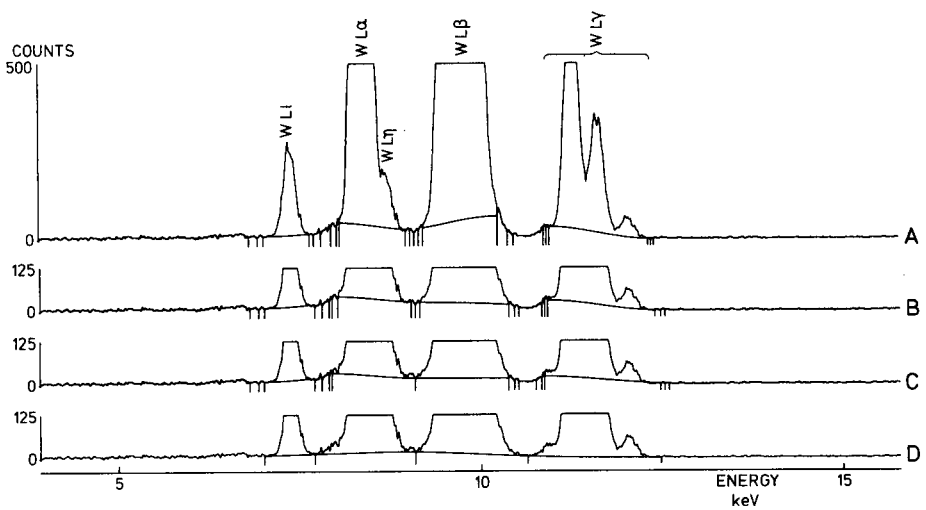

Fig. 1. Estimated backgrounds in the spectrum of tungsten. A, B and C are based on the Butland interpolant and the LM algorithm with FWHM factors of 3.0, 3.5 and 4.0, respectively. D is based on spline 2 and the GM algorithm with a FWHM factor of 4.0. The knots used by the splines are indicated.

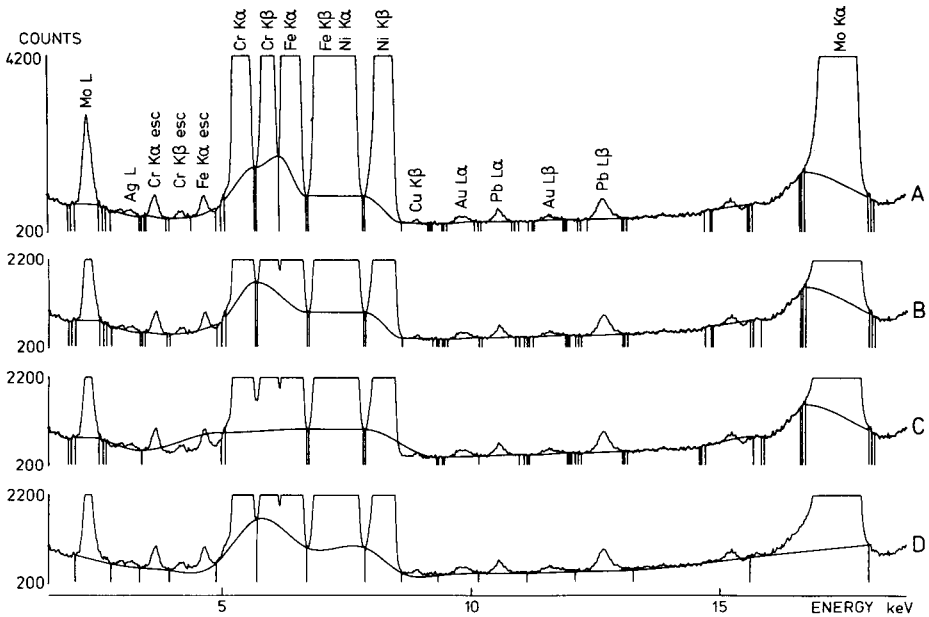

Fig. 2. Estimated backgrounds in the spectrum of the NBS SRM 1201 steel alloy. A, B and C are based on the Butland interpolant and the LM algorithm with FWHM factors of 2.5, 3.0 and 3.5, respectively. D is based on spline 2 and the GM algorithm with a FWHM factor of 3.0. The knots used by the splines are indicated.

2 and based on the GM algorithm are also shown. A close examination of the cubic spline 2 reveals that this method produces a curve which displays excursions in amplitude that markedly exceed the boundaries established by the knots. It was found that these excursions were considerably reduced if the calculations were based on the LM algorithm rather than the GM algorithm. This shortcoming is believed to be a result of the condition that the second derivative be a continuous function. In the case of the Butland interpolant, no excursions were observed. In fact, it can be shown that between two knots, the Butland interpolant is monotonic. Backgrounds estimated by the Butland interpolant and the GM algorithm were useless and will therefore not be discussed. For a more detailed investigation of different splines suitable for an empirical calculation of background curves, the work of Tervo et al. [5] should be consulted. It was found that the Butland interpolant together with the LM algorithm produced useful background estimates in peak regions. For all samples, it was found that the reproducibility of the background obtained was satisfactory when this procedure was used, i.e., the standard deviation for the summation of counts in a peak region after background subtraction was found to be less than what would be expected from the counting statistics.

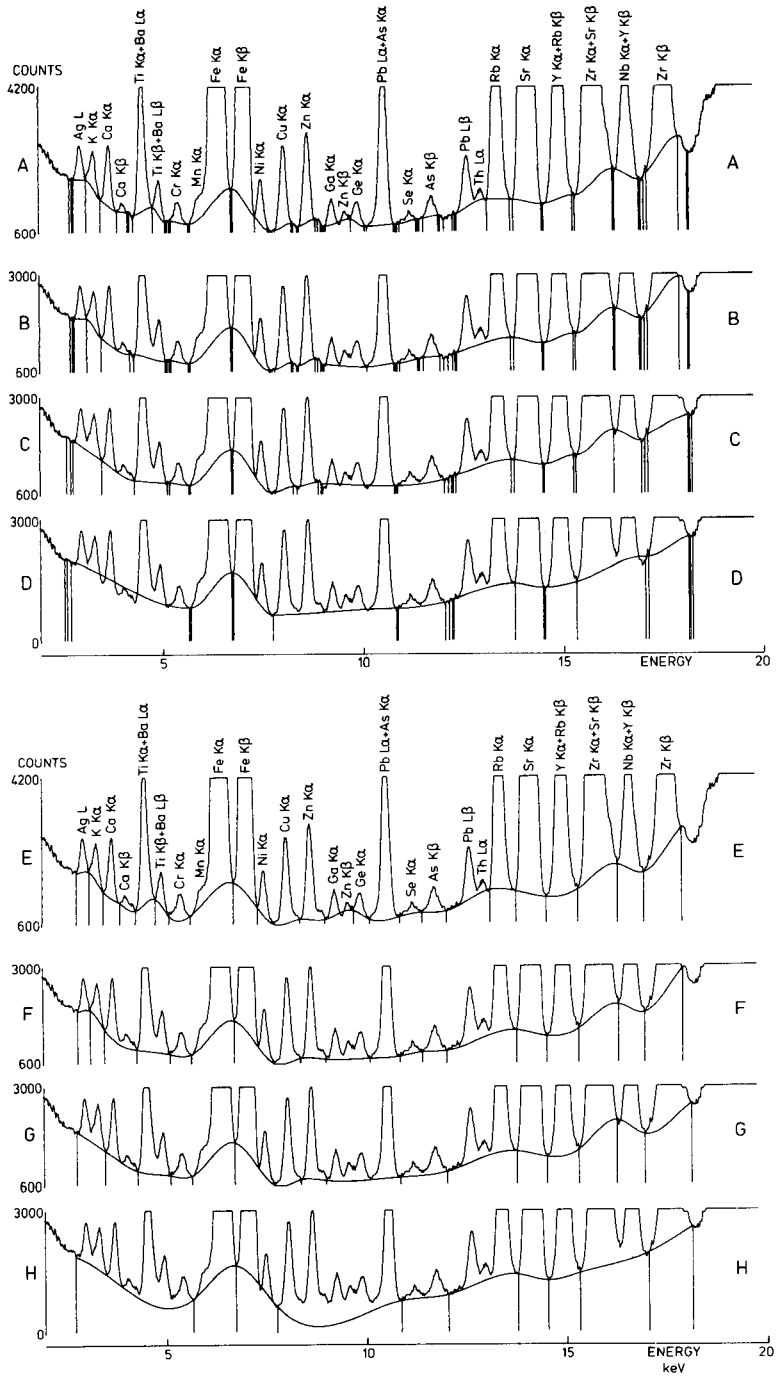

Fig. 3. Estimated backgrounds in the spectrum of coal fly ash. A, B, C and D are based on the Butland interpolant and the LM algorithm with FWHM factors of 1.5, 2.0, 2.5 and 3.0, respectively. E, F, G and H are based on spline 2 and the GM algorithm with FWHM factors of 1.5, 2.0, 2.5 and 3.0, respectively. The knots used by the splines are indicated.

The FWHM factor

The value of the FWHM factor was found to be critical for the background estimates. Its value was found to depend on the peak density in the spectra. No automatic way of selecting the FWHM factor was found, but some general lines for choosing suitable factors are outlined below.

Figures 1—3 show spectra with different peak densities as well as backgrounds obtained by the use of different values for the FWHM factor. The spectrum of tungsten in Fig. 1 shows a number of peaks of varying intensity, and also well-defined background regions. The peak density is low in this spectrum. The spectrum in Fig. 2 has a higher peak density; there is a group of intense peaks and the remaining peaks are closer to each other than in the tungsten spectrum. Visually, the background in Fig. 2 seems well-defined. The spectrum of coal fly ash in Fig. 3 has the highest peak density, and the background level is less clear. In case of extreme peak overlap, the peak search may detect a group of peaks as one peak, e.g., the W-L_β lines in Fig. 1. In the latter case, additional information about a few more L_β lines was added to the peak list by the operator. If the peaks to be added to the peak list are listed in the program, then the peak list can be extended automatically (after a qualitative analysis). With increasing peak density, the best value of the FWHM factor decreases. The effect of decreasing the FWHM factor is to decrease the peak area. For the tungsten lines in Fig. 1, a change of the factor value from 4 to 3 reduced the peak areas by 1—2%. The lines in the tungsten spectrum are intense; in contrast, some of the lines in Figs. 2 and 3 are small. For these small lines, the peak areas were reduced as much as 30% by decreasing the FWHM factor from 2.5 to 1.5 (Fig. 3). However, such extreme reductions were observed only in cases where one peak region was sliced into two peak regions as a consequence of the decrease in the FWHM factor. For example, in Fig. 3, the Se-K_α and As-K_β lines are handled in one peak region for a FWHM factor of 2.5 and in individual regions for a FWHM-factor of 1.5. When the peak regions were not sliced, the reduction in peak areas was less than 5%.

The peak areas of the lines in the SRM 1201 spectrum were used for quantitative evaluation by means of the VAP program [10]; in the mode used, the calculation of the calibration constant was included in the iterative procedure. When the peak areas were obtained after background subtraction with different FWHM factors, the concentrations found were alike within an absolute deviation of 0.1% (w/w). The absence of the normal effect of decreasing peak areas on the quantitative results is a consequence of treating the calibration constant as a scaling factor. In the case of the fly ash spectrum, the qualitative analysis is incomplete, and consequently, a previously established absolute calibration has to be used in the quantitative calculation. In this case, the resulting concentrations are affected in the usual way.

Effect of acquisition time

Figure 4 shows the calculated backgrounds obtained by the LM algorithm and the Butland interpolant in four selenium spectra with acquisition times

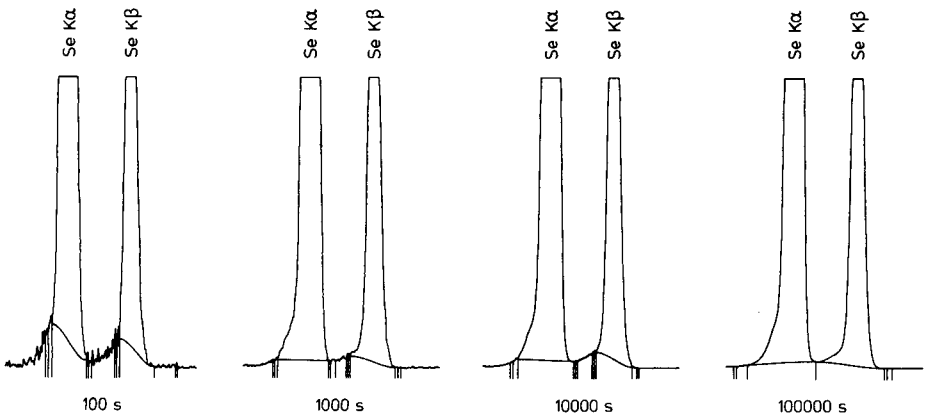

Fig. 4. Estimated backgrounds in spectra of selenium from 1.5% (w/w) Se/98.5% (w/w) binder. The backgrounds are based on the Butland interpolant and the LM algorithm with a FWHM factor of 3.0. The acquisition times for the spectra are indicated as are the knots used by the spline.

of 100 s, 1000 s, 10 000 s and 100 000 s, respectively. The counts in the Se-K_α peaks are are about ten times the counts in the background. For the 100-s spectra, large statistical fluctuations produce local minima on the low energy tail and not on the true background. This drawback is eliminated if the counting time is increased to give suitable counting statistics in the channels at the foot of the peak. For the present case, the counts per unit time increased 2% from the 100-s spectrum to any of the other spectra. The increase from the 1000-s spectrum to the 100 000-s spectrum was less than 0.05%.

APPENDIX. CALCULATION OF THE CUBIC SPLINES

The cubic spline connects a set of $N + 1$ knots using N cubic polynomials, $P_k(x)$, of the form:

$$P_k(x) = A_k + B_k(x - X_k) + C_k(x - X_k)^2 + D_k(x - X_k)^3 \text{ (for } X_k \leqslant x \leqslant X_{k+1})$$

where k refers to the interval number, given by the adjacent two knots (X_k, Y_k) and (X_{k+1}, Y_{k+1}); X is the channel number and Y is the count value assigned to the channel. Here, $\Delta X_k = X_{k+1} - X_k$ is defined as the difference between channel numbers and $\Delta Y_k = Y_{k+1} - Y_k$ as the difference between counts; S_k and S_{k+1} are the slopes in the two knots defining the interval. Thus the coefficients on P_k are calculated from:

$$A_k = Y_k$$

$$B_k = S_k$$

$$C_k = (3\Delta Y_k/\Delta X_k - S_{k+1} - 2S_k)/\Delta X_k$$

$$D_k = (S_{k+1} + S_k - 2\Delta Y_k/\Delta X_k)/(\Delta X_k)^2$$

Case 1. For the Butland interpolant, the slopes [5] are determined locally:

$1/S_k = \alpha/(\Delta Y_{k-1}/\Delta X_{k-1}) + (1-\alpha)/(\Delta Y_k/\Delta X_k)$ if $(\Delta Y_{k-1}/\Delta X_{k-1})(\Delta Y_k/\Delta X_k) > 0$

$S_k = 0$ if $(\Delta Y_{k-1}/\Delta X_{k-1})(\Delta Y_k/\Delta X_k) < 0$

with

$\alpha = 1/3(1 + (X_{k+1} - X_k)/(X_{k+1} - X_{k-1}))$

S_{k+1} is found analogously to S_k. In the first and last knots, the slopes are given by $S_1 = \Delta Y_1/\Delta X_1$ and $S_{N+1} = \Delta Y_N/\Delta X_N$.

Case 2. The cubic spline 2 is determined from the conditions that the spline itself, the slope (first derivative) and the curvature (second derivative) are continuous functions. The slopes in all knots are found simultaneously by solving $N-1$ equations of the form [9]:

$$\Delta X_m S_{m-1} + 2(\Delta X_{m-1} + \Delta X_m)S_m + \Delta X_{m-1}S_{m+1} = 3(\Delta X_m \Delta Y_{m-1}/\Delta X_{m-1} + \Delta X_{m-1}\Delta Y_m/\Delta X_m)$$

where $m = 2, 3, \ldots\ldots, N$. For the first and last knots, the slopes are given as in case 1.

REFERENCES

1 H. L. Bank, A. J. Forst and C. F. Lam, Ultramicrosc., 5 (1980) 153.
2 M. J. Koskelo, P. A. Aarnio and J. T. Routti, Nucl. Instrum. Methods, 190 (1981) 89.
3 E. Marageter, W. Wegscheider and K. Muller, Nucl. Instrum. Methods, B1 (1984) 137.
4 D. D. Burgess and R. J. Tervo, Nucl. Instrum. Methods, 214 (1983) 431.
5 R. J. Tervo, T. J. Kennet and W. V. Prestwich, Nucl. Instrum. Methods, 216 (1983) 205.
6 B. B. Jensen and N. Pind, Anal. chim. Acta, 171 (1985) 101.
7 S. Brodersen, Procedure TOP (MATBIB; VAX 11/780), Department of Chemistry, Aarhus University, Denmark, 1984 (available on request).
8 S. J. B. Reed, in V. D. Scott and G. Love (Eds.), Quantitative Electron-Probe Microanalysis, Horwood, Chichester, 1983, p. 90.
9 S. D. Conte and C. de Boor, Elementary Numerical Analysis Algorithmic, an Approach, 3rd edn., McGraw-Hill, London, 1980, p. 289.
10 B. B. Jensen, J. N. Marcussen and N. Pind, Anal. Chim. Acta, 161 (1984) 175.
11 L. H. Christensen, S. E. Rasmussen, N. Pind and K. Henriksen, Anal. Chim. Acta, 116 (1980) 7.
12 C. J. Sparks, Jr., Adv. X-ray Anal., 19 (1976) 19.

Analytica Chimica Acta, 184 (1986) 143—149
Elsevier Science Publishers B.V., Amsterdam — Printed in The Netherlands

COMPUTER-ASSISTED STRUCTURE/TASTE STUDIES ON SULFAMATES BY PATTERN RECOGNITION METHODS

YOSHIKATSU MIYASHITA, YOSHIMASA TAKAHASHI[a], CHIYOZO TAKAYAMA, TAKEHIKO OHKUBO, KIMITO FUNATSU and SHIN-ICHI SASAKI*

Laboratory for Chemical Information, School of Materials Science, Toyohashi University of Technology, Tempaku-cho, Toyohashi 440 (Japan)

(Received 3rd February 1986)

SUMMARY

Structure/taste relationships for fifty carbosulfamates were investigated by means of pattern recognition. The SIMCA method was used to classify the compounds into sweet or unsweet categories. As a result of feature selection, four descriptors were shown to be significant in modelling the sweet compounds. A compound predicted to be sweet by the model equation was synthesized and found to be three times sweeter than sucrose.

In order to develop satisfactory new synthetic sweeteners, it is desirable to investigate the structure/taste relationships of sweeteners. Cyclohexylsulfamate (cyclamate) was widely used as an artificial sweetener. The structure/taste relationships of sulfamates ($R—NHSO_3Na$) were studied by Pautet and Nofre [1] and by Spillane and co-workers [2, 3]. Pautet and Nofre reported that if sulfamates were to be sweet, then certain steric conditions of R were required.

The structure/taste relationships of perillartines [4, 5] and aspartyl dipeptides [6] have been investigated by means of pattern-recognition methods. In this paper, structure/taste relationships of fifty carbosulfamates were investigated by using the pattern-recognition method, SIMCA.

CHEMICAL STRUCTURE AND PATTERN REPRESENTATION

Fifty compounds (14 sweet, 36 not sweet) were used to analyze the structure/taste relationships. The chemical structures of the compounds, with the references from which the data were taken, are shown in Table 1. The sweet compounds are assigned to class 1 and the unsweet compounds to class 2.

In order to apply pattern-recognition techniques, chemical structures can be represented by several descriptors. It is known that the taste response is a

[a]Present address: Research Center for Chemometrics, Toyohashi University of Technology, Tempaku-cho, Toyohashi 440, Japan.

0003-2670/86/$03.50

function of the size, shape and functional groups of a molecule. Therefore, molar refractivity (MR) was used to represent the size, the STERIMOL parameters (L, B_1, B_0, B_r and B_l) were used to represent the shape, and Taft's σ^* was used to represent the functionality of the R group of the carbosulfamate molecule. The pattern vector is thus seven-dimensional:

$$X = (MR, L, B_1, B_0, B_r, B_l, \sigma^*)$$

Here, the naming of some of the STERIMOL parameters has been changed, because the STERIMOL B parameters contain no information about direction; L is the length of substituent R; the B parameters are the widths in the direction perpendicular to the L axis, B_1 being the minimum width of a substituent, B_0 being the parameter in the opposite direction to B_l, and B_r and B_l the right- and left-hand widths, respectively. In the case of the cyclohexyl group, these parameters are illustrated in Fig. 1.

The SIMCA method

The class-modelling technique SIMCA [20] describes the similarities between the objects of a class by a principal component model based on r_q components for class q:

$$x_{ik}^{(q)} = \alpha_k^{(q)} + \sum_{\beta=1}^{r_q} z_{i\beta}^{(q)} t_{k\beta}^{(q)} + \epsilon_{ik}^{(q)} \tag{1}$$

where $x_{ik}^{(q)}$ is the measurement of variable k for object i in class q, $\alpha_k^{(q)}$ is the mean value of a descriptor k in class q, $t_{k\beta}^{(q)}$ is the loading giving the correlation of variable k with the principal component β, $z_{i\beta}^{(q)}$ is a factor depending only on the object i, and $\epsilon_{ik}^{(q)}$ is the residual describing that part of the data which cannot be explained by the class model q; r_q is the number of components in class q and is estimated by the cross-validation technique. The confidence interval of class q is given by $RSD^{(q)}$, which is defined by

$$RSD^{(q)} = [\sum_{i}^{n_q} \sum_{k}^{d} \epsilon_{ik}^{(q)^2} / (n_q - r_q - 1)(d - r_q)]^{1/2} \tag{2}$$

where n_q is the number of compounds in class q, and d is the number of descriptors.

Each data vector x_{ik} can be fitted to the class parameters by multiple regression:

$$x_{ik} - \alpha_k^{(q)} = \sum_{\beta=1}^{r_q} u_{i\beta}^{(q)} t_{k\beta}^{(q)} + e_{ik}^{(q)}$$

How well the data vector fits the model is expressed by its residual standard deviation, $D_i^{(q)}$:

$$D_i^{(q)} = [\sum_{k}^{d} e_{ik}^{(q)^2} / (d - r_q)]^{1/2} \tag{3}$$

TABLE 1

Descriptor values for R group of carbosulfamates

No.	NH—R	Taste[a]	*MR*	*L*	B_1	B_0	B_T	B_l	σ^*	Ref.
1	n-Propyl	S	15.0	4.92	1.52	3.49	1.91	1.91	−0.12	7—9
2	n-Butyl	S	19.6	6.17	1.52	4.43	1.92	1.90	−0.13	7—11
3	2-Methylbutyl	S	24.2	6.17	1.52	4.43	3.16	1.90	−0.16	12
4	Isopentyl	S	24.3	6.17	1.52	4.43	3.15	1.92	−0.16	12
5	Isobutyl	S	19.6	4.92	1.52	4.21	3.16	1.90	−0.13	7, 8, 11, 12
6	Neopentyl	S	24.3	4.92	1.52	4.22	3.16	3.15	−0.17	8
7	Cyclohexyl	S	26.7	6.06	1.91	3.24	3.59	2.81	−0.15	13
8	2-Methylcyclohexyl	S	31.3	6.06	1.91	3.24	3.77	3.59	−0.15	13
9	3-Methylcyclohexyl	S	31.3	6.15	1.91	4.47	3.59	3.35	−0.15	12
10	Cyclopentyl	S	21.5	4.90	1.90	4.06	3.42	2.58	−0.20	14
11	2-Methylcyclopentyl	S	26.1	4.90	1.90	4.06	3.62	3.42	−0.20	12
12	3-Methylcyclopentyl	S	26.1	5.91	1.90	4.06	3.42	2.58	−0.20	11, 15
13	Cyclopentylmethyl	S	26.1	6.05	1.52	4.11	2.86	2.86	−0.13	16, 17
14	Phenyl	S	25.4	6.28	1.71	1.71	3.11	3.11	0.60	13
15	Ethyl	NS	10.3	4.11	1.52	2.98	1.91	1.90	−0.10	8—10
16	n-Pentyl	NS	24.3	6.97	1.52	4.94	1.92	1.90	−0.16	8, 9
17	Isohexyl	NS	28.9	6.97	1.52	5.66	3.17	1.90	−0.16	18
18	2,3-Dimethylcyclohexyl	NS	35.9	6.15	1.91	4.47	3.77	3.59	−0.15	2
19	2,5-Dimethylcyclohexyl	NS	35.9	6.06	2.14	3.56	4.42	4.29	−0.15	14
20	2,6-Dimethylcyclohexyl	NS	35.9	6.06	1.91	3.24	4.50	3.77	−0.15	12
21	3,3,5-Trimethylcyclohexyl	NS	40.6	6.26	1.91	4.47	4.50	3.44	−0.15	19
22	2-Ethylcyclohexyl	NS	40.6	6.06	1.91	4.29	4.66	3.59	−0.15	14
23	4-tert-Butylcyclohexyl	NS	40.6	8.20	1.91	4.59	3.52	2.72	−0.15	2
24	4-tert-Pentylcyclohexyl	NS	49.9	8.98	1.91	4.59	3.52	2.72	−0.15	2
25	Cyclobutyl	NS	17.9	4.77	1.77	3.18	3.20	2.04	−0.15	7, 9
26	Cyclohexylmethyl	NS	31.3	6.12	1.52	5.30	3.26	3.14	−0.13	12
27	4-Ethenylcyclohexyl	NS	35.4	8.28	1.91	4.01	3.59	2.81	−0.15	2
28	Benzyl	NS	30.0	4.62	1.52	6.02	3.13	3.10	0.22	10, 11
29	1-Adamantyl	NS	40.6	6.17	3.16	3.16	3.49	3.49	−0.26	7
30	Methyl	NS	5.7	2.87	1.52	2.04	1.90	1.90	0.00	8
31	n-Hexyl	NS	28.9	8.22	1.52	5.88	1.92	1.90	−0.17	7, 13
32	n-Heptyl	NS	33.6	9.03	1.52	6.39	1.92	1.90	−0.17	7
33	n-Octyl	NS	38.2	10.27	1.52	7.33	1.93	1.90	−0.15	8
34	Isopropyl	NS	15.0	4.11	1.91	3.16	2.98	2.76	−0.12	8
35	1-Methylpropyl	NS	19.6	4.92	1.91	3.16	3.49	2.76	−0.21	8
36	1-Methylbutyl	NS	24.3	6.17	1.91	4.39	3.54	2.99	−0.23	8
37	1-Methylpentyl	NS	28.9	6.97	1.90	4.94	3.16	2.76	−0.26	8
38	1-Methylhexyl	NS	33.6	8.22	1.91	5.63	4.30	2.99	−0.27	8
39	1,2-Dimethylhexyl	NS	28.9	6.17	1.91	4.39	3.74	2.99	−0.23	8
40	1,3-Dimethylhexyl	NS	28.9	6.17	1.91	4.42	3.49	2.98	−0.26	8
41	1,4-Dimethylhexyl	NS	28.9	6.97	1.91	4.39	4.50	2.99	−0.26	8
42	1,2,2-Trimethylpropyl	NS	33.5	4.92	1.91	4.40	3.74	2.99	−0.29	8
43	t-Butyl	NS	19.6	4.11	2.77	2.98	3.16	3.15	−0.30	8
44	1,1-Dimethylpropyl	NS	24.2	4.92	2.77	3.49	3.16	3.15	−0.31	8
45	1,1,3,3-Tetramethylbutyl	NS	38.2	6.17	2.60	4.22	3.16	3.15	−0.36	8
46	Cyclopropyl	NS	13.5	4.14	1.55	3.08	3.24	1.81	−0.15	14
47	1-Methylcyclopentyl	NS	26.1	4.90	2.66	3.24	4.09	3.17	−0.30	12
48	1-Methylcyclohexyl	NS	31.3	6.06	2.73	3.48	3.30	3.16	−0.44	12
49	Phenylethyl	NS	34.6	8.33	1.52	3.16	3.12	3.11	0.08	13
50	Phenylpropyl	NS	39.3	6.67	1.52	7.47	3.14	3.10	0.02	13

[a]S, sweet; NS, not sweet.

If an object is part of the class training set, object i is classified by means of an approximate F-test with $(d - r_q)(n_q - r_q - 1)/n_q$ and $(n_q - r_q - 1)(d - r_q)$ degrees of freedom:

$$F = [(n_q - r_q - 1)/n_q] D_i^{(q)^2} / RSD^{(q)^2} \quad (4)$$

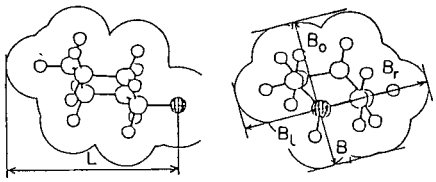

Fig. 1. Modified STERIMOL parameters for the cyclohexyl group.

If an object is not in the class training set, object i is classified by means of an approximate F-test with $(d - r_q)$ and $(n_q - r_q - 1)(d - r_q)$ degrees of freedom:

$$F = D_i^{(q)^2}/RSD^{(q)^2} \tag{5}$$

RESULTS

Fifty carbosulfamates were represented by 7-dimensional vectors. The descriptor values are shown in Table 1. These data were autoscaled. The dimensionality was estimated by the cross-validation method. Only the sweet class model was constructed. For the sweet class the dimensionality is 0. Feature selection was done according to the modelling power $\psi_k^{(q)}$:

$$\psi_k^{(q)} = 1 - S_k^{(q)}/S_{k,x}^{(q)} \tag{6}$$

where $S_k^{(q)}$ is the residual standard deviation of descriptor k for the training set in class q and $S_{k,x}^{(q)}$ is the corresponding standard deviation of the training set x in class q. The modelling power is shown in Table 2. These values indicate that only the MR, L, B_1 and B_0 parameters are significant. Therefore the vector becomes 4-dimensional.

The F statistics were calculated for classification as a sweet sulfamate or unsweet sulfamate. Comparison of the F statistics for each sulfamate in Table 3 shows that 13/14 or 93% of the sweet compounds and 24/36 or 67% of the unsweet compounds were correctly classified by the model. The average recognition rate is 80%.

The distances from each sulfamate to the two class models ($r_1 = 0, r_2 = 0$) are shown in Fig. 2. This Coomans plot shows that some of the sulfamates are outside the residual standard deviation, but all sweet sulfamates are within 2RSD. This indicates the existence of a well-defined cluster of sweet compounds. In order to visualize the four-dimensional descriptor space, the space was transformed to two dimensions by the Karhunen-Loève method. The plot is shown in Fig. 3. Two principal components describe 86% of the variance of the data. The sweet sulfamates cluster in a restricted area, as was suggested by the Coomans plot. The unsweet sulfamates are located around the sweet sulfamates. The structure of the data is asymmetric. Therefore, a classification method such as the linear learning machine cannot discriminate between sweet and unsweet sulfamates.

TABLE 2

Modelling power

Descriptor	MR	L	B_1	B_0	B_r	B_l	σ^*
Modelling power	0.496	0.585	0.513	0.349	0.219	−0.014	−0.354

TABLE 3

F statistics and residual standard deviation (D) for classification

No.	Class	D[a]	F-value[b]	No.	Class	D	F-value
1	1	0.66	1.72	26	2	0.78	2.27
2	1	0.46	0.85	27	2	1.12	4.66
3	1	0.37	0.55	28	2	1.08	4.27
4	1	0.37	0.55	29	2	2.10	16.23
5	1	0.47	0.86	30	2	1.66	10.14
6	1	0.38	0.57	31	2	1.28	6.04
7	1	0.42	0.72	32	2	1.69	10.49
8	1	0.56	1.26	33	2	2.33	19.95
9	1	0.57	1.27	34	2	0.86	2.75
10	1	0.41	0.68	35	2	0.56	1.14
11	1	0.39	0.61	36	2	0.39	0.56
12	1	0.30	0.35	37	2	0.74	2.00
13	1	0.30	0.35	38	2	1.30	4.79
14	1	0.96	3.67	39	2	0.47	0.80
15	2	1.07	4.19	40	2	0.47	0.82
16	2	0.68	1.71	41	2	0.62	1.42
17	2	0.96	3.39	42	2	0.68	1.71
18	2	0.77	2.20	43	2	1.54	8.69
19	2	0.88	2.87	44	2	1.39	7.15
20	2	0.77	2.19	45	2	1.41	7.28
21	2	1.02	3.81	46	2	0.91	3.02
22	2	0.99	3.59	47	2	1.28	6.05
23	2	1.33	6.53	48	2	1.38	7.03
24	2	1.89	13.14	49	2	1.15	4.83
25	2	0.58	1.23	50	2	1.83	12.28

[a]Class 1 RSD = 0.52. [b]For assignment to class 1, $F < F(4, 52)_{\alpha 0.05}$ = 2.55 for class 1, class 2, and test set.

Prediction of sweet taste

The structure requirement for substituents R of the sulfamates to produce a sweet taste is given by the inequality

$$F < F(4, 52)_{\alpha 0.05} \tag{7}$$

where F is given by Eqn. 5 for the test set and D is given by the equation

$$D = \{1/4[(MR - 24.4/8.77)^2 + (L - 5.68/1.46)^2 + (B_1 - 1.69/0.395)^2 + (B_0 - 3.89/1.15)^2]\}^{1/2} \tag{8}$$

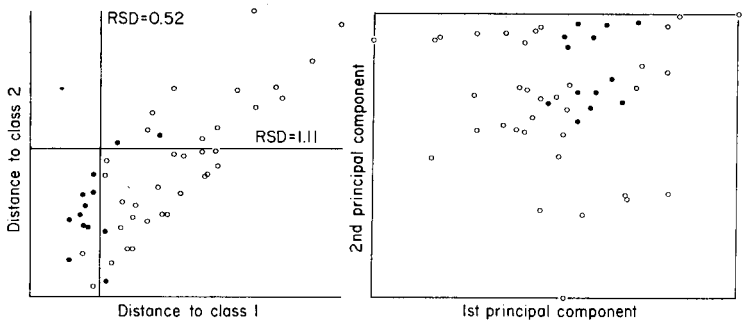

Fig. 2. Coomans plot: (•) sweet; (○) unsweet.

Fig. 3. Karhunen-Loéve plot: (•) sweet; (○) unsweet.

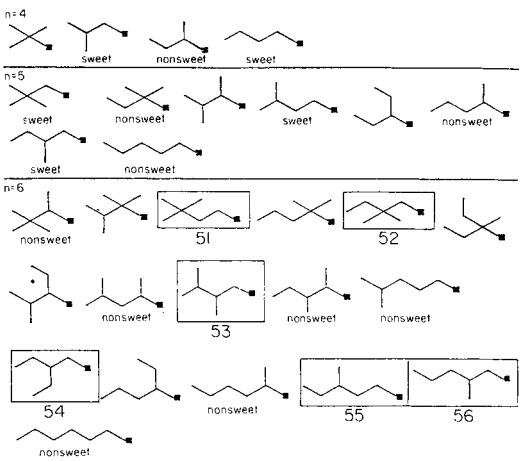

Fig. 4. All possible alkyl groups with n = 4, 5 or 6 for C_nH_{2n+1}—$NHSO_3Na$.

The alkyl groups can be considered as candidate substituents. First, the molar refractivities for C_4H_9, C_5H_{11} and C_6H_{13} are calculated by using the additive rule. The *MR* values (C_nH_{2n+1}) are 19.6, 24.3, and 28.9 for n = 4, 5, and 6, respectively. It is desirable that the *MR* value should be close to 24.4. Therefore, these alkyl groups seem to be proper substituents for producing a sweet taste.

All possible alkyl groups with carbon numbers of 4—6 were enumerated by CHEMICS [21]. The chemical structures are shown in Fig. 4; the taste quality observed is shown under the chemical structures. The sulfamates which have substituents at the α-position are not sweet and can therefore be eliminated from the list of candidate compounds. The six alkylsulfamates (nos. 51—56) remained.

The descriptor values and F statistics for these six test sulfamates are shown in Table 4. The six sulfamates satisfied inequality 7 and were therefore

TABLE 4

Prediction of taste quality

No.	*MR*	*L*	B_1	B_9	*D*	*F*-value
51	28.9	6.17	1.52	4.43	0.45	0.75
52	28.9	6.17	1.52	4.43	0.45	0.75
53	28.9	6.17	1.52	4.43	0.45	0.75
54	28.9	6.17	1.52	5.15	0.67	1.68
55	28.9	6.97	1.52	4.94	0.72	1.95
56	28.9	6.97	1.52	4.94	0.72	1.95

predicted to have sweet taste. Compound 51 was synthesized by the method of Audrieth and Sveda [13]. The sweetness of this compound is three times greater than that of sucrose.

It is concluded that the SIMCA method is powerful for predicting the taste qualities of sulfamates. The class models developed by SIMCA give the required information about the design of sweet sulfamates.

The authors thank the Computer Center, Institute for Molecular Science, for affording facilities for computation.

REFERENCES

1 F. Pautet and C. Nofre, Pharm. Acta Helv., 53 (1978) 231.
2 W. J. Spillane and G. McGlinchey, J. Pharm. Sci., 70 (1981) 933.
3 W. J. Spillane, G. McGlinchey, I. O. Muircheartaigh and G. A. Benson, J. Pharm. Sci., 72 (1983) 852.
4 Y. Takahashi, Y. Miyashita, Y. Tanaka, H. Abe and S. Sasaki, J. Med. Chem., 25 (1982) 1245.
5 Y. Takahashi, Y. Miyashita, Y. Tanaka, H. Hayasaka, H. Abe and S. Sasaki, J. Pharm. Sci., 73 (1984) 737.
6 Y. Miyashita, Y. Takahashi, C. Takayama, K. Sumi, K. Nakatsuka, T. Ohkubo, H. Abe and S. Sasaki, J. Med. Chem., in press.
7 G. A. Benson and W. J. Spillane, J. Med. Chem., 19 (1976) 869.
8 C. Nofre and F. Pautet, Bull. Soc. Chim. Fr., (1975) 686.
9 G. Hamprecht, D. Mangold and K. H. Koing, German Pat. 2164197 (1973).
10 W. W. Thompson, U.S. Pat. 2805124 (1957).
11 H. Yamaguchi, Japanese Pat. 13056 (1963).
12 B. Unterhalt and L. Boschemeyer, Z. Lebensm. Unters.-Forsch., 149 (1972) 227.
13 L. F. Audrieth and M. Sveda, J. Org. Chem., 9 (1944) 89.
14 B. Unterhalt and L. Boschemeyer, Z. Lebensm. Unters.-Forsch., 145 (1971) 93.
15 K. M. Beck and A. W. Weston, U.S. Pat. 2785195 (1957).
16 C. Nofre and F. Pautet, French Pat. 7345385 (1975).
17 C. Nofre and F. Pautet, Naturwissenschaften, 62 (1975) 97.
18 F. Pautet and C. Nofre, Z. Lebensm. Unter.-Forsch., 166 (1978) 167.
19 C. D. Hurd and N. Kharasch, J. Am. Chem. Soc., 68 (1946) 653.
20 S. Wold and M. Sjostrom, in B. R. Kowalski (Ed.), Chemometrics: Theory and Applications (ACS Symp. Ser. No. 52), Am. Chem. Soc., Washington, D.C., 1977, p. 243.
21 Y. Kudo and S. Sasaki, J. Chem. Inf. Comput. Sci., 16 (1976) 43.

Analytica Chimica Acta, 184 (1986) 151—164
Elsevier Science Publishers B.V., Amsterdam — Printed in The Netherlands

DIGITAL SIMULATION AS AN AID TO SAMPLE SCHEDULING IN A ROUTINE LABORATORY FOR LIQUID CHROMATOGRAPHY

BART VAN DE WIJDEVEN and JAAP LAKEMAN

Organon International B.V., Kloosterstraat 6, 5349 AB Oss (The Netherlands)

JO KLAESSENS*, BERNARD VANDEGINSTE and GERRIT KATEMAN

Laboratorium voor Analytische Chemie, Katholieke Universiteit Nijmegen, Toernooiveld, 6525 ED Nijmegen (The Netherlands)

(Received 27th December 1985)

SUMMARY

A computer model is described to aid decision-making in a routine laboratory for liquid chromatography. The managerial demand was to reduce the delay times of the samples in the laboratory despite an increasing sample input. Knowledge derived from records on the laboratory and from the experience of the laboratory staff is used to develop a simulation model of the laboratory. The model is applied to study the effects of several factors on the performance of the laboratory in order to trace the bottlenecks.

The value of analytical information depends on four factors: precision, accuracy, result delay and sampling planning [1]. The chemical or instrumental procedure remains vital, as precision and accuracy largely depend on it. However, because chemical analysis is essentially part of a decision-making process with regard to products or processes, it becomes important to evaluate what information is needed for a given purpose and at what cost. The analytical chemist is an expert who translates the client's problem into analytical constraints (the four factors mentioned above), gathers the optimal amount of information, converts it into common language and finally helps the client to solve the problem.

The result delay is the time lag between the sample entering the laboratory and the result becoming available and is usually governed by the organization of the laboratory. In studies of the operation of routine laboratories, it was found that it is not exceptional that samples requiring only a few hours of working time can remain in the laboratory for weeks [2—4]. Too large a delay time will decrease the value of the result, or even render it worthless.

For instance, if it is considered that, in order to control a chemical process, it has to be monitored more accurately, one would be inclined to increase the sampling frequency. However, the input to the laboratory will then increase and so will the delay times for results. If the laboratory already has a high workload, the increase in delay will be dramatic. The later the analytical

0003-2670/86/$03.50

result becomes available, the less valuable it will be for process control. In order to improve the monitoring of the process, the bottlenecks in the laboratory organization must be traced and removed.

Description of the problem

A routine laboratory can be a rather complex structure governed by implicit and explicit rules. The laboratory to be considered here is an independent section of a quality control laboratory for a producer of pharmaceuticals; liquid chromatography is done by four technical staff. The input of the section is rather complicated because there are four sources of sample, each of which has its own priorities: (1) from production, samples are taken from a batch of products which can only be released after a pharmacist has approved on the basis of the analytical results; (2) samples from a research department; (3) samples from a microbiology department; (4) samples for testing the shelf-life of pharmaceutical products. Most samples originate from production (Table 1). Every morning, the head of the laboratory decides on the samples that are to be analyzed that day, i.e., the workload. A technician takes a sample from the workload and runs the analysis. All four technicians are able to process all types of samples, and, as a consequence, to operate all h.p.l.c. instruments. In the laboratory, a priority rule is applied which is based on the delay times of the samples. In addition, production samples have priority because of their direct commercial consequences; batches of products must be stored until the analytical results become available.

Although the laboratory was facing an increasing sample input, a reduction in delay time (especially of production samples) was desired. Several solutions were possible: more equipment, increase of manpower, change in priority rules, and prior warning of the expected arrival times of the samples which would improve the planning within the laboratory. Because of lack of knowledge about the factors that govern the operation of the laboratory, these alternatives could not be evaluated. However, some knowledge was available: historical data on the laboratory and the experience of the laboratory

TABLE 1

Annual sample input (in sample units; total input of the real laboratory is 100); real laboratory (June 1982—May 1983) and five simulation runs with different random numbers

	Stability	Microbiol.	Research	Production	Total lab.
Real	7.8	4.2	26.1	61.9	100.0
Run 1	6.3	3.9	24.7	61.5	96.4
Run 2	4.6	4.3	30.7	62.1	101.8
Run 3	7.1	3.2	29.7	67.7	107.7
Run 4	4.9	4.3	30.1	65.9	105.2
Run 5	6.4	4.4	29.0	68.8	108.5

staff and personnel. From these sources, a decision support system based on digital simulation was designed. The former type of knowledge must be viewed in relation to commercially available laboratory information management systems (LIMS) [5] which will make the historical data more easily accessible.

CONSTRUCTION OF THE SIMULATION MODEL OF THE LABORATORY

A vast literature on simulation and many textbooks [e.g., 6, 7] are now available. However, only a few applications to clinical laboratories [8, 9] and analytical laboratories [2–4, 10] have been reported. These reports mainly investigate the suitability of digital simulation to describe an analytical laboratory [2] and the impact of various factors on the performance of the laboratory [3, 4, 10]. In the research reported here, the managerial objectives are easily discerned. Because of lack of well structured knowledge, it was decided to design a simulation model of the laboratory.

In the application of digital simulation to problem solving, three phases can be discerned: (1) the modeling phase in which a computer model of the laboratory is constructed; (2) model verification and validation; (3) the experimental phase in which simulation experiments are conducted to support decision making.

The modeling phase: description of the simulation model

An analytical laboratory can be defined as a network of service stations with an input of samples. During the modeling phase, both the network (structure) and the input are translated into a simulation model that approximates reality in its stochastic properties.

In general, a model consists of classes of objects and queues. A class contains rules and attributes and a specific object of this class is created by assigning values to these attributes. For instance, an object of the class "sample" can be specified by its origin, arrival time, due time, working time, etc. Objects can be stored in queues from which they are retrieved when some operation is about to be done, e.g., processing of a sample. To some extent, both translation processes can be considered separately.

In this study, the input generating part of the model was defined as a class of generators, consisting of four objects: the sample sources as previously mentioned. In order to specify the four generators, the real input of the laboratory was analyzed from filed historical data. From these files, approximately 100 different types of sample, characterized by the chromatographic procedure, were discernible. This number is too large to handle efficiently in the model and the low frequencies of many types make it rather unstable. Therefore a cluster analysis [2] was done in close cooperation with the laboratory personnel. This produced a reduction to 18 types, e.g., by combination into one new type of several types that required similar sample preparation and apparatus.

In order to quantify the generators, the main statistical characteristics of the real input were determined, i.e., distributions of input samples according to origin and type, and their mean values and standard deviations. In the model, each generator has a typical distribution of entries per day from which a random value is taken for each morning. Then, the type of every entry is established, also randomly according to a distribution that is specific with respect to the generator. It appeared that some types may enter the system in batches. So, for every entry the batch-size is evaluated according to a distribution that is specific with respect to generator and type. An entry may consist of one sample or of a batch of samples. Table 2 contains the relative input frequencies of the sample types of the production generator. The structure of the generating part of the model is depicted in Fig. 1.

The next step is the translation of the structure of the laboratory. The main building blocks are: a class of samples, a class of liquid chromatographs, a class of technicians and a planner. The planner contains the rules that control the sample throughput; to some extent it is the base of rules for the system. Many of its parameters cannot be reconstructed from the record files and must be estimated in close cooperation with the laboratory personnel. This also applies to many parameters of the other objects in the model. For instance, the preparation times of all sample types and their standard deviations were estimated in a session with the laboratory personnel. From these estimates, uniform distributions of preparation times were created, from which a random value was taken for every sample. Other parameters are well defined, e.g., chromatographic times and injection times.

Several queues are used in the model to store the samples before the different processes (Fig. 2). After generation, the samples are stored in a queue called shelf. Every morning, the planner takes the newly entered samples from the shelf and tries to combine samples of the same type into batches for which the total batch preparation time does not exceed 7 h. Treatment in batches reduces the total processing time in routine work. These combinations concern samples that enter the system simultaneously; they can always be combined if they have the same type; only the total preparation time serves as a restriction. Next, the planner tries to combine

TABLE 2

Production generator (model): types of generated samples and their relative frequencies

Type	Relative frequency	Type	Relative frequency	Type	Relative frequency	Type	Relative frequency
1	0.10	6	0.09	11	0.04	15	0.03
2	0.08	7	0.07	12	0.05	16	0.09
3	0.09	8	0.07	13	0.03	17	0.03
4	0.11	9	0.03	14	0.06	18	0.01
5	—	10	0.03				

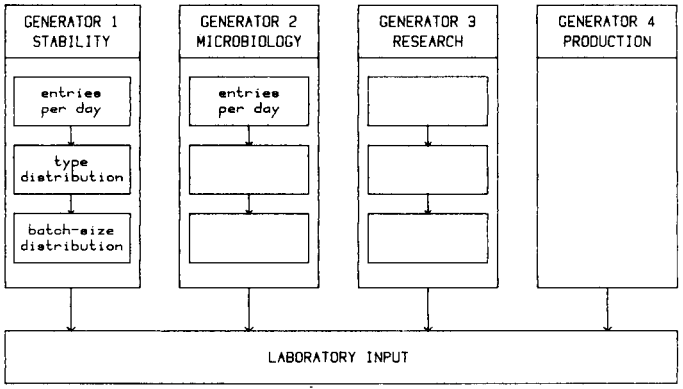

Fig. 1. Model of the input generators.

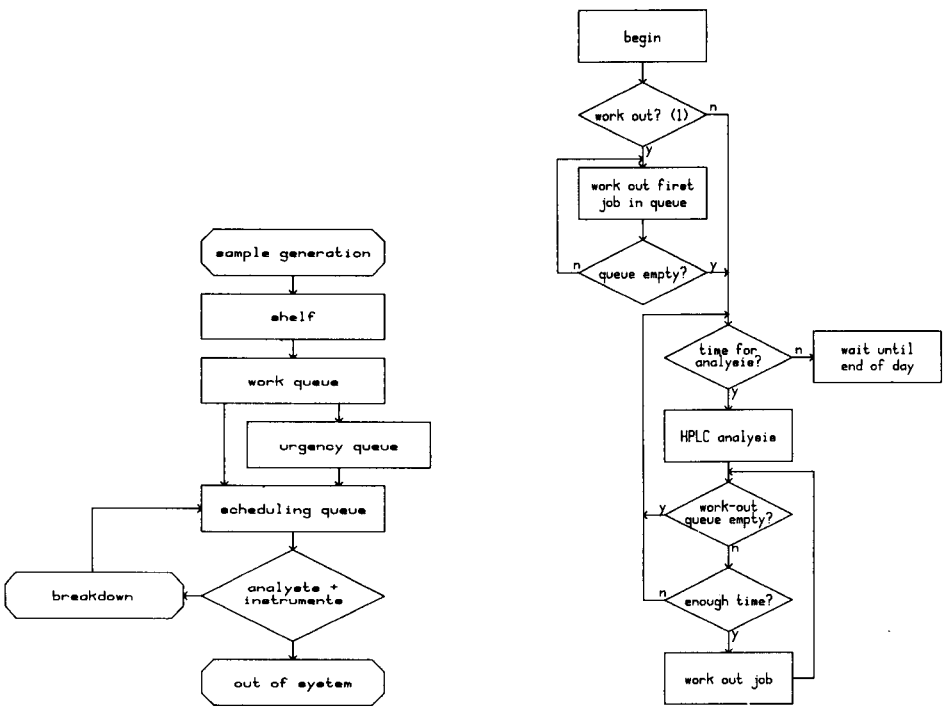

Fig. 2. Sample stream through the laboratory and the hierarchy of the queues (in rectangular boxes).

Fig. 3. Flow sheet of the activities of a technician; work out (1) asks if the total work-out time is longer than 5 h.

the newly entered samples with samples in the work queue that entered the system earlier. Combination of samples of the same type is not always possible at this stage. This was approximated in the model by the introduction of a so-called combination chance. The samples (or batches of combined samples which will also be referred to as samples) are placed in the work queue and ordered according to due time. The planner looks at all samples in the work queue to see if they should be in the urgency queue. Samples to be moved to the urgency queue are mainly production samples whose due time will elapse within a certain period ("urgency factor" days). Apart from these, there are urgent samples which enter the laboratory having short due times, and which may originate from all four generators. They must always be placed in the urgency queue. This reflects the real situation in which information is quickly needed, e.g., to anticipate a halt in a production line.

The planner's next job is to fill the scheduling queue which contains the samples that are to be processed, i.e., the workload of that day. Samples are assigned to all chromatographs that are available or will become available during the day. As many urgent samples as possible must be assigned and the samples will not be suitable for all instruments (varying from 1 to 5), thus establishing the workload is a rather complicated procedure. The technicians take the samples from the scheduling queue as required.

Compared to the planner where many implicit rules had to be stated explicitly, the other objects in the laboratory are relatively simple. A class of six h.p.l.c. instruments was defined. The objects of this class have rules only with respect to three states (active, passive and busy). The class covering technicians contains more activities. There are four technicians, one of whom is working in the model only when the workload is high. In reality, this fourth technician is called from elsewhere at need. The model has an advanced time handling mechanism and the simulation covers all day: the technicians start at 8.00 a.m. and work for eight hours a day. For simplicity, weekends are discarded. The job of the technicians consists of sample preparation and tuning of the chromatographs which actually run overnight. Then, the results must be calculated out and checked, a report is written. If the workload is high, these jobs accumulate until a work-out time limit has been exceeded. Figure 3 contains a flowsheet of the activities.

The model is completed with two disturbance processes in order to simulate the breakdown of an instrument. In case of the first kind of disturbance, immediate correction by the technician is possible after which the running job will be started from the beginning. It models the technician's decision from a first examination that the chromatography must be repeated because of some failure although the instrument did not break down. In the second case (breakdown of an instrument), immediate correction is not possible; the running job is rescheduled and the instrument becomes available again after a randomly distributed disturbance time.

Only a rough description of the simulation model has been given. Many details of the model are not mentioned because they are not essential for understanding the model.

Model verification and validation

A simulation model must gain credibility before it can be used to support decisions, i.e., it must be subjected to a test procedure which involves several steps [11]. Before the construction of the computer model is started, the plausibility of the model must be checked by the laboratory staff who know the organization. Other verification steps involve checking of historical data and checking whether the program runs as planned.

The next stage concerns validation of the model, i.e., its ability to predict the laboratory output if it is fed with input that shows the same statistical characteristics as the real input. Therefore the input generating part of the model must be tested first. Although there is some disagreement about the method to be used, the method of hypothesis testing is commonly adopted, i.e., the null hypothesis H_0 that there is no significant difference between model and reality. Five different simulation runs with different random numbers were used. The total sample input from the four generators is listed in Table 1. Figure 4 shows the real and one of the simulated input distributions of the total laboratory. The χ^2 test ($\alpha = 0.05$) indicated that none of the simulated distributions differed significantly from the real distribution. Autocorrelation functions of the real and simulated input showed that they are not significantly correlated in time.

After the input has been tested, the laboratory performance can be tested by comparing the real and simulated output. Usually, a model contains several parameters that are difficult to estimate beforehand. For instance, in the case of a high workload, a fourth technician is added to the laboratory; it is very difficult to express precisely the criterion to be used. Initially, there will be no agreement between simulated and real output because of these vague parameters, which must be tuned gradually until both outputs match. This process is called model calibration. Only the end results of the calibration are shown below. The simulation was run five times with different random numbers, so as to obtain statistical information about the behaviour of the model. Figure 5 shows the distributions of the delay times of the samples in

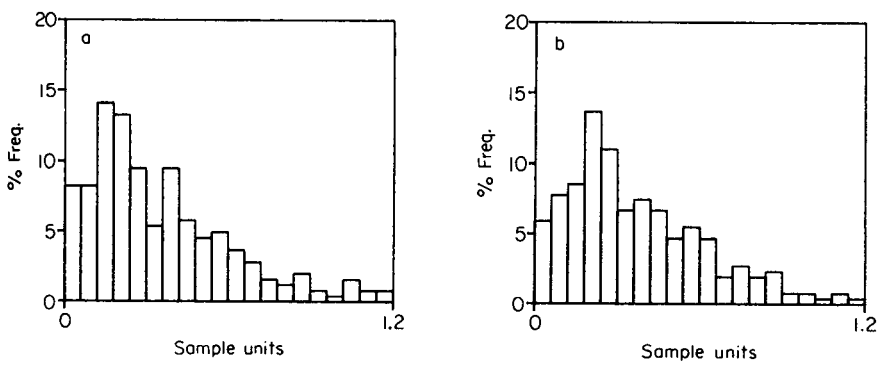

Fig. 4. Input distributions (% frequency vs. sample units) for the total laboratory: (a) real; (b) simulated.

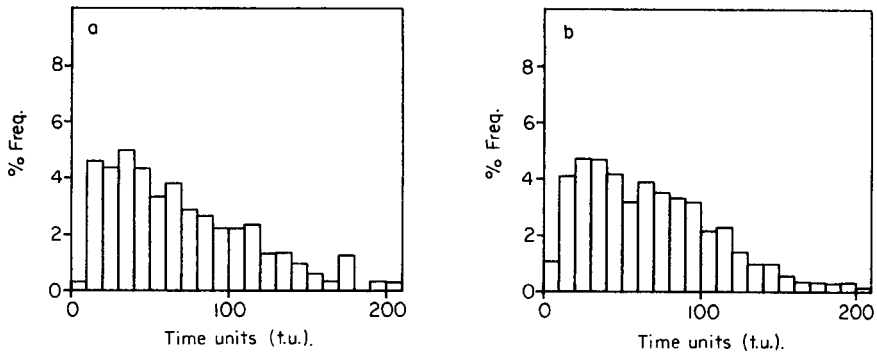

Fig. 5. Distributions (% frequency vs. time units) of the delay times for the total laboratory: (a) real; (b) simulated.

the real and the simulated laboratory; they resemble each other fairly well. The mean values of the delay times and the standard deviations are shown in Table 3; the delay times are correlated in time which may reduce the standard deviation. Therefore, the standard deviation was also calculated from the five simulation runs. Normal distribution of mean delay times was assumed. Because the real mean delay time belongs to the interval $x_m \pm ts$ (x_m and s are the mean value and standard deviation of the simulation runs, respectively, and t is Student's t for $\alpha = 0.05$ and d.f. = 4), there is no significant difference between simulated and real delay times, except for microbiology. The real value for microbiology is affected by some processing errors in the laboratory. As shown in Table 1, microbiology constitutes only a small part of the input and the difference will hardly affect the total performance. Some other factors were used to test the model, i.e., percentage of samples overdue, availability of instruments, mean number of combined samples, and the daily working times of the staff (Table 4).

From these results, reality and model coincide fairly well. Further refinement would be possible but the loss in clarity of the model and the extra cost would probably not compensate for the gain in reliability. The extent of refinement is not governed by what is possible but by what is optimal for managerial purposes. Even before any experiments were done, the simulation approach provided useful information on which parameters were important with regard to laboratory performance. However, better insight was gained from experiments.

EXPERIMENTAL

The model of the laboratory was written in PROSIM [12] which is a special simulation language based on PL/I. The program was run on an IBM 3081 mainframe computer. Simulation of the annual operation of the laboratory took about 30 cpu seconds.

TABLE 3

Mean delay times during the period 1982—1983 (in time units; the mean real delay time is 100) for real laboratory and five simulations. Standard deviations are given in parentheses

	Stability	Microbiol.	Research	Production	Total lab.
Real	258 (183)	20 (43)	147 (145)	66 (45)	100 (114)
Run 1	144 (150)	15 (6)	148 (116)	62 (31)	86 (82)
Run 2	278 (270)	16 (9)	184 (177)	68 (35)	107 (129)
Run 3	297 (232)	14 (6)	188 (142)	62 (33)	108 (121)
Run 4	282 (239)	16 (8)	160 (153)	62 (33)	94 (110)
Run 5	97 (115)	15 (8)	190 (219)	68 (40)	97 (128)
Mean runs	219 (92)	15.3 (1.0)	174 (19)	67 (3)	103 (9)

TABLE 4

Comparison of the performance of real laboratory and five simulations during 1982—1983

	Overdue[a] (%)	Machine av.[b]	Comb.[c]	Daily working hours[d]			
				1	2	3	4
Real	28.5	60—70	2.4	—	—	—	—
Run 1	21.4	61	2.1	6.39	6.58	6.34	2.78
Run 2	13.7	68	2.2	6.45	6.28	6.30	4.58
Run 3	25.8	66	2.4	6.37	6.45	6.35	4.31
Run 4	22.5	63	2.2	6.53	6.52	6.31	3.23
Run 5	24.1	66	2.3	6.24	6.20	6.31	3.26

[a]Percentage of samples with delay times that exceed the planned due time. [b]Mean availability of the instruments (%). [c]Mean number of samples combined into batches. [d]For technicians 1—4.

Historical data were used from the period June 1982—May 1983. A file of magnetic tape contained the arrival times and report times of all samples. A file of sample documents contained the characteristics for the samples: (a) number of independent determinations; (2) preparation time (e.g. an extraction, if needed, takes about 1.5 h); (3) type of chromatograph with its particular mobile phase; (4) number of injections per sample; (5) run time per injection. In addition to these data, many important characteristics of the laboratory were estimated in sessions with the laboratory staff.

APPLICATION OF THE SIMULATION MODEL

Conducting experiments

Experiments with a simulation model must be conducted very carefully. Essentially, the model can be no more than an approximation of the real

laboratory with regard to sample throughput. Because the validation was restricted to a limited time period and no generality in input was pursued, the model has only a limited reliability. Consequently, exploratory experiments can be trusted only if the effect of slight changes in the parameters is measured. These changes should not lead to a situation that is too far removed from the validated structure. However, careful experimentation within these limits will reveal the importance of the variables of interest.

The influence of some variables often depends on the level of the other variables. For instance, the effect of adding a new instrument will be negligible if the number of technicians is the real limiting factor, whereas it can be important if the system retains some flexibility with respect to manpower. With a minimal number of experiments, the interactions between variables can best be measured by means of experimental (or factorial) design. Extensive discussions of experimental designs, along with methods for constructing and evaluating the designs, were given by Davies [13] and Kleijnen [14].

Results of the experiments

In addition to the number of technicians and chromatographs, some other factors that give a better insight into the performance of the system were evaluated: (1) the due time of production samples (i.e., the major part of the input); (2) the fraction of urgent samples, i.e., generated with smaller due times (uniformly distributed from 2 to 10 days); (3) the workload factor (the workload for the next seven days is calculated every day, and if it exceeds the workload factor the fourth technician is called in and stability samples are no longer analysed); (4) the time needed to work out the results of a chromatographic run and to write the report; (5) repetition factor, i.e., the fraction (%) of repetitions of chromatographic jobs, which controls the first of the above-mentioned disturbance processes; (6) the mean interdisturbance time, i.e., the mean value of the negative exponentially distributed time between two instrument breakdowns; and (7) the urgency factor for which the samples are moved from the work queue to the urgency queue if the due time will elapse within a period of "urgency factor" days.

The main effects of these seven factors and some of their interactions can be measured by using a factorial design of 16 experiments. In order to obtain statistical information, each experiment was repeated. The high and low levels of all factors are listed in Table 5. The performance of the system was measured by means of the following entities: the delay times of research and production samples and of the total laboratory, and the total busy time of all technicians per day. The significant effects are listed in Table 6; none of the interactions appeared to be significant. The most important effect is clearly the work-out time. This is as expected; longer work-out times per sample will result in longer busy times. There is also an effect on the delay times which is larger for research samples because production samples have priority. The data indicate that the system is sensitive to changes that concern the workload of the technicians. A change in the urgency factor does

TABLE 5

Levels of the factors in the factorial design as compared to the normal values

Level	High	Low	Normal
Due time production (t.u.)	80	40	60
Urgent sample fraction (%)	20	3	10
Workload factor (h)	180	80	130
Work-out time (units)	1.5	0.5	1
Repetition factor (%)	25.5	4.5	15
Mean int. dist. time (t.u.)	20	10	15
Urgency factor (t.u.)	15	5	10

TABLE 6

Results of the factorial design

Level	Delay times (t.u.)			Busy times[a] (h)
	Research	Production	Lab.	
Due time rel.	—	19[b]	—	—
Urgent sample fraction	−66[c]	—	−18[d]	—
Workload factor	48[d]	—	18[d]	−0.7[c]
Work-out time	98[b]	15[c]	31[b]	3.8[b]
Repetition factor	—	—	—	—
Mean int. dist. time	—	−9[e]	—	0.5[d]
Urgency factor	—	—	—	—
St. dev. effects	22	5	14	0.46

[a]Mean working time per analyst. Student's t test (d.f. = 16); [b]significant $\alpha < 0.005$; [c]significant $0.005 < \alpha < 0.01$; [d]significant $0.01 < \alpha < 0.05$; [e]significant $0.05 < \alpha < 0.1$.

not cause a change in the workload; it appears to have no effect. Increased frequency of repetition obviously increases the workload somewhat, although no effect was measured. A higher frequency of machine breakdowns increases the workload more because the sample preparation has to be repeated. Indeed, some effect was measurable. The effects of the urgent sample fraction can be understood, because research samples normally have low priority but an increase of urgent samples with high priority reduces the mean delay time. Finally, the workload factor controls the activity of the fourth technician and therefore an increase of this factor causes a decrease of the total busy time of the technicians and an increase in the delay times. This factor, however, will strongly affect the delay times of stability samples; the effect was not measured.

All effects support the conclusion that the system is sensitive to changes in workload or, correspondingly, working capacity, and that other factors are less important. To confirm this conclusion, a new factorial design was

tested, a 2^2 design with two factors (number of technicians and number of instruments). The low levels of both factors are equal to the laboratory situation during 1982—1983. The high levels are an extra allround technician and an extra chromatograph. The measurements were made in duplicate. The significant effects are listed in Table 7. This design strongly indicates that a lack of manpower is the real bottleneck in the system.

The same experiments were conducted using the validated model for the period June 1983—May 1984. For this validation, only the input generation had to be adapted to a larger workload. The old and new inputs are compared in Table 8. In spite of the larger input, almost the same factors showed significant effects. For instance, in the 2^2 design with the factors technicians and instruments, only the effect of the number of technicians was significant, this time even more so because of the increased workload.

Conclusion

The most important conclusion to be drawn from the simulation experiments is that the managerial aim to reduce the delay times can best be met by increasing the working capacity of the laboratory. This conclusion was handed over to the laboratory management. The impact of adding extra personnel to a small laboratory is very large, and one must be careful not to

TABLE 7

Significant effects of the 2^2 factorial design (1982—1983); Student's t test (d.f. = 4)

	Delay times (t.u.)		
	Research	Production	Lab.
Technicians (a)	—92[a]	—22[b]	—42[b]
Instruments (b)	—	—	—
Interaction (a—b)	—	—	—
St. dev. effects	19	6	11

[a]Significant $0.005 < \alpha < 0.01$; [b]significant $0.01 < \alpha < 0.05$.

TABLE 8

Comparison of the performance of the real laboratory during 1982/1983 and 1983/1984

Factor	Difference (%)	Factor	Difference (%)
Total input (samples)	6.9	Overdue[a]	15.4
Delay times research	15.5	Samples in lab.	17.0
production	3.8	Technician hours per day[b]	6.9
lab.	7.4		

[a]The percentage of samples with delay times that exceed the planned due time. [b]Results obtained from simulations.

depart too far from the validated model. This would decrease the reliability of the conclusions. Moreover, a very extensive reorganization would not gain the support of the laboratory personnel, which is essential for success.

The best plan is to weigh the cost of extra staff against the profit resulting from the calculated reduction of due times of production samples, and to determine the optimum. In this case, it was optimal to add an extra technician, which could be on a temporary basis. After a while, the new situation can be evaluated to check whether the forecast improvement is real and a permanent settlement may then be established.

The construction of a simulation model is a time- and money-consuming activity. It took about six months to model the laboratory and conduct the experiments. In some applications, the investment would not be profitable if the simulation model were used only once. Mostly, however, the model is easily kept up to date and can be used for decision support over a long time.

Two recent developments may be important with respect to computer-aided decision-making based on digital simulation. First, application of artificial intelligence techniques [15, 16] can facilitate the construction of the model. The second important development is the introduction of a LIMS, which would make historical data more easily accessible and would facilitate the input and analysis. A LIMS offers only poor facilities with regard to decision-making as it cannot evaluate managerial proposals. Implementation of modules for expert modeling and simulation into a LIMS context will offer these facilities.

The authors are grateful to Mr. Rob Sierenberg (Sierenberg & de Gans B.V.) for his professional expertise in the use of PROSIM and his suggestions during the design and construction of the model. We are indebted to Mr. Chris Jansen (Organon International B.V.) for his valuable assistance and helpful comments throughout the project, and also to Mr. Henk van Zwam (Organon International B.V.) for the computer calculations and data reductions.

REFERENCES

1 B. G. M. Vandeginste, Analusis, 12 (1984) 496.
2 T. A. H. M. Janse and G. Kateman, Anal. Chim. Acta, 159 (1984) 181.
3 B. G. M. Vandeginste, Anal. Chim. Acta, 112 (1979) 253.
4 B. G. M. Vandeginste, Anal. Chim. Acta, 122 (1980) 435.
5 R. E. Dessy, Anal. Chem., 55 (1983) 70A, 277A.
6 J. A. Payne, Introduction to Simulation: Programming Techniques and Methods of Analysis, McGraw-Hill, New York, 1982.
7 A. M. Law and W. D. Kelton, Simulation Modeling and Analysis, McGraw-Hill, New York, 1982.
8 I. K. Väänanen, S. Kivitikko, J. Koskenniemi and A. Relander, Methods Inf. Med., 13 (1974) 158.
9 B. Sandblad, in M. H. Hamza (Ed.), Proceedings of the International Symposium and Course Simulation 1975, Acta Press, Calgary, Zürich, 1975, p. 364.
10 J. G. Vollenbroek and B. G. M. Vandeginste, Anal. Chim. Acta, 133 (1981) 85.

11 B. Page, Angew. Inf. Appl. Inf., 25 (1983) 149.
12 R. W. Sierenberg, in L. Dekker, G. Savastano and G. C. Vansteenkiste (Eds.), Simulations of Systems '79, 9th IMACS Congress Sorrento 1979, North-Holland, 1980, p. 997.
13 O. L. Davies (Ed.), The Design and Analysis of Industrial Experiments, Oliver and Boyd, Edinburgh, 1956.
14 J. P. C. Kleijnen, Statistical Techniques in Simulation, Dekker, New York, 1975.
15 J. W. A. Klaessens, G. Kateman and B. G. M. Vandeginste, Trends Anal. Chem., 4 (1985) 114.
16 S. A. Borman, Anal. Chem., 57 (1985) 983A.

Analytica Chimica Acta, 184 (1986) 165—172
Elsevier Science Publishers B.V., Amsterdam — Printed in The Netherlands

CONVERSION TECHNIQUES IN FLOW INJECTION ANALYSIS
Determination of Sulphide by Precipitation with Cadmium Ions and Detection by Atomic Absorption Spectrometry

BO A. PETERSSON, ZHAOLUN FANG[a], JAROMIR RŮŽIČKA* and ELO H. HANSEN
Chemistry Department A, Technical University of Denmark, Building 207, DK-2800 Lyngby (Denmark)

(Received 26th November 1985)

SUMMARY

A flow-injection system is described for on-line conversion of a soluble species to an insoluble compound by means of a tag-material which subsequently can be determined. This approach is used for the determination of sulphide by flame atomic absorption spectrometry, cadmium(II) ions being used as the precipitating tag-reagent. Excess of cadmium(II) is collected on a chelating ion-exchanger and later eluted. The detection limit for sulphide was 10 $\mu g\ l^{-1}$ and the sampling rate was 100 h^{-1}. Typical relative standard deviation was 1.2%. Of the potential interferences tested, only phosphate had any effect.

Determination of sulphide by flow injection analysis (f.i.a.) has been achieved with several detection techniques, such as chemiluminescence (0.4 $\mu g\ l^{-1}$) [1], amperometry (0.5 $\mu g\ l^{-1}$) [2], molecular emission cavity analysis (20 $\mu g\ l^{-1}$) [3], potentiometry with ion-selective electrodes (10^{-4} M) [4, 5], and spectrophotometry (10 $\mu g\ l^{-1}$) [6, 7]; the values in parentheses are the limits of detection. Good sensitivity, high sampling rate (>100 h^{-1}) and relatively cheap instrumentation are the main advantages for most of these techniques. The relative standard deviations are in all cases better than 4%.

The on-line use of ion-exchange columns in f.i.a. combined with atomic absorption spectrometry (a.a.s.) was first described by Olsen et al. in 1983 [8]. Since then, this versatile technique for preconcentration, matrix isolation and subsequent determination of heavy metals has undergone rapid expansion [9—14].

Very recently, a flow-injection conversion method for the determination of cyanide was reported [15]. This novel approach for anion determination is based on an on-line heterogeneous chemical reaction utilizing a flow-injection system comprising a column containing copper(II) sulphide by

[a]Present address: Institute of Forestry and Soil Science, Academia Sinica, Box 417, Shenyang, China.

0003-2670/86/$03.50

means of which the analyte is converted to a copper(I) cyanide complex which is then measured by a.a.s. (Fig. 1A). In the present work, a flow-injection system aimed at assay of anions and including a packed column and detection by a.a.s. is similarly applied. Here, however, the anion is converted to an insoluble compound by means of a cationic tag-material. The method was tested on the determination of sulphide via precipitation by cadmium(II) ions. Sample and reagent are injected simultaneously using the merging zones principle [16]. The excess of cadmium(II) is retained on a miniature ion-exchange column packed with a chelating resin which, after the detection of the cadmium sulphide precipitate, is eluted with nitric acid (Fig. 1B).

EXPERIMENTAL

Apparatus

The atomic absorption spectrometer was a Varian AA-1275 model connected to a Radiometer REC-80 recorder with a REA-112 high-sensitivity module. The sample uptake rate of the nebulizer was adjusted to 4 ml min^{-1}. A Varian cadmium hollow-cathode lamp was used as the light source and the signals at 228.8 nm were recorded.

Two Ismatec Model Mini-S-840 peristaltic pumps with tygon pump tubes were used in the system. The stop-go intervals of the pumps were controlled synchronously by a timer which was actuated by means of a microswitch at each turn of the valve.

The flow injection system (Fig. 2) comprised a rotary valve with 8 ports and furnished with two external loops for metering of the injected volumes of sample and cadmium tag-solution. The sample volume was 200 μl and that of the precipitating reagent (cadmium nitrate) was 250 μl. The ion-exchange column, made as described earlier [12], consisted of a suitable length of 2.5 mm i.d. tygon tube. The section filled with resin was 26 mm long. All connections were made with Microline tubing (0.5 mm i.d.).

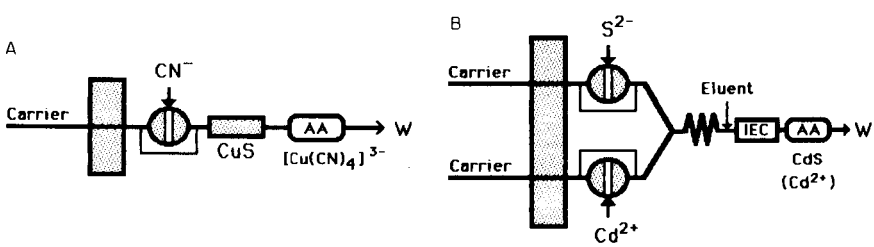

Fig. 1. Principles of conversion methods in f.i.a. (A) A manifold in which the analyte (cyanide) is converted in a packed column of copper(II) sulphide to tetracyanocuprate(I) which is detected by a.a.s. (B) The system in which the analyte (sulphide) is precipitated by cadmium(II) ions; the precipitate passes unhindered through the system and is detected by a.a.s. Excess of cadmium(II) is removed by the ion-exchange column (IEC) and later eluted.

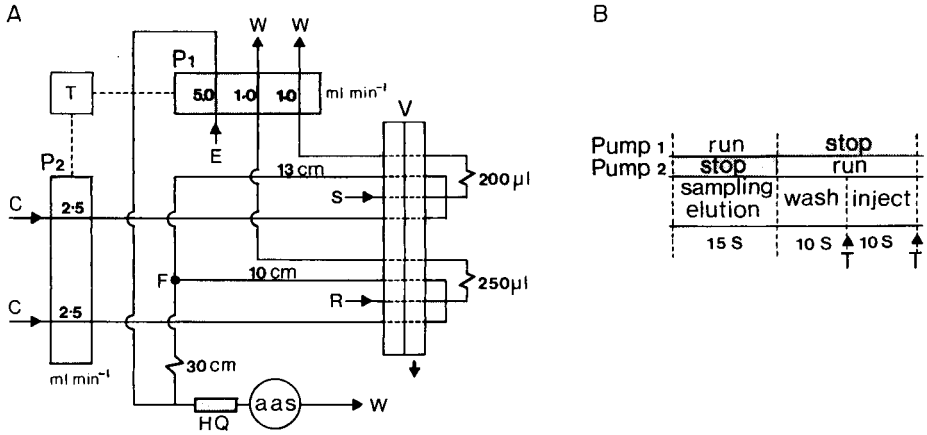

Fig. 2. (A) Flow-injection manifold for the determination of sulphide with detection by a.a.s., comprising two peristaltic pumps (P1 and P2), a timer (T), an injection valve (V) and an ion-exchange column (HQ): S, sample; C, carrier stream; R, reagent; E, eluent; and W, waste. (B) Time-sequencing program for valve operation; the points marked T indicate turn of the valve. For details, see text.

Reagents

A 25 mM ammonium acetate buffer was prepared by aqueous dilution of a 2 M ammonium acetate solution adjusted to pH 9.5 with 25% ammonia solution. An approximately 100 mg l^{-1} sulphide solution was prepared fresh daily by dissolving 0.75 g of sodium sulphide nonahydrate (Merck) in 1 l of the ammonium acetate buffer. The exact sulphide content was determined iodimetrically by titration [17]. Standard solutions of sulphide in the range 0.4—2.4 mg l^{-1} were made from the 100 mg l^{-1} standard solution by serial dilution with the ammonium acetate buffer (added in order to avoid any formation of H_2S). All samples were adjusted to contain 200 mg l^{-1} phosphate (added as disodium hydrogenphosphate).

A 10 mg l^{-1} cadmium solution was prepared by dilution of an aqueous 1000 mg l^{-1} standard solution of cadmium nitrate (BDH Chemicals) with the ammonium acetate buffer.

The 8-quinolinol chelating ion-exchanger was from Pierce Chemicals Co.; the 8-quinolinol is azo-immobilized to controlled-pore glass (CPG, 125—177-µm particle size and 50-nm pore size).

Procedure

The manifold was assembled as shown in Fig. 2, both pumps (P1 and P2) being connected to a timer (T) which controls their sequential operation (Fig. 2B). The lengths of the individual operational steps were as follows: injection 10 s, elution/sampling 15 s, and wash 10 s.

The analysis cycle is initiated by injecting 200 µl of sample solution and 250 µl of cadmium tag-reagent into two separate lines of carrier stream C

(25 mM ammonium acetate buffer of pH 9.5) propelled forward by pump P2. The cadmium nitrate and the sample are mixed when the injected zones merge at point F. If the sample contains sulphide, insoluble cadmium sulphide is formed. The mixture of cadmium sulphide and excess of cadmium(II) ions then flows through the ion-exchange column (HQ). All free cadmium ion is retained on the column while the cadmium sulphide passes through the column and into the a.a.s. instrument where cadmium is detected by measuring the absorption at 228.8 nm. When the recorded signal has reverted almost to the baseline level (after 10 s), the valve (V) is turned manually to the elution position which prompts the timer to trigger the operation of pump P1 and the stop of P2. During this sequence, all the cadmium(II) retained on the ion-exchange column is redissolved by the eluant (E, 1 M nitric acid) and transported to the nebulizer yielding a second peak (cf. Fig. 3). Simultaneously with the elution procedure, the next sample (S) and a fresh portion of cadmium(II) reagent solution (R) are aspirated into the loops of the valve. The elution/sampling period is completed after 15 s, whereupon pump P2 resumes action and P1 is stopped, allowing the system to be thoroughly washed by the slightly alkaline carrier solution. After 10 s, when the system is completely restored, the next sampling sequence can be initiated. The flow rates actually used are shown in Fig. 2.

Before closing down, the entire system is washed by pumping distilled water through all lines.

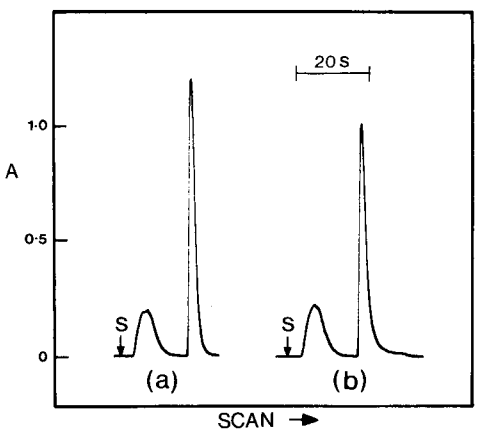

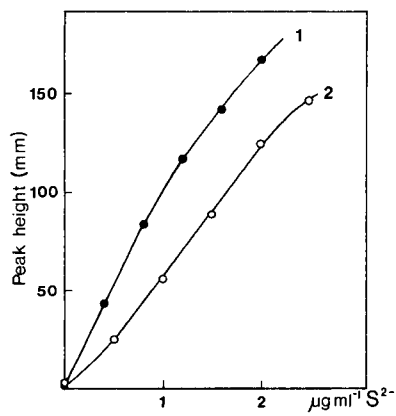

Fig. 3. Rapid-scan response curves obtained by injecting a sample containing 2 mg l^{-1} sulphide: (a) with 8-quinolinol (immobilized on controlled-pore glass) as the ion-exchanger; (b) with a column packed with 122 ion-exchange resin. In both cases, the first peak is due to cadmium sulphide, while the second peak is the signal produced on elution of excess of cadmium(II).

Fig. 4. Calibration graphs for sulphide, obtained by using the manifold depicted in Fig. 2: (1) sulphide standards which all contain 200 mg l^{-1} phosphate; (2) sulphide standard solutions containing no phosphate. All samples were prepared in 25 mM ammonium acetate buffer (pH 9.5).

RESULTS AND DISCUSSION

The metal ion selected for the conversion of free sulphide to an insoluble species for f.i.a./a.a.s. determination must fulfil several requirements. First, the solubility product of the metal sulphide formed must be low. Secondly, the sensitivity of the measurement of the selected cation must be high. Additionally, interferences caused by precipitation, possible coprecipitation, and complex formation with other ions must be considered.

Originally, silver was selected as the precipitating reagent because the measurement of silver by a.a.s. is very sensitive, yet this turned out to be of limited potential because of the strong interferences encountered from halides. Especially chloride, which is ubiquitous in most practical samples, caused interference by formation of silver chloride resulting in an increase of response. Consequently, cadmium(II) was chosen as the precipitating reagent, because the solubility product of cadmium sulphide is low (2×10^{-28}), the sensitivity of measurement of cadmium by a.a.s. is good, and, besides sulphide, very few anions form insoluble cadmium(II) compounds.

The manifold for the detection of free sulphide is shown in Fig. 2; a total flow rate of 5 ml min^{-1} was chosen because of the requirements of the nebulizing system of the spectrometer. Sample and precipitating reagent are injected as individual zones which downstream merge synchronously. It is important to note that the volume of the precipitating reagent is larger than that of the injected sample so that the sample zone is completely surrounded by the zone of cadmium solution, thereby ensuring that all the sulphide is converted to insoluble cadmium sulphide before passing through the ion-exchange column. If free sulphide were to be allowed to enter the column, the sulphide would react with the cadmium(II) withheld on it, leading to in situ formation of cadmium sulphide which then tends to be retained within the structure of the complexing material; this lowers the ion-exchange capacity, increases the flow resistance of the column and causes poor reproducibility of results. When the cadmium sulphide is formed before entering the column, this problem does not arise, very likely because the precipitate generated is primarily in a colloidal form.

The performance of various ion-exchange resins was investigated with respect to their ability to retain cadmium(II) and their ease of elution. The Dowex-50 and the Chelex-100 resins turned out to require long elution periods because of their strongly acidic characteristics. The weakly acidic 122 resin, which has a phenol-formaldehyde base with salicylate functional groups [13], showed excellent complexing ability for cadmium(II) ions and the elution was very fast. The 8-quinolinol chelating exchanger, which is immobilized on controlled-pore glass, turned out to be an even better choice than the 122 resin because of the pellicular character of the ion-exchange layer. The behaviour of the 122 and the 8-quinolinol resins is illustrated in Fig. 3.

Potential interferences to the proposed determination of sulphide can be divided into two groups: (a) anions which form insoluble or stable complex species with cadmium(II); and (b) cations which interfere through competition with the cadmium(II) retained on the column. Fourteen different ionic species were tested (Table 1), amongst which phosphate was found to constitute the only source of interference. The reason for the interference from phosphate may be ascribed to the low solubility product of tricadmium diphosphate ($K_{sp} = 10^{-32.6}$). Because phosphate is a commonly encountered species, its interference was investigated in greater detail. Surprisingly, it was found that phosphate alone did not yield any response when injected in a "blank" sample, i.e., in the absence of sulphide. A possible explanation of this phenomenon is that only in the presence of sulphide and ensuing precipitation of cadmium sulphide does cadmium orthophosphate coprecipitate, thereby giving rise to a positive error. This theory is confirmed by comparison of the respective peak heights for the elution peak in the presence and in the absence of phosphate. Further, it was found that it was possible to overcome the phosphate interference provided that the phosphate concentration in all samples was increased by addition of 200 mg l^{-1} orthophosphate. Raising the phosphate level by adding another 50 mg l^{-1} orthophosphate increased the response by only 5%. Generally, addition of phosphate results in a slight increase in sensitivity (Table 2) but also in a narrower linear range of measurement (Fig. 4), yet it has no influence on the limit of detection. A typical run for calibration is shown in Fig. 5.

Conclusion

A new conversion technique based on f.i.a. is described for the determination of anions by a.a.s. The novelty of the present approach is that it is based not on a heterogeneous exchange reaction (such as the previously described conversion of insoluble copper sulphide to the soluble detectable tetracyano-

TABLE 1

Determination of sulphide in the presence of potential interfering species
(All samples contained 2 mg l^{-1} sulphide in 25 mM ammonium acetate buffer.)

Ion[a]	Conc. added (mg l^{-1})	Interference (%)	
		A[b]	B[c]
Cl^-, NH_4^+, CO_3^{2-}, SCN^-, Ca^{2+}, Mg^{2+}, NO_3^-, SO_3^{2-}, SO_4^{2-}, $S_2O_3^{2-}$	100	0	0
PO_4^{3-}	100	+84	+5[d]
CN^-	2	0	0
I^-, Br^-	10	0	0

[a]Ions tested individually. [b]No phosphate originally present in samples. [c]200 mg l^{-1} phosphate added to all samples. [d]Only a further 50 mg l^{-1} phosphate added.

TABLE 2

Evaluation of the performance of the flow-injection system comprising a column containing different chelating resins, as used for the determination of sulphide in samples with and without addition of phosphate

Resin	Addition of 200 mg l^{-1} phosphate to sample	Characteristic conc. (mg l^{-1})	Detection limit (mg l^{-1})	R.s.d. (%)	Sampling frequency (h^{-1})
8-Quinolinol	—	0.040	0.007	1.3	100
	+	0.025	0.010	1.2	100
122	—	0.037	0.015	0.9	75
	+	0.030	0.013	1.2	75

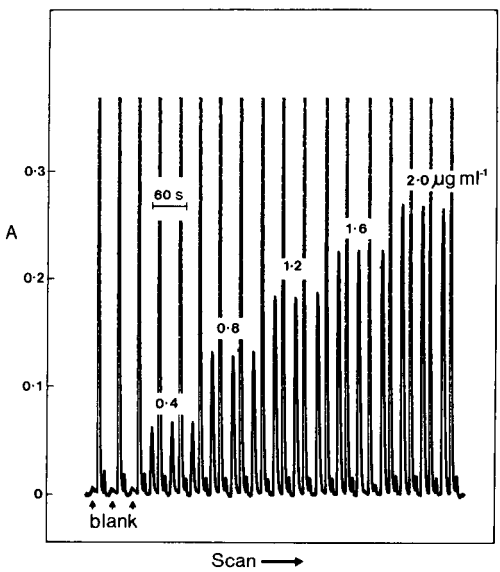

Fig. 5. Calibration run for sulphide in the concentration range 0—2 mg l^{-1} with the manifold depicted in Fig. 2. The elution peaks were all out of range of the recorder and so they appear to be of equal heights.

cuprate(I) ion [15]), but on a precipitation reaction with subsequent separation of unreacted excess of reactant by means of an ion-exchange column. The column material is not consumed (i.e., it does not become exhausted) because it is renewed during each cycle. In addition to the precipitate formed, only negatively charged complexes can pass through the cation-exchange column.

Atomic absorption spectrometers are available in most analytical laboratories. These new conversion techniques make it possible to increase the range of species accessible with such spectrometers. Apart from the determination of sulphide, the approach described in this paper could be applied

for the determination of other anions, such as fluoride or sulphate via precipitation of calcium fluoride or barium sulphate which are notorious in gravimetric analysis for initial precipitation in a colloidal form. Particular advantages of the proposed method are that it is based on simple chemical manipulations and requires limited ancillary apparatus.

The properties of the ion-exchanger are of great importance. Strongly acidic resins require longer elution periods than the weakly acidic chelating resins. Immobilisation of the chelating reagents on porous glass beads results in a faster ion-exchange process because of the pellicular character of the ion-exchanging layer. This type of preparation is therefore to be preferred to the conventional resin products.

The authors wish to express their appreciation to Inge Marie Johansen for conscientious technical assistance and to the Danish Council for Industrial and Scientific Research for partial financial support.

REFERENCES

1 J. L. Burguera and A. Townshend, Anal. Chim. Acta, 114 (1980) 209.
2 H. Ma and H. Yan, Kexue Tongbao, 27 (1982) 959.
3 J. L. Burguera and M. Burguera, Anal. Chim. Acta, 157 (1984) 177.
4 E. J. Duffield, G. J. Moody and J. D. R. Thomas, Anal. Proc., 17 (1980) 533.
5 M. G. Glaister, G. J. Moody and J. D. R. Thomas, Analyst (London), 110 (1985) 113.
6 M. O. Babiker and J. A. W. Dalziel, Anal. Proc., 20 (1983) 609.
7 D. J. Leggett, N. H. Chen and D. S. Mahadevappa, Anal. Chim. Acta, 128 (1981) 163.
8 S. S. Olsen, L. C. R. Pessenda, J. Růžička and E. H. Hansen, Analyst (London), 108 (1983) 905.
9 S. S. Jørgensen and K. Petersen, Paper presented at the 9th Nordic Atomic Spectroscopy and Trace Elements Conference, Reykjavik, Iceland, 1983.
10 F. J. Krug, B. F. Reis and S. S. Jørgensen, Proc. Workshop Locally Prod. Lab. Equip. Chem. Educ., Copenhagen, Denmark, 1984, p. 121.
11 F. Malamas, M. Bengtsson and G. Johansson, Anal. Chim. Acta, 160 (1984) 1.
12 Z. Fang, S. Xu and S. Zhang, Anal. Chim. Acta, 164 (1984) 41.
13 Z. Fang, J. Růžička and E. H. Hansen, Anal. Chim. Acta, 164 (1984) 23.
14 E. B. Milosavljevic, J. Růžička and E. H. Hansen, Anal. Chim. Acta, 169 (1985) 321.
15 A. T. Haj-Hussein, G. D. Christian and J. Růžička, Anal. Chem., 58 (1986) 38.
16 J. Růžička and E. H. Hansen, Flow Injection Analysis, Wiley, New York, 1981.
17 J. Williams, Handbook of Anion Determinations, Butterworths, London, 1979.

Analytica Chimica Acta, 184 (1986) 173—185
Elsevier Science Publishers B.V., Amsterdam — Printed in The Netherlands

AXIAL DISPERSION IN COILED TUBULAR REACTORS

DENYS F. LECLERC, PETER A. BLOXHAM[a] and E. CLIFFORD TOREN, JR.*

Department of Pathology, University of South Alabama, 2451 Fillingim Street, Mobile, AL 36617 (U.S.A.)

(Received 8th January 1986)

SUMMARY

A theoretical and experimental treatment of axial dispersion in coiled tubes is presented. The dispersion, δ, is related to the theoretical plate height divided by four times the radius of the tube ($H/4r$). This parameter, when plotted against the product of the Reynolds number and the Schmidt number ($ReSc$), accurately predicts maxima in dispersion curves. Variations in the boundary layer thickness and the velocity profile cause the dispersion to pass through a maximum at a constant value of log ($De^2Sc^{1\cdot14}$) equal to 6.13 for unretained solutes (De is the Dean number). A new measure of dispersion is proposed; the reduced dispersion, $\epsilon = 256/(Re^{0.667}Sc)$, is derived from the experimental behavior of dispersion at values of log ($De^2Sc^{1\cdot14}$) smaller than 6.13. The logarithm of ϵ is found to be approximately zero for $2.2 < \log (De^2Sc^{1\cdot14}) < 6.1$ and to decrease linearly with log ($De^2Sc^{1\cdot14}$) at higher values. Experiments with four solutes that have a wide range of molecular diffusivities are reported. Results agree with theory.

Secondary flow occurs when fluid passes through a curved tube. In conformity with Poiseuille flow, the greatest fluid velocity is found at the center of the channel; therefore, centrifugal forces will act there with maximum effect. The parabolic flow pattern is deflected toward the outer wall of the channel by radial or secondary flow. This creates a recirculating pattern in which fluid flows back inwardly along the walls. The recirculation generates two strong symmetrical patterns that effectively divide the tube into two cells. There is little exchange of liquid between the two halves. This results in markedly reduced axial dispersion [1] because diffusion occurs over smaller distances. Secondary flow also stabilizes laminar flow. Turbulent flow develops at much higher Reynolds numbers than that for straight tubes [2]. This lowering of axial dispersion is of considerable interest in chromatography, flow-injection systems and post-column reactor design.

Over the last ten years, many workers have studied dispersion phenomena in straight as well as coiled tubes. Dispersion in straight tubes is better characterized than for coiled tubes, because the theory for secondary flow is more difficult. The early phases of Poiseuille flow (viscosity-controlled) were

---

[a]Present address: Agricultural Chemicals Dept., E. I. du Pont de Nemours, Co., La Porte Plant, P.O. Box 347, La Porte, TX 77571, U.S.A.

0003-2670/86/$03.50

studied in straight tubes by Golay and Atwood [3]. The dispersion of a sample plug was simulated under varying conditions of flow rates. Elution profiles were found to approach a Gaussian distribution when more than thirty theoretical plates were generated. A sizable deviation from a Gaussian profile was observed with less than ten theoretical plates; indeed, doubly-peaked profiles were seen. Hoffman and Halasz [4, 5] studied mass transfer in straight and coiled open tubes. Plate heights at higher fluid velocities were much lower for coils than for similar straight tubes. It is well known that the velocity profile assumes a trapezoidal shape under the influence of secondary flow [6], and lies at a constant inclination from the general direction of flow. Truesdell and Adler [7] have numerically simulated the stream function that arises from this flow pattern; they used loose and tight coils, as well as solutes with various diffusivities. Austin and Seader [8] extended this work to higher Dean numbers. Trivedi and Vasudeva [9] have shown that coiling can reduce axial dispersion by as much as 500 times, under laminar flow conditions. Their data were obtained by changing the aspect ratio, λ, the ratio of the tube radius to that of the coil. Although the scatter of the points was quite high as the fluid velocity increased, a maximum in the dispersion curve was clearly visible. This had not been predicted by earlier theoretical treatments. Mass transfer in coiled tubes is usually evaluated by comparing the observed plate height, H, with the theoretical plate height, H_o, that would be obtained under similar conditions in a straight tube. (Notations and definitions are summarized in Table 1.) This is done by calculating a ratio, H/H_o, and plotting it against De^2Sc, where De represents the Dean number and Sc the Schmidt number of the solute. This ratio is assumed to be identical to a parameter, κ, that depends on the velocity profile. Jannsen [10] was the first to link (H/H_0) to De^2Sc. Other workers [11—13] have also calculated this ratio to characterize dispersion in coiled tubes, but no maximum could be predicted. Experimental data, when plotted in terms of (H/H_o) against De^2Sc, are widely scattered at intermediate and high values of De^2Sc, instead of falling on a common curve. However, this situation does not apply to lower velocities. For example, in the region where $210 < De^2Sc < 2300$, experimental data can be made to fit a common curve which is a function of $(De^2Sc)^{-1/3}$ [11—13]. Also, theory [14, 15] and experiment [16] show that Taylor dispersion behavior [17] occurs only for very low fluid velocities, i.e., for $De^2Sc < (2072/\pi^2)$ [16].

Tijssen [18] developed corrections for coiling effects on dispersion at intermediate and high fluid velocities. A correlation based on Sherwood numbers was used over a wide range of velocities to account for the behavior of κ. The behavior of the diffusion coefficient ratio is also related to the change in boundary layer thickness with increasing fluid velocity; however, predictions for plate heights drawn from the resulting equations were found to disagree by as much as a factor of ten too low [18]. Dispersion maxima are also predicted for velocities three times lower than those experimentally observed. The dispersion curve unexpectedly undergoes a change of slope at

TABLE 1

Notations and definitions

$C(\theta)$	C-curve profile function
d	Column diameter (cm)
D	Hypothetical axial diffusivity ($cm^2\ s^{-1}$)
D_r	Effective radial mass transfer number ($cm^2\ s^{-1}$)
D_s	Secondary flow component of D ($cm^2\ s^{-1}$)
D_m	Molecular diffusion coefficient ($cm^2\ s^{-1}$)
De	Dean number (dimensionless) ($Re\ \lambda^{1/2}$)
$f(k)$	Retention function (dimensionless) (= $[1 + 6k + 11k^2]/[1 + k]$)
H	Plate height (coiled tubes) (cm)
H_o	Plate height (straight tubes) (cm)
k	Column efficiency (dimensionless)
L	Column length (cm)
$Pe(r)$	Peclet number (dimensionless) (= $\bar{u}d\ D^{-1}$)
r	Column radius (cm)
R	Coil radius (cm)
Re	Reynolds number (dimensionless) (= $2r\bar{u}[\rho/\eta]$)
Sc	Schmidt number (dimensionless) (= $\eta/[\rho D_m]$)
Sh	Sherwood number (dimensionless)
t	Time (s)
$\bar{u}$	Mean fluid velocity ($cm\ s^{-1}$)
u_x	Component of fluid velocity in the axial direction
u_r	Component of fluid velocity in the radial direction
u_ϕ	Component of fluid velocity in the angular direction
x	Axial direction coordinate
δ	Intensity of dispersion (dimensionless) (= $D/\bar{u}d$)
ϵ	Reduced dispersion (dimensionless) (= $256DD_m/[(\bar{u}d)^{5/3}\ (\eta/\rho)^{1/3}]$)
η	Viscosity (poise)
Θ	Reduced time (dimensionless) (t/μ_1)
κ	Velocity profile parameter (dimensionless)
λ	Aspect ratio (dimensionless) (= r/R)
μ_1	First moment of elution profile (s)
μ_2	Second moment of elution profile (s^2)
ρ	Density ($g\ cm^{-3}$)
σ^2	Axial variance of a sample peak
ϕ	Angular cylindrical coordinate

velocities well below the maximum. That is, the experimental slope of the dispersion versus $ReSc$ on the ascending part was found to be 2/3 while the decreasing part of the curve has a slope of −4/3. Tijssen's theoretical development predicts the slope to be 1 and −1, respectively.

Tijssen's development warrants further research, because the equations he used were suitable only for an infinite retention situation. Some of the numerical constants used in the equations are inappropriate because the experiments were done without a stationary phase. In this paper, it is shown that, if the equations are modified to account for an unretained solute, theoretical predictions agree much more closely with experiments. Results were obtained over a wide range of flow rates and for four different solutes.

Results were also obtained from a novel dual-detector system that increases the precision and accuracy of plate-height measurements.

THEORY

According to Golay [19], the plate height, H, for straight, open columns is described by

$$H = (2D_m/\bar{u}) + (2\kappa_0 r^2)\,(f[k])_0\,\bar{u}/D_m \tag{1}$$

where D_m is the molecular diffusion coefficient, $\bar{u}$ the mean fluid velocity, κ the velocity profile factor, r the column radius and $f[k]$ the retention function. In straight tubes, the velocity profile is parabolic and κ becomes a constant, κ_0. The first term generally vanishes, because it is very small compared to the others. The retention function for straight tubes, $(f[k])_0$, becomes unity when there is no retention in the stationary phase. Hence

$$H_0 = (2\kappa_0 r^2 \bar{u})/D_m \tag{2}$$

where $\kappa_0 = 1/48$. In coiled tubes, the contribution from radial convection results in an additional term in the denominator of Eqn. 2. As diffusion processes are modified by radial flow, the molecular diffusion coefficient, D_m, becomes

$$D_r = D_m + D_s \tag{3}$$

where D_r is an effective mass transfer number having the units of diffusivity and D_s is the additional contribution of convection generated by secondary flow.

Following Tijssen [18], this concept can be used to modify the formal mass balance equation. For cylindrical coordinates [20] with x as the direction of flow,

$$\partial C/\partial t = D_m \nabla^2 C - [u_x(\partial C/\partial x)] + [u_r(\partial C/\partial r)] + [u_\phi(\partial C/r\partial\phi)] \tag{4}$$

to form

$$\partial C/\partial t = D\nabla^2_{r,\phi} C - u_x(\partial C/\partial x) \tag{5}$$

where D is a hypothetical axial diffusivity which in a plug-flow model [21] gives the same value of axial variance, σ_x^2, as in the real, three-dimensional case. The first term in D_m has been omitted, because $D_m \ll D$. The solution of Eqn. 5 is in a form similar to Eqn. 2:

$$H \approx (2\kappa r^2 \bar{u})/D_r \tag{6}$$

where the value of κ depends on the velocity profile. The function that describes D assumes different forms over several ranges of velocity. According to Tijssen [18], both sides of Eqn. 6 are divided by $4r$ and its right-hand side is multiplied by $(\rho/\eta)(\eta/\rho)$. Then, both the numerator and the denominator

are divided by D_m to obtain

$$H/4r = [2\kappa r\bar{u}(\rho/\eta)(\eta/\rho D_m)]/4(D_r/D_m) \quad (7)$$

where ρ is the fluid density and η its viscosity. With the usual definitions of the dimensionless Reynolds and Schmidt numbers, the equation can be written as

$$\delta = \kappa(ReSc)/4(D_r/D_m) \quad (8)$$

The dimensionless group, δ, is equal to $H/4r$ and is identical to the reciprocal of the radius-based Peclet number, $Pe(r)$, which is equal to $\bar{u}d/D$. The parameter δ can be expressed as $D/\bar{u}d$, where d is the tube diameter. This parameter is also related to the vessel dispersion number, $D/\bar{u}L$, by the geometric factor, (d/L), where L is the length of the tube [21].

Tijssen [22] found that the definition of the Sherwood number, Sh, for heat transfer also applies to mass transfer. Thus, κ can be expressed as

$$\kappa = [Shf(k)]^{-1} \quad (9)$$

In an unretained situation ($k = 0$), the retention function is unity and

$$\kappa = Sh^{-1} \quad (10)$$

whereas in Tijssen's derivation a situation of infinite retention is assumed, with $f(k = \infty) = 11$, and the velocity profile parameter becomes

$$\kappa = [11\,Sh]^{-1} \quad (11)$$

This equation is suitable only for infinite retention and has been erroneously used to discuss results obtained with no retentive stationary phase. Still following Tijssen [22] and the work by Kalb and Seader [23] and Dravid et al. [24], Eqn. 10 becomes

$$\kappa = 2.666\,De^{-1/2}Sc^{-0.14} \quad (12)$$

Because there is an uncertainty of at least a factor of two in the evaluation of a Sherwood number [18] (the exponent 0.14 is an average), the original equation was modified accordingly by multiplying the original constant 1.333 by 2. Equation 12 predicts a square-root decrease in κ with increasing velocity. Although κ can be different from κ_0, it is nonetheless considered a constant at velocities below the dispersion maximum. Likewise, the parameter (D_r/D_m) is constant at lower velocities. Diffusion distances are lower by a factor of two because the tube is divided into two parallel halves by the circulation pattern. Therefore, $D_r/D_m = 4$. At higher flow rates, the boundary layer thickness varies with fluid velocity [18] so that

$$D_r/D_m = (De^{1.5}Sc)/8000 \quad (13)$$

Finally, Eqn. 8 can be modified on the basis of the experimental data presented by Tijssen [18] to account for the actual dispersion observed

$$\delta = \kappa(Re^{0.667}Sc)/4(D_r/D_m) \quad (14)$$

This relationship seems to apply when $De^2Sc > 2300$.

Axial dispersion in coiled tubes with increasing fluid velocity will therefore be controlled by the behavior of the parameters κ and (D_r/D_m). Dispersion behavior can be predicted over a wider range of experimental conditions, based on the above. In liquids, the mass-transfer term is much more important than the molecular-diffusion term; therefore, two types of behavior are expected, given the experimental conditions encountered in this work.

At high flow rates, inertial forces distort the velocity profile. The combination of velocity profile modification and radial mixing causes a nonlinear increase in axial dispersion. Therefore, Eqn. 14 gives a more accurate description and

$$\delta = (Re^{0.667}Sc)/256 \quad \text{when } (ReSc > 10^4) \tag{15}$$

where $\kappa = 1/16$ and $D_r/D_m = 4$. This is in agreement with an estimate of $\kappa = 1/20$ by Tijssen and Wittebrood [25]. At yet higher flow rates, κ and D_r/D_m change with fluid velocity. Replacing κ and D_r/D_m in Eqn. 14 by the corresponding expressions in Eqns. 12 and 13 results in

$$\delta = (16000/3)/(Re^{1.333}Sc^{0.14}\lambda) \tag{16}$$

Consequently, a maximum in the dispersion curve can be predicted at the intersection of Eqns. 15 and 16. This occurs at a value of

$$\log De^2Sc^{1.14} = 6.13 \tag{17}$$

whereas Tijssen [18] obtained 5.4733, using a value of (D_r/D_m) equal to 6.39 and the factor of 11 given in Eqn. 11.

Here a new parameter, ϵ, is introduced, for which any dispersion maximum corresponds to the same value of that parameter versus $De^2Sc^{1.14}$. Because the intensity of dispersion, δ, is described by Eqn. 15 at lower velocities, it can be shown that for any solute

$$\log \epsilon \approx 0 \quad (\text{for } \log De^2Sc^{1.14} < 6.13) \tag{18}$$

and from Eqn. 16

$$\log \epsilon = 6.13 - \log De^2Sc^{1.14} \quad (\text{for } \log De^2Sc^{1.14} > 6.13) \tag{19}$$

The reduced dispersion is

$$\epsilon = 256\delta/(Re^{0.666}Sc) = (256\, DD_m)/[(\bar{u}d)^{1.666}(\eta/\rho)^{0.333}] \tag{20}$$

Trivedi and Vasudeva [9] used a similar parameter, $K_c = (DD_m)/(\bar{u}d)^2$ and obtained a curve whereas a plot of log ϵ against log $De^2Sc^{1.14}$ should show that all data points lie on a straight line. It is now clear that the excess curvature shown in their work is due to the extraneous factor $(\bar{u}d)^{-1/3}$ present in K_c.

The vessel dispersion number, $D/\bar{u}L$, can be expressed as

$$D/\bar{u}L = H/2L = \delta(d/L) \tag{21}$$

A very accurate estimate of $D/\bar{u}L$ can be obtained by convolving an upstream

detector response into a simulated downstream detector response. The simulated response is compared with the actual elution profile. The vessel dispersion number is changed iteratively until a good fit is obtained. Because a flow-through cell is used in ultraviolet detection, only the component of concentration that is parallel to the direction of flow is detectable; therefore, the form of Eqn. 5 changes to

$$\partial C/\partial t = D(\partial^2 C/\partial x^2) - u_x(\partial C/\partial x) \quad (22)$$

Substitution of the dimensionless parameters, $z = x/L$ and $\theta = t\bar{u}/L$, gives the analytically solvable equation

$$\partial C/\partial \theta = ([D/\bar{u}L][\partial^2 C/\partial z^2]) - (\partial C/\partial z) \quad (23)$$

This is an equation analogous to Fick's Second Law and has the exponentially-modified Gaussian (EMG) solution [21]

$$C(\theta) = [4\pi\theta(D/\bar{u}L)]^{-1/2} \quad \exp[-(1-\theta)^2/4\theta(D/\bar{u}L)] \quad (24)$$

The parameter θ is also expressed as t/μ_1, where μ_1 is the first moment of the sample profile $C(\theta)$. Plate heights obtained from the simulation can be used to validate results obtained from the moments measured at each detector.

Dispersion data obtained from solutes that have widely different Schmidt numbers should exhibit a dispersion maximum at approximately the same value of the parameter $De^2Sc^{1.14}$. Many authors [11—13, 18] have stated that the plate-height ratio (H/H_o), calculated from Eqns. 2 and 6, is a function of De^2Sc. Because of the Sherwood correlation dependence on $Sc^{0.14}$, (H/H_o) is better expressed as depending on $De^2Sc^{1.14}$. The (H/H_o) curves obtained from different solutes would be expected to fall on the same curve.

EXPERIMENTAL

Apparatus

An illustration of the apparatus is available in the paper by Fulton et al. [26]. A Varian Model 8500 HPLC gradient system (Varian Instrument Division, Palo Alto, CA, U.S.A.) was used as the carrier delivery unit. This system can supply continuous, pulseless flow throughout the system, under controlled flow conditions. Injections of 20-μl samples were made with a Rheodyne 7010 injector valve. A dual-detector system similar to the one shown earlier [26] was used. A pre-delay coil, 1790-cm long, was installed between the first detector and the injector. The main reactor coil, 2955-cm long, was installed between the first and second detectors. Both coils were 508-μm (i.d.) 316 stainless steel (Alltech Associates, Deerfield, IL). The coils were fabricated by winding the tubing around PVC pipes having an o.d. of 4.76 cm. The coils were maintained at a constant temperature (20 ± 1°C) by a Forma Scientific Model 2095 thermostated bath (Marietta, Ohio). The absorbance was measured at two different locations with two Micromeritics Model 787 variable-wavelength detectors with optically matched 12-μl flow

cells (Micromeritics Instruments Co., Norcross, GA). The output from each detector was monitored by a Kipp & Zonen BD41 dual-channel recorder (Kipp Analytica, Emmen, Holland).

Reagents

Protein solutions (1.2—1.6 g l^{-1}) were prepared as described by Walters et al. [27] in a 0.08 M sodium sulfate/0.02 M sodium acetate buffer, pH 7.0. The buffer was also used as the carrier for protein experiments. It was filtered through a 0.5-μm filter before use. Bovine serum albumin (A-5003, Sigma Chemical Co.), thyroglobulin (T1126, Sigma), and horse heart cytochrome C (no. 2666, Mol-Ranger, Pierce Chemical Co.) were used as macromolecular samples. An aqueous 4.31 mM phenol solution was prepared from phenol (Gold Label Grade 99.9%; Aldrich Chemicals).

Methods

All samples were passed through the coils at flow rates ranging from 0.05 to 24 ml min^{-1}. Most of the runs were made in triplicate, except for the very long experiments, in which case a single well-controlled run was made. Data acquisition was begun within 0.2 s of injection. The detection wavelengths were 214 nm for the proteins and 270 nm for phenol.

Data acquisition and software. The data-acquisition rate was constrained by the duration of the experiment and a maximum capacity of 5000 points per detector; thus, rates ranged from 0.05 to 20 Hz for all experiments. The signal from each detector was stored separately, using the program described below. The output from the detector was set to the integrator mode that gave a maximum signal of 5.12 V at full scale. A DECLAB 11/V03 with a 12-bit analog-to-digital converter (Digital Equipment Corp.) used a modified version of the acquisition program described earlier [26]. Data were reduced and displayed with a Digital Equipment Corporation GT-46 system that used a VT-11 graphic terminal system for display [26]. Parts of both software systems were substantially modified to accommodate greater storage capacity and to improve calculations. The algorithms pertaining to these calculations are discussed below.

Calculations. The plate height, H, can be calculated from the ratio of the first and second moments, μ_1 and μ_2, of the sample profile, $H = (\mu_2/\mu_1^2)L$, in which μ_1 and μ_2 are calculated according to Grushka's exponentially modified Gaussian model [28] which accounts for both peak asymmetry and tailing. The algorithm for this calculation was presented by Yau [29]. The influence of noise in the calculations is diminished by a threshold criterion that limits integration to peak regions in which the signal is higher than a preset value. The data were displayed and the baseline was established by the light pen on the VT-11 graphics monitor. Approximate peak boundaries were also given. Actual peak-profile boundaries were then obtained by software with baseline and threshold criteria. Plate heights were calculated in three different ways. Moments were first evaluated for each detector. The difference in variance

between the two detectors was also used. This was possible because of the additivity of variance. Finally, plate-height values were obtained from the vessel dispersion number calculated by numerically convolving and curve-fitting the simulated response of detector 1 with the actual profile from detector 2.

Theoretical calculations were made for each solute, using values of diffusion coefficients given by Walters et al. [27] for the protein solutes and by Bacon and Adams [30] for phenol. The Schmidt numbers were corrected to account for the slightly different density and viscosity of the buffer solution compared to pure water at 20°C. These data are presented in Table 2.

RESULTS AND DISCUSSION

The vessel dispersion numbers, $D/\bar{u}L$, were experimentally calculated for phenol and are shown in Fig. 1. They were obtained from plate-height measurements using peak moments. The results were compared with values obtained from the simulation method. The validation was performed for the phenol dispersion curve. These values for phenol were plotted against the estimates obtained by moments as shown in Fig. 1. Some scattering is visible although a linear fit gives a slope close to unity. Values of the intercept and of the slope for the eight lowest flow rates are 3.3×10^{-5} and 0.97, respectively. Plotting the difference between the two sets of values against the flow rate reveals (Fig. 2) that most of the scatter occurs at high flow rates, because of greater errors in measuring the moments as a peak becomes narrower. It is difficult to evaluate moments correctly with very narrow peaks because the acquisition rate is limited to 20 Hz which results in fewer points per peak. In this case, the convolution method is very successful in evaluating plate heights. For example, even when the number of plates drops below 30 and the profile becomes distinctly non-Gaussian, the simulation successfully convolves a doubly-peaked profile into a simulated curve that agrees very well with the experimental curve observed at the downstream detector. Figure 3 illustrates this point for thyroglobulin near its dispersion maximum. The relative discrepancy in variance between the actual and simulated profiles was 3.25% for the EMG function, 13.65% for the symmetrical Gaussian model proposed by Levenspiel [21] and 6.25% for the N-tanks-in-series model for

TABLE 2

Molecular weights, diffusion coefficients and Schmidt numbers of solutes

Compound	Molecular weight	D_m (10^{-7} cm^2 s^{-1})	Schmidt number
Phenol	94	84—77	1200—1300
Cytochrome C (horse heart)	13,500	11.6	8500
Albumin (bovine serum)	66,500	6.29	15,700
Thyroglobulin	650,000	3.45—2.65	28,600—37,300

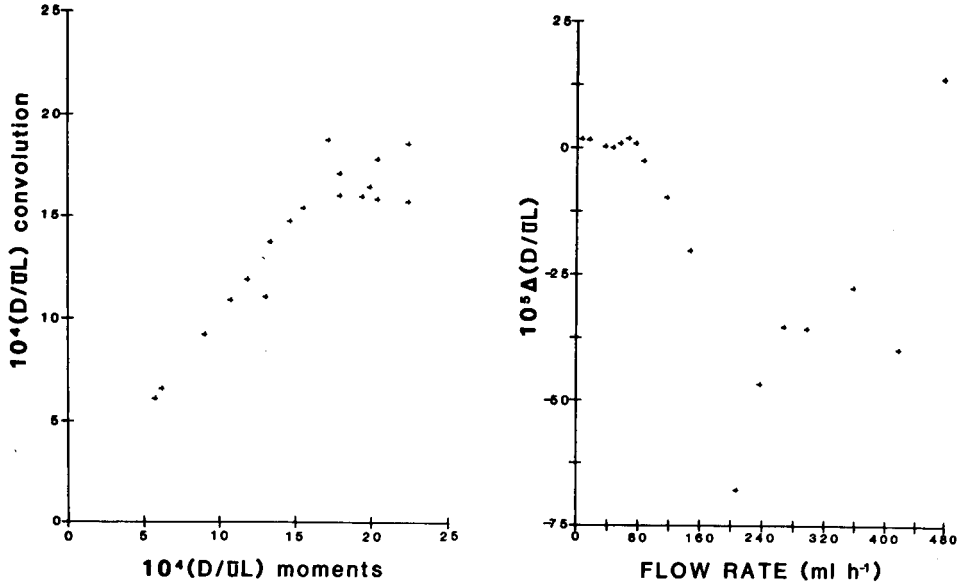

Fig. 1. Validation of the simulation method. $D/\bar{u}L$ values for phenol obtained from the convolution method are plotted against their corresponding value obtained from the moment method. Eight-point least-squares fits for lowest flow rates: slope, 0.97; intercept, 3.3×10^{-5}.

Fig. 2. Change in $(D/\bar{u}L)$ for phenol, obtained from Fig. 1, as a function of fluid velocity.

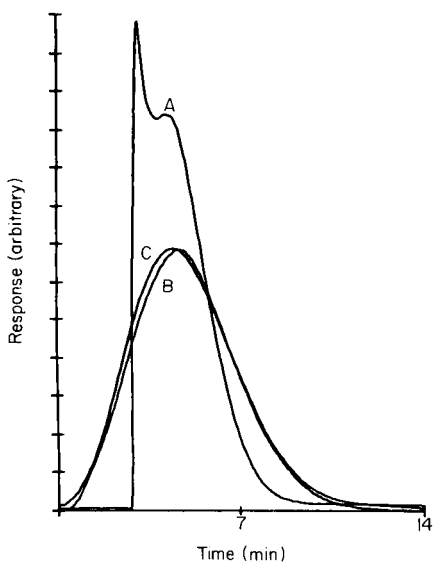

Fig. 3. Convolution simulation for thyroglobulin near its dispersion maximum. Curves: (A) detector 1 profile; (B) actual detector 2 profile; (C) simulated detector 2 profile with $D/\bar{u}L$ = 0.0165. Ordinate is expressed in arbitrary units such that the areas under the peaks are equal. Flow rate is 0.83 ml min^{-1}.

N = 30. Therefore, the EMG model seems to correspond very well to experiment, as it gives the smallest discrepancy between the two profiles.

Plate-height ratios (H/H_o) for all four solutes as a function of $De^2Sc^{1.14}$ are shown in Fig. 4. Agreement is good at low and high flow rates, but not for intermediate values. This was also observed by Tijssen [11, 18] even though the discrepancy was then attributed to the measurement technique. Peak widths and retention times were used; it was assumed that the scatter would disappear if moments were used instead. This is now shown not to be the case. The greatest spread is obtained at a value of log $De^2Sc^{1.14}$ equal to 6, which is quite close to the value predicted by Eqn. 17; therefore, plotting log (H/H_o) against log $De^2Sc^{1.14}$ is not the most appropriate way to characterize axial dispersion in coiled tubes. No maximum in the curve can be predicted with this method.

Conversely, a much more coherent picture is obtained by plotting the logarithm of the intensity of dispersion, δ ($D/\bar{u}d$), against the logarithm of the parameter $ReSc$ as shown in Fig. 5. Equations 15 and 16 were used because $ReSc$ was greater than 10^4 for all of the data. It is readily seen that agreement between theory and experiment is close, especially for the three globular proteins.

The plateau seen at higher flow rates (210—360 ml h^{-1}) seems to occur for a plate height approximately equal to $2\pi R$, where R is the radius of the coil. Increasing the flow rate beyond 30 ml h^{-1} again decreases the plate height.

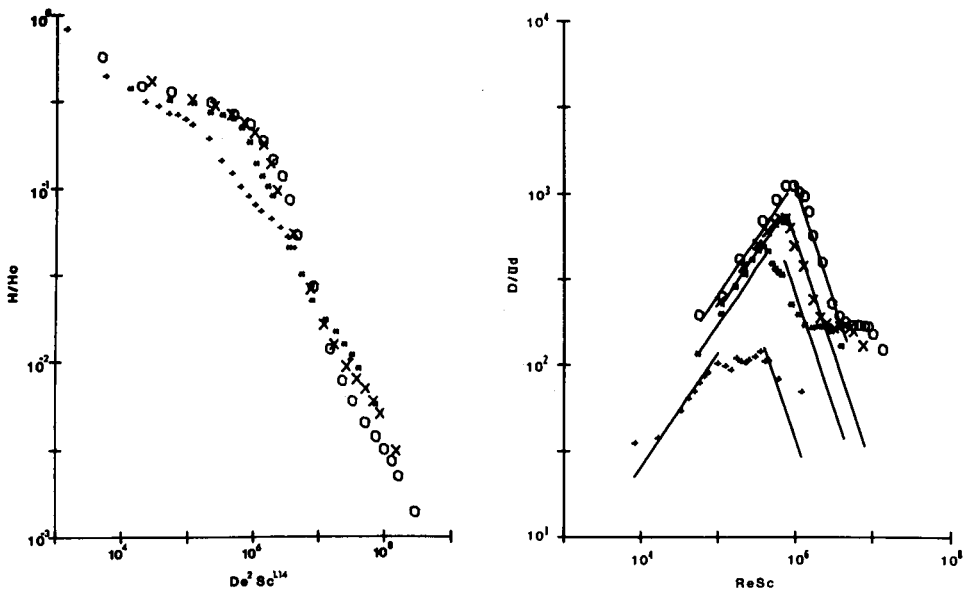

Fig. 4. Plate-height ratios (H/H_o) as a function of $De^2Sc^{1.14}$: (+) phenol (Sc = 1200); (*) cytochrome C; (×) albumin; (○) thyroglobulin (Sc = 37300).

Fig. 5. Intensity of dispersion, $D/\bar{u}d$, as a function of $ReSc$: (+) phenol (Sc = 1300); (*) cytochrome C; (×) albumin; (○) thyroglobulin (Sc = 28600). Theoretical curves were calculated from Eqns. 15 and 16.

Dispersion maxima are thus accurately predicted by Eqn. 17. Plate heights are also well characterized. Figure 6 shows even more clearly that dispersion maxima occur at a constant value of $De^2Sc^{1.14}$. This is the natural outcome of D_r/D_m increasing linearly with $(\bar{u})^{1.5}$ and of the square root decrease of κ with velocity. Thus there is a need to verify the behavior of the reduced dispersion, $256\ DD_m/[(\bar{u}d)^{5/3}(\eta/\rho)^{1/3}]$ which, as shown earlier, should decrease linearly as a function of $De^2Sc^{1.14}$. This is seen in Fig. 7. A 14-point linear regression fit of the parameters predicted for Eqn. 19 gives an intercept of 6.13 ± 0.39 and a slope of -0.99 ± 0.06. The agreement with theory is excellent and thus confirms that the form of Eqn. 15 is correct. A second fit done for the data beyond the plateau yielded a similar slope. Notwithstanding the theoretical uncertainty about the factor $Sc^{0.14}$, the spread is much smaller than for the parameter (H/H_o). The latter ratio is in fact proportional to $Re^{-0.333}$ for $\log De^2Sc^{1.14} < 6.13$ and inversely proportional to $De^2Re^{0.333}Sc^{1.14}$ for higher values. It must be remembered that previous measurements of (H/H_o) did not take into account the additional factor, $Sc^{0.14}$. Ignoring this factor leads to a discrepancy of 60% in the respective abscissa values of the phenol and thyroglobulin curves. Data obtained from molecules with low Schmidt numbers (higher D_m) are indeed spread out in the original data [11–13, 18].

It is therefore possible to describe axial dispersion adequately in coiled tubes. Equations 18 and 19 appear to be quite successful in the progress toward a more definitive theoretical treatment.

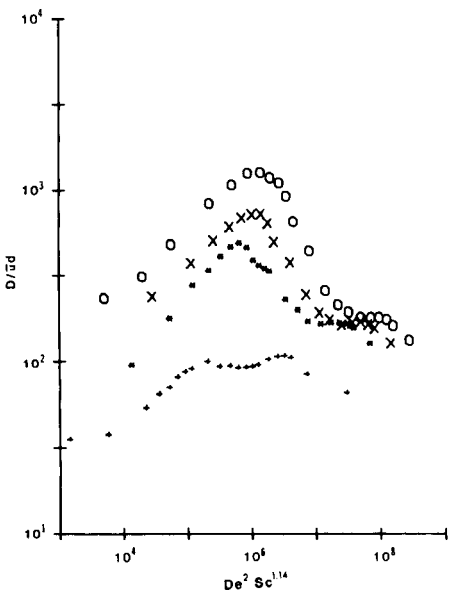

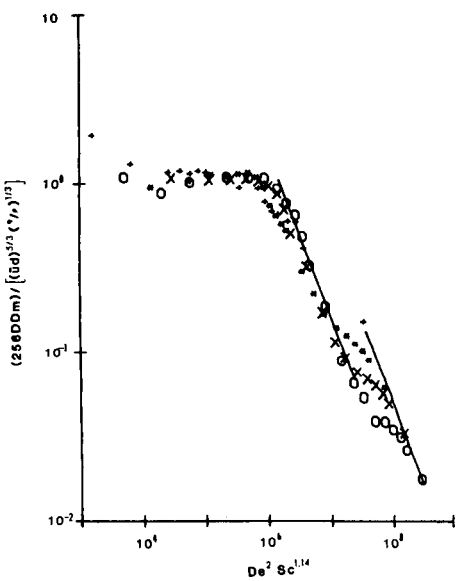

Fig. 6. Intensity of dispersion, $D/\bar{u}d$, as a function of $De^2Sc^{1.14}$. Symbols as for Fig. 4.

Fig. 7. Reduced dispersion, ϵ, as a function of $De^2Sc^{1.14}$. Symbols as for Fig. 5.

Dispersion maxima in coiled post-column reactors can thus be accurately predicted. The flow rate in a post-column reactor can be increased beyond a certain critical velocity in order to reduce the additional dispersion contributed by the presence of a reactor. The coiling radius can also be adjusted to accommodate a given range of molecular weights of solutes. In general, a very tight coil will contribute little additional dispersion for macromolecules when moderately high flow rates (ca. 3 ml min^{-1}) are used.

We are indebted to Dorothy N. Vacik and Joe Ann Thomas for their technical assistance. This work was supported by Grant no. CHE-81101123 of the National Science Foundation.

REFERENCES

1 J. A. Koutsky and R. J. Adler, Can. J. Chem. Eng., 42 (1964) 239.
2 G. I. Taylor, Proc. R. Soc. London, Ser. A, 124 (1929) 243.
3 M. J. E. Golay and J. G. Atwood, J. Chromatogr., 186 (1979) 353.
4 K. Hofmann and I. Halasz, J. Chromatogr., 173 (1979) 211.
5 I. Halasz, J. Chromatogr., 173 (1979) 229.
6 M. Adler, Z. Angew. Math. Mech., 14 (1934) 257.
7 L. C. Truesdell, Jr. and R. J. Adler, Am. Inst. Chem. Eng. J., 16 (1970) 1010.
8 L. R. Austin and J. D. Seader, Am. Inst. Chem. Eng. J., 19 (1973) 85.
9 R. N. Trivedi and K. Vasudeva, Chem. Eng. Sci., 30 (1975) 317.
10 L. A. M. Jannsen, Chem. Eng. Sci., 31 (1976) 215.
11 R. Tijssen, Anal. Chim. Acta, 114 (1980) 71.
12 R. S. Deelder, M. G. F. Kroll, A. J. B. Beeren and J. H. M. van den Berg, J. Chromatogr., 149 (1978) 669.
13 J. H. M. van den Berg, R. S. Deelder and H. G. M. Egberink, Anal. Chim. Acta, 114 (1980) 91.
14 R. J. Nunge, T. S. Lin and W. N. Gill, J. Fluid Mech., 51 (1972) 363.
15 M. J. E. Golay, J. Chromatogr., 186 (1979) 341.
16 J. G. Atwood and J. Goldstein, J. Phys. Chem., 88 (1984) 1875.
17 G. I. Taylor, Proc. R. Soc. London, Ser. A, 219 (1953) 186.
18 R. Tijssen, Sep. Sci. Technol., 13 (1978) 681.
19 M. J. E. Golay, in D. H. Desty (Ed.), Gas Chromatography, Butterworths, London, 1958, p. 36.
20 R. B. Bird, W. E. Stewart and E. N. Lightfoot, Transport Phenomena, Wiley, New York, 1960, p. 559.
21 O. Levenspiel, Chemical Reaction Engineering, 2nd edn., Wiley, New York, 1972, Chap. 9.
22 R. Tijssen, Ph.D. Dissertation, Technical University, Delft, The Netherlands, 1979.
23 C. E. Kalb and J. D. Seader, Am. Inst. Chem. Eng. J., 20 (1974) 340.
24 A. N. Dravid, K. A. Smith, E. W. Merrill and P. L. T. Brian, Am. Inst. Chem. Eng. J., 17 (1971) 1114.
25 R. Tijssen and R. T. Wittebrood, Chromatographia, 5 (1972) 286.
26 J. A. Fulton, T. D. Schlabach, J. E. Kerl, E. C. Toren, Jr. and A. R. Miller, J. Chromatogr., 175 (1979) 269.
27 R. R. Walters, J. F. Graham, R. M. Moore and D. J. Anderson, Anal. Biochem., 140 (1984) 190.
28 E. Grushka, Anal. Chem., 44 (1972) 1733.
29 W. W. Yau, Anal. Chem., 49 (1977) 395.
30 J. Bacon and R. N. Adams, Anal. Chem., 42 (1970) 524.

Analytica Chimica Acta, 184 (1986) 187—196
Elsevier Science Publishers B.V., Amsterdam — Printed in The Netherlands

SEPARATION OF TRACE RARE EARTHS AND OTHER METALS FROM URANIUM BY LIQUID-LIQUID EXTRACTION WITH QUANTITATION BY INDUCTIVELY-COUPLED PLASMA/MASS SPECTROMETRY

MARGO D. PALMIERI, JAMES S. FRITZ, JOSEPH J. THOMPSON and ROBERT S. HOUK*

Ames Laboratory-USDOE and Department of Chemistry, Iowa State University, Ames, IA 50011 (U.S.A.)

(Received 2nd December 1985)

SUMMARY

N,N-Dihexylacetamide in toluene was used to extract uranium selectively from an aqueous phase containing 30 elements at 10 or 100 $\mu g\ l^{-1}$ concentrations. After three extractions, the uranium level fell from 119 000 mg l^{-1} (0.5 M) to less than 3 mg l^{-1}. An inductively-coupled plasma/mass spectrometer (i.c.p./m.s.) was used to determine recoveries of the trace elements in the aqueous phase, which, in most cases, were in the range 90—110%. This combination of liquid-liquid extraction with i.c.p./m.s. offers determinations at the 10 ng g^{-1} level in uranium for most of the elements studied.

Uranium purity is of extreme importance in the nuclear industry. Trace impurities, especially those with high neutron-capture cross-sections, can hinder a fission chain reaction in addition to altering the metallurgical characteristics of the uranium metal.

Several methods have been developed which are still used to determine trace metals in uranium. The classical method, carrier distillation, has been used extensively but suffers from lack of sensitivity for those elements which form involatile or refractory oxide species [1]. The direct excitation and detection of impurities in uranium samples has been tried [2], but interference from uranium spectral lines severely restricts the number of elements which can be determined with reasonable detection limits.

Recently, several methods of determining trace elements in uranium have been developed by using chemical separation and detection by inductively-coupled plasma/atomic emission spectrometry (i.c.p./a.e.s.). The commonest separation method is liquid-liquid extraction. Separation schemes followed by i.c.p./a.e.s. have been developed with such complexing agents as tributylphosphate (TBP) [3], tri-n-octylphosphine oxide (TOPO) [4], tri-(2-ethylhexyl)phosphate (TEHP) [5—8], and tri(iso-octyl)amine [9].

One class of uranium extractants which has not been widely used is the *N,N*-dialkyl-substituted alkylamides. Gasparini and Grossi [10] have noted that these compounds are easy to synthesize, extract as well as TBP, are

0003-2670/86/$03.50

more resistant to radiolytic degradation, and the degradation products do not interfere with the extraction. One such extractant developed is *N,N*-dihexylacetamide (DHA) [11]. It displays all the advantages of the *N,N*-dialkyl-substituted alkylamides, and its starting materials are relatively inexpensive and readily available.

Inductively-coupled plasma/mass spectrometry (i.c.p./m.s.) is a new technique for multielement determinations in solution [12—15]. Now that commercial instrumentation is available, i.c.p./m.s. is being evaluated for its ability to solve difficult analytical problems. Both i.c.p./m.s. and i.c.p./a.e.s. are capable of multielement quantitation, but in the present application, i.c.p./m.s. has two main advantages over i.c.p./a.e.s. Spectral interferences from uranium are not a problem in i.c.p./m.s., in that U^{2+} (m/z = 117, 117.5 and 119) is the only uranium species observed in the m/z range corresponding to analyte elements. In contrast, excitation of uranium in the i.c.p. produces thousands of emission lines [16] that obstruct analyte lines even at moderate uranium concentrations. A second advantage of i.c.p./m.s. is its very low detection limits (10—100 ng l^{-1}), which are an order of magnitude better than i.c.p./a.e.s. for most elements [15]. At present, however, i.c.p./m.s. exhibits greater ionization suppression effects than does i.c.p./a.e.s. [15]. Uranium has been found to be one of the worst elements at suppressing the ionization of analytes [17]. Thus, the combination of efficient liquid-liquid extraction with i.c.p./m.s. greatly improves the value of this technique for quantitation of elements in uranium. This paper reports the determination of very low levels of impurities in uranium by extraction with DHA and i.c.p./m.s. detection.

EXPERIMENTAL

Equipment

The Sciex ELAN commercial i.c.p./m.s. (Model 250) was used with the operating parameters listed in Table 1. Figure 1 illustrates the location of the lens elements named in Table 1. The quantitative characteristics of this particular device have recently been described in detail [18]. The mass analyzer was operated in a "peak-hopping" mode. In this mode, the mass analyzer made a 0.1-s measurement at each of three m/z positions spaced 0.1 dalton apart on the top of a chosen peak. The mass analyzer then jumped to the next chosen peak, on top of which another three measurements were made at 0.1-dalton intervals. This sequence was repeated until the dwell time accumulated for each channel was 0.5 s. The three count rates for each peak were then averaged and divided by the average count rate for the internal standard to yield one "determination". Typically, six such determinations were made for each of ten elements. Therefore, the total time for each sample was approximately 90 s, i.e., the mass spectrometer acquired data for a total of 9 s for each element. The standard deviations for individual sample concentrations were based on the average of the six determinations.

TABLE 1

Sciex i.c.p./m.s. operating parameters

I.c.p. torch	Ames Laboratory design [19], torch extended 1½ in. from aerosol injector
Outer argon flow rate	12 l min^{-1}
Auxiliary flow rate	0.8 l min^{-1}
I.c.p. forward power	1.30 kW
Aerosol flow rate	1.2 l min^{-1}
Solution uptake rate	2.5 ml min^{-1}
Sampling position	20 mm above load coil, centered on axial channel
Sampler orifice	1.2-mm diameter
Skimmer orifice	0.90-mm diameter
Pressure, quadrupole chamber, i.c.p. on	4×10^{-5} torr
Ring lens (1 in Fig. 1)	Setting: 07 (−4.38 V at TP[a])
A.c. rods (2)	Grounded
Ion shield (3)	Grounded
Lens 4	Setting: 20 (−4.00 V at TP)
Lens 5	Setting: 65 (+6.19 V at TP)
Lens 6	Setting: 79 (−15.78 V at TP)
Entrance AC rods (7)	−5.10-V bias (at TP)
Mass filter (8)	Zero DC bias
Exit AC rods (9)	−5.10-V bias (at TP)
Exit shield lens (10)	−5.00 V (at TP)
Exit lens (11)	−130 V (at TP)
Deflector	+3370 V (at TP)
Electron multiplier	−2790 V (−4.18 V at TP)

[a]TP = test point. Test point voltages are not necessarily identical to the voltages actually supplied to the device.

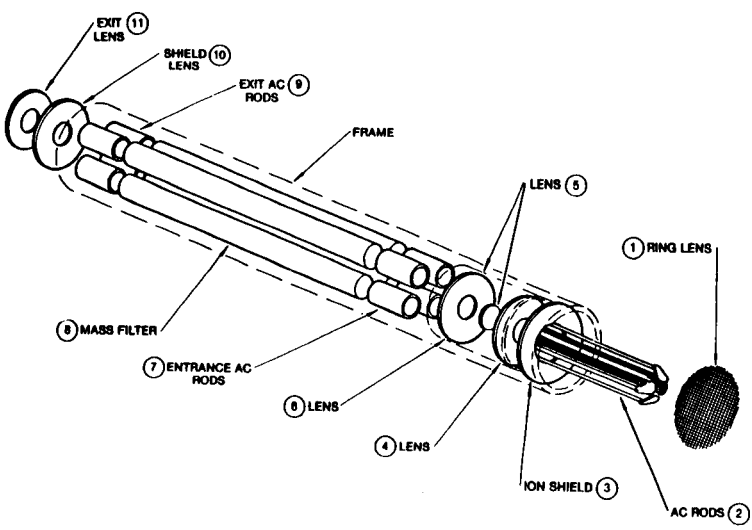

Fig. 1. Sciex ion lens and mass analysis system; see Table 1 for appropriate voltages.

Two modifications were made to the instrumentation before it was used in these experiments. The i.c.p. torch was replaced with one of Ames Laboratory design [19], with the torch extending 1.5 inches from the tip of the aerosol injector tip. The Ames Laboratory torch contained a jet-type orifice in the central injection tube in contrast to the capillary-type injector supplied by Sciex. The standard concentric pneumatic nebulizer was replaced with a continuous-flow ultrasonic one (with aerosol desolvation) [20, 21]. These additions made it easier to control matrix interference and drifting effects, which are discussed below in the interference section.

Reagents and standards

N,N-Dihexylacetamide was synthesized by the method outlined by Fritz and Orf [11]. Reagent-grade or better chemicals were used. Reagent-grade uranyl nitrate was obtained from Mallinkrodt and Fisher.

Multielement standards were prepared by combining and diluting single-element reference stock solutions. The rare earths were obtained at Ames Laboratory, dried, weighed (as oxides) and dissolved in dilute nitric acid (in deionized water). The purity of these standards was verified by i.c.p./m.s. by scanning the entire mass spectrum of a 1000 mg l^{-1} solution. No impurities were found in the concentrated standards above a 10 μg l^{-1} level. Other stock solutions came from Fisher Scientific. The 1% (v/v) nitric acid used to dilute all samples and standards was made from the reagent-grade acid (Fisher Scientific), except for the experiments in which the low mass blanks became substantial at the 10 μg l^{-1} level. For those experiments, sub-boiling distilled nitric acid, made in an all-quartz apparatus, was required. Deionized water came from either a Millipore Milli-Q water purifier or from a Barnstead Nanopure-II system. The digital pipettes (Rainin) used in dilution and in the addition of the internal standard were calibrated gravimetrically and found to be within the manufacturer's specifications for precision and accuracy (better than 2% at all the volumes used).

Quantitative procedures

In the determination of the distribution coefficients, 500 mg l^{-1} solutions were prepared in 2 M nitric acid and were extracted with an equal volume of 2 M DHA in toluene. The mixture was placed on a Burrel Wrist Action shaker and equilibrated for 1 h. The aqueous phase was removed, diluted and tested for metal ion content. Atomic absorption spectrometry was used to determine the concentrations of Cs, Ag, Sr, Ba, and Cr. The metals, Cu, Hg, Ni, Zn, Mn, Co, Pb, and Cd, were determined spectrophotometrically at pH 9.2 with 4-(pyridylazo)resorcinol (Aldrich Chemical) [22]. Uranium was determined by the method of Fritz and Johnson-Richard [23]. An ASTM method was used in the determination of iron [24]. The remaining metals were determined by the methods outlined by Phillips [25].

For the separation and quantitation of trace metals in a uranium matrix, a 119 000 mg l^{-1} (0.5 M) solution of uranium in 2 M nitric acid was prepared

from uranyl nitrate. Various trace metals were added to the uranium solution so that their final concentrations were either 100 or 10 $\mu g\ l^{-1}$ (0.84 or 0.084 $\mu g\ g^{-1}$ of uranium). An aliquot of the spiked uranium solution was then extracted three times with an equal volume of 2 M DHA in toluene. An aliquot of the aqueous phase was taken, evaporated almost to dryness, dissolved in 1% nitric acid spiked with the internal standard, and examined by i.c.p./m.s. Lutetium was the internal standard for the rare earths and rubidium and holmium were used as internal standards for other metals.

The instrument was adjusted to give optimal performance as follows. Approximate settings of the aerosol flow rate and forward power were made, such as those that had worked on the previous day. A solution containing 10 $\mu g\ l^{-1}$ of both Ho and Lu in 1% nitric acid was introduced and the ratio Ho/Lu was measured several times. This ratio was then compared to that from a 10 $\mu g\ l^{-1}$ solution made up in 50 mg l^{-1} uranium. If the ratios were significantly different, the forward power was slowly changed until the ratios coincided. Then the Ho/Lu ratio was monitored for about 10 min to see if it would drift. If it did, by more than 5%, a slightly different aerosol flow rate was chosen, and the procedure was repeated.

The standards used were not run through the extractions with the samples. Instead, a single blank was taken through the procedure along with 3—4 samples. This ensured that trace impurities in the 0.5 M uranium, which might be substantial at the 10 $\mu g\ l^{-1}$ level, would be detected. Standards contained either 10 or 100 $\mu g\ l^{-1}$ of the internal standard, and were matrix-matched to contain the same amount of uranium as the samples. Calibration curves were prepared by using 2, 5, 10, and 30 $\mu g\ l^{-1}$ standards (or ten times higher for the high blank metals). During the procedure, the 10 $\mu g\ l^{-1}$ standard was reintroduced after each sample to verify that the calibration curve had not shifted. If there had been a small drift, the data could be used to normalize subsequent sample concentrations.

The reported detection limits were calculated as the analyte concentration necessary to yield a net (blank-subtracted) signal equal to three times the standard deviation of the blank count rate.

RESULTS AND DISCUSSION

Distribution coefficients

Table 2 lists the distribution coefficients (D_c) for various metal ions in 2 M nitric acid with 2 M DHA in toluene as the extractant. The extraction conditions were chosen on the basis of the work by Fritz and Orf [11] so that extraction of uranium was efficient while good separation of the phases was retained. Nitric acid was used instead of sodium nitrate so that it could be evaporated after extraction, thereby eliminating interference effects caused by high salt concentrations. However, the D_c value for uranium is much higher (624) in sodium nitrate than in nitric acid, probably because of a salting-out effect. For most of the elements listed, D_c is either very small or zero, which indicates the wide applicability of DHA in separating trace metal

TABLE 2

Distribution coefficients for elements in 2 M HNO_3 with 2 M DHA in toluene as the extractant[a]

Metal ion	D_c	Metal ion	D_c	Metal ion	D_c
Ag^+	0.054	Hg^{2+}	0.44	Th^{4+}	5.25
Bi^{3+}	2.55	Ni^{2+}	<0.01	UO_2^{2+}	57.8
Cu^{2+}	<0.01	Pb^{2+}	0.043	Zr^{4+}	0.24

[a]The following ions had zero D_c values: Zn^{2+}, Mn^{2+}, Co^{2+}, Cd^{2+}, La^{3+}, Tm^{3+}, Gd^{3+}, Pr^{3+}, Cs^+, Sr^{2+}, Ba^{2+}, Y^{3+}, Fe^{3+}, Ti^{4+}, Cr^{3+}, Al^{3+}, V^{5+}.

ions from uranium. Of the metals listed, only uranium, thorium, and bismuth were extracted significantly under the chosen conditions, with uranium being extracted much more efficiently (98.3%) than the other elements. With the exception of thorium and bismuth, quantitative data for other metals which have non-zero D_c values can be corrected for extraction in the recovery studies.

After extraction experiments with uranium, the DHA was recycled by back-extracting the uranium in the organic phase with several portions of a saturated sodium hydrogencarbonate solution, and then washing the organic phase with 2 M nitric acid before use in further extractions. The DHA solution was used several times with little loss in efficiency of uranium extraction.

Interferences and stability

Two initial problems with the Sciex instrument were drift of calibration curves and severe matrix effects from uranium even at concentrations as low as 100 mg l^{-1} (0.01%). Internal standardization, by itself, did not correct these problems. However, replacing the pneumatic nebulizer with the ultrasonic one facilitated selection of forward power and aerosol flow rate such that internal standardization would compensate for these effects. Aerosol flow rate is a critical parameter in i.c.p./m.s. [18, 26]. It was much easier to optimize performance by adjusting the aerosol flow rate with the ultrasonic nebulizer than to change the relatively fixed flow rate from the pneumatic. Furthermore, this optimization could be done without affecting the nebulization efficiency, thereby preserving detection limits to some extent. As noted above, these conditions enabled 10 μg l^{-1} rare earth ratios to be kept constant (within 3%) for concomitant uranium concentrations up to 50 mg l^{-1} over a 2-h period. In other words, the same set of conditions alleviated both the drifting and interference problems at once, the only drawback being a 3- to 4-fold increase in detection limits.

After two extractions with DHA, the uranium concentration was found to be about 150 mg l^{-1}. With the Sciex instrument set at the conditions noted above, it was difficult to quantify trace elements in this matrix; 10 μg l^{-1} was very close to the detection limit with these conditions. However, after three

extractions, the uranium concentration was below 3 mg l^{-1}. Long-term drift of the analyte signal and ratios was then the main problem, along with contamination of the samples by the organic phase. Spectral interference by metal oxide ions (MO^+) was not a problem at the 10 $\mu g\ l^{-1}$ level because the ratio MO^+/M^+ was less than 1% under the conditions used. The background mass spectrum obtained was similar to that reported previously [15].

Recovery of trace elements

Table 3 lists the relative amounts of metals in the deionized water, distilled nitric acid, and evaporated 2 M nitric acid compared to a 2 $\mu g\ l^{-1}$ Co signal. Values in this table are only semiquantitative in nature, because they are not corrected for the different isotopic abundances of the elements and other sensitivity factors. The blank-corrected recoveries of the trace elements added to the uranium solution are listed in Tables 4 and 5. The amount of spiked material originally added was varied according to the level of trace impurities present in the blank in order to avoid the imprecision of subtracting two numbers of nearly equal magnitude. The high blanks for Al, Ba, and Pb are likely due to impurities in the nitric acid which have been concentrated in the evaporation step (see Table 3). The uranium used in the recovery studies was identical to the "unknown" in Table 6. Therefore, the metals which exhibit high blanks could either be native impurities in the uranium or traces which may not have been fully back-extracted from the organic phase before the extractant was used again. Thorium was extracted too efficiently to

TABLE 3

Background signal from various elements relative to 2 $\mu g\ l^{-1}$ cobalt[a]

Element	*m/z*	Deionized H_2O	Distilled 1% HNO_3	Evaporated distilled 2 M HNO_3
Al	27	0.1	0.3	6.5
Ba	138	0.1	0.1	9.4
Cd	114	0.3	0.3	0.1
Cr	52	0.2	0.4	0.4
Cs	133	0.05	0.09	0.1
Cu	63	0.4	0.4	0.5
Mn	55	0.07	0.1	0.3
Pb	208	1.5	5	6
Sr	88	0.1	0.1	1.5
Ti	48	0.06	0.1	0.2
Th	232	0.3	0.3	0.4
Y	89	0.05	0.1	0.1
Zn	66	0.05	0.1	2.5
Zr	90	0.06	0.2	1.7

[a]Values are not corrected for isotopic abundances or other sensitivity factors but merely reflect approximate levels of trace impurities in the reagents used for comparison purposes.

TABLE 4

Recoveries of rare earth elements[a] from a 119 000 mg l^{-1} U solution

Metal	*m/z*	Average recovery (%)[b]	Metal	*m/z*	Average recovery (%)[b]
Ce	140	90 (12)	La	139	92 (13)
Dy	163	93 (5)	Nd	146	90 (13)
Er	166	97 (4)	Sm	152	95 (16)
Eu	153	95 (16)	Tb	159	95 (9)
Gd	157	92 (11)	Tm	169	99 (5)
Ho	165	97 (5)	Yb	174	100 (3)

[a]All the rare earths were recovered at the 0.084 $\mu g\ g^{-1}$ of uranium (10 $\mu g\ l^{-1}$) level. [b]Based on 10 trials conducted on three different days; relative standard deviations are given in parentheses.

TABLE 5

Recoveries of other metals from 119 000 mg l^{-1} U solution

Metal	*m/z*	Recovery levels ($\mu g\ g^{-1}$ U)	Number of trials[a]	Average recovery (%)	Relative standard deviation (%)
Al	27	0.84	8	112	21
Ba	138	0.84	8	104	7
Cd	114	0.084	13	105	16
Cs	133	0.084	14	97	10
Co	59	0.084	14	98	20
Cr	52	0.84	11	107	10
Mn	55	0.084	14	95	16
Pb	208	0.84	11	112	24
Sr	88	0.084	14	99	16
Ti	48	0.084	14	87	13
V	51	0.84	8	95	15
Y	89	0.084	14	98	8
Zn	66	0.84	8	99	24
Zr	90	0.84	14	106	33

[a]Obtained on 3 or 4 different days.

permit reliable evaluation of its recovery. Attempts to find recoveries for iron and copper at 100 $\mu g\ l^{-1}$ were precluded by significant background in the i.c.p./m.s. itself at these masses. Boron could not be determined with the ultrasonic nebulizer used, probably because of loss of boron in the desolvation system.

The relative standard deviation (r.s.d.) for individual samples was usually less than 3%, which reflects the short-term stability of the instrument. The r.s.d. within a run of 3—4 samples (separately extracted) was between 3 and

TABLE 6

Concentration of trace elements in a uranyl nitrate sample

Metal	Average concn.[a] (ng g^{-1} U)	Detection limit[b] (ng g^{-1} U)	Metal	Average concn.[a] (ng g^{-1} U)	Detection limit[b] (ng g^{-1} U)
Al	360 (190)	9	Nd	<2.4	0.8
Ba	940 (37)	0.5	Pb	400 (87)	0.8
Cd	31 (11)	2	Pr	<0.7	0.3
Ce	2.8 (0.6)	0.3	Sm	<1.3	0.8
Co	55 (6)	2	Sr	86 (10)	0.2
Cr	620 (68)	7	Tb	<0.2	0.2
Cs	<0.3	0.3	Ti	120 (35)	5
Dy	<1.3	0.8	Tm	<0.5	0.2
Er	<0.9	0.4	V	110 (8)	4
Eu	<0.4	0.4	Y	120 (13)	0.2
Gd	<0.8	0.8	Yb	<0.3	0.3
Ho	<0.1	0.1	Zn	560 (280)	8
La	<1.0	0.4	Zr	67 (35)	0.8
Mn	130 (13)	3			

[a]Average of 4 trials with standard deviation (ng g^{-1} of uranium) in parentheses. [b]Detection limits in $\mu g\ l^{-1}$ are 0.088 × ng g^{-1} U.

10%. However, the day-to-day variation was larger, as is reflected by the r.s.d. values in Tables 4 and 5. In general, those elements with lower blanks, or with one major isotope, had better r.s.d.'s in their recoveries. Lead and zirconium had higher relative standard deviations probably because of differences in their extraction efficiencies from sample to sample. The large amount of uranium present, especially in the initial extraction, could affect the extractability of lead and zirconium into the organic phase.

Once the recoveries had been demonstrated, the method was used to determine the level of impurities in reagent-grade Fisher uranyl nitrate. The results in ng g^{-1} of uranium are given in Table 6. The standard deviations are rather high because of the low levels of the elements present as well as the high blanks (from the nitric acid) and drift of the analyte signal. The detection limits for elements in a 2-mg l^{-1} uranium solution (i.e., the same uranium concentration as the samples) are also given in Table 6. The uranium in the standards and blanks used to evaluate these detection limits was not extracted. Therefore, the native impurities in the uranyl nitrate were still present, but at levels below detectability. These detection limits are 10- to 100-fold better than those for similar extraction/detection experiments reported in the literature [3, 5, 9]. Thus, the utility of the present method is clear, especially if modest increases in precision could be made.

This paper was presented in part at the Winter Conference on Plasma Spectrochemistry, Kona, Hawaii, 1986. The research was supported in part

by the Institutional Supporting Research and Development Program at Los Alamos National Laboratory, which is operated by the University of California. It was also supported in part by the Director of Energy Research, Office of Basic Energy Sciences. The Ames Laboratory is operated by Iowa State University for the U.S. Department of Energy under contract No. W-7405-Eng-82. We wish to thank the following people who have contributed to this project in one way or another: Jose Olivares, Edward DeKalb, Robert Staggs, Rodney Walters, Daniel Wiederin, Robert Bachman, and Robert Jackson and the Sciex Customer Service department.

REFERENCES

1 B. F. Scribner and H. R. Mullen, J. Res. Natl. Bur. Stand., 37 (1946) 379.
2 C. E. Pepper, A Review of Spectrochemical Emission Methods and Associated Problems for the Determination of Impurities in Nuclear Grade Uranium, Atomic Energy Commission NLCO-999, 1967.
3 J. P. Maney, V. Luciano and A. F. Ward, Jarrell-Ash Plasma Newsl., 2 (1979) 11.
4 B. R. Bear, M. C. Edelson, B. Gopalan and V. A. Fassel, Anal. Chem. Spectrosc. Symp. Ser., 19 (1984) 187.
5 M. A. Floyd, R. W. Morrow and R. B. Farrar, Spectrochim. Acta, Part B: 38 (1983) 303.
6 C. J. Coleman, Anal. Chem. Spectrosc. Symp. Ser., 19 (1984) 195.
7 A. A. Halouma, R. B. Farrar, E. A. Hester and R. W. Morrow, Anal. Chem. Spectrosc., Symp. Ser., 19 (1984) 201.
8 B. W. Short, H. S. Spring and R. L. Grant, Determination of Trace Impurities in Uranium Hexafluoride by an Inductively Coupled Argon Plasma Spectrometer, Goodyear Atomic Corporation, Piketon, OH, CAT-T-3184, 1983.
9 J. K. Seshagiri, Y. Babu, M. L. Jayanth Kumar, A. G. I. Dalvi, M. D. Sastry and B. D. Joahi, Talanta, 31 (1984) 773.
10 G. M. Gasparini and G. Grossi, Sep. Sci. Tech., 15 (1980) 825.
11 J. S. Fritz and G. Orf, Anal. Chem., 47 (1975) 2043.
12 R. S. Houk, V. A. Fassel, G. D. Flesch, H. J. Svec, A. L. Gray and C. E. Taylor, Anal. Chem., 52 (1980) 2283.
13 R. S. Houk, Anal. Chem., 58 (1986) 97A.
14 A. R. Date and A. L. Gray, Analyst (London), 108 (1983) 1033.
15 D. J. Douglas and R. S. Houk, Prog. Anal. At. Spectrosc., 8 (1985) 1.
16 R. K. Winge, V. A. Fassel, V. J. Peterson and M. A. Floyd, Inductively Coupled Plasma Atomic Emission Spectrometry: An Atlas of Spectral Information, Elsevier, New York, 1985.
17 D. J. Douglas, Short Course on Inductively Coupled Plasma Mass Spectrometry, Winter Conference on Plasma Spectrochemistry, Kona, HI, 1986.
18 G. Horlick, S. H. Tan, M. A. Vaughan and C. A. Rose, Spectrochim. Acta, Part B: 40 (1985) 1555.
19 R. H. Scott, V. A. Fassel, R. N. Kniseley and D. E. Nixon, Anal. Chem., 46 (1974) 75.
20 K. W. Olson, W. J. Haas and V. A. Fassel, Anal. Chem., 49 (1977) 632.
21 B. R. Bear, M.S. Thesis, Iowa State University, Ames, IA, 1983.
22 F. D. Snell, Photometric and Fluorometric Methods of Analysis, Wiley-Interscience, New York, 1978.
23 J. S. Fritz and M. Johnson-Richard, Anal. Chim. Acta, 20 (1959) 164.
24 ASTM, 1974 Annual Book of ASTM Standards, 26 (1974) 543.
25 R. J. Phillips, Ph.D. Dissertation, Iowa State University, Ames, IA, 1980, p. 142.
26 J. A. Olivares and R. S. Houk, Appl. Spectrosc., 39 (1985) 1070; Anal. Chem., 57 (1985) 2674.

Analytica Chimica Acta, 184 (1986) 197—203
Elsevier Science Publishers B.V., Amsterdam — Printed in The Netherlands

SPECIATION OF n-BUTYLTIN COMPOUNDS BY ATOMIC ABSORPTION SPECTROMETRY WITH AN ELECTROTHERMAL QUARTZ FURNACE AFTER HYDRIDE GENERATION

LOUISE RANDALL, OLIVIER F. X. DONARD[a] and JAMES H. WEBER*

Chemistry Department, Parsons Hall, University of New Hampshire, Durham, NH 03824 (U.S.A.)

(Received 15th December 1985)

SUMMARY

A method is described for the speciation of n-butyltin compounds. The compounds are volatilized from aqueous solution, trapped on a chromatographic packing material contained in a teflon column, and separated on the basis of differing boiling points. The column is attached directly to an electrothermal quartz furnace of an atomic absorption spectrometer for detection at 224.61 nm. Absolute detection limits (3σ) are 11—45 pg as tin, calibration curves are linear to 13 ng, and reproducibility at the 2-ng level ranges from 5% for mono-n-butyltin to 18% for tri(n-butyl)tin.

The extensive use of n-butyltin compounds [1] allows the ready introduction of these compounds into the environment [2]. Extremely low levels of alkylated tin compounds are acutely toxic to non-target organisms [3]. In France, for example, leaching of tri(n-butyl)tin compounds from marine antifouling paints is considered to affect oyster larvae adversely [4].

Thompson et al. [1] reviewed techniques for the determination of low concentrations of n-butyltin compounds. Atomic absorption (or emission) spectrometry (a.a.s.) without prior separation has detection limits of 0.3 ng ml^{-1} tin [5] but does not speciate n-butyltin compounds [1]. Gas chromatography of aquated n-butyltin compounds with a modified flame photometer [6—8], mass spectrometer [9], or flame ionization-quenching [10] as detector, involves derivatization prior to detection [1]. Ebdon et al. [11] speciated tin compounds by coupled high-performance liquid chromatography/flame a.a.s. Hodge et al. [12] used hydride derivatization and separation on a glass wool column, followed by a.a.s. detection. Donard et al. [13] reported the speciation of methyltin and n-butyltin compounds by hydride generation, cryogenic trapping, separation on chromatographic packing material, and detection by a.a.s. with a quartz furnace.

---

[a]Present address: Laboratoire de Chimie Physique A, Université de Bordeaux I, 33405 Talence Cedex, France.

0003-2670/86/$03.50

The chromatographic/a.a.s. technique for aqueous solution is further developed here by using a column attached directly to the quartz furnace to obtain simultaneous detection limits (3σ) of 11—45 pg for n-butyltin compounds with linear calibration from sub-nanogram to nanogram quantities. The detection limit of 45 pg for tri(n-butyl)tin is a factor of 4 lower than previously reported [13] and the technique requires a minimum of sample manipulation. Determination of tetra(n-butyl)tin as well as direct and simultaneous determination of methyl- and n-butyltin compounds are possible.

EXPERIMENTAL

Apparatus

Butyltin hydrides were detected with a Perkin-Elmer Model 503 atomic absorption spectrometer fitted with a Westinghouse electrodeless discharge lamp (EDL) for tin, operated on continuous mode by a Westinghouse EDL power supply. The hydride generator (5 × 7 cm, 100-ml sample size), hydride trap (35 cm, 0.4-cm i.d.), and quartz furnace (10.5 cm, 1.1-cm i.d.) are illustrated in Fig. 1. Butyltin hydrides were trapped at −196°C (liquid nitrogen) on 2.5 g of Chromosorb G AW-DMCS (45—60 mesh) coated with 3% SP-2100 packed in the U-shaped teflon trap. The trap was prepared from Cole-Parmer Type T-6407-44 teflon TFE tubing, and was wrapped with nichrome wire (26 gauge, 0.088 ohm cm^{-1} resistance). The major inlet of the previously described furnace [13] was wrapped with the same type of nichrome wire. Two heated flexible transfer lines were prepared from teflon PTFE tubing. The inner tube (0.3-cm o.d., 0.1-cm wall) was inserted into the outer tube (0.5-cm o.d., 0.05-cm wall), which was wrapped with nichrome wire (28

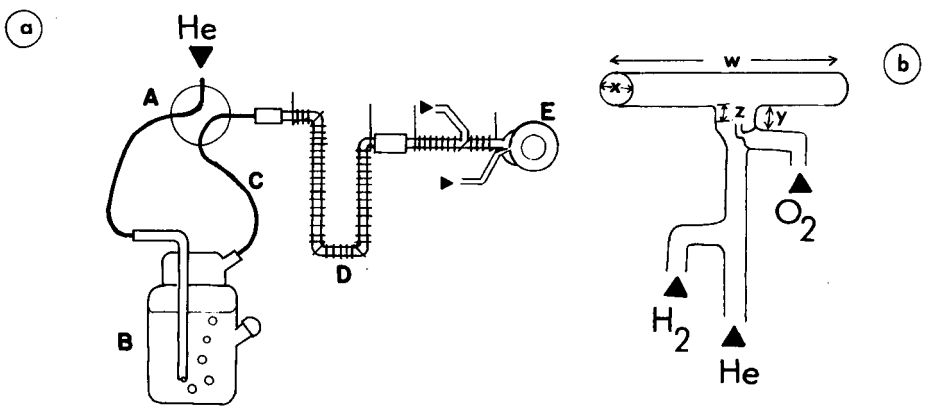

Fig. 1. (a) Apparatus for the speciation of n-butyltin compounds: A, four-way valve; B, hydride generator; C, heated transfer lines; D, separation trap in liquid nitrogen; E, quartz furnace. (b) Dimensions of optimum quartz furnace: W, 10.5 cm; X, 1.2 cm; Y, 1.5 cm; Z, 0.5 cm.

gauge, 0.35 ohm cm^{-1} resistance) and insulated with teflon tape. A Hamilton four-way valve allows the helium carrier gas to by-pass the hydride generator. Teflon-to-teflon and teflon-to-quartz connections were made with Omnifit teflon variable-bore connectors. Power to the transfer lines, trap, furnace inlet, and furnace was individually supplied by Variacs. The output signal (1 V full deflection) was amplified 10-fold, filtered by a low-pass filter, and integrated by a Hewlett-Packard Model 3392 A integrator. The hydrogen and helium flow rates were controlled by Cole Parmer flow meters and the oxygen flow rate by a precise Brooks flow meter.

Operating parameters determined by Simplex optimization were gas flow rates of helium = 400, oxygen = 21, and hydrogen = 833 ml min^{-1}. The tin EDL was used at 10 W in continuous mode. The spectrometer was operated at 224.61 nm with a 1-mm slit and an 0.3-s integration repeat mode. The output signal was amplified 10-fold and filtered at 1.3 Hz. The Variac outputs were set at 50 V for transfer lines, 5—30 V for the trap, 8 V for the furnace inlet and 19 V for the furnace. Temperatures were 150°C in the transfer lines, 20—300°C in the trap, and 750°C in the furnace. Temperatures were measured with a chromel/alumel thermocouple. Integrator parameter settings were 8 for attenuation and threshold, 0.16 for peak width, and a chart speed of 1.5 cm min^{-1}.

Reagents and standards

The water used in all experiments was deionized three times and then distilled through a Corning Megapure still. All glassware was soaked in 7% (v/v) nitric for at least 12 h and rinsed with water. Nitric acid solutions (5 M) were prepared from Fisher 70% nitric acid. Aqueous 6% (w/v) sodium tetrahydroborate was prepared from the Aldrich (99+%) reagent. The solution was filtered through a 0.2-μm Nuclepore filter, and allowed to stand for at least 12 h in a glass flask to reduce the tin blank. Methanol was Fisher certified A.C.S. Spectroanalyzed grade.

Mono- and di(n-butyl)tin chlorides, tetra(n-butyl)tin, and triethyltin bromide were from Alfa Ventron, and tri(n-butyl)tin hydride and tri(n-butyl)-tin chloride from Aldrich. Standards (total concentration 50 μg ml^{-1} as tin) were prepared (without purification) by dissolving the required compounds in 10 ml of methanol and storing them in 10-ml Hypovials sealed with crimp-on teflon-lined septa. All solutions stored in the dark at 4°C were stable over several months. The standards were injected through the septum of the hydride generator by a Hamilton 0.5-μl syringe.

Operating procedure

Water (100 ml) and nitric acid (2 ml, 5 M) were introduced into the hydride generator. The magnetic stirrer was started at a medium speed, the trap (heating coil set at 5 V) was lowered into the liquid nitrogen, and helium was bubbled through the solution for 2 min. The n-butyltin standards and the triethyltin internal standard, followed by 2.5 ml of the tetrahydroborate

solution, were added via the septum. The stirrer was turned to high for 2 min, the stirrer speed was reduced, and then a further 2.5 ml of the tetrahydroborate solution was added. After the bubbling had decreased, the stirrer speed was increased and the solution was purged for 4 min. The hydride generator was then by-passed via the four-way valve, the trap was removed from the liquid nitrogen, and after 2 min, 30 V was applied with the Variac.

RESULTS AND DISCUSSION

Hydride generation, optimization of atomization and furnace design

The reaction of tetrahydroborate and alkyltin compounds was described earlier [13], but additional information is noted here. The solution pH was initially 1.6, rising to 2.2 after addition of the tetrahydroborate. Additional injections of tetrahydroborate solution did not generate more n-butyltin hydrides at the concentrations studied. A comparison of peak area of $(n\text{-}Bu)_3SnH$ formed from $(n\text{-}Bu)_3SnCl$ and of $(n\text{-}Bu)_3SnH$ indicated a 100 ± 5% recovery from $(n\text{-}Bu)_3SnCl$.

Removal of the trap and connection of the hydride generator directly to the furnace allowed optimization of atomization conditions. The $(n\text{-}Bu)_3Sn^+$ peak area and peak height were observed for changing values of helium, oxygen and hydrogen. (For brevity, the cationic form $(n\text{-}Bu)_3Sn^+$ is used here for all tri(n-butyl)tin species detected as the hydride.) The gas flow rates were initially checked by trial and error, and then fixed by using Simplex optimization [14]. Peak areas yielded slightly better reproducibility than peak heights. The reproducibility of the three highest peak areas was checked. The helium flow rate was critical for $(n\text{-}Bu)_3Sn^+$, but a high flow rate resulted in excessive back-pressure. A flow of 400 ml min^{-1} was most suitable. Optimum oxygen and hydrogen flow rates were 21 and 833 ml min^{-1}, respectively.

The furnace design yielding the highest atomization efficiency is illustrated in Fig. 1. The low volatility of $(n\text{-}Bu)_3Sn^+$ (b.p. 80°C at 0.4 mm Hg) required minimization of "cold spots". A white deposit on the furnace inlet and a smaller $(n\text{-}Bu)_3Sn^+$ peak were noted for furnaces having the oxygen inlet at a distance of more than 2 cm from the atomizing region. Heating the inlet also increased the $(n\text{-}Bu)_3Sn^+$ peak. In the previous experiments [13], a stream of inert gas was used to blanket the furnace to extend the furnace lifetime. A stream of inert gas was not used here because the furnace temperature was 200°C lower.

Development of the method

Several systems based on glass rather than teflon were investigated. The technique previously described [13] had a detection limit of 200 pg for $(n\text{-}Bu)_3Sn^+$ based on 3σ of background and 100-ml samples. In an attempt to reduce this limit, Chromosorb T 45—60 mesh was used to replace the Chromosorb G packing, but the column was easily blocked under the conditions

used. Silanized glass wool gave a separation of the n-butyltin compounds, but after three experiments, sensitivity decreased rapidly. Similarly, glass beads did not give a reproducible separation. An empty g.c.-type column (1-mm i.d., 150-cm length) coated with 3% SP-2100 gave an excellent separation with high sensitivity, but was again irreproducible. Silanizing the column prior to coating did not improve reproducibility. Use of a two-column system incorporating a U-tube containing glass wool or 5A molecular sieve and a g.c.-type column also suffered problems. The U-tube and g.c.-type column did not give reproducible results and the molecular sieves resulted in no detection of n-butyltin compounds. Activation of the wet (and heated) glass surface by the alkaline sodium tetrahydroborate and subsequent loss of n-butyltin compounds is a possible reason for the lack of reproducibility. The teflon columns used gave a reproducibility of 18% for 2 ng of $(n\text{-}Bu)_3Sn^+$ and detection limit of 45 pg as Sn (3σ). However, the sensitivity decreased after 15 experiments because of deterioration of the SP-2100-coated Chromosorb G.

Separation conditions

The Chromosorb G with a mesh size of 45—60 was the most suitable for the helium flow rate used, and a coating of 3% provided a good separation of the n-butyltin compounds (Fig. 2). Separation of stannane (1.2 ng), trimethyltin (0.2 ng), mono-n-butyltin (2 ng), triethyltin (2.2 ng), di(n-butyl)tin (2.6 ng), tri(n-butyl)tin (1.8 ng), and tetra(n-butyl)tin (2.2 ng) occurs within 4 min (Fig. 2). Teflon transfer lines allowed a high temperature to be maintained through the lines. Typical retention times of the hydrides (3% reproducibility) for 2-min heating at a rate of $0.8°C\ s^{-1}$ followed by heating at $2.4°C\ s^{-1}$ were: stannane (0.50 min), mono-n-butyltin (2.08 min), triethyltin (2.63 min), di(n-butyl)tin (2.85 min), tri(n-butyl)tin (3.35 min) and tetra(n-butyl)tin (3.43 min). Redistribution of the compounds did not occur. The stannane results mainly from contamination of the sodium tetrahydroborate by inorganic tin. The tin blank of 1.2 ng can be further reduced by purging the tetrahydroborate solution with nitrogen [13]. Splitting of the inorganic tin peak occurred occasionally as before [13]. Splitting of the tri(n-butyl)tin hydride peak, noted when a 2% coating of SP-2100 was used, probably indicates desorption from different sites on the packing material.

Sensitivity and selectivity

Table 1 illustrates calibration data for triethyltin and n-butyltin compounds at 224.61 nm in water. The sensitivity to the n-butyltin compounds decreases with increasing numbers of n-butyl groups. The linear calibration range extends from subnanogram quantities to ca. 12 ng. The range can be extended by using a less sensitive wavelength such as 235.48 nm [13]. The detection limit of 45 pg for $(n\text{-}Bu)_3Sn^+$ is among the lowest reported, and a minimum of sample manipulation is needed. Triethyltin was chosen as an internal standard because it undergoes the same reduction process as mono-,

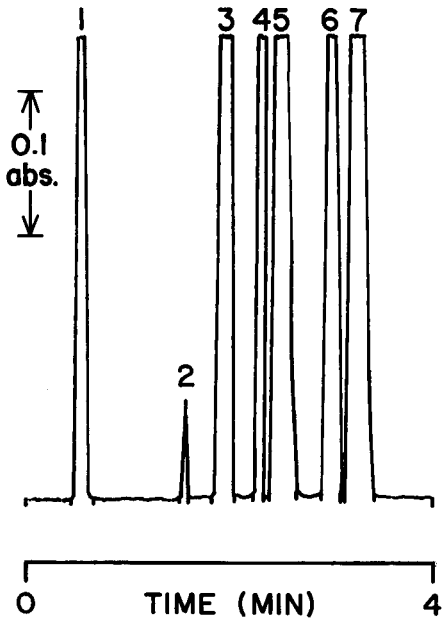

Fig. 2. Chromatogram of inorganic tin, trimethyl-, triethyl- and n-butyl-tin compounds. Peaks (and amounts as ng Sn): (1) inorganic tin (1.2); (2) trimethyltin (0.2); (3) mono-n-butyltin (2); (4) triethyltin (2.2); (5) di(n-butyl)tin (2.6); (6) tri(n-butyl)tin (1.8); (7) tetra(n-butyl)tin (2.2).

TABLE 1

Data for linear range, detection limits, and reproducibility for triethyltin and n-butyltin compounds

Compound	Linear range[a] (ng)	Slope[b] $\times 10^{-7}$	Intercept[c] $\times 10^{-7}$	$S_{est(y)}$[d]	Detection limit[e] (pg)
$(n\text{-Bu})Sn^{3+}$	0.03—12	0.747 (5)	—0.107 (6)	0.005	11
Et_3Sn^+	0.06—5	0.321 (7)	—0.305 (1)	0.003	22
$(n\text{-Bu})_2Sn^{2+}$	0.04—13	0.558 (12)	—0.056 (14)	0.009	14
$(n\text{-Bu})_3Sn^+$	0.10—8	0.159 (18)	—0.096 (21)	0.004	45

[a]From 10σ of blank to limit of linearity. [b]Correlation coefficients are greater than 0.99. Slope values are ng Sn (arbitrary relative units)$^{-1}$. RSD (%), given in parentheses, is for 2 ng, as tin ($n = 5$). [c]Arbitrary relative units. [d]Standard error of estimate. [e]Based on 3σ of background and 100-ml samples.

di-, and tri-(n-butyl)tin, has a retention time between mono- and di-(n-butyl)-tin, and is not known to occur in the environment. By using a slower rate of heating, determination of methyltin compounds is possible, but with a slight loss of sensitivity for n-butyltin compounds.

Conclusion

The method allows the simultaneous speciation of n-butyltin compounds with little sample manipulation at detection limits of 11 pg for mono-, 14 pg for di-, and 45 pg for tri-(n-butyl)tin. The detection of methyltin compounds is also possible. The technique incorporates the flexibility and selectivity of a.a.s. as the detector, with detection limits lower than those reported previously [8, 12, 13]. The internal standard for the proposed method confirms proper operation and allows direct calibration for each individual compound. Speciation of n-butyltin compounds from complex matrices is under study.

This research was funded in part by the Office of Sea Grant, National Oceanic and Atmospheric Administration, and in part by EPA grant R 809416. It is contribution UNHMP-JR-SG-85-18 from the University of New Hampshire Sea Grant Program.

REFERENCES

1 J. A. J. Thompson, M. G. Sheffer, R. C. Pierce, Y. K. Chau, J. J. Cooney, W. R. Cullen and R. J. Maguire, Organotin Compounds in the Aquatic Environment, 1985, NRCC/CNRC 22494 Ottawa, Canada.
2 P. J. Craig, in G. Wilkinson (Ed.), Comprehensive Organometallic Chemistry, Vol. 2, Pergamon Press, Oxford, 1982, p. 979.
3 R. B. Laughlin, Jr. and W. J. French, Bull. Environ. Contam. Toxicol., 25 (1980) 802.
4 G. E. Walsh, L. L. McLaughlan, E. M. Lores, M. K. Louie and C. H. Deans, Chemosphere, 14 (1985) 383.
5 P. Hocquellet, At. Spectrosc., 6 (1985) 69.
6 R. J. Maguire and H. Huneault, J. Chromatogr., 209 (1981) 458.
7 R. J. Maguire, Environ. Sci. Technol., 18 (1984) 291.
8 R. J. Maguire and R. J. Tkacz, J. Chromatogr., 268 (1983) 99.
9 H. A. Meinema, T. Burger-Wiersma, G. Versluis-de Haan and E. Ch. Gevers, Environ. Sci. Technol., 12 (1978) 288.
10 D. R. Hansen, C. H. Lillie and H. H. Hill, Jr., J. Chromatogr. Sci., 23 (1985) 208.
11 L. Ebdon, S. J. Hill and P. Jones, Analyst (London), 110 (1985) 515.
12 V. F. Hodge, S. L. Seidel and E. D. Goldberg, Anal. Chem., 51 (1979) 1256.
13 O. F. X. Donard, S. Rapsomanikis and J. H. Weber, Anal. Chem., 58 (1986) 772.
14 S. Rapsomanikis, O. F. X. Donard and J. H. Weber, Anal. Chem., 58 (1986) 35.

Analytica Chimica Acta, 184 (1986) 205—212
Elsevier Science Publishers B.V., Amsterdam — Printed in The Netherlands

DETERMINATION OF ARSENIC IN GLYCERINE BY FLOW INJECTION, HYDRIDE GENERATION AND INDUCTIVELY-COUPLED PLASMA/ ATOMIC EMISSION SPECTROMETRY

NGEE-HENG TIOH[a], YECHESKEL ISRAEL[b] and RAMON M. BARNES*

University of Massachusetts, Department of Chemistry, GRC Towers, Amherst, MA 01003-0035 (U.S.A.)

(Received 2nd November 1984)

SUMMARY

The determination of low concentrations of arsenic in glycerine is investigated with flow injection for the introduction of analyte and tetrahydroborate reagent for arsine generation, separation in a vapor-liquid flow cell, and inductively-coupled plasma/atomic emission spectrometry (i.c.p./a.e.s.). Peak areas are used to quantify arsenic in the concentration range 0.12—3.0 $\mu g\ ml^{-1}$. Peak areas for prepared standards exhibited average deviations of about 1.4% for this concentration range. The slope and intercept for a least-squares fit of area (nanocoulombs) vs. concentration ($\mu g\ ml^{-1}$) were 10.9 ± 0.17 and 0.46 ± 0.3, respectively.

Hydride generation with inductively-coupled plasma/atomic emission spectrometry (i.c.p./a.e.s.) is advantageous for the determination of hydride-forming volatile elements, owing to the reduced detection limits [1, 2]. This is attributed to the separation of the volatile hydride from the analyte matrix, thus increasing the concentration of hydride in the gas reaching the plasma. The detection limit for arsenic is improved 100-fold compared to nebulization of arsenic from aqueous solution [1, 2]. However, manually controlled hydride generation with i.c.p./a.e.s., although accurate, demands close operator attention and proficiency to obtain consistent results. Moreover, the evolution of hydrogen into the i.c.p. requires that appropriate background changes be evaluated [3].

The introduction of sample solutions by flow injection with various detectors is a valuable approach and is utilized extensively for rapid routine quantitation [4, 5]. Thompson et al. [1, 6, 7] described a continuous-flow hydride-generation technique with a flow cell for separation of arsenic and other volatile hydrides. Pruszkowska et al. [8] evaluated the performance of a similar flow cell with a commercial flow-injection processor interfaced to a

---

[a]On leave from the Chemistry Department, University of Malaya, Kuala Lumpur 22-11, Malaysia.
[b]On leave from IMI Institute for Research and Development, Haifa 31002, Israel.

0003-2670/86/$03.50

sequential i.c.p. for the quantitation of arsenic and selenium in a water standard and samples. Liversage et al. [9] described a flow-injection/hydride-generation system for i.c.p./a.e.s. which produced minimal hydrogen evolution by injecting both the tetrahydroborate reagent and the sample into a distilled-water carrier.

Glycerine is a water-soluble compound that has wide applications in the pharmaceutical industry [10]. Determination of the arsenic content in this compound is of interest for quality control on the maximum permissible concentration, 1.5 $\mu g\ g^{-1}$ [10]. Preliminary studies were conducted in this laboratory to determine arsenic in industrial glycerine by batch hydride generation with i.c.p./a.e.s., and it was demonstrated that no significant difference was obtained in the results for arsenic in glycerine whether or not the procedure included acid digestion. These results served as the basis for the present approach incorporating flow injection with hydride generation and i.c.p./a.e.s. However, the conditions associated with the use of the flow-injection procedure required that all chemical and instrumental operating parameters be evaluated. These parameters included initial dilution of the glycerine sample, tetrahydroborate and acid reagent concentrations, and their volume ratio. Results for the determination of arsenic in industrial glycerine are presented.

EXPERIMENTAL

Apparatus

The commercial flow-injection instrument used (Fiatron Systems, Model SHS-200) includes an all-teflon, dual-channel sample injector consisting of electronically driven, microminiature solenoid valves. A multiroller, variable-speed pump is situated before the valves and can be operated in continuous-flow or in stopped-flow modes. The continuous-flow mode was used. A diagram of the arrangement is given in Fig. 1. Four of the multiroller pump streams (P) were used. Usually two of the multiroller streams were used for pumping the acid reagent, which was subsequently merged at Y_1, a Y-shaped connector. Both of these streams by-passed the instrument valve system (V). The two remaining streams were applied in the normal flow-injection mode through the valve system (V) to pass the tetrahydroborate carrier (C) and the analyte (S) either through the first loop (L_1, Fig. 1A) or through the second loop (L_2, Fig. 1B) and subsequently to merge at Y_2, the second Y-shaped connector, with the acid streams of Y_1. In some preliminary experiments, only one acid stream was used, and only three streams of the multiroller pump and one Y-connector were required.

Two sizes of manifold tubing (Fisherbrand Accu-Rated PVC) were used for the pump with flow rates of 2.24 ml min^{-1} and 8.75 ml min^{-1} at 100% motor speed. The latter served as one of the acid streams. With these conditions, the volume ratio of acid to tetrahydroborate was 4.9:1 when two channels were used for the acid. Various injection volumes for the analyte were examined, but usually 10-s injection was chosen, corresponding to 374 μl.

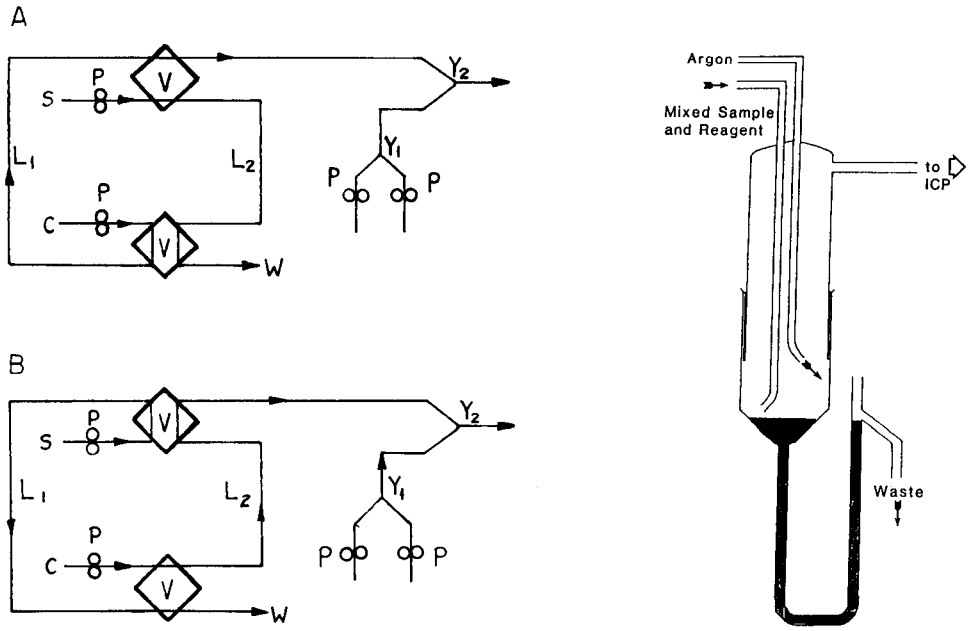

Fig. 1. Diagram of flow-injection apparatus. (A) Flow of sample and carrier through sampling loop L_1. (B) Flow of sample and carrier through sampling loop L_2.

Fig. 2. Hydride/liquid phase separator cell.

The glass flow cell for vapor-liquid separation, patterned after the one described by Thompson et al. [1], is depicted in Fig. 2. The inlet of the mixed sample plus reagents is connected directly to Y_2 in Fig. 1. Vapor-liquid separation is initiated in Y_2 and continued in the flow cell. The argon carrier gas flushed the vapors through the upper outlet side tube directly into the base of the plasma torch. The U-shaped tube at the bottom of the flow cell was filled by the liquid (Fig. 2) and its excess drained to waste.

Instrumentation for i.c.p./a.e.s. was as described previously [11, 12], although a nebulizer was not needed. BASIC software was developed for data acquisition, for digital smoothing, and for calculating mean values from sets of consecutive measurements. Intensity/time curves were plotted (Hewlett-Packard 7221 B), with or without digital smoothing. Peak heights or peak areas (in nanocoulombs (nC)) (for a specified time span of 105-s) were calculated along with the relative standard deviation (s_b) of the background current.

Flow-injection operating conditions for the determination of arsenic in glycerine are listed in Table 1. They result from the adaptation of previously determined operating conditions for hydride generation using Simplex optimization [11, 13].

TABLE 1

Operating conditions for quantitation of arsenic in glycerine

Flow system		*Spectrometer*	
Flow rate, carrier	2.24 ml min^{-1}	Wavelength	193.70 nm
acid (stream 1)	8.75 ml min^{-1}	Power	0.65 kW
acid (stream 2)	2.24 ml min^{-1}	Argon flow rate	
Glycerine in injected solution	200 g l^{-1}	outer	15.30 l min^{-1}
Injected volume	374 µl	central	0.39 l min^{-1}
$NaBH_4$ carrier	1.1% (w/v)	intermediate	0.10 l min^{-1}
Acid/BH_4^-	4.9:1 (v/v)	Mean observation height	16 mm
Peak area computation time	105 s	Slit height	5 mm
Data collection time for duplicates	270 s	Image magnification	1
		Monochromator slit widths	50 µm

Reagents and solutions

Analytical grade hydrochloric acid, sodium hydroxide, and deionized distilled water were used. Hydrochloric acid was distilled isothermally.

Various solutions of sodium tetrahydroborate (0.4—2.0%) (MCB reagents) were prepared in either 0.2 M, or in 0.5 M sodium hydroxide. The cloudy solutions were pressure-filtered through 0.45-µm membrane filters. Sodium hydroxide stabilized the sodium tetrahydrohydrate solution [14].

Purified arsenic trioxide (Mallinckrodt) was dissolved in hydrochloric acid and was then diluted (1 + 99) with deionized distilled water.

Arsenic-free glycerine, as well as industrial glycerine samples, were supplied by Procter and Gamble (Cincinnati, OH) [15]. Glycerine samples had to be diluted with deionized distilled water before injection. Various dilutions were made to select an appropriate viscosity which can be handled by the flow-injection instrument. Concentration of glycerine greater than 200 g l^{-1} seemed too viscous, therefore two dilutions of 200 g l^{-1} and 100 g l^{-1} were prepared and examined. A series of standard solutions of glycerine was prepared from the arsenic-free reagent for each one of the above dilutions by adding the calculated volume of the acidic arsenic trichloride solution to give final solutions containing 0.12—3.0 µg As g^{-1} of glycerine (either in 200 g l^{-1} or in 100 g l^{-1} glycerine solutions).

RESULTS AND DISCUSSION

Operating conditions

A 2% (w/v) solution of sodium tetrahydroborate, previously found to be most suitable for hydride generation [11], was too concentrated for the proposed system because the discharge was unstable. Therefore, lower concentrations were examined with aqueous standard solutions of arsenic (0.7 µg ml^{-1}). The results are listed in Table 2. With 0.4% sodium tetrahydroborate solutions, the peak-area measurements were low, and no significant change in the signals was observed when the concentration of sodium tetrahydroborate exceeded 1.2%. For glycerine solutions, a suitable concentration range for

TABLE 2

Dependence of arsenic peak-area measurements on the concentration of sodium tetrahydroborate and sodium hydroxide in the carrier

$NaBH_4$ (%)	NaOH (M)	Peak area[a] (nC)	s_b[b] (%)	$NaBH_4$ (%)	NaOH (M)	Peak area[a] (nC)	s_b[b] (%)
0.4	0.5	0.866	3.3	1.2	0.5	2.024	2.2
0.4	0.5	0.792	3.0	1.2	0.5	2.060	2.9
0.8	0.2	1.683	1.8	1.5	0.5	2.070	2.4
0.8	0.2	1.568	2.1	1.5	0.5	2.095	2.4
1.0	0.5	1.870	2.5				

[a]Average of two determinations. [b]Relative standard deviation of background (Fig. 4); 0.7 μg As ml^{-1} in aqueous 4 M HCl.

sodium tetrahydroborate was 1.0—1.2%, and a 1.1% solution was adopted. While a hydrochloric acid dilution of 1 + 2 was adequate both for hydride generation and for flow-injection/hydride generation with aqueous arsenic solutions, when glycerine solutions were used, a 1 + 1 dilution of 6 M hydrochloric acid was preferred. A volume ratio of HCl to tetrahydroborate of 4.9:1 was used for best results. No significant difference existed between the results obtained when the tetrahydroborate solutions were prepared in 0.2 M and 0.5 M sodium hydroxide, provided that this reagent was used within a few days after preparation.

There were no advantages in using a 100 g l^{-1} solution of glycerine compared to 200 g l^{-1}. Similar blanks were observed for both solutions, and the more dilute solution promoted more bacterial growth when left standing at room temperature for a few days. Accordingly, subsequent work was done with 200 g l^{-1} glycerine solutions.

Injecting an arsenic-free glycerine blank produced a small signal, the area of which averaged 0.33 nC for a time span of 105 s (Fig. 3, curve a) while the average area of a peak for a glycerine solution containing 0.4 μg As g^{-1} was 5.03 nC after blank correction (Fig. 3, curve b). However, superimposing the well-defined transient signal (curve b) on the blank reveals a negative signal for the blank, which coincides with the peak of curve (b), and the origin of which is unknown. In contrast to the well-defined transient of curve (b), the transient signals observed for higher concentrations of arsenic, for both the standard solutions and the samples, exhibited signal pulsations and broadening at half-peak heights, accompanied by some degree of flickering of the plasma (Fig. 4). In addition, the reproducibility of the peak heights for the same analyte was poor. Linearity of peak heights with arsenic concentration in glycerine was observed to 2.0 μg As g^{-1}. Variation of the shapes and time dispersions of the peaks along with the deviation of peak heights from linearity with arsenic concentration is inconsistent with conventional flow-injection behavior. The reason for this deviation from conventional

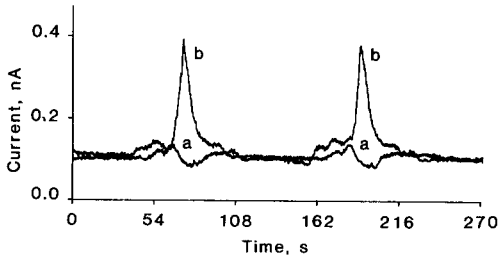

Fig. 3. Response for glycerine sample with 1.1% $NaBH_4$ and 1 + 1 HCl in duplicate: (a) arsenic free; (b) containing 0.4 μg As g^{-1} glycerine.

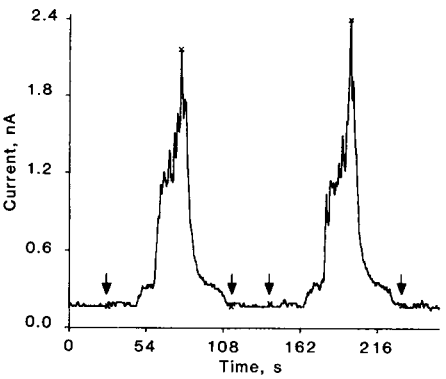

Fig. 4. Duplicate arsenic signals for a glycerine sample containing 3.0 μg As g^{-1} glycerine. The arrows indicate the start and end of the integration period. Peak areas are 34.5 nC and 36.5 nC, s_b for the two injections was 1.4% and 5.6%, and the calculated limits of detection were 0.03 and 0.1 ng ml^{-1}, respectively.

behavior stems from the added complexity of the hydride generation and separator which involves a three-stage process. The time-dependent transient shape is most likely influenced by the effects of vapor (arsine and H_2) formation on the flow patterns in both the liquid stream and the argon carrier gas to the i.c.p. Although it might be possible to modify the flow-injection system to permit peak heights to be used for higher arsenic concentrations [16] this possibility was not examined here and peak areas were used.

Glycerine samples

Glycerine solutions containing known amounts of arsenic were processed as described above. The reproducibility of peak areas for concentrations between 0.7 and 3.0 μg As g^{-1} glycerine exhibited an average difference of ±1.4% for duplicate samples. A least-squares fit of the peak areas (nC) vs. concentration (0.12—3.0 μg As g^{-1}, see Fig. 5) gave a slope of 10.96 nCg μg^{-1}, with a standard deviation of ±0.17, and an intercept of 0.46 ± 0.30 nC.

Industrial glycerine samples were processed in a similar manner, and results are listed in Table 3. The results obtained for samples 1 and 3 are in excellent

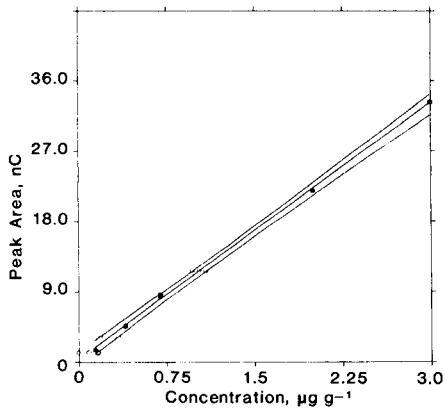

Fig. 5. Calibration graph of arsenic emission peak area (nC) for concentration of arsenic in glycerine standard solutions (•). Confidence bands at the 95% level are indicated with intersection of curves at peak area values corresponding to samples 1—3 in Table 3 (○).

TABLE 3

Arsenic in industrial glycerine

Sample	Peak area[a] (nC)	Glycerine concn.[b] ($\mu g\ g^{-1}$)			
		Added	Found	Difference	Literature [15]
1	1.31	0.1	0.08 ± 0.08	0.02	0.08
2	3.06	0.5	0.26 ± 0.08	—0.24	0.46
3	11.71	1.0	1.03 ± 0.05	0.03	1.1
4	63.22[c]	7.0	5.73 ± 0.27	—1.27	7.4

[a]Blank area corrected. [b]Concentration range based on 95% confidence band limits of calibration function (Fig. 5). [c]Beyond the range of the calibration.

agreement. The large deviation for sample 4 probably results from the peak area exceeding the maximum linear range of the calibration curve. The result for sample 2 is anomalously low. However, if peak height instead of peak area were used, the concentration of sample 2 would be 0.47 μg As g^{-1}. In view of the results for sample 2, further investigation of the flow cell design to reduce signal variations (Fig. 4) is warranted.

We thank Baird Corporation for the loan of the Fiatron instrument. Research was supported by the ICP Information Newsletter, and Department of Energy Contract DE-AC02-77EV-0432. Paper presented at the 1984 Winter Conference on Plasma Spectrochemistry, January 1984, San Diego, CA.

REFERENCES

1 M. Thompson, B. Pahlavanpour, S. J. Walton and G. F. Kirkbright, Analyst (London), 103 (1978) 568.
2 T. Nakahara, Prog. Anal. Atom. Spectrosc., 6 (1983) 163.
3 P. Fodor and R. M. Barnes, Spectrochim. Acta, Part B: 38 (1983) 229.
4 J. Růžička and E. H. Hansen, Flow Injection Analysis, Wiley, New York, 1981, pp. 15—17 and 146—176.
5 D. Betteridge, Anal. Chem., 50 (1978) 832A.
6 M. Thompson, B. Pahlavanpour, S. J. Walton and G. F. Kirkbright, Analyst (London), 103 (1978) 705.
7 M. Thompson and B. Pahlavanpour, Anal. Chim. Acta, 109 (1979) 251.
8 E. Pruszkowska, P. Barrett, R. Ediger and G. Wallace, Atom. Spectrosc., 4 (1983) 94.
9 R. Liversage, J. C. Van Loon and J. C. De Andrade, Anal. Chim. Acta, 161 (1984) 275.
10 U.S. Pharmacopeia, 20th revision, U.S. Pharmacopeal Convention, Rockville, MD, 1980, p. 353.
11 L. R. Parker, Jr., N. H. Tioh and R. M. Barnes, Appl. Spectrosc., 39 (1985) 45.
12 H. S. Mahanti and R. M. Barnes, Anal. Chem., 55 (1983) 405.
13 L. R. Parker, Jr., M. R. Cave and R. M. Barnes, Anal. Chim. Acta, 175 (1985) 231.
14 J. R. Knechtel and J. L. Fraser, Analyst (London), 103 (1978) 104.
15 A. H. Ullman, J. Am. Oil Chem. Soc., 60 (1983) 614.
16 G. S. Pyen, S. Long and R. F. Browner, Appl. Spectrosc., 40 (1986) 246.

Analytica Chimica Acta, 184 (1986) 213—218
Elsevier Science Publishers B.V., Amsterdam — Printed in The Netherlands

DETERMINATION OF ARSENIC BY HYDRIDE GENERATION WITH A LONG ABSORPTION CELL FOR ATOMIC ABSORPTION SPECTROMETRY

W. J. WANG, S. HANAMURA and J. D. WINEFORDNER*
Department of Chemistry, University of Florida, Gainesville, FL 32611 (U.S.A.)
(Received 21st October 1985)

SUMMARY

A method is described for the determination of arsenic involving hydride generation and atomic absorption spectrometry with an improved long graphite-tube furnace capable of considerably higher temperatures than the conventional quartz-tube heaters. Arsine is generated with sodium tetrahydroborate, held in a nitrogen-cooled trap and then swept with helium into an alumina tube (19 cm long) placed within the graphite furnace. The optimum conditions for determination of arsenic are given. The detection limit is 0.2 ng ml^{-1} with RSD of 2—3%. Results for various NBS Standard Reference Materials agreed well with expected values and were as follows: orchard leaves, 10 ± 1 $\mu g\ g^{-1}$; tomato leaves, 0.28 ± 0.03 $\mu g\ g^{-1}$; bovine liver, 0.046 ± 0.005 $\mu g\ g^{-1}$.

Graphite electrothermal atomizers are commonly used as absorption cells in atomic absorption spectrometry. Most graphite furnaces are designed to vaporize and atomize the sample into a relatively small volume so as to improve sensitivity. L'vov [1] and Woodriff and co-workers [2, 3] have given quantitative relationships for absorption with respect to length, temperature, and pressure. These workers as well as others have shown that the overall sensitivity is proportional to the 3rd power of the length and that analyte loss by diffusion is less serious with long closed tubes than it is for tubes with openings near the center.

Ng and Caruso [4] recently reviewed electrothermal vaporization for sample introduction in atomic spectrometry and stressed the importance of independent control of vaporization and atomization which results in higher sensitivity and more efficient atomization of analyte in different sample types introduced into the atom reservoir. Hydride generation is one means of independent introduction of suitable analytes into furnaces, flames, and plasmas. Nakahara [5] has reviewed the principles and applications of hydride-generation techniques in atomic absorption spectrometry. Improvements in detectability of hydride generation over direct introduction of sample solutions were obtained in most cases [6, 7]. In this paper, a hydride-generation system coupled with a long-tube graphite furnace is used to quantify arsenic and is evaluated with respect to optimum conditions and quantitative applications.

0003-2670/86/$03.50

The long-tube furnace achieves a much higher temperature (>1200°C) than is possible with conventional quartz vessels. Thus atomization is much more efficient for many elements.

EXPERIMENTAL

Apparatus

A Hitachi Model 180-80 atomic absorption spectrometer equipped with a tube graphite furnace (14 cm long), hollow-cathode lamp (Hamamatsu), and a Hitachi Model 056 strip-chart recorder were used. General aspects of the absorption cell are shown in Fig. 1.

The apparatus used for the generation of arsine is similar to the one described by Uthus et al. [9]. Helium is used as the arsine carrier because it has a lower boiling point than liquid nitrogen, which avoids clogging that would take place with argon. The line from the gas cylinder is split with a glass Y-joint into two lines provided with separate flowmeters. One line is connected to the left side inlet of the graphite tube to sweep the helium/arsine mixture into the furnace; the other line is connected to the quartz tube as a sheath gas to minimize degradation of the graphite heater tube. Because of the outer diameter of the long tube furnace, the magnet of the Zeeman spectrometer could not be used and so background correction was made separately from sample measurements. A new long tube furnace is now being designed for use with the Zeeman magnet to allow background correction.

Reagents

A standard stock solution of arsenic was prepared by dissolving arsenic trioxide (SRM 83b, National Bureau of Standards). High-purity hydrochloric

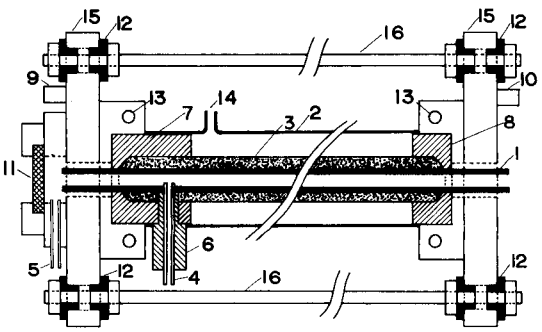

Fig. 1. Cross-sectional view of long absorption cell: (1) inner tube (i.d. 2.4 mm, o.d. 6.5 mm, length 19 cm, alumina); (2) quartz tube (o.d. 27 mm, length 14 cm); (3) heater tube (i.d. 6.5 mm, o.d. 9.5 mm, length 14 cm, graphite); (4) sample gas inlet tube (alumina); (5) argon carrier gas inlet tube (brass); (6) sample gas inlet tube holder (graphite); (7, 8) graphite electrodes; (9, 10) terminals; (11) quartz window; (12) insulator; (13) electrode cooling water tube; (14) sheath gas inlet; (15) electrode assembly holder (brass); (16) electrode assembly holder binding bar (brass).

and nitric acids were prepared by using the sub-boiling method [10]. The aqueous 10% (w/v) sodium tetrahydroborate solution was prepared by dissolving the sodium salt (A.C.S. grade, Fisher Scientific) in aqueous 0.5% (w/v) potassium hydroxide (86%, Mallinckrodt). This solution was filtered through No. 41 filter paper (Whatman) before use. An aqueous 20% (w/v) potassium iodide (A.C.S. grade, Fisher Scientific) solution was used. Deionized water was used throughout.

Preparation of NBS Standard Reference Materials (SRM)

Standard reference materials (NBS) were dried in a desiccator for 2 days over phosphorus pentoxide. Approximately 250 mg of sample (orchard leaves, SRM 1571; tomato leaves, SRM 1573; bovine liver, SRM 1577) was weighed into a 300-ml round-bottom flask, and then 10 ml of high-purity nitric acid and 1 ml of sulfuric acid were added. The sample/acid mixture was digested with a condenser and a laboratory-constructed nitric acid reservoir. The side-arm reservoir was used to collect the condensed nitric acid after the production of sulfur trioxide fumes; the flask was then cooled and the condensed nitric acid solution was returned to the sample mixture. The digesting procedure was repeated until the residual solution became clear. The solution was transferred to a teflon beaker and evaporated to white fumes. Finally, the digested solution was transferred to a 50-ml volumetric flask and diluted with deionized water to the mark. This sample was then used directly for arsenic measurements. Standard calibration solutions were prepared in 100-ml flasks from a 1000-mg l^{-1} stock solution of arsenic containing 4% (v/v) hydrochloric acid.

Arsenic generation

Figure 2 shows the block diagram of the arsine generation system. The 1-ml sample was placed in the 100-ml round bottom flask with 1 ml of the iodide solution, 2 ml of water, and 1 ml of 6 M hydrochloric acid. The solution was stirred, 1 ml of the tetrahydroborate solution was added, and the arsine was collected by the liquid nitrogen trap; this process required about 6 min. Power was applied to the graphite furnace, which was adjusted to a constant temperature before the liquid nitrogen dewar flask was replaced by a beaker which was filled with water at room temperature.

RESULTS AND DISCUSSION

The optimum amounts and concentrations of hydrochloric acid, iodide and tetrahydroborate were selected from previous studies [9, 11, 12]. The effects of the flow rates of argon and helium carrier gas on peak height are shown in Fig. 3. An argon flow rate of 120 ml min^{-1} and a helium flow rate of 55 ml min^{-1} gave maximum absorption for the samples used.

The arsine signal for 1 ng of arsenic was shown to reach a plateau over the range 6—10 min trapping time, indicating complete generation, trapping, and

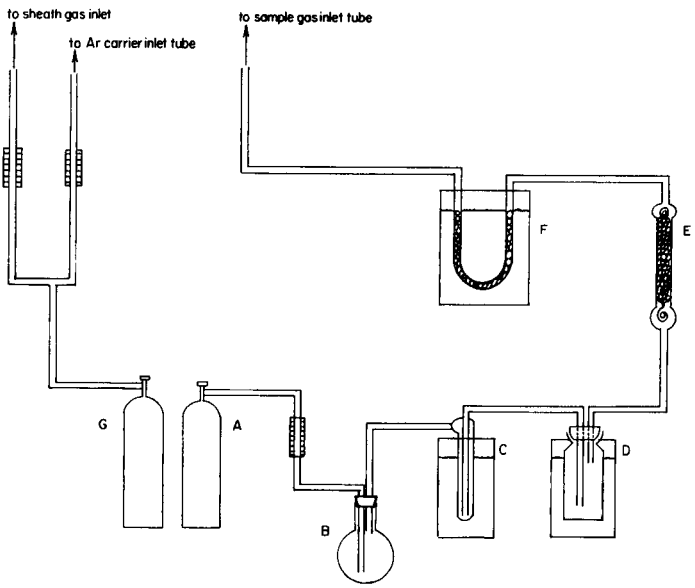

Fig. 2. Block diagram of arsine generation system: (A) helium; (B) generating flask; (C, D) dry ice/acetone cold traps to collect water; (E) $CaCl_2$ drying tube; (F) liquid nitrogen cold trap; (G) argon.

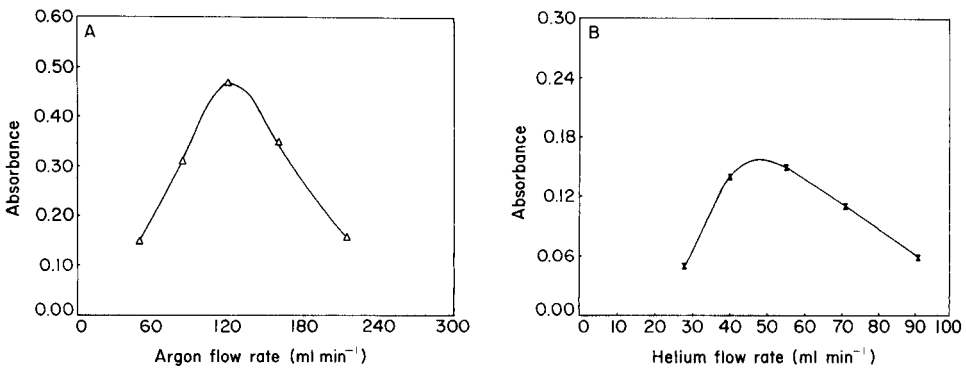

Fig. 3. Absorbance vs. flow rate: (A) argon for 10 ng As; (B) helium for 1 ng As.

release of the arsine. This result agreed with the results of Shaikh and Tallman [13]. The trapping time limited the sampling rate of the method; in the present system, it is about 6 samples per hour.

With the long absorption cell, the limit of detection was 0.2 ng ml^{-1} (S/N = 3). The arsenic content of various NBS standards was also determined (Table 1). The values obtained for six determinations agreed well with the certified values. According to Kang and Valentine [14], residual sulfuric acid below 5% in the final biological sample solution did not interfere with the determination of arsenic as long as the arsine was collected in a suitable trap and released rapidly for measurement.

TABLE 1

Arsenic content of NBS Standard Reference Materials

SRM	Arsenic content ($\mu g\ g^{-1}$)	
	Present study[a]	Certified value
1571: orchard leaves	10 ± 1	10 ± 2
1573: tomato leaves	0.28 ± 0.03	0.27 ± 0.05
1577: bovine liver	0.046 ± 0.005	0.055 ± 0.005

[a]Mean and standard deviation for 6 determinations on dried samples.

Sturgeon and Berman [15] found that an increase of the partial pressure of oxygen in the graphite furnace suppressed the rate of condensed-phase thermal dissociation of analyte oxides, resulting in thermal shifting of the absorption pulses by the reaction $M_xO_y(s, l) \rightarrow xM(g) + y/2O_2$. The availability of carbon atoms on graphite to adsorb oxygen resulted in an increase in the number of gas-phase analyte atoms. It was not sufficient to consider only the interaction between oxygen and the graphite surface, because graphite formed intercalation or lamellar compounds. Koreckova et al. [16] showed that 45% of ^{74}As was left after pretreatment of the regular graphite tube at 1400°C for 90 s. Figures 4 and 5 show the effect of using the regular graphite tube alone and using an inner alumina tube with the graphite outer tube. It is clear that the inner alumina tube can prevent any interaction between graphite and arsenic, so that the sensitivity is increased.

Figure 6 shows a plot of the absorption signal vs. furnace temperature; the furnace temperatures were measured with an optical pyrometer. It is apparent that the arsine dissociates as the temperature increases above 1150—1200°C.

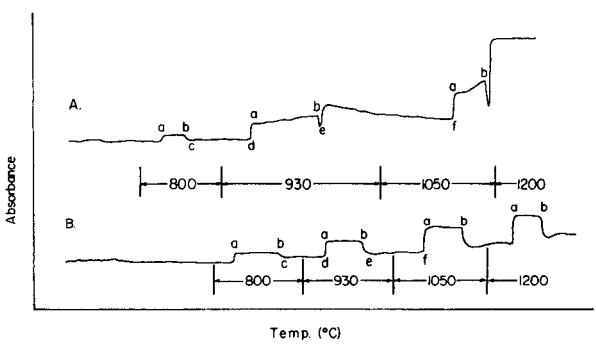

Fig. 4. Effect of inner tube material on absorbance for cylinder arsine at a flow rate of 10 ml min^{-1}: (a) AsH_3 turned on; (b) AsH_3 turned off; (c, d) temperature increased from 800 to 930°C; (e, f) temperature increased from 930 to 1050°C. (A) Graphite inner surface; (B) graphite outer tube with alumina inner surface.

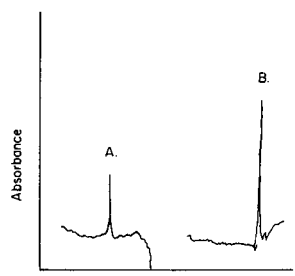

Fig. 5. Effect of inner tube material on absorbance from 10 ng As (1330°C, liquid nitrogen trapping time 6 min). A and B as in Fig. 4.

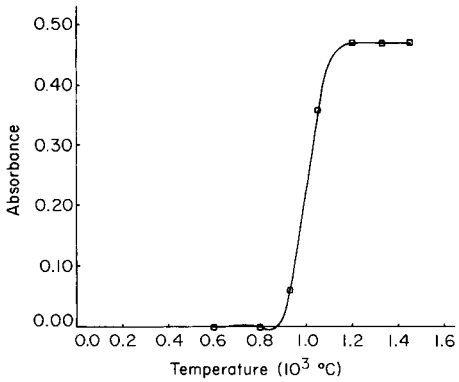

Fig. 6. Absorbance vs. furnace temperature for 10 ng of arsenic.

Two atomization mechanisms have been proposed [8, 17] for arsine; for both mechanisms, the appearance temperature was around 900°C. When tank arsine was used, a plot similar to that in Fig. 6 was obtained. This implies that the atomization mechanism based on reduction of arsine with hydrogen to arsenic [17] is not likely, but the mechanism involving thermal dissociation of the As_4 and As_2 species [8] is a possibility.

This research was supported by EPA-R-810387-01-1.

REFERENCES

1 B. V. L'vov, Atomic Absorption Spectrochemical Analysis, Elsevier, New York, 1970.
2 R. Woodriff, Appl. Spectrosc., 28 (1974) 413.
3 S. R. Lawson, F. G. Dewalt and R. Woodriff, Prog. Anal. At. Spectrosc., 6 (1983) 1.
4 K. C. Ng and J. A. Caruso, Appl. Spectrosc., 39 (1985) 719.
5 T. Nakahara, Prog. Anal. At. Spectrosc., 6 (1983) 163.
6 K. C. Thompson and D. R. Thomerson, Analyst (London), 99 (1974) 595.
7 M. H. Hahn, K. A. Wolnik, F. L. Fricke and J. A. Caruso, Anal. Chem., 54 (1982) 1048.
8 S. Akman, O. Genc and T. Balkis. Spectrochim. Acta, Part B: 37 (1982) 903.
9 E. O. Uthus, M. E. Collings, W. E. Cornatzer and F. H. Nielsen, Anal. Chem., 53 (1981) 2221.
10 E. C. Kuehner, R. Alvarez, P. J. Paulsen and T. J. Murphy, Anal. Chem., 44 (1972) 2050.
11 J. Aggett and A. C. Aspell, Analyst (London), 101 (1976) 341.
12 T. Inui, S. Terada and H. Tamura, Fresenius' Z. Anal. Chem., 305 (1981) 189.
13 A. U. Shaikh and D. E. Tallman, Anal. Chem., 49 (1977) 1093.
14 H. K. Kang and J. L. Valentine, Anal. Chem., 49 (1977) 1829.
15 R. E. Sturgeon and S. S. Berman, Anal. Chem., 57 (1985) 1268.
16 J. Koreckova, W. Frech, E. Lundberg, J. Persson and A. Cedergren, Anal. Chim. Acta, 130 (1981) 267.
17 B. Welz and M. Melcher, Analyst (London), 108 (1983) 213.

Analytica Chimica Acta, 184 (1986) 219—226
Elsevier Science Publishers B.V., Amsterdam — Printed in The Netherlands

EFFECTIVE ENERGY COUPLING FOR 200-MHz PULSED RADIOFREQUENCY SPECTROSCOPIC DISCHARGES

DAVID M. COLEMAN* and MARIO A. SAINZ[a]
Department of Chemistry, Wayne State University, Detroit, MI 48202 (U.S.A.)
(Received 15th November 1985)

SUMMARY

The introduction of various new radiofrequency electrical discharges has placed increased emphasis on circuit design which provides optimal energy transfer between a generator and its corresponding spectroscopic "load". This technology is well developed for high-frequency (ca. 27 MHz) inductively-coupled plasma discharges and for cavity discharges which operate in the microwave region (e.g., 2450 MHz). The 200-MHz very high frequency (VHF) region has received less attention. New circuitry is described which allows effective transfer of high power (5-kW), pulsed (2.5-μs), VHF (200-MHz) energy into a plasma suitable for analytical purposes. A triple-stub tuner is used in this circuitry. Comparison with other approaches and applicability to a variety of discharge systems are discussed.

Recent experiments which segregate the "sampling" step from the "excitation" step in a spark discharge have resulted in spectral simplification, minimization of background continuum, and narrow line emission [1]. This system involved a unidirectional spark which ablated a metal surface followed by inductively-coupled re-excitation of the resultant toroidal port-discharge environment [2]. A 2.5-μs burst of 200-MHz radiofrequency energy was used. Although emission intensities corresponding to re-excitation of the post-discharge torus are weak, compared to direct spark emission, signal-to-background ratios are often improved by several orders of magnitude. Photographic integrations exceeding 1-h duration were typical. [The time/space/wavelength-resolved spectrometer system used to collect such data operates with an optical time resolution of ca. 80 ns at a discharge repetition rate of 360 Hz. Thus, a "1-h exposure" corresponds to an integrated exposure of events totaling approximately 100 ms. The system will be described at a later date.] This research indicated the need for more efficient transfer of power for re-excitation purposes. Discharge luminosity was used to indicate optimum performance.

Instrumentation reported here dramatically improves such energy transfer.

---

[a]Present address: Allied Analytical, 590 Lincoln St., Waltham, MA 02154, U.S.A.

Instrumentation

Effective energy transfer requires that the impedance of the energy source be equal to the impedance of the load. In addition to limiting effective energy transfer to the load coil and plasma, the presence of load mismatch also results in reflected power transferred back to the generator, causing component failure.

A variety of impedance-matching networks to transform the source impedance into that of the load have been described for 27-MHz inductively-coupled plasma (i.c.p.) discharges (see, e.g. [3, 4]). Operation with these same devices at 200 MHz presents complications. In particular, the inductive and capacitive reactance of each element, resulting in parasitic oscillatory tank circuits, component placement relative to each other and to ground planes, and circuit losses, become very critical and difficult to predict at higher frequencies.

The voltage standing wave ratio (VSWR) is a direct measure of the ratio of forward (E_i) to reflected (E_r) voltage [5]:

$$\text{VSWR} = E_{max}/E_{min} = (E_i + E_r)/(E_i - E_r) \tag{1}$$

The total power actually delivered to the load is given by

$$P/P_i = (P_i - P_r)/P_i = (E_i^2 - E_r^2)/E_i^2 = 4(\text{VSWR})/(\text{VSWR} + 1)^2 \tag{2}$$

where P is the power delivered to the load and P_i and P_r are the incident and reflected powers, respectively. Figure 1 illustrates P calculated as a function of VSWR values assuming that P_i = 5 kW (this latter power level is typical for operation in this laboratory). Thus, a VSWR of 8 implies a badly mismatched circuit with less than 40% of generator forward output power delivered to the load. This level of reflected power can result in catastrophic damage to the output device.

Accurate measurement of VSWR at 200 MHz is also difficult. The envelope of generator output (terminated in a 50-Ω resistive dummy load) is shown in Fig. 2. The transient, non-ideal nature of this waveform contributes to measurement difficulties. It was noted in earlier work [1] that instrumentation was not available to measure the effectiveness of forward power transfer. As a result, it was possible only to correlate "optimum" power transfer with re-excitation emission intensities. This approach can be misleading as indicated by data presented here. Efforts to design a pulsed-radiofrequency (r.f.) monitoring facility were abandoned when a preproduction model of a Bird (Bird Electronic Corporation, 30303 Aurora Road, Cleveland, OH 44139) Model 4391 Power Analyst, was acquired. This instrument is designed for pulsed radar and similar applications and is an insertion-type digital r.f. bi-directional wattmeter designed to measure peak or average power, load mismatch (VSWR), and modulation properties in 50-Ω coaxial transmission lines. Directional plug-in units are available for a variety of frequency ranges and power levels. This instrument was used in acquiring all data reported here.

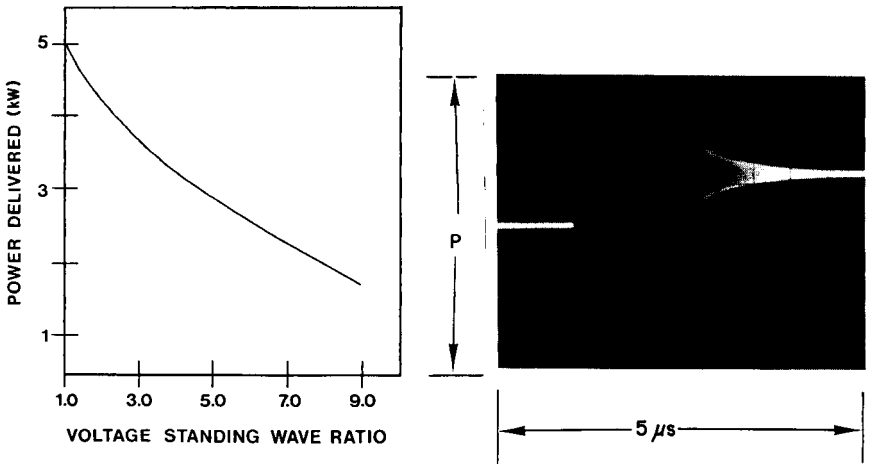

Fig. 1. Power delivered as a function of VSWR.

Fig. 2. Envelope of the 200-MHz radiofrequency pulse used for the inductive-coupling spectroscopic experiments described earlier [1]. The ordinate is relative power. The zero-offset after pulse turn-off is a characteristic property of the power-sensing circuit in the Heath (Benton Harbor, MI Model HN-31) 50-Ω resistive dummy load.

EXPERIMENTAL

The earlier experiments [1] used standard i.c.p.-type L-network impedance matching circuitry consisting of a micrometer-driven adjustable 1000-pF air dielectric-load capacitor to ground and a three-quarter-turn air-core indicator in series with the plasma load coil. This capacitor was fabricated from two ground and polished aluminum plates (5-cm diameter) supported on teflon standoffs and adjusted to be parallel to within ±0.0025 cm. This first-generation device sustained high losses. Further, this apparatus was temporally unstable, susceptible to temperature and humidity changes, and sensitive to static electricity effects. Based on an assumption that the air dielectric capacitor resulted in significant losses, this prototype unit was reconfigured with a low-loss, variable-drive, vacuum capacitor (Jennings Radio UCS300; 0—300 pF; glass-housing vacuum bellows-driven capacitor). As will be noted, this approach improved energy transfer, but acceptable VSWR levels were not possible.

The application of coaxial line tuners [6] was investigated as a new approach to improved performance. Components such as stub tuners, stub stretchers, and phase shifters are linear passive devices intended to introduce variable impedance and/or phase into a transmission line. These units are used in the range 0.1—10 GHz. A triple-stub tuner is outlined in Fig. 3. This device is theoretically capable of matching all impedances. Operation of the triple-stub tuner is based on the principle that mismatch in a coaxial transmission system can be cancelled by the introduction of another mismatch,

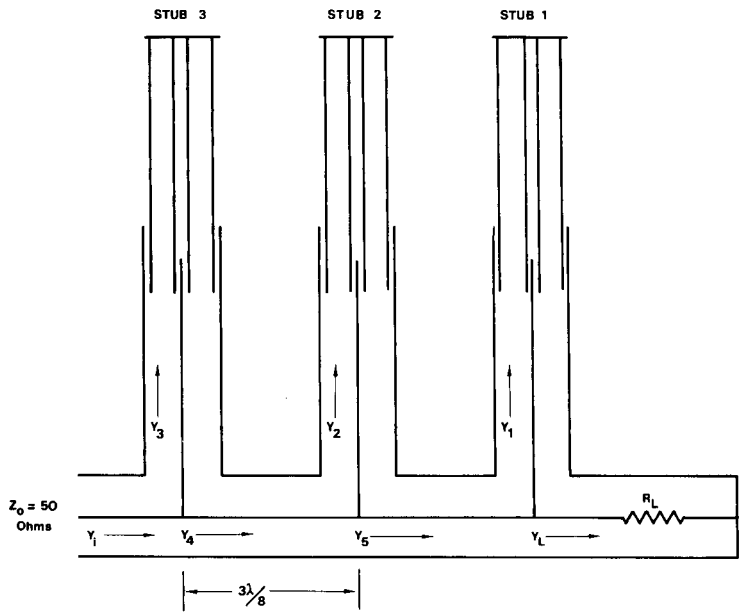

Fig. 3. Schematic representation of a triple-stub tuner. The input impedance is 50 Ω. R_L represents the load to be matched. The distance between stubs is approximately 3/8 λ.

the reflection coefficient of which is in antiphase with the load mismatch, thereby cancelling the reflected wave. Thus a stub tuner produces both a variable mismatch and a variable phase. The triple-stub tuner consists of three variable-position short circuits positioned along the central transmission line. Depending on the position of each stub along the line, the resultant reactance can be either capacitive or inductive, with total stub impedance adjustable from zero to infinity in an ideal lossless system. An exact mathematical description of the triple-stub tuner operation is complicated [7] and is beyond the scope of this paper. Lance [7] gives an approximate sequential description of single- and double-stub tuner operation based on Smith charts. Circuit properties are calculated in terms of normalized load admittances.

A Microlab/FXR (Livingston, NJ 07039) model S3-02N triple-stub tuner was manufactured for these experiments. Specifications are detailed in Table 1. Each stub allows 75 cm of travel. To facilitate adjustment without increasing the overall dimensions of the tuner, the outer conductor of each stub is slotted to permit adjustment of stub position. The entire unit is silver-plated and beryllium/copper contacts assure good electrical contact and long mechanical life.

RESULTS AND DISCUSSION

Results of several approaches to impedance matching at 200 MHz are summarized in Table 2. Measurements of VSWR were made with P_f set to

TABLE 1

Summary of electronic components (cf. Fig. 3)

High-frequency pulsed power generator	
Model	Model PH40K, Applied Microwave Division, EPSCO, Westwood, MA 01810
Mainframe power capability	40 kW, peak
Mainframe frequency range	150 to 6100 MHz (with 20 optional r.f. oscillator plug-in units)
Plug-in r.f. oscillator	EPSCO Model 1701H4, traveling wave tube oscillator. (Custom engineered for enhanced output at 200 MHz)
Plug-in oscillator r.f.	150—300 MHz
Plug-in oscillator peak power	15 kW (variable)
Output impedance	50 Ω
Load VSWR	1.5:1 max.
Maximum duty cycle	0.001
Frequency stability	0.5% h^{-1}
Power stability	±0.5 dB
Pulse duration	0.4—25 μs
Repetition rate	10 to 10 000 Hz (externally triggered at 360 Hz)
Rise time	100 ns max.
Full time	200 ns max.
Droop	0.5% μs^{-1}
Isolator	
Model	PAMTECH Model VTC2047, Canoga Park, CA
Peak power capacity	15 kW
Isolation	20 dB
Insertion loss	(—0.3 dB)
Frequency of optimum isolation	200 ± 10 MHz
Triple-stub tuner	
Model	Microlab/FXR Model S3-02N, Livingston, NJ 07039
Power rating, average	100 W
Power rating, peak	5 kW
Frequency range	0.2—1.0 GHz
Impedance	50 Ω
Maximum insertion loss	0.2 dB
Finish	Silver QQ-S-365
Coupling inductor L	
Specification	ca. 1-cm diameter. Turns (1—10) and turn spacing depend on experiment specifications
Series resistor R	
Value	20—45 Ω
Power rating, average composition	2 W carbon, noninductive
Miscellaneous	
Connectors	All r.f. connections made with type N, or equivalent
Cable	RG-214/M

TABLE 2

Results of impedance-matching study

Mode	VSWR
Simple L-network	8.2
Simple L-network with vacuum capacitor	3.8
Triple-stub tuner	2.1
Triple-stub tuner with quarter-wave termination	1.05

4.0 kW peak envelope power (PEP) as measured with the Bird Model 4391 reflectometer. Measurements reported were made on the 2-turn coupling load coil shown in Fig. 2 of the earlier paper [1]. Standard deviations of ±0.2 VSWR are normal.

Improved circuit design and enhanced component quality markedly improve the observed VSWR. Equivalent matching performance, in terms of VSWR, was also obtained for matching coupling coils with up to 10 turns. It is evident that simple LC networks do not provide adequate impedance-matching performance.

The triple-stub tuner, placed between the generator and the load coil, provides improved impedance matching. Although adjustments are interactive, the tuner is simple to operate. When the Bird digital reflectometer is used to optimize power transfer, an infinite number of combinations of stub positions will result in an acceptable match. Under these operational conditions, the VSWR was reduced to ca. 2.0. This circuit also eliminates the instability and static electricity effects which characterized the previous LC networks. Preliminary VSWR adjustments are made at reduced power levels (ca. 0.5 kW) to avoid internal arcing within the triple-stub tuner under high mismatch conditions.

The operational configuration used here is shown in Fig. 4. Components are identified in Table 1. For optimum performance, proper termination of the stub tuner into the load is important. Theoretically, the load can be positioned at any reasonable distance from the tuner. However, if the generator exhibits a small degree of frequency instability, and the length of the coaxial termination is many wavelengths long, small changes in frequency can result in large changes in impedance. The resultant instability is termed the long-line effect. This effect is minimized by terminating the stub tuner into the load through a coaxial cable section cut to be one quarter-wavelength long [5]. A 2-W, carbon-composition resistor is included in series with the load coil. Values between 20 and 45 Ω are selected experimentally depending on the configuration of the coupling coil.

As shown in Fig. 4, an isolator is normally placed between the pulsed r.f. generator and the impedance-matching circuitry. The isolator is a protective device with a directional port which channels reflected power into an internal

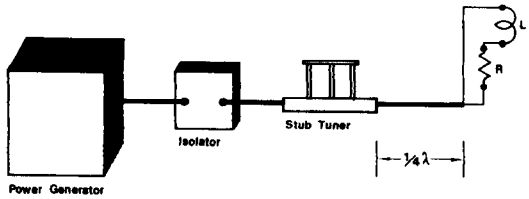

Fig. 4. Final impedance-matching circuitry to allow optimum power transfer of the inductive-coupling load coil at 200 MHz. Components are identified in Table 1.

resistive dummy load. This protection avoids catastrophic damage to the traveling-wave-tube output of the generator under conditions of high VSWR (including open or short circuits at the load). An insertion loss of 0.3 dB was experimentally verified. A limitation of the isolator is that effective isolation is only provided over a narrow frequency range (±10 MHz), limiting the flexibility to investigate r.f. coupling over wide frequency ranges. As a result of improved VSWR performance, experiments were often run with the isolator removed from the circuit.

The procedure now used for impedance matching is to optimize generator output directly into a calibrated 50-Ω resistive "dummy load"; to connect the stub tuner with quarter-wave coaxial termination to the load coil, to minimize VSWR with interactive stub-tuner adjustments using a bidirectional reflectometer, to readjust the generator frequency to minimize VSWR (±2 MHz), and to recheck forward power and return to the step for minimizing VSWR. If these conditions are met, VSWR values of 1.05:1 (±0.01) are routinely achieved.

It should be noted that the estimated generator peak power reported earlier [1] was based on the plate voltage, and the instrumentation described here indicates that these earlier data were actually taken with a peak forward power of about 2.5 kW and a VSWR of about 8. An exposure time of 60 min was required to produce the re-excitation data shown in Figs. 7 and 8 of the earlier paper [1]. Current experiments were typically run with 5-kW peak forward power and a VSWR of 1.05. Spectroscopically, this reduces exposure times to 15 s with re-excitation intensities equivalent to those reported earlier [1]. This performance has had a major impact on current research efforts by increasing available coupling energy and by reducing experiment times. Higher available energies can also be used to enhance upper electronic state populations of species contained in the torus. These studies are in progress.

The instrument has been run for several hundred hours using the triple-stub tuner matching a 200-MHz generator output of 5 kW. No degradation in performance has been observed. Although the triple-stub-tuner ratings have been exceeded, recent operations have included a 10-kW peak forward power, with a VSWR of 1.06, for continuous periods of up to 10 h, without deleterious effect on generator or tuner.

Results of these investigations may prove useful in other experiments in which pulsed high-frequency energy is advantageously coupled into atomic plasmas.

We are indebted to Lee Peterson, Milt Shopnick, Albert Wilson, and Eugene Snowden of the Wayne State University, Liberal Arts and Sciences Machine Shops, for their continuing efforts in the fabrication of specialized instrumentation. Discussions with Mark E. Grandy are acknowledged. Gifts in the form of electronic and optical instrumentation and components from Allied Analytical (formerly Jarrell-Ash), Waltham, MA and from Baird Corporation (Bedford, MA) are appreciated. Part of this work was funded by the National Science Foundation under Grant CHE-80-16148.

REFERENCES

1 D. M. Coleman, M. A. Sainz and H. T. Butler, Anal. Chem., 52 (1980) 746.
2 D. M. Coleman and J. P. Walters, J. Appl. Phys., 48 (1977) 3297.
3 R. G. Schleicher and R. M. Barnes, Anal. Chem., 47 (1975) 724.
4 C. D. Allemand and R. M. Barnes, Spectrochim. Acta, Part B: 33 (1978) 513.
5 J. D. Snyder, Network Lines and Fields, Prentice-Hall, New York, 1955.
6 F. A. Benson, Millimetre and Submillimetre Waves, Iliffe, London, 1969.
7 A. L. Lance, Introduction to Microwave Theory and Measurements, McGraw-Hill, New York, 1964.

Analytica Chimica Acta, 184 (1986) 227—234
Elsevier Science Publishers B.V., Amsterdam — Printed in The Netherlands

DETERMINATION OF IODATE AND PERIODATE AT THE MICROGRAM LEVEL BY A KINETIC METHOD

A. GARRIDO, M. SILVA and D. PÉREZ-BENDITO*

Department of Analytical Chemistry, Faculty of Sciences, University of Córdoba, Córdoba (Spain)

(Received 12th November 1985)

SUMMARY

A procedure is reported for the kinetic determination of iodate/periodate mixtures based on the reduction of these anions by the iron(II)/dipyridylglyoxal dithiosemicarbazone complex in an acidic medium. The reaction is monitored spectrophotometrically at 410 nm (absorption maximum of the iron(III) complex formed). Mixtures of these anions at $\mu g\ ml^{-1}$ levels for iodate/periodate ratios from 5:1 to 1:4 can be determined with a r.s.d. of ca. 3%. Molybdate is used to mask periodate to allow iodate to be determined alone. The sum of both anions is obtained in the absence of molybdate. Chromate, hypochlorite and hexacyanoferrate(III) interfere seriously.

Iodate and periodate have been extensively used as ingredients for indicator reactions in catalytic-kinetic analysis involving redox processes. However, there are few methods for their kinetic determination. The kinetic methods reported so far for determination of iodate are mainly based on two catalytic reactions. The first of these relies on the catalytic action of iodate on the reduction of the monothiocyanate complex of iron(III) in the presence of sodium nitrite and nitric acid [1, 2]. Because this reaction is also catalyzed by iodide, several procedures have been suggested for the resolution of iodide/iodate mixtures [3—5]. The second type is based on the well-known iodide-catalyzed reaction between cerium(IV) and arsenic(III). Although iodate is inactive as a catalyst, both iodide and iodate can be determined by reducing iodate to the catalytically active form with arsenic(III) [6]. This determination has been automated by Truesdale and co-workers and applied to the determination of these species in water samples [7, 8]. The only report on the kinetic determination of periodate involves a fixed-time procedure based on the uncatalyzed redox reaction between dimedone bisthiosemicarbazone monohydrochloride and periodate [9]; it was suggested that iodate and periodate might be distinguished by the different pH dependences of their reactions.

This paper describes a kinetic/spectrophotometric method for the determination of iodate/periodate mixtures. It is based on the oxidation of the iron(II)/dipyridylglyoxal dithiosemicarbazone (DGT) complex to the iron(III)

0003-2670/86/$03.50

complex. No synergic effects were apparent when both anions were present, so the resolution of these mixtures was accomplished by using two sets of experimental conditions (in the presence and absence of molybdate, which masks the action of periodate [10]). No reference has been found to the kinetic determination of iodate/periodate mixtures, and only one reference to the determination of mixtures of species with redox properties involved in the reversible transformation of ferroin/ferriin-type complexes [11]. That method was based on the simultaneous kinetic analysis of uric acid/ascorbic acid mixtures by means of a stopped-flow technique, with tris(2,2′-bipyridyl)-iron(III).

EXPERIMENTAL

Reagents and equipment

The reagents were of analytical-reagent grade and distilled water was used in the preparation of solutions. Standard solutions (1000 μg ml^{-1}) of iodate or periodate were prepared by dissolving pure potassium iodate or sodium metaperiodate in water. A solution of iron(II) (2000 μg ml^{-1}) was prepared by dissolving ammonium iron(II) sulphate in dilute sulphuric acid (pH 2.0). This solution was standardized by photometric titration with potassium dichromate, using diphenylaminosulphonic acid as indicator, and stored in an argon atmosphere to avoid atmospheric oxidation. Solutions (0.05 and 0.0375% w/v) of dipyridylglyoxal dithiosemicarbazone (DGT) were prepared by dissolving the appropriate amount of recrystallized reagent in 100 ml of ethanol. This reagent was synthesized from dipyridylglyoxal and thiosemicarbazide [12]. A stock buffer solution of pH 2.3 was prepared from monochloroacetic acid and sodium monochloroacetate.

Kinetic runs were examined and spectra were measured with a Perkin-Elmer 575 u.v.-visible spectrophotometer equipped with 10-mm glass or silica cells and with Peltier thermostat attachment. A Mettler Memotitrator DL-40 photometric titrator and a Radiometer PHM62 pH meter with a combined glass/calomel electrode were also used.

Procedure

To a 10-ml volumetric flask, add 4.0 ml of 0.05% DGT solution, 1.0 ml of the buffer solution and 0.5 ml of 250 μg ml^{-1} iron(II) solution, and then start the stopwatch. Dilute to the mark with distilled water and after 1 min transfer two 2.5-ml portions of this solution to the spectrophotometer cells, maintained at 25 ± 0.1°C. Wait for 1 min and add 40 μl of a solution containing 2.5—12.5 μg of iodate and 2.5—10 μg of periodate to the sample cell. Stir this solution magnetically and wait for 1 min before starting to record the absorbance (at λ_{max} = 410 nm) as a function of time. Calculate the slope of the linear plot, which is proportional to the iodate plus periodate concentration in the sample. In another experiment, add 2.0 ml of 0.02 M sodium molybdate after the iron(II) solution in order to mask the periodate, and

proceed as above. The difference between the two rates represents the periodate content.

For the determination of periodate alone, follow the procedure as above without molybdate addition; for iodate alone, add 4.0 ml of 0.0375% (w/v) DGT solution and 0.4 ml of 250 μg ml^{-1} iron(II) solution instead of the amounts used above.

RESULTS AND DISCUSSION

Formation and spectrophotometric characteristics of the iron complexes

The DGT forms strongly coloured complexes with iron(II) in a process which is strongly pH-dependent. In acidic medium (pH 2.5), iron(II) forms a red-violet complex (λ_{max} = 550 nm) in which DGT behaves like a ferroin-type reagent, whereas in an ammonia/ammonium chloride buffer (pH 10) it forms a green-blue complex (λ_{max} = 610 nm) in which the sulphur atoms take part in the co-ordination. The reagent also forms a yellow chelate with iron(III) which has an absorption maximum at 410 nm. The iron(II) complexes have been used previously for the spectrophotometric determination of iron [13].

The spectrophotometric characteristics of the iron(III) complex were studied here. At any pH, this chelate has a 1:1 iron(III)/DGT ratio, the sulphur atoms binding as in the green-blue iron(II) complex. The iron(III) complex is very stable, more so than the iron(II) complex. The lesser stability of the iron(II) complex can be used in kinetic analysis as the basis of an indicator reaction. Thus, this complex can readily be oxidized to the yellow chelate by several oxidants. In addition, its atmospheric oxidation is fast at pH 3.0 (Fig. 1). Its reduction is only feasible in the presence of high

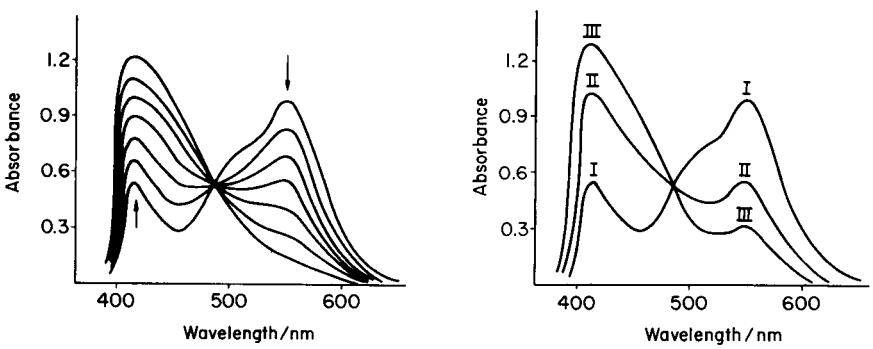

Fig. 1. Spectra showing the air-oxidation of the iron(II)/DGT complex. Curves recorded at 5-min intervals. Conditions: 2.2 x 10^{-4} M Fe^{2+}, 5.6 x 10^{-4} M DGT, pH 3.1, 25°C.

Fig. 2. Absorption spectra of the iron(II)/DGT complex in the presence of: (I) ascorbic acid; (II) 4.0 μg ml^{-1} periodate; (III) 4.0 μg ml^{-1} iodate. Curves recorded after reaction for 5 min under the recommended conditions.

concentrations of reductants such as ascorbic acid. Consequently, only the determination of oxidants is of analytical interest.

Kinetic study of the oxidation reactions

As stated above, the iron(II)/DGT complex can be oxidized to the iron(III)/DGT complex in an acidic medium by the action of one of several oxidants. When iodate or periodate is used, this reaction takes place sufficiently rapidly for application in kinetic analysis. Thus, the oxidizing action of iodate and periodate on the red-violet iron(II) complex is used here for the kinetic determination of both anions individually and in mixtures.

Figure 2 shows the effect of both anions (each at 4.0 μg ml^{-1}) on the spectrum after a reaction time of 5 min. It shows that the oxidation is much faster with iodate than periodate. For kinetic measurements, the absorbance/time curves were monitored at the absorption maximum of the iron(III) complex (410 nm) because the molar absorptivity of the iron(III) complex was higher than that of the iron(II) complex. A kinetic study of the influence of variables on the oxidation rate was made in order to develop kinetic methods for the determination of iodate and periodate.

Effect of reaction variables

The determination of iodate/periodate mixtures is influenced by several variables which were studied for each ion separately by means of initial rate/concentration plots.

The influence of temperature was examined in the range 10—40°C. The plots of initial rate vs. temperature were similar in both cases, with maxima at 25 and 30°C for periodate and iodate, respectively. The decrease in reaction rate at higher temperatures can be ascribed to the air-oxidation of the iron(II) complex used as reference solution. These temperatures were chosen for the recommended procedure. By plotting log (initial rate) against the inverse absolute temperature, activation energies of 26.6 and 24.6 kJ mol^{-1} were obtained for periodate and iodate, respectively.

A decrease in the initial rate with increasing pH was observed for both reactions. However, the change was less above pH 3.0, so that a working pH of 3.1 was chosen (Fig. 3a). The use of a buffer solution of pH 2.3 (2.0 ml) gave this final pH in the reaction vessel in the presence of 40% (v/v) ethanol. Under these conditions, the partial order in hydrogen ion concentration was 0.5 for both reactions.

The DGT concentrations that gave the greatest initial rate for each system were 5.6×10^{-4} M (4.0 ml of 0.05% solution) for periodate and 4.8×10^{-4} M (4.0 ml of 0.0375% solution) for iodate (Fig. 3b). For iodate, the reaction order with respect to DGT was 1 below 4.8×10^{-4} M and —0.5 above this concentration. Under the experimental conditions set for periodate, the reaction orders were 0.5 and —0.5 at DGT concentrations below and above 5.6×10^{-4} M, respectively.

The iron concentration was varied from 0.5 to 3.5×10^{-4} M while the other variables were maintained constant. A plot of initial rate vs. iron

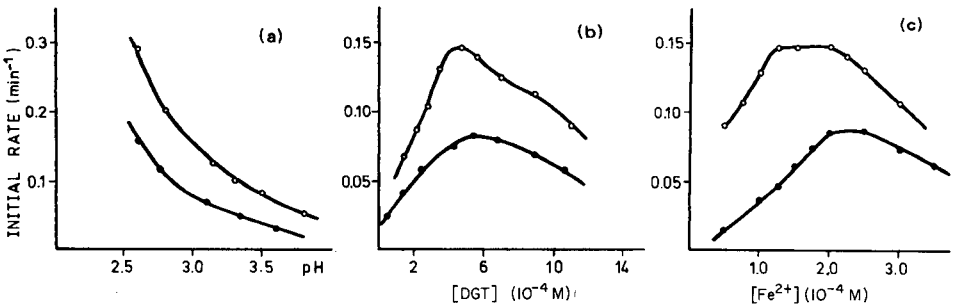

Fig. 3. Effect of variables on the reaction rate: (○) 4.0 μg ml^{-1} iodate; (●) 4.0 μg ml^{-1} periodate. (a) Effect of pH; (b) effect of DGT concentration; (c) effect of iron(II) concentration. See text for details.

concentration is shown in Fig. 3(c). In both cases, a zero-order dependence region is obtained for iron concentrations around the DGT:iron(II) stoichiometric ratio; this can be attributed to the greater lability of the iron(II) complex under the conditions fixed for its oxidation with iodate or periodate. This is also in agreement with the decrease in the analytical signal at iron concentrations outside the plateau (Fig. 3c), representative of an excess of DGT (left portion) or iron(II) (right portion). Consequently, because of the more powerful oxidation action of iodate, the zero-order region is wider and is attained at higher DGT:iron(II) ratios than for periodate. This suggests that the dissociation of the iron(II) complex takes place prior to oxidation by iodate or periodate. In order to keep precision as high as possible, an iron concentration of 1.8×10^{-4} M for iodate and 2.2×10^{-4} M for periodate is recommended. Regarding the kinetic dependence on the iron concentration at values outside the plateau, partial orders of 0.5 and −1 for iodate and 1 and −1 for periodate were found (left and right portions, respectively).

Adjustment of the ion strength to 0.3 M with potassium chloride or potassium nitrate did not affect either method. The effect of ethanol on the rate was studied in the range 25—60% (v/v). The rate of both reactions increased with increasing ethanol content up to 40% and remained virtually constant at higher values. Therefore, 40% is recommended; this is achieved by the amount of ethanol added as the DGT solution.

Absorbance/time curves were recorded for solutions containing different amounts of iodate and periodate, under the recommended experimental conditions. The reaction was found to be first-order with respect to iodate and periodate. The following kinetic equations are suggested for the procedure recommended for the determination of iodate and periodate:

$$d[Fe^{3+}\text{—DGT}]/dt = k_1[\text{DGT}]^{1/2}[H^+]^{1/2}[IO_4^-]$$

$$d[Fe^{3+}\text{—DGT}]/dt = k_2[\text{DGT}][H^+]^{1/2}[IO_3]$$

where [Fe^{3+}—DGT] is the concentration of the product and k_1 and k_2 are the conditional rate constants for the oxidation reactions.

Individual kinetic determination of iodate and periodate

Three methods were applied under the recommended experimental conditions for the determination of low levels of iodate and periodate (Table 1), the initial-rate method, the fixed-time method (1.5 min for both anions) and a fixed-absorbance approach (0.200 for iodate and 0.250 for periodate). For both anions, the initial-rate method was selected for further experiments because it had the highest precision. The sensitivities were (calibration slope) 7.64×10^{-3} and 4.85×10^{-3} min^{-1} M^{-1} for iodate and periodate, respectively.

Determination of iodate/periodate mixtures

The determination of iodate/periodate mixtures is based on two facts: no synergic effects were found when an iodate/periodate mixture was treated with the iron(II)/DGT complex, and the effect of periodate can be masked with molybdate [14]. Thus, two sets of reaction conditions allowed both iodate and periodate to be determined: in the absence of molybdate both anions were determined; after molybdate had been added, iodate only was determined. The recommended conditions for the determination of periodate alone were used for the analysis of the mixtures. The amount of sodium molybdate required to achieve the complete masking of periodate was studied on samples containing 4.0 μg ml^{-1} each of iodate and periodate. The results showed that 2.0 ml of 0.02 M sodium molybdate was enough to ensure the desired effect.

The results obtained for several synthetic mixtures of iodate and periodate are summarized in Table 2. As can be observed, the determination of iodate/periodate mixtures is feasible in the weight ratio range 1:4 to 5:1 (with a maximum relative error of 5%). When the recommended procedure was applied to eleven samples containing 2.0 μg ml^{-1} each of iodate and periodate, the r.s.d. was 2.9% for iodate and 3.5% for periodate.

The effects of other ions are shown in Table 3. Iodate/periodate mixtures can be determined in the presence of 100-fold amounts of several related anions such as bromate, chlorate and perchlorate. The most serious interferences were those of chromate, hypochlorite and hexacyanoferrate(III),

TABLE 1

Kinetic determination of iodate and periodate

Ion	Method	Range (μg ml^{-1})	R.s.d. (%)[a]
Iodate	Initial rate	2—14	1.32
	Fixed time	3—9	3.14
	Fixed absorbance	7—16	5.68
Periodate	Initial rate	2—8	0.84
	Fixed time	2—12	1.19
	Fixed absorbance	4—16	5.19

[a]For 11 samples containing 6.0 μg IO_4^- ml^{-1} and 4.0 μg IO_3^- ml^{-1}.

TABLE 2

Analysis of mixtures of iodate and periodate

Concentrations (μg ml^{-1})			
Taken		Found	
Iodate	Periodate	Iodate	Periodate
1.00	1.00	1.02	1.00
1.00	2.00	1.05	1.95
1.00	4.00	1.01	4.07
3.00	1.00	2.97	1.00
5.00	1.00	4.97	1.03

TABLE 3

Tolerance limits for foreign anions in the kinetic determination of 2.0 μg ml^{-1} each of iodate and periodate

Tolerance limit (μg ml^{-1})	Foreign anion
200	Cl^-, Br^-, NO_3^-, BrO_3^-, ClO_3^-, SO_4^{2-}, PO_4^{3-}, ClO_4^-, acetate, citrate, tartrate
100	SO_3^{2-}, CO_3^{2-}
50	F^-, SCN^-
10	$S_2O_8^{2-}$, I^-, $Fe(CN)_6^{4-}$
2	CrO_4^{2-}, ClO^-, $Fe(CN)_6^{3-}$

which interfere at a concentration similar to that of iodate and periodate through oxidation of the iron(II)/DGT complex, thus causing a positive interference.

Recoveries of iodate and periodate added to sea water, river water and drinking water, previously filtered and acidified with nitric acid were measured. Concentrations of 1.0—4.0 μg ml^{-1} gave recoveries from 96 to 103.3%, with an average of 100.1% for iodate and 99.8% for periodate. The standard deviations of the recoveries were 2.2% and 3.0% for iodate and periodate, respectively, for nine determinations of each.

Conclusions

Iodate/periodate mixtures can be determined in the μg ml^{-1} range by initial-rate measurements on an uncatalyzed redox reaction. Methods for the determination of iodate reported in the literature are more sensitive because they use catalytic reactions; however, these sometimes require the prior conversion of iodate to an active catalytic species such as iodide. Regarding the kinetic determination of periodate alone, the method proposed herein shows advantages of sensitivity and selectivity over the previous method [9].

REFERENCES

1 I. Iwasaki, S. Utsumi and T. Ozawa, Bull. Chem. Soc. Jpn., 26 (1953) 108.
2 S. Utsumi, M. Shiota, N. Yonehara and I. Iwasaki, J. Chem. Soc. Jpn., Pure Chem. Sect., 85 (1964) 32.
3 I. Iwasaki, S. Utsumi and N. Yonehara, J. Chem. Soc. Jpn., Pure Chem. Sect., 85 (1964) 36.
4 N. Yonehara, Bull. Chem. Soc. Jpn., 37 (1964) 1101.
5 C. P. Sivaraman and S. Rajeswari, Indian J. Mar. Sci., 12 (1983) 177.
6 P. A. Rodriguez and H. L. Pardue, Anal. Chem., 41 (1969) 1376.
7 V. W. Truesdale and P. J. Smith, Analyst (London), 100 (1975) 111.
8 S. D. Jones, C. P. Spencer and V. W. Truesdale, Analyst (London), 107 (1982) 1417.
9 M. Callejon-Mochon and J. A. Muñoz-Leyva, Anal. Chim. Acta, 140 (1982) 271.
10 D. Burnel, Compt. Rend., 261 (1965) 1982.
11 E. Pelizzetti and E. Mentasti, Anal. Chim. Acta, 108 (1979) 441.
12 J. L. Bahamonde, D. Pérez-Bendito and F. Pino, Inf. Quim. Anal. (Madrid), 26 (1972) 7.
13 J. L. Bahamonde, D. Pérez-Bendito and F. Pino, Talanta, 20 (1973) 694.
14 R. Belcher and A. Townshend, Anal. Chim. Acta, 41 (1968) 395.

Analytica Chimica Acta, 184 (1986) 235—242
Elsevier Science Publishers B.V., Amsterdam — Printed in The Netherlands

ENZYMATIC DETERMINATION OF CHOLESTEROL, L-AMINO ACIDS AND LINOLEIC ACID WITH A NOVEL REDOX INDICATOR SYSTEM

J. PEINADO and F. TORIBIO

Department of Biochemistry, Faculty of Veterinary Sciences, University of Córdoba, Córdoba (Spain)

D. PÉREZ-BENDITO*

Department of Analytical Chemistry, Faculty of Sciences, University of Córdoba, Córdoba (Spain)

(Received 17th December 1985)

SUMMARY

A sensitive kinetic fluorimetric system is proposed for the determination of hydrogen peroxide produced by enzymatic oxidation of cholesterol, L-amino acids and linoleic acid. 2-Hydroxynaphthaldehyde thiosemicarbazone (HNTS) is oxidized by hydrogen peroxide or hydroperoxides in an ammoniacal medium in a Mn(II)-catalyzed reaction to give a fluorescent product (λ_{ex} = 390 nm, λ_{em} = 450 nm). The lowest concentration of hydrogen peroxide determined is 50 pmol. Cholesterol was determined in egg yolk, cod liver oil and horse serum. The ranges of concentration for substrates were 0.33—3.74 μM cholesterol; 0.3—10 μM, 0.6—15 μM and 0.75—10 μM, for L-leucine, L-phenyalanine and L-serine, respectively; and 15—150 μM linoleic acid.

The determination of substances of clinical interest such as glucose, cholesterol or uric acid in serum is now usually based on enzymatic reactions. In many such reactions, enzymatically generated hydrogen peroxide is determined spectrofluorimetrically, or less often fluorimetrically, after the oxidation of an indicator reagent or reaction between a chromogenic hydrogen donor and a coupling agent, both in the presence of peroxidase. In a recent paper, a very sensitive spectrofluorimetric determination of hydrogen peroxide was described, based on the oxidation of 2-hydroxynaphthaldehyde thiosemicarbazone (HNTS) by hydrogen peroxide or other hydroperoxides in an ammoniacal medium, catalyzed by manganese(II) [1]. This system is applied here to the determination of cholesterol, L-amino acids and linoleic acid by use of the corresponding cholesterol and L-amino acid oxidases, which generate hydrogen peroxide, and soybean lipoxidase (L-1 isoenzyme), which forms 13-hydroperoxolinoleate. The procedure can determine as little as 50 pmol of hydrogen peroxide, takes only 5 min and does not require peroxidase.

0003-2670/86/$03.50

EXPERIMENTAL

Reagents and apparatus

All common reagents used were of analytical grade, and all water was twice-distilled. Ethanolic 0.01% (w/v) HNTS, 0.5 mM hydrogen peroxide and (1 + 5) ammonia solutions were prepared daily. The peroxide solution was standardized by permanganate titration in acidic solution. A standard manganese(II) solution (1.0 g l^{-1}) was prepared by dissolving a suitable amount of the metal in the minimum volume of (1 + 1) hydrochloric acid and diluting with (1 + 9) hydrochloric acid. All the enzymes, cholesterol, cholesterol oleate and sodium taurocholate, were from Sigma Chemical Co. The cholesterol oxidase solution was prepared by dissolving 1.2 mg of enzyme in 1.2 ml of 0.2 M sodium chloride/0.8 ml of 1 M ammonium sulphate (the stock solution contained 17.4 U ml^{-1}). Cholesterol esterase (3.5 U ml^{-1}) was dissolved in 0.1 M potassium phosphate, pH 7.0. L-Amino acid oxidase (2 U ml^{-1}) was stored as an aqueous solution. Soybean lipoxidase (1620 U ml^{-1}) was dissolved in 0.168 M sodium borate buffer, pH 9.0. All the enzyme solutions were stored in a refrigerator. A 20 mM solution of sodium linoleate was prepared as described by Axelrod et al. [2]; 1 and 4 mM L-phenylalanine (Phe), L-leucine (Leu), L-serine (Ser) and L-glycine (Gly) solutions were prepared in a 0.4 M Tris-HCl buffer, pH 7.8.

All spectrofluorimetric measurements (λ_{ex} = 390 nm, λ_{em} = 450 nm) were made in an Aminco-Bowman spectrofluorimeter, with 16.5-nm excitation and emission slits and a 11.0-nm photomultiplier slit. Under these conditions, a 0.1 $\mu g\ l^{-1}$ solution of quinine sulphate in 0.05 M sulphuric acid gave an intensity of 8 mV.

Procedures

Cholesterol determination. Cholesterol oleate (ca. 10 mg) was hydrolyzed by dissolution in 10 ml of a 0.5 M potassium hydroxide solution in methanol in a 50-ml round-bottomed flask. After heating under reflux for 25 min, the contents of the flask were cooled and transferred to a 25-ml volumetric flask by pipette. The former flask was washed several times with isopropanol, the washing solution being transferred to the volumetric flask, which was made up to volume with isopropanol and cooled for 20 min in a refrigerator. The solution was filtered and 10 μl of this were assayed. This procedure was also applied to egg yolk and cod liver oil.

A reaction mixture consisting of 0.46 ml of 0.5 M 3-(*N*-morpholino)-propane-sulfonic acid (MOPS) buffer, pH 7.0, 10 μl of cholesterol sample, and 20 μl of cholesterol oxidase was prepared. For horse serum samples, 20 μl of cholesterol esterase and 20 μl of 50 mM sodium taurocholate were also added. The mixture was incubated at 30°C for 4 min. The mixture was transferred to a 10-ml flask containing 1.5 ml of ethanolic HNTS solution; 5 ml of ethanol and 0.5 ml of (1 + 5) ammonia were added, the solution was made up to the mark with water and a solution containing 2.5 μg of

manganese(II) added. A portion of the solution was transferred to a 10-mm quartz cell, and the fluorescence intensity was recorded as a function of time 15 s after initiation. The blank reaction was monitored under similar conditions (no cholesterol present). The reaction rate was calculated from the difference between the slopes of the fluorescence vs. time plots for the sample and blank experiments. A calibration graph of rate vs. cholesterol concentration was prepared.

L-Amino acid determination. For calibration, a mixture of 125 − x μl of 0.4 M Tris-HCl buffer, 25 μl of L-amino acid oxidase and x μl (3—25 μl) of 1 or 4 mM L-amino acid solution was incubated, with shaking, at 37°C for 15 min. The mixture was transferred to a 10-ml flask containing 1.5 ml of HNTS solution and monitored as above. A blank solution containing no L-amino acid was also monitored in the same way, and calibration graphs of net rate vs. amino acid concentration were prepared.

Linoleic acid determination. A mixture of 0.47 ml of 0.2 M borate buffer, 15 μl of sodium linoleate solution and 15 μl of lipoxidase was incubated at 30°C for 1 min. The mixture was transferred to a 10-ml flask containing 1.5 ml of HNTS solution, 1 ml of ethanol and 0.5 ml of (1 + 5) ammonia solution were added, and the solution was diluted to the mark with redistilled water, after which 2.5 μg of manganese(II) was added (the ethanol and water were preheated to 30°C in a thermostatted bath). The fluorescence intensity was recorded as a function of time after 15 s. Because the linoleic acid is auto-oxidized in this medium, the rate of the enzyme-catalyzed reaction was calculated from the difference between the slopes of the fluorescence vs. time plots of the reaction rate of the sample with enzyme and the reaction rate of the sample without enzyme added.

RESULTS AND DISCUSSION

Assay for cholesterol

The enzymatic reaction is temperature-dependent. The limiting rate is attained in 6 min at 20°C and in only 4 min at 25 or 30°C. Thus, a temperature of 30°C was chosen for the coupled reaction (Table 1). Under the recommended conditions, the calibration graph for cholesterol was linear, with an equation $y = 3.02[\text{cholesterol}] + 0.36$, where y is the initial rate expressed as mV min^{-1}, and the cholesterol concentration is in μM. The slope obtained for hydrogen peroxide under similar conditions was: $y = 3.30[H_2O_2] + 0.31$, which indicates ca. 90% recovery of hydrogen peroxide from cholesterol. When five samples of 1.5×10^{-6} M cholesterol were processed, the relative standard deviation was 1.3%.

The cholesterol content of egg yolk, cod liver oil and horse serum was determined. As cholesterol is mostly present as an ester, prior alkaline hydrolysis for egg yolk and cod liver oil was needed. Initially, cholesterol oleate was examined by this method. The results in Table 2 show good recoveries. The results obtained for egg and cod liver oil, also shown in

TABLE 1

Effect of temperature on the activity of cholesterol oxidase (1.5×10^{-6} M cholesterol)

Temp. (°C)	Initial rate ($mV\ min^{-1}$)	H_2O_2 generated ($\times 10^{-6}$ M)[a]
20	4.1	1.24
25	4.8	1.45
30	4.9	1.49
35	4.0	1.19
40	2.9	0.85

[a]After 4 min.

TABLE 2

Determination of cholesterol in foodstuffs and serum

Sample	Cholesterol present	Cholesterol found[a]
Cholesterol oleate	10.0 mg	9.8 ± 0.54 mg
Egg yolk	13.4 mg g^{-1} [b]	13.8 ± 0.82 mg g^{-1}
Cod liver oil	878.0 mg/100 g[b]	850.0 ± 7.51 mg/100 g
Horse serum	179.0 mg dl^{-1} [c]	187.0 ± 9.20 mg dl^{-1}

[a]Mean of four separate determinations with standard deviation. [b]Average values in Geigy Scientific Tables. [c]Determined by the Seralyzer automatic method of Ames Division, Miles Laboratories.

Table 2, are within the expected range. A prior enzymatic hydrolysis was required for horse serum samples. So, the reaction mixture contained cholesterol esterase and cholesterol oxidase. The sera were diluted 12-fold to lighten the colour of the sample and to obtain a cholesterol concentration within the calibration range. The concentration in serum was checked by an automatic method involving reaction of hydrogen peroxide, MBTH and primaquine phosphate in the presence of peroxidase, to obtain a pink colour which is monitored at 560 nm [3]. This process involves narrow plastic strips.

Assay for L-amino acids

This is derived from the method described by Lichtenberg and Wellner [4], based on the measurement of the decrease in fluorescence intensity of scopoletin, which is oxidized to an unfluorescent product in the presence of peroxidase. Figure 1 shows the calibration graphs obtained for the different L-amino acids assayed. L-Leucine is oxidized fastest; this result was not expected because L-phenylalanine is the best substrate for L-amino acid oxidase in snake venom [5]. In the present conditions, $0.3—10 \times 10^{-6}$ M L-leucine in the final solution could be determined, with a mean r.s.d. of

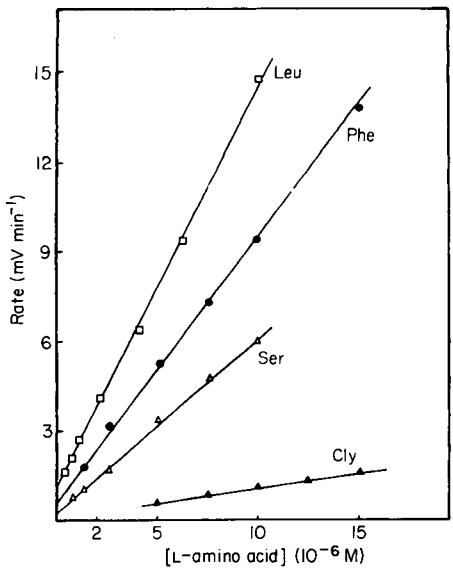

Fig. 1. Calibration plots by the initial-rate method: (□) L-leucine; (●) L-phenylalanine; (△) L-serine; (▲) glycine.

1.5%. At higher concentrations of substrate, the calibration graph was not linear. The method proposed herein allows the determination of amounts of L-leucine as low as 0.3 nmol, a lower concentration than obtained with two other methods [4, 5].

The ratios of the turnover rates for the various L-amino acids can be estimated by comparing the slopes of their calibration graphs (Fig. 1), i.e., Leu = 100, Phe = 67, Ser = 43, Gly = 7. Linear calibration ranges were 0.6—15 μM Phe and 0.75—10 μM Ser.

Assay for linoleic acid

The enzymatic activity of soybean lipoxidase was that of the L-1 isoenzyme, which converts linoleic acid to 13-hydroperoxolinoleate [6]. The activity of the L-1 isoenzyme can be distinguished from that of other soybean lipoxidase isoenzymes (L-2, L-3a and L-3b) on the basis of the optimum pH of the L-1 isoenzyme, which is 9.0—9.5.

A study of the influence of temperature on enzymatic activity (Fig. 2) showed that the maximum rate is attained between 25 and 30°C. Because the latter coincides with that of the coupled reaction, it was used in all further studies.

The assay time of the enzymatic activity was studied under the experimental conditions described in the procedure. The maximum rate of the coupled reaction is attained after 1 min and then diminishes; 1 min was chosen as the reaction time. This indicates that the concentration of

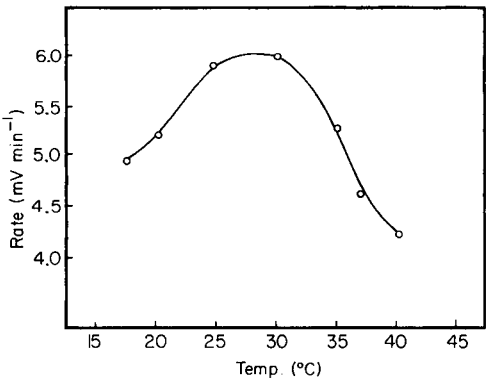

Fig. 2. Effect of the temperature on the activity of soybean lipoxidase.

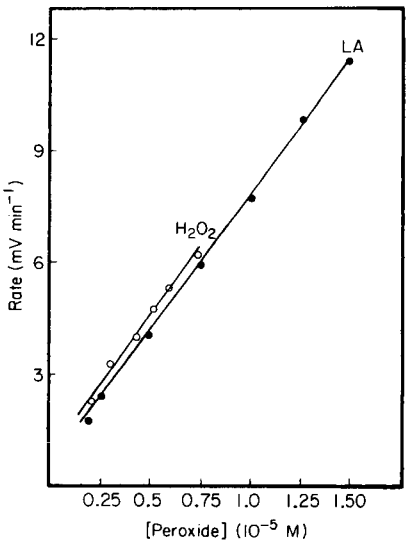

Fig. 3. Calibration graphs for the determination of linoleic acid (LA) and hydrogen peroxide.

13-hydroperoxolinoleate is greatest at 1 min, after which it decreases owing to secondary reactions catalyzed by the isoenzymes of soybean lipoxidase. For example, the L-1 isoenzyme catalyzes the reaction between linoleic acid and 13-hydroperoxolinoleate [7] yielding keto-dienes. These byproducts are not peroxo compounds and cannot oxidize HNTS. Table 3 shows the dependence of the initial rate on the time allowed for the enzymatic reaction.

The experimental conditions for HNTS oxidation by hydroperoxolinoleate (indicator-coupled reaction) are different from those used in the determination of hydrogen peroxide. The difference arises because the linoleic acid is auto-oxidized in the ammoniacal ethanolic medium. When the ethanol content is 65%, the rate of the reaction without enzyme proceeds at the same rate as the reaction with enzyme. By decreasing the ethanol content to $\leqslant 25\%$, the difference between the sample and the blank rates becomes appreciable. Table 4 shows the effect of different ethanol concentrations. Under these conditions, the linear calibration range for linoleic acid is 0.15–1.5×10^{-5} M (mean r.s.d. = 1.4%) (Fig. 3).

To check whether hydroperoxolinoleate was as reactive an oxidant of HNTS as hydrogen peroxide, this last compound was assayed under the conditions used for linoleic acid (with an ethanol content of 25%). Figure 3 shows very similar slopes of the calibration graphs for hydrogen peroxide and linoleic acid. This indicates that both are equally reactive.

Tests were made to establish whether linoleic acid formed the peroxide in the absence of lipoxidase. Unsaturated fatty acids are particularly prone to

TABLE 3

Effect of assay time for soybean lipoxidase on the rate

Assay time (s)	10	30	60	90	150
Rate (mV min^{-1})	0.8	5.6	6.0	5.9	4.7

TABLE 4

Effect of ethanol content on the rate for hydroperoxolinoleate

Ethanol added (ml)	Ethanol content (%)	Initial rate (mV min^{-1})		
		Sample	Blank	Difference
5.0	65	6.0	5.7	0.3
4.0	55	5.7	4.0	1.7
3.0	45	5.5	2.9	2.6
2.0	35	5.3	2.4	2.9
1.5	30	5.1	1.8	3.3
1.0	25	5.0	1.2	3.8
0.5	20	4.4	0.8	3.6

oxidation. Their auto-oxidation can be catalyzed by metals such as copper, iron, manganese and nickel [8]. As manganese is present in the reaction medium, it may be assumed that it will accelerate the oxidation of linoleic acid to hydroperoxolinoleate. In order to check this, a series of samples of grape oil (rich in linoleic acid) was prepared, and the hydroperoxolinoleate content was assayed [9]. In the presence of manganese, the content in lipid hydroperoxides was found to be increased threefold. However, ethanol interacts with manganese(III) to form acetaldehyde and hydrogen peroxide, as described by Denisov et al. [10]. This was confirmed by determination of the acetaldehyde [11]. Thus, the hydrogen peroxide formed could interact with the linoleic acid [12], giving rise to the effect exerted by ethanol on linoleic acid auto-oxidation.

REFERENCES

1 J. Peinado, F. Toribio and D. Pérez-Bendito, Anal. Chem., in press.
2 B. Axelrod, T. M. Cheesbrough and S. Laakso, Methods Enzymol., 71 (1981) 441.
3 E. Chang, Clin. Chem., 25 (1979) 1091.
4 L. A. Lichtenberg and J. Wellner, Anal. Biochem., 26 (1968) 313.
5 G. Guilbault and J. Hieserman, Anal. Biochem., 26 (1968) 1.
6 J. P. Christopher, E. K. Pistorius, F. E. Regner and B. Axelrod, Biochim. Biophys. Acta, 289 (1972) 82.
7 G. A. Veldink, J. F. Vliegenthart and J. Boldingh, Prog. Chem. Fats Other Lipids, 15 (1977) 31.
8 J. Frank, J. V. Geil and R. Freaso, Food Technol., (1982) 71.

9 J. Peinado, F. Toribio and D. Pérez-Bendito, Talanta, in press.
10 E. T. Denisov, N. I. Mitskevitch and V. E. Agabekov, Liquid Phase Oxidation of Oxygen-Containing Compounds, 1977, cited in R. A. Sheldon and J. K. Kochi, Metal-Catalyzed Oxidations of Organic Compounds, Academic Press, New York, 1981, p. 351.
11 A. I. Cederbaum, E. Dicker and G. Cohen, Biochemistry, 17 (1978) 3058.
12 E. M. Kellog and I. Fridovich, J. Biol. Chem., 250 (1975) 8812.

Analytica Chimica Acta, 184 (1986) 243—250
Elsevier Science Publishers B.V., Amsterdam — Printed in The Netherlands

SPECTROPHOTOMETRIC FLOW-INJECTION DETERMINATION OF ASCORBIC ACID BY GENERATION OF TRIIODIDE

J. HERNÁNDEZ-MÉNDEZ*, A. ALONSO MATEOS, M. J. ALMENDRAL PARRA and C. GARCÍA DE MARÍA

Department of Analytical Chemistry, Faculty of Chemistry, University of Salamanca, Salamanca (Spain)

(Received 3rd July 1985)

SUMMARY

A method is proposed for the flow-injection determination of ascorbic acid (0.1—40 μg ml^{-1}). Iodine is generated in the flow system as triiodide ion or the triiodide/starch complex giving a steady spectrophotometric signal at 350 or 580 nm, respectively; inverse peaks caused by ascorbic acid samples are measured. The method is applied to the determination of ascorbic acid in a fruit juice, jam and vitamin C preparation.

Many procedures are used for the selective determination of ascorbic acid or of total reductant concentration, of which it is a major component, as in fruit juices, foods and wines. Titration with oxidants such as 2,6-dichlorophenolindophenol, iodine or chloramine-T [1—3] and direct [4—6] or indirect [7—14] spectrophotometric methods based on the reduction of compounds such as molybdate, 1,2-phenylenediamine and ferroin are most commonly used. Recently, Fogg et al. [15] proposed a method for its determination by flow injection with amperometric detection.

In the present paper, ascorbic acid is determined spectrophotometrically by using a stream of triiodide generated in a flow system as the reagent. Apart from the advantages inherent in the flow-injection technique, the method proposed is more readily applied than the flow method based on electrochemical detection, although the sensitivity is similar.

The redox potential of the I_3^-/I^- system, its independence of the pH of the medium used below 8, and the kinetics of most of the reactions in which it is involved confer on it interesting characteristics regarding its selectivity, rapidity and field of application. Nevertheless, conventional determinations with this system have certain drawbacks stemming from the indicator systems and because of the instability of iodine (volatility, low solubility in aqueous media, photosensitivity, etc.) and iodide solutions (atmospheric oxidation). This paper proposes a procedure for the generation of a steady stream of iodine in a flow system which can be applied, for example, to the determination of ascorbic acid.

0003-2670/86/$03.50

EXPERIMENTAL

Reagents and apparatus

Solutions of potassium iodate (1.000 g l^{-1}), 0.20 M potassium iodide, 0.20 M sulphuric acid, 2.00 g l^{-1} starch and 8.06×10^{-4} M 2,6-dichlorophenol-indophenol were prepared from analytical- or spectrophotometric-grade products. A 100.0 μg ml^{-1} ascorbic acid solution was stabilized with 0.1 g l^{-1} EDTA and 4.0 g l^{-1} formic acid. These reagents were prepared in and diluted, when necessary, with deionized water.

Eyela MP-3 peristaltic pumps (Tokyo Rikakikai Co.) were fitted with Isoversinic 1 × 3 pump tubes. Injection was via a PTFE L-100-1 rotary valve (Tecator; injection volume 126 μl). The detector was a Pye Unicam SP1800 u.v./visible spectrophotometer equipped with an AR-25 linear recorder, and a 30-μl Suprasil I flow cell of 10-mm optical path (Hellma). All other tubing and coils were of PTFE (0.5 mm i.d.) with the exception of coil R_1 which had an inner diameter of 0.7 mm. PVC-flanged tube fittings (Rheodyne) and home-made plexiglas T-connectors were used.

Flow system

For the study of the variables affecting the generation and stability of triiodide, the system shown in Fig. 1 was used. Generation of triiodide was based on the oxidation of iodide by iodate:

$$IO_3^- + 8I^- + 6H^+ \leftrightharpoons 3I_3^- + 3H_2O$$

Triiodide was measured spectrophotometrically at 350 nm. Alternatively, the triiodide/starch complex was formed by adding starch to channel C_1. In this case, the absorbance was measured at 580 nm.

For determination of ascorbic acid (0.5—20 μg ml^{-1}), the manifold described in Fig. 1 was used, with the injection valve inserted in C_3 after the pump. The recommended conditions are as follows: channel C_1, 0.08 M potassium iodide (and 1.20 g l^{-1} starch), flow rate 1.5 ml min^{-1}; channel C_2, 10.0 mg l^{-1} (4.6×10^{-5} M) potassium iodate in 1×10^{-3} M sulphuric acid, flow rate 1.5 ml min^{-1}; channel C_3, carrier solution at pH 1.5—11.0, flow

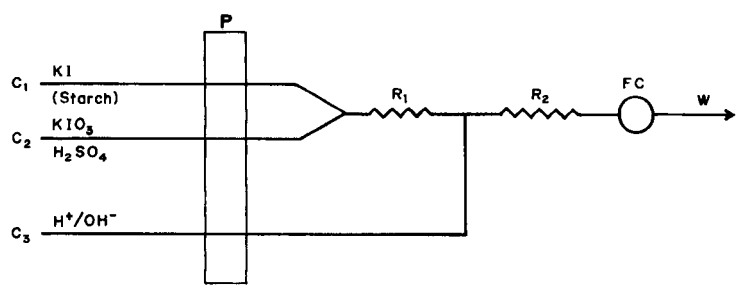

Fig. 1. Flow system for generation of triiodide. P, Peristaltic pump; FC, flow cell; R_1, R_2, reactors; W, waste.

rate 3.0 ml min^{-1}; R_1, 0.7 mm i.d., 300 cm long coiled around a 9 mm o.d. glass tube; R_2, a knotted PTFE tube, 0.5 mm i.d. and 130 cm long. Slight modifications to the procedure allowed other ranges of ascorbic acid to be determined. Hence if the concentration of potassium iodate was 4.0 mg l^{-1}, 0.1—7.0 μg ml^{-1} ascorbic acid could be determined.

RESULTS AND DISCUSSION

Generation and stability of triiodide

In all experiments, fixed flow rates of 1.5 ml min^{-1} were used for C_1 and C_2 and 3.0 ml min^{-1} of deionized water for C_3. The influence of acidity was investigated in experiments with 0.08 M potassium iodide in C_1 and 5.0, 10.0 or 20.0 mg l^{-1} potassium iodate in 1.5×10^{-6}—1.6×10^{-2} M sulphuric acid pumped in C_2. The concentration of triiodide generated was found to increase with increase in acidity up to 1×10^{-3} M acid (pH 2.7) because of increased reaction rate; above this acidity it remained constant at all concentrations of iodate employed (Fig. 2). Below this acidity, the triiodide absorbance also depended on the length of R_1 and R_2; the longer R_1 or R_2, the greater the triiodide absorbance. Further, the greater the length of R_1 or R_2, the smaller the fluctuations of the triiodide absorbance signal because of the improved mixing of the different streams. Therefore, in all further experiments, R_1 = 300 cm, R_2 = 130 cm (knotted PTFE tube) and 1×10^{-3} M sulphuric acid were used. These conditions ensured maximum triiodide generation and minimum fluctuations of the absorbance signal.

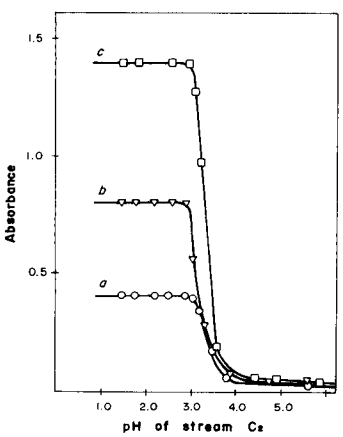

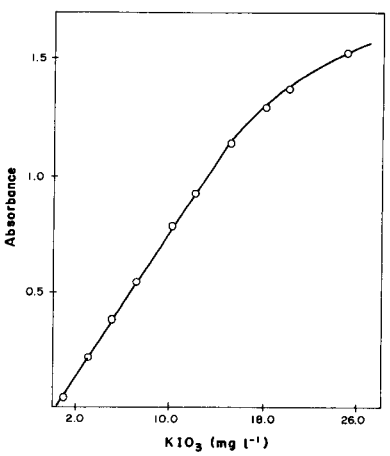

Fig. 2. Effect of the pH of stream C_2 at 0.08 M KI with different concentrations of KIO_3: (a) 5.0; (b) 10.0; (c) 20.0 mg l^{-1} (350 nm).

Fig. 3. Effect of KIO_3 concentration on triiodide absorbance (0.08 M KI, 1×10^{-3} M H_2SO_4 in C_2; 350 nm).

The effect of potassium iodate concentration was investigated by passing 0.08 M potassium iodide through C_1 and 1×10^{-3} M sulphuric acid containing 1.0—25.0 mg l^{-1} potassium iodate through C_2. Figure 3 shows the triiodide absorbances obtained; the reaction used leads to a mixture of triiodide, which absorbs at 350 nm, and molecular iodine, which does not absorb at this wavelength ($I_2 + I^- \rightleftharpoons I_3^-$; K = 708 l mol^{-1}). The concentration of molecular iodine increases with iodate concentration and for $\leqslant$15 mg l^{-1} potassium iodate the absorbance varies linearly with iodate concentration; at concentrations >15 mg l^{-1}, the linearity disappears because of an appreciable level of molecular iodine in the triiodide stream. In no case was there an increase in absorbance on increasing the acidity or the residence time (by stopping the flow), indicating that the absorbance was not limited by kinetic factors but only by the iodate concentration.

The effect of iodide concentration (0.01—0.10 M) was studied with 10 mg l^{-1} potassium iodate solutions in 1×10^{-3} M sulphuric medium. The results showed that the concentration of triiodide generated increases swiftly with iodide concentration up to 0.03 M iodide and then gradually up to 0.06 M iodide, above which it remained constant. An increase in residence time or acidity for <0.06 M iodide increased the triiodide concentration generated. At higher iodide concentrations the effect did not occur, for the reasons mentioned above.

The effect of pH in stream C_3 on the triiodide generated was investigated. This was done under the following conditions: a 0.08 M solution of potassium iodide was introduced through C_1 and a 10.0 mg l^{-1} solution of potassium iodate in 1×10^{-3} M sulphuric acid through C_2; solutions of sulphuric acid or sodium hydroxide over the pH range 1.5—12.5 were added through C_3. It was found that the pH of the C_3 stream could be varied between 1.5 and 11.0 without modifying the absorbance signal obtained. At pH >11 the absorbance decreased rapidly to zero because of the formation of hypoiodite, which is practically complete at pH >12.2.

Generation of triiodide in the presence of starch

Applications based on the detection of triiodide at 350 nm are not possible in the presence of substances which also absorb at this wavelength. In such cases, it is feasible to use the triiodide/starch complex which has an absorbance maximum at 580 nm and has a redox behaviour similar to that of the triiodide ion. To study the influence of starch concentration, a solution containing 10.0 mg l^{-1} potassium iodate in 1×10^{-3} M sulphuric acid was passed through C_2, and solutions of 0.08 M potassium iodide with a starch content ranging from 0.02 to 1.50 g l^{-1} were pumped through C_2. Only deionized water was pumped through C_3. The results (Fig. 4) show that formation of the triiodide/starch complex increased with starch concentration up to a starch content in C_1 of 1.20 g l^{-1}, above which the absorbance signal was constant.

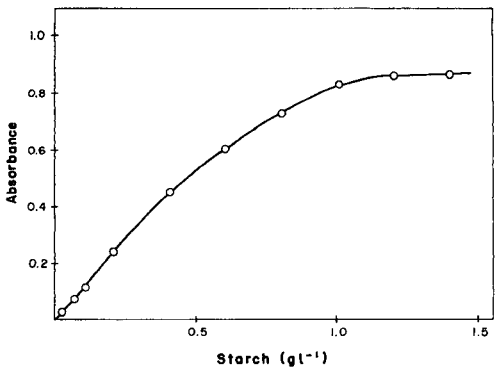

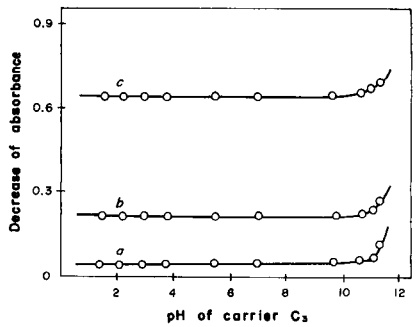

Fig. 4. Effect of starch concentration on absorbance (conditions as in text).

Fig. 5. Effect of pH of carrier stream C_3 on the response to ascorbic acid: (a) 1.0; (b) 5.0; (c) 15.0 μg ml^{-1} (conditions as in text).

Application to the determination of ascorbic acid

Ascorbic acid, when injected into stream C_3, gave a negative peak after merging with the generated triiodide stream. Such peaks were used to determine ascorbic acid. The influence of experimental variables on this procedure was also studied. Those variables related to the generation of triiodide, already optimized above, were maintained at 0.08 M potassium iodide in C_1, 1 $\times$ 10^{-3} M sulphuric acid in C_2, and R_1 = 300 cm (0.7 mm i.d.). Flow rates were kept at 1.5 ml min^{-1} for C_1 and C_2 and 3.0 ml min^{-1} for C_3.

To study the influence of carrier stream (C_3) acidity, 10 mg l^{-1} potassium iodate was used with R_1 = 130 cm. Standard samples of 1.0, 5.0 and 15.0 μg ml^{-1} ascorbic acid were introduced into C_3. The results are shown in Fig. 5. For all samples of ascorbic acid, the decrease in absorbance remained constant up to pH 10. Stopped flow measurements below pH 10 did not lead to a further decrease in absorbance.

The effect of 4.0, 7.0, 10.0, 15.0 and 20.0 mg l^{-1} potassium iodate on samples of ascorbic acid (1.0, 5.0, 10.0 and 15.0 μg ml^{-1}) was studied. The peaks obtained (Fig. 6) and the plots obtained therefrom (Fig. 7) revealed that the greatest decrease in absorbance occurred when the iodate concentration was close to 10 mg l^{-1}. For concentrations >10 mg l^{-1}, the negative peaks were smaller because of the presence of molecular iodine in the triiodide stream; molecular iodine reacts with ascorbic acid in a similar way to triiodide, but its disappearance does not contribute to negative peaks at 350 nm. The precision of the measurements decreased on increasing the potassium iodate concentration (Table 1).

The effect of reaction time was measured under the conditions described above for 10 mg l^{-1} potassium iodate. The reaction time (the residence time of the samples in R_2) was modified either by varying the length of R_2 or by stopping the flow. Samples of ascorbic acid (1.0, 5.0 or 15.0 μg ml^{-1}) were

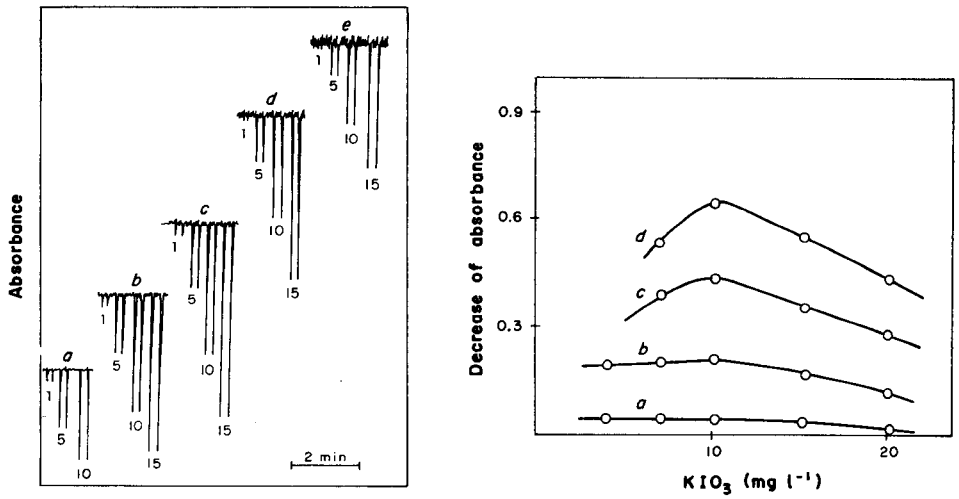

Fig. 6. Effect on peaks at 350 nm of different KIO_3 concentrations: (a) 4.0; (b) 7.0; (c) 10.0; (d) 15.0; (e) 20.0 mg l^{-1}. The number on each peak indicates the ascorbic acid concentration ($\mu g\ ml^{-1}$).

Fig. 7. Effect of KIO_3 concentration on inverse peak heights at different ascorbic acid concentrations: (a) 1.0; (b) 5.0; (c) 10.0; (d) 15.0 $\mu g\ ml^{-1}$.

TABLE 1

Precision of ten determinations of 5.0 $\mu g\ ml^{-1}$ ascorbic acid, for different concentrations of potassium iodate (R_2 = 130 cm; 350 nm)

KIO_3 (mg l^{-1})	4	7	10	15	20
R.s.d. (%)	1.5	1.8	2.0	5.0	8.0

injected, the length of R_2 being varied between 30 and 170 cm in each case. It was found that the extent of the redox reaction did not increase when the length of R_2 was increased; there was only a slight decrease in peak height resulting from increased dispersion. This indicated that the redox reaction was rapid and was practically complete for the smallest R_2 reactor used. However, the precision of the measurements increased with the length of R_2 (Table 2). In later studies, a knotted tube, 130 cm long, was used as R_2. Stopping the flow for 3—60 s did not affect the absorbance signal.

Five series of experiments were conducted with 4.0, 7.0, 10.0, 15.0 and 20.0 mg l^{-1} potassium iodate, respectively. For each series, standard samples of ascorbic acid (0.05—40 $\mu g\ ml^{-1}$) were injected and the absorbances were recorded at 350 nm. Figure 8 shows the calibration curves obtained. There

TABLE 2

Precision of ten determinations of 5.0 μg ml^{-1} ascorbic acid, for different lengths of R_2 (KIO_3 = 10 mg l^{-1}; 350 nm)

Length of R_2 (cm)	30	70	130	170
R.s.d. (%)	6.0	4.0	2.0	1.5

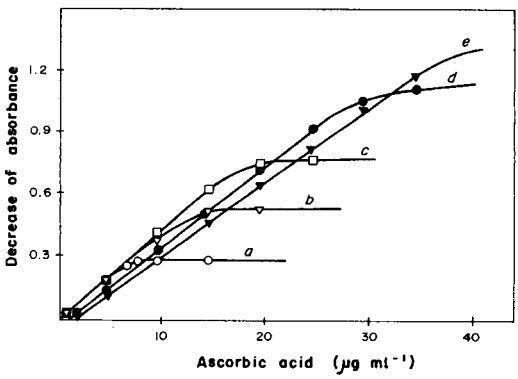

Fig. 8. Calibration graphs for ascorbic acid at different KIO_3 concentrations: (a) 4.0; (b) 7.0; (c) 10.0; (d) 15.0; (e) 20.0 mg l^{-1}.

are different linear ranges, limited by the triiodide concentration. For >10 mg l^{-1} potassium iodate, the sensitivity of the method decreased because of the presence of molecular iodine in the stream of triiodide, as mentioned above.

Because the method is indirect, the maximum concentration of analyte that can be determined is governed by the concentration of iodate employed. For samples with small concentrations of ascorbic acid, it is advisable to use low concentrations of iodate. In this way, there are fewer fluctuations in the continuous triiodide signal and a lower concentration of molecular iodine. The limits of determination corresponding to each series are shown in Table 3.

If there are interferences at 350 nm, the method can be modified by adding starch and measuring at 580 nm. Starch (1.20 g l^{-1}) was introduced into the system through channel C_1 with the potassium iodide. The method thus modified had detection limits and sensitivity similar to those obtained in the absence of starch.

The proposed method was applied to the determination of the ascorbic acid content of a vitamin C preparation, a canned jam and pineapple juice. The results were compared with those obtained by direct titrimetry with 2,6-dichlorophenolindophenol, the method recommended for these kinds of samples. The samples were suitably diluted and stabilized with EDTA and formic acid (0.1 and 4 g l^{-1} respectively, after dilution), filtered when necessary and injected into the flow system. Their concentration was determined by previous calibration in the presence and absence of starch. In a

TABLE 3

Determination limits for ascorbic acid at different concentrations of potassium iodate (350 nm)

KIO_3 (mg l^{-1})	4.0	7.0	10.0	15.0	20.0
Ascorbic acid (μg ml^{-1})	0.1—7	0.2—12	0.5—20	1—30	2—40

TABLE 4

Determination of ascorbic acid in various samples

Sample	Flow injection[a,b]		Titrimetry[a]
	350 nm	580 nm	
Vial vitamin C (mg/vial)	1070 ± 14	1070 ± 14	1074
Pineapple juice (mg l^{-1})	136 ± 4	137 ± 4	136
Jam (mg kg^{-1})	671 ± 14	675 ± 14	670

[a]Mean of 3 determinations. [b]With 95% confidence limits.

parallel series of experiments, aliquots of the samples were titrated with 8.06 × 10^{-4} M 2,6-dichlorophenolindophenol in acetic acid. The results obtained by the different methods are shown in Table 4. The flow methods gave satisfactory results for all the samples, and significant advantages over conventional methods: the reagents are stable, they do not need to be standardized or deoxygenated and their concentration can range considerably without affecting the results. Furthermore, up to 300 samples per hour can be injected, which is very suitable for routine analysis.

REFERENCES

1 J. Tillmans, Z. Unters. Lebensm., 54 (1972) 33.
2 H. Leonhardt and W. Moeser, Z. Anal. Chem., 122 (1941) 3.
3 G. S. Sastry and G. G. Rao, Talanta, 19 (1972) 212.
4 Ying Sing Fung and Shin Fai Luk, Analyst (London), 110 (1985) 201.
5 T. Tono and S. Fukita, Agric. Biol. Chem., 45 (1981) 2947; 46 (1982) 2953.
6 A. F. A. Moussa, Pharmazie, 32 (1977) 724.
7 J. H. Roe and C. A. Kuether, J. Biol. Chem., 147 (1943) 399.
8 G. Szepesi, Fresenius' Z. Anal. Chem., 265 (1973) 334.
9 S. S. M. Hassan, M. H. Abad el Fatlah and M. T. M. Zaki, Fresenius' Z. Anal. Chem., 277 (1975) 369.
10 T. Kamangar, A. B. Fawzi and R. H. Magjssoudi, J. Assoc. Off. Anal. Chim., 60 (1977) 528.
11 B. Jaselski and S. J. J. Nelapaty, Anal. Chem., 44 (1972) 379.
12 N. Delaporte and J. J. Macheix, Chim. Anal., 50 (1968) 187.
13 K. L. Bajaj and G. Kaur, Analyst (London), 106 (1981) 117.
14 H. Mohr, Mitt. Geb. Lebensmittelunters. Hyg., 47 (1956) 20.
15 A. G. Fogg, M. A. Summan and M. A. Fernández Arciniega, Analyst (London), 110 (1985) 341.

Analytica Chimica Acta, 184 (1986) 251—258
Elsevier Science Publishers B.V., Amsterdam — Printed in The Netherlands

OPTICAL SENSOR FOR SODIUM BASED ON ION-PAIR EXTRACTION AND FLUORESCENCE

Z. ZHUJUN[a], J. L. MULLIN[b] and W. R. SEITZ*

Department of Chemistry, University of New Hampshire, Durham, NH 03824 (U.S.A.)

(Received 21st October 1985)

SUMMARY

A reagent phase that responds to sodium ion is used in a sodium-selective fiber-optic sensor. The components of the reagent phase are the ammonium salt of 8-anilino-1-naphthalenesulfonic acid (ANS), copper(II)—polyethyleneimine, and a commercial sodium-selective ionophore [*N,N',N''*-triheptyl-*N,N',N''*-trimethyl-4,4',4''-propylidynetris(3-oxabutyramide)] immobilized on silica. In the absence of sodium, the ANS binds to the copper(II) polyelectrolyte and fluorescence is quenched. When sodium (20—200 mM) is added, it forms a cationic complex which forms ion-pairs with some of the ANS, causing it to fluoresce. Response is linear at the lower sodium concentrations but tends to curve toward the concentration axis at higher concentrations. The sensitivity and the range of linear response depend on ANS concentration. Typically, it takes 1—3 min to reach 90% of steady-state response. The response time increases with decreasing temperature, increasing amounts of immobilized ionophore, and higher sodium concentrations. The selectivity of the sensor is established by the selectivity of the ionophore.

There is considerable interest in the development of chemical sensors consisting of an immobilized reversible indicator on the end of optical fiber(s). They offer advantages relative to electrical sensors in that they are free from electrical interference, do not require a reference electrode, and are potentially more stable with respect to calibration. Recent reviews summarize progress in this field [1—4].

For the advantages of optical sensors to be achieved in practice, it is necessary to develop immobilized indicator phases that are selective and respond reversibly to analyte over the concentration range of interest. This paper reports the development of a sensor that responds selectively to sodium ion. The components of the indicator phase are an anionic fluorophor, a copper(II)—polyethyleneimine complex and a neutral sodium-selective ionophore immobilized on a solid substrate. These reagents are confined by a dialysis membrane that is permeable to alkali metal ions but not to copper(II)—polyethyleneimine. In the absence of sodium ion, the anionic fluorophore binds

---

[a]Present address: Department of Chemistry, Shaansi Normal University, Xian, Shaansi, People's Republic of China. [b]Present address: Department of Chemistry, University of Wisconsin, Eau Claire, WI 54701, U.S.A.

0003-2670/86/$03.50

to the cationic copper(II)—polyethyleneimine polyelectrolyte. On the polyelectrolyte, the paramagnetic copper(II) ion causes fluorescence to be quenched. When sodium ion is added, some of the sodium combines with the neutral ionophore causing it to become cationic. The cationic surface forms an ion-pair with some of the anionic fluorophor, pulling it away from the quenching polyelectrolyte and rendering it fluorescent. Fluorescence intensity serves as a measure of alkali metal-ion concentration. The approach is a variation of ion-pair extraction for alkali metal ions, which has been reported for both nonaqueous solvents [5—7] and solid-phase reagents [8]. However, the present system is designed so that ion-pair formation occurs reversibly as the alkali metal concentration varies.

The ion-pairing approach offers several attractive features. It has the selectivity of the ionophore and the sensitivity of fluorescence. By varying the concentrations of anionic fluorophor and copper(II)—polyethyleneimine, it is possible to vary the effective equilibrium constant for ion-pair formation and thus alter the working range of the sensor. The approach can be applied with other ionophores.

THEORY

The three reactions occurring in the immobilized reagent phase and their associated equilibrium constants are represented as

$$\mathrm{Na} + \mathrm{I} = \mathrm{NaI}; \quad K_1 = [\mathrm{NaI}]/[\mathrm{Na}][\mathrm{I}] \tag{1}$$

$$\mathrm{P} + \mathrm{F} = \mathrm{PF}; \quad K_2 = [\mathrm{PF}]/[\mathrm{P}][\mathrm{F}] \tag{2}$$

$$\mathrm{NaI} + \mathrm{F} = \mathrm{NaIF}; \quad K_3 = [\mathrm{NaIF}]/[\mathrm{NaI}][\mathrm{F}] \tag{3}$$

where Na is the sodium ion, I is the ionophore, P is the cationic polyelectrolyte, and F is the anionic fluorophor. The concentrations, [P] and [PF], refer to the concentrations of cationic binding sites on the polyelectrolyte that are free and associated with anionic fluorophor, respectively. It is assumed that the binding of fluorophor to cationic sites on the polyelectrolyte can be characterized by a single equilibrium constant.

The mass balances for the system are:

$$C_{\mathrm{I}} = [\mathrm{I}] + [\mathrm{NaI}] + [\mathrm{NaIF}] \tag{4}$$

$$C_{\mathrm{P}} = [\mathrm{P}] + [\mathrm{PF}] \tag{5}$$

$$C_{\mathrm{F}} = [\mathrm{PF}] + [\mathrm{F}] + [\mathrm{NaIF}] \tag{6}$$

where C_{I}, C_{P} and C_{F} are the total concentrations of ionophore, polyelectrolyte binding sites, and fluorophor, respectively.

The species monitored is NaIF because the polyelectrolyte-associated fluorophor is quenched. In deriving an expression for the relationship between the concentration of NaIF and the sodium ion concentration, it is assumed that $[\mathrm{PF}] \gg [\mathrm{F}], [\mathrm{NaIF}]$. Because cationic polyelectrolytes strongly bind

organic counterions, [F] is small. In the experiments reported here, the amounts of ionophore, fluorophor and polyelectrolyte were chosen so that [NaIF] $\ll$ [PF] even in the presence of high sodium concentrations. It is also assumed that the concentration of sodium in the sample is not affected by the amount of sodium that is extracted by the ionophore and thus can be considered a constant. Under the conditions of these experiments this is a valid assumption.

With the first assumption, the mass balances on polyelectrolyte and fluorophor become $C_P = [P] + [C_F]$ and $C_F = [PF]$. These equations combined with Eqn. 2 yield

$$[F] = [PF]/[P]K_2 = C_F/(C_P - C_F)K_2 \tag{7}$$

Substituting for [F] in Eqn. 3

$$K_3 = [NaIF](C_P - C_F)K_2/[NaI]C_F \tag{8}$$

Substituting for [NaI] using Eqn. 1 and rearranging yields

$$[Na] = [NaIF](C_P - C_F)K_2/[I]C_F K_1 K_3 \tag{9}$$

Rearranging Eqn. 4, the mass balance on ionophore, and substituting for [NaI] using Eqn. 1 yields

$$[I] = C_I - K_1[Na][I] - [NaIF]$$

which can be rearranged to

$$[I] = (C_I - [NaIF])/(1 + K_1[Na]) \tag{10}$$

Substituting for [I] in Eqn. 9 and rearranging yields

$$[NaIF] = [Na]C_I C'K'/(1 + K_1[Na] + C'K'[Na]) \tag{11}$$

where $C' = C_F/(C_P - C_F)$ and $K' = K_1K_3/K_2$.

Equation 11 provides the desired relationship between the measured parameter and analyte concentration. Several features of this equation are noteworthy. First, for low sodium concentrations, $K_1[Na] + C'K'[Na] \ll 1$ and the response is expected to be linearly proportional to sodium concentration. As the magnitude of $K_1[Na] + C'K'[Na]$ approaches and exceeds unity, response becomes curved and ultimately flat when $K_1[Na] + C'K'[Na] \gg 1$. This corresponds to saturation of the ionophore with alkali metal ion. Secondly, the C' term can be varied at will, proving a means of adjusting the reagent phase composition to achieve response over a particular concentration range. This is possible only if $C'K' > K_1$. Otherwise the $K_1[Na]$ term in the denominator dominates response. This corresponds to the situation in which the anionic fluorophor is more strongly attracted to the polyelectrolyte than it is to the cationic complex so that it remains on the polyelectrolyte even when the cationic complex is formed. Finally, the K' term includes the three equilibrium constants. The first, K_1, reflects the affinity of the ionophore for sodium ion. The larger K_1, the more sensitive the response, as

would be expected. The ratio K_3/K_2 reflects the relative affinities of the ionophore complex and the cationic polyelectrolyte for the anionic fluorophor. This will depend on the structures of the polyelectrolyte, ionophore and fluorophor.

EXPERIMENTAL

Apparatus

The fiber-optic fluorimeter is similar in design to the instrument used in earlier work [9]. It includes a tungsten-halogen source, interference filters for wavelength selection and a photomultiplier detector. In all experiments, the excitation and emission wavelengths were 380 and 460 nm, respectively.

The configuration of the reagent phase at the common end of the fiber optic is shown in Fig. 1. A thin layer of approximately 0.1 mg of solid substrate on cellophane tape is held on the fiber optic by an O-ring. A distance of 0.5 mm between the tape and the end of the fiber bundle was found to give the greatest sensitivity. A piece of dialysis membrane (Spectrapor 2, molecular weight cutoff 12—14 × 10^3) is positioned below the cellophane tape and held in place by a piece of Tygon tubing. There is a 1.0-mm gap between the dialysis membrane and the immobilized reagent on the cellophane tape. This gap is filled with 1.0 ml of a solution of anionic fluorophor and copper(II)—polyethyleneimine complex.

An Orion 501 digital pH meter was used to measure pH.

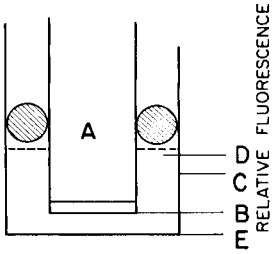

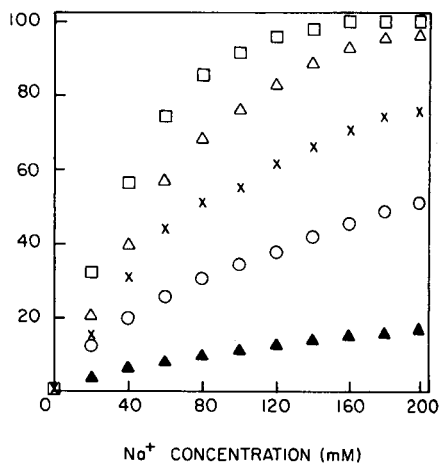

Fig. 1. Reagent phase for the sodium detector: A, common end of the birfurcated fiber optic; B, cellophane tape that holds silica used as immobilization substrate; C, glass tubing; D, internal filling solution; E, dialysis membrane.

Fig. 2. Relative fluorescence intensity as a function of sodium concentration. Concentration of ANS in the internal filling solution: (▲) 0.005 mM; (○) 0.01 mM; (×) 0.05 mM; (△) 0.1 mM; (□) 0.5 mM.

Reagents

Sodium ionophore I (*N,N',N''*-triheptyl-*N,N',N''*-trimethyl-4,4',4''-propylidynetris(3-oxabutyramide)) and sodium ionophore II (*N,N'*-dibenzyl-*N,N'*-diphenyl-1,2-phenylenedioxydiacetamide) were purchased from Fluka. These are neutral sodium-selective ionophores developed for use in liquid-membrane electrodes [10, 11]. Silica-gel powder (60—200 mesh; Baker) was ground to 400-mesh size before use. Polyethyleneimine, 50% solution in water, and the ammonium salt of 8-anilino-1-naphthalenesulfonic acid (ANS) were from Aldrich.

Standard 2.000 M and 0.500 M sodium solutions were prepared by weighing reagent-grade sodium chloride.

The internal filling solution of the reagent phase was prepared by pipetting 50.0 ml each of 1.0 mM ANS, 1.0 mM copper(II) sulfate, 0.010 M tris(hydroxymethyl)aminomethane buffer and 0.50 g l^{-1} polyethyleneimine into a 500-ml volumetric flask. After adjustment of the pH by addition of either 2.0 M hydrochloric acid or 2.0 M lithium hydroxide, the solution was diluted to the mark with water. In some experiments, the volume of ANS was varied as indicated later.

Immobilization of ionophores. Sodium ionophores were immobilized by dissolving weighed amounts in 5.0 ml of tetrahydrofuran and adding 1.0 g of 400-mesh silica. After being stirred for 2 h, the silica was put into a vacuum desiccator and evaporated to dryness under reduced pressure at room temperature. Unless otherwise indicated, the immobilized phase contained 0.10 mmol sodium ionophore II per gram of silica.

RESULTS AND DISCUSSION

Choice of system

Various possibilities were investigated before deciding on the final composition of the internal filling solution of the sodium sensor. Copper(II)—polyethyleneimine was chosen as the cationic quenching polymer because copper(II) is an efficient quencher. Also, because copper(II) forms strong complexes with polyamines, there will be very little free copper(II) in solution and a slow rate of loss of copper(II) through the dialysis membrane. The composition of the filling solution corresponds to one copper(II) per 11.6 monomer units. This is about half the total binding capacity of polyethyleneimine for copper(II). A study of polyethyleneimine interactions with copper(II) and other metal ions is reported elsewhere [12].

In addition to ANS, the other compounds evaluated as the anionic fluorophor in the internal filling solution were the sodium salts of 1-pyrenebutyric acid, 1-pyrenesulfonic acid, eosin, and 1,4-dihydroxy-3-amino-2-anthraquinonesulfonic acid (Nuclear Fast Red). While response was observed for all fluorophors, ANS gave the smallest signal in the absence of immobilized ionophore and the presence of salt. At high ionic strength, the other fluorophors either did not completely associate with the quenching polymer or they were not completely quenched when associated with polymer.

Alkyl-bonded silica was evaluated as a substrate for ionophore immobilization. However, it was observed that the response time was shorter when the ionophore was immobilized on unmodified silica.

Effect of ionophore structure. Under otherwise equivalent conditions, response was 5-fold more sensitive for sodium ionophore II than for sodium ionophore I. This is attributed to π—π interactions between ANS and the aromatic groups of sodium ionophore II which enhance the tendency for the fluorophor to form an ion-pair with the immobilized complex. The value of K_3 is larger for sodium ionophore II. This observation illustrates the importance of ionophore structure in designing a system that will show maximum sensitivity. Because the sensitivity proved greater for sodium ionophore II, this ligand was used in developing a sensor even though it is significantly less selective for sodium than sodium ionophore I [10].

Response to sodium concentration and response time

Figure 2 shows the intensity of ANS fluorescence at 460 nm as a function of sodium ion concentration for five different ANS levels. As predicted by Eqn. 11, response is linear at low concentrations but the slope decreases at higher concentrations. Changing the level of ANS changes the C' term of Eqn. 11. As predicted, an increase in C' increases the sensitivity and saturation occurs at a lower sodium concentration. This illustrates how the useful range of the sensor can be changed by appropriate choice of the composition of the internal filling solution. For measurements of sodium in serum, 0.1 mM ANS yields linear response over the concentration range of interest.

The time required to reach 90% of steady-state response varies with sodium concentration, temperature, and the amount of immobilized ionophore. Typically the response time is in the range 1—3 min. It is shorter for lower amounts of added sodium. Figure 3 shows response as a function of time

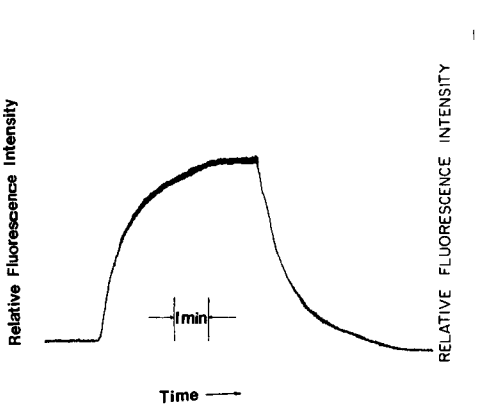

Fig. 3. Raw data showing change in intensity with time after the concentration was changed from 0 to 20 mM sodium ion and then back to 0.

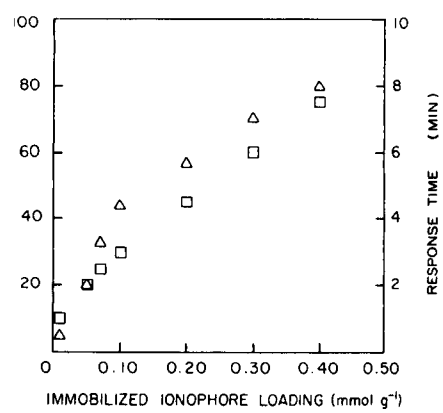

Fig. 4. Effect of the amount of immobilized ionophore on relative fluorescence intensity (△) and response time (□) for 20.0 mM sodium ion.

after an injection of 5.0 μl of 2.000 M standard sodium chloride into 5.0 ml of Tris buffer. The restoration time is also shown.

If the dialysis membrane is removed and the entire sample chamber is filled with the internal filling solution, then the response time decreases from 2.5 to 1 min when sodium is added to a stirred solution under otherwise equivalent conditions.

Figure 4 shows that both intensity and response time increase with the amount of immobilized ionophore. The increase in intensity is predicted by Eqn. 11. The strong dependence of response time on amount was not expected. It suggests that the process that governs the response time is the rate at which ANS leaves the polymer. If the rate at which ANS leaves the copper(II)—polyethyleneimine associate is constant, the response time will depend on how much ANS has to leave. This is also consistent with the observation that the response time is longer for larger changes in sodium concentration. The time required for mass transfer of ANS in the internal filling solution to the immobilized ionophore on the silica surface will also contribute to the observed response time.

Effects of pH and temperature

Figure 5 shows that sensitivity increases as pH is varied from 3 to 11. This implies that at higher pH, ANS either has a stronger tendency to form an ion-pair or is less strongly bound to the copper(II)—polyethyleneimine. Because the ion-pairing chemistry does not involve hydrogen ion, this suggests that protonation of the cationic polyelectrolyte is responsible for the variation in intensity with pH. As pH is decreased, some of the free amino groups on copper(II)—polyethyleneimine may be protonated, creating new positive sites on the polyelectrolyte which can bind ANS. If this explanation is correct, it means that ANS bound to protonated sites is still close enough to

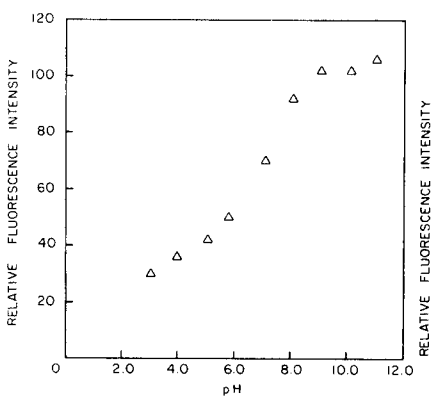

Fig. 5. Effect of pH on relative fluorescence intensity for 20.0 mM sodium ion.

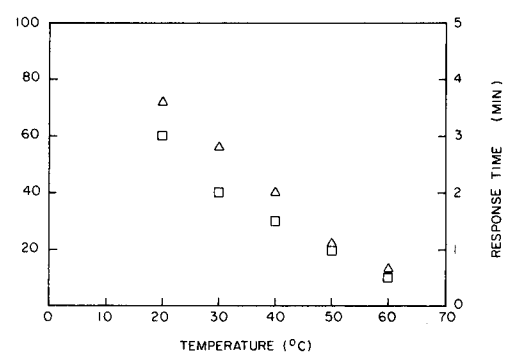

Fig. 6. Effect of temperature on relative fluorescence intensity (△) and response time (□) for 20.0 mM sodium ion.

copper(II) sites so that its fluorescence is quenched. Other factors may contribute to the variation in response with pH. The surface charge on the silica will change with pH, which could influence response. Changes in ionic strength might also influence response; however, the experimental results shown in Fig. 5 were performed at essentially constant ionic strength.

Figure 6 shows that both the sensitivity and response time depend strongly on temperature. As expected, increasing temperature accelerates the rates of the processes required for response, thereby reducing the time required to reach a steady-state signal. The decrease in sensitivity with temperature is also expected because fluorescence quantum efficiencies normally decrease with increasing temperature. In addition, there must also be significant changes in the equilibrium constants of the reactions required for response which also would affect sensitivity.

Stability and interferences

The usable lifetime of an immobilized reagent phase was established by the rate of swelling of the glue on the cellophane tape holding the silica. The swollen glue tended to cover the surface of the silica, resulting in slower response and reduced sensitivity. The longest a particular reagent phase was used was three days. Over this period, there was no evidence that significant amounts of either ANS or Cu(II) diffused out of the dialysis membrane.

The sensor responds also to potassium and calcium. The selectivities for sodium are 1.2 and 1.7 relative to potassium and calcium, respectively. This is consistent with literature selectivity values [10] and is adequate for applications in which sodium is present in large excess. Magnesium (5 mM), chloride (200 mM), hydrogencarbonate (120 mM), phosphate (100 mM), sulfate (100 mM) and bovine serum albumin (2%) did not measurably affect the response observed for 20 mM sodium ion at pH 7.30. The anions were all tested as the lithium salts.

This work was supported by Instrumentation Laboratory, Inc., Lexington, MA.

REFERENCES

1 W. R. Seitz, Anal. Chem., 56 (1984) 16A.
2 J. I. Peterson and G. G. Vurek, Science, 224 (1984) 123.
3 O. S. Wolfbeis, Trends Anal. Chem., 4 (1985) 184.
4 W. R. Seitz, Sensors, 2(8) (1985) 6.
5 A. Sanz-Medel, D. Blanco Gomis and J. R. Garcia Alvarez, Talanta, 28 (1981) 425.
6 L. M. Tsay, J. S. Shih and S. C. Wu, Analyst (London), 108 (1983) 1108.
7 H. Nishida, Y. Katayama, H. Katsuki, H. Nakamura, M. Takagi and K. Ueno, Chem. Lett., (1982) 1853.
8 S. C. Charlton, R. L. Fleming and A. Zipp, Clin. Chem., 28 (1982) 1857.
9 L. A. Saari and W. R. Seitz, Anal. Chem., 54 (1982) 821.
10 R. A. Steiner, M. Oehme, D. Amman and W. Simon, Anal. Chem., 51 (1979) 351.
11 W. Simon, E. Pretsch, D. Amman, W. E. Morf, M. Gueggi, R. Bissig and M. Kessler, Pure Appl. Chem., 44 (1975) 613.
12 S. D. Dowling, J. L. Mullin and W. R. Seitz, Macromolecules, 19 (1986) 344.

Analytica Chimica Acta, 184 (1986) 259—269
Elsevier Science Publishers B.V., Amsterdam — Printed in The Netherlands

USE OF A FLOW-INJECTION SYSTEM IN THE EVALUATION OF THE CHARACTERISTIC BEHAVIOR OF NEUTRAL CARRIERS IN LITHIUM ION-SELECTIVE ELECTRODES

ROBERT Y. XIE, VICTOR P. Y. GADZEKPO[a], AZZA M. KADRY[b], YEHIA A. IBRAHIM[c], JAROMIR RŮŽIČKA[d] and GARY D. CHRISTIAN*

Department of Chemistry, BG-10, University of Washington, Seattle, WA 98195 (U.S.A.)

(Received 25th November 1985)

ABSTRACT

A flow-injection system based on microconduits is used to investigate electrode characteristics such as selectivity, detection limit, and response and equilibrium times of the new ionophore, *N,N,N',N'*-tetraisobutyl-5,5-dimethyl-3,7-dioxanonane diamide, in lithium ion-selective electrodes. These characteristics were compared with those of the ionophore *N,N'*-diheptyl-*N,N'*,5,5-tetramethyl-3,7-dioxanone diamide. The new ionophore has superior detection limits and shorter response and equilibrium time, but the other exhibits better selectivity for lithium with respect to sodium. Values of K^{Pot}_{LiNa} for the new ionophore vary from 0.0450 to 0.566, depending on the methods of measurement and solution conditions. This phenomenon is discussed. Stop-flow experiments effectively demonstrated the response and equilibrium time differences between these two ionophore membranes.

Flow-injection techniques have found wide application in several areas of analytical chemistry. In the area of ion-selective electrodes, they offer advantages of increased sensitivity, decreased chemical and mechanical interferences, fast response time and very good reproducibility of results [1]. Flow-injection techniques with potentiometric detection have been applied to the determination of ions in blood serum [2—4]. Few studies have used this technique to characterize electrode behavior. This paper describes an investigation of the characteristic behavior of a new compound, *N,N,N',N'*-tetraisobutyl-5,5-dimethyl-3,7-dioxanonane diamide (ionophore 1), as the ionophore in a lithium ion-selective electrode. Its behavior is compared to that of the previously reported *N,N'*-diheptyl-*N,N'*,-5,5-tetramethyl-3,7-dioxanonane diamide (ionophore 2) by using flow-injection measurements.

Zhukov et al. [5] prepared several lipophilic diamides and investigated

---

[a]Present address: Department of Applied Chemistry, The University of Wales, Institute of Science and Technology, Cardiff CF1 3X1, Great Britain. [b]On leave from Department of Chemistry, Faculty of Pharmacy, Zagazig University, Egypt. [c]Fulbright Scholar, on leave from Department of Chemistry, Faculty of Science, Cairo University, Egypt. [d]Permanent address: Chemistry Department A, The Technical University of Denmark, 2800 Lyngby, Denmark.

0003-2670/86/$03.50

[1] [2] [3]

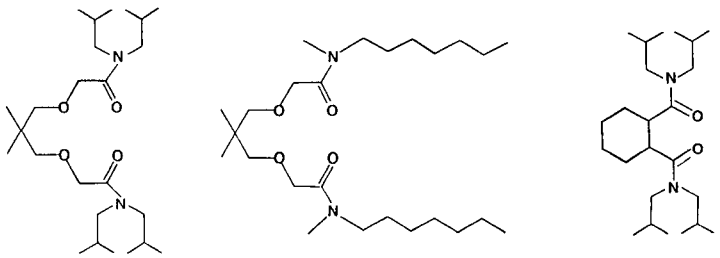

their characteristic behavior as neutral carriers in lithium ion-selective electrodes. The compounds included ionophore 2 and ionophore 3 and it was reported that ionophore 3 showed an improved selectivity for lithium ions [5] compared to ionophore 2 [6]. It was of interest to prepare ionophore 1 which resembles ionophores 2 and 3, combining features of both (backbone or side chains).

Ionophores 1 and 2 were synthesized and their characteristics compared in lithium ion-selective electrodes using a flow-injection system with microconduits. These characteristics include slope, linear range, detection limit, response and equilibrium times, and selectivity coefficients for lithium with respect to sodium, K^{pot}_{LiNa}, under different measurement and solution conditions.

EXPERIMENTAL

Reagents and syntheses

All solutions were prepared from salts of reagent grade, with deionized water. The chlorides of the metals were used.

Synthesis of ionophores. For the synthesis of ionophore 1, a solution of the acid chloride [7] (1.0 g, 0.0039 mol) in benzene (10 ml) was added dropwise with stirring and cooling (ice bath) to a solution of diisobutylamine (1.10 g, 0.0085 mol) in dichloromethane (15 ml) and triethylamine (3 ml). After addition was complete, the reaction mixture was left at room temperature overnight and then dichloromethane (50 ml) was added. The solution was washed twice with water, twice with distilled water, twice with hydrochloric acid (20 ml, 5 M), once with saturated sodium hydrogen carbonate solution, and finally with water. The organic layer was dried over anhydrous sodium sulfate and concentrated under vacuum to give the product as a yellow oil (1.8 g; yield ca. 82%). This was purified by column chromatography on silica gel, eluting first with petroleum ether (30—60 fraction; 100 ml), followed by a 2:1 mixture of petroleum ether (30—60) and chloroform to collect the product. The yield was 1.4 g (64%). Elemental content of the product (vs. theoretical) was as follows: 67.5% C (67.8%); 11.5% H (11.4%).

Ionophore 2 was synthesized and characterized as described by Zhukov et al. [5].

Plasticizer/PVC stock solution. Poly(vinyl chloride) (0.6 g) was mixed with 1.36 g of tris(2-ethylhexyl)phosphate as described earlier [8]. Cyclohexanone (7.5 ml) was added and the mixture was shaken until all the PVC had dissolved.

Membrane preparation. A 10.6-mg portion of ionophore 1 and about 3.6 mg of potassium tetrakis(*p*-chlorophenyl)borate (about 30% mole ratio with respect to ionophore 1) were dissolved in 500 μl of the PVC stock solution and mixed very well using a vortex mixer. For ionophore 2, 9.7 mg of the ionophore and 3.2 mg of potassium tetrakis(*p*-chlorophenyl)borate were dissolved in 500 μl of the stock PVC solution. These solutions were used to prepare the electrodes.

Apparatus, sample cell, and electrode preparation

Figure 1 shows the apparatus arrangement. Microconduits made from PVC blocks were used as the sample cell [9]. The channels on the block were engraved with a Dremel drill (model 210). The channel radius was 0.6 mm. A clear plastic sheet was tightly glued on the top of these channels with double-sided adhesive tape inserted between the microconduit and the sheet to seal the microconduit. The carrier solution was pumped via an air-pressurized reservoir which, because of its simplicity, stability and versatility, is superior to a peristaltic pump or chromatographic pump. An attempt to use a peristaltic pump or a chromatographic pump failed, as noise was introduced into the system by the static electricity generated. Unless otherwise stated, a sample of 100 μl was injected into the carrier stream, with a flow rate of 0.9 ml min^{-1} easily controlled by adjusting the air pressure. A Beckman model 3500 digital pH meter and a Corning model 146 digital pH meter were used for simultaneous potential measurements with both electrodes on a given injected sample. No significant differences were observed in potential measurements when the two pH meters were used separately with a single

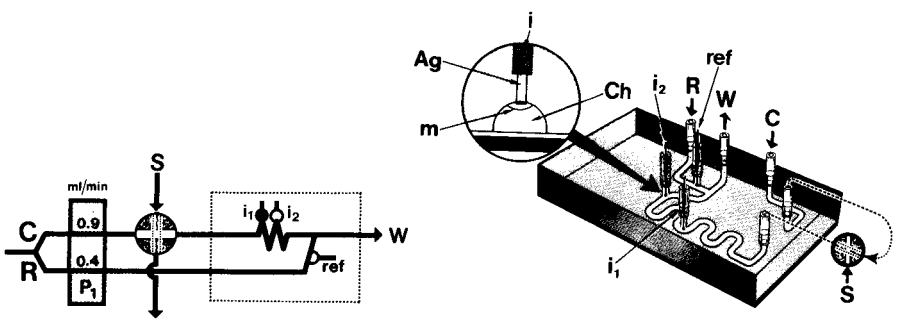

Fig. 1. Manifold and microconduit design: C, carrier stream; P, pump; S, sample solution; i_1, ion-selective electrode 1; i_2, ion-selective electrode 2; R, reference stream; ref, reference electrode; W, waste; i, gold pin; Ag, silver wire; m, membrane; Ch, channel of microconduit.

electrode. Responses were recorded on a chart recorder (Linear model 385).

Silver wires were inserted and glued to various positions, as shown in Fig. 1, with tetrahydrofuran, as described by Růžička and Hansen [9]. The ends of the silver wires were next inserted into gold pins for electrical contact. The surface of the silver wire in the conduit was oxidized with a few drops of a solution prepared by dissolving equal amounts of sodium chloride and sodium phosphate (0.3 g) in about 5 ml of bleach solution (Clorox); this deposited a reference layer of silver chloride on the silver surface. The wire was then washed with water and methanol and allowed to dry. The PVC solution containing the neutral carrier was applied to the surface of the silver wire under a microscope. Three layers were applied with drying between applications. Thus, a rugged miniature ion-selective electrode was constructed in the microconduit. The reference electrode was prepared in the same manner except that no PVC solution was applied to the silver wire surface.

Selectivity coefficients (K^{Pot}_{LiNa})

The selectivity coefficients were determined by following three different methods [10—12]. Potentials were taken from the recorded peaks.

Method 1 [10]. Equal concentrations of lithium or sodium were separately injected into the carrier stream. The potential changes with respect to the baseline were recorded and the selectivity was calculated from the equation $\log K^{Pot}_{LiNa} = (E_{Na} - E_{Li})/S$, where S is the slope of lithium response.

Method 2 [11]. A plot of voltage vs. logarithm of the lithium concentration (calibration graph) was first constructed by injecting pure lithium standards. Then a known concentration of pure sodium solution (C'_{Na}) was injected into the carrier stream, and the potential response was recorded. The lithium concentration (C'_{Li}) corresponding to this potential was obtained from the lithium calibration curve. The selectivity coefficient then is given by $K^{Pot}_{LiNa} = C'_{Li}/C'_{Na}$. The reverse approach can be used when a known concentration of lithium is injected.

Method 3 [12]. Several lithium solutions with known concentrations, prepared in carrier solution, were injected into the carrier stream and the changes in potential were recorded. A known concentration of sodium prepared in the carrier solution was next injected and the potential was recorded. A calibration plot of potential vs. logarithm of the lithium concentration was constructed and from this curve the concentration of lithium corresponding to exactly the potential of the sodium in the carrier solution was determined. In the case of lithium carrier solution, the following two forms of the Nicolsky equation are applied to the potential, E_1, measured on injection of sodium in lithium carrier solution, and to the potential, E_2, measured in constructing the calibration ($C_{Li\ total}$) plot:

$$E_1 = \text{const} + RT\,(zF)^{-1} \ln (C_{Li\ carrier} + K^{Pot}_{LiNa} C_{Na})$$

$$E_2 = \text{const} + RT\,(zF)^{-1} \ln C_{Li\ total}$$

Because E_1 and E_2 are equal, $C_{\text{Li total}} = C_{\text{Li carrier}} + K^{\text{Pot}}_{\text{LiNa}} C_{\text{Na}}$. Thus, the selectivity coefficient, $K^{\text{Pot}}_{\text{LiNa}}$, in lithium carrier stream is

$$K^{\text{Pot}}_{\text{LiNa}} = (C_{\text{Li total}} - C_{\text{Li carrier}})/C_{\text{Na}}$$

In the case of sodium carrier solution, the equations are

$$E_3 = \text{const} + RT\,(zF)^{-1} \ln K^{\text{Pot}}_{\text{LiNa}} C_{\text{Na total}}$$

$$E_4 = \text{const} + RT\,(zF)^{-1} \ln (C_{\text{Li}} + K^{\text{Pot}}_{\text{LiNa}} C_{\text{Na carrier}})$$

where E_3 is the potential measured for injection of sodium in sodium carrier solution and E_4 is the potential measured in constructing the plot of potential vs. lithium concentration (C_{Li}) in sodium carrier solution. Because E_3 and E_4 are again equal, $K^{\text{Pot}}_{\text{LiNa}} C_{\text{Na total}} = C_{\text{Li}} + K^{\text{Pot}}_{\text{LiNa}} C_{\text{Na carrier}}$. Thus, the selectivity coefficient, $K^{\text{Pot}}_{\text{LiNa}}$, in the sodium carrier stream is

$$K^{\text{Pot}}_{\text{LiNa}} = C_{\text{Li}}/(C_{\text{Na total}} - C_{\text{Na carrier}}).$$

In these equations, R, T, z and F are defined as in the classical Nicolsky equation; $C_{\text{Li total}}$ and $C_{\text{Na total}}$ are the net concentration changes plus carrier solution concentrations of lithium and sodium, respectively; $C_{\text{Li carrier}}$ and $C_{\text{Na carrier}}$ are the lithium carrier and sodium carrier solution concentrations, respectively; C_{Li} and C_{Na} are the lithium concentration in the sodium carrier solution and the sodium concentration in the lithium carrier solution, respectively. This is basically the matched potential method [12]. A major and important difference from method 2 is that the lithium and sodium solutions are prepared in the carrier solution and so the carrier concentration remains constant throughout the response peak.

RESULTS AND DISCUSSION

Measurement conditions

Fast and very reproducible results were obtained for electrodes containing ionophore 1, with rise times in the order of 6 s. The response dependence on the flow rate and the sample volume was investigated. An optimum response was obtained using a flow rate of 3 ml min^{-1}. The response was increased 32% by increasing the flow rate from 0.9 ml min^{-1} to 3 ml min^{-1}.

To minimize diffusion of the sample plug into the carrier stream, it was necessary to decrease the dispersion as much as possible. This was done by increasing the sample volume from 50 μl to 100 μl. Further increases in sample volume did not increase the signals. Under these conditions, the electrodes reach the equilibrium potential while the sample plug flows through the electrodes. The flat portion of the responses shown in Fig. 2A corresponds to the equilibrium potential. It is clear that the dispersion, D, is equal to one and there is no mixing of the sample plug with the carrier solution.

Economy of carrier solution was weighed against the increase in response by the increase of flow rate. It was more economical to use a flow rate of 0.9 ml min^{-1} and increase the signal by an increase in sample volume to 100 μl.

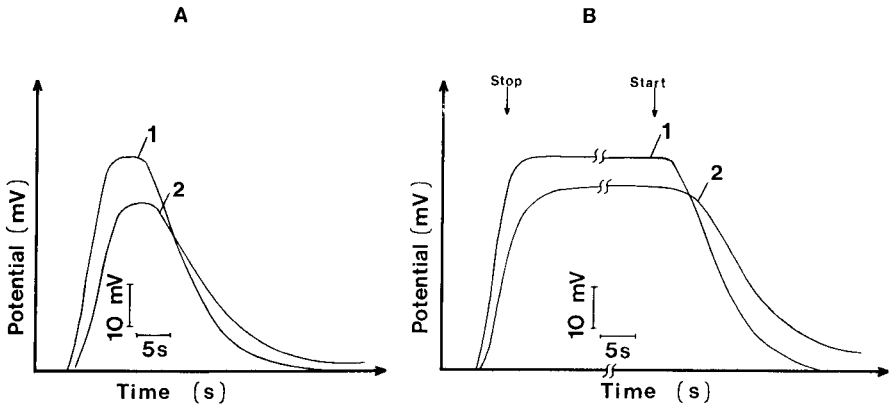

Fig. 2. (A) Flow curves for electrodes 1 and 2; (B) stop-flow curves for electrodes 1 and 2. In both cases, the carrier was 1.4 mM lithium and 10 mM lithium was injected.

Comparison of the relative peak heights for injection of lithium into an aqueous unbuffered 1.4 mM lithium carrier stream revealed substantially higher signals than for injection of the same concentration of sodium. This gives quick quantitative information about the selectivity of the electrode. One advantage in the use of the flow-injection technique with ion-selective electrodes employing microconduits, as described here, is the possibility of having more than one electrode implanted in the cell. Two different ionophore-membrane electrodes can be easily monitored and compared at the same time and with the same sample injection, which eliminates the possibility of error from concentration inaccuracy of the sample solution or previous electrode treatment (history).

Response and equilibrium times

A stop/flow experiment was used to study the response behaviors of two electrodes. Figure 2B shows the stop/flow curves for injection of 10 mM lithium into a 1.4 mM lithium carrier solution. Although electrode 2 (ionophore 2 membrane) is upstream 0.4 s, under the applied flow rate of 0.9 ml min^{-1} with respect to electrode 1 (ionophore 1 membrane), electrode 1 responds first at 4.8 s after injection; electrode 2 responds at 5.2 s after injection, so there is a real difference in their response times of 0.8 s. Differences between equilibrium times for electrodes 1 and 2 can be observed in both the flow curve and stop/flow curves (Fig. 2). As determined from the flow curve, electrode 1 reaches equilibrium potential at 11.8 s after sample injection (10 mM lithium) and electrode 2 appears to do so at 13.9 s, a total real difference of 2.5 s. Note that the maximum response for electrode 2 is only about 90% that of the equilibrium response achieved under stopped-flow conditions, indicating that true equilibrium was not reached under flow conditions; i.e., the true response for electrode 2 is even slower. This is more

evident from the stop/flow curve. Electrode 1 reaches equilibrium potential at 15.6 s after injection and electrode 2 does so at 21.5 s when the flow is stopped at 10 s, a total real difference of 6.4 s. It may be noted that the dynamic flow system does decrease the apparent equilibrium time of the electrodes, demonstrating one of the advantages of the flow-injection method compared to the batch method. When flow is continued after a period of being stopped, electrode 1 returns to the background potential significantly faster than electrode 2 does. Thus, it is concluded that the rate constants ($\vec{k}$, $\overleftarrow{k}$) [13] of ion transport from aqueous solution to the membrane phase for electrode 1 are larger than for electrode 2. In addition, the relative membrane permeabilities (permeability $P = (\vec{k}/\overleftarrow{k})C_s$, where C_s is the free ionophore concentration in the membrane) of the two electrodes differ in proportion to the difference in K_{ij}^{Pot} values (= P_1/P_2) [13]. Alternatively, one might expect the diffusion coefficient for ionophore 2 and its lithium ion complex to be lower in the membrane phase than for ionophore 1, resulting in longer equilibrium times for electrodes using ionophore 1 [13].

Figures of merit

Figure 3 illustrates the linear range, sensitivity (slope) and detection limit [14] of electrode 1 in 1.4 mM lithium carrier stream. Table 1 summarizes the linear ranges, slopes and detection limits of electrodes 1 and 2 in 1.4 and 14 mM lithium streams. These three characteristic behaviors of electrodes are all dependent upon the composition of the carrier solution. Higher concentration of lithium in the carrier solution reduces the observed sensitivity of the electrodes, increases the values of observed detection limits, and reduces the observed linear ranges for both electrodes. In 1.4 mM lithium carrier stream, electrode 1 has a larger linear range than that of electrode 2, and its observed detection limit is 40% lower than that of electrode 2.

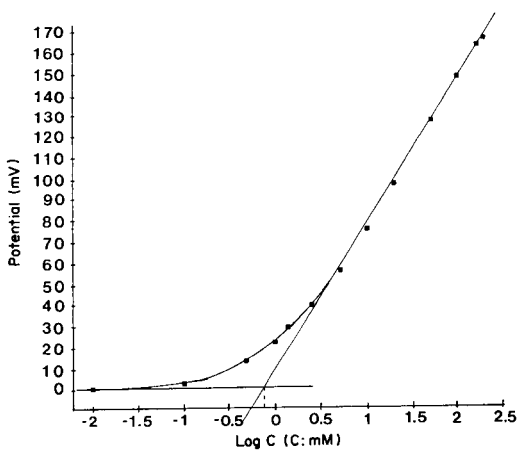

Fig. 3. Logarithmic lithium concentration (mM) vs. millivolt curve for the electrode based on ionophore 1 in unbuffered 1.4 mM Li carrier solution.

TABLE 1

Figures of merit for electrodes

	1.4 mM Li carrier stream		14 mM Li carrier stream	
	Ionophore 1	Ionophore 2	Ionophore 1	Ionophore 2
Range (mM)[a]	2.5—1000	5.0—1000	10—1000	10—1000
Slope (±s.d.)	68.9 (±0.7)	69.1 (±0.7)	53.7 (±1.1)	47.5 (±1.5)
Standard error of estimate (mV)	1.6	1.3	1.9	2.0
Correlation coefficient	1.000	1.000	0.999	0.994
Detection limit (±s.d.) (mM)	0.74 (±0.07)	1.2 (±0.1)	4.5 (±0.9)	4.7 (±1.5)

[a]Linear range of potential response vs. logarithm of concentration plot.

Selectivity coefficients

Table 2 summarizes the K_{ij}^{Pot} values calculated by methods 1, 2, and 3, respectively, for electrode 1 and electrode 2 in different carrier streams with a series of lithium or sodium solution injections. Methods 1 and 2 are separate-solution methods, because pure lithium or sodium is injected and $D = 1$ was deliberately set in the flow system. Method 3, the matched-potential method, is a revised fixed-interference method or a revised fixed primary-ion method, depending on the carrier solution used. When sodium carrier solutions are used, method 3 is experimentally similar to the method recommended by IUPAC and the uncertainty of this method is better than that of the IUPAC method in the present application. Direct comparison of K_{ij}^{Pot} values by the three methods may not be appropriate because solution conditions are quite different, and it is impossible to use exactly the same set of concentrations of lithium and sodium to calculate K_{ij}^{Pot} values by the three methods. However, the general trend is that method 1 gives the largest range of K_{ij}^{Pot} values, methods 2 and 3 give a smaller range of K_{ij}^{Pot} values, and similar solution conditions seemed to give similar K_{ij}^{Pot} values by the three different methods. In each method, electrode 2 shows a better selectivity for lithium.

Selectivity and carrier solution composition

Four different carrier solutions were used in this study, and the choice of 14 mM and 140 mM sodium carrier solutions was based on the practical purpose of application to determination of lithium in blood. In different carrier solutions, K_{ij}^{Pot} values for the PVC hydrophobic membrane electrode varied. For a perfect PVC liquid membrane, a bulk membrane model [13] can be used. The membrane potential (E_m) is [15]

$$E_m = \text{const.} + RT\,(zF)^{-1} \ln \left(\sum_n K_{in} a_i + \sum_n K_{jn} a_j\right) \quad (1)$$

TABLE 2

Values of selectivity coefficients (K_{ij}^{Pot}) calculated by the three methods

Carrier stream	Method 1						Method 2						Method 3				
	Li^+ (mM)	Na^+ (mM)	Ionophore 1		Ionophore 2		Li^+ (mM)	Na^+ (mM)	Ionophore 1		Ionophore 2		Na^+ (mM)	Ionophore 1		Ionophore 2	
			K	$1/K$	K	$1/K$			K	$1/K$	K	$1/K$		K	$1/K$	K	$1/K$
1.4 mM Li^+	10	10	0.302	3.31	0.287	3.48		10	0.254	3.93	0.197	5.07	2	0.319	3.13	0.357	2.80
	20	20	0.236	4.23	0.188	5.33		20	0.227	4.40	0.150	6.60	5	0.272	3.68	0.212	4.72
	100	100	0.134	7.47	0.0907	11.0		100	0.145	6.90	0.0906	11.03	10	0.235	4.26	0.169	5.90
	200	200	0.114	8.77	0.0752	13.3		200	0.113	8.83	0.0815	12.28	—	—	—	—	—
14 mM Li^+	10	10	0.566	1.77	0.601	1.66		10	0.334	3.00	0.360	2.78	20	0.268	3.73	0.183	5.46
	25	25	0.385	2.60	0.381	2.62		25	0.268	3.74	0.242	4.13	50	0.222	4.51	0.146	6.85
	100	100	0.178	5.62	0.163	6.15		100	0.182	5.50	0.162	6.16	100	0.174	5.74	0.166	8.65
	200	200	0.145	6.88	0.0982	10.2		200	0.164	6.09	0.112	8.97	—	—	—	—	—
14 mM Na^+	16	16	0.283	3.53	0.166	6.01	1.00	—	—	—	0.193	5.19	2	0.185	5.41	0.136	7.35
	18	18	0.290	3.45	0.169	5.90	1.88	—	0.220	4.54	0.171	5.85	4	0.225	4.44	0.162	6.17
	20	20	0.277	3.61	0.159	6.30	2.50	—	0.219	4.57	—	—	6	0.218	4.59	0.141	7.09
140 mM Na^+	160	160	0.0450	22.2	0.0219	45.6	5		0.184	5.45	0.117	8.55	20	0.110	9.09	0.0632	15.82
	180	180	0.0467	21.4	0.0214	46.7	10		0.174	5.75	0.0986	10.1	40	0.126	7.94	0.0638	15.68
	200	200	0.0464	21.5	0.0220	45.3	—		—	—	—	—	60	0.118	8.47	0.0652	15.34

Here, a_i and a_j are single ion activities of ions I^+ and J^+, n is the number of ionophores complexed with I^+ or J^+, and K_{in} and K_{jn} are the equilibrium constants of the reactions

$$I^+(aq) + nS(membrane) \overset{K_{in}}{\rightleftharpoons} IS_n^+(membrane)$$

$$J^+(aq) + nS(membrane) \overset{K_{jn}}{\rightleftharpoons} JS_n^+(membrane)$$

where S is the ionophore in the membrane phase. It is reasonable to assume that only 1:1 complexes are formed, thus $n = 1$ in the above chemical equations and from Eqn. 1 the selectivity coefficient compared to the classical Nicolsky equation reads $K_{ij}^{Pot} = K_j/K_i$.

Further consideration shows that K_j or K_i are functions of β_{js} or β_{is}, K_{js} or K_{is}, as well as a_s and k_s:

$$K_j = \beta_{js}K_{js}(a_s/K_s) \text{ and } K_i = \beta_{is}K_{is}(a_s/K_s)$$

where β_{js} or β_{is} is the stability constant of the complex JS^+ or IS^+ in aqueous solution, and K_{js} or K_{is} is the equilibrium constant for transfer of the complex into the membrane; K_s is an equilibrium constant for transfer of free ligands into the boundary layer and a_s is the activity of free ionophore, S, in the membrane. Combining these last three equations yields

$$K_{ij}^{Pot} = [\beta_{js}K_{js}(a_s/K_s)]/[\beta_{is}K_{is}(a_s/K_s)] \quad (2)$$

Equation 2 can further be reduced to

$$K_{ij}^{Pot} = \beta_{js}K_{js}/\beta_{is}K_{is} \quad (3)$$

as it can be assumed that the concentration of ionophore in the membrane is not changed.

Equation 3 shows that K_{ij}^{Pot} is a constant only when the membrane condition which determines K_{js}/K_{is} is not altered by any external conditions. However, in many practical cases, the membrane condition is altered by external conditions such as composition of solutions used for activation or storage of electrodes. During use, electrodes are always conditioned by different electrolyte solutions, often in a haphazard way, especially if operated batchwise. In a flow-injection system, when various carrier solutions are passed through the electrode cell, the solution composition can be maintained with a high reproducibility and it is therefore of interest to investigate it in more detail. Thus, for each carrier solution, the membrane is altered such that a different set of K_{js} and K_{is} values apply in Eqn. 3. This is evidenced by the changes in K_{ij}^{Pot} value in different carrier solutions. Even when the electrodes are exposed to different solutions for a short time, the electrode membrane properties are slightly altered, as evidenced by the variation in K_{ij}^{Pot} values observed when different concentrations of lithium and sodium are injected in the same carrier stream. The dependence of K_{ij}^{Pot} values on solution conditions has been reported for other ion-selective electrodes, in which a beaker method was employed for measurements [10].

In summary, many factors such as the choice of measurement method (1—3) used, the carrier solution composition and injected solution composition affect the value of the selectivity coefficient. Under the present measurement conditions, the new ionophore *N,N,N',N'*-tetraisobutyl-5,5-dimethyl-3,7-dioxanonane diamide exhibits selectivity coefficients K^{Pot}_{LiNa} from 0.566 to 0.0450. It is apparent that the selectivity coefficient should be determined under conditions that are similar to those of analytical measurements. Comparing the selectivities for electrodes with ionophores **1** and **2**, the response of ionophore **2** toward lithium ion relative to sodium ion is comparable to that of ionophore **1**, but the detection limit and response and equilibrium times of the new ionophore electrode are superior to those with ionophore **2**.

REFERENCES

1 E. Pungor, K. Toth and A. Hrabeczy-Pall, Trends Anal. Chem., 3(1) (1984) 28.
2 P. C. Meier, D. Ammann, H. F. Osswald and W. Simon, Med. Progr. Technol., 5 (1977) 1.
3 J. Růžička, E. H. Hansen and E. A. G. Zagatto, Anal. Chim. Acta, 88 (1977) 1.
4 M. E. Meyerhoff and P. M. Kovach, J. Chem. Educ., 60 (1983) 767.
5 A. F. Zhukov, D. Erne, D. Amman, M. Guggi, E. Pretsch and W. Simon, Anal. Chim. Acta, 131 (1981) 117.
6 M. Guggi, U. Fiedler, E. Pretsch and W. Simon, Anal. Lett., 8 (1975) 857.
7 N. L. Kirsch, R. J. J. Funck, E. Pretsch and W. Simon, Helv. Chim. Acta, 60 (1977) 2326.
8 V. P. Y. Gadzekpo and G. D. Christian, Anal. Lett., 16 (1983) 1371.
9 J. Růžička and E. H. Hansen, Anal. Chim. Acta, 161 (1984) 1.
10 K. Srinivasan and G. A. Rechnitz, Anal. Chem., 41(10) (1969) 1203.
11 G. J. Moody and J. D. R. Thomas, Analyst (London), 95 (1970) 919.
12 V. P. Y. Gadzekpo and G. D. Christian, Anal. Chim. Acta, 164 (1984) 279.
13 W. E. Morf, The Principles of Ion-Selective Electrodes and of Membrane Transport, Elsevier, Amsterdam, 1981, pp. 113—149 and 375—400.
14 IUPAC, Pure Appl. Chem., 48(1) (1976) 1.
15 W. R. Morf, The Principles of Ion-Selective Electrodes and of Membrane Transport, Elsevier, Amsterdam, 1981, pp. 264—336.

Analytica Chimica Acta, 184 (1986) 271—280
Elsevier Science Publishers B.V., Amsterdam — Printed in The Netherlands

DETERMINATION OF TRACE METALS IN RAIN WATER BY DIFFERENTIAL-PULSE STRIPPING VOLTAMMETRY

L. VOS, Z. KOMY[a], G. REGGERS, E. ROEKENS and R. VAN GRIEKEN*
Department of Chemistry, University of Antwerp (UIA), B-2610 Antwerp-Wilrijk (Belgium)

(Received 29th November 1985)

SUMMARY

Differential-pulse stripping voltammetry is applied to measure zinc, cadmium, lead and copper by anodic stripping and selenium(IV) by cathodic stripping in rain water at pH 2; subsequently, at pH 9.1, manganese is measured by anodic stripping on the same portion, and cobalt and nickel are measured in the adsorptive mode after formation of their dimethylglyoximates. The instrumental parameters are optimized. The linear ranges, mutual interferences and detection limits are studied. Excellent accuracy is demonstrated; the standard deviation is around 15% at 2.5—50 $\mu g\ l^{-1}$ levels. The method is shown to be applicable for rain water.

The determination of heavy metals in atmospheric deposition is of interest in studies of the biogeochemical cycles of trace elements. This determination is of importance in the context of the current problem of "acid rain" for several reasons. First, trace element measurements are mandatory to establish the chemistry of precipitation in general. Second, acids from rain mobilize heavy metals in surface water, thus constituting a major environmental hazard of acid rain, so that it is necessary to assess the importance of the direct heavy-metal supply from polluted rain relative to this mobilization effect. Finally, trace metals could be considered as tracers for the origin of the air masses producing acid rain. Indeed, Rahn and Lowenthal [1] have recently shown that the relative concentrations of, e.g., Mn, Se, Zn, V, As, Sb and In in atmospheric aerosols can be used as a characteristic signature of the source of a polluted air mass, which can be followed several thousand kilometers downwind, and it would seem that this method could be applied in an even more straightforward way to the precipitation itself.

Various methods are available for the multi-element trace analysis of rain water. The nuclear-based methods (neutron activation, photon-induced techniques, etc.) have recently been reviewed by Landsberger et al. [2]. Inductively-coupled plasma atomic emission spectrometry has also been proposed [3].

---

[a]On leave from the Department of Chemistry, Assiut University, Egypt.

0003-2670/86/$03.50

In view of the large number of rain-water samples that a routine measurement program usually involves, and because of its high speed, simplicity, low cost, sensitivity and multi-element character, differential-pulse stripping voltammetry (d.p.s.v.) could offer a viable alternative. Zinc, cadmium, lead and copper have been determined simultaneously in rain water by using differential-pulse anodic stripping voltammetry (d.p.a.s.v.) by Nguyen et al. [4] and Nürnberg [5]. Lingerak et al. [6] computerized this method and removed organic interferences on an activated carbon filter. Selenium has been measured in rain water [4] by differential-pulse cathodic stripping voltammetry (d.p.c.s.v.), and cobalt and nickel by adsorption differential-pulse voltammetry (a.d.p.v.) [5] after formation of the dimethylglyoximates [7].

In this paper, extensions to the d.p.s.v. techniques are reported so that a suite of eight trace elements can be determined in one run in rain water. Determining the maximum number of elements in a certain volume of water is highly relevant because studies of washout phenomena can require analysis of several fractions of a rain shower, which can limit the available amount of sample.

EXPERIMENTAL

Apparatus and chemicals

The voltammetric measurements were done with a microprocessor-controlled PAR polarographic analyzer model 264 (E.G. and G. Princeton Applied Research). This device controls a PAR model 303 static mercury drop electrode system (SMDE) and magnetic stirrer and an x-y recorder. The SMDE is provided with a 10-ml glass or teflon sample cup and a three-electrode system including an Ag/AgCl reference electrode and a teflon-covered Pt auxiliary electrode; the mercury working electrode was used in the hanging drop mode (HMDE). Before measurements, the sample solution was deaerated by bubbling for 4 min with nitrogen. During measurements, an inert atmosphere over the solution was maintained by flushing with nitrogen. During the deposition step, the solution was stirred automatically.

The samples were filtered under air pressure in a Sartorius filtration device (SM 16510) with 47-mm active diameter, through precleaned Sartorius membrane filters (0.45 μm pore size) or Nuclepore membranes (0.40 μm pore size).

The reagents used for the preparation of the supporting electrolytes were Merck Suprapur substances except ammonia and ammonium chloride, which were Baker Analytical Grade. The standard solutions were prepared by diluting Ventron AAS standards (1000 mg l^{-1}) or Baker Dilut-it standards. The ultrapure water was prepared in a Millipore Milli-Q water-purification unit.

Procedures

Sample preparation. All vessels (beakers for collection, polythene bottles for storage, flasks) were cleaned by keeping them for a month in diluted

(1 + 1) hydrochloric acid, rinsing thoroughly with purified water and then keeping them for another month in diluted (1 + 1) nitric acid. Before use, they were rinsed again with purified water.

The rain water was collected in 5-l beakers. During a rain period, the beakers were emptied normally in fractions of 20—50 ml. This also prevented contamination by dry fall-out. Samples were also taken on a weekly basis by a wet deposition collector, as described elsewhere [8]. After measurement of pH, the samples were filtered through a cleaned Sartorius filter or a Nuclepore membrane and the filtrate was acidified with hydrochloric acid (Suprapur) and stored in polythene bottles until required.

Determination of Zn, Cd, Pb and Cu; Se, Mn, Co and Ni. A study of the relevant literature [4—6, 9—14] and some optimization experiments (see below) led the following recommended procedure.

After filtration and acidification to pH 2 with hydrochloric acid, Zn, Cd, Pb and Cu were determined directly in a 10-ml portion of the sample. After deaeration for 4 min, these elements were deposited at a potential of −1.2 V with deposition times ranging between 1 and 3 min. After a rest interval of 30 s, the HMDE was polarized in the differential-pulse mode in the anodic direction to 0.0 V. Subsequently, selenium was determined in the same solution by cathodic stripping voltammetry. The preconcentration is done at 0.0 V for 2—5 min; after the rest interval of 30 s, the HMDE was polarized in the cathodic direction to −0.8 V. Then the pH was adjusted to 9.0—9.1 by adding 100 μl of a 10 M NH_3/NH_4Cl buffer, in which manganese was determined; after deposition at −1.7 V for 5 min, the potential was scanned to −1.30 V. Finally, cobalt and nickel were determined after adding dimethylglyoxime (DMG) to give a concentration of 10^{-4} M; the resulting complexes with DMG were adsorbed on the mercury drop at a potential of −0.7 V for 2 min and the voltammogram was recorded by scanning in the cathodic direction to −1.3 V.

Quantification was done by standard addition, using three spikes for each element.

Typical voltammograms of a rain-water sample are shown in Fig. 1. As can be seen, the stripping peaks are sufficiently separated so that the determination of these elements is possible over a wide concentration range without obvious mutual interference problems. The determination of copper is hampered somewhat by the oxidation wave of mercury; this can be overcome by working in nitric acid medium.

RESULTS AND DISCUSSION

Optimization of the instrumental parameters

The influence of the d.p.a.s.v. parameters on the analytical results was studied for solutions containing 100 $\mu g\ l^{-1}$ of Zn, Cd, Pb and Cu. A sodium acetate buffer (pH 4.5 and 0.1 M) was used as the supporting electrolyte. Under these conditions, the d.p.a.s.v. peaks of the ions appeared at ca. −1.00,

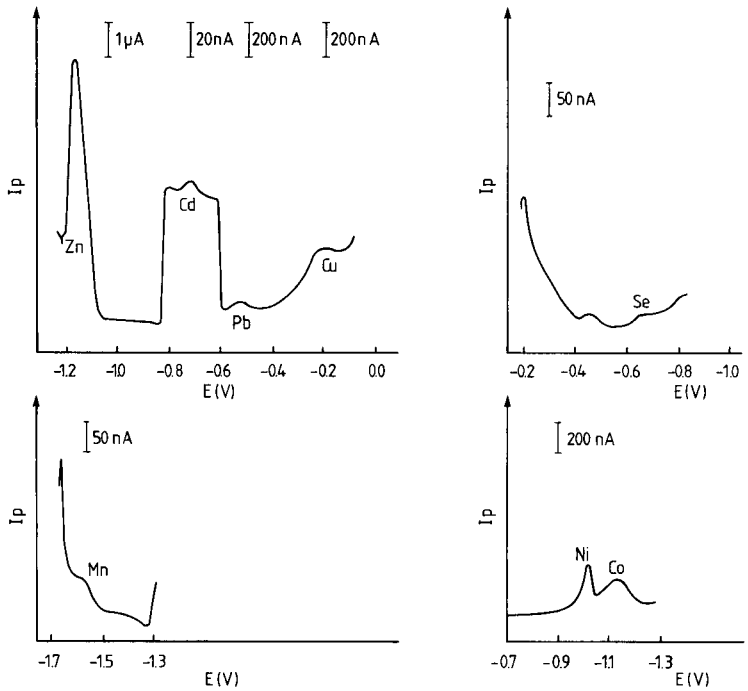

Fig. 1. Typical stripping voltammograms of a rain sample, under the selected experimental conditions.

—0.59, —0.42 and 0.00 V, respectively, versus the Ag/AgCl reference electrode. The deposition potential must be more negative than —1.00 V, to allow a simultaneous determination of the four elements. The peak height of zinc measured at different deposition potentials between —1.10 V and —1.40 V was constant in the interval —1.20 V to —1.40 V; hence a deposition potential of —1.20 V was chosen.

The influence of the scan speed, pulse amplitude, drop size, stirring speed and pulse repetition time on the peak height and on the full width at half maximum (FWHM) of the peaks was studied. The results are summarized in Table 1. In each experiment, one parameter was varied while the others were kept constant. A higher scan speed resulted in a decrease in resolution and peak height. At low scan speeds, the analysis time became prohibitively long, so that a compromise was needed. When high resolution was required, a scan speed of 2 mV s^{-1} was used; otherwise 10 mV s^{-1} was used. An increase in pulse amplitude increased the sensitivity but decreased the resolution; 50 mV was mostly used as a good compromise. The drop size affected the peak height but not the resolution; the large drop size provided greatest sensitivity for obvious reasons but was unstable; therefore the medium drop size was used. Higher stirring speeds increased the sensitivity, but the drop

TABLE 1

Influence of the instrumental parameters on the d.p.a.s.v. determination of Zn^{2+}, Cd^{2+}, Pb^{2+} and Cu^{2+}

(The default parameters were 5 mV s^{-1} scan speed, 50-mV pulse amplitude, medium drop size, slow stirring speed and 0.2-s pulse repetition time.)

Parameter	Peak height (mm)				FWHM (mm)			
	Zn	Cd	Pb	Cu	Zn	Cd	Pb	Cu
Scan speed (mV s^{-1})								
1	72	50	30	76	6	6	5	6
2	70	49	31	76	6	6	6	6
5	71	43	26	74	7	7	6	7
10	70	39	23	62	8	7	7	8
20	61	33	19	50	11	9	8	10
Pulse amplitude (mV)								
25	43	27	16	45	6	6	5	6
50	73	44	26	76	7	7	6	7
100	94	55	33	100	9	10	10	10
Mercury drop size								
Small	55	33	20	57	5	6	6	7
Medium	70	43	25	73	6	6	7	7
Large	100	59	35	99	6	6	7	7
Stirring speed								
Slow	72	44	26	73	7	6	6	7
Fast	84	51	29	83	7	6	7	8
Pulse repetition time (s)								
0.2	73	44	26	76	7	6	6	6
0.5	70	41	24	69	8	7	7	7
1.0	67	37	22	61	9	8	8	8

became so unstable that the slow speed was mostly selected. The smaller the pulse repetition time, the better the sensitivity and the better the resolution; therefore, a pulse repetition time of 0.2 s was always used.

Because 0.01 M HCl is a suitable medium for the simultaneous determination of Zn, Cd, Pb and Cu and subsequent analysis for Se(IV) [5], the same parameters were also examined for a solution of 10 $\mu g\ l^{-1}$ Zn, Cd, Pb and Cu in 0.01 M HCl. Similar results were obtained.

Linearity of the d.p.s.v. responses and interelement interferences

Figure 2 illustrates the dependence of the d.p.a.s.v. peaks of Zn, Cd, Pb and Cu (each at 5 $\mu g\ l^{-1}$) on the deposition time between 0.5 and 16 min. For all these elements, a linear relationship was obtained up to a deposition time of 8 min. For a deposition time of 16 min, the stripping peaks of Cu and Zn became smaller probably because of the formation of the intermetallic Cu/Zn compound. The linear range for all four elements thus goes much

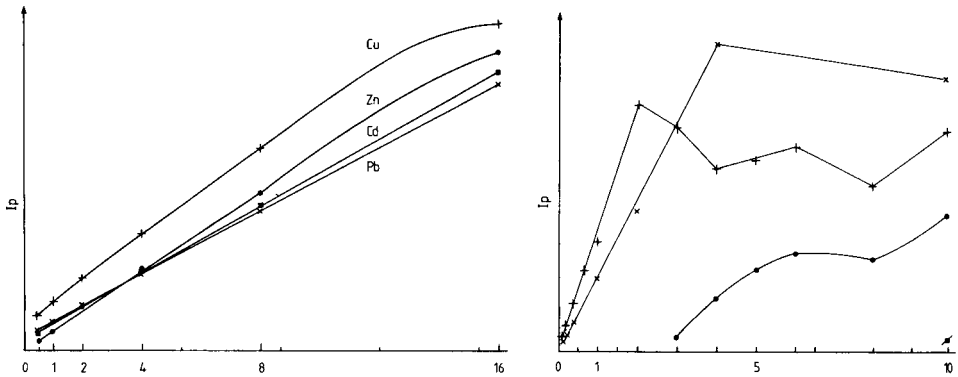

Fig. 2. Influence of the deposition time on the d.p.a.s.v. peak heights for Zn (•), Cd (▪), Pb (×) and Cu (+).

Fig. 3. Dependence of d.p.c.s.v. peak height on the concentration of Se(IV). Deposition potential: (+, •) −0.20 V; (×, ▪) 0.0 V. Peak potential: (+, ×) −0.52 V; (•, ▪) −0.75 V.

further than the deposition time of 1—3 min actually used, but low deposition times shorten the analysis time and reduce the risks of the interferences found in conventional linear-scan stripping voltammetry as well as the risks of drop instability.

The influence of diverse metal ions was studied. The concentration of Zn^{2+}, Cd^{2+}, Pb^{2+} and Cu^{2+} was varied between 1 and 10 $\mu g\ l^{-1}$; the concentration of Ni^{2+}, Co^{2+}, Sb^{3+} or Mn^{2+} was 25 $\mu g\ l^{-1}$ and the concentration of Fe^{2+} was around 200 $\mu g\ l^{-1}$. No apparent decrease in the peak height of Zn, Cd, Pb or Cu was found when these ions were added.

In hydrochloric acid medium of pH 2, selenium(IV) can be determined by d.p.c.s.v. The electrochemical preconcentration is achieved by formation of a HgSe layer on the HMDE at 0 V (vs. Ag/AgCl) and during the cathodic stripping selenium is released back to the solution [4, 12]. The influence of the concentration on the peak height was studied for two deposition potentials (−0.2 V and 0.0 V) in the concentration range between 0.1 and 10 $\mu g\ l^{-1}$ Se(IV) with a deposition time of 2 min (Fig. 3). With the deposition potential of −0.2 V, the curve of the stripping peak at −0.52 V remained linear up to 2 $\mu g\ l^{-1}$; above this level an additional peak appeared at a potential of −0.75 V. This was studied by Jarzabek and Kublik [12], who eliminated the peak splitting by preconcentrating at 0.0 V in concentrated hydrochloric acid. By deposition at 0.0 V in hydrochloric acid medium of pH 2, it proved possible to extend the linear range (Fig. 3) but at 4 $\mu g\ l^{-1}$ the peak at −0.75 V still appeared and the peak at −0.52 V became asymmetric. The influence of other metal ions on the stripping peak of selenium from a 0.2 $\mu g\ l^{-1}$ solution was also studied; Cu, Zn, As and Te had no influence up to 10 $\mu g\ l^{-1}$ levels. A concentration of 2 $\mu g\ l^{-1}$ cadmium or lead caused a decrease of 10%, and 10 $\mu g\ l^{-1}$ Cd or Pb caused a decrease of 40% on the intensity of the selenium

stripping peak. Only low concentrations can be measured in rather dilute samples; if the selenium concentration is high, the deposition time must be kept short. This also implies that this method is impractical for routine purposes. In rain-water samples a selenium peak is often found at a potential of —0.65 V (see Fig. 1).

The d.p.a.s.v. determination of manganese at mercury electrodes was studied and optimized by O'Halloran and Blutstein [9] and O'Halloran [10]. Manganese is only slightly soluble in mercury (0.0018% w/w); Mn_2Hg_5 may precipitate as a dispersed phase in the mercury electrode once the saturation level has been reached. Below the saturation level, a simple quasi-reversible charge transfer mechanism is involved with $\alpha = 0.9$. The consequences of this extreme charge-transfer asymmetry on a.s.v. were considered by O'Halloran and Blutstein [9]; they found that slow scan rates allowed satisfactory determinations of Mn(II) at very low concentrations. In an optimized procedure for the determination of manganese in sea water in tetraborate buffer at a mercury film electrode (MFE), a detection limit of 0.01 $\mu g\ l^{-1}$ was obtained and it was observed that 1 $\mu g\ l^{-1}$ Co, Cr, Ni or 10 $\mu g\ l^{-1}$ Cu suppressed the manganese peak for a 1 $\mu g\ l^{-1}$ solution by 50% [9, 10]. It was found here that manganese could be determined satisfactorily in an ammoniacal buffer of pH 9.1. The dependence of the peak height on the manganese concentration is illustrated in Fig. 4A for a deposition time of 5 min. The linear range extends to 30 $\mu g\ l^{-1}$, i.e., much higher than the concentration usually found in rain water. The influence of 10 $\mu g\ l^{-1}$ Co, Cr, Ni and Cu on the stripping peak of 5 $\mu g\ l^{-1}$ Mn was studied. None of these elements appeared to influence the peak height for manganese.

Nickel and cobalt were determined in the ammoniacal buffered medium with dimethylglyoxime (DMG) as a complexing agent. The preconcentration involves interfacial accumulation of an adsorption layer of the nickel and cobalt bis(-dimethylglyoximate) at the surface of the HMDE. The reduction of Ni(II) and Co(II) proceeds from this adsorbed state. The electrode reduc-

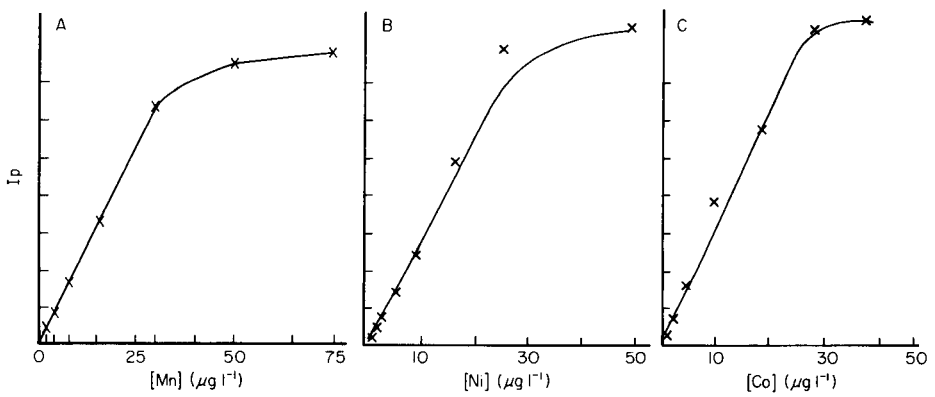

Fig. 4. Dependence of stripping peak heights on concentration: (A) manganese by anodic stripping; (B) nickel by adsorption stripping; (C) cobalt by adsorption stripping.

tion is totally irreversible and the transfer of the second electron is the rate-determining step of the reduction with an overall uptake of two electrons reducing the chelated nickel(II) and cobalt(II) to elemental nickel and cobalt [11]. The relation between the peak height and the concentration is shown in Fig. 4B and C for a 0.2 M NH_3/NH_4Cl buffer containing 10^{-4} M DMG with an adsorption time of 2 min. The relation is linear for concentrations lower than 30 $\mu g\ l^{-1}$. The range can be extended by increasing the buffer concentration but this is not necessary for the analysis of rain water because the concentrations are usually very low.

Blank levels, detection limits, precision and accuracy

It appeared that during filtration of a 50-ml sample with Sartorius filters, heavy metals were leached from the filter resulting in concentrations for Zn, Cd, Pb, Cu, Ni and Co of 5, 0.06, 1.2, 0.1, 1.4 and 2 $\mu g\ l^{-1}$, respectively. Therefore the filters were cleaned by rinsing with 50 ml of 0.1 M hydrochloric acid (Suprapur) followed by 100 ml of purified water. The levels of the leached heavy metals were then reduced to 0.75, <0.02, 0.6, <0.1, 0.7 and 0.7 $\mu g\ l^{-1}$ for Zn, Cd, Pb, Cu, Ni and Co, respectively.

The blank levels with their standard deviation found after filtration through Nuclepore filters, where no significant leaching of the studied elements was observed, were 0.75 ± 0.39, 0.11 ± 0.08, 0.89 ± 0.47, 0.28 ± 0.14, 0.087 ± 0.003, 0.21 ± 0.08, 0.60 ± 0.26 $\mu g\ l^{-1}$ for Zn, Cd, Pb, Cu, Se, Ni and Co, respectively in a normal laboratory environment. The resulting detection limits, obtained by taking three times the standard deviation, were 1.2, 0.23, 1.4, 0.41, 0.01, 0.24, 0.78 $\mu g\ l^{-1}$, respectively. It is obvious that, especially for selenium, the practical detection limit will often be set by the blank level.

To estimate the accuracy and precision of the proposed method, we participated in an intercomparison run on IAEA/W-4 Simulated Fresh Water [15]. The test portion was analyzed six times for Zn, Cd, Pb, Cu, Ni and Co; Se and Mn could not be determined because the solution had been acidified with nitric acid. The results are given in Table 2. The agreement between the

TABLE 2

Results of analyses of IAEA/W-4 Simulated Fresh Water

Element	Input value ($\mu g\ l^{-1}$)	Results of d.p.s.v.[a]	
		Average ($\mu g\ l^{-1}$)	RSD (%)
Zn	50.0	50.7	15
Cd	5.00	5.07	10
Pb	25.0	24.1	17
Cu	25.0	25.4	14
Co	2.5	2.27	22
Ni	2.5	2.74	12

[a]Average of 6 determinations with relative standard deviation per measurement.

TABLE 3

Results of rain-water analyses[a]

	Wilrijk (n = 10)			Maasmechelen (n = 12)			Mechelen (n = 13)		
	Mean	Min.	Max.	Mean	Min.	Max.	Mean	Min.	Max.
pH	4.3	4.0	4.7	4.4	4.0	5.2	6.2	4.7	7.3
Zn	66	10	163	73	10	347	33	10	71
Cd	3.5	0.16	22	1.3	0.12	4.3	0.92	0.19	2.6
Pb	47	5.1	110	41	6.0	180	19	1.7	72
Cu	15	0.9	58	5.5	<0.2	18	5.3	1.3	14
Se	—	—	—	—	—	—	0.4	<0.1	1.6
Mn	15	<1	55	23	<0.2	90	—	—	—
Co	2.6	1.0	4.3	2.3	0.33	4.5	1.3	0.18	2.3
Ni	8.4	1.0	37	16	0.68	>500	5.6	0.35	21

[a]The elemental concentrations are in $\mu g\ l^{-1}$.

present results and the input values is very satisfactory. The average relative standard deviation per measurement appears to be around 15% for the elaborate analytical procedure.

Applicability

Rain water was sampled at three different sites in Belgium: at Wilrijk on the university campus which is in a residential zone some 10 km south of the center of Antwerp, at Maasmechelen in a rural zone in the northeast of Belgium, and at Mechelen, a middle-size town some 25 km south of Antwerp. The samples at Wilrijk and Maasmechelen were taken on a daily basis during August and September 1984 and at Mechelen on a weekly basis between February and July 1985. The mean values are summarized in Table 3.

A very high pH value was measured in Mechelen, where the samples were taken near an historic cathedral in a study to assess the influence of acid rain on the weathering process of the building stones. This high pH value may be caused by neutralization of the rain water by calcium carbonate particles released from the building into the atmosphere [8]. The metal concentrations found in the rain water in Wilrijk and Maasmechelen are of the same order of magnitude and are generally a little higher than the concentrations found in the rain water sampled in Mechelen. Slanina et al. [16] measured in North Holland a slightly higher Zn level (95 $\mu g\ l^{-1}$) but lower Cd (0.46 $\mu g\ l^{-1}$), Pb (1.3 $\mu g\ l^{-1}$), Cu (4.1 $\mu g\ l^{-1}$) and Mn (5.4 $\mu g\ l^{-1}$) levels. The annual average heavy metal concentrations in rain water reported in the Germany Wet Deposition Program were in the lower $\mu g\ l^{-1}$ range for Zn, Cu, Pb and between 0.1 and 1 $\mu g\ l^{-1}$ for cadmium [14].

Part of this work was supported by the Belgian Ministry of Science under contract 84-89/67, the European Economic Community under grant ENV-768-B/RS, and the Flemish Ministry of Culture.

REFERENCES

1 K. A. Rahn and D. H. Lowenthal, Science, 223 (1984) 132.
2 S. Landsberger, R. E. Jerves and S. Monaro, in J. F. Lawrence (Ed.), Trace Analysis, Vol. 4, Academic Press, Orlando, 1985, p. 237.
3 J. R. Garbanino and H. E. Taylor, in J. F. Lawrence (Ed.), Trace Analysis, Vol. 4, Academic Press, Orlando, 1985, p. 185.
4 V. D. Nguyen, P. Valenta and H. W. Nürnberg, Sci. Total Environ., 12 (1979) 151.
5 H. W. Nürnberg, Sci. Total Environ., 37 (1984) 9.
6 W. A. Lingerak, A. M. v. Wensween-Leuter and J. Slanina, Int. J. Environ. Anal. Chem., 19 (1985) 85.
7 P. Nangniot, Ind. Chim. Belge, 32 (1967) 1323.
8 E. Keppens, E. Roekens and R. Van Grieken, Proc. Vth Int. Congr. Deterioration Conserv. Stone, Vol. 1, Presses Polytechniques Romandes, Lausanne, 1985, p. 499.
9 R. J. O'Halloran and H. Blutstein, J. Electroanal. Chem., 125 (1981) 261.
10 R. J. O'Halloran, Anal. Chim. Acta, 140 (1982) 51.
11 B. Pihlar, P. Valenta and H. W. Nürnberg, Fresenius' Z. Anal. Chem., 307 (1981) 337.
12 G. Jarzabek and Z. Kublik, Anal. Chim. Acta, 143 (1982) 121.
13 H. W. Nürnberg, Anal. Chim. Acta, 164 (1984) 1.
14 H. W. Nürnberg, P. Valenta, V. D. Nguyen, M. Godde and E. Urano de Carvalho, Fresenius' Z. Anal. Chem., 317 (1984) 314.
15 L. Pszonicki, A. N. Hanna and O. Suschny, Report on Intercomparison IAEA/W-4 of the Determination of Trace Elements in Simulated Fresh Water, I.A.E.A. Rep., IAEA/RL/118 (1985).
16 J. Slanina, J. J. Möls, J. H. Board, H. A. Van der Cloot and J. G. Raaphorst, Int. J. Environ. Anal. Chem., 7 (1979) 161.

Analytica Chimica Acta, 184 (1986) 281—286
Elsevier Science Publishers B.V., Amsterdam — Printed in The Netherlands

Short Communication

SIMULTANEOUS EVALUATION OF ELECTROACTIVE MEMBRANES ON A FOUR-FUNCTION ISFET BY A CONSTANT DILUTION METHOD

A. K. COVINGTON* and P. D. WHALLEY

Electrochemistry Research Laboratories, Department of Physical Chemistry, University of Newcastle, Newcastle upon Tyne, NE1 7RU (Great Britain)

(Received 26th November 1985)

Summary. Multifunctional ISFETs are used in testing the performance of several nitrate-sensitive polymeric membranes simultaneously. By mounting the ISFET in a miniature flow-through cell, a continuous dilution technique can be used to obtain calibration curves and selectivity coefficient data for several membranes under identical conditions.

Evaluation of new electroactive materials for ion-sensitive electrodes (ISEs) and ion-sensitive field effect transistors (ISFETs) is of fundamental importance. Usually [1], this involves the preparation of a series of discrete solutions of the primary ion, and mixtures of the primary ion and various interfering ions to establish calibration curves and derive selectivity coefficients for each different membrane. The precision of these measurements is limited by the number of solutions used over the concentration range of the primary ion (typically <10). A constant dilution technique has been suggested [2] for calibrating ISEs. By monitoring the output of an electrode pair whilst diluting a solution of the primary ion at a constant rate with distilled water, a continuous calibration curve can be generated. Selectivity coefficients can be estimated by introducing a fixed concentration of the interfering ion in the initial solution containing the primary ion and in the diluent (i.e., the mixed solution method [1]).

Multifunction ISFETs [3] readily permit the simultaneous comparison of differing electroactive membranes sensitive to the same species. By incorporating an ISFET into a miniature V-shaped flow cell, and using the constant dilution technique, rapid and precise membrane appraisal can be achieved. Data collection and evaluation are facilitated by the use of a microcomputer. To demonstrate the advantages of the constant dilution method, using ISFETs for electroactive membrane evaluation, four nitrate-sensitive membranes with different compositions are compared.

Experimental

Membranes. Nitrate-sensitive membranes were prepared from tetradodecylammonium nitrate (TDDA-N) [4] and Aliquat-336 nitrate [5]. The TDDA-N

0003-2670/86/$03.50

was prepared from the bromide salt (Fluka) by repeated exchange with analytical-grade potassium nitrate followed by recrystallisation from ethanol. Elemental analysis on the product confirmed its composition. A polymeric plasticizer (Elvaloy 742, DuPont de Nemours) was used instead of dibutyl phthalate in membrane B. Tetrahydrofuran/cyclohexanone mixture was used as the casting solvent for the membranes. Membrane compositions are given in Table 1.

Fabrication of the flow cell. A four-function ISFET (Eμ 144), described elsewhere [3], was used. The chip was mounted in a 16-pin dual-in-line ceramic header (Shinko CA-P16003-S Dage Intersem). Successful encapsulation depends on the cleanliness of the chip surface. An ultrasonic cleaning routine with detergent, distilled water (twice) and propan-2-ol, followed by blow drying with nitrogen, was used prior to the attachment of the gold bond wires and subsequent encapsulation. A polyimide/photoresist composite encapsulation method [3] was used to restrict exposure to the four individual gates of the ISFET, whilst preventing solution contact with the chip metallization, etc. All devices were checked for electrical integrity after encapsulation by applying a varying bias potential (−2 to +5 V) to a reference electrode and monitoring any resulting leakage current. This method of encapsulation ensured leakage currents below the realistic detection limit of the measuring apparatus (typically <10 pA) [3].

The etched holes in the encapsulation above the ISFET gates provided a natural well for the electroactive membranes. Care was taken with the membrane deposition to prevent any contact between adjacent membranes. Several applications of each membrane were necessary to produce an estimated thickness of 20—50 μm. After membrane deposition, the devices were stored for several days under vacuum to ensure removal of the cyclohexanone/tetrahydrofuran solvent mixture.

The V-shaped glass caps for the flow cells were cemented in position on to the ceramic headers with silicone rubber (Dow-Corning RTV 3145). The tubing between the dilution vessel and the flow cell was 0.5 mm i.d.

Signal processing. The drain current from the ISFET was passed through a current-to-voltage amplifier and the signal linearized by using a matched

TABLE 1

Membrane compositions

Membrane	Composition[a]
A	TDDA-N (4%); DBP (68%); PVC (28%)
B	TDDA-N (4%); Elvaloy (68%); PVC (28%)
C	Aliquat-336 (52%); DBP (26%); PVC (22%)
D	Aliquat-336 (52%); HA (26%); PVC (22%)

[a]DBP, dibutyl phthalate; HA, hexyl adipate; Elvaloy, Elvaloy 742; TDDA-N, tetradodecylammonium nitrate.

MOSFET by means of a circuit described earlier [3]. Buffering the outputs from the four ISFET channels before analogue switching, provided fast multiplexing without any adverse effects. Output from the ISFET interface was fed to a single-pen chart recorder (Linseis) and a high-resolution digital multimeter (Hewlett-Packard model HP-3468A). Data collection and control of the ISFET interface were achieved with a Hewlett-Packard HP-86B microcomputer.

Operation of the constant dilution system. A schematic diagram of the constant dilution apparatus and the ISFET interface with computer link is shown in Fig. 1. The use of a flow cell instead of dip electrodes enabled a sealed glass dilution vessel to be used, thus avoiding any difficulties associated with volume fluctuations in an open vessel. Rapid solution mixing in the dilution vessel was achieved by using a magnetic stirrer and follower. This was verified visually by the introduction of a dye into the dilution stream. The volume of the dilution vessel (ca. 16 cm^3) was measured by weighing.

The ISFET flow cell was mounted as close as possible to the dilution vessel. A saturated calomel electrode (Russell, type CR) was situated downstream from the flow cell and connected to the stream via a glass T-piece filled with saturated potassium chloride and the liquid junction was restrained with a ceramic frit sealed into the glass T-piece. A multi-roller peristaltic pump gave a flow rate of between 4.5 and 5.5 $cm^3\ min^{-1}$ which was measured several times for each dilution. All experiments were done at ambient temperature (typically 20°C).

Solutions were prepared from degassed distilled water to reduce the possibility of bubble formation from dissolved gas within the flow cell. Selectivities were estimated with a constant interferent concentration of 10^{-3} mol dm^{-3} during the dilution of the primary ion.

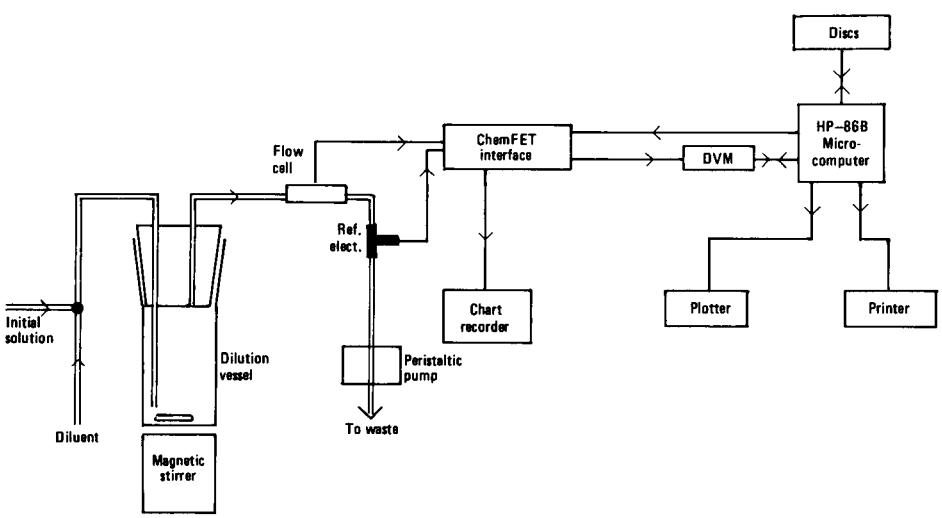

Fig. 1. Computer-controlled constant-dilution apparatus.

The relationship between the flow rate and the initial concentration of the primary ion has been given by Horvai et al. [2]. The four channels were switched every 30 s, the output of each channel being averaged over 5 readings of the digital multimeter at 0.1 s intervals. A total of approximately 100 data points was collected over the concentration range 10^{-1}—10^{-6} mol dm^{-3}. The time taken for a calibration was typically 50 min. Nitrate activities were estimated using a Debye-Hückel expression for activity coefficients.

Results and discussion

The time required for a dilution depends on the speed of response of the membrane. A critical requirement of the constant dilution method is that the sensor response is fast relative to the rate of change of concentration of the primary ion.

Examples of continuous nitrate calibration curves and of the effects of nitrite and chloride interferences on the responses of the four membranes are shown in Figs. 2 and 3. Typical selectivity data for the four membranes used are given in Table 2. The TDDA-N membranes were found to be superior to the Aliquat-336 membranes. The selectivity coefficients for the membranes containing TDDA-N were in reasonable agreement with those given by Nielsen and Hansen [4], and by Wright and Bailey [6] for conventional ISEs. Electrode slopes were in the range 52—57 mV/decade at 20°C. No appreciable differences were observed between membranes plasticized with dibutyl phthalate or Elvaloy 742, but membranes prepared with the latter were found to be physically stronger. As with ISEs, there are inevitable variations in slope and selectivity coefficients between nominally identical polymeric membranes on ISFETs.

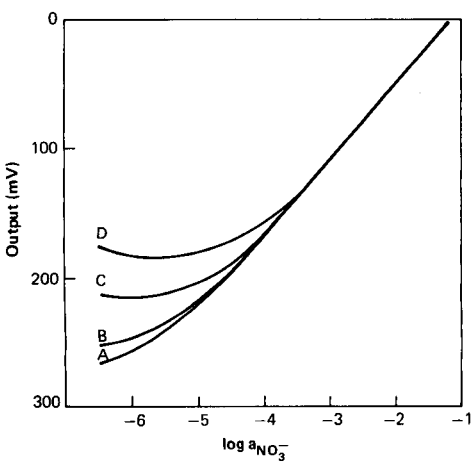

Fig. 2. Simultaneous nitrate calibration curves for membranes A—D (see Table 1 for membrane compositions).

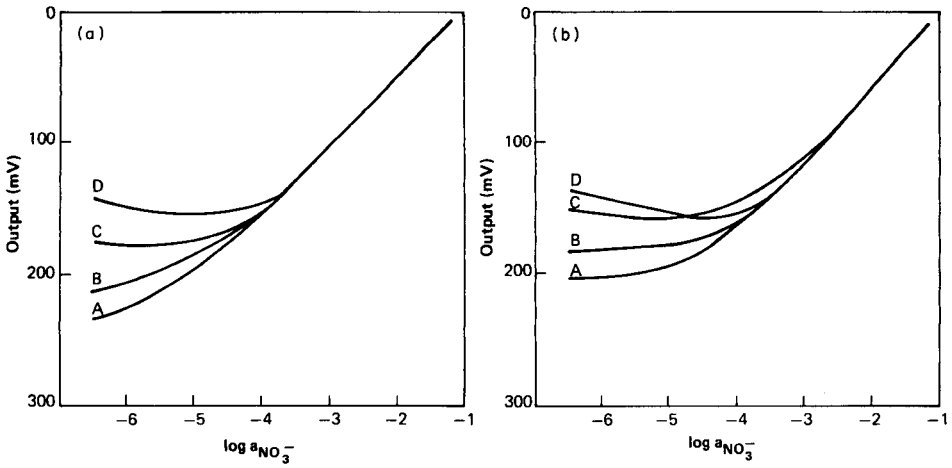

Fig. 3. Interference effects on the nitrate response: (a) chloride with $a_{Cl^-} = 10^{-3}$ mol dm^{-3}; (b) nitrite with $a_{NO_2^-} = 10^{-3}$ mol dm^{-3}.

TABLE 2

Selectivity data

Membrane	$-\log K_{NO_3^-,X}$		
	Chloride	Nitrite	Hydrogencarbonate
A[a]	2.7, 2.1	1.6, 1.8	2.6, 2.7
B[a]	2.3, 2.0	1.0, 1.8	2.8
C[a]	1.5	0.8	—
D[a]	0.8	0.7	—
TDDA-N [4][b]	2.30	1.15	>3.30
Aliquat-336 [6][b]	2.30 (2.5)	1.35	(3.55)

[a]Interferent concentrations 10^{-3} mol dm^{-3}. [b]Interferent concentrations 10^{-2} mol dm^{-3}, except for the values in parentheses, which were obtained at 10^{-1} mol dm^{-3}.

Device stability varied considerably between different ISFETs with nitrate membranes but no definite pattern was discernible. There are at least three possible explanations of instability and observed drift with polymeric membrane devices: (a) leaching out of electroactive material, (b) hydration, or solution penetration, of the membrane with associated internal pH changes, and (c) release of impurities or stabilizers from the PVC matrix. The problem of membrane internal pH change is potentially the most critical in ISFET applications because of the pH sensitivity of the silicon nitride surface. Any pH changes in the membrane will result in a shift in the potential difference at the membrane/silicon nitride interface. This change in potential difference would be superimposed on that observed at the ISFET/solution interface.

Conclusion

The constant dilution technique is an efficient and reliable method for calibrating ISFETs and ISEs. By incorporating a multi-function ISFET in a miniature flow cell, different membrane compositions sensitive to the same ion can be evaluated simultaneously under identical conditions.

The authors acknowledge financial support from the Water Research Centre. We are grateful to Dr. A. Sibbald for his advice, to Prof. P. Meares for the Elvaloy 742 sample and to T. R. Harbinson for preparing the Aliquat nitrate sample.

REFERENCES

1 A. K. Covington in, A. K. Covington (Ed.), Ion-Selective Electrode Methodology, Vol. 1, CRC Press, Boca Raton, 1979, p. 1.
2 G. Horvai, K. Toth and E. Pungor, Anal. Chim. Acta, 82 (1976) 45.
3 A. Sibbald, P. D. Whalley and A. K. Covington, Anal. Chim. Acta, 159 (1984) 47.
4 H. J. Nielsen and E. H. Hansen, Anal. Chim. Acta, 85 (1976) 1.
5 C. J. Coetzee and H. Freiser, Anal. Chem., 40 (1968) 2071.
6 J. A. Wright and P. Bailey, in E. Pungor (Ed.), Ion-Selective Electrodes, Elsevier, Amsterdam, 1978, p. 603.

Analytica Chimica Acta, 184 (1986) 287—290
Elsevier Science Publishers B.V., Amsterdam — Printed in The Netherlands

Short Communication

AMPEROMETRIC DETERMINATION OF SULFITE WITH SULFITE OXIDASE IMMOBILIZED AT A PLATINUM ELECTRODE SURFACE

TEKUM FONONG

Department of Chemistry, Illinois State University, Normal, IL 61761 (U.S.A.)

(Received 11th December 1985)

Summary. Sulfite oxidase is immobilized on collagen membrane at the surface of a platinum electrode and catalyzes the oxidation of sulfite to sulfate with stoichiometric production of hydrogen peroxide. The hydrogen peroxide is detected amperometically at the platinum electrode at an applied potential of 700 mV. The system responds linearly to sulfite in the range 1—150 μM, with a detection limit of 0.2 μM. The enzyme retains over 95% of its activity for three weeks if stored at −20°C when the probe is not in use.

Sulfite is widely used in the food and pharmaceutical industries as an inhibitor of bacterial growth and as an anti-oxidant. In large quantities, sulfite is a pollutant in ground and wastewaters. Recent approaches used for the determination of sulfite include molecular emission cavity analysis [1], chemiluminescence [2], spectrophotometry [3], titrimetry [4] and ion chromatography [5]. However, other fast, simple, and accurate procedures will be useful.

The purpose of the work described here was to design a sensitive enzyme probe for the quantitation of small concentrations of sulfite. The conditions of optimum operation of the system are reported.

The method utilizes the enzyme-catalyzed oxidation of sulfite to sulfate with stoichiometric production of hydrogen peroxide:

$$SO_3^{2-} + O_2 + H_2O \xrightarrow{\text{sulfite oxidase}} SO_4^{2-} + H_2O_2$$

The hydrogen peroxide is monitored amperometrically via its oxidation at a platinum anode. The measured current is proportional to the concentration of hydrogen peroxide produced and so to the concentration of sulfite in the sample solution.

Experimental

Apparatus and reagents. All measurements of current were made with the YSI-Clark 2510 Oxidase Probe and the Model 25 Oxidase Meter (Yellow Springs Instrument Company, Yellow Springs, OH). A Fisher Scientific Model 4512BF strip-chart recorder was used to record current traces. A Fisher Model 80 constant-temperature circulator was used to control the

0003-2670/86/$03.50

temperature of a 50-ml capacity double-jacketed sample glass cell at 25.0 ± 0.1°C. Collagen membranes were obtained from YSI. Cellulose acetate membranes were prepared by established methods [6]. Phosphate buffers of 0.10 M concentration were prepared in deionized water. Reagent-grade sodium sulfite was used to make standard solutions. Sulfite oxidase (E.C. 1.8.3.1; from chicken liver, Lot No. 104F-0590; Sigma Chemical Co.) was used.

Procedures. In experiments to determine the optimum pH of enzyme activity, initial buffer volumes of 5 ml were used. The enzyme solution was used as received. To each buffer was added 10 μl (3.6 units) of enzyme and the solution was thermostatted at 25 ± 0.5°C with constant stirring. Then aliquots of a standard sulfite solution were added to give final concentrations of sulfite of 1×10^{-4} M. The probe current was measured after 3 min for each solution. Calibration graphs for sulfite were obtained by addition of aliquots of a freshly prepared standard sulfite solution to 50 ml of pH 8.50 phosphate buffer after the immersed enzyme probe had reached thermal equilibrium and the residual current had been offset on the meter.

To minimize the nonenzymatic oxidation of sulfite to sulfate, buffered sample solutions were purged of oxygen by bubbling nitrogen through for about 5 min and maintaining them under a nitrogen atmosphere. Sulfite solutions were either stabilized against air oxidation by preparing them in buffer solutions containing glycerol or prepared freshly for each experiment.

Preparation of the enzyme probe. The YSI-Clark 2510 Oxidase Probe used consists of a platinum anode surrounded by a silver cathode. The probe operates at an applied potential of 700 mV. The collagen membrane used to immobilize the enzyme was first chemically activated as described by Coulet et al. [7].

An ultrafine cellulose acetate membrane was first placed over the amperometric probe. Sulfite oxidase solution (3.6 units) was pipetted onto the center of this membrane, over the circular platinum anode of the probe. The enzyme layer was then covered with an activated collagen membrane (2.5 cm diameter) held in place with an O ring. The probe was then conditioned in a pH 8.50 phosphate buffer for about 2 h or until a steady background current was obtained. This current, which was less than 5 nA, was offset on the instrument.

Results and discussion

Increased sensitivity to a 1×10^{-4} M sulfite solution was observed with increased immobilized sulfite oxidase (0.5—3.6 units). The maximum amount of enzyme used for subsequent studies (3.6 units) was limited by the surface area of the platinum electrode.

The pH profile of sulfite oxidase is shown in Fig. 1. Maximum enzyme activity is observed at pH 8.50 and subsequent experiments were done at this pH. It was found that tris(hydroxy)methylaminomethane buffers of pH > 8 generated high background currents, thus phosphate buffers were used.

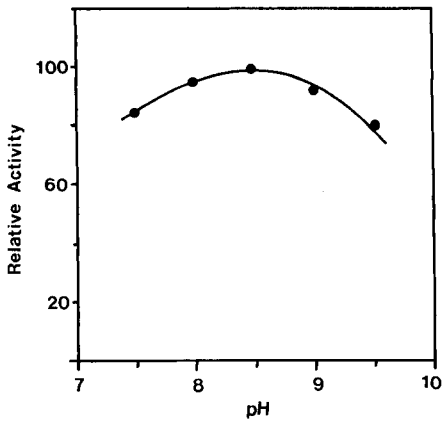

Fig. 1. pH profile of immobilized sulfite oxidase electrode at 25°C with activity reported as percent of maximum.

Ascorbic acid ($>10^{-3}$ M) interfered significantly with the probe. However, the use of ultrafine cellulose acetate membrane and a reaction medium of pH > 7 minimized the problem [8]. Ammonium ion ($>4 \times 10^{-2}$ M) produced a signal which was about 10% of that generated from 2×10^{-4} M sulfite.

The calibration graph of the logarithm of current (y) against the logarithm of the concentration (x) had the linear regression equation $y = (1.019 \pm 0.013)x + 5.71 \pm 0.07$ with $S_{yx} = 0.03$ and $r = 0.9995$. The plot was linear in the range 1—150 μm sulfite. The upper limit was imposed by the instrument which could detect a maximum current of 100 nA. Solutions containing sulfite concentrations >150 μM were diluted before measurements were made.

The enzyme probe was stored at —20°C in buffer when not in use. Calibration graphs were prepared and recovery studies were done daily for three weeks. During this period, the slope of the calibration graph decreased by 5% although the linear range was maintained. The detection limit for sulfite was found to be 0.2 μM. Freshly prepared sulfite solutions were used in these tests; sulfite solutions stabilized with glycerol were adequate for only two days. The titre of a 5×10^{-2} M sulfite solution was found to decrease by 20% on overnight storage at 4°C.

Randomly selected known concentrations of sulfite between 0.16 and 10.45 μg ml^{-1} were quantified by using the probe. The sample volumes varied from 5 to 40 ml. A least-squares fit of experimental concentrations (y) vs. the known values (x) gave $y = (1.011 \pm 0.002)x - (0.005 \pm 0.011)$ μg ml^{-1} with $S_{yx} = 0.02$ μg ml^{-1} and $r = 0.9999$. The relative errors ranged from 1.1 to 6.3% and the within-run relative standard deviations for five determinations ranged from ±1.0% to ±7.2% with an average of ±2.5%.

The level of the final, stable current reading and the time required to attain it depends on whether the enzyme is placed in the bulk solution or isolated behind the membrane. In the bulk solution, the enzyme is relatively

less concentrated so that a longer time is required to attain a steady-state current but the final current is higher because substrate conversion is essentially complete. Behind the membrane, the enzyme is highly concentrated but converts only the substrate that has diffused through the membrane; the steady-state current is reached more quickly but the final current is lower. It took 3.5 min to reach a final stable current of 4 nA when 1 unit of the enzyme was added to 1×10^{-4} M sulfite. This time was reduced to about 0.5 min and the current reading was 3.4 nA when the same amount of enzyme was immobilized at the probe.

A definite advantage of the immobilized enzyme is the shorter time required to obtain a steady-state response, thus reducing the extent of non-enzymatic air oxidation of sulfite in the bulk solution.

REFERENCES

1 S. L. Bogdanski, A. Townshend and B. Yenigul, Anal. Chim. Acta, 115 (1980) 361.
2 M. Yamada, T. Nakada and S. Suzuki, Anal. Chim. Acta, 147 (1983) 401.
3 S. Rama Bhat, J. M. Eckert, R. Geyer and N. A. Gibson, Anal. Chim. Acta, 108 (1979) 293.
4 P. Bruno, M. Caselli, A. Difano and A. Traini, Anal. Chim. Acta, 104 (1979) 379.
5 M. Lindgren and A. Cedegren, Anal. Chim. Acta, 141 (1982) 279.
6 Instruction Manual, YSI Model 25 Oxidase Meter, Yellow Springs Instr. Co., Yellow Springs, OH, U.S.A., p. 8.
7 P. R. Coulet, J. H. Julliard and D. C. Gautheron, Biotech. Bioeng., 16 (1974) 1055.
8 V. S. Srinivasan, T. J. Povsic and J. L. Huntington, Am. Clin. Prod. (Rev.), May/June (1983) 14.

Analytica Chimica Acta, 184 (1986) 291—293
Elsevier Science Publishers B.V., Amsterdam — Printed in The Netherlands

Short Communication

DIAGRAM, A DRAWING PROGRAM FOR LOGARITHMIC CONCENTRATION/pH PLOTS

J. MAIMÓ J. A. GARCÍA-RASO, J. M. ESTELA and V. CERDÁ*

Department of Analytical Chemistry, Faculty of Sciences, Universidad de Palma de Mallorca, Palma de Mallorca (Spain)

(Received 1st October 1985)

Summary. DIAGRAM provides graphic display of acid-base equilibria based on logarithmic concentrations of the species involved. Various subroutines facilitate calculation of α and concentration values of the different species in a system and successive protonations can be superimposed on the output.

Graphic presentation is widely used in the treatment of ionic equilibria and its importance has been stressed by numerous authors [1—6]. Several computer programs, e.g., MINIQUAD [7] and SQUAD [8] give graphic information about ionic equilibria but were designed primarily for the refinement of equilibrium constants, rather than to provide graphic information under any desired consitions. Other programs, e.g., COMPLEX [9], are useful to calculate the pH dependence of the concentrations of free species in complex systems, using known values of the equilibrium constants. When the pH range is scanned, the concentration or percentage of all free species in a system can be represented versus pH, giving compact information about the predominance of the different species.

In this communication, a new program, DIAGRAM, is described for plotting logarithmic concentration and distribution diagrams of acid-base equilibria, as well as for calculation of α_i fractions or concentrations of all species present at any desired pH value. Several systems can be superimposed in the same figure.

Description of the program

The program comprises a main program, PRINCIPAL, and nine subroutines. In the PRINCIPAL program, the task to be done is specified. In the LOG subroutine, logarithmic concentration diagrams are produced. First, the analytical concentrations (c_a) of the system are input and then the maximum degree of protonation, n, of the system and the pK values are introduced through the DATA subroutine, together with the selected intervals of the x and y scales, and the required resolution. In the N/D subroutine, the expression

$$\alpha_i = h^{n-i}K_1K_2 \ldots K_{n-i}/(h^n + K_1h^{n-1} + K_1K_2h^{n-2} + \ldots + K_1 \ldots K_n)$$

0003-2670/86/$03.50

is calculated, and values of log $[x_i] = c_a\alpha_i$ are obtained in the LOG subroutine. Here, h is the protonic concentration.

Once all the points to be represented have been obtained, the program jumps to the DRAW subroutine, where the kind of representation can be selected (printer, plotter or both). Without changing scales, other systems can be superimposed on the same diagram, which allows comparison of different systems or performance of calculations from line interceptions. Once all the systems required have been introduced, the program returns to PRINCIPAL.

In the DIST subroutine, the flow diagram is very similar to that of the LOG subroutine: α_i is represented directly versus pH, and the plot is independent of analytical concentrations. The distribution diagrams can be shown on a printer, a plotter or both. Different systems can be superimposed and diagrams can be produced in different sizes, vertically or horizontally or both. When no further systems need to be represented, the program returns to PRINCIPAL.

In the CONCS subroutine, the data for a given system (analytical concentrations and pK values) are introduced and then the free concentrations of all species are calculated for a selected pH value. When no more pH values need to be studied, the program returns to PRINCIPAL. The ALFAS subroutine is similar to CONCS, but α_i values are obtained instead of concentrations. A HELP subroutine summarizes the different possibilities of the programs. Subroutine GSTORE is used when the diagram shown on the display has to be filed. Subroutine GLOAD recovers a stored diagram for display.

The program will run on a desk computer with 32 kbytes of RAM. Both

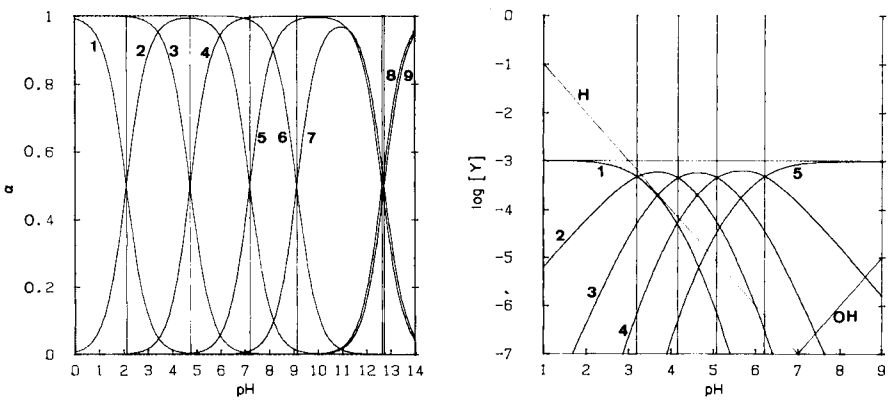

Fig. 1. Distribution diagram for the components of Prideaux buffers made from acetic, phosphoric and boric acids [10]: (1) H_3PO_4; (2) $H_2PO_4^-$; (3) CH_3COOH; (4) CH_3COO^-; (5) HPO_4^{2-}; (6) H_3BO_3; (7) $H_2BO_3^-$; (8) PO_4^{3-}; (9) HBO_3^{2-}.

Fig. 2. Logarithmic concentration diagram for 1×10^{-3} M ethylenediaminetetraacetoamidooxime (Y) [11] at ionic strength 0.1 M (25°C) with $pK_{a1} = 3.19$, $pK_{a2} = 4.16$, $pK_{a3} = 5.08$ and $pK_{a4} = 6.21$: (1) H_4Y^{4+}; (2) H_3Y^{3+}; (3) H_2Y^{2+}; (4) HY^+; (5) Y.

HP-85 and HP-86 microcomputers have been used; the first gives hard copies on thermal paper, the second on DIN A4 paper with a 7470A plotter. (Cassette or floppy disc of both versions are available on request at nominal costs.)

The program can deal with a maximum of nine protonation numbers, because the equilibrium constant array was not dimensioned. This can easily be changed if necessary.

Results

Experience with the DIAGRAM program has been satisfactory. The program has been used to obtain logarithmic concentrations and distribution diagrams to represent systems whose pK values were obtained during our researches.

In Figs. 1 and 2, two examples are represented.

REFERENCES

1 A. Johansson, Talanta, 20 (1973) 89.
2 D. W. Barnum, J. Chem. Educ., 59 (1982) 809.
3 L. Sucha and S. Kotrly, Solution Equilibria in Analytical Chemistry, Van Nostrand/Reinhold, London, 1972.
4 H. Freiser and Q. Fernando, Ionic Equilibria in Analytical Chemistry, Wiley, New York, 1963.
5 M. Valcárcel and J. M. López, Metodología Gráfica en el tratamiento de los equilibrios iónicos en disolución, Circulo Editor Universo, Barcelona, 1978.
6 E. Hogfeldt, in I. M. Kolthoff and P. J. Elving (Eds.), Treatise on Analytical Chemistry, Part I — Theory and Practice, Vol. 2, 2nd edn., Wiley-Interscience, New York, 1979, Chaps. 15 and 16.
7 A. Sabatini, A. Vacca and P. Gans, Talanta, 21 (1974) 53.
8 D. J. Leggett, Anal. Chem., 49 (1977) 276.
9 G. Ginzburg, Talanta, 23 (1976) 149.
10 C. Mongay and V. Cerdá, Talanta, 24 (1977) 747.
11 F. Borrull, E. Casassas, V. Cerdá and J. Guash, Quim. Anal., to be published.

Analytica Chimica Acta, 184 (1986) 295—297
Elsevier Science Publishers B.V., Amsterdam — Printed in The Netherlands

Short Communication

DETERMINATION OF CHLORPROMAZINE HYDROCHLORIDE IN TABLETS BY MOLECULAR EMISSION CAVITY ANALYSIS

ISSAM M. A. SHAKIR
Chemistry Department, College of Science, University of Salah Al-Deen, Arbil (Iraq)
(Received 9th October 1985)

Summary. Sulphur in chlorpromazine hydrochloride (2—50 mg) is oxidized by dichromate in condensed phosphoric acid (CPA) to sulphate, which in turn is reduced to hydrogen sulphide by heating with tin dissolved in CPA. The gas is carried by nitrogen to a steel cavity situated in a hydrogen/nitrogen flame and the S_2 emission is measured at 384 nm. The method is applied to determine the drug in powdered tablets. No sample pretreatment is needed; the procedure takes 10 min.

Chlorpromazine hydrochloride (I; 2-chloro-10-(3-dimethylaminopropyl)-phenothiazine) is used as a tranquillizer and antiemetic. It can be determined

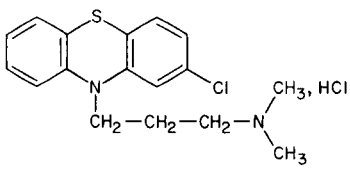

I

spectrophotometrically by extraction with flavianic acid from a neutral aqueous medium over the range 7—70 $\mu g\ ml^{-1}$ [1]. Reaction with alizarin red S in dilute sulphuric acid gives a 1:1 adduct, the absorbance of which can be measured at 420 nm [2]. Sodium nitrite forms a violet or pink colour in strongly acidic media with chlorpromazine hydrochloride, and 98.8—104.3% recoveries were obtained by spectrophotometry [3]. Other reagents include chloranil [4], tungstophosphoric acid [5] and iron(III) chloride [6]. Numerous chromatographic methods have been suggested [7—11].

Molecular emission cavity analysis (m.e.c.a.) has been used to determine compounds containing various elements, especially sulphur compounds [12], including chlorpromazine [13]. A method for reducing sulphate to hydrogen sulphide for m.e.c. detection was developed [14]. This is used in the present communication to generate hydrogen sulphide from the reduction of sulphate procuded by oxidation of chlorpromazine. Chlorpromazine hydrochloride was oxidized by chromium(VI) in condensed phosphoric acid to sulphate. Excess of chromium(VI) was destroyed, and the sulphate reduced by tin dis-

0003-2670/86/$03.50

solved in condensed phosphoric acid to hydrogen sulphide [14]. The hydrogen sulphide generated was swept from the reaction vessel, by a stream of nitrogen, to the cavity via a condenser which removed any spray that might otherwise reach the detector.

Experimental

The arrangement of the apparatus is shown in Fig. 1. Flame gases were 1.5 l H_2 min^{-1} and 1.75 l N_2 min^{-1}, with 15 ml N_2 min^{-1} as carrier. The

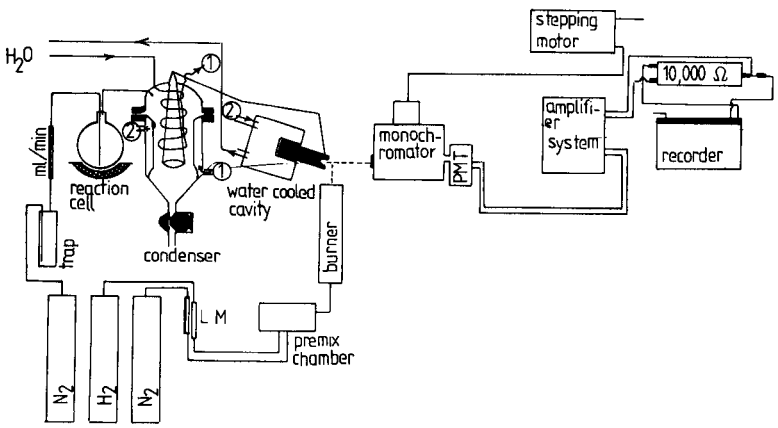

Fig. 1. Schematic diagram of the m.e.c. detector with the reaction cell and condenser: (1, 2) indicate points connected for water flow; L, M are flow meters.

spectrometer was similar to that described previously [14], with a water-cooled stainless steel cavity and a stepping motor device for wavelength scanning.

Preparation of oxidant and reductant. Concentrated phosphoric acid (analytical grade; 500 ml) was placed in an open round-bottomed flask heated by an isomantle until the temperature reached 285°C as measured by a protected thermometer, dipped into the acid. The "condensed" phosphoric acid was cooled and potassium dichromate (100 g) was dissolved in it by heating on a water bath. This reagent will be referred to as Cr/CPA. The reductant was prepared by adding 100 g of tin granules to the same amount of cool CPA prepared as above, and heating to 290°C [14]; this reagent is termed Sn/CPA.

Calibration. To a 100-ml round-bottomed flask, weighed mg-amounts of chlorpromazine hydrochloride were added, followed by 20 ml of Cr/CPA. The mixture was heated on a water bath until all powder had dissolved. To remove excess of Cr/CPA, the solution was heated on an isomantle until it turned deep green owing to the formation of chromium(III). The solution was left to cool to room temperature, and 20 ml of Sn/CPA added. The flask was fixed to the vapour transport system and heated to produce hydrogen

sulphide. The generated gas was passed to the detector where the S_2 emission at 384 nm was measured as a function of time. The maximum intensity was plotted as a function of the mass of drug.

Determination of chlorpromazine hydrochloride in tablets. Largopromactil tablets contain 10 or 50 mg of chlorpromazine hydrochloride as the active ingredient. Fourteen tablets that each contained 10 mg of drug were weighed and ground separately until the powder passed a 200-mesh sieve. The same procedure was adopted for 50-mg tablets. A weighed amount of each powder was treated as the calibration procedure. The maximum S_2 intensity was measured, and the amount of chlorpromazine found from the calibration graph.

Results and discussion

The calibration graph for chlorpromazine hydrochloride is linear for 2—50 mg of drug. Maximum intensity was obtained after heating for 9—10 min under the conditions used. For seven 10-mg drug tablets, when the weights added to the reaction vessel were 177.4 mg, the peak height obtained was 38.9 ± 1.1 mV, corresponding to 10.5 mg of chlorpromazine hydrochloride; for 380 mg of 50-mg drug tablets, the average peak height was 182.0 ± 1.8 mV, which is equivalent to 49.5 mg of chlorpromazine hydrochloride. These results are in good agreement with the expected values, which indicates that other tablet components do not affect the chlorpromazine recovery.

The author thanks the Samarra-Iraq company for their kind help in supplying samples.

REFERENCES

1 M. Tarasiewicz, E. Staniszewska and H. Puzanowska-Tarasiewicz, Acta Pol. Pharm., 37 (1980) 427.
2 M. Tarasiewicz, E. Staniszewska and H. Puzanowska-Tarasiewicz, Chem. Anal., 25 (1980) 591.
3 R. T. Sane, S. S. Kamat, V. S. Narkar, A. Y. Sathe and J. G. Mhalas, Indian Drugs, 18 (1980) 19.
4 T. S. Al-Ghabsha, S. K. Ibrahim and M. Q. Al-Abachi, Microchem. J., 28 (1983) 501.
5 P. G. Ramappa, H. S. Gowda, A. N. Nayak, Microchem. J., 28 (1983) 286.
6 V. N. Gandi and H. Shah, Indian Drugs, 21 (1984) 354.
7 D. J. Smith, J. Chromatogr. Sci., 19 (1981) 65.
8 K. K. Midha, J. K. Cooper, I. J. McGilveray, A. G. Butterfield and J. W. Hubbard, J. Pharm. Sci., 70 (1981) 1043.
9 A. C. Metha, Analyst (London), 106 (1981) 1119.
10 J. K. Cooper, G. McKay and K. K. Midha, J. Pharm. Sci., 72 (1983) 1259.
11 C. M. Davis and C. A. Harrington, J. Chromatogr. Sci., 22 (1984) 71.
12 M. Burguera, A. Townshend and S. L. Bogdanski, CRC Crit. Rev. Anal. Chem., 10 (1981) 10.
13 M. Q. Al-Abachi, Proc. Anal. Div. Chem. Soc., 14 (1977) 251.
14 S. L. Bogdanski, I. M. A. Shakir, W. I. Stephen and A. Townshend, Analyst (London), 104 (1979) 886.

Analytica Chimica Acta, 184 (1986) 299—306
Elsevier Science Publishers B.V., Amsterdam — Printed in The Netherlands

Short Communication

EFFECT OF RADIOFREQUENCY POWER ON LASER INDUCED FLUORESCENCE AND EMISSION SPECTROMETRY WITH AN EXTENDED-SLEEVE INDUCTIVELY-COUPLED PLASMA TORCH

X. HUANG[a], D. MO[b], K. S. YEAH and J. D. WINEFORDNER*
Department of Chemistry, University of Florida, Gainesville, FL 32611 (U.S.A.)
(Received 21st October 1985)

Summary. Relative laser-excited fluorescence and emission intensities as a function of RF power were measured for the Ca-I, Ca-II, Ba-I, Ba-II, Mg-I, Mg-II, Na-I and Cu-I lines with an extended inductively-coupled plasma (ICP) torch. In most cases, the relationships were different from those found in previous studies with a conventional short ICP torch. In some cases, unexpected double maxima or minima occurred. A study of the effect of an easily ionized element, potassium, on the fluorescence at the Ca-I and Ca-II lines with the extended-sleeve torch showed a considerably larger ionization interference than exists with the conventional short torch. The extended torch has found some use in laser-excited fluorescence and ICP-excited fluorescence, but researchers should be wary of unexpected variations with power and substantial ionization interferences.

The effects of radiofrequency (RF) power on the signal level in inductively-coupled plasma (ICP) fluorescence and emission spectrometry have not been thoroughly investigated previously for the extended-sleeve torch. Demers and co-workers [1, 2] found that the atomic fluorescence signals of easily dissociated but difficultly ionizable elements such as As, Pb, Tl, Cu, Fe and Zn increased only slightly as RF power increased, whereas easily ionized elements, such as sodium, decreased with increased RF power. Kosinski et al. [3] found that, with increased RF power, the atomic fluorescence signals of gallium decreased and those of molybdenum reached a peak, whereas the ionic fluorescence signals of Ca, Sr, and Ba changed little and those of Y and Zr increased. Apparently, the influence of RF power on fluorescence signals has not been studied with the short (conventional) torch. However, several RF-power studies have been done with the short torch for emission [4—12].

The previous emission studies [4—12] showed no unusual behavior with variation in RF power, and in fact in previous similar studies here, no unusual behavior was observed for either emission or fluorescence measurements with variation of RF power using a short torch, i.e., the emission or fluorescence

[a] On leave from Institute of Chemical Metallurgy, Academia Sinica, Beijing, China.
[b] On leave from Institute of Geochemistry, Academia Sinica, Guiyang, Guizhou Province, China.

0003-2670/86/$03.50

signals continually increased with RF power, or increased with RF power reaching a plateau or a maximum value, or decreased slightly with increased RF power. However, recent studies with an extended-sleeve torch (40 mm longer than the short torch) in both fluorescence and emission spectrometry resulted in different power-dependencies (i.e., more than one maximum and/or minimum in the fluorescence or emission signal vs. RF power plots) which are reported here. The unusual behavior must be taken into account when the extended torch is used in fluorescence or emission spectrometry.

Experimental

Apparatus. The laser system consisted of an XeCl excimer pumped dye laser. For the excimer laser (Lumonics Model 860; Lumonics Research, Ontario, Canada), the pulsed output at 308 nm was 80 mJ. The dye laser (Molectron Model DL-II; Molectron Corp., Sunnyvale, CA) was operated in both the fundamental region of 360—950 nm and the frequency-doubled region of 217—360 nm. Table 1 shows the laser dyes, wavelength ranges, and elements/lines investigated.

The 27.2-MHz ICP system was a Plasma-Therm Model HFP-2000-D (Plasma-Therm, Kresson, NJ). The extended plasma torch was 40 mm longer than usual (Baird Corp., Bedford, MA). The nebulizer was a Meinhard Model TR-30-A3 (J. E. Meinhard Assoc., Santa Ana, CA).

The optical system between the dye laser and the plasma consisted of two mirrors and a small aperture to align and direct the beam into the ICP. The axis of the plasma was aligned with the entrance slit and the central cross-section was imaged 1:1 onto the entrance slit of a 0.3-m monochromator (Model 700, GCA McPherson Instrument, Acton, MA); a photomultiplier detector (Model R1414, Hamamatsu TV Co., Middlesex, NJ) was used. The detector output was transferred to a preamplifier (Model 4163, Evans

TABLE 1

Laser dyes, wavelength ranges and element lines investigated

Dye and solvent	Wavelength range[a] (nm)	Element and excitation line (nm)	
Rhodamine 590 (methanol)	566—610	Mg I	285.2[b]
Rhodamine 560 (methanol)	542—578	Mg II	279.6[b]
Bis-MSB (1,4-dioxane)	411—431	Ca I	422.7
PBBO (1,4-dioxane)	386—420	Ca II	393.4
Coumarin 540A (methanol)	521—605	Ba I	553.5
Coumarin 450 (methanol)	430—482	Ba II	455.4
Rhodamine 590 (methanol)	566—610	Na I	589.0
Crystal violet 670 (methanol)	634—690	Cu I	324.7[b]

[a]The data are taken from Laser Dyes, Exciton Chemical Co., Dayton, Ohio. [b]Fluorescence was measured at the doubled frequencies.

Associates, Berkeley, CA) with a 1-kΩ input resistor and then to a boxcar averager (Model 162/165, Princeton Applied Research, Princeton, NJ). All measurements were made on a potentiometric chart recorder (Model Servo/Riter 2, Texas Instruments, Houston, TX).

Reagents. The elements investigated were Ca, Ba, Mg, Na, and Cu. Stock (aqueous) solutions containing 1000 $\mu g\ ml^{-1}$ of each were prepared from their chloride or nitrate salts. These solutions were diluted to 1, 10, 50 and 100 $\mu g\ ml^{-1}$ for fluorescence and emission measurements as indicated in Table 2.

Procedures. The operating conditions for the instrumental system are given in Table 3. The high coolant flow rate of 18 l min^{-1} was needed to avoid melting of the extended-sleeve torch. The torch was adjusted so that the top of the inner aerosol tube was positioned between the first and second turns of the load coil.

All fluorescence measurements were made at the same wavelength as excitation (resonance transition) to allow comparison with emission at the same wavelength.

Results and discussion

Figure 1 shows the influence of RF power on the relative resonance fluorescence intensities (RFI) and relative emission intensities (REI) for all the elements listed in Table 1. The data are the results of triplicate measurements taken over a 3-month period and normalized with respect to the relative fluorescence and emission intensities. The features of interest can be summarized as follows. The fluorescence increases with RF power reaching a single maximum (0.7—0.9 kW) and then decreases significantly for Mg I, Mg II, Ca II, Ba II and Cu I; in the cases of Mg II, Ca II and Cu I, the curves approach a plateau region at high powers. The fluorescence reaches two maxima (≈0.7—0.8 kW and ≈1—1.2 kW) for Ca I and most likely Ba I. The fluorescence for Na I seems to decrease gradually until ≈0.9 kW and then increases rapidly. The emission of Mg I, Mg II, and Na I decreases with power reaching a minimum (≈0.8—1.0 kW) and then increases slightly. The emission of Ca II, Ba II, and Ba I increases with RF power, as expected. Finally, the emission of Ca I decreases and then increases and that for Cu I increases to a maximum at ≈0.7 kW and finally increases rapidly with power.

TABLE 2

Concentrations of solutions used for different experiments

Concentration ($\mu g\ ml^{-1}$)	Lines tested	
	Fluorescence	Emission
1	Ca I, Ca II, Ba II, Mg II	Ca I, Ca II, Ba II
10	Na I	Mg I, Mg II, Na I, Cu II
50	Cu I	—
100	Ba I, Mg I	Ba I

TABLE 3

Operating conditions for instrumental system

Parameter	Operating conditions
Pump laser energy	50 mJ
Dye laser energy	
Fundamental	0.8—1.2 mJ/pulse
Frequency-doubled	1—8 μJ/pulse
Laser beam diameter at plasma	≈3 mm
ICP forward power	0.6—1.2 kW
Observation height	10 mm above the tip of torch (50 mm above the load coil)
Radial position	Optimized for maximum signal
Plasma argon flow rates	18 l min^{-1} coolant, 0.7 l min^{-1} nebulizer (no auxiliary)
Monochromator	
Slit width	1000 μm for fluorescence; 25—50 μm for emission
Slit height	1 mm for fluorescence and emission
Photomultiplier	−800 V

The variation of emission and fluorescence signals with RF power (Fig. 1) normally obeys one of the following two trends; either the signal drops as power increases, because of a decrease in the ground-state population and increases in excited-state and ionic populations, as with Cu, Na, and Zn, or the signal increases with power as with B, P, and Zr, where dissociation of stable oxide molecules increases with power. The fluorescence plots where one maximum occurs (Mg I, Mg II, Ca II, Ba II, and Cu I, and possibly Ca I if it were redrawn to intersect the points below a power of ≈1.0 kW), can be interpreted in the same way as for refractory elements (B, P, and Zr) to explain the increasing signal at low RF powers and in the same way as for non-refractory elements (Cu, Mo, and Zn) at high RF powers. Certainly the Na I and Ba I fluorescence plots in Fig. 1 do not conform to previous studies or to the interpretation of the other fluorescence plots. The emission/power plots generally show the expected increase in signal with increase in power (Ca II, Ba II, Ba I, Cu I); however, the Mg I, Mg II, Na I, and Ca I plots show unexpected decreases with increase in power, reaching minima at RF powers of ≈0.8—1.0 kW and the emission signal increases with further increase in power. The Mg I and Mg II plots are similar and difficult to explain. The Ca I and Na I plots are probably a convolution of two effects; a decrease in excited-state populations caused by ionization and an increase in excitation efficiencies at high power.

In Fig. 2, the influences of RF power on the fluorescence signal-to-background ratio, *S/B*, are compared with the RFI plots for Na I, Ba I, Ba II, Ca I and Ca II. For the Ba and Ca lines, the *S/B* vs. power plots increase as do the RFI vs. power plots, whereas for Na I, the *S/B* vs. power plot drops because of the abnormal increase in background with RF power increase.

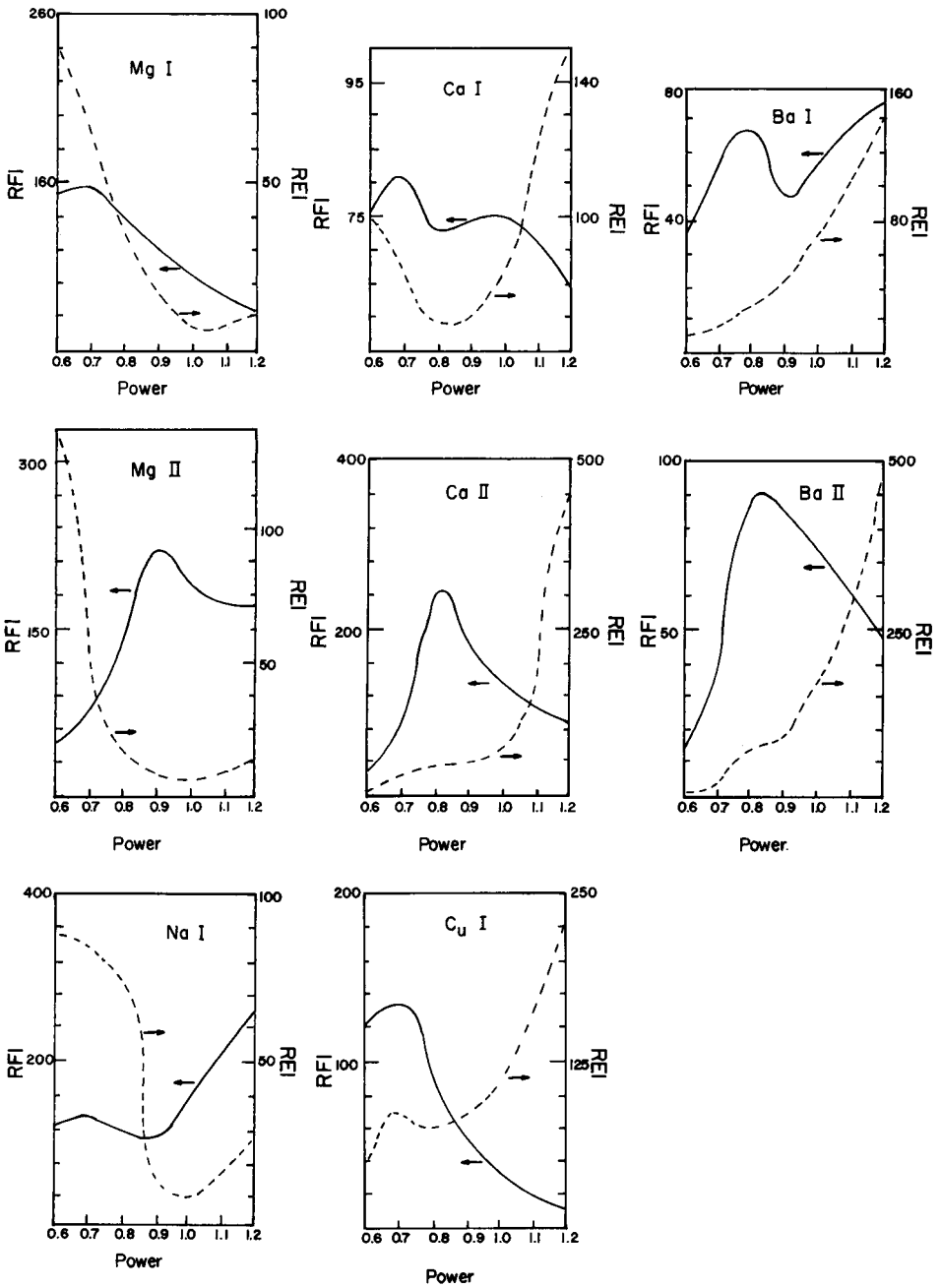

Fig. 1. Comparisons of the effects of RF power on resonance fluorescence and emission: (——) RFI; (— — —) REI. The lines used are listed in Table 1. Power is given in kW.

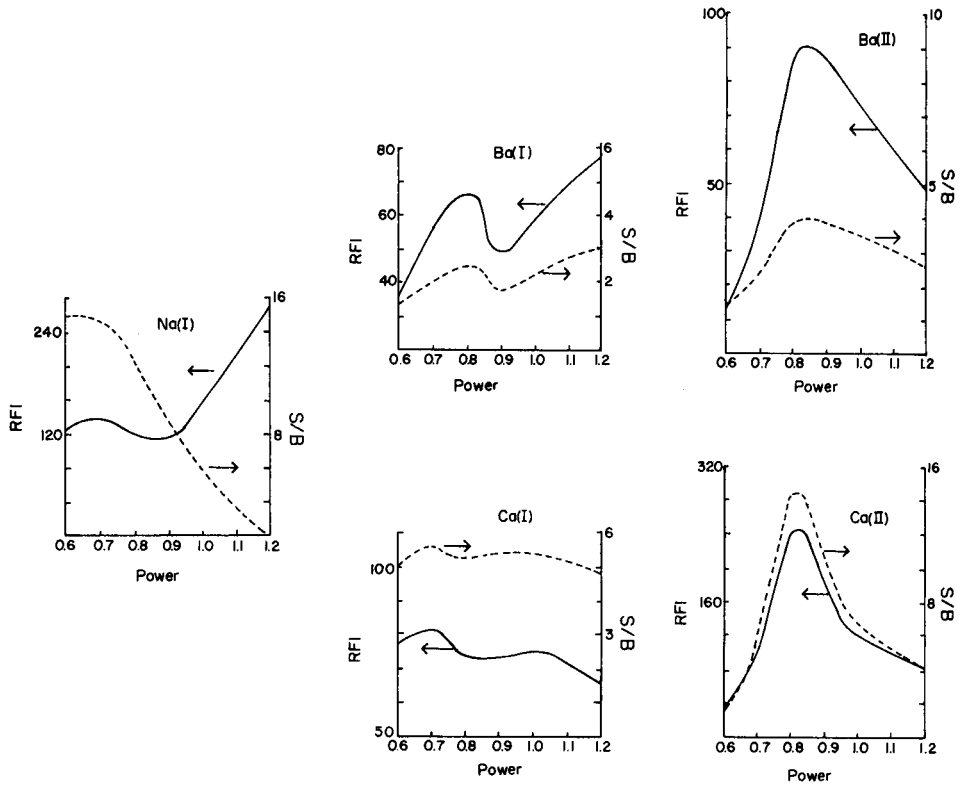

Fig. 2. The effect of RF power (given in kW): (——) on relative fluorescence intensity; (— — —) on signal-to-background ratio, *S/B*.

In Fig. 3, the influence of an easily ionized element, potassium, on the fluorescence of calcium as a function of RF power is given, with recorder tracings of the calcium fluorescence with and without 1000 μg ml^{-1} potassium added. The striking effect of potassium ion on the Ca-I line, i.e., an increase by ca. 4-fold, and on the Ca-II line, i.e., a decrease of >100-fold, should be noted. This is in contrast to the much smaller effect of potassium ion on elements measured by emission with the conventional (short) torch. The effect of RF power on the relative intensity of the Ca-I line shows a steep maximum at ≈0.8 kW as opposed to the rather flat plot without potassium present.

The increased effect of an easily ionized element on an element like calcium with the extended torch is likely due to the lower electron number density [13] (perhaps ≈10^{12} electrons cm^{-3}) and the lower plasma temperature [3]. As a result, the easily ionized element contributes significantly to the electron number density of the cooler plasma. In fact, the plasma produced with the extended torch would be expected to have characteristics between the conventional short-torch ICP at about 15 mm above the load

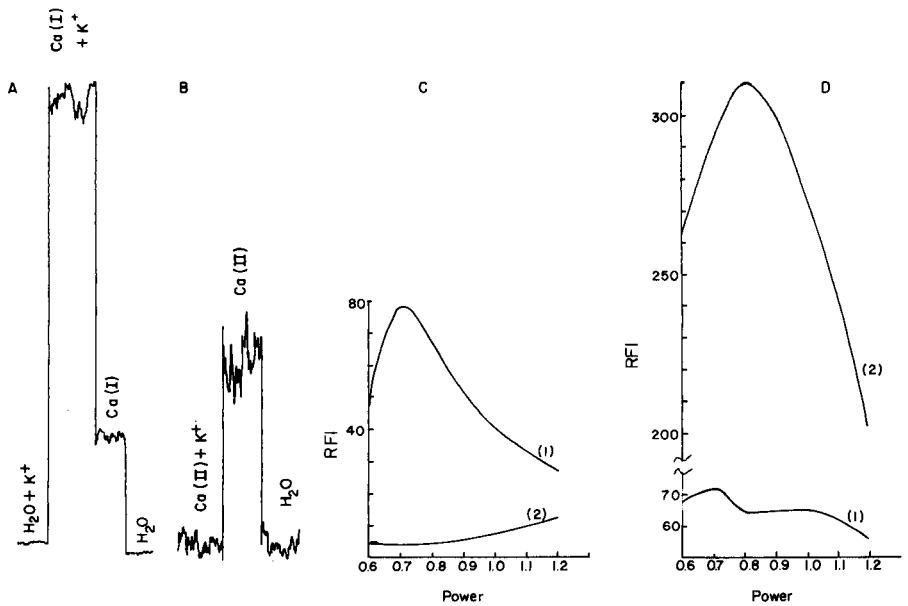

Fig. 3. Effects of potassium ion (1 g l^{-1}) on the fluorescence intensities of calcium. (A) Ca-I line with and without K^+ added at 0.7 kW power; (B) Ca-II line with and without K^+ added at 0.7 kW power. (C) Effect of RF power (in kW) on Ca-II line without (curve 1) and with (curve 2) addition of K^+; (D) as for C at the Ca-I line. The calcium concentration in these tests was 1 mg l^{-1}.

coil and a hot combustion flame, e.g., nitrous oxide/acetylene. The unexpected but reproducible effects observed with power variation in Fig. 1 for both emission and fluorescence are difficult to explain based on previous models of the ICP atomization/ionization/excitation mechanism. The major points to stress here are that: (i) the extended-sleeve-torch plasma is not well understood; (ii) RF power variations can lead to unexpected variations of emission and fluorescence indicating a need for stable RF power; and (iii) ionization interferences are larger than for the short torch.

This work was supported by AF-AFOSR-F49620-84C-0002.

REFERENCES

1 D. R. Demers and C. D. Allemand, Anal. Chem., 53 (1981) 1915.
2 D. R. Demers and A. I. Priede, ICP Inf. Newsl., 3 (1977) 221.
3 M. A. Kosinski, H. Uchida and J. D. Winefordner, Talanta, 30 (1983) 339.
4 P. W. J. M. Boumans and F. J. De Boer, Spectrochim. Acta, Part B: 30 (1975) 309; 32 (1977) 365.
5 T. E. Edmonds and G. Horlick, Appl. Spectrosc., 31 (1977) 536.
6 S. S. Berman and J. W. McLaren, Appl. Spectrosc., 32 (1978) 372.
7 R. N. Savage and G. M. Hieftje, Anal. Chem., 52 (1980) 1267.

8 H. Kawaguchi, T. Ito, K. Ota and A. Mizuike, Spectrochim. Acta, Part B: 35 (1980) 199.
9 H. Kawaguchi, T. Ito and A. Mizuike, Spectrochim. Acta, Part B: 36 (1981) 615.
10 M. W. Blades and G. Horlick, Spectrochim. Acta, Part B: 36 (1981) 861, 881.
11 P. W. J. M. Boumans and M. Ch. Lux-Steiner, Spectrochim. Acta, Part B: 37 (1982) 97.
12 R. Rezaaiyaan, J. W. Olesik and G. M. Hieftje, Spectrochim. Acta, Part B: 40 (1985) 73.
13 B. L. Caughlin and M. W. Blades, Spectrochim. Acta, Part B: 40 (1985) 987.

Analytica Chimica Acta, 184 (1986) 307—310
Elsevier Science Publishers B.V., Amsterdam — Printed in The Netherlands

Short Communication

FLUORESCENCE QUANTUM EFFICIENCIES OF HALOGEN-SUBSTITUTED BENZOIC ACID ISOMERS[a]

I. M. KHASAWNEH[a] and J. D. WINEFORDNER*
Department of Chemistry, University of Florida, Gainesville, FL 32611 (U.S.A.)
(Received 15th October 1985)

Summary. The fluorescence of halogen-substituted benzoic acid isomers is enhanced by the addition of an aliphatic acid to chloroform as the solvent. The molar absorptivities of these isomers at the wavelength of maximum absorbance are reported. The fluorescence quantum efficiencies of the fluorescent species from these isomers in 5% acetic acid/chloroform are also reported.

Absolute fluorescence quantum efficiencies of many compounds have been evaluated by different methods [1]. Many difficulties are associated with these methods [2]. Therefore, the quantum efficiencies of many compounds are determined relative to a standard which has a known quantum efficiency. Parker [3] reported the excitation wavelengths and the quantum efficiencies of benzene, anthracene, and naphthalene in ethanol as solvent. The quantum efficiencies of toluene in cyclohexane [4] and of acetylsalicylic acid [5] have been reported. The fluorescence quantum efficiencies of many compounds depend on the experimental conditions [6—9], such as temperature, solvent, excitation wavelength, degassing of the solvent, and the concentration of the compound used for measurements.

In other work [10], it was found that halogen-substituted benzoic acid isomers do not fluoresce to a measurable degree in pure chloroform at room temperature. However, the addition of 5% acetic acid to the pure chloroform enhances their fluorescence to a considerable degree. The main purpose of the present communication is to report the effect of the addition of acetic acid and the halogen substitution on the fluorescence quantum efficiency of benzoic acid. The relative fluorescence quantum efficiencies of these isomers were determined by using 9,10-diphenylanthracene (DPA) as a standard. The quantum efficiency for DPA has been reported at different excitation wavelengths, temperature, and solvents [11—15]. The present measurements were done at room temperature and without degassing the solution. Therefore, based on previous work [16], the quantum efficiency of DPA used here was

[a]Present address: Department of Chemistry, Yarmouk University, Irbid, Jordan.

0003-2670/86/$03.50

0.66, although values between 0.76 and 1 have been reported in different solutions.

The fluorescence quantum efficiency, ϕ, is calculated by using the equation

$$\phi_c = \phi_s(A_s/A_c)(F_c/F_s)(I_s^0/I_c^0)(n_c^2/n_s^2) \quad (1)$$

where the subscripts c and s denote the test compound and the standard, respectively; A is the absorbance of the species at the respective excitation wavelengths, F is the area under the emission spectrum corrected for the blank, I^0 is the relative excitation flux at the excitation wavelength, and n is the refractive index of the solvent.

The fluorescence quantum efficiencies of these halogen-substituted benzoic acid isomers are compared with each other and with the parent molecule (benzoic acid) as described below.

Experimental

Apparatus and reagents. A Perkin-Elmer spectrofluorimeter (LS-5) interfaced with a Model 3600 data station was used to measure fluorescence and a Sargent-Welch recorder (Model SRG) was used to record the fluorescence spectra. All measurements were made by using a 10 × 10 mm quartz cuvette. A Pye-Unicam spectrophotometer (SP-8-100) was used to obtain the absorption spectra.

The sources of the isomers were the same as reported earlier [10]. The standard DPA was from Aldrich; absolute ethanol was obtained locally.

All glassware was placed for 45 min in a supersonic cleaner (Cole Parmer, Chicago), rinsed five times with distilled water and three times with deionized water (Barnstead Nanopure System), dried for 24 h and rinsed with solvent five times before use. The automatic micropipettes and absorption/fluorescence cuvettes were dried and rinsed five times with sample before measurements.

Procedures. A solution containing the isomer (50 μg ml^{-1}) in 5% acetic acid/chloroform and one containing 10 μg ml^{-1} DPA in ethanol were prepared. Three diluted solutions with concentrations of 5, 3 and 1 μg ml^{-1} of each compound were prepared by dilution of the concentrated solution, and one solution containing 1 μg ml^{-1} DPA was prepared; successive dilutions contained 0.5 and 1.0 ng ml^{-1} of DPA. The fluorescence spectra of all these solutions were recorded to obtain the corrected spectrum for each compound; the area-corrected spectrum for each compound was calculated and the fluorescence quantum efficiencies were calculated with Eqn. 1.

Results and discussion

The peak absorbance wavelength, the molar absorptivities and the fluorescence quantum efficiencies of benzoic acid and some fluoro and chloro derivatives are given in Table 1. The molar absorptivities of the (*o*-, *m*- and 2,6-di-fluoro isomers are only moderate (>1000), while that of benzoic acid is smaller. The molar absorptivities of DPA at different wavelengths are ca. 10^4 l mol^{-1} cm^{-1}.

TABLE 1

Fluorescence quantum efficiencies of halogen-substituted benzoic acid isomers

Compound	λ_{max}[a] (nm)	Molar absorptivity (mol^{-1} l cm^{-1})	ϕ_f[b]	Relative change of ϕ_f[c]
Benzoic acid	276	8.95×10^2	0.0068	—
o-Fluorobenzoic acid	280	1.58×10^3	0.0072	5.9
m-Fluorobenzoic acid	281	1.60×10^3	0.0069	1.5
2,6-Difluorobenzoic acid	284	1.02×10^3	0.0015	−78
o-Chlorobenzoic acid	282	1.14×10^3	0.0019	−72
m-Chlorobenzoic acid	284	1.10×10^3	0.0032	−53
p-Chlorobenzoic acid	280	4.10×10^3	0.0030	−56
2,5-Dichlorobenzoic acid[d]	288	3.65×10^2	—	—

[a]Absorption maxima precise to ±2 nm. [b]9,10-Diphenylanthracene: λ_{max} = 330, 351, 370, 390 nm with corresponding $\epsilon_{max} = 7.98 \times 10^3$, 1.75×10^4, 2.84×10^4, 2.68×10^4 l mol^{-1} cm^{-1}. [c]Relative change compared to benzoic acid, i.e., ϕ_F (isomer)/ϕ_F (benzoic acid); the negative sign means depression of fluorescence. [d]No measurable fluorescence.

It was found earlier [10—16] that the addition of acetic acid to chloroform enhanced the fluorescence of benzoic acid and its derivatives significantly. This enhancement was thought to be due to the formation of rigid species in the excited state as a result of hydrogen bonding between the carboxyl groups of the benzoic and acetic acids which decreased the intersystem crossing. In this work, the influence of acetic acid was evaluated by determining the fluorescence quantum efficiencies of halogen-substituted benzoic acid and comparing them with the parent molecule. Table 1 shows that the quantum efficiencies of the *o*-fluoro and *m*-fluoro isomers are higher than that of benzoic acid while the others are smaller. This is caused by steric effects and by the localization of the electron density of the ring, decreasing the electron density of the carboxyl group and thus increasing the acidity. All these effects decrease the possibility of hydrogen bonding between carboxylic groups and lead to lower fluorescence quantum efficiencies relative to benzoic acid. In spite of this, Table 1 shows that the *o*-fluoro isomer has a higher fluorescence quantum efficiency than benzoic acid and the other isomers. The possibility of intramolecular hydrogen bonding between the fluorine atom and the carboxyl group of benzoic acid most likely increases the fluorescence by decreasing intersystem crossing. The quantum efficiencies of the *m*-fluoro isomer and benzoic acid are similar because the former does not undergo intramolecular hydrogen bonding; its ability to withdraw the electron density of the carboxyl group and steric effects are less than in the *o*-fluoro isomer. The 2,6-difluoro isomer has the lowest quantum efficiency because the localization, the withdrawing ability, and the steric effect are greater than in the *o*-fluoro isomer.

All the chloro isomers have lower quantum efficiencies than benzoic acid. Because the electronegativity of chlorine is less than that of fluorine, the

localization and the withdrawing ability are less; however, the steric effect is larger. Data in Table 1 show that the *o*-chloro isomer has lower quantum efficiency than the *m*- and *p*-isomers, which is attributed mainly to the electron-withdrawing ability and the steric effect. This is in good agreement with the concept of hydrogen bonding where it is more difficult to form such bonds in the *o*-isomer than in *m*- and *p*-isomers. In the case of 2,6-dichloro isomer, the withdrawing ability, localization, and steric effects are greater than in the *o*-isomer, so that the dichloro isomer shows no detectable fluorescence. The chloro isomers quench the fluorescence more than the fluoro isomers, mainly because chlorine does not form an intramolecular hydrogen bond such as fluorine does in the case of the *o*-fluoro isomer.

No exact correlation can be drawn between the fluorescence and structure of these compounds. The fluorescence is sufficient to detect and quantify each isomer at concentrations in the ng ml^{-1} range. For example, a detection limit of 10 ng ml^{-1} was obtained for the *m*-fluoro isomer [10].

This research was supported by NIH grant GM 11373-22.

REFERENCES

1 J. N. Demas, in K. D. Mielenz (Ed.), Measurement of Photoluminescence, Vol. 3, Optical Radiation Measurements, Academic Press, New York, 1982.
2 C. A. Parker, Photoluminescence of Solutions, Elsevier, Amsterdam, 1968.
3 C. A. Parker, Anal. Chem., 34 (1962) 502.
4 W. Young and E. K. S. Lee, J. Chem. Educ., 46 (1969) 277.
5 C. I. Miles and G. H. Schenk, Anal. Chem., 42 (1970) 656.
6 R. F. Chen, Anal. Biochem., 19 (1967) 374.
7 W. H. Melhuish, J. Phys. Chem., 64 (1960) 762.
8 H. C. Borresen and C. A. Parker, Anal. Chem., 38 (1966) 1073.
9 I. B. Berlman, Handbook of Fluorescence Spectra of Aromatic Molecules, Academic Press, New York, 1965.
10 I. M. Khasawneh and J. D. Winefordner, Can. J. Spectrosc., in press.
11 G. Heinrich, S. Schoof and H. Gusten, J. Photochem., 13 (1974) 315.
12 J. R. Huber, M. A. Mahaney and W. W. Mantulin, J. Photochem., 12 (1973) 67.
13 J. Ferguson and A. M. H. Man, Chem. Phys. Lett., 14 (1972) 245.
14 J. V. Morris, M. A. Mahaney and J. R. Huber, J. Phys. Chem., 80 (1976) 969.
15 C. A. Parker and T. A. Joyce, Chem. Commun., (1967) 744.
16 I. M. Khasawneh and G. H. Schenk, unpublished work, Wayne State University, Detroit.

Analytica Chimica Acta, 184 (1986) 311—315
Elsevier Science Publishers B.V., Amsterdam — Printed in The Netherlands

Short Communication

FLOW-INJECTION DETERMINATION OF IRON(II), IRON(III) AND TOTAL IRON WITH CHEMILUMINESCENCE DETECTION

E. G. SARANTONIS[a] and ALAN TOWNSHEND*
Department of Chemistry, University of Hull, Hull HU6 7RX (Great Britain)
(Received 7th October 1985)

Summary. Iron(II) (1.0×10^{-9}—1.0×10^{-6} M) is determined by the production of chemiluminescence in a luminol system in the absence of added oxidant. Iron(III) (2.0×10^{-8}—2.0×10^{-6} M) is determined after reduction to iron(II) in a silver reductor mini-column in the flow system. Cobalt, chromium, copper and manganese interfere.

Various methods have been proposed for the sensitive determination of iron(II) and iron(III) on the basis of chemiluminescence reactions. Iron(II) can be determined by its reported catalytic effect on the oxidation of luminol by dissolved oxygen [1, 2] or lucigenin [3]. Iron(III) can be determined by its catalytic effect on the oxidation of lucigenin [4] or luminol [5] by hydrogen peroxide.

This communication reports the flow-injection determination of iron(II) (1.0×10^{-9}—1.0×10^{-6} M) by its effect on the oxidation of luminol in the absence of added oxidants and measurement of the emitted radiation. Iron(III) is determined after reduction to iron(II) in a silver-containing mini-column incorporated in the flow system. The use of such mini-columns in flow-injection systems has been proposed for reduction of iron(III) to iron(II) [6] and copper(II) to copper(I) [7] for spectrophotometric determination, as well as for the production of unstable oxidation states of metal ions [8—10]. Iron(II) and iron(III) are determined in mixtures by first analyzing the sample without reduction, thus determining iron(II) and then passing a second portion of sample to flow through the reductor before measurements, so that total iron is determined.

Experimental

Reagents. All chemicals were of analytical-reagent grade and deionized distilled water was used throughout. A buffer solution was prepared by addition of small increments of 0.5 M ammonium chloride to 0.5 M ammonia solution to bring the final pH to 11.4. A 1.00×10^{-2} M luminol solution was prepared

[a]On study leave from the Department of Chemistry, Laboratory of Analytical Chemistry, University of Athens, 106 80 Athens, Greece.

0003-2670/86/$03.50

by dissolving 0.1772 g of luminol (Sigma Chemical Co.) in the buffer solution and diluting with buffer solution to exactly 100 ml. More-dilute solutions were prepared daily by dilution with the buffer solution. Stock solutions of 1.00×10^{-2} M iron(II) or iron(III) were prepared by dissolving 0.2780 g of $FeSO_4 \cdot 7H_2O$ or 0.2703 g of $FeCl_3 \cdot 6H_2O$ in 0.010 M hydrochloric acid and diluting each with 0.010 M hydrochloric acid to exactly 100 ml. More dilute solutions were prepared daily by dilution with 0.010 M hydrochloric acid.

Apparatus. The silver reductor mini-column was prepared as described previously [7] and the flow injection chemiluminescence analyzer was the same as described elsewhere [11]. The flow manifold used is shown in Fig. 1. A peristaltic pump (Ismatec Mini S-820) was used and sample solutions were introduced via an injection valve (Rheodyne RH-5020, Anachem) with a 40-μl sample loop. The silver reductor was placed in the sample stream and a similar column packed with glass beads (GBC) was placed in the by-pass stream to achieve an equal pressure drop and similar dispersion of sample in the two streams.

Procedures. A 5.0×10^{-3} M luminol solution was continuously pumped into the manifold. Iron(II) was determined by injection of the sample into a water stream, and directed through the GBC via a switching valve. The peak height emission was measured. Iron(III) was determined by injection of the sample into a 0.010 M hydrochloric acid stream and directed through the reductor via the switching valve. Calibrations were done under the same conditions.

When mixtures of iron(II) and iron(III) were to be analyzed, sample solutions were injected into the 0.010 M hydrochloric acid stream and either passed through the reductor (total iron) or directed through the GBC (iron-(II)). Because 0.010 M hydrochloric acid was used as the carrier stream in both cases, it was also used for calibration for iron(II) and total iron.

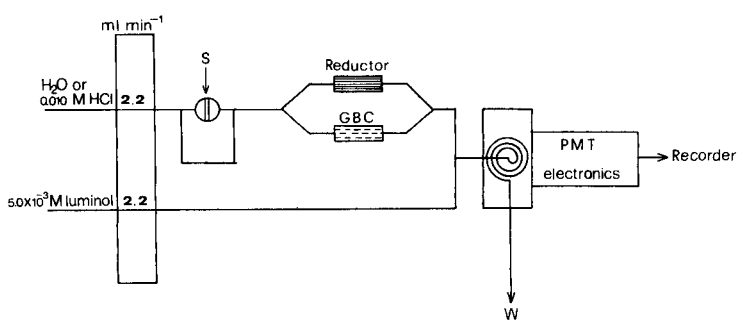

Fig. 1. Manifold used for the determination of iron(II) and total iron: (S) sample injected (40 μl); (GBC) glass beads column; (W) waste; (PMT) photomultiplier tube.

Results and discussion

Optimization. The effect of total flow rate on the emission intensity from 1.0×10^{-6} M iron(II) is shown in Fig. 2. A total flow rate of 4.4 ml min^{-1} (2.2 ml min^{-1} for each stream) is recommended because at >4.4 ml min^{-1} the signal was noisy and irreproducible. The effect of luminol concentration is shown in Fig. 3; 5.0×10^{-3} M luminol is recommended and was used throughout. The pH of the luminol solution was found to be very critical. At pH 9.5 no emission was observed from 1.0×10^{-6} M iron(II). The emission intensities from 1.0×10^{-7} M iron(II) at pH 10.0 and 11.4 were 8.2 and 14.1 mV, respectively. Above pH 11.4, no increase of the emission intensity was observed.

Dissolved oxygen was necessary for oxidation of luminol and production of chemiluminescence as stated by Klopf and Nieman [2], because the intensity was found to decrease as the partial pressure of oxygen decreased. Table 1 shows how the emission obtained by injection of iron(II) decreased in a sequence of injections into deaerated solutions, as residual oxygen in the system was consumed.

Iron(III) can be determined after reduction to iron(II) within the silver reductor mini-column. Maximum peak height was obtained with a 20 mm long column. Shorter columns gave smaller peaks because of incomplete reduction of iron(II); longer columns increased sample dispersion so also decreasing the peak height. Therefore, a 20-mm column (2.5 mm i.d.) was used for all further measurements. Hydrochloric acid was needed for reduction of iron(II) to take place within the reductor. At <0.010 M acid, peak heights were smaller owing to incomplete reduction; at >0.010 M HCl, the

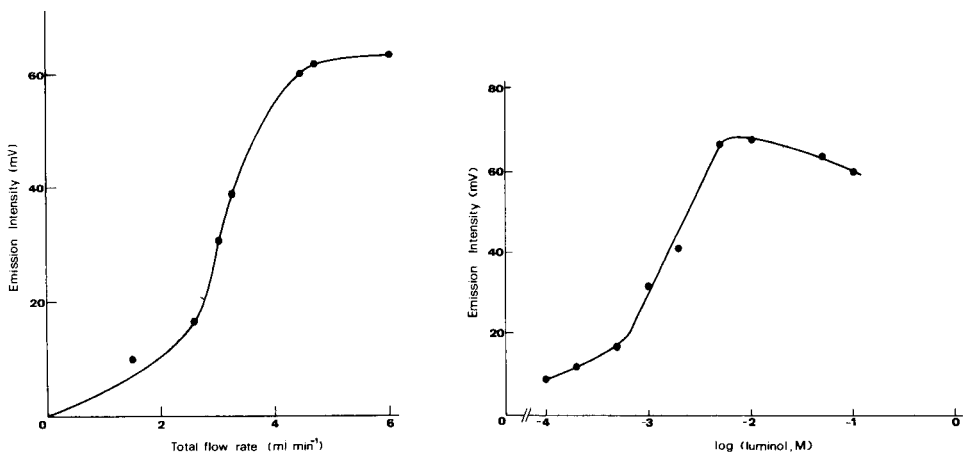

Fig. 2. Emission intensity for 1.0×10^{-6} M iron(II) and 5.0×10^{-3} M luminol as a function of total flow rate.

Fig. 3. Emission intensity for 1.0×10^{-6} M iron(II) as a function of luminol concentration.

TABLE 1

Effect of rapid sequential injections into deaerated solutions on the emission intensity from 1.0×10^{-6} M iron(II)

Injection number	1	3	5	7	9	11
Emission intensity[a]	72	47	42	27	12	12

[a]Intensity from non-deaerated solutions taken as 100.

emission intensity was decreased because the pH of the luminol solution, after mixing, was decreased below the optimum value (pH 11.4). Therefore, 0.010 M HCl is recommended. However, the heat evolved during reaction with the alkaline luminol solution gives rise to a 20-fold increase in noise and increases the limit of detection for iron(II) from 5.0×10^{-10} M to 2.0×10^{-8} M iron(II).

Analytical characteristics. Under the optimized conditions, the calibration graph of emission intensity (I, mV) vs. molarity was linear for iron(II) injected into a water stream in the range 1.0×10^{-9}—1.0×10^{-6} M ($I = 2.5 \times 10^{9}$ [Fe(II)] − 53.4; $r = 0.994$, $n = 7$) and the relative standard deviation for determination of 1.0×10^{-8} M iron(II) was 2.9% ($n = 10$). The limit of detection (signal-to-noise = 2) was 5.0×10^{-10} M. When iron(II) was injected into the hydrochloric acid stream, or when iron(III) was determined after reduction to iron(II), the calibration graph for both ions was linear in the range 2.0×10^{-8}—2.0×10^{-6} M ($I = 6.6 \times 10^{7}$ [Fe] − 0.20; $r = 0.999$, $n = 7$) and the relative standard deviation for determination of 2.0×10^{-7} M iron(III) was 2.4% ($n = 10$). The limit of detection was 2.0×10^{-8} M iron(III), which is mainly set by the iron impurities in hydrochloric acid and the heating effect referred to earlier. By using the same calibration graph, iron(II), iron(III) and total iron can be readily determined. Some results are shown in Table 2. The column could be used for ca. 3000 determinations, and 60 samples per hour could be analyzed.

Interferences. Interferences were investigated by determining 1.0×10^{-8} M iron(II) in the presence of 100-fold (weight) concentration of potential

TABLE 2

Determination of iron(II) and iron(III) in mixtures

Added ($\times 10^{-8}$ M)		Found ($\times 10^{-8}$ M)	
Fe(II)	Fe(III)	Fe(II)	Fe(III)
2.0	2.0	2.1	1.9
5.0	5.0	4.8	4.9
10.0	10.0	10.0	10.0
20.0	20.0	21.0	21.0
50.0	50.0	52.0	51.0

TABLE 3

Effect of interfering ions on the chemiluminescence intensity for 1.0×10^{-8} M iron(II)

Ion	Response change (%) with $1-10 \times 10^{-7}$ M ion			
	1.0×10^{-7}	2.0×10^{-7}	5.0×10^{-7}	10.0×10^{-7}
Cr^{3+}	0	−20	−48	−67
Mn^{2+}	−60	−95	−100	−100
Cu^{2+}	−80	−100	−100	−100
Co^{2+}	+100	+150		

interferents. The responses were compared with those obtained from an uncontaminated iron solution. No effect was observed from K^+, Na^+, Mg^{2+}, Ca^{2+}, Ba^{2+}, Cd^{2+}, Hg^{2+}, Zn^{2+}, Al^{3+}, Ni^{2+} or Pb^{2+}. Cobalt(II) is also reported to catalyze the reaction [1]; it interfered severely (Table 3). Copper(II), Mn^{2+} and Cr^{3+} decreased the response from iron(II) (Table 3). The same ions had similar effects on the determination of iron(III).

E. G. Sarantonis is grateful to the University of Athens for financial support.

REFERENCES

1 W. R. Seitz and D. M. Hercules, Anal. Chem., 44 (1972) 2143.
2 L. Klopf and T. A. Nieman, Anal. Chem., 55 (1983) 1080.
3 L. I. Dobovenko and A. Y. Nazarenko, Ukr. Khim. Zh., 41 (1975) 1205; Chem. Abstr., 85 (1976) 13303j.
4 A. P. Tovmasyan, Mater. Konf. Molodykh. Uch. Spets., Acad. Nauk. Arm. SSR, 1972, 188; Chem. Abstr., 83 (1975) 187424a.
5 J. E. Klinichensko and M. O. Grichenko, Ukr. Khim. Zh., 36 (1970) 610.
6 A. T. Faizullah and A. Townshend, Anal. Chim. Acta, 167 (1985) 225.
7 A. T. Faizullah and A. Townshend, Anal. Chim. Acta, 172 (1985) 291.
8 R. C. Schothorst, J. M. Reijn, H. Poppe and G. den Boef, Anal. Chim. Acta, 145 (1983) 197.
9 R. C. Schothorst, M. van Son and G. den Boef, Anal. Chim. Acta, 162 (1984) 1.
10 R. C. Schothorst and G. den Boef, Anal. Chim. Acta, 153 (1983) 133.
11 A. T. Faizullah and A. Townshend, Anal. Proc., 22 (1985) 15.

Analytica Chimica Acta, 184 (1986) 317—322
Elsevier Science Publishers B.V., Amsterdam — Printed in The Netherlands

Short Communication

SPECTROPHOTOMETRIC DETERMINATION OF TIN(IV) BY EXTRACTION OF THE TERNARY TIN/IODIDE/5,7-DICHLORO-8-QUINOLINOL COMPLEX

A. M. GUTIERREZ*, M. V. LAORDEN and A. SANZ-MEDEL[a]

Departamento de Química Analítica, Facultad Ciencias Químicas, Universidad Complutense, 28040-Madrid (Spain)

J. L. NIETO

Instituto Estructura de la Materia, Consejo Superior de Investigaciones Científicas, Serrano 119, 28006-Madrid (Spain)

(Received 12th November 1985)

Summary. The characteristics of the ternary complexes formed by fluoride, bromide, iodide and thiocyanate with tin(IV) and 5,7-dichloro-8-quinolinol (HCQ) have been studied. A spectrophotometric method is proposed for the determination of tin(IV) (1—20 $\mu g\ ml^{-1}$), based on the extraction into chloroform of the tin/iodide/HCQ complex. Aluminium, bismuth and lead do not interfere, but antimony, copper, iron(III) and fluoride do. Copper and iron can be eliminated by preliminary extraction in the absence of iodide.

One of the major problems encountered in the spectrophotometric determination of tin is that preseparation of the tin is usually needed. Reagents commonly used are catechol violet [1—3] and quercetin [4], the tin first being extracted as tin(IV) iodide into toluene or cyclohexane [5, 6]. Previous work [7, 8] showed that tin(IV) can be extracted into chloroform by formation of a ternary complex with 5,7-dichloro-8-quinolinol (HCQ) and chloride ion. The extraction was from a strongly acidic medium, which ensured good selectivity. It was thought, however, that by using halide ions less electronegative than chloride, a ternary complex with increased molar absorptivity could be extracted, thus allowing a more sensitive spectrophotometric determination of tin whilst maintaining the selectivity obtained when chloride was used. For this reason, and in order to round off the previous studies [7, 8], an extractive-spectrophotometric study of the complexes formed by tin(IV) with HCQ and bromide, iodide and thiocyanate, as well as fluoride, was initiated. The iodide complex showed the highest molar absorptivity, and its stoichiometry and optimal conditions for its formation were examined.

---

[a]Present address: Departamento Química Analítica, Facultad de Ciencias, Universidad Oviedo, Oviedo, Spain.

0003-2670/86/$03.50

As a result, an improved extractive-spectrophotometric method for tin is proposed.

Experimental

Apparatus and solutions. A Beckman DK-2A spectrophotometer with 1-cm glass cells, a Metrohm E-516 pH meter with glass and saturated calomel reference electrodes, and 100-ml separating funnels were used.

All chemicals were of analytical-reagent grade. Standard tin(IV) solutions were freshly prepared by dilution of a 1000 μg ml^{-1} stock solution obtained by dissolving tin metal in sulphuric acid [7]. The tin content was checked gravimetrically [8]. The HCQ solution, 1% (w/v) was in chloroform. All halide solutions were 1.0 M, except for the potassium iodide, which was 0.5 M.

Procedure. Pipette a portion of the sample solution containing 25—200 μg of tin into a separating funnel, add sufficient perchloric acid (to ensure a 1 M final concentration in the aqueous phase) and 1 ml of the halide solution. Adjust the final volume to ca. 10 ml with distilled water. Add 10 ml of the HCQ solution with gentle manual shaking, allow to stand for 5—10 min, and extract the tin by shaking the funnel for 4 min. Allow the phases to separate, filter the chloroform solution through a dry Whatman No. 1 filter paper and measure the absorbance at 401 nm against a blank prepared in the same way but free from added tin(IV).

Results and discussion

Formation of the ternary complexes. Mixed ligand ternary complexes of tin(IV) with HCQ and bromide, iodide or thiocyanate were formed in acidic media; the ternary fluoride complex was not, probably because of the high stability of the hexafluorostannate(IV) ion. The spectral characteristics of the complexes are shown in Table 1. The molar absorptivity decreased in the order $I^- > Br^- > SCN^- > Cl^-$. The shapes of the spectra of all the complexes were very similar to that obtained with iodide (Fig. 1).

The influence of the anion concentration on the concentration of complex extracted from 1 M perchloric acid is shown in Fig. 2. For iodide and bromide, the concentration extracted is nearly independent of the halide

TABLE 1

Spectral characteristics of tin(IV)/anion/HCQ complexes

Anion	λ_{max} (nm)	Molar absorptivity (10^4 l mol^{-1} cm^{-1})
Cl^-	403	0.47
Br^-	402	0.61
I^-	401	0.83
SCN^-	400	0.51

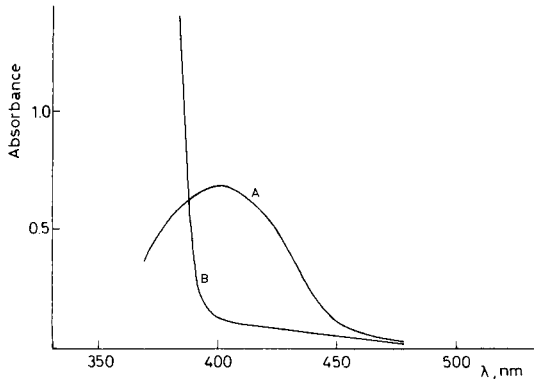

Fig. 1. Absorption spectra: (A) tin(IV)/iodide/HCQ complex against reagent blank (10 μg Sn ml^{-1}); (B) reagent blank against chloroform as reference.

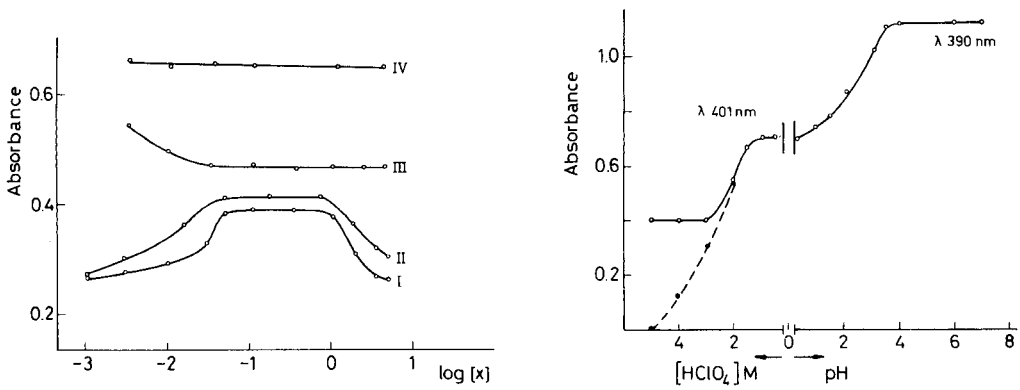

Fig. 2. Influence of anion concentration on the extraction of the tin(IV)/X/HCQ complex. Anion (X^-): (I) Cl^-; (II) SCN^-; (III) Br^-; (IV) I^- (measured at λ_{max} for each complex, 10 μg Sn ml^{-1}).

Fig. 3. Effects of perchloric acid concentration and pH on the extraction of the tin(IV)/iodide/HCQ complex (10 μg Sn ml^{-1}). Reference solution: (○) chloroform; (●) reagent blank.

concentration over most of the range studied, but for thiocyanate and chloride, extraction is maximum only in the range 0.05—1 M anion. These data confirm that the iodide complex should provide the most sensitive determination of tin, which would be least affected by variation of the anion concentration. This system was selected for further work.

Effect of experimental conditions on the extraction. Four mineral acids (perchloric, sulphuric, nitric and hydrochloric) were used to acidify the aqueous phase. Hydrochloric acid was unsuitable because the blank absorbance was too high. This was because ion pairs of the type $H_2CQ^+Cl^-$ [9],

extractable into chloroform, were formed. Nitric acid nitrates some of the HCQ, giving coloured species in both phases. The use of perchloric or sulphuric acids presented no special problems, the former being slightly advantageous because perchlorates are generally more soluble than sulphates, thus decreasing the risk of formation of precipitates when real samples are analyzed.

The effect of perchloric acid concentration on the extraction of the tin/iodide/HCQ complex was studied in the range 0.5—5 M. As shown by Fig. 3, final concentrations of 0.5—1.2 M perchloric acid in the aqueous phase produced constant absorbance so a perchloric acid concentration of 1 M is recommended. In >3 M perchloric acid, the constant absorbance observed is due to formation and extraction of iodine. As iodine is also formed in the blank, measurement of absorbance against the reagent blank (represented by the dotted line in Fig. 3) shows the effect of acidity on complex extraction which is similar to that observed for the ternary chloride complex [7].

The pH of the aqueous phase was varied in the range 0.3—9.0. Its influence on the extent of extraction is also shown in Fig. 3. As the pH increases the absorption maximum shifts to shorter wavelengths (Table 2). Above pH 2, the absorption spectrum of the extracted species changes to the typical spectrum of the complex extracted in the absence of halide, i.e., $SnO(CQ)_2 \cdot HCQ$ [8], showing that with increasing pH, iodide ions are gradually replaced by hydroxide.

Maximum absorbance was achieved with 1% (w/v) HCQ in the organic phase for 10 μg Sn(IV) ml^{-1}. A larger excess of HCQ increases the blank absorbance without increasing the net signal. A manual shaking time of 4 min was required to obtain maximum absorbance; the extract obtained exhibited constant absorbance for at least 24 h.

The stoichiometry of the extracted species was studied by Job's method of continuous variations extended to a two-phase system [10] and the mole ratio method [11]. Both gave tin/iodide/HCQ ratios of 1:2:2.

Analytical performance. The extracted complex obeyed Beer's law for 1—20 μg Sn ml^{-1} in aqueous solution. The apparent molar absorptivity at 401 nm was $(0.83 \pm 0.01) \times 10^4$ l mol^{-1} cm^{-1}. The relative standard deviation as evaluated from six determinations of 100 μg of tin(IV) was 1.2%.

TABLE 2

Effect of pH on the absorption maximum and absorbance of the tin(IV)/iodide/HCQ complex (10 μg Sn ml^{-1} in aqueous solution)

pH	λ_{max} (nm)	Abs. at λ_{max}	pH	λ_{max} (nm)	Abs. at λ_{max}
0.3	401	0.70	3.5	390	1.10
1.0	401	0.74	4.0	390	1.12
1.5	400	0.78	6.0	390	1.12
2.1	395	0.87	7.0	390	1.12
3.1	390	1.02			

TABLE 3

Tolerance limits for various ions in the determination of tin (10 μg ml^{-1})

Ion added	Tolerance limit Ion/Sn(IV) (w/w)
Al^{3+}	100
Pb^{2+}	5000[a]
Bi^{3+}	500
Mn^{2+}, Mg^{2+}	20
Zn^{2+}, Ni^{2+}, Co^{2+}	7
Sb(V), Sb(III), Fe^{3+}, Cu^{2+}	Interfere[b]
Nitrate, sulphate	5000[a]
Tartrate	20
Fluoride, EDTA	Interfere[b]

[a]Maximum ratio tested. [b]Indicates significant interference at a 1:1 ratio.

Tin (10 μg ml^{-1}) was determined by the recommended procedure in the presence of possible interfering ions. The results are shown in Table 3. Aluminium, bismuth and lead are tolerated even if present in great excess. However, copper, antimony, iron(III), fluoride and EDTA seriously interfered. The copper and iron(III) interferences could be eliminated by their preextraction with HCQ from 1 M perchloric acid in the absence of iodide, as described above. Once these cations had been removed, iodide was added and the tin was extracted into chloroform as before. The selectivity of the proposed method (Table 3) is similar to that of the less sensitive method based on chloride [7], except for the effect of antimony, which is greater in the present method, and the possibility of oxidation of iodide.

The method was tested by analyzing a certified lead-based sample supplied by the Instituto del Hierro y el Acero (CENIM-CSIC, Spain). The sample was dissolved with a nitric/tartaric acid mixture [12], and tin content was determined by following the new procedure. The mean value of nine determinations of the tin content of the sample was 0.098% (2% relative standard deviation), which compares favourably with the certified value, 0.100%.

REFERENCES

1 W. J. Ross and J. C. White, Anal. Chem., 33 (1961) 421.
2 Analytical Methods Committee, Analyst (London), 92 (1967) 320.
3 L. E. Coles, Pure Appl. Chem., 54 (1982) 1737.
4 A. Engberg, Analyst (London), 98 (1973) 137.
5 E. J. Newman and P. D. Jones, Analyst (London), 91 (1961) 406.
6 K. Tanaka and N. Takagi, Anal. Chim. Acta, 48 (1969) 357.
7 A. Sanz-Medel and A. M. Gutiérrez, Analyst (London), 103 (1978) 1037.
8 A. M. Gutiérrez, R. Gallego and A. Sanz-Medel, Anal. Chim. Acta, 149 (1983) 259.
9 J. Duplessis, F. Nasr and R. Guillaumont, Analusis, 6 (1978) 446.

10 H. Irving and T. B. Pierce, J. Chem. Soc., (1959) 2565.
11 J. M. Yoe and A. L. Jones, Ind. Eng. Chem. Anal. Ed., 16 (1944) 111.
12 J. L. Jiménez, A. Gómez and M. T. Dorado, Rev. Metal. (Madrid), 5 (1969) 603.

Analytica Chimica Acta, 184 (1986) 323—327
Elsevier Science Publishers B.V., Amsterdam — Printed in The Netherlands

Short Communication

SPECTROPHOTOMETRIC DETERMINATION OF ADVANCED PRODUCTS OF NON-ENZYMATIC GLYCOSYLATION OF LYSINE BY MEANS OF THEIR REACTION WITH DIAZONIUM SALTS

GIOVANNI CANDIANO*, GIAN MARCO GHIGGERI, GEROLAMO DELFINO and CARLO QUEIROLO

Department of Internal Medicine and Hemodialysis Service, Hospital of Lavagna, Lavagna (GE) (Italy)

FABRIZIO GINEVRI

Gaslini Institute, Genoa (Italy)

(Received 15th October 1985)

Summary. A typical product (glycosyl lysine) formed by reaction of lysine with glyceraldehyde is measured at 490 nm after coupling with diazotized sulfanilic acid. Reaction with 4-dimethylaminobenzaldehyde was less satisfactory.

Non-enzymatic glycosylation has been shown to occur in vivo with various proteins and to affect protein functions in several ways [1, 2]. The reaction between sugars and proteins involves the initial binding of the aldehyde and amino groups, with the formation of an aldimine, followed by an Amadori rearrangement and some further steps, which are not well characterized [3]. The whole process, known as the Maillard reaction, has been extensively studied in food chemistry as the main cause of deterioration of some preserved foods and loss of bioavailability of their nutrients. It has been the subject of much investigation, of reviews [4, 5] and of a recent meeting [6]. The final Maillard products (or browning compounds), which occur during food processing under obviously unphysiological conditions, have the structure of reductones, furfural and pyrroles and share some optical and fluorescent properties (λ_{max}(absorbance) = 340 nm; fluorescent emission at 440 nm for excitation at 370 nm).

Recently, it has been demonstrated that the major consequence of hyperglycemia in diabetes mellitus is excessive non-enzymatic glycosylation of proteins and that the end-products of advanced glycosylation may form in vivo from Amadori products, through a series of further reactions, rearrangements and dehydrations [1, 7, 8]. Post-Amadori glycosylation products accumulate on longer-lived proteins, producing structural effects in many tissues. Advanced glycosylation end-products can be detected by using spectrophotometric and fluorescence techniques, but direct quantitation of particular chemical products has not yet been possible.

0003-2670/86/$03.50

Procedures to detect browning compounds are of vital importance for studying the relevance of such compounds in pathological conditions such as diabetes mellitus. The present communication shows that the browning products, obtained by reacting lysine (the most reactive amino acid) with glyceraldehyde (the most reactive "sugar") under physiological conditions [9], are reactive towards a diazonium salt and produce a chromophore with maximum absorbance at 490 nm. Diazonium salts may therefore be used to detect these "late" products of the glycosylation of proteins in vivo.

Experimental

Chemicals. Lysine, hystidine and glyceraldehyde were obtained from Fluka; sulfanilic acid, sodium nitrite, 4-dimethylaminobenzaldehyde and hydroxymethylfurfural were from Merck; pyrrole, 2,5-dimethylpyrrole, pyrrole-carboxylic acid, furan, furan-2-carboxyl-Cl, imidazole, *N*-acetylimidazole, 3-ethylimidazole and 2-hydroxybenzimidazole were from Serva.

Incubation. Browning products were prepared by incubating lysine (40 mmol l^{-1}) with various amounts of glyceraldehyde (20—400 mmol l^{-1}) at 37°C in pH 8.0 phosphate buffer, in the dark, and were characterized by their absorption and fluorescence spectra.

Reaction of glycosyl lysine with 4-dimethylaminobenzaldehyde. For the reaction with 4-dimethylaminobenzaldehyde, 1 g of this compound was dissolved in 100 ml of acetone and hydrochloric acid (10 mol l^{-1}) was added to give a final concentration of 2 mol l^{-1}. Alternatively, phosphoric acid (85% final concentration) was added instead of hydrochloric acid. To 50 µl of sample, 500 µl of the benzaldehyde reagent was added and the mixture was kept at 37°C for 30 min before its absorbance was measured at 540 nm.

Reaction of glycosyl lysine with sulfanilic acid and sodium nitrite. After many variations (see Results) had been tested, the following conditions for the assay with a diazonium salt were found to give the highest absorbance. The sample (200 µl) was mixed with 100 µl of 0.029 mol l^{-1} sodium nitrite and 1 ml of a 32 mmol l^{-1} solution of sulfanilic acid in 165 mmol l^{-1} hydrochloric acid. After incubation at 37°C for 1 h, 100 µl of 5 mol l^{-1} sodium hydroxide was added and the mixture was kept for a further 45 min at 37°C before the absorbance was measured at 492 nm. Lysine (40 mmol l^{-1}) and glyceraldehyde (20 mmol l^{-1}) were used separately as blanks. Spectra were recorded with a Cary 219 spectrophotometer (Varian, Palo Alto, CA).

Results and discussion

Reaction of browning compounds with diazonium salts. In the search to find a simple assay for browning compounds in vivo, a pair of very reactive substances (lysine and glyceraldehyde) was chosen. The final reaction products [6] (with the absorption and fluorescence characteristics of browning compounds) were tested with two reagents commonly used to detect pyrrole structures in molecules of biological importance, 4-dimethylaminobenzaldehyde and a diazonium salt. The former reagent proved to be unreactive with

the glycosylated structure in the presence of 2 mol l^{-1} hydrochloric acid and only weakly reactive when 85% (final concentration) phosphoric acid was present in the reaction mixture. The diazonium salt, however, was strongly reactive and led to the formation of a chromophore with an absorbance maximum at 490 nm (Fig. 1). The absorbance correlated almost linearly with the amount of glyceraldehyde added to the incubation medium (Fig. 2), and showed that the maximum production of pyrrole rings corresponded to one mole of pyrrole per mole of lysine. Comparison of the rates of formation of browning compounds and of pyrrole showed that the reaction was almost complete after 2 h while after 96 h all the glyceraldehyde had reacted (cf. the difference in diazonium salt reactivity between 96 and 158 h, Fig. 2).

Optimization for sensitivity and reproducibility of the reaction conditions. The reaction of glycosyl lysine with diazonium salts was optimized by testing various amounts of reagents in the assay. Figure 3 shows that the absorbance

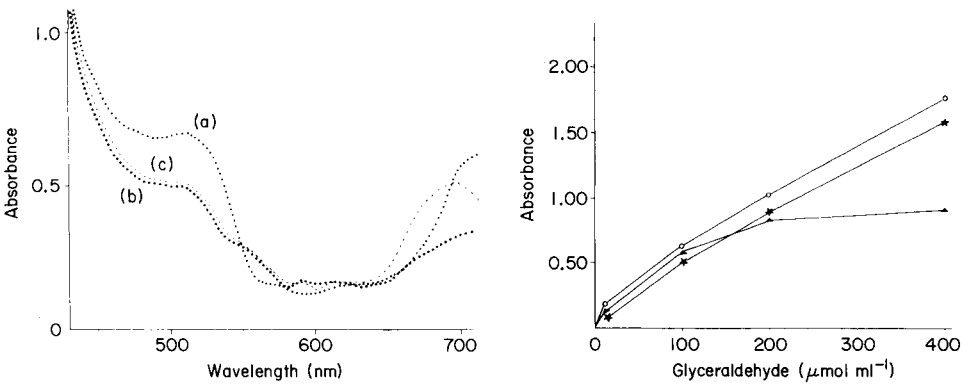

Fig. 1. Absorption spectra: (a) glycosyl lysine; (b) pyrrole; (c) imidazole (after reaction with a diazonium salt under the recommended conditions).

Fig. 2. Absorbance at 492 nm of lysine/glyceraldehyde adducts when reacted with a diazonium salt. Lysine (40 mmol l^{-1}) was incubated with various concentrations of glyceraldehyde (20—400 mmol l^{-1}) at 37°C in the dark for 1, 96 and 158 h. Different times: (▲) 1 h; (★) 158 h; (○) 96 h.

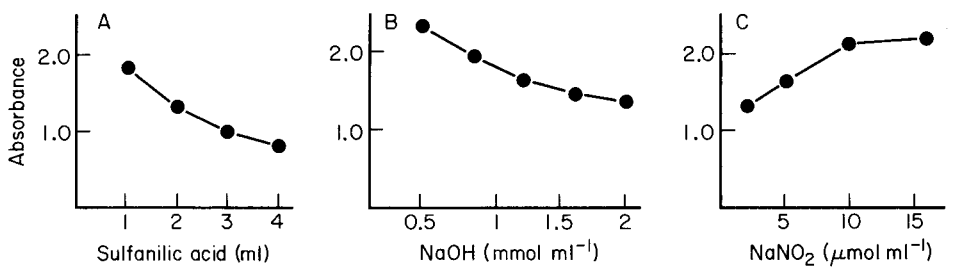

Fig. 3. Effect of reagent concentrations on the absorbance obtained for 40 mmol l^{-1} lysine, and glyceraldehyde (20 mmol l^{-1}), under the recommended conditions except for the variable under investigation. Reagent: (a) sulfanilic acid; (b) sodium nitrite; (c) sodium hydroxide.

TABLE 1

Reactivity of diazonium salts with molecules having a pyrrole or imidazole group but different substituents

Compound	Absorbance at 490 nm[a]	Compound	Absorbance at 490 nm[a]
Pyrrole	0.55	2-Hydroxybenzimidazole	0.36
Pyrrol-2-carboxylic acid	0.61	Furan	0.62
2,5-Dimethylpyrrole	0.59	Furan-2-carboxylic acid	0.71
Imidazole	0.60	5-Hydroxymethyl-2-furaldehyde	0.26
1-Acetylimidazole	0.39	Histidine	0.56
2-Ethylimidazole	0.35		

[a]For a 1 nmol ml^{-1} solution.

increases on decreasing the amount of sulfanilic acid and sodium hydroxide, and by increasing the concentration of sodium nitrite. The recommended conditions gave relative standard deviations within and between assays (on 10 determinations) of less than 5%, and good calibration linearity between 50 and 500 nmol ml^{-1} pyrrole.

Site of reaction of diazonium salt with pyrrolic molecules. Diazonium salts are strongly electrophilic compounds which react with activated aromatic rings. For analytical purposes, they are generally used to quantify pyrrole or imidazole-like structures based on their supposed preferential site of attack on C-2 in these molecules. Based on the difference in reactivity between the diazonium salt and 4-dimethylaminobenzaldehyde, it was questioned whether this had any structural significance, because the two reagents attack at different sites on the aromatic structure. Therefore the reactivity of the diazonium salt was tested with numerous pyrrole- or imidazole-like molecules in which the various carbon atoms were alternately blocked. As listed in Table 1, all the molecules tested reacted with the diazonium salt, indicating that there is no preferential site of attachment of the diazonium ion, which, because of its own high electrophilicity, may bind the pyrrole structure at any of the four carbon atoms or the nitrogen. Accordingly, the low reactivity of 4-dimethylaminobenzaldehyde may be explained by the lower electrophilicity of the reagent compared to the diazonium salt.

The authors acknowledge the continuous interest of Prof. G. Romussi.

REFERENCES

1 H. F. Bunn, D. N. Hanney and S. Kamin, J. Clin. Invest., 57 (1976) 1652.
2 L. Kennedy and J. W. Baynes, Diabetoligia, 26 (1984) 93.
3 A. S. Acharya and J. M. Manning, J. Biol. Chem., 255 (1980) 7218.
4 J. E. Hodge, J. Agri. Food Chem., 1 (1953) 928.
5 T. M. Reynolds, Adv. Food Res., 12 (1963) 1.

6 G. R. Waller and M. S. Feather (Eds.), The Maillard Reaction in Foods and Nutrition, American Chemical Society, Washington, 1983.
7 V. M. Monnier and A. Cerami, Science, 211 (1981) 491.
8 V. M. Monnier, R. R. Kohn and A. Cerami, Proc. Natl. Acad. Sci. U.S.A., 81 (1984) 583.
9 G. Candiano, G. M. Ghiggeri, G. Delfino, C. Queirolo, C. Cuniberti, E. Gianazza and P. G. Righetti, Carbohydr. Res., 145 (1985) 99.

Analytica Chimica Acta, 184 (1986) 329–333
Elsevier Science Publishers B.V., Amsterdam — Printed in The Netherlands

Short Communication

COLORIMETRIC DETERMINATION OF ALUMINIUM(III) WITH CHROME AZUROL S AND THE REACTIVITY OF HYDROLYSED ALUMINIUM SPECIES

J. A. KENNEDY and H. K. J. POWELL*
Chemistry Department, University of Canterbury, Christchurch (New Zealand)
(Received 1st October 1985)

Summary. The metallochromic reagent chrome azurol S, when used in hexamine buffer at pH 4.9, reacts rapidly with monomeric and small polymeric forms of aluminium(III) in aged hydrolysed solutions. It is unreactive toward the polymer $Al_{13}(OH)_{32}^{7+}$ and colloidal $Al(OH)_3$ and the hydroxyaluminosilicates, imogolite and allophane. The reagent is appropriate for rapid semi-quantitative analysis of labile aluminium in acid lake waters or acid soils.

For the spectrophotometric determination of aluminium(III), the reagent chrome azurol S (CAS) has distinct advantages over other possibilities such as aluminon, 8-quinolinol and eriochrome cyanine R. These advantages include rapid colour development, sensitivity, use at room temperature, colour stability and simple experimental procedure [1]. The studies with this reagent reported here relate to a general interest in developing field tests for rapid qualitative or semi-quantitative visual estimation of metal ions in natural samples such as soils (e.g., KCl-exchangeable aluminium) and waters. The colour observed for CAS/Al(III) solutions results from absorption by the CAS/Al(III) complex, and by the unreacted (excess) CAS. Under suitable conditions, the colour of the solution changes rather than its intensity as the aluminium concentration is varied. The CAS/Al(III) test is attractive because of the rapid formation of distinctive colours at low aluminium concentrations. For example, with 2.0×10^{-4} M CAS at pH 4.9, the solutions become amber, red-brown, and mauve instantaneously for 0, 0.4—0.8, and $\geqslant 1.2$ mg l^{-1} Al, respectively; with 4.0×10^{-5} M CAS, the colours are light amber, red-brown and mauve for 0, 0.15—0.2 and $\geqslant 0.3$ mg l^{-1} Al, respectively (after 30 s); with 1×10^{-5} M CAS, the colours are light amber, pink and mauve at 0, 0.08—0.12 and $\geqslant 0.20$ mg l^{-1}, respectively; and with 2.5×10^{-6} M CAS, a pink or mauve solution (after 120 s) indicates $\geqslant 0.02$ mg l^{-1} Al.

In this communication, the following aspects are considered: (i) the stoichiometry of the CAS/Al(III) complex; (ii) the optimal type and concentration of buffer for colour development; (iii) the order of reagent addition; (iv) colour stability; (v) interferences; and (vi) the Al(III) species which react

0003-2670/86/$03.50

with CAS at pH 4.9. The reactivity of CAS toward a series of partially hydrolysed Al(III) solutions and the amorphous aluminosilicates imogolite and allophane was examined.

Experimental

Chemicals. Chrome azurol S was purified as its tetra-acid (H_4R) by recrystallisation (twice) from a concentrated solution (20% w/v) in 6 M hydrochloric acid as described by Langmyhr [2]. Purity was checked by pH titration and elemental analysis. A distinct end-point at pH 5.5—7.5 corresponding to titration of 3 protons indicated a formula weight of 608 ± 16, i.e., $H_4CAS \cdot 4H_2O$ (found 44.8% C, 3.2% H, 5.0% S; required for the tetrahydrate 45.1% C, 3.3% H, 5.2% S).

Analytical reagent-grade chemicals and CO_2-free double-distilled water were used throughout. Aluminium chloride solution (1000 mg l^{-1}) was prepared from aluminium chloride hexahydrate in 10^{-2} M hydrochloric acid (to suppress hydrolysis). This stock solution was standardized gravimetrically by the conventional 8-quinolinol method [3] and working solutions were made by suitable dilution with a micrometer syringe. Hexamine buffer was prepared by adjusting the pH of 1.0 M hexamine to 4.9 with hydrochloric acid.

Hydrolysed aluminium(III) species. These were prepared at 25°C from aqueous acidic solutions of Al^{3+} (1×10^{-4} M) and KCl (1 M); they were aged in polypropylene bottles. [The 1 M KCl medium was chosen because it is used as an extractant for exchangeable aluminium in soils [4]; hydrolysis constants ($\log \beta_m$) are available for Al(III) in this medium [5]. The species included in the hydrolysis calculations were Al^{3+}, $Al(OH)^{2+}$, $Al(OH)_2^+$, $Al(OH)_3(aq)$, $Al(OH)_4^-$, $Al_2(OH)_2^{4+}$, $Al_3(OH)_4^{5+}$ and $Al_{13}(OH)_{32}^{7+}$.] Solutions with pH values in the range 4.5—6.5 were prepared under nitrogen purging by addition of potassium hydroxide (micrometer syringe); the pH was monitored until steady values (±0.02) were recorded (up to 3 days).

Imogolite. Imogolite was prepared in polypropylene bottles by the method of Farmer and Fraser [6] from silicon tetraethoxide and a perchloric acid-hydrolysed solution of aluminium tri-sec-butoxide. The product was recovered by freeze-drying and characterized by the distinctive i.r. absorption at 348 cm^{-1} for a sample in a KBr disc [7] (3 mg/500 mg/KBr, heated at 150°C for 16 h).

Results and discussion

Complex stoichiometry. Titration of an Al(III)/CAS solution (1:2.2) gave a distinct end-point at pH 6.5 corresponding to the loss of one weakly acidic (phenolic) proton per Al(III) ion. Mole ratio plots based on the absorption of the Al/CAS complex at 546 nm established formation of a 1:1 complex at pH 6.5 (and pH 4.9). The persistence of a 1:1 complex at pH 6.5 implies that a second ligand group has bound with the aluminium, as in $Al_2(CAS)_2^{2-}$. The molar absorptivity for the complex increased from zero at pH <2 to a maximum at pH 3—4 and then decreased to about 50% of this value at pH 6.5; λ_{max} remained constant at 546 nm. These observations are consistent with

formation of $Al(CAS)^-$ at pH <3 followed by dimerisation to $Al_2(CAS)_2^{2-}$ at pH >4. In contrast, other workers have referred to the formation of bis complexes $Al(HR)_2^{3-}$ and AlR_2^{5-} [8].

At pH >7.5 additional buffering occurs; the absorbance of the complex diminishes rapidly and at pH 8 the solution is yellow and the spectrum is identical to that of CAS only, indicating that the Al-CAS complex has dissociated.

Buffer conditions. Pakalns [1] used a pH 4.6 acetate buffer (0.7 M). Colour development was instantaneous, but absorbance not only decreased by 2% h^{-1} on standing but was dependent on buffer concentration. This interference by acetate was confirmed at pH 4.9. With hexamine buffer the absorbance was found to be much less variable with buffer concentration, e.g., there was an 8% decrease in absorbance at 546 nm from 0.1 to 0.2 M hexamine compared to a 29% decrease for acetate. Electrolyte concentration (0.1—0.5 M KCl) in the final solution did not affect absorbance measurably.

In this work, a 1 M hexamine buffer was used, diluted to a final concentration of 0.2 M (pH 4.9).

Colour stability. Absorbances for Al/CAS solutions decreased by 10% over 24 h, but were then stable for some days. Colour development was 97% complete in 1 min for a final reagent concentration of 1.6×10^{-4} M and was complete in 10 min for a CAS concentration of 5.3×10^{-5} M (spectrophotometric working range 0.05—0.8 mg l^{-1} Al). Beer's law was obeyed at 567.5 nm (molar absorptivity, 25.2×10^3 l mol^{-1} cm^{-1}, but not at 546 nm, as noted by Pakalns [1]. Absorbance readings at 567.5 nm were corrected for the contribution from unreacted CAS by reference to the decrease in absorbance at 442 nm for uncoordinated CAS.

Addition of reagents. The absorbance developed by an aluminium(III) solution is independent of the order in which the reactants (CAS, buffer, Al) are mixed. This contrasts with pyrocatechol violet for which a pH 6.2 buffer is used [9]; initial mixing of buffer with Al(III) may lead to zero change in absorbance because of rapid formation of non-labile hydroxy-aluminium polymers and colloidal $Al(OH)_3$. At pH 4.9 hydroxyaluminium polymer formation is negligible in dilute solution [5], thus the integrity of the more acidic sample solutions is maintained; further, at pH 4.9, the hydrogen ion concentration is not sufficient to give rapid decomposition of polymers existing in less acidic analyte solutions.

Interferences. Pakalns [1] reported several interferences and methods adopted for masking. Interferences from the environmentally significant species silicate and fulvic acid were examined here. At 6 mg l^{-1}, fulvic acid caused no suppression of absorbance for a 0.5 mg l^{-1} Al solution. With H_4SiO_4 at 20 and 200 mg l^{-1}, the suppression was 4% and 85%, respectively. In soils and natural waters, the most significant interferences will be from iron(III), which can be masked by reduction to iron(II) with ascorbic acid (10 mg/100 ml final solution) added before [1] or after colour development, phosphate (—41% at 80 mg l^{-1} with 0.5 mg l^{-1} Al) and fluoride (—94% at 1.9 mg l^{-1}).

Other severe interferences are from citric acid (—58% at 1.9 mg l^{-1}) and dihydrogenpyrophosphate (—58% at 1.8 mg l^{-1}).

Reaction with hydrolysed aluminium(III) species. Three tests were applied on each of the aged hydrolysed aluminium solutions. To establish the content of labile soluble aluminium, a sample was centrifuged (2500 rpm) for 30 min; an aliquot from the top 1 cm of the supernatant liquid was analysed by the CAS/hexamine method. The absorption spectra were found to remain constant when monitored for 60 min. For total dissolved aluminium, another aliquot of the same supernatant liquid was acidified (pH 2, HCl) and digested on a steam bath for 30 min; after cooling and dilution to volume, an aliquot was taken through the CAS/hexamine procedure. To estimate the content of total labile aluminium, a sample was added to CAS/hexamine and then centrifuged (2500 rpm, 10 min); absorption spectra were measured for the supernatant liquids and found to remain constant with time (60 min).

The results are plotted in Fig. 1. Total dissolved aluminium (curve a) passed through a minimum near pH 6; this is consistent with the (calculated) solubility curve for amorphous $Al(OH)_3$. Data on curve (b), derived from the difference between total dissolved aluminium and labile soluble aluminium, represents soluble CAS-unreactive or non-labile aluminium. The similarity between curves (b) and (c) for the concentration of $Al_{13}(OH)_{32}^{7+}$ calculated for solutions with compositions given by curve (a), implies that unreactive dissolved aluminium can be approximated to the polymer $Al_{13}(OH)_{32}^{7+}$.

Results for the total reactive (labile) aluminium in solution and for the labile soluble aluminium in the supernatant liquid agreed within 10—20%. This implied that colloidal phases were not significantly reactive under the conditions used. For a solution aged at pH 6.5, the test for total labile aluminium produced a reddish-blue precipitate, possibly $Al(OH)_3$ plus adsorbed/complexed CAS.

Reactivity of aluminosilicates. The hydrous aluminosilicate imogolite is often found in the fine clay fraction of soils, acting as a cementing or coating material [10]. It has a tubular structure with an outer hydroxo-oxo-aluminium surface [11]. Imogolite is frequently found in acid soils such as podzols and

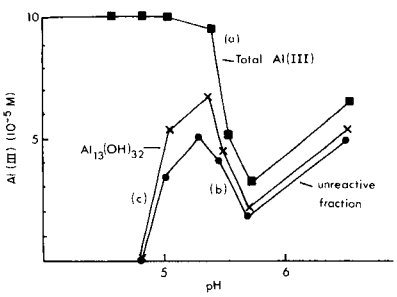

Fig. 1. Reactivity of hydrolysed Al(III) solutions with CAS: (a) total dissolved Al(III); (b) soluble non-labile (CAS-unreactive) Al(III); (c) $Al_{13}(OH)_{32}^{7+}$ concentration computed for each solution.

it is inferred that its low molecular weight precursor proto-imogolite [6] may be one form in which aluminium is translocated down acid soil profiles [10]. Proto-imogolite is a possible component of acid soil waters.

A sample of imogolite (3 mg) was suspended in distilled water for 16 h, and then treated with a calculated excess of CAS/hexamine reagent. There was no evidence of rapid dissolution and/or reaction of imogolite. There was no visible colour change in the CAS solution (hours). The imogolite sample was recovered unchanged (i.r.) from the centrifuged freeze-dried solution, but its blue colour indicated a surface reaction with CAS. A similar result was obtained for a natural allophane sample (Silica Springs allophane) [12].

Conclusions

Chrome azurol S in hexamine buffer at pH 4.9 is well suited to rapid estimations of aluminium in environmental samples. The reagent is appropriate for determinations of labile aluminium in acid lake waters [13] and in soils, and for examination of soil pedology. The order of addition of reagents is not important; thus for semiquantitative field tests, subsequent additions of CAS or analyte can be made to enhance the colour development. The CAS does not react with non-labile polymeric species ($Al_{13}(OH)_{32}^{7+}$), with colloidal $Al(OH)_3$ or colloidal aluminosilicates (imogolite). Interference from fulvic acid and silicate at environmental concentrations is negligible.

The use of CAS at appropriate concentrations allows rapid visual detection of Al(III) ion at 0.02 mg l^{-1} (2.5×10^{-6} M CAS) to >1.2 mg l^{-1} (2.0×10^{-4} M CAS). Unknowns can be assigned to small ranges of concentration by visual comparison with the colours of standard aluminium solutions, permitting a semiquantitative estimate of labile aluminium in natural samples.

REFERENCES

1 P. Pakalns, Anal. Chim. Acta, 32 (1965) 57.
2 F. Langmyhr, Anal. Chim. Acta, 29 (1963) 149.
3 A. I. Vogel, A Textbook for Quantitative Inorganic Analysis, 3rd edn., Longmans Green and Co., London, 1961.
4 B. W. Bache and G. S. Sharp, Geoderma, 15 (1976) 91.
5 R. E. Mesmer and C. F. Baes, The Hydrolysis of Cations, Wiley, New York, 1976.
6 V. C. Farmer and A. R. Fraser, in M. M. Mortland and V. C. Farmer (Eds.), International Clay Conference 1978, Elsevier, Amsterdam, 1979.
7 V. C. Farmer, A. R. Fraser, J. D. Russell and N. Yoshinaga, Clay Miner., 12 (1977) 55.
8 D. D. Perrin, Stability Constants of Metal Ion Complexes, Part B, IUPAC Chemical Data Series No. 22, Pergamon, Oxford, 1979.
9 W. K. Dougan and A. L. Wilson, Analyst (London), 99 (1974) 431.
10 H. A. Anderson, M. L. Berrow, V. C. Farmer, A. Hepburn, J. D. Russell and A. D. Walker, J. Soil Sci., 33 (1982) 125.
11 V. C. Farmer, A. R. Fraser and J. M. Tait, J. Chem. Soc. D: (1979) 462.
12 N. Wells, C. W. Childs and C. J. Downes, Geochim. Cosmochim. Acta, 41 (1977) 1497.
13 G. D. Howells and A. S. Kallend, Chem. Br., 20 (1984) 407.

Analytica Chimica Acta, 184 (1986) 335—346
Elsevier Science Publishers B.V., Amsterdam — Printed in The Netherlands

Book Reviews

Y. Marcus. *Ionic Solvation.* Wiley-Interscience, Chichester, 1985 (ISBN 0-471-90756-1). viii + 306 pp. Price £42.00.

This book presents an up-to-date account of theoretical and practical aspects of the interactions between ions and a solvent. It starts with a discussion of the simplest example of ion solvation — that of gaseous ions interacting with gaseous solvent molecules. This can be studied both theoretically and experimentally and the results then applied to the more familiar liquid phase. Theoretical treatments of ion solvation are based upon a number of models, and the nature of these together with their limitations is presented. The results of experimental work on ion solvation is described not only for the most commonly used solvent, water, but also for nonaqueous solvents and for mixed solvents where selective solvation is observed. Possibly of greatest interest to analytical chemists will be the final "applications" chapter where, among other topics, liquid-liquid extraction and electrochemistry in various solvents are discussed. The book contains many tables of physical data connected with solvation. For example, for 110 different solvents it lists 28 different properties ranging from boiling point to molecular collision diameter. For the data tables alone, this book will prove very useful. The data tables and text are provided with many references to original sources and, in all, this book is a fine starting point for someone wishing to find out about any aspect of ion solvation. It is written at the advanced undergraduate/graduate student level.

J. R. Chipperfield

H. G. Barth (Ed.), *Modern Methods of Particle Size Analysis (Vol. 73* in *Chemical Analysis).* Wiley, New York, 1984 (ISBN 0-471-87571-6). x + 309 pp. Price £58.50.

This book, volume 73 in Chemical Analysis, A Series of Monographs on Analytical Chemistry and its Applications, consists of nine chapters written by eleven contributors. The first two chapters give a very useful review of modern instruments and techniques in the field of particle size analysis, the second concentrating on methods used to characterise sub-micrometre particles. Not all available methods are dealt with in the same depth and whilst most of them are "modern" the latest version of an instrument is not always depicted. The time-dependent light-scattering method, photon correlation spectroscopy, is the subject of Chapter 3 and the application of the photon correlation function to the determination of molecular weight distributions of polymers in solution follows. Chapter 5 presents a readable,

detailed study of the Fraunhofer diffraction method whilst Chapter 6 describes sizing particles from 0.1 to 1000 μm using instruments of one particular company. The principles of field flow fractionation are introduced in Chapter 7. Hydrodynamic chromatogrpahy, another technique not yet in the main stream of particle sizing, which is described at some length in the early chapters, is used to analyse polydisperse polymers in the final chapter, detection systems for particle chromatography having been previously described. A total of 359 references and 35 instrument manufacturers are listed.

The book, which concentrates on more recent particle-sizing techniques of interest rather than those most widely practised nowadays, is a useful addition to the literature on the subject of particle size analysis — at a price!

J. E. C. Harris

Alan Wiseman (Ed.), *Handbook of Enzyme Biotechnology, 2nd edn.* Horwood, Chichester, 1985 (ISBN 0-85312-420-5). 457 pp. Price £42.50.

The first edition of this book was published in 1975. It was an immediate success. It pointed the way ahead in a subject which has since become very topical, and has continued to develop rapidly. The book stimulated ten subsequent volumes on "Topics in Enzyme and Fermentation Biotechnology", also edited by Dr. Wiseman. The time is ripe, therefore, for a complete revision of the foundation volume. The new text is divided into two sections. The first deals with principles, the second with details and data. In each section, there are chapters on large-scale extraction and purification of enzymes, and industrial enzymology. Of more immediate interest to analytical chemists are the chapters on enzyme immobilization (Kennedy and White) and enzymes in clinical analysis (Gould and Rocks), although there is a dearth of post-1980 references in the former chapter. Taken as a whole, the book provides a comprehensive and readable account of the widest range of applications of enzymes. Analytical chemists, in particular, are becoming increasingly appreciative of enzyme-catalyzed processes, and will be stimulated by the information collected in the immobilization and analytical chapters. But they will also find much of value in the industrial section. There is no doubt that the new edition is a worthy successor to the previous version.

Alan Wiseman (Ed.), *Topics in Enzyme and Fermentation Biotechnology, Vol. 10.* Horwood, Chichester, 1985 (ISBN 0-85312-767-0). 218 pp. Price £31.00.

The 10th volume in the series contains five articles, a brief introduction by the Editor, a subject index, and a cumulative subject index for Volumes 6—9.

Two chapters deal with immobilized living cells. The first (by E. Concoron) describes the production and use of immobilized microbial cells, mainly by entrapment in various matrices. Chemically-immobilized bacteria have been used analytically in certain electrodes, but this application is not discussed, and chemical immobilization receives but cursory attention. Nevertheless, the information provided will be useful to forward-looking analytical chemists. The article on immobilized plant cell cultures (M. J. C. Rhodes) is of little immediate relevance to analysis, and likewise those on the Koji solid state-fermentation process and fermentation techniques in xanthan gum production. The final article is entitled "Covalent Chromatography in Biochemistry and Biotechnology" (K. Brocklehurst, J. Carlsson and M. P. J. Kierstan). Essentially the technique involves selective covalent bonding of a component or components to a support (e.g., via —S—S— bond formation) and subsequent elution by bond breakage (possibly in sequence, according to bond strength). This is undoubtedly an interesting separatory technique, but it should not be called chromatography. It will be very useful, however, for numerous separations, and its wider exposure will be beneficial.

A. Townshend

J. C. Miller and J. N. Miller, *Statistics for Analytical Chemists.* Horwood, Chichester, 1984 (ISBN 0-85312-662-3). 202 pp. Price £18.50 (Paperback £7.90).

For analytical techniques ranging from the simplest manual titration through to the most sophisticated computer-controlled instrumentation, the treatment and interpretation of the resultant data is an integral part of the total analytical process. It is, therefore, of prime importance that all persons associated with the analytical process are cognizant of statistical methods and their practical applications. Unfortunately, the general level of understanding is poor, and one reason for this is the dearth of readable literature aimed specifically at practising analytical chemists. Two major attractions of this text are, therefore, the use of real analytical results to illustrate each of the statistical methods discussed and the general readability of the text.

In order to appeal to the growing number of students specializing in analytical chemistry and to the practising analyst, all of the important statistical techniques are covered, and their treatment requires no prior knowledge of statistics. For those readers relatively unfamiliar with the subject there is an introduction covering accuracy and precision and experimental errors. This is followed by three chapters dealing with important statistical concepts for classical and instrumental analysis, including standard deviations, confidence limits, significance tests, regression and correlation.

There is also a chapter on non-parametric methods dealing with data that do not follow the normal (Gaussian) distribution and a final chapter which

discusses experimental design, optimization techniques and pattern recognition. Each chapter also contains a bibliography and a set of exercises, again with a distinct analytical flavour, that the reader is encouraged to work through.

This book is therefore highly recommended to all practising analytical chemists and students of the subject. The comment that there is not a suitable text on statistics for analytical chemists is no longer a valid one.

P. J. Worsfold

P. M. Marcus and F. Jona (Eds.), *Determination of Surface Structure by LEED*. Plenum Press, New York, 1984 (ISBN 0-306-416646). 565 pp. Price $89.50.

This book is therefore highly recommended to all practising analytical of the Conference on Determination of Surface Structure by LEED, held in June, 1980. Comparing the date of the symposium with the publication year makes the reader wonder why it took so long to prepare this volume. The editors give at least a partial explanation. The authors were asked to write the papers after the Symposium and prepare "full and detailed discussions" of various aspects of LEED. The result is a thorough coverage of basic principles and applications of LEED for the determination of the surface structure of a material.

The papers are grouped into four sections: discussions of the mathematical formulation of intensity theory and computational procedures to implement the theory; presentation of data-fitting processes and the reliability of parameter determination; reviews of new instrumentation and new techniques for data acquisition; and discussions of complex aspects of LEED intensities arising from defects, in other words LEED patterns of imperfectly ordered "real" surfaces.

The paper contained in this volume are written by leading experts, mostly from the USA and Western Europe. The book is, therefore, not only at a top-level standard but represents the field in a truly international manner. The individual contributions do have the character of state-of-the-art and progress reports. They are written for the specialist in the field and for scientists concerned with the determination of surface structure. For those, this volume presents LEED at an up-to-date level. For the analytical chemist concerned with the characterization of surfaces wanting to study the potential of LEED, more introductory texts are better suited.

M. Grasserbauer

J. A. Butt, D. F. Duckworth and S. G. Perry (Eds.), *Characterisation of Spilled Oil Samples, Purpose, Sampling, Analysis and Interpretation.* Published on behalf of The Institute of Petroleum, London by Wiley, Chichester, 1986 (ISBN 0-471-90890-8). ix + 95 pp. Price £17.50.

There have been several major changes in the oil industry since the early 1970s, particularly the development of North Sea oil production, which have increased potential pollution problems for the United Kingdom. The past decade has also seen significant advances in analytical techniques relating to oil characterization and an increased awareness of environmental pollution. This text is therefore a timely successor to the 1974 Institute of Petroleum publication "Marine Pollution by Oil". It is a short text written at a very general level and is easy to read, but lacks the practical details of its predecessor.

There are brief chapters on the administrative aspects of oil pollution analysis, the fate of oily pollutants in the environment and the chemical composition of petroleum. There is a more detailed chapter on sampling, sample storage and sample treatment and a final chapter (consisting of almost half the book) outlining the various analytical techniques available for oil spill identification. The key techniques discussed are gas chromatography, computerised gas chromatography/mass spectrometry, infrared spectroscopy, elemental analysis and fluorimetry.

This book is intentionally aimed at a broad readership which includes company management, legislators, journalists and laymen. It is therefore somewhat disappointing from an analytical viewpoint in that it only contains an overview of analytical techniques, with little critical comment. The absence of an index and a lack of consistency in presentation is also irritating.

P. J. Worsfold

F. L. Boschke (Ed.), *Analytical Chemistry Progress (Vol. 126* in *Topics in Current Chemistry).* Springer-Verlag, Berlin, 1984 (ISBN 3-540-13596-0). 122 pp. Price DM 78.00.

This is a collection of five review articles on a variety of analytical or potentially analytical topics. The first, laser-induced ionization spectrometry of elements in a flame (R. B. Green), is a novel and, as yet, little exploited technique which has a theoretical detection limit approaching 1 pg ml^{-1}. Laser spectrometry of biomolecules (A. Anders) dealing with chlorophyll, nucleic acids, haemoglobin, rhodopsin, etc., is perhaps better known, and certainly provides a powerful diagnostic tool. The remaining three articles cover aspects of thin layer chromatography (TLC). The chapter on ion-pair reversed-phase TLC (D.-G. Volkmann) describes separations of drugs, peptides, amines, etc., on various phases in the presence of various counter ions.

S. Ebel discusses evaluation and calibration in quantitative TLC, covering subjects such as regression, peak height and area measurement, standard-addition procedures, etc. Finally, I. M. Böhrer covers evaluation systems, i.e., densitometers of various types. Each article is concise but informative, and provides essential information on theory, instrumentation and applications. I suspect in compilations of this type, personal sales would be increased if there was less diversity of subjects in a given volume. Nevertheless, as a source of review information, the concept is fine. This volume also has the cumulative index to Volumes 101—126.

A. Townshend

K. J. Voorhees (Ed.), *Analytical Pyrolysis: Techniques and Applications.* Butterworths, London, 1984. 486 pp. £35.00.

This is a volume based on fifteen invited lectures presented at the 5th International Symposium on Analytical Pyrolysis held in Colorado. It has been printed from the authors' typescripts; this may minimise publication delays, but must easily have doubled the number of pages that would have been required with normal typesetting. And what of the contents? In his preface, the editor states that "the aim of this book is to present an up-to-date overview of analytical pyrolysis applied to geochemistry, polymers, biomass and biology, as well as to provide information on state-of-the-art analytical pyrolysis".

To attain this objective, a truly international list of contributors has been assembled and the general standard of presentation, both with respect to the science and also the layout, is quite high. Apart from one contribution (which discusses general problems of heat transfer in analytical pyrolysis), the papers are oriented towards the analytical techniques used, which are principally Fourier-transform infrared, gas-liquid chromatography, mass spectrometry, or a combination of the last two. The quality of this analytical equipment, and the general standard of interpretation, are undoubtedly high, and at least one paper (that by Tsuge and Ohtani on stereospecific polypropylenes) will be quoted as a classic. Unfortunately, the quality of the pyrolysis equipment in nearly all cases is relatively crude, and in most cases this restricts the potential of the overall technique. In particular, far too many workers seem to have misplaced confidence in Curie-point heating. This is by no means a reliable way of attaining a specified ("Curie") temperature; the latter may be not attained, or may be exceeded, depending on the r.f. energy used. The implications of this are that the most successful papers are those characterizing differences between similar samples (e.g., between different fossil fuels or different bacterial samples). However, every one of the contributions is worth reading, and this book should be in the library of every laboratory concerned with characterization, analysis, or pyrolysis. There are minor irritations which should have been eliminated by more careful editing or

proofreading. Thus there are frequent errors of spelling (only a few of which are Americanisms), a missing reference (p. 41, ref. 20), some text missing (between pp. 204 and 205), and one paper where the English is sufficiently quaint to have benefitted from some editorial attention. The price is not unreasonable by today's standards.

R. S. Lehrle

P. Zuman and R. C. Patel, *Techniques in Organic Reaction Kinetics.* Wiley-Interscience, New York, 1984 (ISBN 0-471-03556-4). 340 pp. Price £57.25.

The volume is intended to provide the necessary information on data treatment and measurement in a kinetic study as a means for investigation of organic reaction mechanisms. Based on a sound discussion of experimental techniques for monitoring time-dependent concentration changes it covers the whole area of analysing kinetic data and studying fast reactions.

The techniques for concentration measurements range from direct chemical measurements to physicochemical methods based on absorbance, thermometric, conductimetric, potentiometric and polarographic measurements or on magnetic resonance spectrometry (NMR, ESR) and chromatography. What follows is a very valuable guide to the obligatory tools for handling organic reaction kinetics, i.e., establishing reactants, products and intermediates, deriving rate equations for the reaction under study, determing reaction orders and rate constants, and considering effects of pH (coupled acid-base equilibria and catalyzed reactions), of solvents (including the more recent concept of donor numbers), temperature, ionic strength or treating structural effects. The last chapter, which is devoted to studying fast reactions (less than 10 s), contributes well to exploring the whole time scale of organic reactions. It deals with modified classical methods, with techniques based on rapid mixing of reactants, on competitive methods, on NMR- and ESR-measurements, and on relaxation methods as well.

The authors have put in the volume all their experience in investigating the mechanisms of organic reactions, revealing a stimulating in-depth description of the exciting field of chemical kinetics. The book is written concisely since the authors do not attempt to cover the whole theory of reaction kinetics. I would not have missed the chapter on analog computers for, as the authors state themselves, "they are less easily accessible in most chemical laboratories" (p. 136).

The book serves a good purpose for the elucidation of reaction mechanisms, filling a gap in the literature on kinetics, and can be recommended to anyone who has an interest in organic reaction kinetics, especially to undergraduate and graduate students and young researchers, but to readers with only peripheral interest as well.

M. Otto

M. S. Verrall (Ed.), *Discovery and Isolation of Microbial Products.* Published for the Society of Chemical Industry by Horwood, Chichester, 1985 (ISBN 0-85312-748-4). 198 pp. Price £23.50.

The most recent estimate of the number of antibiotic compounds (according to Janos Berdy, the author of the first chapter of this book) is 10986 which includes some 7653 microbial metabolites. The number of other microbial products which are not bioactive must almost be the same again. As probably less than 20% of all microbial genera have been investigated in any degree of thoroughness, the potential for future discovery of useful microbial compounds is enormous. It is no wonder therefore that the exploration of microbial products remains a high priority in the research of most of the large pharmaceutical companies throughout the world. The protocols which are to be used in isolating microbial products must, therefore, be carefully thought out so that the screening can both be rapid and accurate.

The current volume is based on a two-day meeting organized in October 1984 by the Society of Chemical Industry; it covers a wide range of topics and deals not only with the isolation of small molecular weight microbial metabolites, but also in the isolation of proteins and enzymes from various sources. The book begins with two chapters on the screening for microbial antibiotics; the first (by Berdy) is from Budapest and the second (by S. J. Box) from Beechams in Surrey. Thereafter, the book is more concerned with the isolation of proteins and enzymes though in the middle of the book, another chapter suddenly appears from Pirotta (Rohm & Haas, Milan) which reverts back to the original topic of antibiotics. The key chapter to the whole book is probably that by A. R. Thomson (Biochemistry Group, Harwell) who describes and discusses the possibilities which are now being opened up in biotechnology by the use of recombinant DNA techniques and how these may be applied to integrate the process of fermentation with that of the recovery of the microbial product. If you can get the process right by appropriate DNA procedures, then product recovery becomes much less complicated. A number of chapters are from commercial companies (Pharmacia, Alfa-Laval and Westfalia) which all unashamedly extol the virtues of their own companies' technologies.

The Editor is to be congratulated on producing a lively and interesting volume which has both breadth and depth of coverage. The inclusion of a chapter devoted specifically to a discussion of the safety and regulatory aspects applying to industrial companies in this field was a very deft touch. The contribution from Nourish and Brace of the Health and Safety Executive, will be read with a great deal of interest by many people. There is much here for both the specialist as well as the newcomer to the field. It presents the plethora of analytical techniques which are now being used by biotechnologists; the speed at which biotechnology is developing then throws increasing pressure upon the people concerned with isolating microbial products as well as monitoring their yield and biological performance.

Colin Ratledge

L. J. Berliner and J. Reuben (Eds.), *Biological Magnetic Resonance, Vol. 5.* Plenum Press, New York, 1983 (ISBN 0-306-41293-4). 303 pp. Price $45.00.

This series has established a reputation for authoritative surveys of important topics in the very active area of the application of magnetic resonance methods to biochemistry, and this volume continues that tradition. The first chapter, by Baxter, Mackenzie and Scott, is a somewhat dated review of the usefulness of ^{13}C as an NMR probe for metabolic pathways in vivo. This material is of interest primarily to biochemists. Of considerably wider interest are the chapters on ^{15}N-NMR in biological systems (Blomberg and Rüterjans) and NMR work on biophosphates involving ^{17}O and ^{18}O isotopes (Tsai and Bruzik). The former survey covers amino acids and proteins, nucleotides and related molecules, and other compounds such as vitamins and antibiotics, providing extensive tabulations of ^{15}N chemical shifts and coupling constants. Similar tabulations are given for ^{17}O data in the chapter on biophosphates, which also discusses, inter alia, oxygen isotope effects and the investigation of the stereochemistry of enzyme reactions at phosphorus. Some of this material is repeated in the review by Rao of ^{13}P-NMR studies of enzyme systems but this chapter is mainly concerned with line-shape analysis and is likely to be of interest only to enzymologists. The largest chapter in this volume is a very thorough survey by Devaux of lipid-protein interactions as studied by ESR and NMR methods. Although inevitably showing some overlap with material presented elsewhere, this review provides an excellent summary of recent work concerning the study of protein diffusion by saturation transfer ESR, the effect of proteins on lipid order (by ESR), and the nature of the boundary lipid-protein interaction (by ESR and ^{2}H-NMR). This chapter will be of interest to biochemists and analytical chemists investigating the many unsolved problems in the area of membrane chemistry and biochemistry.

D. F. Ewing

T. H. Ryan (Ed.), *Electrochemical Detectors, Fundamental Aspects and Analytical Applications.* Plenum, New York, 1984 (ISBN 0-306-41727-8). viii + 172 pp. Price $39.50.

This book comprises eleven papers presented at the fifth biannual Anglo-Czech Symposium in Electrochemistry held as long ago as 1981! In it, Albery and Hagget summarize their work on detection of proteins, anaesthetic gases and catecholamines in vivo, and Trojanek describes voltammetric flow-through detectors. Four articles (Samuel and Webber, Richards, van Oort et al. and Roger Smith) discuss various aspects of electrochemical detection in h.p.l.c. Jiři Tenygl confronts the problem of renewable electrode surfaces in electrochemical sensors, and Volke gives an extended account of the voltammetry of organic molecules at a variety of electrodes. The remaining

three articles discuss tensammetry in combination with adsorptive accumulation of surface-active compounds on the electrode surface (Kalvoda), analytical applications of immiscible electrolyte interfaces (Mareček) and the impedance of small Li—CuO primary cells (Leek et al.). A subject index is included.

The main subject of the book was (and remains) very timely, and much of the text provides a useful guide to work in the area of electrochemical detection. Thus, unlike many conference proceedings, which are merely a memory of an enjoyable meeting, this book fulfils a useful educational function. The presentation, too, is consistently good.

Bruno Sansoni (Ed.), *Instrumentelle Multielementanalyse.* VCH, Weinheim, 1985 (ISBN 3-527-26225-3). xviii + 782 pp. Price DM 160.

This book has been written around the papers presented at a symposium on instrumental multielement analysis held at Jülich in April, 1984. There are 90 papers reproduced from camera-ready copy. The first four are introductory articles. One (Sansoni) covers generalities and comparisons (54 pp.), the others (Morrison, Laqua and Ohls) describe selected opportunities, multielement capabilities and routine applications, respectively. The remaining papers cover a wide range of subjects (applications, techniques — most spectroscopic techniques are covered — standards, data processing, etc.). Almost 50% of the text is in English, the remainder in German, as might be expected from the preponderance of German authors, although there is a fair sprinkling of other Europeans.

The presentation of the book is good, and the editor has taken pains to ensure that it is more than just a record of a successful symposium. There are subject and technique indexes, extensive compilations of acronyms, photographs of apparatus and details of suppliers. Whether this is the best way to present an account of modern multielement analysis is open to question, but to the practitioner in this field, it does provide a timely account of the state of the art, at a relatively low price per page.

Curt M. White (Ed.), *Nitrated Polycyclic Aromatic Hydrocarbons.* Hüthig, Heidelberg, 1985 (ISBN 3-7785-1029-0). xii + 376 pp. Price DM 128.

It is an indication of the growing awareness of scientists of the environmental significance of nitrated polycyclic aromatic hydrocarbons that this substantial monograph can be devoted entirely to them. It includes contributions by a number of authors on analytical aspects (gas, liquid and thin-layer chromatography, chromatographic detectors, and mass spectrometry) including sampling of atmospheric particulates. Other chapters deal with synthesis of the compounds (including labelled species) and the characterization of the

products, and with their mutagenic and carcinogenic effects. The book concludes with a data collection (m.p., b.p., dipole moment, references to spectroscopic information, CAS numbers) and a subject index. The information provided is very detailed, but the book presents a very readable, up-to-date and comprehensive account of the subject. It should be available in all laboratories where air pollution is studied, and the information it contains will not be without relevance to analyses for other, similar pollutants.

K. L. Kompa and J. Wanner (Eds.), *Laser Applications in Chemistry*. Plenum Press, New York, 1984 (ISBN-0-306-41622-0). ix + 273 pp. Price $45.00.

This is a collection of papers presented at the NATO Advanced Study Institute at Pisa in 1982. It has four main themes, one of which is "laser applications to analytical chemistry". Of the five short articles in this section, four are by J. C. Wright, on absorption (9 pp.), fluorescence (7 pp.), multiphoton ionization (5 pp.) and coherent non-linear spectroscopic techniques (7 pp.). The other paper is about laser measurements of trace gases in the atmosphere and laboratory (12 pp.). The other themes are "laser and related light sources" (4 papers), "spectroscopic and dynamic studies" (14 papers) and "approaches to laser synthesis" (4 papers). Many of the articles they contain could be analytically relevant. The book concludes with a list of the participants and a subject index.

E. Pungor and I. Buzás (Eds.), *Ion-selective Electrodes, 4. (Analytical Chemistry Symposium Series, Vol. 22)*. Elsevier, Amsterdam, 1985 (ISBN 0-444-99553-6). xvi + 766 pp.

This volume contains a comprehensive account of the proceedings of the fourth international symposium on ion-selective electrodes, held at Mátrafüred, Hungary in October, 1984. The proceedings focussed on theoretical aspects of the subject, but practical applications were also covered. Fifty-one plenary, keynote and discussion lectures are presented, together with questions and comments for several papers. Publication is from camera-ready copy but the text and figures are generally very clear.

The subjects of the four plenary lectures presented were: chemical sensor mechanisms (R. P. Buck), polarization studies with ion-selective electrodes (K. Cammann and G. A. Rechnitz), flow analysis using ion-selective liquid membrane electrodes (N. Ishibashi et al.) and clinical applications of polymer membrane ion-selective electrodes (U. Oesch et al.). Other presentations covered a broad spectrum of ion-selective electrode theory and applications, including papers on chemically modified electrodes and chemically sensitive field effect transistors. This would, therefore, be a useful up-date volume for those working in the area of ion-selective electrodes.

P. J. Worsfold

Eric Reid and J. P. Leppard (Eds.), *Drug Metabolite Isolation and Determination*. Plenum Press, New York, 1983 (ISBN 0-306-41265-9). xii + 289 pp. Price £42.50.

This text is Volume 12A in the series of "Methodological Surveys in Biochemistry and Analysis". As such, it provides excellent, detailed, individual accounts of a range of problems relating to the determination of drugs and their metabolites in body fluids. It surveys the various chromatographic techniques, and deals with drugs, metabolites and conjugates, including a number of brief notes describing the experiences of individual authors. The book is based on the proceedings of the 4th Bioanalytical Forum held at the University of Surrey in 1981. This text, like some of its predecessors, is valuable in that it provides both good background articles on topics under discussion, and detailed analytical information which can be applied directly to the often difficult problems of particular drug or metabolite determination. In addition, this volume has a cumulative index of compound types covering Volumes 5, 7, 10 and 12A, and corrections to Volume 10 (Trace-Organic Sample Handling) and 11.

David R. Rossington, Robert A. Condrate and Robert L. Snyder (Eds.), *Advances in Materials Characterization, Materials Science Research, Vol. 15.* Plenum Press, New York, 1983 (ISBN 0-306-41347-7). xi + 680 pp. Price $89.50.

This volume comprises camera-ready copy of the proceedings of the Conference on Advances in Materials Characterization at Alfred University, New York, August, 1982. It contains 47 papers on the applications of surface spectroscopy, surface characterization, i.r. and raman spectroscopy, microscopy, x-ray techniques, mechanical and acoustic properties and crystallography to solid samples (glass, ceramics, oxides, etc.). In general, the reproduction of the papers is of a high standard, especially the numerous figures and photographs. Overall, the book presents an impressive account of the power of modern instrumental techniques in studying the solid state.

ANALYTICA CHIMICA ACTA, VOL. 184 (1986)

AUTHOR INDEX

ACA announcements

ANNOUNCEMENTS OF MEETINGS

38th PITTSBURGH CONFERENCE AND EXPOSITION ON ANALYTICAL CHEMISTRY AND APPLIED SPECTROSCOPY, ATLANTIC CITY, NJ, U.S.A., MARCH 9–13, 1987

Each year the Pittsburgh Conference proudly presents an intensive program of technical papers and symposia covering the newest and most innovative techniques in analytical chemistry and applied spectroscopy. Advances in methodology, instrumentation and theory, as well as challenges yet to be met, are presented and discussed in the Technical Program. The Technical Program for the 1987 Pittsburgh Conference and Exposition will consist of approximately 30 symposia and 900 contributed papers. Contributed papers are a vital part of the overall program. You are encouraged to participate in the 1987 programme as the author of a contributed paper. Abstracts may be submitted on all areas of analytical chemistry, spectroscopy and associated fields. The Program Committee will review each abstract in order to maintain the excellent quality of our Technical Program. Contributed papers may take the form of either posters or formal, oral presentations.

Four (4) copies of a 500-word abstract must be submitted for review; the deadline for receipt of abstracts is August 1, 1986. All abstracts will be carefully evaluated. The abstract should clearly state: (a) the objective of the work, (b) equipment and procedures used and (c) results and conclusions. Abstracts must include sufficient content for adequate evaluation by the Conference Program Committee. The Pittsburgh Conference reserves the right to reject any paper. The designated speaker will be notified of acceptance or rejection of the paper in November, 1986. Specific references to vendor products in the titles of papers are not permitted and will be automatically eliminated. No conference proceedings will be published. Authors may publish their papers after the conference. A second abstract will be required for reproduction in book form for distribution to the conferees. Forms and instructions concerning this second abstract will be sent to the designated speaker with the notification of acceptance of the paper. The second abstract will be due December 12, 1986. The title of the paper and the author information originally submitted cannot be changed for the Second Abstract; therefore, be sure you have the desired title and author information on the original abstract.

The 1987 program will also include a variety of short and mini-courses designed to maximize the educational value of the Pittsburgh Conference. Further information on the topics to be covered will appear in the update in October.

Authors wishing to present papers in the 1987 Pittsburgh Conference and Exposition Technical Program should submit four (4) copies of a 500-word abstract by August 1, 1986 to: Mrs. Alma Johnson, Program Secretary, 12 Federal Drive, Suite 322, Pittsburgh, PA 15235, U.S.A.

SCIENTIFIC COMPUTING AND AUTOMATION (EUROPE), AMSTERDAM, THE NETHERLANDS, MAY 13–15, 1987

This will be Europe's first conference and exhibition specifically for computing and automation in the sciences. Scientific Computing and Automation (Europe) will be the European counterpart to its successful sister meeting in the U.S.A. carrying the same name.

SCA Europe will be supported by a number of European societies, among them the Royal Society of Chemistry, and will be held at the RAI Congress Centre in Amsterdam, on 13–15th May, 1987. A full scientific programme will form the backbone of the meeting. The programme will be set up by a distinguished scientific board under the chairmanship of Prof. D.L. Massart from the Vrije Universiteit of Brussels, Brussels, Belgium. Workshops and short courses will be run in conjunction with the conference.

SCA Europe will devote parallel sessions to the latest advances in computing and automation in different scientific areas. These include chemistry (pharmaceutical, analytical, clinical, synthesis), the life sciences (clinical, microbiological), engineering and technology (bio, materials, chemical) and physics (mainly applied geophysics). Within the framework of these specialist fields, the programme will be concerned with computing (artificial intelligence, expert systems, image analysis, Computer Aided Learning (CAL), pattern recognition, molecular graphics, databases, simulation and off-the-shelf software, etc.), automation (LIMS, networking, data acquisition, sensors, process control, etc.) and robotics (laboratory products).

All the plenary and disciplinary sessions will be chaired by specialists in their own field who will also sit on the scientific programme committee and thus ensure the high quality of submitted papers. You are invited to send your abstracts to: Prof. D.L. Massart, Vrije Universiteit of Brussels, Laarbekelaan 103, B-1090 Brussels, Belgium.

For further information please contact: K. Foley, Scientific Computing and Automation, P.O. Box 330, 1000 AH Amsterdam, The Netherlands. Tel: (020) 5862 828.

1st INTERNATIONAL SYMPOSIUM ON THE INTERFACE BETWEEN ANALYTICAL CHEMISTRY AND MICROBIOLOGY; APPLICATIONS OF CHROMATOGRAPHY AND MASS SPECTROMETRY, COLUMBIA, SC, U.S.A., MAY 24–27, 1987

This new international symposium will serve to forge connections between analytical chemistry and microbiology at a level that emphasizes both the fundamental development and practical application of chromatographic and mass spectrometric methods. The depth of growing interdisciplinary efforts by both analytical chemists and microbiologists necessitates a symposium where both groups of researchers can meet on a common ground. The symposium will be planned with ample opportunity for discussion in large groups as well as in informal settings. Plenary lectures will be presented by speakers invited by the International Organizing Committee. Contributions in the forms of presented papers and posters are also solicited from participants. A book of the symposium papers will be published after a normal editing and review process.

The site of the meeting will be at the conference facilities of the University of South Carolina in Columbia, SC, U.S.A.

The symposium will have an interdisciplinary flavor, emphasizing analytical chemical applications of chromatography and mass spectrometry in microbiology, including the following topics: chemotaxonomy; direct analysis of chemical markers for microorganisms; GC, LC and MS in environmental microbiology; applications of GC, LC, and MS to food microbiology; analysis of tissues and fluids for bacteria and fungi; rapid detection and identification of biological materials; clinical microbiology applications; computer assisted pattern recognition/data handling; sample handling/preparation; pyrolysis GC, pyrolysis MS, pyrolysis, GC–MS of microorganisms; derivatization methods coupled to GC, GC–MS, LC, and LC–MS; headspace analysis of volatile fermentation products; GC and MS monitoring of fermentation; high resolution MS methods; and new detection methods.

The registration fee ($150 if paid by February 24, 1987; $180 if paid after February 24, 1987) will cover the cost of attending the meeting and include a copy of the symposium proceedings book when published, the banquet, and hospitality mixers.

Further information can be obtained from: 1st International Symposium on the Interface between Analytical Chemistry and Microbiology, P.O. Box 7126, Columbia, SC 29202, U.S.A.

WORKING PARTY ON ANALYTICAL CHEMISTRY (WPAC/FECS)

EUROPEAN ANALYTICAL COLUMN 9

In January 1986, the WPAC membership remained at the same high level as the year before; 29 chemical societies from 23 European countries are represented by 27 delegates. Spain is now represented by the "Spanish Society for Analytical Chemistry" in addition to the "Spanish Royal Society for Chemistry". Only the Society of Luxembourg Chemists and the Pancyprian Union of Chemists among the FECS members are not yet active in the WPAC. The chemical societies of Egypt, the G.D.R., Israel and Rumania as well as IUPAC have observer status.

The 16th meeting of the WPAC was held in Vienna, November 24, 1985, and was attended by 21 delegates (Chairman: Prof. E. Pungor).

The following activities of the WPAC should be noted.

Euroanalysis Conferences

Euroanalysis V, August 26–31, Cracow, Poland. President: Prof. A. Hulanicki. The proceedings of this conference contain all but one of the fourteen invited lectures and are available now in the series "Review on Analytical Chemistry" from Akademiai Kiado, Budapest, Hungary.

Euroanalysis VI, September 7–11, 1987, Paris, France. President: Prof. E. Roth with Prof. A. Hulanicki, Prof. H. Malissa. The first circular including information on selected topics and special sessions is available. Please contact Prof. E. Roth, or GAMS, 88, Bd. ds Malesherbes, F-75008 Paris, France.

Euroanalysis VII, August 27–31, 1990, Vienna, Austria. President: Prof. J.F.K. Huber, Host Society: Austrian Society for Microchemistry and Analytical Chemistry.

Events sponsored or supported by WPAC in 1985

4th Scientific Session on Ion Selective Electrodes, October 8–12, 1984, Matrafüred, Hungary. Chairman: Prof. E. Pungor. Proceedings containing all plenary, keynote and discussion lectures are available now from Akademiai Kiado and Elsevier.

12th International Competition in Analytical Chemistry, May 13–15, 1985, Veszprem, Hungary. Chairman: Prof. J. Inczedy. Students from European countries participated; this meeting will be repeated in 1986 in Szeged.

1st International Symposium on Philosophy and History in Analytical Chemistry, November 22–23, 1985, Vienna/Schallaburg, Austria. Chairmen: Prof. H. Malissa and Prof. F. Szabadvary. In the stimulating historic environment, 54 participants from 18 countries discussed the impact and importance of selected time periods and philosophical aspects in the development of analytical chemistry; the philosophical papers will be published.

Education in Analytical Chemistry. The WPAC brochure has been distributed to all 229 participating institutions; a few further copies are available at the secretariat.

Further activities sponsored or supported by WPAC

COBAC IV, September 15–19, 1986, Graz, Austria. Chairmen: Doz. W. Wegscheider, Doz. K. Varmuza. The first circular is available as well as detailed information on the programme.

Symposium on Bioelectroanalysis, October 6–8, 1986, Matrafüred, Hungary, organized by the Electroanalytical Committee of the Hungarian Academy of Sciences.

6th International Conference on Fourier-Transform Spectroscopy, August 24–28, 1987, Vienna, Austria. Chairman: Prof. G. Zerbi, Milan, Italy. Programme Chairman: Dr. G. Guelachvili, Paris, Secretary: Prof. R. Kellner, Technical University Vienna, Institute for Analytical Chemistry, Getreidemarkt 9, A-1060, Wien, Austria. The first circular is available from the Secretariat.

European Conference on Molecular Spectroscopy (EUCMOS 18), August 30–September 4, 1987, Amsterdam, The Netherlands. President: Prof. Orville-Thomas. The first circular was sent out recently. The coordinative effort of WPAC has made it possible to link the FTS-Conference in Vienna, EUCMOS in Amsterdam and Euroanalysis VI in Paris without time clashes.

8th European Symposium on Polymer Spectroscoy (ESOPS 8), 1988, Budapest, Hungary, organized by the Hungarian Academy of Sciences.

For any further informations related to WPAC activities, please contact the secretary, Prof. Dr. R. Kellner, Institute for Analytical Chemistry, Technical University Vienna, Getreidemarkt 9, A-1060 Wien, Austria.

SCIENTIFIC SOFTWARE

SOFTWARE AVAILABLE FROM AUTHORS

A new section of this journal has started, which will give authors of computer progams the opportunity to announce software that they are willing to share with their colleagues. The aims of the section have been outlined in an Editorial (*Anal. Chim. Acta*, 173 (1985) 1). The programs offered will be listed in this section of the journal, as information becomes available.

Further details and forms for entry are available from Professor J.T. Clerck, Universität Bern, Pharmazeutisches Institut, Baltzerstrasse 5, CH-3102 Bern, Switzerland.

CALENDAR OF FORTHCOMING MEETINGS

July 7–10, 1986
Bordeaux, France

2nd International Meeting on Chemical Sensors
Contact: Dr. Claude Lucat, 2nd International Meeting on Chemical Sensors, Université de Bordeaux I, 351, cours de la Libération, 33405 Talence, Cedex, France.

July 14–17, 1986
Ottawa, Canada

10th International CODATA Conference
Contact: Mrs. Lois Baignée, Executive Secretary CODATA '86, Conference Services, National Research Council of Canada, Montreal Road, Ottawa, K1A OR6 Canada. (Further details published in Vol. 172.)

July 20–26, 1986
Bristol, U.K.

SAC 86 – International Conference and Exhibition on Analytical Chemistry
Contact: Miss P.E. Hutchinson, Royal Society of Chemistry, Analytical Division, Burlington House, London W1V 0BN, U.K. Tel.: (01) 734-9971. (Further details published in Vol. 169.)

July 28–Aug. 1, 1986
New Hampton, NH, U.S.A.

Gordon Research Conference on Statistics in Chemistry and Chemical Engineering
Contact: Conference Chairman, Gary Blau, The Dow Chemical Company, 1776 Building, Midland, MI 48640, U.S.A. Tel.: (517) 636-5170.

Aug. 10–17, 1986
Ottawa, Canada

6th International Congress of Pesticide Chemistry
Contact: T.H.G. Michael, Chemical Institute of Canada, 151 Slater Street, Suite 9065, Ottawa, Ontario, Canada K1P 5H3. Tel.: (613) 233-5623. Telex: 053-4306 AIC.

Aug. 17–21, 1986
Seattle, WA, U.S.A.

6th International Conference on Methods in Protein Sequence Analysis
Contact: MPSA, Conference Management, GH-22 University of Washington, Seattle, WA, U.S.A. Tel.: (206) 543-2300, telex: (910) 474 0096 UW UI.

Aug. 17–23, 1986
The Hague, The Netherlands

15th International Symposium on the Chemistry of Natural Products
Contact: Dr. G.J. Koomen, Secretary, 15th IUPAC International Symposium on the Chemistry of Natural Products, Laboratorium voor Organische Scheikunde, Universiteit van Amsterdam, Nieuwe Achtergracht 102, 1018 WS Amsterdam, The Netherlands.

Aug. 25–29, 1986
Antwerp, Belgium

10th International Symposium on Microchemical Techniques
Contact: Dr. R. Dewolfs, University of Antwerp, Department of Chemistry, Universiteitsplein 1, B-2610 Wilrijk, Belgium. Tel.: 03/828.25.28 (ext. 204), telex: 33646. (Further details published in Vol. 169.)

Aug. 26–27, 1986 Antwerp, Belgium	**3rd International Laser Microprobe Mass Spectrometry Workshop 1986** Contact: L. Van Vaeck, UIA-University of Antwerp, Department of Chemistry, Universiteitsplein 1, B-2610 Wilrijk, Belgium. Tel.: (03) 828 25 28, telex: 33646.
Aug. 26–29, 1986 Dunedin, New Zealand	**10th Conference of the Australian and New Zealand Society for Mass Spectrometry** Contact: Dr. J. Cutfield, Department of Biochemistry, University of Otago, Box 56, Dunedin, New Zealand. (Further details published in Vol. 175.)
Aug. 31–Sept. 5, 1986 Eugene, OR, U.S.A.	**10th International Conference on Raman Spectroscopy** Contact: Prof. Warner L. Peticolas, Department of Chemistry, University of Oregon, Eugene, OR 97403-1210, U.S.A.
Sept., 1986 Graz, Austria	**4th Conference on Computer Based Analytical Chemistry** Contact: Dr. Wolfhard Wegscheider, Institut für Analytische Chemie, Mikro- und Radiochemie, Technische Universität, Technikerstrasse 4, A-8010 Graz, Austria. Tel: (0316) 7061-8300/8301. (Further details published in Vol. 172.)
Sept. 8–10, 1986 Freiburg, F.R.G.	**4th International Symposium on Bioluminescence and Chemiluminescence** Contact: Dr. J. Schölmerich, Medizinische Universitätsklinik, D-7800 Freiburg, F.R.G.
Sept. 9–12, 1986 London, U.K.	**5th Meeting of the International Electrophoresis Society, "Electrophoresis '86"** Contact: Dr. M.J. Dunn, Muscle Research Unit, Royal Postgraduate Medical School, DuCane Road, London W12 0HS, U.K. Tel.: 01-743-2030 ext. 338.
Sept. 9–12, 1986 Preveca, Greece	**2nd International Symposium on Kinetics in Analytical Chemistry** Contact: Prof. N. Evmirides, Laboratory of Analytical Chemistry, Chemistry Department, University of Ioannina, Ioannina, Greece.
Sept. 15–18, 1986 Houston, TX, U.S.A.	**22nd International Symposium on Advances in Chromatography** Contact: Professor A. Zlatkis, Chemistry Department, University of Houston, Houston, 77004 TX, U.S.A. Tel.: (713) 749 2633. (Further details published in Vol. 178, No. 2.)
Sept. 15–19, 1986 Reading, U.K.	**7th International Symposium on Analytical and Applied Pyrolysis** Contact: Dr. C.S. Gutteridge, Cadbury Schweppes Plc, The Lord Zuckerman Research Centre, The University, Whiteknights, P.O. Box 234, Reading RJ6 2LA, U.K.
Sept. 25–26, 1986 Cambridge, U.K.	**International Conference on Enzyme Engineering** Contact: Miss Fiona Spindlove, IBC Technical Services Ltd., Bath House, 56 Holborn Viaduct, London, EC1A 2EX, U.K. Tel.: (01) 236 4080, telex: 888870.
Sept. 29–Oct. 3, 1986 St. Louis, MO, U.S.A.	**FACSS '86, Federation of Analytical Chemistry and Spectroscopy Societies 1986 Meeting** Contact: Dr. Marshall Fishman, U.S. Department of Agriculture, 600 E. Mermaid Lane, Wyndmoor, PA 19118, U.S.A. Tel.: (215) 233-6450. (Further details published in Vol. 178, No. 2.)
Oct. 6–8, 1986 Mátrafüred, Hungary	**Bioelectroanalytical Symposium 1986** Contact: Organizing Committee of Bioelectroanalytical Symposium 1986, Institute for General and Analytical Chemistry, Technical University, Gellért tér 4, 1502 Budapest, Hungary.

Oct. 6–9, 1986 Gaithersburg, MD, U.S.A.	**1986 Meeting of the National Conference of Standards Laboratories; 25 Years of Measurement Progress** Contact: Ernest L. Garner, B362 Physics Building, National Bureau of Standards, Gaithersburgh, MD 20899, U.S.A. Tel.: (301) 921 2805.
Oct. 6–10, 1986 Biarritz, France	**5th International Conference on Reliability and Maintainability** Contact: Secretariat of the Conference, A.D.E.R.A.-C.E.A., B.P. 48, 33166 Saint-Médard-en-Jalles Cedex, France. Tel.: 56 05 84 25-256, telex: 560 715 F.
Oct. 7–11, 1986 Seattle, WA, U.S.A.	**5th International Symposium on New Spectroscopic Methods for Biomedical Research and Short Courses on Biomedical ESCA and Biomedical FTIR** Contact: Buddy D. Ratner, Ph.D., Department of Chemical Engineering, BF-10, University of Washington, Seattle, WA 98195, U.S.A. Tel.: (206) 545 1005.
Oct. 8–10, 1986 Palma de Mallorca, Spain	**3rd Symposium on Handling of Environmental and Biological Samples in Chromatography** Contact: Prof. Dr. R.W. Frei, Department of Analytical Chemistry, Free University, De Boelelaan 1083, 1081 HV Amsterdam, The Netherlands. Tel.: (020) 5485379. (Further details published in Vol. 181.)
Oct. 16–17, 1986 London, U.K.	**3rd European Seminar and Exhibition on Computer-Aided Molecular Design** Contact: Miss Fiona Spindlove, IBC Technical Services Ltd., Bath House, 56 Holborn Viaduct, London, EC1A 2EX, U.K. Tel.: (01) 236 4080, telex: 888870.
Oct. 19–22, 1986 Boston, MA, U.S.A.	**4th International Symposium on Laboratory Robotics** Contact: Gerald L. Hawk, Ph.D. and Janet Strimaitis, Zymark Corporation, Zymark Center, Hopkinton, MA 01748, U.S.A. Tel.: (617) 435-9501.
Oct. 20–22, 1986 Baden-Baden, F.R.G.	**6th International Symposium on High-Performance Liquid Chromatography of Proteins, Peptides and Polynucleotides** Contact: Secretariat 6th ISPP, P.O. Box 3980, D-6500 Mainz, F.R.G
Oct. 20–24, 1986 New York, NY, U.S.A.	**The Silver Jubilee Eastern Analytical Symposium** Contact: Dr. S. David Klein, EAS Publicity, 642 Cranbury Cross Road, North Brunswick, NJ 08902, U.S.A. Tel.: (201) 846-1582. (Further details published in Vol. 178, No. 2.)
Oct. 21–23, 1986 Gaithersburg, MD, U.S.A.	**32nd Annual Conference on Bioassay, Analytical and Environmental Radiochemistry** Contact: Kenneth Inn, C114 Radiation Physics Building, National Bureau of Standards, Gaithersburg, MD 20899, U.S.A. Tel.: (301) 921 2383.
Oct. 22–24, 1986 Montreux, Switzerland	**4th Symposium on Liquid Chromatography–Mass Spectrometry and Mass Spectrometry–Mass Spectrometry** Contact: Professor Dr. R.W. Frei, Department of Analytical Chemistry, Free University, De Boelelaan 1083, 1081 HV Amsterdam, The Netherlands. Tel.: (020) 5485379. (Further details published in Vol. 181.)
Oct. 23–24, 1986 Graz, Austria	**IFAC Workshop on Mass Spectrometry in Biotechnological Process Analysis and Control** Contact: IFU-MS-Workshop, Elisabethstrasse 11, A-8010 Graz, Austria. Tel.: (0316) 36030-17.

Nov. 11–13, 1986 Stockholm, Sweden	**International Symposium on Immunoassays – Present Status and Future Perspectives** Contact: The Swedish Academy of Pharmaceutical Sciences, P.O. Box 1136, S-111 81 Stockholm, Sweden.
Nov. 12–14, 1986 Gaithersburg, MD, U.S.A.	**1986 International Workshop on Moisture Measurement and Control for Microelectronics** Contact: Stanley Ruthberg, A331 Technology Building, National Bureau of Standards, Gaithersburg, MD 20899, U.S.A. Tel.: (301) 921 3625.
Nov. 17–20, 1986 Gaithersburg, MD, U.S.A.	**Scientific Software for Supercomputing** Contact: Francis E. Sullivan, A151 Technology Building, National Bureau of Standards, Gaithersburg, MD 20899, U.S.A. Tel.: (301) 921 3395.
Nov. 18–20, 1986 Teddington, U.K.	**4th International Conference on Quantitative Surface Analysis, Techniques and Applications and VAMAS Workshop** Contact: Conference Secretary, Dr. G.C. Smith, Division of Materials Applications, National Physical Laboratory, Teddington, Middlesex, TW11 0LW, U.K. Tel.: (01) 977 3222, telex: 262344. (Further details published in Vol. 178, No. 2.)
Nov. 18–21, 1986 Atlanta, GA, U.S.A.	**10th Symposium on Flue Gas Desulferization** Contact: Brooke Eldredge, Symposium Coordinator, Electric Power Research Institute, 3412 Hillview Avenue, P.O. Box 10412, Palo Alto, CA 94303, U.S.A. Tel.: (415) 855 7919.
Nov. 25–29, 1986 Milan, Italy	**26th MAC, International Exhibition of Chemistry, Analysis, Research, Test Equipment and Biotechnology** Contact: MAC '86 General Secretariat, Via Domenichino 11, 20149 Milan, Italy. Tel.: (02) 4815541.
Nov. 26–29, 1986 Milan, Italy	**ATB '86, Advanced Technology for the Clinical Laboratory and Biotechnology (2nd European Edition of the Oak Ridge Conference)** Contact: MAC '86, Dott. Laura Pinna Berchet, Via Domenichino 11, 20149 Milan, Italy.
March 9–13, 1987 Atlantic City, NJ, U.S.A.	**38th Pittsburgh Conference and Exposition on Analytical Chemistry and Applied Spectroscopy** Contact: Mrs. Alma Johnson, Program Secretary, 12 Federal Drive, Suite 322, Pittsburgh, PA 15235, U.S.A.
April 6–9, 1987 Cardiff, U.K.	**International Symposium on electroanalysis in Biomedical, Environmental and Industrial Sciences** Contact: Short Courses Section, UWIST, P.O. Box 68, Cardiff CF1 3XA, Wales, U.K. Tel.: (0222) 42588, ext. 2213. (Further details published in Vol. 178, No. 2.)
April 27–May 1, 1987 Sydney, Australia	**9th Australian Symposium on Analytical Chemistry** Contact: The Secretary 9AC, Mr. John Eames, P.O. Box 137, North Ryde, N.S.W. 2133, Australia. Tel.: (02) 887-8688. (Further details published in Vol. 178, No. 2.)
May 11–14, 1987 Ghent, Belgium	**2nd International Symposium on Quantitative Luminescence Spectrometry in Biomedical Sciences** Contact: Dr. W. Bayens, State University of Ghent, Laboratory of Pharmaceutical Chemistry and Drug Quality Control, Harelbekestraat 72, B-9000 Ghent, Belgium. (Further details published in Vol. 178, No. 2.)

May 13–15, 1987 Amsterdam, The Netherlands	**Scientific Computing and Automation (Europe)** Contact: K. Foley, Scientific Computing and Automation, P.O. Box 330, 1000 AH Amsterdam, The Netherlands. Tel.: (020) 5862 828.
May 17–22, 1987 Tokyo, Japan	**CHEMRAWN VI, World Conference on Advanced Materials Needed for Innovations – Energy, Transportation and Communications** Contact: Mr. H. Hamada, Executive Director, The Chemical Society of Japan, 1-5 Kanda-Suragadi, Chiyoda-ku, Tokyo, Japan.
May 24–27, 1987 Columbia, SC, U.S.A.	**1st International Symposium on the Interface between Analytical Chemistry and Microbiology** Contact: 1st International Symposium on the Interface between Analytical Chemistry and Microbiology, P.O. Box 7126, Columbia, SC 29202, U.S.A.
June 17–19, 1987 Fort Collins, CO, U.S.A.	**Conference on Chemically Modified Surfaces** Contact: W. Collins, Mail Stop C41C00, Dow Corning Corporation, Midland, MI 48686-0994, U.S.A.
June 21–26, 1987 Toronto, Canada	**XXV Colloquium Spectroscopium Internationale** Contact: Mr. L. Forget, Executive Secretary CSI XXV, National Research Council of Canada, Ottawa, K1A 0R6 Canada. Tel.: (613) 993-9009, telex: 053-3145. (Further details published in Vol. 172.)
June 28–July 4, 1987 Amsterdam, The Netherlands	**HPLC '87, 11th International Symposium on Column Liquid Chromatography** Contact: Organisatie Bureau Amsterdam bv, Europaplein, 1078 GZ Amsterdam, The Netherlands. Tel.: (31) 20-440807, telex: 13499 raico nl. (Further details published in Vol. 181.)
July 13–18, 1987 Sofia, Bulgaria	**31st IUPAC Congress** Contact: Dr. R. Vlahov, Institute of Organic Chemistry, Bulgarian Academy of Sciences, 1113 Sofia, Bulgaria. Telex: 22729 ECHBAN BG. (Further details published in Vol. 181.)
Aug. 24–28, 1987 Vienna, Austria	**6th International Conference on Fourier Transform Spectroscopy** Contact: Interconvention, P.O. Box 80, A-1107 Vienna, Austria. Tel.: (222) 57 63 05, 57 62 88, telex: 11 12 10.
Aug. 25–30, 1987 Beijing, China	**8th International Conference on Computers in Chemical Research and Education** Contact: Cheng Qian, 345 Lingling Road, 200032 Shanghai, China. Telex: 33354 SIOC CN.
Aug. 30–Sept. 4, 1987 Amsterdam, The Netherlands	**EUCMOS XVIII, 18th European Congress on Molecular Spectroscopy** Contact: EUCMOS XVIII, c/o Municipal Congress Bureau, P.O. Box 2289, 1000 CG Amsterdam, The Netherlands. Tel.: (3120) 552 3459, telex: 16460 anal. chem.
Sept. 7–11, 1987 Paris, France	**Euroanalysis VI, European Conference on all Aspects of Analytical Sciences** Contact: G.A.M.S., 88 Boulevard Malesherbes, 75008 Paris, France. (Further details published in Vol. 181.)
Sept. 28–Oct. 1, 1987 Gaithersburg, MD, U.S.A.	**Accuracy in Trace Analysis – Accomplishments, Goals, Challenges** Contact: Harry Hertz, A309 Chemistry Building, National Bureau of Standards, Gaithersburg, MD 20899, U.S.A. Tel.: (301) 921 2851. (Further details published in Vol. 181.)

Sept. 28–Oct. 2, 1987 Amsterdam, The Netherlands	**2nd Amsterdam *HPLC* Summercourse** Contact: Dr. J.C. Kraak, Laboratory for Analytical Chemistry, University of Amsterdam, Nieuwe Achtergracht 166, 1018 WV Amsterdam, The Netherlands.
Oct. 19–23, 1987 Fellbach, F.R.G.	**ECASIA '87, European Conference on Applications of Surface and Interface Analysis** Contact: U. Nagorny, Max-Planck-Institut für Metallforschung, Institut für Werkstoffwissenschaften, Seestrasse 92, D-7000 Stuttgart 1, F.R.G.
April 18–21, 1988 Las Vegas, NV, U.S.A.	**Flow Analysis IV, An International Conference on Flow Analysis** Contact: Dr. Gilbert E. Pacey, Department of Chemistry, Miami University, Oxford, OH 45056, U.S.A. (Further details published in Vol. 181.)

tinued from outside back cover)

CONTENTS

(Abstracted, Indexed in: Anal. Abstr.; Biol. Abstr.; Chem. Abstr.; Curr. Contents Phys. Chem. Earth Sci.; Life Sci.; Index Med.; Mass Spectrom. Bull.; Sci. Citation Index; Excerpta Med.)

(continued on inside back cove